Rupture de symétrie et formation de structures dans certaines équations de champs neuronaux

Grégory Faye

UNIVERSITY OF NICE - SOPHIA ANTIPOLIS
DOCTORAL SCHOOL SFA
SCIENCES FONDAMENTALES APPLIQUEES

P H D T H E S I S

to obtain the title of

PhD of Science

of the University of Nice - Sophia Antipolis
Specialty : Applied Mathematics

Defended by

Grégory Faye

Symmetry breaking and pattern formation in some neural field equations

Thesis Advisors:
- Pascal Chossat
- Olivier Faugeras

prepared at INRIA Sophia Antipolis, NeuroMathComp Team

defended on June 11, 2012

Committee :

Reviewers :	Martin Golubitsky	-	MBI Ohio State University
	Arnd Scheel	-	University of Minnesota
Examinators :	Stephen Coombes	-	University of Nottingham
	Yves Frégnac	-	UNIC, Gif-sur-Yvette
	Reiner Lauterbach	-	University of Hamburg
	Benoit Perthame	-	University Pierre et Marie Curie

Abstract

The aim of this Thesis is to give a deeper understanding of pattern formation in neural field equations with symmetry, and to understand the significance of these symmetries in modeling the visual cortex. Neural field equations are mesoscopic models that describe the spatio-temporal activity of populations of neurons. They were introduced in the 1970s and are often called the Wilson-Cowan-Amari equations in reference to their authors. From a mathematical point of view, neural field equations are integro-differential equations set on domains particular to the modeled anatomical / functional properties. The first part of the Thesis is an introduction to mesoscopic modeling of the visual cortex and presents a model of the processing of image edges and textures. The second part is dedicated to the study of spatially periodic solutions of neural field equations, in different geometries, with applications to visual hallucination patterns. The results developed are general enough to be applied to other pattern formation problems. Finally, the last part is centered on the study of localized solutions of neural field equations set on unbounded domains.

Résumé

Cette thèse se propose de comprendre la formation de structures dans les équations de champs neuronaux en présence de symétrie ainsi que la conséquence pour la modélisation du cortex visuel. Les équations de champs neuronaux sont des modèles mésoscopiques qui décrivent l'activité spatio-temporelle de populations de neurones. Elles ont été introduites dans les années 1970 et sont souvent appelées les équations de Wilson-Cowan-Amari en référence à leurs auteurs. D'un point de vue mathématique, les équations de champs neuronaux sont des équations intégro-différentielles posées sur des domaines qui dépendent des propriétés anatomiques et/ou fonctionnelles modélisées. Dans la première partie, nous rappelons quelques éléments de biologie du cortex visuel, dérivons les équations de champs neuronaux de manière générale et introduisons ensuite une nouvelle classe de champs neuronaux pour le problème de modélisation de la perception des textures. La seconde partie de cette thèse est dédiée à l'étude de formation de structures en géométrie non-euclidienne et s'appuie principalement sur la théorie des systèmes dynamiques en dimension infinie en présence de symétrie. Cette seconde partie est relativement indépendante des autres et est écrite de manière suffisamment générale pour pouvoir être appliquée de façon systématique à tout problème de formation de structures en géométrie non-euclidienne satisfaisant certaines conditions de généricité. Enfin, dans la dernière partie, nous étudions l'existence de solutions localisées pour une certaine classe de champs neuronaux définis sur des domaines non bornés.

Acknowledgments

I would like to thank the members of my committee: Martin Golubitsky, Arnd Scheel, Stephen Coombes, Yves Frégnac, Reiner Lauterbach and Benoît Perthame. Your work has been a constant source of inspiration for my research. I would like to deeply thank my reviewers Martin Golubitksy and Arnd Scheel for taking the time to read carefully, comment and criticize this thesis. I am extremely grateful to Benoît Perthame for his constant support and advice since my master degree. I warmly thank Yves Frégnac for his patience in listening to me talking about mathematical modeling of "texture" and answering my questions about biology. I have a special thought for Stephen Coombes who has always been very kind with me, especially during conferences, I am really pleased you accepted to be in my committee. Finally, I would like to thank Reiner Lauterbach for accepting to be in my committee despite extremely busy schedule. I would also like to thank him for providing a GAP program to determine the biquaternionic representation of the octagonal group as well as its four-dimensional irreducible representations.

I would like to thank James Rankin for his numerical support. Most of the figures in the last part of this Thesis would have been impossible without his help.

My last acknowledgment goes to David Lloyd. He has been the first to introduce me into the world of localized patterns in the Swift-Hohenberg equation. I am sure that our collaboration initiated in May 2011 during the SIAM Conference on Dynamical Systems will lead us to new and exciting problems. I would also like to thank him for the careful reading of the last part of my Thesis and for all the hours spent on AUTO problems.

This work was partially funded by the ERC advanced grant NerVi number 227747 and by the European Union Seventh Framework Program (FP7/2007- 2013) under grant agreement no. 269921 (BrainScaleS).

Remerciements

Mes premiers remerciements vont tout particulièrement à mes deux directeurs de thèse Pascal Chossat et Olivier Faugeras qui m'ont tous deux guidé dans mes premiers pas dans le monde de la recherche depuis mon stage de M2 jusqu'à l'aboutissement de cette thèse. Olivier a toujours su me proposer des sujets de recherche passionnants, souvent à l'interface entre mathématiques appliquées et modélisation. Si son soutien et ses conseils ont toujours été précieux, j'ai également beaucoup apprécié la confiance et la très grande liberté qu'il m'a accordées. Je ne le remercierai jamais assez pour m'avoir permis de réaliser un de mes rêves: donner des cours de M2 à l'ENS Paris le temps d'un demi-semestre. Quant à Pascal, il m'a ouvert les yeux sur un domaine entier des mathématiques appliquées que je ne connaissais pas avant de le rencontrer: le monde des brisures de symétries spontanées et/ou forcées dans les systèmes dynamiques. Il m'a également permis de voir à quel point la frontière entre les mathématiques dites pures et appliquées était perméable. Travailler à ses côtés a toujours été extrêment enrichissant pour moi. Je les remercie chaleureusement pour leur générosité et leur investissement.

Je tiens également à remercier Benoît Perthame et Robert Eymard pour tout le temps qu'ils m'ont accordé depuis mon M2.

La liste des autres personnes à remercier serait inifinie mais je me dois de commencer par Romain et Mathieu avec qui j'ai passé un nombre incroyable d'heures à parler de nos problèmes mathématiques et qui ont toujours été présents lorsque j'ai eu besoin d'eux. Je tiens également à remercier toutes les personnes (permanents et étudiants) des équipes NeuroMathComp et Athéna, avec une pensée toute particulière pour Pierre pour les heures passées à soulever de la fonte dans la joie et la bonne humeur. Je voudrais enfin souligner la gentillesse de Marie-Cécile sans qui bien des choses auraient été plus compliquées.

Je remercie chaleureusement James, Chloé et Astrid pour tous les délicieux moments passés ensemble, sans oublier Emilien et Danièle pour leur infinie gentillesse.

Je voudrais finalement remercier tous ceux, famille et amis qui à Lyon, Paris, Antibes ou ailleurs ont été à mes côtés pendant ces années avec amour et amitié.

Mes derniers mots vont pour mes parents et ma soeur. Merci pour votre éducation et tous les moments que nous avons pu passer ensemble et pour ceux qui arriveront encore. Je trépigne d'impatience de vous voir venir dans mon nouveau chez moi aux Etats-Unis... Quant à toi, petite soeur, merci d'avoir toujours été là lorsque j'en ai eu besoin et de m'avoir accepté tel que je suis.

Finalement, je tiens à embrasser ma femme Barbara qui a été d'un éternel soutien tout au long de cette thèse. Je lui suis mille fois reconnaissant d'avoir toujours accepté de me suivre où que j'aille: de Paris à Antibes puis maintenant d'Antibes à Minneapolis. Je lui dédie cette thèse.

To my wife Barbara,
For her support,
For her love.

Introduction

This Thesis is oriented toward the study of mesoscopic models of cortical activity through the symmetries that these models possess. This work is at the frontier between mathematical neuroscience and applied mathematics as it provides specific results for some neuronal models and also general theoretical results that can also be applied to models in a more general context. Throughout this Thesis, we will use neural fields equations which model the spatio-temporal activity of populations of neurons. These equations are a first approximation of the mean membrane potential of populations of neurons that are distributed in the cortex and should be thought of has elementary mean field equations. We will be interested in the spontaneous activity of the cortex and thus will assume that our models work without any external input. In general, we aim to characterize the different possible solutions that can emerge from homogeneous state with respect to the symmetries that we assume in the model. We now give a brief summary of each part of the Thesis.

Part I: Mesoscopic modeling of the visual cortex

This part is an introduction to mesoscopic modeling of the visual cortex. The first chapter 1 is focused on the biology: it gives an overview of visual processing and highlights the notion of a cortical column in the primary visual cortex. The nonlinear dynamics of individual neurons forming these columns are taken into account in chapter 2 where we present the neural field formalism that will be used throughout this Thesis. In the last chapter 3, we introduce a model of processing of image edges and textures together with all the mathematical background related to this modeling. The study of some particular solutions of this model acts as a guideline for the results developed in the following parts.

Part II: Symmetry breaking mechanism in neural field equations

Neural field equations are infinite dimensional dynamical systems that can be defined on various state spaces. In this Thesis we consider unbounded state spaces that can have either a Euclidean or hyperbolic geometry. Neural field equations display stationary solutions which are interpreted as time independent cortical activity. In these equations, there is a connectivity function which describes the coupling between different populations of neurons. In particular, we will consider connectivities which only depend upon the distance between two points in the state space. This will naturally induce an invariance of the system with respect to the symmetries of the domain that are transfered in some way to the solutions of the equations. However, depending on the parameters, the neural field equations can

have multiple stationary solutions which have less symmetries than the symmetries of the original equations. This type of bifurcation with symmetries is known as spontaneous symmetry-breaking mechanism. This part focuses on the study of spontaneous symmetry-breaking mechanism for stationary solutions which are assumed to be periodic with respect to a given lattice. More precisely, we apply tool from equivariant bifurcation theory to classify stationary solutions, with respect to their symmetries, in the cases where the state space is the Euclidean plane, the Poincaré disk and the direct product of the Euclidean plane and the Poincaré disk. The main contribution of this part is a complete analysis of nonlinear pattern formation in the Poincaré disk for a regular octagonal tiling. We have applied our results to a neural fields model describing a network of interacting hypercolumns of "structure tensors" (see chapters 3 and 8) which has led to the description of new visual cortical hallucination planforms.

Part III: Localized states on unbounded neural field equations

In part II, we have studied spatially periodic solutions of unbounded neural field equations with respect to some given lattices. In this part, we show the existence of an other type of solution that emerges naturally in systems set on unbounded domains, namely localized solutions. In the neuroscience community, this class of solutions are considered to be the analog of short-term memory and thus are of particular interest. The main results of this part are proof of the existence of localized states for different state spaces: the real line, the Euclidean plane and the Poincaré disk. For the one dimensional case, the results rely on the theory of homoclinic bifurcation with reversible symmetry and are illustrated with "snaking" bifurcation diagrams. For the two dimensional problems (Euclidean plane and Poinacré disk), we only deal with radially symmetric solutions and the proofs are drawn on the methods developed in [Scheel 2003, Lloyd 2009, McCalla 2010] for the Swift-Hohenberg equation.

Publications

A part of the work in chapter 3 is published in [Faye 2011b]. Chapter 6 on pattern formation in the Poincaré disk is published in [Chossat 2011]. The study of the irreducible representations of dimension four is published in [Faye 2011a]. The spatialized model of interacting hypercolumns of chapter 8 has been submitted to the journal Networks and Heterogeneous Media [Faye 2012b]. The study of localized solutions on the real line with smooth firing-rate function is a collaboration with James Rankin and has been published in the Journal of Mathematical Biology [Faye 2012c]. The PDE method developed in the Poincaré disk is published in [Faye 2012a].

Introduction (Version française)

Cette thèse a pour but d'étudier des modèles mésoscopiques de l'activité corticale à travers les symétries que possèdent ces modèles. Ce travail se situe à la frontière entre les neurosciences mathématiques et les mathématiques appliquées puisqu'il donne des résultats pour des modèles neuronaux spécifiques et également des résultats théoriques généraux qui peuvet être appliqués dans d'autres types de modèles. Tout au long de cette thèse, nous utiliserons le formalisme des équations de champs neuronaux. Ces équations sont des modèles corticaux décrivant l'activité spatio-temporelle de populations de neurones. Ces équations sont une première approximation du potentiel de membrane de populations de neurones distribuées dans le cortex et doivent être considérées comme des équations de champ moyen simplifiées. Nous nous intéresserons à l'activité spontanée du cortex et supposerons donc que nos modèles ne reçoivent aucun signal du monde extérieur. Nous allons caractériser les différentes solutions possibles qui peuvent émerger à parti d'un état homogène en fonction des symétries que l'on suppose présentent dans le modèle considéré. Nous donnons maintenant un rapide résumé de chaque partie.

Partie I: modélisation mésoscopique du cortex visuel

Cette première partie est une introduction à la modélisation mésoscopique du cortex visuel. Le premier chapitre est une introduction à la biologie du cortex où l'on donne une vue d'ensemble du traitement de l'information dans les aires visuelles. Nous donnons également des définitions précises sur la notion de colone corticale. La dynamique nonlinéaire de chaque neurone formant ces colones est prise en compte dans le chapitre 2 où nous présentons le formalisme des équations de champs neuronaux qui va être utilisé tout au long de cette thèse. Dans le dernier chapitre, nous introduisons un modèle qui prend en compte le traitement des contours et des textures pour les images ainsi que tout le matériel mathématique requis pour aborder cette modélisation. L'étude de certaines solutions de ce modèle constituera le fil conducteur de cette thèse.

Partie II: brisures de symétries dans quelques équations de champs neuronaux

Les équations de champs neuronaux sont des systèmes dynamiques de dimension infinie qui peuvent être définies sur de nombreux espaces d'états. Dans cette thèse, nous considérons des espaces d'état non bornés qui peuvent avoir soit une géométrie euclidienne soit une géométrie hyperbolique. Leurs solutions stationnaires sont interpétées comme des activités stationnaires corticales. Dans ces équations, il existe une fonction de connectivité qui décrit le couplage entre les différentes populations

de neurones. En particulier, nous considèrerons des connectivitésqui ne dénpent que de la distance entre deux points de l'espace d'états. Cela induira naturellement une invariance du système par rapport aux symétries du domaine qui seront tranférées aux solutions d'une certaine manière. Cepdendant, en fonction de certains paramètres, les équations de champs neuronaux peuvent avoir de multiples solutions qui possèdent moins de symétries que l'équation de départ. Ce type de phénomène est plus communément appelé méchanisme de brisures spontanées de symétries. Cette partie se concentre sur l'étude de tels méchanismes sur les solutions stationnaires de certaines équations de champs neuronaux qui sont supposées être périodiques par rapport à un réseau donné. Plus précisémment, nous appliquons la théorie des bifurcations équivariantes pour classifier ces solutions stationnaires en fonction de leurs symétries dans les cas où l'espace des états est le plan euclidiean, le disque de Poincaré et le produit direct du plan euclidien et du disque de Poincaré. La contribution principale de cette partie est l'analyse complète du problème de formation d'états structurés dans le disque de Poincaré pour le cas du réseau octagonal. Nous avons également appliqué nos résultats à l'étude d'un modèle de champs neuronaux décrivant l'activité corticale d'un réseau d'hypercolones de "tenseurs de structure " (voir les chapitres 3 et 8) qui a conduit à la description de nouveaux types d'hallucinations visuelles.

Partie III: solutions localisées dans les équations de champs neuronaux non bornés

Dans la première partie, nous avons étudié les solutions spatialement périodiques de certaines équations de champs neuronaux non bornés. Dans cette partie, nous montrons l'existence d'un autre type de solutions qui apparaissent naturellement dans les systèmes définis sur des domaines non bornés: ce sont les solutions dites localisées. Dans la communauté des neurosciences, cette classe de solutions a une importance toute particulière puisqu'elles sont reliées à certains méchanismes de mémoire à courts termes. Les résultats principaux de cette partie sont des résultats d'existence de solutions localisées pour différents espaces d'états: la droite réelle, le plan euclidien et le disque de Poincaré. Pour le cas unidimensionel, les résultats reposent sur la théorie des bifurcations homoclines avec symétrie de réversibilité et sont illustrés avec des diagrames de bifurcation ayant une forme de "serpent". Pour les problèmes de dimension deux (plan euclidien et le disque de Poincaé), nous nous intéressons uniquement à la classe des solutions radialement symétriques et les preuves sont adaptées des méthodes développées dans [Scheel 2003, Lloyd 2009, McCalla 2010] pour l'équation de Swift-Hohenberg.

Publications

Une partie du chapitre 3 est publiée dans [Faye 2011b]. Le chapitre 6 concernant la formation de structures dans le disque de Poincaré est publié dans [Chossat 2011].

L'étude des représentations irréductibles de dimension quatre est publiée dans [Faye 2011a]. Le modèle spatialisé d'hypercolones du chapitre 8 est soumis dans le journal Networks and Heterogeneous Media [Faye 2012b]. L'étude numérique des solutions localisées sur la droite réelle avec une fonction de taux de décharge lisse est issue d'une collaboration avec James Rankin et a été publiée dans Journal of Mathematical Biology [Faye 2012c]. La méthode de type EDP dans le disque de Poincaré du chapitre 11 est publiée dans [Faye 2012a].

Contents

I Mesoscopic modeling of the visual cortex **1**

1 Cortical organization of the visual cortex **3**
1.1 Overview of visual processing 4
1.1.1 The retina 4
1.1.2 From the retina to the visual cortex 5
1.2 Cortical column 9
1.2.1 The anatomical column 9
1.2.2 Cortical column as physiological units 10
1.2.3 From anatomical to functional units 10
1.3 Cortical connections in V1 14
1.3.1 Vertical intra-columnar connections 14
1.3.2 Horizontal inter-colmunar connections 14

2 Neural field modeling **17**
2.1 Synaptically coupled networks of spiking neurons 17
2.1.1 Conductance based model of a neuron 18
2.1.2 Synaptic processing 19
2.2 From neural networks to neural fields 20
2.2.1 Rate-based neural network models 20
2.2.2 The continuum models 22
2.3 The “Mexican/Wizard-hat” model 24

3 Textures modeling and structure tensor formalism **25**
3.1 Visual edges and textures modeling 26
3.1.1 Introduction 26
3.1.2 The structure tensor as a representation of edges and textures 27
3.1.3 Biological evidence of structure tensors in visual areas? . . . 30
3.1.4 Structure tensor neural field equation 30
3.2 The mathematical structure of the set of structure tensors 33
3.2.1 A Riemannian framework 34
3.2.2 The Poincaré disk model 34
3.2.3 Isometries of the Poincaré disk 37
3.2.4 Polar map and Poincaré disk formalism 39
3.3 Theoretical and general results for structure tensor neural field equation 41
3.3.1 Existence and uniqueness of a solution 41
3.3.2 Stationary solutions 43
3.4 Conclusion 45

II Symmetry breaking mechanism in some neural field equations **47**

4 Introduction to bifurcation theory in infinite dimensional system **49**
4.1 Elementary bifurcation . . . 50
4.1.1 Saddle-node bifurcation . . . 50
4.1.2 Pitchfork bifurcation . . . 51
4.1.3 Transcritical bifurcation . . . 52
4.2 Center manifold and normal form . . . 52
4.2.1 Notations and definitions . . . 52
4.2.2 Local center manifold . . . 53
4.2.3 Parameter-dependent center manifold . . . 55
4.2.4 Empty unstable spectrum . . . 56
4.2.5 Normal forms . . . 57
4.3 Equivariant bifurcation . . . 58
4.3.1 Definitions . . . 58
4.3.2 Equivariant center manifold . . . 58
4.3.3 Equivariant Branching Lemma . . . 59

5 Pattern formation in the Euclidean case **61**
5.1 Planforms on the Euclidean plane . . . 63
5.1.1 Lattices and lattice patterns . . . 63
5.1.2 Steady-state bifurcation on a lattice . . . 64
5.2 Visual hallucination patterns of a square superlattice . . . 69
5.2.1 Simplified Ermentrout-Cowan model . . . 69
5.2.2 Theoretical results . . . 71
5.2.3 Network behaviour . . . 73
5.3 Conclusion . . . 75

6 Pattern formation in the Poincaré disk **77**
6.1 Introduction to harmonic analysis in the Poincaré disk . . . 78
6.1.1 The Laplace-Beltrami operator on the Poincaré disk . . . 78
6.1.2 Helgason-Fourier transform . . . 80
6.1.3 Convolutional operator on the Poincaré disk . . . 80
6.2 Spontaneous symmetry breaking in the Poincaré disk . . . 82
6.2.1 Periodic lattices . . . 82
6.2.2 Periodic eigenfunctions of the Laplace-Beltrami operator . . . 84
6.2.3 Bifurcation of patterns in the Poincaré disk . . . 86
6.3 A case study: the octagonal lattice . . . 88
6.3.1 The octagonal lattice and its symmetris . . . 89
6.3.2 Irreducible representation of the octagonal group . . . 92
6.3.3 Octagonal H-planforms . . . 95
6.4 Computation of hyperbolic planforms . . . 99
6.4.1 Introduction . . . 99

6.4.2 Desymmetrization of the octagon for the 1D case 100
6.4.3 Numerical experiments 101
6.5 Application to the structure tensor formalism 107
6.5.1 Bifurcation problem 108
6.5.2 Elementary results 110
6.6 Conclusion 110

7 Study of the four-dimensional representations 113
7.1 Basic facts and results 114
7.1.1 Steady-state bifurcations with $\mathcal{G}$ symmetry 114
7.1.2 Octagonal H-planforms in the 4D case 116
7.1.3 Bifurcation with submaximal isotropy 118
7.1.4 Presentation with biquaternions 122
7.1.5 Molien series 124
7.2 Bifurcation diagrams in the case of the representation χ_{12} 126
7.2.1 Equivariant structure of the equations on the center manifold 126
7.2.2 Isotropy types and fixed points subspaces 127
7.2.3 Bifurcation analysis 128
7.3 Bifurcation diagrams in the case of the representation χ_{11} 131
7.3.1 Equivariant structure of the equations on the center manifold 131
7.3.2 Isotropy types and fixed points subspaces 132
7.3.3 Bifurcation analysis 133
7.4 Bifurcation of a heteroclinic network in the χ_{11} case 140
7.4.1 Existence 140
7.4.2 Quotient network 141
7.4.3 Asymptotic stability 142
7.4.4 Computation of the stability conditions 147
7.5 Conclusion 148

8 Application to spontaneous pattern formation in V1 using structure tensor formalism 151
8.1 The continuum models of V1 and their symmetries 152
8.1.1 The model equations 153
8.1.2 Symmetries of the model 153
8.1.3 The Poincaré disk model 154
8.1.4 Two complementary approaches 155
8.2 Problem 1: weak anisotropic coupling on a bounded structure tensor space 156
8.2.1 Eigenfunctions of the Laplace-Beltrami operator on Ω 156
8.2.2 Study of an isolated hypercolumn 159
8.2.3 Weak lateral interactions 162
8.3 Problem 2: bifurcation of doubly periodic planforms in both $\mathbb{R}^2$ and $\mathbb{D}$166
8.3.1 Bifurcation problem 167
8.3.2 Bifurcations of octagonal H-planforms 168

8.3.3 Bifurcation diagrams for one hypercolumn . . . 172
8.3.4 Symmetry-breaking bifurcations on lattices . . . 177
8.3.5 Group actions . . . 178
8.3.6 Selection and stability of patterns . . . 180
8.3.7 Pictures of axial planforms Σ_1 and Σ_2 . . . 181
8.3.8 Forced symmetry breaking . . . 184
8.4 Conclusion . . . 186

III Localized states on unbounded neural field equations 189

9 General introduction 191

10 Localized states of NFEs on the real line 195
10.1 Wizard hat model . . . 196
10.1.1 Connectivity function . . . 197
10.1.2 Linear stability analysis of the trivial state . . . 198
10.1.3 Bifurcation of the trivial state for the full system . . . 199
10.2 Reversible Hopf bifurcation with 1:1 resonance . . . 200
10.2.1 PDE methods . . . 200
10.2.2 Reversible-Hopf bifurcation . . . 202
10.2.3 Normal form theory . . . 202
10.2.4 Existence of homoclinic orbits . . . 204
10.3 Stability of localized solutions . . . 205
10.3.1 Asymptotic stability . . . 205
10.3.2 Stability against perturbations in the connectivity function . 209
10.4 Numerical results . . . 211
10.4.1 Tuning the parameters . . . 211
10.4.2 Numerical computation of the stability of localized solutions 211
10.4.3 Snaking behaviour and localized solutions varying μ . . . 212
10.4.4 Regions of localized solutions in the parameter plane . . . 214
10.5 Conclusion . . . 216

11 Radially symmetric localized states 219
11.1 Localized patterns in Euclidean geometry . . . 220
11.1.1 The model . . . 220
11.1.2 Linear stability analysis of the trivial state . . . 221
11.1.3 PDE method . . . 222
11.1.4 The equation near the core . . . 222
11.1.5 The far-field equations . . . 226
11.1.6 Matching the core and the far-field . . . 228
11.2 Localized patterns in the Poincaré disk . . . 232
11.2.1 Choice of the connectivity function . . . 232
11.2.2 Linear stability of the trivial state . . . 234

11.2.3 PDE methods in the Poincaré disk . . . 234
11.2.4 The equation near the core . . . 235
11.2.5 The far-field equations . . . 243
11.3 Conclusion . . . 246

IV Conclusion 247

12 General conclusion 249

V Appendix 253

A Appendix for the four-dimensional representations 255
A.1 Computation of low-order equivariants . . . 255
A.1.1 Computational part of the proof of theorem 7.2.1 . . . 255
A.1.2 Computational part of the proof of theorem 7.3.1 . . . 257
A.2 Fixed-point subspaces . . . 258
A.2.1 Proof of Lemma 7.2.3 . . . 258
A.2.2 Proof of Lemma 7.3.3 . . . 259

B Appendix for chapter 8 261
B.1 Computation of ϖ in 8.2.2.2 . . . 261
B.2 Proof of Lemma 8.3.1 . . . 263
B.3 Calculation of cubic equivariants . . . 265

C Proofs of chapter 10 267
C.1 Proof of Lemma 10.1.1 . . . 267
C.2 Proof of Lemma 10.1.2 . . . 268
C.2.1 Computation of ν . . . 268
C.2.2 Computation of χ . . . 268
C.3 Proof of Lemma 10.2.2 . . . 269
C.3.1 Computation of c_3^0 . . . 270
C.3.2 Computation of β and c . . . 271
C.3.3 Computation of γ . . . 273

Bibliography 275

Part I

Mesoscopic modeling of the visual cortex

Chapter 1

Cortical organization of the visual cortex

Contents

1.1 Overview of visual processing 4
1.1.1 The retina 4
1.1.2 From the retina to the visual cortex 5
1.2 Cortical column 9
1.2.1 The anatomical column 9
1.2.2 Cortical column as physiological units 10
1.2.3 From anatomical to functional units 10
1.3 Cortical connections in V1 14
1.3.1 Vertical intra-columnar connections 14
1.3.2 Horizontal inter-colmunar connections 14

Neurons are a particular type of brain cells that process the inputs from sensory pathways. Their coordinated activity is the basis of brain functions. The aim of this chapter is to identify some basic structures of the visual cortex and identify a functional scale to study populations of connected neurons that will be necessary for the modeling chapters 2 and 3. We first give an overview of visual processing from the retina to the visual cortex. Then we introduce the notion of a cortical column from an anatomical to a functional point of view. Finally, we discuss the different cortical connections within the primary visual cortex.

This chapter does not give a complete and general introduction to the biology of vision but rather highlights some anatomical and functional principles at a mesoscopic level. Indeed, we will treat cortical units or blocks composed of at least one hundred neurons (minicolumn see 1.2.1) and at most one hundred thousand neurons (hypercolumn see 1.2.3) [Chemla 2010b]. The nonlinear dynamics of individual neurons forming these units will only be taken into account in chapter 2. Our intention in this Thesis is to model cortical columns and cortical areas composed of such mesoscopic blocks. The choice of the mesoscopic scale presents the advantages that lots of biophysical data are available in particular mesoscopic intra-columnar and inter-columnar connectivity data. Such data are still missing at the level of single neurons. For a review on cortical circuits see [Kandel 2000, Grimbert 2008, Chemla 2010b].

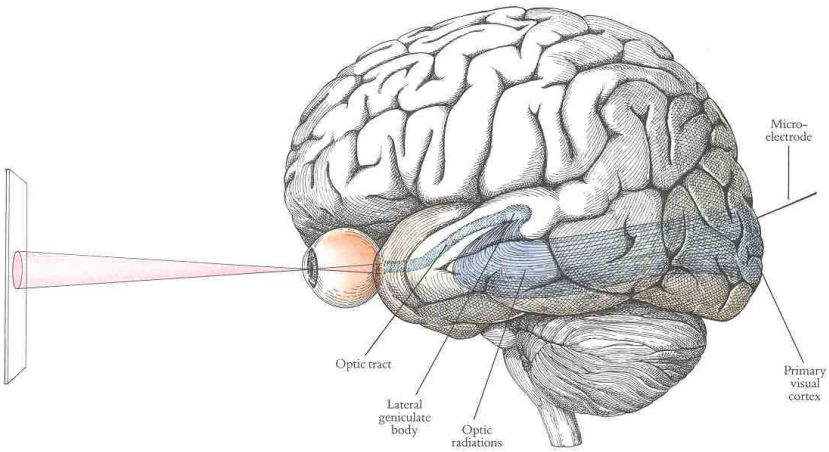

Figure 1.1: Main elements of the visual pathway.

1.1 Overview of visual processing

1.1.1 The retina

Visual processing begins in the retina, *i.e.* the receptive surface inside the back of the eye. Light enters the eye, passes through the layers of cells in the retina before reaching the photoreceptors (cone cells for daylight vision and rod cells for twilight vision) which are located at the back of the retina. Light activates the photoreceptors, which modulate the activity of bipolar cells. As a first approximation, bipolar cells, in turn, connect with ganglion cells located at the front of the retina. The axons of these output cells form the optic nerve, which carries information to the brain see figures 1.1 and 1.2.

Definition 1.1.1. *The receptive field (RF) of a neuron is defined as the region of the retina or its equivalence in visual space, within which a stimulus evokes a change in the discharge of the neuron.*

Therefore, a RF characterizes the transformation between the visual image and neuronal activity. The receptive field of neurons is usually subdivided in subregions ON (resp. OFF) which are excitatory (resp. inhibitory) in that they increase (resp. decrease) the stimulus response.

The RFs of most ganglion cells display a characteristic, roughly circular center-surround architecture where the center is excitatory (resp. inhibitory) and the surround is inhibitory (resp. excitatory) [Rodieck 1965], see figure 1.3. Moreover, the ON/OFF subregions are usually associated with particular wavelengths of light. Hence, the ganglion cells act as local spatial contrast detectors. For primates, ganglion cells can also be divided into two functional classes according to their size: M cells and P cells (respectively for *magni* and *parvi*), thus providing the magno- and parvocellular pathways. The magnocellular pathway carries information from the large retinal ganglion cells to the large cells in the thalamus and from there

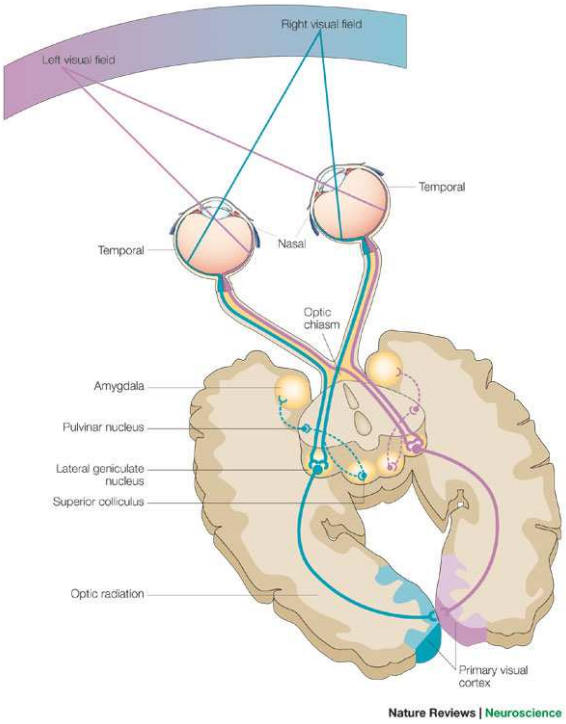

Figure 1.2: Horizontal section of the visual pathway. Redrawn from [Hannula 2005].

to the primary visual cortex (V1). This M-pathway carries all transient, motion related and low contrast black-and-white visual information and is responsive to low spatial frequencies and high temporal frequencies. The parvocellular pathway from the small retinal ganglion cells is color sensitive, has lower contrast sensitivity and is responsive to higher spatial frequencies and lower temporal frequencies. For more details on the retina, see [Wohrer 2008].

Hence, we could think of the retina, as a first approximation, as a spatiotemporal contrast detector. Indeed, transmitting the same information constantly is useless, it is changes in the information flow that are important.

1.1.2 From the retina to the visual cortex

The thalamus is the entrance portal for all sensory information passed to the cortex and the lateral geniculate nucleus (LGN) is the part of the thalamus concerned with vision see figures 1.1 and 1.2. The magno- and parvocellular pathways remain segregated in the LGN, providing the magno- and parvocellular layers, respectively forming by projection of the above M and P ganglion cells. More information about the LGN anatomy can be found in [Sherman 1996]. Note that in these layers, the RFs of thalamic neurons have the same concentric center-surround organization (see figure 1.4) as the retinal ganglion cells that feed into them. However, their sensitivity to stimulus features, e.g. color contrast, luminance contrast, spatial and

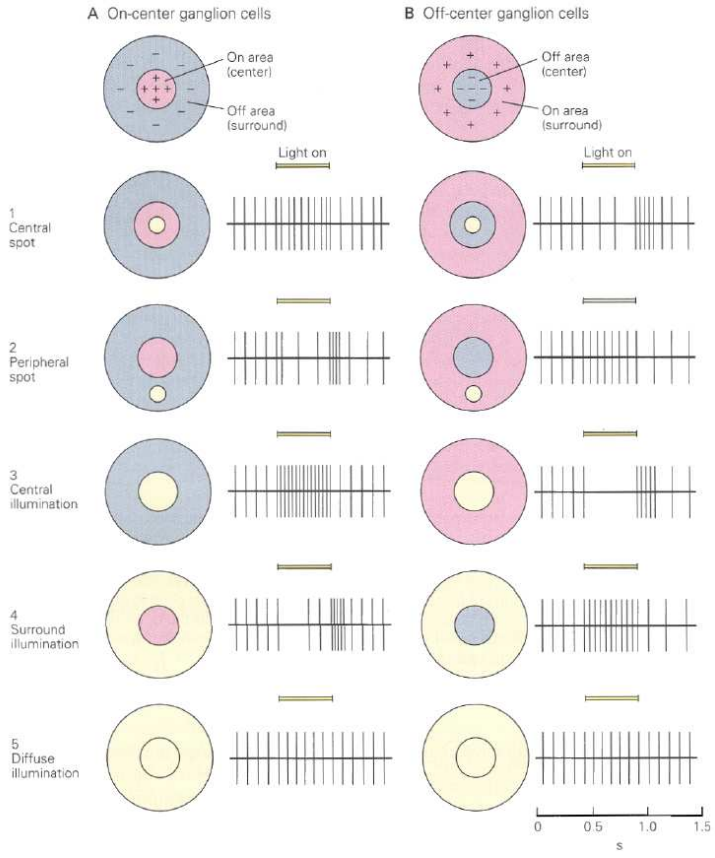

Figure 1.3: Schematic of the receptive field properties of a ganglion cell. Ganglion cells have circular receptive fields divided into two subregions: a central area and a surrounding ring. ON-center cells (left) are excited when the center is illuminated by a spot of light and inhibited when stimulated in the surround, whereas off-center cells (right) are excited when the surround is illuminated and inhibited when stimulated in the center [Rodieck 1965]. Redrawn from [Kandel 2000].

temporal frequency, are quite different. The pathways segregation continues in layer IV of the primary visual cortex.

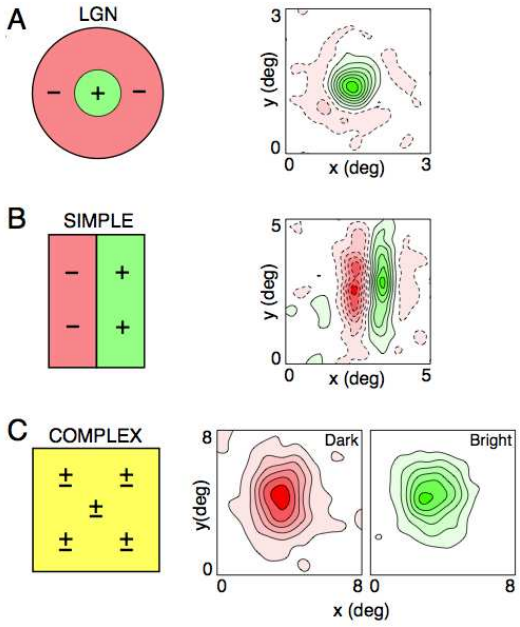

Figure 1.4: Spatial arrangement of receptive fields of cat LGN and V1 cells. Schematic (left) and two-dimensional spatial (x-y) (right) RF profiles A: ON-center LGN neuron. The RF has a central ON region, surrounded by an antagonist OFF region B: V1 simple (linear) cell RF exhibits an alternating arrangement of elongated excitatory and inhibitory subregions that are responsive to either bright (green, +) or dark (red, -) stimuli. C: V1 complex (non-linear) cell RF do not present net subdivision between excitatory and inhibitory subregions. Redrawn from [DeAngelis 1995b].

The cortex is a folded sheet of width 2cm known as the grey matter. It contains the somas of the neurons. The white matter is made of the myelinated axons of the grey matter. The cortex shares many features of the LGN. It is a layered structure, 6 layers that have been identified by [Brodmann 1909] see figures 1.5 and 1.8, which is also retinotopically organised (see figure 1.6 where the retinotopy is shown). The mapping between the visual field and the cortical coordinates is approximatively log-polar (see [Schwartz 1977]). From the LGN, the information is transmitted to the visual cortex located at the back of the head (see figures 1.1 and 1.2), mostly to the primary visual area V1.

Let us consider V1 more precisely. By using extracellular recordings of single cells in the visual cortex of anesthetized cats and simple set of geometric test stimuli, Hubel and Wiesel [Hubel 1962] mainly classified them into two groups: simple and complex. They proposed the following definition. The RF of the simple cells is more elongated than the RF of the LGN cells which accounts for their selectivity for the orientation of the stimulus. It is also comprised of ON/OFF subregions (see

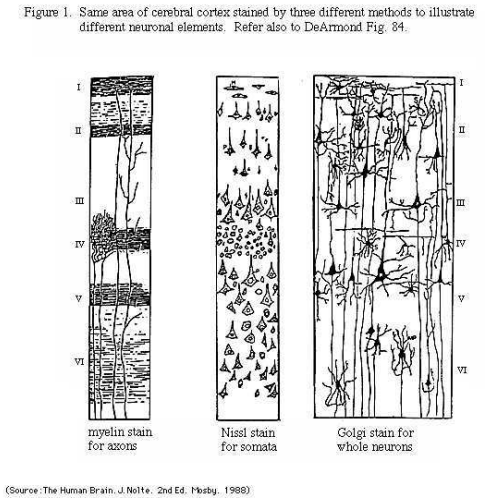

Figure 1.5: Layer organization of the cortex (a) Weigert's coloration shows myelinated fibers (axons) and so the connections inside and between layers, (b) Nissl's coloration only reveals cell bodies (c) Golgi's coloration shows the whole cells (From [Nolte 2001]).

figure 1.4). It has been shown that these cells better respond to bars than to spots. Simple (linear) cells are selective to orientation and position. On the other hand, the complex cells are not so well characterized by their RF (see figure 1.4) despite being responsive to which eye is stimulated, the orientation, the spatial frequency of the stimulus and other properties. Complex (non-linear) cells show some kind of position invariance and generalize orientation selectivity across receptive field extent.

Neurons in the primary visual cortex can actually be selective along many stimulus dimensions, such as spatial position, phase, temporal and spatial frequency, orientation, direction of movement, binocular disparity. Based on the retinotopy property, it is interesting to compare the preferred stimulus of V1 cells and see how it is spatially organised in the cortex. Since the 1950s, thanks to the work of Mountcastle [Mountcastle 1957], we know that the cerebral cortex has also a columnar organization. Indeed, using a microelectrode in cat primary somatosensory cortex, he found that neurons responding to the same stimulation, *i.e.* sharing common receptive field properties, were arranged vertically into columns, crossing the six layers of the cortical tissue. In 1960s and 1970s, Hubel and Wiesel followed Mountcastle's discoveries by showing that ocular dominance and orientations are organized in a columnar manner in cat and monkey visual cortex [Hubel 1962, Hubel 1965, Hubel 1977]. The individual cortical column was then considered to be the elementary unit of organization in the cerebral cortex. Today, the term "cortical column" is very confusing and one can find in the literature: minicolumns, microcolumns, hypercolumns, macrocolumns, orientation columns, ocular dominance bands, barrels, blobs, stripes... The aim of the next section is to give a

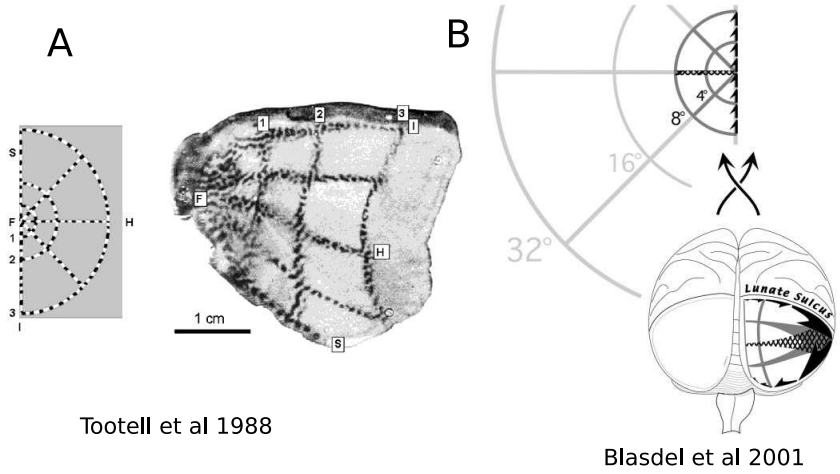

Figure 1.6: Retinotopic organization of the macaque striate cortex.

precise meaning of what we will call *cortical column* throughout this Thesis.

1.2 Cortical column

1.2.1 The anatomical column

Many cortical neurons throw their axons and dendrites from the cortex surface to the white matter thereby forming the anatomical basis of the columnar organization in the cortex, see figure 1.7. Nervous fibers from the thalamus mostly end in layer IV where they are connected to stellate neurons. These neurons throw their axons towards the surface of the cortex, parallel to apical dendrites of neighboring pyramidal neurons, and establish connections with them. The thalamocortical input is therefore conducted within a thin column of strongly connected cells so that the same information is shared throughout the depth of the cortex perpendicular to its surface [Kandel 2000].

Definition 1.2.1. *Minicolumns, sometimes also called microcolumns, are narrow vertical chains of about one hundred neurons, barely more than one cell diameter wide, i.e. 20 up to 50 µm, which are formed during brain development, due to radial migration of neurons [Buxhoeveden 2002, Nolte 2001].*

However minicolumns do not solve the problem of defining cortical columns. They have not been extensively observed among species, nor among cortical areas. Moreover, at this spatial scale, individual microcolumns have no reason to be considered as functional entities and classical electrophysiological techniques limit the research.

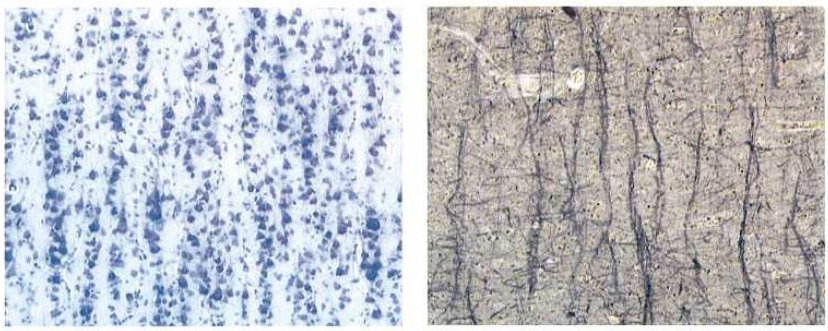

Figure 1.7: The anatomical column. Left: Nissl-stained tissue reveals vertically aligned cells, suggesting the existence of minicolumns in the developing cortex. Right: Myelinated fibre bundles in the same region of human cortex. The correlation between myelin bundles and cell soma aggregates is clear. Redrawn from [Buxhoeveden 2002].

1.2.2 Cortical column as physiological units

In 1957 Mountcastle [Mountcastle 1957], discovered a columnar organization in the cortex. However this columnar organization differs from the anatomical column defined above, especially regarding the diameter of the column. With electrode recordings, he showed that neurons inside columns of 300 to 500 μm of diameter displayed similar activities, which is much larger than the diameter of the microcolumn. Those physiological units are usually called *macrocolumns* and defined as a continuum of many minicolumns from 0.4 to 1 mm.

1.2.3 From anatomical to functional units

At the spatial scale of the macrocolumn, many experiments investigated the possible relation between physiological columns and sensory functions [Mountcastle 1957, Hubel 1962, Hubel 1965, Hubel 1977, Kandel 2000, Lund 2003]. Indeed, a cortical column can also be defined on the basis of functional features, e.g. columns of cortical cells all responding to the same stimulus property. Besides, columns, barrels, blobs, and stripes have all been called *cortical modules*, as any repeated functional clusters in different areas of the brain.

Visual cortical cells are also sensitive to orientation, meaning that they will selectively respond to stimuli, e.g. bars, edges, at particular orientations. Hubel and Wiesel [Hubel 1962, Hubel 1965, Hubel 1977] showed that orientation preference of neurons remains constant in vertical electrode penetrations through the entire thickness of the cortex, while gradually changes when moving the electrode obliquely, see figure 1.8. It thus led to the definition of *cortical column of orientation*. The point-by-point sampling with microelectrodes of cells preferences, performed by Hubel and Wiesel, has since been supplemented by the optical imaging method of intrinsic signals (see [Blasdel 1986, Grinvald 1986]) which reveals that the orien-

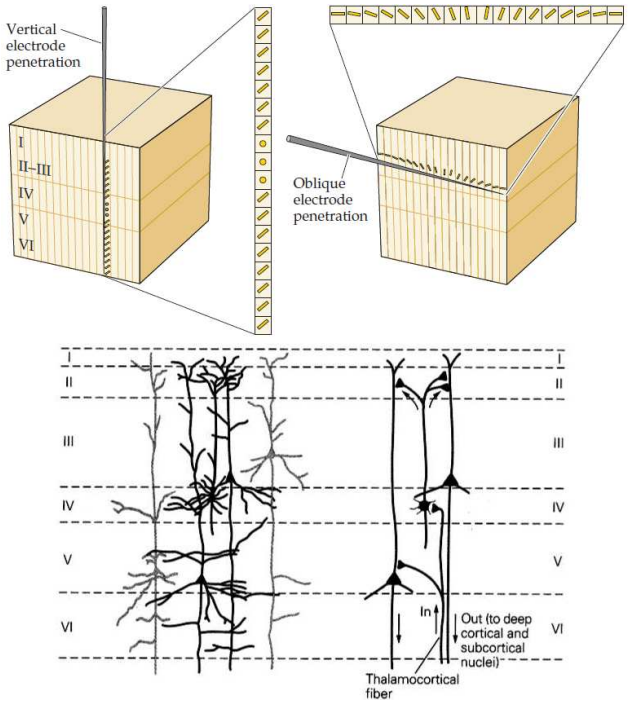

Figure 1.8: Top left: orientation preference of neurons remains constant in vertical electrode penetrations. Top right: orientation preference of neurons gradually changes when moving the electrode obliquely. Bottom left: Morphology of relay cells from layers III to V. Stellate neurons (layer IV) receive information from the thalamus and transmit it to neighboring pyramidal cells in superficial layers of the cortex. Pyramidal cells throw their axons towards deep layers of the cortex and other cortical or sub-cortical regions. They also establish horizontal connections with neighboring columns sharing the same physiological properties. Bottom right: diagram of intra-cortical excitatory circuitry. Redrawn from [Kandel 2000] based on the original work of Hubel and Wiesel [Hubel 1962, Hubel 1965, Hubel 1977].

tation preference map is composed of pinwheel-like structures as shown in figure 1.9 for the tree shrew visual cortex. A similar structure has been shown for the macaque primary visual cortex (see [Blasdel 1986]) and the cat visual cortex (see [Bonhoeffer 1991]). In figure 1.9 B, the color indicates the preferred orientation of neurons in the underlying column. This figure was obtained by combining the cortical responses for different orientation stimulus as shown in figure 1.9 A. The striking feature, already found by Huber and Wiesel, is the existence of particular points called pinwheels (see figure 1.9 C Right) where all orientations are represented, which are singularities in the orientation map. Between these pinwheels (or singularities), there are smooth and continuous zones with orientation preference gradient where the local orientation preference does not have radial organization (see figure 1.9 C Left).

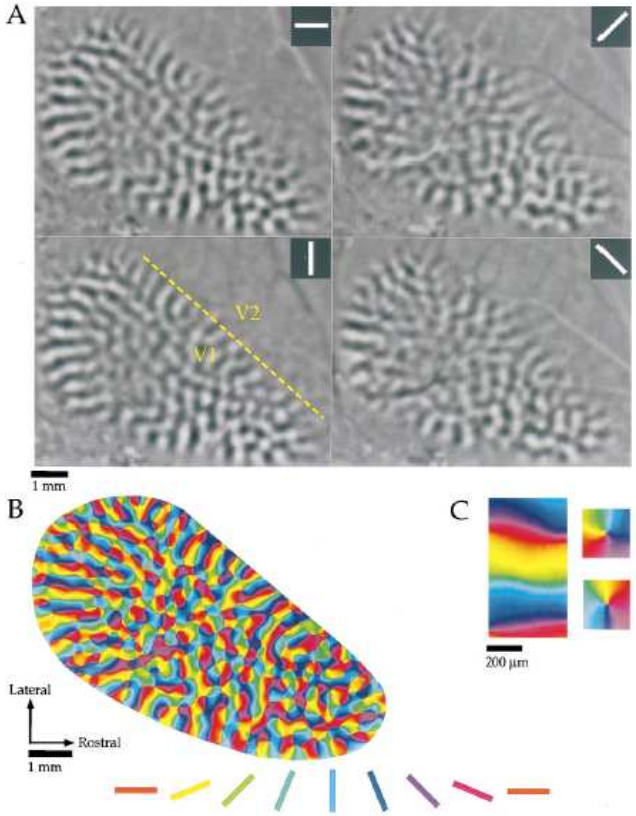

Figure 1.9: Optical imaging of intrinsic signals in tree shrew visual cortex. A, Difference images obtained for four stimulus angles. Dark signal indicates areas that were active during presentation of the stimulus. B, Orientation preference map. Orientation preference of each location is color-coded according to the key shown below the map. C, Portions of the orientation preference map shown in B have been enlarged to demonstrate that the orientation preference maps contained both smooth and continuous zones (left), and pinwheel arrangements (right) that are functional singularities. Redrawn from [Bosking 1997].

In addition to the pinwheel structure, there are ocular preference domains, in effect large bands, that show to which stimulated eye the columns are more responsive. The two maps of orientation preference and ocular preference can be superposed as in figure 1.10 from [Hubener 1997] (in the cat). It becomes clear that both systems are spatially related: many iso-orientation lines cross the borders between ocular dominance columns close to right angles, and the pinwheel centers are preferentially located in the middle of the ocular dominance columns.

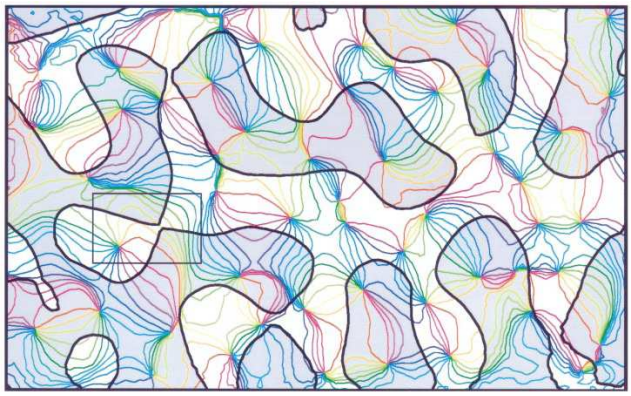

Figure 1.10: Relationship between ocular dominance and orientation maps. The colored iso-orientation lines were derived from the orientation preference map. All points on lines with a given color prefer the same orientation. The contours of the ocular dominance columns were obtained from the ocular dominance map of the same cortical region, using an objective automated procedure; grey denotes contralateral eye dominance. Redrawn from [Hubener 1997] for the cat.

Following the observation that orientation columns did not show discrete boundaries, Hubel and Wiesel [Hubel 1977] defined a *hypercolumn* as the structure which contains representations of all orientations for both eyes. The idea is that the module periodicity is usually in the millimeter range. The primary visual cortex of many mammals species is thus arranged with several superimposed functional maps that represent the visuotopic position, orientation, ocular dominance, spatial frequency, spatial disparity or movement direction, of visual stimuli. This columnar organization implies that all feature maps are "superimpose" on the 2D cortical sheet.

To finish our discussion on functional columns, it is to be noted that these structures have not been observed in all regions of mammals cortex and show species dependency. For example, there is no orientation preference columnar structure in rat primary visual cortex, which means that locally, cells with all orientation preference are represented [Ohki 2005].

1.3 Cortical connections in V1

We now focus on the intra-cortical connections within the primary visual cortex. Let us first mention that the term *horizontal* or *lateral* connectivity is used for the inter-column connections between columns, parallel to the cortical surface, whereas the *vertical* or *local* connectivity is used for intra-column connections.

1.3.1 Vertical intra-columnar connections

In a general manner, over a spatial scale of about 800 μm, neighboring columns exhibit strong physiological short-range connections (excitatory and inhibitory) with each other, independently of any visual feature selectivity, and connection strength (or synaptic weight) decrease with cortical distance [Das 1999]. This particular organization of local connectivity together with the structure of orientation maps (as in figure 1.9) implies that these connections play a different role depending on the place of the neurons in the pinwheel map (see [Shelley 2002, Mariño 2005, Nauhaus 2008]). Indeed, the homogeneous connections provide a uniform sampling of the neighbouring neurons. In the linear zones, the neurons are mainly connected to neurons sharing the same orientation preference, whereas near pinwheels the neurons are connected to neurons with different orientations.

1.3.2 Horizontal inter-colmunar connections

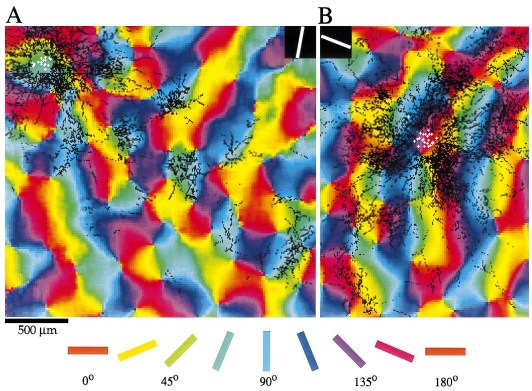

Figure 1.11: The patchy nature of horizontal connections in the tree shrew visual cortex. Axonal bouton distribution (black dots) after biocytin injection in layer II/III. A: Pyramidal neurons (white crosses) of the injected site have a preferred orientation of 80 degree. B: The injected site has an orientation preference of 160 degree. For both case, except for the region immediately adjacent to the injection sites, the labeled boutons are clustered in regions that have orientation preferences similar to that of the injection site, *i.e.* orientation columns are connected by long-range horizontal connections. Redrawn from [Bosking 1997].

Lateral connections are mainly made by excitatory neurons and long-range projections can extend to about 3000 μm. The global distribution of excitatory synaptic boutons with respect to lateral distances from the injection site (see figure 1.11 left), revealed dense local connections with exponential decline of bouton density with radial distance from the injection site, surrounded by patches of long-range connections. Thus, lateral connections are patchy and regular, and thought to be linked to the regularity of functional domains. The clearest relationship between anatomical connectivity and functional domains concerns excitatory long-range lateral connections and orientation columns. Several studies in different mammals (cats, ferrets, monkeys) have shown long-distance clustered horizontal connections that preferentially link columns with similar orientation preference [Malach 1993, Lund 2003], see figure 1.11.

Chapter 2

Neural field modeling

Contents

2.1 Synaptically coupled networks of spiking neurons 17
2.1.1 Conductance based model of a neuron 18
2.1.2 Synaptic processing 19
2.2 From neural networks to neural fields 20
2.2.1 Rate-based neural network models 20
2.2.2 The continuum models 22
2.3 The "Mexican/Wizard-hat" model 24

In this chapter, we present the neural field formalism that will be used throughout this Thesis. The current mathematical approach for understanding coarse-grained activity of large ensembles of neurons in cortex is based around the work of Wilson and Cowan [Wilson 1972, Wilson 1973] and Amari [Amari 1975, Amari 1977]. Because the number of neurons and synapses is vast, a natural first approximation is to take continuum limit and treat cortical space as continuous, giving rise to the notion of a neural field model. These models typically take the form of integro-differential equations. Compared to spiking neural networks, the neural field model presents the advantages that various techniques from the analysis of partial differential equations (PDEs) can be adapted to study the nonlinear dynamic behaviours and that few parameters are needed. The sorts of dynamical behaviour that are typically observed in neural field models include spatially and temporally periodic patterns [Ermentrout 1979, Tass 1995], localized regions of activity [Laing 2002, Kishimoto 1979] and traveling waves [Pinto 2001a, Laing 2005, Kilpatrick 2008]. Neural fields have been used to model a wide range of neurobiological phenomena such as visual hallucinations [Ermentrout 1979, Bressloff 2001a], mechanisms for short term memory [Laing 2002, Laing 2003a] and feature selectivity in the visual cortex [Ben-Yishai 1995]. For a review on neural field models, see [Ermentrout 1998, Coombes 2005b, Coombes 2010, Bressloff 2012].

2.1 Synaptically coupled networks of spiking neurons

We start this section by briefly describing the biological components of synaptically coupled networks of spiking neurons. We only consider conductance-based models of action potential generation and synaptic processing.

2.1.1 Conductance based model of a neuron

The structure of a cortical neuron typically consists of three parts: (i) the cell body (or soma); (ii) a branching output structure known as the axon; (iii) and a branching input structure known as the dendritic tree, see figure 2.1.

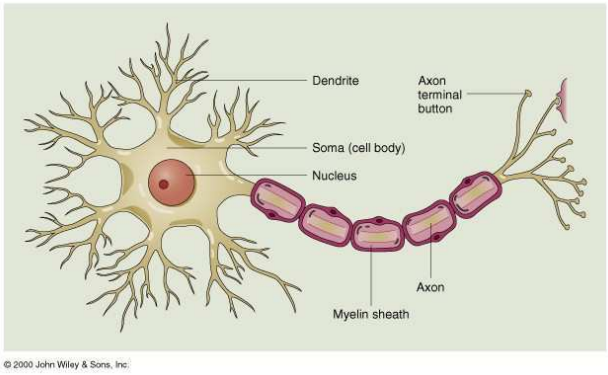

Figure 2.1: Basic structure of a neuron.

Neurons mainly communicate with each other by sending action potentials along their axons, action potentials are initiated at a specialized region of the soma called the axon hillock. Axons make contacts on the dendrites of other neurons via microscopic junctions known as synapses. There are two kind of synapses, the chemical and the electrical (also called gap junctions). We will not consider electrical synapses in this Thesis. When the somatic potential across the membrane reaches a threshold, a sequence of action potentials (also called spikes) is produced at the axon hillock. This sequence is then transmitted, without alteration, to the axon terminals where the synapses with the targeted neuron are located.

The standard biophysical model describing the dynamics of single neuron with somatic membrane potential V is based upon the conservation of electric charge:

$$C\frac{dV}{dt} = -I_{con} + I_{syn} + I_{ext}, \tag{2.1}$$

where C is the cell capacitance, I_{con} is the membrane current, I_{syn} denotes the sum of synaptic currents entering the cell and I_{ext} describes any externally injected currents. The membrane current through a specific channel varies approximately linearilly with changes in the potential V relative to some reversal potential that mediates the synaptic current. Summing over all channel types, the total membrane current leaving the cell through the cell membrane is

$$I_{con} = \sum_s g_s(V - V_s), \tag{2.2}$$

where g_s is the conductance due to channels of type s and V_s the corresponding reversal potential. Three different types of ion channels are taken into account: Na^+, Ca^{2+} and K^+. The conductance g_s for ion channels of type s is taken to be

the product $g_s = \bar{g}_s P_s$ where $\bar{g}_s$ is equal to the density of channels in the membrane multiplied by the conductance of a single channel and P_s is the fraction of open channels.

2.1.2 Synaptic processing

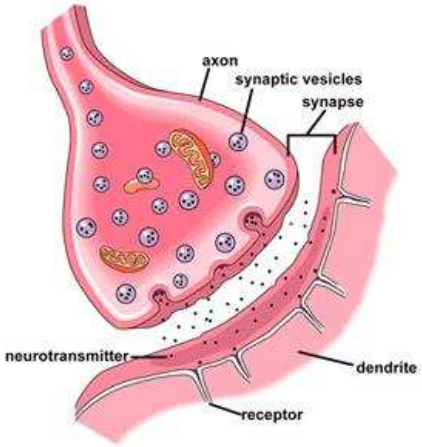

Figure 2.2: Basic structure of a synapse.

When a spike arrives at a synapse, it triggers the release of neurotransmitter in the synaptic cleft, see figure 2.2. These neurotransmitters bind to specific receptors on the postsynaptic neuron. The binding causes ion channels to open (or close), thus changing the ability of ions to flow through the postsynaptic membrane. Hence, the binding of neurotransmitters alters the conductance of the postsynaptic membrane. A single synaptic event due to the arrival of an action potential at time T induces a synaptic current of the form

$$I_{syn}(t) = g_{syn}(t-T)\left(V_{syn} - V(t)\right), \tag{2.3}$$

where V is the voltage of the postsynaptic neuron, V_{syn} is the synaptic reversal potential and $g_{syn}(t)$ is the change in synaptic conductance with $g_{syn}(t) = 0$ for $t < 0$. A typical form for $g_{syn}(t)$ is the difference of exponentials

$$g_{syn}(t) = \bar{g}\left(\frac{1}{\tau_d} - \frac{1}{\tau_r}\right)^{-1}\left(e^{-t/\tau_d} - e^{-t/\tau_r}\right)H(t), \tag{2.4}$$

where $H(t)$ is the Heaviside function, $\bar{g}$ a constant conductance and $\tau_{d,r}$ are time constants. Two limits are commonly used

$$\begin{aligned} g_{syn}(t) &= \bar{g}\alpha^2 t e^{-\alpha t}H(t), \text{ in the limit } \tau_d \to \tau_r = \alpha^{-1}, \\ g_{syn}(t) &= \bar{g}e^{-t/\tau_d}H(t), \text{ in the limit } \tau_r \ll \tau_d. \end{aligned} \tag{2.5}$$

2.2 From neural networks to neural fields

Following the lines of Ermentrout and Bressloff [Ermentrout 1998, Ermentrout 2010a, Bressloff 2012], we highlight a sequence of approximations that can be made to reduce a network of spiking neurons to an effective rate-based model. Finally, we derive the neural field equations in the continuum limit.

2.2.1 Rate-based neural network models

Let us now consider a network of synaptically coupled cortical neurons labeled $i = 1, \dots, N$. If we denote the sequence of firing times of the jth neuron by $\{T_j^m, m \in \mathbb{Z}\}$, then the net synaptic current into postsynaptic neuron i due to innervation by the spike train from presynaptic neuron j is taken to have the general form $\sum_m \mathrm{PSP}_{ij}(t - T_j^m)$, where $\mathrm{PSP}_{ij}(t)$ represents the temporal filtering effects of synaptic and dendritic processing. Assuming that the spikes' contributions sum linearilly, the average membrane potential of the ith neuron, which we denote by $u_i(t)$, is

$$u_i(t) = \sum_{j=1}^{N} \sum_m \mathrm{PSP}_{ij}(t - T_j^m) = \sum_{j=1}^{N} \int_{-\infty}^{t} \mathrm{PSP}_{ij}(t - s) a_j(s) ds, \tag{2.6}$$

where we have set

$$a_j(t) = \sum_{m \in \mathbb{Z}} \delta(t - T_j^m), \tag{2.7}$$

$\delta(t)$ being the delta Dirac function. In order to obtain a closed set of equations, we have to determine the firing times T_i^m. This takes the form of a threshold condition

$$T_i^m = \inf\{t, t > T_i^{m-1} \mid V_i(t) = \kappa, \dot{V}_i(t) > 0\}, \tag{2.8}$$

where κ is the firing threshold and the somatic membrane potential $V_i(t)$ evolves according to the conductance based model

$$C \frac{dV_i}{dt} = -I_{con,i}(V_i, \dots) + u_i. \tag{2.9}$$

Under the simplifying assumption that synapses are sufficiently slow, we can carry out a short term temporal averaging of equation (2.6) in which we approximate the output spike train $a_j(t)$ by the instantaneous firing rate $a_j(t) = S_j(u_j(t))$ with S_j the corresponding firing rate function. Equation (2.6) reduces to

$$u_i(t) = \sum_{j=1}^{N} \int_{-\infty}^{t} \mathrm{PSP}_{ij}(t - s) S_j(u_j(s)) ds. \tag{2.10}$$

In neural network models, S_j is usually approximated by the sigmoidal function

$$S_j(x) = \frac{1}{1 + e^{-\mu_i(x - \theta_i)}} \tag{2.11}$$

where μ_i is the nonlinear gain and θ_i is the threshold.

There are two main simplifying assumptions that appear in the literature [Ermentrout 1998, Pinto 1996] and produce two different models that we describe below.

The voltage based model The assumption is that the postsynaptic potential has the same shape no matter which presynaptic population caused it. This leads to the relation

$$\mathrm{PSP}_{ij}(t) = w_{ij}\mathrm{PSP}_i(t).$$

w_{ij} denotes the synaptic strenght of the connection from neuron j to neuron i and $\mathrm{PSP}_i(t)$ determines the time course of the input, which is assumed to depend only on properties of the postsynaptic cell i. The shape of $\mathrm{PSP}_i(t)$ is often approximated by a simple exponential decay $\mathrm{PSP}_i(t) = e^{-t/\tau_i}H(t)$, or equivalently that

$$\tau_i \frac{d\mathrm{PSP}_i(t)}{dt} + \mathrm{PSP}_i(t) = \delta(t). \tag{2.12}$$

Combining equations (2.12) together with (2.10) leads to a system of differential equations for the current $u_i(t)$:

$$\tau_i \frac{du_i(t)}{dt} + u_i(t) = \sum_{j=1}^{N} w_{ij} S_j(u_j(t)). \tag{2.13}$$

We introduce the $N \times N$ matrix $\mathbf{J}$ such that $\mathbf{J}_{i,j} = w_{i,j}/\tau_i$, and the function $\mathbf{S} : \mathbb{R}^N \to \mathbb{R}^N$ such that $\mathbf{S}(\mathbf{U})$ is the vector of coordinates $S_i(u_i)$ if $\mathbf{U} = (u_1, \ldots, u_N)$. We rewrite (2.13) in vector form and obtain the following system of N differential equations

$$\dot{\mathbf{U}}(t) = -\mathbf{L}\mathbf{U}(t) + \mathbf{J}\mathbf{S}(\mathbf{U}(t)) + \mathbf{I}_{\mathrm{ext}}(t), \tag{2.14}$$

where $\mathbf{L}$ is the diagonal matrix $\mathbf{L} = \mathrm{diag}\,(1/\tau_1, \ldots, 1/\tau_N)$ and $\mathbf{I}_{\mathrm{ext}}(t)$ is an added external current such that $\mathbf{I}^i_{\mathrm{ext}}(t)$ models the non-local connections of population i.

The activity based model The assumption is that the shape of the postsynaptic potential depends only on the nature of the presynaptic cell, that is

$$\mathrm{PSP}_{ij}(t) = w_{ij}\mathrm{PSP}_j(t).$$

As above, we suppose that $\mathrm{PSP}_j(t)$ satisfies equation (2.12) and define the time-averaged firing rate to be

$$A_i(t) = \int_{-\infty}^{t} \mathrm{PSP}_i(t-s) S_i(u_i(s)) ds. \tag{2.15}$$

Combining equations (2.12) together with (2.15) leads to a system of differential equations for $A_i(t)$:

$$\tau_i \frac{dA_i(t)}{dt} + A_i(t) = S_i\left(\sum_{j=1}^{N} w_{ij} A_j(t)\right). \tag{2.16}$$

We can rewrite in vector form and introduce an external current $\mathbf{I}_{\text{ext}}(t)$

$$\dot{\mathbf{A}}(t) = -\mathbf{L}\mathbf{A}(t) + \mathbf{S}\left(\mathbf{J}\mathbf{A}(t) + \mathbf{I}_{\text{ext}}(t)\right). \tag{2.17}$$

2.2.2 The continuum models

So far we have not made any assumptions about the topology of the underlying neural network, that is, the structure of the weight matrix $\mathbf{J}$. If one looks at a region of the primary visual cortex, one finds that it has a characteristic spatial structure: neurons are distributed according to an approximately two-dimensional architecture. That is, the physical location of a vertical column of neurons within the two-dimensional cortical sheet often reflects the specific information processing role of that population of neurons. This suggests labeling neurons according to their spatial location in cortex. We now combine the rate-based neural networks to form a continuum of neural fields, *e.g.*, in the case of a model of significant part Ω of the cortex. We consider $\Omega \subset \mathbb{R}^d$, $d = 1, 2, 3$ which we assume to be connected.

We denote $\mathbf{U}(\mathbf{r}, t)$ (respectively $\mathbf{A}(\mathbf{r}, t)$) the N-dimensional state vector at the point $\mathbf{r}$ of the continuum. We introduce the $N \times N$ matrix function $\mathbf{J}(\mathbf{r}, \mathbf{r}')$ which describes how neural mass at point $\mathbf{r}'$ influences that at point $\mathbf{r}$. We call $\mathbf{J}$ the connectivity function. Equation (2.14) can be extended to

$$\frac{d}{dt}\mathbf{U}(\mathbf{r}, t) = -\mathbf{L}\mathbf{U}(\mathbf{r}, t) + \int_\Omega \mathbf{J}(\mathbf{r}, \mathbf{r}')\mathbf{S}(\mathbf{U}(\mathbf{r}', t))d\mathbf{r}' + \mathbf{I}_{\text{ext}}(\mathbf{r}, t), \tag{2.18}$$

and equation (2.17) to

$$\frac{d}{dt}\mathbf{A}(\mathbf{r}, t) = -\mathbf{L}\mathbf{A}(\mathbf{r}, t) + \mathbf{S}\left(\int_\Omega \mathbf{J}(\mathbf{r}, \mathbf{r}')\mathbf{A}(\mathbf{r}', t)d\mathbf{r}' + \mathbf{I}_{\text{ext}}(\mathbf{r}, t)\right). \tag{2.19}$$

When $d = 1$ we deal with one-dimensional sets of neural fields. Even though this appears to be of limited biological interest, this is one of the most widely studied cases because of its relative mathematical simplicity and because of the insights one can gain of the more realistic situations.

When $d = 2$ we discuss properties of two-dimensional sets of neural fields. This is perhaps more interesting from a biological point of view since Ω can be viewed as a piece of cortex where the third dimension, its thickness, is neglected. This case has received by far less attention than the previous one, probably because of the increased computational difficulty.

Finally $d = 3$ allows us to discuss properties of volumes of neural fields, *e.g.* cortical sheets where their thickness is taken into account[Kandel 2000, Chalupa 2004].

Some remarks

(i) Unfortunately, there does not currently exist an analysis that provides a rigorous derivation of neural field equations, although some progress has been made in this direction [Deco 2008, Bressloff 2009, Faugeras 2009a, Baladron 2011].

(ii) Moreover, heuristic approaches have been used to incorporate mechanisms such as synaptic depression/facilitation in neural field formalism [Tsodyks 1998, Kilpatrick 2010a, Kilpatrick 2010b], spike frequency adaptation [Curtu 2004, Coombes 2003, Coombes 2005a, Kilpatrick 2010c] and axonal propagation delays [Venkov 2007, Hutt 2006, Faye 2010, Veltz 2011].

(iii) A significant amount of work has been devoted to the study of equations (2.18) and (2.19) in the case of unbounded cortical domains $\Omega = \mathbb{R}^d$, $d = 1, 2, 3$. Recent reviews of this work, and much more, can be found in the papers of Coombes [Coombes 2005b] and Bressloff [Bressloff 2012]. Amari [Amari 1977] investigated the problem in the case $d = N = 1$ when the sigmoid function is approximated by a Heaviside function and the connectivity function has a "Mexican-hat shape". He proved the existence of stable localized stationary solutions in this case. His work has been extended to different firing-rate and connectivity functions [Gutkin 2000, Laing 2002, Laing 2003b, Rubin 2004, Guo 2005a, Guo 2005b]. The case $N = 2$, $d = 1$ has been considered by several authors including [Pinto 2001a, Pinto 2001b] for general firing-rate functions and Gaussian-like connectivity functions, and [Blomquist 2005] when the firing-rate functions are approximated by Heaviside functions. Extending these analyses to two- or three-dimensional continuum is difficult because of the increase in the degrees of freedom in the choice of the connectivity function. The case $N = 1, d = 2$ has been studied in [Werner 2001, Folias 2005, Owen 2007] when the firing-rate functions are approximated by Heaviside functions and the connectivity function is circularly symmetric. Let us also point out that some work has also been done for the theoretical study of stationary solutions with bounded compact domain Ω [Faugeras 2008, Faugeras 2009b, Veltz 2010b].

(iv) Note that equations of the type of (2.18) and (2.19) have been studied in pure mathematics, see [Hazewinkel 2001]. They are of the Hammerstein type [Hammerstein 1930, Tricomi 1985]. This type of equations has received some recent attention, see [Appell 2006], and progress have been made toward a better understanding of their solutions.

(v) As explained in the introduction of this chapter, neural field equations have been used to model a wide range of neurobiological phenomena. One of the major modeling issues is to determine how these phenomena depend on the connectivity function $\mathbf{J}$. It is usually assumed that $\mathbf{J}$ depends on the Euclidean distance between interacting cells within the 2D cortical sheet so that $\mathbf{J}(\mathbf{r}, \mathbf{r}') = \mathbf{J}(\|\mathbf{r} - \mathbf{r}'\|)$, but it can also depend on the distance between two points within a feature space (see chapter 3). The dependence, with respect to the connectivity function, of the existence of stationary localized solution of equation (2.18) in the case $N = 1$ and $\Omega = \mathbb{R}$ will be discussed in 10.

2.3 The "Mexican/Wizard-hat" model

In most of the models presented in this Thesis, we use a one-layer model in which nearby neurons excite each other while more distant pairs have an inhibitory effect. Then the connectivity function has a "Mexican-hat" or a "Wizard-hat" shape depending if it is a difference of Gaussian or exponential functions. It is possible [Ermentrout 1998, Pinto 2001b] to interpret this one-layer model as an approximation of a two layers system as follows.

Let us consider two populations of excitatory and inhibitory neurons spread along a single spatial domain $\Omega = \mathbb{R}$ (see [Pinto 2001b]). We write the neural field equation (2.18) without any input as

$$\begin{aligned} \tau_e \frac{d}{dt} u_e(x,t) &= -u_e(x,t) + \int_{\mathbb{R}} w_{ee}(x-y) S_e(u_e(y,t)) dy - \int_{\mathbb{R}} w_{ie}(x-y) S_i(u_i(y,t)) dy \\ \tau_i \frac{d}{dt} u_i(x,t) &= -u_i(x,t) + \int_{\mathbb{R}} w_{ei}(x-y) S_e(u_e(y,t)) dy. \end{aligned} \tag{2.20}$$

For simplicity we have neglected the term describing recurrent inhibition. We also assume that time constant of inhibition is smaller than that of excitation. For instance, with instantaneous inhibition (*i.e.* , $\tau_i = 0$) we arrive at a single equation on the excitation:

$$\tau_e \frac{d}{dt} u_e = -u_e + w_{ee} * S_e(u_e) - w_{ie} * S_i \left(w_{ei} * S_e(u_e) \right), \tag{2.21}$$

where $*$ stands for the convolution over the real line.

This equation can still be further simplified. Supported by experimental data comparing the firing properties of excitatory versus inhibitory neurons in cortex [McCormick 1985], we may assume that the firing rate function for the inhibitory population is linear such that $S_i(x) = \alpha x$ for some positive constant $\alpha > 0$ being the gain of the sigmoid function S_i. We finally obtain the reduced equation

$$\begin{aligned} \tau_e \frac{d}{dt} u_e &= -u_e + (w_{ee} - \alpha w_{ie} * w_{ei}) * S_e(u_e) \\ &\stackrel{def}{=} -u_e + w * S_e(u_e). \end{aligned} \tag{2.22}$$

For example, if the connectivities $w_{kl}(x) = e^{-x^2/2\sigma_{kl}}$ are Gaussian functions then $w_{ie} * w_{ei}$ is also a Gaussian function. Hence in effect, w in equation (2.22) is a difference of Gaussian functions also called the "Mexican-hat" connectivity function when $w(0) > 0$. In some models, it is more convenient to work with a difference of exponential functions as in chapter 10 and in that particular case w is called a "Wizard-hat" connectivity function.

Finally, we have seen that a one-layer model with "Mexican-hat" or "Wizard-hat" connectivity function can actually be regarded as a two-layer model in which the inhibition is linear and very fast.

Chapter 3

Textures modeling and structure tensor formalism

Contents

3.1 Visual edges and textures modeling 26
3.1.1 Introduction 26
3.1.2 The structure tensor as a representation of edges and textures 27
3.1.3 Biological evidence of structure tensors in visual areas? . . . 30
3.1.4 Structure tensor neural field equation 30
3.2 The mathematical structure of the set of structure tensors 33
3.2.1 A Riemannian framework 34
3.2.2 The Poincaré disk model 34
3.2.3 Isometries of the Poincaré disk 37
3.2.4 Polar map and Poincaré disk formalism 39
3.3 Theoretical and general results for structure tensor neural field equation 41
3.3.1 Existence and uniqueness of a solution 41
3.3.2 Stationary solutions 43
3.4 Conclusion 45

The selectivity of the responses of individual neurons to external features are often the basis of neuronal representations of the external world. For example, neurons in the primary visual cortex respond preferentially to visual stimuli that have a specific orientation [Ben-Yishai 1995, Hansel 1997, Bressloff 2000], spatial frequency [Bressloff 2003b], velocity and direction of motion [Orban 1986], color [Hubel 1968]. A local network in the primary visual cortex, roughly 1 mm^2 of cortical surface, is assumed to consist of neurons coding for a given position in the retina for a full functional set of orientations and ocular dominance. These subgroups are the so-called Hubel and Wiesel hypercolumns of V1 defined in 1.2.3. Chossat and Faugeras have introduced in [Chossat 2009] a new approach to model the processing of image edges and textures in the hypercolumns of area V1 that is based on a nonlinear representation of the image first order derivatives called the structure tensor [Bigun 1987, Knutsson 1989]. It was suggested that this structure tensor was represented by neuronal populations in the hypercolumns of V1 and that the time evolution of this representation was governed by equations similar to those proposed by Wilson and Cowan [Wilson 1972, Wilson 1973].

The aim of this chapter is to present in detail the structure tensor model introduced by Chossat and Faugeras in [Chossat 2009] and give all the mathematical background related to this modeling. The structure of this chapter is as follows. In the first section 3.1, we expose the structure tensor formalism for edges and textures detection and introduce the main equations of this Thesis in subsection 3.1.4. In section 3.2, we present the mathematical structure of the set structure tensors and show the non-Euclidean geometry of the model. The last section is devoted to a preliminary theoretical study of the structure tensor neural field equation: existence, uniqueness of a solution together with some general properties of stationary solutions.

3.1 Visual edges and textures modeling

3.1.1 Introduction

Visual perception, computational or biological, depends upon the extraction from the raw flows of images incoming on the retina of a number of image features such as edges, corners, textures, or direction of motion, at a variety of spatio-temporal scales. The definition of edges, corners and direction of motion is natural whereas the notion of texture is less intuitive and needs some explanations. A wood's slice, a zebra's stripes and a field of sand all define a visual structure, that we call a *texture*, whose organization into coherent parts is fundamental to many aspects of computer vision. This class of patterns is common in both natural and man-made objects (see figure 3.1) and for centuries it has been used by artists as a tool to convey both the shape and shading of smoothly varying surfaces and their discontinuities.

Figure 3.1: Examples of textures in real images.

All these features (edge, corner, texture and direction of motion) involve comparing some functions of the incoming intensity values at nearby spatio-temporal locations and this points strongly to the notion of derivatives. The idea of constructing the image representations from various derivatives of the intensity flow is

at the heart of the concept of the primal sketch put forward in the seventies by Marr [Marr 1982] or the concept of k-jets borrowed from mathematics by Koenderink and his colleagues [Koenderink 1987, Florack 1996] and applied in mathematical neuroscience by Petitot [Petitot 2009]. There is also strong evidence that the visual system of many species is organized in such way that quantities related to image derivatives are extracted, and hence represented by neuronal activity. Indeed, a great variety of cells respond to a stimulus on the retinal plane. The receptive field of a visual neuron is classically defined as the domain of the retina to which it is connected through the neural connections of the retino-geniculo-cotrical pathways and whose stimulation elicits a spike response. A receptive field is decomposed into ON (positive contrast) and OFF (negative contrast) zones according to the type of response to light and dark luminance stimulations. There exists therefore a receptive profile of the visual neuron which is simply its impulse response as a filter kernel. It is a classical result [DeAngelis 1995a] that the receptive profiles of the retinal ganglion cells are like Laplacians of Gaussians. On the contrary, simple cells of V1 are oriented and often interpreted as Gabor patches. These neurophysiological results emphasize the fact that image derivatives can be extracted.

In their article [Chossat 2009], Chossat and Faugeras began the development of a mathematical theory of the processing of image edges and textures in the hypercolumns of area V1 that is based on the assumptions, (i) that image derivatives are represented in the visual pathway and (ii) in a nonlinear fashion. They proposed to use a structure tensor formalism, *i.e.* a nonlinear representation of the image first order derivatives, to locally describe edges and textures.

Their study was motivated by the work of Bressloff, Cowan, Golubitsky, Thomas and Wiener [Bressloff 2001b, Bressloff 2002c] on the spontaneous occurrence of hallucinatory patterns under the influence of psychotropic drugs, and its possible extension to the structure tensor model. A further motivation was the spherical model of Bressloff and Cowan [Bressloff 2002b, Bressloff 2002a, Bressloff 2003b] which is an extension of the ring model of orientation of Ben-Yishai [Ben-Yishai 1995] and Hansel, Sompolinsky [Hansel 1997] as it includes both orientation and spatial frequency.

This modeling has also to be connected to some previous work by Ben-Shahar *et al.* [Ben-Shahar 2003a] who discuss the representation and processing in V1 of a larger set of visual features including edges, textures, shading and stereo. Ben-Shahar and Zucker [Ben-Shahar 2003b, Ben-Shahar 2004] pursue these ideas for the texture flow from a viewpoint of differential geometry as described by Petitot in [Petitot 2003a, Petitot 2009]. These approaches are complementary and should be brought together as explained in chapter 12.

3.1.2 The structure tensor as a representation of edges and textures

Definition In the computer vision community [Bigun 1987, Knutsson 1989], the structure tensor is a way of representing the edges and textures of an image. Let $I(x, y)$ denote the original image intensity function, where x and y are two spa-

tial coordinates. Let I^{σ_1} denote the scale-space representation of I obtained by convolution with the Gaussian kernel $g_\sigma(\mathbf{x}) = \frac{1}{2\pi\sigma^2} e^{-\frac{x^2+y^2}{2\sigma^2}}$ where $\mathbf{x} = (x, y) \in \mathbb{R}^2$ and

$$I^{\sigma_1} = I * g_{\sigma_1}.$$

The gradient ∇I^{σ_1} is a two-dimensional vector of coordinates $I_x^{\sigma_1}$, $I_y^{\sigma_1}$ which emphasizes image edges. One then forms the 2×2 symmetric matrix of rank one $\mathcal{T}_0 = \nabla I^{\sigma_1} (\nabla I^{\sigma_1})^{\mathbf{T}}$, where $^{\mathbf{T}}$ indicates the transpose of a vector. The set of 2×2 symmetric positive semidefinite matrices of rank one will be noted $\mathbf{S}^+(1, 2)$ throughout this Thesis (see [Bonnabel 2009] for a complete study of the set $\mathbf{S}^+(p, n)$ of $n \times n$ symmetric positive semidefinite matrices of fixed-rank $p < n$). By convolving $\mathcal{T}_0$ componentwise with a Gaussian g_{σ_2} we finally form the tensor structure as the symmetric matrix:

$$\mathcal{T}(\mathbf{x}) = \mathcal{T}_0 * g_{\sigma_2}(\mathbf{x}) = \begin{pmatrix} \langle (I_x^{\sigma_1})^2 \rangle_{\sigma_2} & \langle I_x^{\sigma_1} I_y^{\sigma_1} \rangle_{\sigma_2} \\ \langle I_x^{\sigma_1} I_y^{\sigma_1} \rangle_{\sigma_2} & \langle (I_y^{\sigma_1})^2 \rangle_{\sigma_2} \end{pmatrix} (\mathbf{x}), \tag{3.1}$$

where we have set for example:

$$\langle (I_x^{\sigma_1})^2 \rangle_{\sigma_2} = (I_x^{\sigma_1})^2 * g_{\sigma_2}.$$

Since the computation of derivatives usually involves a stage of scale-space smoothing, the definition of the structure tensor requires two scale parameters. The first one, defined by σ_1, is a local scale for smoothing prior to the computation of image derivatives. The structure tensor is insensitive to noise and details at scales smaller than σ_1. The second one, defined by σ_2, is an integration scale for accumulating the nonlinear operations on the derivatives into an integrated image descriptor. It is related to the characteristic size of the texture to be represented, and to the size of the receptive fields of the neurons that may represent the structure tensor.

A local texture descriptor By construction, $\mathcal{T}$ is symmetric and non negative as $\det(\mathcal{T}) \geq 0$ by the inequality of Cauchy-Schwarz, then it has two orthonormal eigenvectors $\mathbf{e}_1$, $\mathbf{e}_2$ and two non negative corresponding eigenvalues λ_1 and λ_2 which we can always assume to be such that $\lambda_1 \geq \lambda_2 \geq 0$. Furthermore the spatial averaging distributes the information of the image over a neighborhood, and therefore the two eigenvalues are typically positive: $\lambda_1 \geq \lambda_2 > 0$. Thus, the set of the structure tensors lives in the set of 2×2 symmetric positive definite matrices, noted $\mathbf{SPD}(2, \mathbb{R})$ throughout the Thesis. The distribution of these eigenvalues in the (λ_1, λ_2) plane reflects the local organization of the image intensity variations. Indeed, each structure tensor can be written as the linear combination:

$$\begin{aligned} \mathcal{T} &= \lambda_1 \mathbf{e}_1 \mathbf{e}_1^{\mathbf{T}} + \lambda_2 \mathbf{e}_2 \mathbf{e}_2^{\mathbf{T}} \\ &= (\lambda_1 - \lambda_2) \mathbf{e}_1 \mathbf{e}_1^{\mathbf{T}} + \lambda_2 (\mathbf{e}_1 \mathbf{e}_1^{\mathbf{T}} + \mathbf{e}_2 \mathbf{e}_2^{\mathbf{T}}) \\ &= (\lambda_1 - \lambda_2) \mathbf{e}_1 \mathbf{e}_1^{\mathbf{T}} + \lambda_2 \mathbf{I}_2 \end{aligned} \tag{3.2}$$

where $\mathbf{I}_2$ is the identity matrix and $\mathbf{e}_1\mathbf{e}_1^{\mathbf{T}} \in \mathbf{S}^+(1,2)$. Some easy interpretations can be made for simple examples: constant areas are characterized by $\lambda_1 = \lambda_2 \approx 0$, straight edges are such that $\lambda_1 \gg \lambda_2 \approx 0$, their orientation being that of $\mathbf{e}_2$, corners yield $\lambda_1 \geq \lambda_2 \gg 0$. The coherency c of the local image is measured by the ratio $c = \frac{\lambda_1 - \lambda_2}{\lambda_1 + \lambda_2}$, large coherency reveals anisotropy in the texture.

Visualization by ellipses Since the structure tensor is positive definite matrix, it follows that equation

$$(\xi - \mathbf{x})^{\mathbf{T}} \mathcal{T}(\mathbf{x})(\xi - \mathbf{x}) = 1 \text{ with } \xi, \mathbf{x} \in \mathbb{R}^2 \tag{3.3}$$

defines an ellipse centered at $\mathbf{x}$. The semi-axes of this ellipse are the square roots of the inverse of the eigenvalues (λ_1, λ_2) of $\mathcal{T}(\mathbf{x})$, while the orientations of the axes give the directions of the corresponding eigenvectors $\mathbf{e}_1, \mathbf{e}_2$. In figure 3.2, we plot on an original image ellipses corresponding to the local structure tensor for some pixels. We recover the fact that, close to edges, ellipses are thin and aligned with the local orientations while, in uniform regions, ellipses have a ball shape.

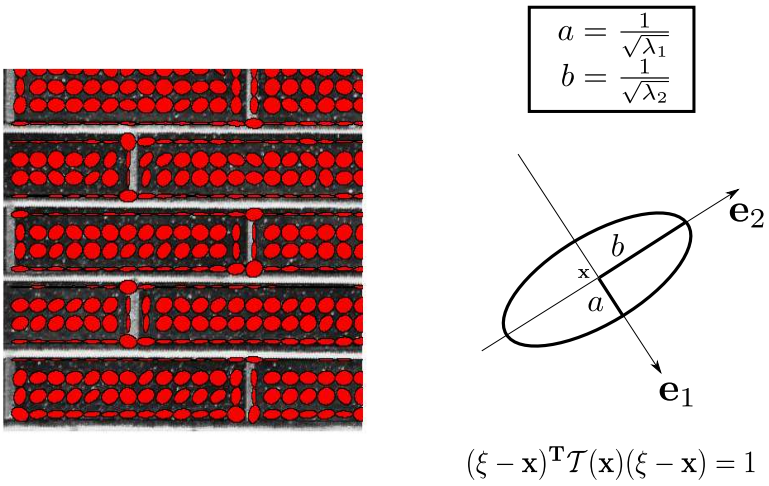

Figure 3.2: Visualization of structure tensor by plain red-colored ellipses for some pixels of an image.

Discussion The structure tensor offers three advantages. Firstly, the matrix representation of the image gradient allows the integration of information from a local neighbourhood without cancellation effects. Such effects would appear if gradients with opposite orientation were integrated directly. Secondly, smoothing the resulting matrix field yields robustness under noise by introducing an integration scale. This scale determines the local neighbourhood over which an estimation at

a certain pixel is performed. Thirdly, the integration of local orientations creates additional information, as it becomes possible to distinguish areas where structures are oriented uniformly, like in regions with edges, from areas where structures have different orientations, like in corner regions.

3.1.3 Biological evidence of structure tensors in visual areas?

The question of whether some populations of neurons in such a visual area as V1 can represent the structure tensor cannot be answered at this point in a definite manner and is still an open question. At the stage of this chapter we can nonetheless argue as follows. Cytochrome oxydase (CO) blobs and their neighbourhoods seem good candidates since their distribution appears to be correlated with a number of periodically repeating feature maps in which local populations of neurons respond preferentially to stimuli with particular properties such as orientation, spatial frequency, brightness and contrast [Blasdel 1992, Blasdel 1986, Bonhoeffer 1995, Issa 2000, Kaplan 2004, Casagrande 2004]. It has thus been suggested that the CO blobs could be the sites of functionally and anatomically distinct channels of visual processing [Edwards 1995, Livingstone 1984, Sincich 2002, Tootell 1988]. Bressloff and Cowan [Bressloff 2003a, Bressloff 2003b] introduced a model of a hypercolumn in V1 consisting of orientation and spatial frequency preferences organized around a pair of pinwheels. One pinwheel is centered at a CO blob and encodes coarse to medium coarse scales, the other is centered at a region that encodes medium coarse to fine scales. Such a hypercolumn is therefore a good candidate for representing the structure tensor at several scales as well as the local orientations at various spatial frequencies. As a consequence of this discussion, we make the following assumption.

Assumtion 3.1.1. *We assume that a hypercolumn of V1 can represent the structure tensor in the receptive field of its neurons as the average membrane potential values of some of its membrane populations.*

3.1.4 Structure tensor neural field equation

Hypercolumnar model Let $\mathcal{T}$ be a structure tensor. The time evolution of the average potential $V(\mathcal{T},t)$ for a given hypercolumn is a scalar function defined from $\mathbf{SPD}(2,\mathbb{R})\times\mathbb{R}^+$ to $\mathbb{R}$. $V(\mathcal{T},t)$ is governed by the following neural field equation adapted from equation (2.18):

$$\frac{d}{dt}V(\mathcal{T},t) = -V(\mathcal{T},t)+\int_{\mathbf{SPD}(2,\mathbb{R})} W_{loc}(d_{\mathbf{SPD}(2,\mathbb{R})}(\mathcal{T},\mathcal{T}'))S(V(\mathcal{T}',t))d\mathcal{T}'+I_{ext}(\mathcal{T},t). \tag{3.4}$$

Equation (3.4) is a rescaled version in time of equation (2.18), such that we have taken $\tau = 1$. S is a sigmoidal function as defined in equation (2.11). The properties of the connectivity function W_{loc} will be explained in section 3.3. We provide in the next section a precise mathematical definition of the set $\mathbf{SPD}(2,\mathbb{R})$. The volume element $d\mathcal{T}'$ and the distance $d_{\mathbf{SPD}(2,\mathbb{R})}$ will also be defined in the next section.

Before making precise all these quantities, we now explain how equation (3.4) can be spatialized in order to provide a cortical field model that could describe the spatio-temporal activity of V1 related to the representation of edges and textures.

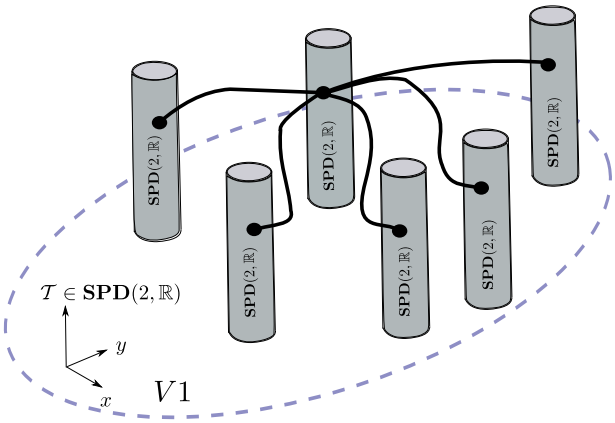

Figure 3.3: The primary visual cortex abstracted as $V^1 = \mathbb{R}^2 \times \mathbf{SPD}(2,\mathbb{R})$. Adapted from [Ben-Shahar 2004].

Spatialized model Let us assume the existence of a continuous distribution of such hypercolumnar systems [Swindale 2000, Das 2000] in a domain Ω modeling a piece of a flat cortex as it is sketched in figure 3.3. As it has been done in [Bressloff 2001b], we will further assume that $\Omega = \mathbb{R}^2$ is the whole Euclidean plane. The average membrane potential of a population of neurons at a cortical position $\mathbf{r} \in \mathbb{R}^2$ at time t is characterized by the real valued function $V(\mathbf{r}, \mathcal{T}, t)$, where $\mathbf{r}$ labels a point in the visual cortex and $\mathcal{T}$ is a structure tensor. All possible textures are represented at every position: $\mathbf{r}$ and $\mathcal{T}$ are independent variables [Bosking 2002]. The average membrane potential evolves according to a generalization of equation (3.4):

$$\frac{d}{dt}V(\mathbf{r},\mathcal{T},t) = -V(\mathbf{r},\mathcal{T},t) + \int_{\mathbb{R}^2}\int_{\mathbf{SPD}(2,\mathbb{R})} W(\mathbf{r},\mathcal{T} \mid \mathbf{r}',\mathcal{T}')S(V(\mathbf{r}',\mathcal{T}',t))d\mathcal{T}'d\mathbf{r}' + I_{ext}(\mathbf{r},\mathcal{T},t), \tag{3.5}$$

where $d\mathbf{r}'$ is the usual Euclidean area element.

A crucial point in this model is the choice of the connectivity function $W(\mathbf{r},\mathcal{T} \mid \mathbf{r}',\mathcal{T}')$ which reflects the underlying functional structure of V1 through its cortical circuits. So far, two different types of cortical circuit have been experimentally found: a local and a lateral. The local circuit, operating at sub-hypercolumn dimensions, consists of a mixture of intra-cortical excitation and inhibition. Such circuit provides a substrate for the recurrent amplification and sharpening of the

tuned response of cells to local visual stimuli (for example the ring model of orientation where the inhibitory connections are more broadly tuned with respect to orientation than the excitatory connections [Ben-Yishai 1995, Hansel 1997]). The lateral circuit, operating between hypercolumns, anisotropically connects cells with similar functional properties: cells in different hypercolumns tend to connect in directions parallel to their common preferred orientation (see figures 1.11 and 3.4). Based on these anatomical structures, Bressloff *et al.* [Bressloff 2001b, Bressloff 2002b] took into account the orientation of cortical neurons and abstracted the visual cortex as $\mathbb{R}^2 \times \mathbf{S}^1$. Their analysis recovered thin line hallucinations such as cobwebs and honeycombs.

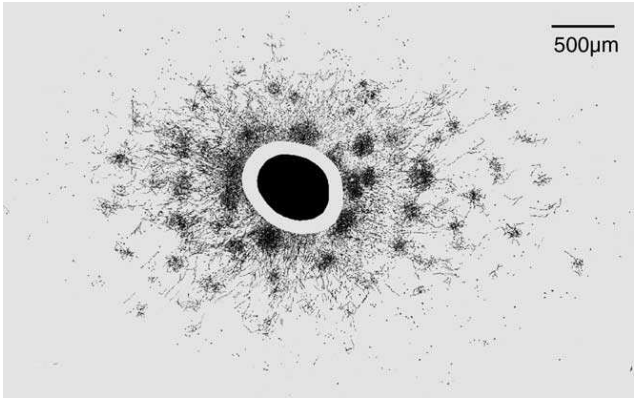

Figure 3.4: Patchy isotropic horizontal connections in layers 2/3 of macaque area V1. Redrawn from [Lund 2003].

However, the anisotropic nature of cortical long-range connections can be weak upon species. For macaques (see figure 3.4) anisotropy tends to be weaker than for tree shrews (see figure 1.11). This remark has been incorporated into numerous models of cortical map development [Wolf 1998, Kaschube 2008, Kaschube 2010]. Following these ideas we decompose the connectivity function $W(\mathbf{r}, \mathcal{T} \mid \mathbf{r}', \mathcal{T}')$ into local (within the hypercolumns) and long-range parts according to:

$$W(\mathbf{r}, \mathcal{T} \mid \mathbf{r}', \mathcal{T}') = W_{loc}(d_{\mathbf{SPD}(2,\mathbb{R})}(\mathcal{T}, \mathcal{T}'))\delta_{\mathbf{r},\mathbf{r}'} + \beta(1-\delta_{\mathbf{r},\mathbf{r}'})W^{\varepsilon}_{lat}(\mathbf{r}, \mathcal{T} \mid \mathbf{r}', \mathcal{T}'). \quad (3.6)$$

Microelectrode recordings suggest that β is small and therefore that the lateral connections modulate rather than drive the cortical activity. The sign of β will determine whether the lateral connections have a net excitatory or inhibitory effect. Note that when $\beta = 0$, we recover equation (3.4). The rules of long-range connections are given by:

$$W^{\varepsilon}_{lat}(\mathbf{r}, \mathcal{T} \mid \mathbf{r}', \mathcal{T}') = \mathcal{J}\left(\sqrt{(\mathbf{r}-\mathbf{r}')^{\mathbf{T}}(\mathbf{I}_2 + \varepsilon\mathcal{T})(\mathbf{r}-\mathbf{r}')}\right)\mathcal{K}\left(d\left(\mathcal{T}, \mathcal{T}'\right)\right) \quad (3.7)$$

The first factor $\mathcal{J}$ incorporates the observation that the density patches tends to decrease monotonically with cortical separation and lies along the direction of

their feature preference. for definiteness, we take $\mathcal{J}$ to be a Gaussian $\mathcal{J}(x) = \mathcal{N}e^{-x^2/2\xi^2}$. For an illustration purpose, in figure 3.5, we plot the profile of $\mathbf{r} \to \mathcal{J}\left(\sqrt{\mathbf{r}^\mathbf{T}(\mathbf{I}_2 + \varepsilon\mathcal{T})\mathbf{r}}\right)$, for specific values of the parameters and a diagonal structure tensor $\mathcal{T} = \text{diag}(50, 0.2)$ which has a preferred orientation at $\frac{\pi}{2}$. Note that first Bressloff in [Bressloff 2003c] and then Baker and Cowan in [Baker 2009] use a similar anisotropic function for a continuum model of V1 with long-range horizontal connections without feature space. The second factor of the horizontal connectivity ensures that the long-range connections link cells with similar feature preferences, and is taken to be an even positive, narrowly tuned distribution with $\mathcal{K}(x) = 0$ for all $|x| \geq k_c$. In the limit $k_c \to 0$, $\mathcal{K}$ is taken to be the δ-dirac function. The parameter ε controls the degree of anisotropy.

These models will be studied in great details in chapter 8. The hypercolumnar model defined in equation (3.4) is a direct generalization of both the ring model of orientations [Ben-Yishai 1995, Hansel 1997] and the spherical model of Bressloff and Cowan [Bressloff 2003a, Bressloff 2003b].

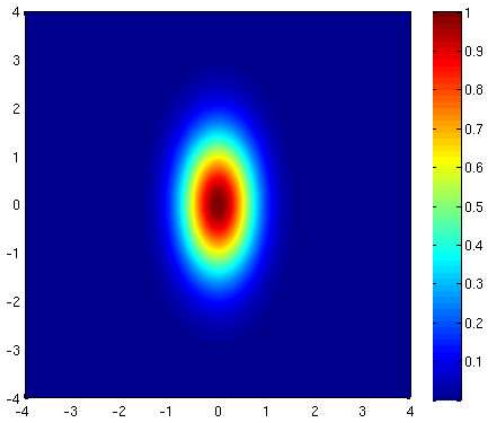

Figure 3.5: Plot of $\mathbf{r} \to \mathcal{J}\left(\sqrt{\mathbf{r}^\mathbf{T}(\mathbf{I}_2 + \varepsilon\mathcal{T})\mathbf{r}}\right)$ in the definition of long-range connections. $\mathcal{N} = \xi = 1$, $\varepsilon = 0.05$ and $\mathcal{T} = \text{diag}\,(50, 0.2)$.

3.2 The mathematical structure of the set of structure tensors

We present in this section some important properties of the set of structure tensors. These properties are essential to our forthcoming part of pattern formation in cortical tissue.

The key observation is that the structure tensors naturally live in a hyperbolic space of dimension 3 that can be peeled into sheets of dimension 2, each sheet corresponding to a constant value of the determinant of the element inhabiting in it. We are therefore led to study hyperbolic spaces of dimension 2 which turn out

to enjoy a very simple representation in the open unit disk $\mathbb{D}$ of the complex plane, the so-called Poincaré disk, with its non-Euclidean geometry that arises from the Riemannian structure of the set of structure tenors. In the first part of this section, we introduce the Riemannian framework of the set of structure tensors and present in a second part its relationships with the Poincaré disk. The last part is devoted to the study of the group of isometries of the Poincaré disk and their corresponding action on structure tensors.

3.2.1 A Riemannian framework

The set of structure tensors is isomorphic to $\mathbf{SPD}(2,\mathbb{R})$ the set of 2×2 symmetric positive definite matrices. This set is a solid open cone in $\mathbb{R}^3$ and a Riemannian manifold with the distance defined as follows [Moakher 2005]. Given $\mathcal{T}_1$ and $\mathcal{T}_2$ in $\mathbf{SPD}(2,\mathbb{R})$, the Riemannian distance $d_{\mathbf{SPD}(2,\mathbb{R})}(\mathcal{T}_1,\mathcal{T}_2)$ can be expressed as the Frobenius norm (the Frobenius norm of a real matrix is the square root of the sum of the square of its elements) of the principal logarithm of $\mathcal{T}_1^{-1}\mathcal{T}_2$:

$$d_{\mathbf{SPD}(2,\mathbb{R})}(\mathcal{T}_1,\mathcal{T}_2) = \|\log \mathcal{T}_1^{-1}\mathcal{T}_2\|_F = \left(\sum_{i=1,2}\log^2\lambda_i\right)^{1/2}, \tag{3.8}$$

where the λ_i's are the eigenvalues of the matrix $\mathcal{T}_1^{-1}\mathcal{T}_2$.

This definition of the distance between two tensors can be motivated from a biological viewpoint. A tensor is a symmetric 2×2 matrix, hence it can be thought of as a three-dimensional vector (a,b,c). The natural distance between two such vectors (representing the tensors $\mathcal{T}_1$ and $\mathcal{T}_2$) is the usual Euclidean distance $\left((a_1-a_2)^2+(b_1-b_2)^2+(c_1-c_2)^2\right)^{1/2}$. However, change of coordinate system does not leave in general the Euclidean distance invariant whereas it does leave $d_{\mathbf{SPD}(2,\mathbb{R})}$ invariant. This invariance is a very desirable feature since the measure of similarity between two tensors should not depend on the particular coordinate system used to evaluate their components.

3.2.2 The Poincaré disk model

Now any $\mathcal{T}\in\mathbf{SPD}(2,\mathbb{R})$ can be written $\mathcal{T}=\Delta\tilde{\mathcal{T}}$ with $\Delta>0$ and $\det\tilde{\mathcal{T}}=1$. Therefore $\mathbf{SPD}(2,\mathbb{R}) = \mathbb{R}_*^+\times\mathbf{SSPD}(2,\mathbb{R})$, the two-dimensional submanifold of symmetric positive definite matrices whose determinant is equal to 1. It can be shown in [Chossat 2009] (see figure 3.6) that the surface $\mathbf{SSPD}(2,\mathbb{R})$ equipped with the Riemannian structure induced by the metric of $\mathbf{SPD}(2,\mathbb{R})$, is isomorphic to the hyperbolic plane which is itself isomorphic to the disk $\mathbb{D}=\{z\in\mathbb{C}\mid |z|<1\}$ equipped with the hyperbolic distance

$$d_{\mathbb{D}}(z,z') = 2\text{arctanh}\frac{|z-z'|}{|1-\bar{z}z'|} \quad \text{(Poincaré disk)}. \tag{3.9}$$

Therefore, there is an isomorphism between the space of structure tensors and the product space $\mathbb{R}_*^+\times\mathbb{D}$. It is a straightforward computation to see that the distance

in $\mathbf{SPD}(2,\mathbb{R})$ can be written in $(\Delta, z) \in \mathbb{R}_*^+ \times \mathbb{D}$ coordinates as

$$d_{\mathbf{SPD}(2,\mathbb{R})}(\mathcal{T},\mathcal{T}') = \sqrt{2\log\left(\frac{\Delta}{\Delta'}\right)^2 + 2d_{\mathbb{D}}(z,z')^2}. \tag{3.10}$$

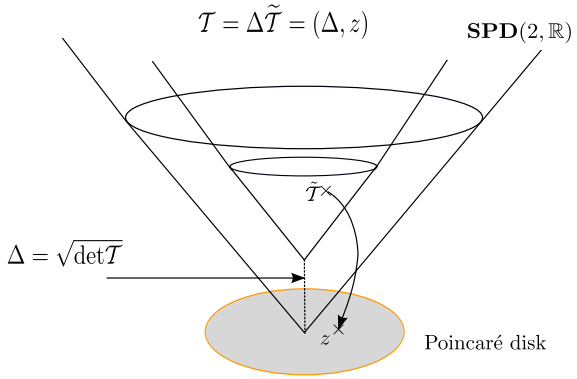

Figure 3.6: Illustration of the isomorphism between $\mathbf{SPD}(2,\mathbb{R})$ and $\mathbb{R}_*^+ \times \mathbb{D}$.

Relationships between $\mathbf{SSPD}(2,\mathbb{R})$ and $\mathbb{D}$ We now detail the relationships between $\mathbf{SSPD}(2,\mathbb{R})$ and its representation in the Poincaré disk $\mathbb{D}$. A unit determinant structure tensor $\mathcal{T}$ is a 2×2 symmetric positive definite matrix defined as

$$\mathcal{T} = \begin{pmatrix} a & c \\ c & b \end{pmatrix}$$

with $ab - c^2 = 1$. The corresponding point in $\mathbb{D}$ is given by:

$$z = \frac{a - b + 2ic}{a + b + 2} \tag{3.11}$$

where z satisfies

$$0 \leq |z| = \frac{a + b - 2}{a + b + 2} < 1.$$

Conversely given a point $z = z_1 + iz_2$ representing a point of $\mathbb{D}$, the corresponding tensor coordinates are given by:

$$\begin{aligned} a &= \frac{(1+z_1)^2 + z_2^2}{1 - z_1^2 - z_2^2} \\ b &= \frac{(1-z_1)^2 + z_2^2}{1 - z_1^2 - z_2^2} \\ c &= \frac{2z_2}{1 - z_1^2 - z_2^2}. \end{aligned} \tag{3.12}$$

Note that equation (3.11) is the "$\mathbf{SSPD}(2,\mathbb{R})$ to $\mathbb{D}$" dictionary that allows us to translate statements about structure tensors to statements to points in the Poincaré disk and (3.12) is the "$\mathbb{D}$ to $\mathbf{SSPD}(2,\mathbb{R})$" dictionary.

Volume element We now express the volume element $d\mathcal{T}$ introduced in neural field equations (3.4) and (3.5).

Proposition 3.2.1. *The volume element in $\mathcal{T} = (\Delta, z)$ coordinates is*

$$d\mathcal{T} = 8\sqrt{2}\,\frac{d\Delta}{\Delta}\,\frac{dz_1\,dz_2}{(1-|z|^2)^2} \text{ with } z = z_1 + iz_2. \tag{3.13}$$

Corollary 3.2.1. *The volume element in $z \in \mathbb{D}$ coordinates is*

$$dm(z) = \frac{4dz_1\,dz_2}{(1-|z|^2)^2} \text{ with } z = z_1 + iz_2. \tag{3.14}$$

Proof. Let $\mathcal{T}$ be a structure tensor

$$\mathcal{T} = \begin{pmatrix} x_1 & x_3 \\ x_3 & x_2 \end{pmatrix},$$

Δ^2 its determinant, $\Delta \geq 0$. $\mathcal{T}$ can be written

$$\mathcal{T} = \Delta\tilde{\mathcal{T}},$$

where $\tilde{\mathcal{T}}$ has determinant 1. Let $z = z_1 + iz_2$ be the complex number representation of $\tilde{\mathcal{T}}$ in the Poincaré disk $\mathbb{D}$.

In order to compute the volume element in (Δ, z_1, z_2) space, we need to express the metric $g_{\mathcal{T}}$ in these coordinates. This is obtained from the inner product in the tangent space $T_{\mathcal{T}}$ at point $\mathcal{T}$ of $\mathbf{SPD}(2,\mathbb{R})$. The tangent space is the set $\mathcal{S}(2)$ of symmetric matrices and the inner product is defined by:

$$g_{\mathcal{T}}(A,B) = \mathrm{tr}(\mathcal{T}^{-1}A\mathcal{T}^{-1}B), \quad A,\, B \in \mathcal{S}(2),$$

We note that $g_{\mathcal{T}}(A,B) = g_{\tilde{\mathcal{T}}}(A,B)/\Delta^2$. We note g instead of $g_{\tilde{\mathcal{T}}}$. A basis of $T_{\mathcal{T}}$ (or $T_{\tilde{\mathcal{T}}}$ for that matter) is given by:

$$\frac{\partial}{\partial x_1} = \begin{pmatrix} 1 & 0 \\ 0 & 0 \end{pmatrix} \quad \frac{\partial}{\partial x_2} = \begin{pmatrix} 0 & 0 \\ 0 & 1 \end{pmatrix} \quad \frac{\partial}{\partial x_3} = \begin{pmatrix} 0 & 1 \\ 1 & 0 \end{pmatrix},$$

and the metric is given by:

$$g_{ij} = g_{\tilde{\mathcal{T}}}(\frac{\partial}{\partial x_i}, \frac{\partial}{\partial x_j}),\ i,j = 1,2,3.$$

The determinant $G_{\mathcal{T}}$ of $g_{\mathcal{T}}$ is equal to G/Δ^6, where G is the determinant of $g = g_{\tilde{\mathcal{T}}}$. G is found to be equal to 2. The volume element is thus:

$$d\mathcal{T} = \frac{\sqrt{2}}{\Delta^3}\,dx_1\,dx_2\,dx_3.$$

We then use the relations:

$$x_1 = \Delta\ a, \quad x_2 = \Delta\ b, \quad x_3 = \Delta\ c,$$

where a, b and c are given by the "$\mathbb{D}$ to $\mathbf{SSPD}(2,\mathbb{R})$" dictionary of equations (3.12). The absolute value of the determinant of the Jacobian of the transformation $(x_1, x_2, x_3) \to (\Delta, z_1, z_2)$ is found to be equal to:

$$\frac{8\Delta^2}{(1-|z|^2)^2}.$$

Hence, the volume element in (Δ, z_1, z_2) coordinates is

$$d\mathcal{T} = 8\sqrt{2}\,\frac{d\Delta}{\Delta}\,\frac{dz_1\,dz_2}{(1-|z|^2)^2}.$$

□

3.2.3 Isometries of the Poincaré disk

We now describe the isometries of $\mathbb{D}$, i.e the transformations that preserve the distance $d_{\mathbb{D}}$. We refer to the classical textbooks in hyperbolic geometry for details, e.g, [Katok 1992]. The direct isometries (preserving the orientation) in $\mathbb{D}$ are the elements of the special unitary group, noted $\mathbf{SU}(1,1)$, of 2×2 Hermitian matrices with determinant equal to 1. Given:

$$\gamma = \begin{pmatrix} \alpha & \beta \\ \bar{\beta} & \bar{\alpha} \end{pmatrix} \text{ such that } |\alpha|^2 - |\beta|^2 = 1, \tag{3.15}$$

an element of $\mathbf{SU}(1,1)$, the corresponding isometry γ in $\mathbb{D}$ is defined by:

$$\gamma \cdot z = \frac{\alpha z + \beta}{\bar{\beta} z + \bar{\alpha}}, \quad z \in \mathbb{D}. \tag{3.16}$$

Orientation reversing isometries of $\mathbb{D}$ are obtained by composing any transformation (3.16) with the reflection $\kappa : z \to \bar{z}$. The full symmetry group of the Poincaré disc is therefore:

$$\mathbf{U}(1,1) = \mathbf{SU}(1,1) \cup \kappa \cdot \mathbf{SU}(1,1).$$

The action of the group $\mathbf{SU}(1,1)$ on the Poincaré disk is equivalent to the conjugation on the set of structure tensors. We call it the lifted action of $\mathbf{SU}(1,1)$ to the set of structure tensors. Indeed, let

$$\gamma = \begin{pmatrix} \alpha & \beta \\ \bar{\beta} & \bar{\alpha} \end{pmatrix} \text{ with } \alpha = \alpha_1 + i\alpha_2, \quad \beta = \beta_1 + i\beta_2,$$

be an element of $\mathbf{SU}(1,1)$ whose action on $\mathbb{D}$ is given by equation (3.16), then it can be shown by an easy computation that the lifted action on the corresponding structure tensor $\mathcal{T}$ is

$$\tilde{\gamma} \cdot \mathcal{T} = \tilde{\gamma}^{\mathbf{T}} \mathcal{T} \tilde{\gamma}, \tag{3.17}$$

where

$$\tilde{\gamma} = \begin{pmatrix} \alpha_1 + \beta_1 & \alpha_2 + \beta_2 \\ \beta_2 - \alpha_2 & \alpha_1 - \beta_1 \end{pmatrix} \in \mathbf{SL}(2,\mathbb{R}). \tag{3.18}$$

Equation (3.17) shows that the lifted action on a given structure tensor of an isometry of $\mathbb{D}$ is a simple change of coordinates in the image plane. We show below that these changes of coordinate systems have simple interpretations for many of the subgroups that generate $\mathbf{SU}(1,1)$.

Let us now describe the different kinds of direct isometries acting in $\mathbb{D}$. We first define the following one parameter subgroups of $\mathbf{SU}(1,1)$:

$$\begin{cases} K \overset{def}{=} \{\mathrm{r}_\phi = \begin{pmatrix} e^{i\frac{\phi}{2}} & 0 \\ 0 & e^{-i\frac{\phi}{2}} \end{pmatrix}, \phi \in \mathbb{S}^1\}, \\ A \overset{def}{=} \{a_\tau = \begin{pmatrix} \cosh(\tau/2) & \sinh(\tau/2) \\ \sinh(\tau/2) & \cosh(\tau/2) \end{pmatrix}, \tau \in \mathbb{R}\}, \\ N \overset{def}{=} \{n_s = \begin{pmatrix} 1+is & -is \\ is & 1-is \end{pmatrix}, s \in \mathbb{R}\}. \end{cases}$$

Note that $\mathrm{r}_\phi \cdot z = e^{i\phi} z$ for $z \in \mathbb{D}$ and also $a_\tau \cdot 0 = \tanh(\tau/2)$. The corresponding lifted elements of $\mathbf{SL}(2,\mathbb{R})$ are according to (3.18):

$$\begin{cases} \widetilde{\mathrm{r}}_\phi = \begin{pmatrix} \cos\left(\frac{\phi}{2}\right) & \sin\left(\frac{\phi}{2}\right) \\ -\sin\left(\frac{\phi}{2}\right) & \cos\left(\frac{\phi}{2}\right) \end{pmatrix}, \\ \tilde{a}_\tau = \begin{pmatrix} e^{\tau/2} & 0 \\ 0 & e^{-\tau/2} \end{pmatrix}, \\ n_s = \begin{pmatrix} 1 & 0 \\ -2s & 1 \end{pmatrix}. \end{cases}$$

They generate three subgroups, respectively noted $\tilde{K}, \tilde{A}$ and $\tilde{N}$ of $\mathbf{SL}(2,\mathbb{R})$. The following decomposition holds (see [Iwaniec 2002]).

Theorem 3.2.1 (Iwasawa decomposition).

$$\boldsymbol{SU}(1,1) = KAN \text{ and } \boldsymbol{SL}(2,\mathbb{R}) = \tilde{K}\tilde{A}\tilde{N}.$$

This theorem allows us to decompose any isometry of $\mathbb{D}$ as the product of at most three elements in the groups, K, A and N. Then, it is possible to express each point $z \in \mathbb{D}$ in hyperbolic polar coordinates: $\mathrm{r}_\phi a_\tau \cdot O = \tanh(\tau/2)e^{i\phi}$ with $\tau = d_{\mathbb{D}}(z,0)$. An other useful coordinate system is the horocyclic coordinates: $z = n_s a_\tau \cdot O \in \mathbb{D}$, where n_s are the transformations associated with the group N ($s \in \mathbb{R}$) and a_τ the transformations associated with the subgroup A ($\tau \in \mathbb{R}$).

The group K is the orthogonal group $\mathbf{SO}(2)$ which fixes the center O of $\mathbb{D}$. Its orbits are concentric circles. The orbits of A converge to the same limit points of the unit circle $\partial\mathbb{D}$, $b_{\pm 1} = \pm 1$ when $r \to \pm\infty$. The elements of A are sometimes called *boosts* in the theoretical Physics literature [Balazs 1986]. They are circular arcs in $\mathbb{D}$ going through the points b_1 and b_{-1}. The orbits of N are the circles inside $\mathbb{D}$ and tangent to the unit circle at b_1. These circles are called *horocycles* with base point b_1. N is called the horocyclic group. These orbits are shown in figure 3.7.

The lifted action of the groups K and A have very intuitive interpretations in term of structure tensors. Unfortunately, there is no corresponding interpretation for the horocyclic group N.

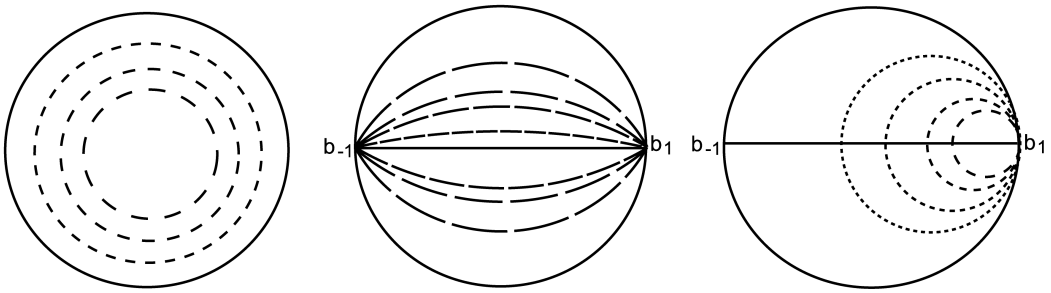

Figure 3.7: The orbits in the Poincaré disk of the three groups K, A and N.

(i) The action $\mathrm{r}_\phi \cdot z$ lifts to the conjugation $\widetilde{\mathrm{r}}_\phi^{\mathbf{T}} \mathcal{T} \widetilde{\mathrm{r}}_\phi$ of the structure tensor $\mathcal{T}$ represented by z. This is equivalent to say that we rotate by $\phi/2$ the orthonormal basis $(\mathbf{e}_1, \mathbf{e}_2)$ in which the coordinates of $\mathcal{T}$ are expressed.

(ii) The action $a_\tau \cdot z$ lifts to the conjugation $\widetilde{a}_\tau^{\mathbf{T}} \mathcal{T} \widetilde{a}_\tau$ of the structure tensor $\mathcal{T}$ represented by z. This is equivalent to say that we scale the first vector of the orthonormal basis $(\mathbf{e}_1, \mathbf{e}_2)$ in which the coordinates of $\mathcal{T}$ are expressed by $e^{\tau/2}$ and the second by $e^{-\tau/2}$.

3.2.4 Polar map and Poincaré disk formalism

Most of the time, we will drop the Δ component of structure tensor $\mathcal{T} = (\Delta, z)$ and only work with neural field equation (3.4) set on the Poincaré disk:

$$\frac{d}{dt}V(z,t) = -V(z,t) + \int_{\mathbb{D}} W_{loc}(d_{\mathbb{D}}(z,z'))S(V(z',t))\mathrm{dm}(z') + I_{ext}(z,t), \qquad (3.19)$$

where $\mathrm{dm}(z')$ is defined through equation (3.14). As in the previous subsection 3.1.3, it is important to look at biological evidence of representation of the Poincaré disk within the primary visual cortex. A plausible answer comes with the notion of polar map.

In optical imaging ([Chemla 2010a] for a review), a polar map is obtained by combining the color code for preferred orientation with a brightness code representing the strength of orientation tuning, see figure 3.8(a). Dark regions represent areas of weak tuning, whereas bright areas represent strong orientation preference. Dark areas are prevalent in pinwheel centers. The polar map is a functional map that assigns each location $\mathbf{r}$, a complex number $z(\mathbf{r})$. The values of $z(\mathbf{r})$ are calculated from the orientation map as follows. Let $(\varphi_j)_{j=1\ldots p}$ be p equidistant orientations presented to the animal, let $S_{\mathbf{r}}^{\varphi_j}$ denote the cortical response at location $\mathbf{r}$ evoked by orientation φ_j.

$$z(\mathbf{r}) = \rho(\mathbf{r})e^{i\theta(\mathbf{r})} = \frac{2}{p}\sum_{j=1}^{p} S_{\mathbf{r}}^{\varphi_j} e^{i\varphi_j},$$

where $\theta(\mathbf{r})$ is the preferred orientation at location $\mathbf{r}$ and the magnitude measures the degree to which the response at location $\mathbf{r}$ is modulated by the stimulus's orientation. This is the *selectivity* of location $\mathbf{r}$. When moving from a point far from the pinwheel towards the pinwheel, the selectivity is gradually reduced, resulting in a large range of selectivity values. For each preferred orientation there is a wide range of selectivities. It was shown in [Nauhaus 2008] that neurons in regions of homogeneous orientation preference (iso-orientation domains) have much sharper tuning than in heterogeneous regions of the map (near pinwheel centers), see figure 3.8(b). These anatomical experiments lead us to identify a point of the polar map $z(\mathbf{r})$ with a point in the Poincaré disk seen as a structure tensor of determinant equal one. The point $z = 0$ of the Poincaré disk is interpreted as a point where all orientations are represented with low selectivity and then corresponds to a pinwheel center, whereas a point $z = |z|e^{i\theta}$ close the boundary $\mathbb{D}$ has a preferred orientation θ and a very high selectivity.

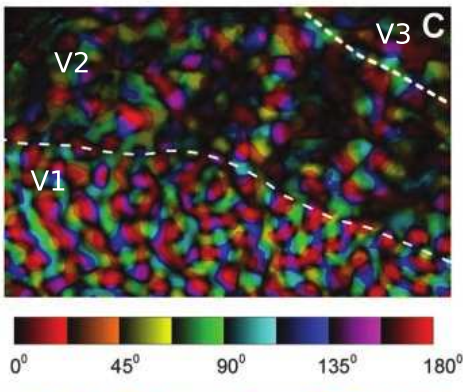

(a) Redrawn from Xu *et al.* [Xu 2004].

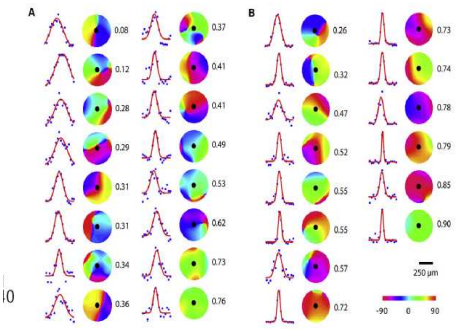

(b) Redrawn from Nauhaus *et al.* [Nauhaus 2008].

Figure 3.8: Left. Polar map for the data obtained by [Xu 2004] for owl monkey. Right. Examples of orientation tuning curves and their location within the orientation map. Tuning width decreases with increasing values of the local homogeneity index (selectivity).

As we have identified the modulus of a point in the Poincaré disk to the selectivity, it is now natural to see if it has an interpretation in term of structure tensor. From the computer vision point of view, the modulus can also be linked to the coherence of the corresponding structure tensor. We have already introduced the coherence of a structure tensor in 3.1.2 and explain that it measures the degree of anisotropy of the two eigenvalues of the structure tensor. For a given structure tensor $\mathcal{T}$, the coherence is defined as the ratio $\frac{\lambda_1-\lambda_2}{\lambda_1+\lambda_2}$, where $\lambda_1 \geq \lambda_2 > 0$ are the two eigenvalues of $\mathcal{T}$. In the case of a structure tensor $\mathcal{T}$ with determinant equal to 1 which is identified to a point $z \in \mathbb{D}$, we have $\frac{\lambda_1-\lambda_2}{\lambda_1+\lambda_2} = \frac{2|z|}{1+|z|^2}$. Then, the notion of coherence for an image and the notion of selectivity to an orientation are directly linked with our Poincaré disk formalism which has certainly a good biological flavor.

3.3 Theoretical and general results for structure tensor neural field equation

In this section we provide theoretical and general results of existence and uniqueness of a solution of (3.4) together with some properties of the stationary solutions. The detailed proof of the theorems can be found in [Faye 2011b].

3.3.1 Existence and uniqueness of a solution

From now on, we use the (Δ, z)-coordinates for a structure tensor $\mathcal{T}$ introduced in the previous section. Using the definition of the distance $d_{\mathbf{SPD}(2,\mathbb{R})}$ of equation (3.10) and the volume element $d\mathcal{T}$ of equation (3.13), we can rewrite equation (3.4) as:

$$\left(\frac{d}{dt}+1\right)V(\Delta,z,t)=\int_{\mathbb{R}_*^+\times\mathbb{D}}\mathcal{W}\left(\log\left(\frac{\Delta}{\Delta'}\right),d_{\mathbb{D}}(z,z')\right)S(V(\Delta',z',t))\frac{d\Delta'}{\Delta'}\mathrm{dm}(z') + I_{ext}(\Delta,z,t), \tag{3.20}$$

where we have set

$$\mathcal{W}\left(\log\left(\frac{\Delta}{\Delta'}\right),d_{\mathbb{D}}(z,z')\right)\overset{def}{=}2\sqrt{2}W_{loc}\left(\sqrt{2\log\left(\frac{\Delta}{\Delta'}\right)^2+2d_{\mathbb{D}}(z,z')^2}\right).$$

We introduce the following mapping $f:(\phi)\to f(\phi)$ such that:

$$f(\phi)(\Delta,z)=\int_{\mathbb{R}_*^+\times\mathbb{D}}\mathcal{W}\left(\log\left(\frac{\Delta}{\Delta'}\right),d_{\mathbb{D}}(z,z')\right)S(\phi(\Delta',z'))\frac{d\Delta'}{\Delta'}\mathrm{dm}(z'). \tag{3.21}$$

Our aim is to find a functional space $\mathcal{F}$ where (3.20) is well-defined and the function f maps $\mathcal{F}$ to $\mathcal{F}$ for all ts. A natural choice would be to take ϕ as a $\mathrm{L}^p(\mathbb{R}_*^+\times,\mathbb{D})$-integrable function of the space variable with $1\leq p<+\infty$. Unfortunately, the homogeneous solutions (constant with respect to (Δ,z)) and the periodic solutions do not belong to that space. Moreover, a valid model of neural networks should only produce bounded membrane potentials. That is why we focus our choice on the functional space $\mathcal{F}=\mathrm{L}^\infty(\mathbb{R}_*^+\times\mathbb{D})$. As $\mathbb{R}_*^+\times\mathbb{D}$ is an open set of $\mathbb{R}^3$, $\mathcal{F}$ is a Banach space for the norm: $\|\phi\|_{\mathcal{F}}=\sup_{z\in\mathbb{D}}\sup_{\Delta\in\mathbb{R}_*^+}|\phi(\Delta,z)|$.

Hypothesis 3.3.1. *We suppose that $\mathbf{W}\in L^1(\mathbb{R}_*^+\times\mathbb{D})$, with the measure element given in equation (3.13), where $\mathbf{W}(\Delta,z)=\mathcal{W}(\log(\Delta),d_{\mathbb{D}}(z,0))$ for all $(\Delta,z)\in\mathbb{R}_*^+\times\mathbb{D}$.*

Proposition 3.3.1 (Well posedness). *If $\mathcal{W}$ satisfies hypothesis 3.3.1 then f is well-defined and is from $\mathcal{F}$ to $\mathcal{F}$.*

We rewrite (3.20) as a Cauchy problem of the form:

$$\begin{cases}\partial_t V(\Delta,z,t)=-\alpha V(\Delta,z,t)+f(V(\Delta,z,t))+I_{ext}(\Delta,z,t) & t\geq 0,\\ V(\Delta,z,0)=V_0(\Delta,z).\end{cases} \tag{3.22}$$

Theorem 3.3.1 (Existence). *Let J be an open interval containing 0. If the external current I_{ext} belongs to $\mathcal{C}(J,\mathcal{F})$ and $\mathcal{W}$ satisfies hypothesis 3.3.1, then fo all $V_0 \in \mathcal{F}$, there exists a unique solution of (3.22) defined on a subinterval J_0 of J containing 0 such that $V(z,\Delta,0) = V_0(z,\Delta)$ for all $(\Delta,z) \in \mathbb{R}_*^+ \times \mathbb{D}$.*

Proof. Direct application of the Cauchy-Lipschitz theorem, see [Faye 2011b]. □

Remark 3.3.1. *Our result is quite similar to those obtained by Potthast and Graben in [Potthast 2010]. The main differences is that our space features is no longer $\mathbb{R}^n$ but a Riemannian manifold. In their article, Potthast and Graben also work with a different functional space by assuming more regularity for the connectivity function $\mathcal{W}$ and then obtain more regularity for their solutions.*

Corollary 3.3.1. *If the external current I_{ext} belongs to $\mathcal{C}(\mathbb{R}^+,\mathcal{F})$ and if $\mathcal{W}$ satisfies hypothesis 3.3.1 with $J = \mathbb{R}^+$, then for all $V_0 \in \mathcal{F}$, there exists a unique solution of (3.22) defined on $\mathbb{R}^+$ such that $V(z,\Delta,0) = V_0(z,\Delta)$ for all $(\Delta,z) \in \mathbb{R}_*^+ \times \mathbb{D}$.*

It is also possible to prove a result on the boundedness of a solution of (3.20). We first denote $\mathcal{W}_0 = \|\mathbf{W}\|_{L^1}$ and $S^m = \sup_{x\in\mathbb{R}} |S(x)|$. Moreover, if the external current I_{ext} satisfies $\sup_{t\in\mathbb{R}^+} \|I_{\text{ext}}(t)\|_{\mathcal{F}} < +\infty$, we can define ρ as:

$$\rho = 2\left(S^m\mathcal{W}_0 + \sup_{t\in\mathbb{R}^+} \|I_{\text{ext}}(t)\|_{\mathcal{F}}\right).$$

Proposition 3.3.2. *If the external current I_{ext} belongs to $\mathcal{C}(\mathbb{R}^+,\mathcal{F})$ and is bounded in time $\sup_{t\in\mathbb{R}^+} \|I_{ext}(t)\|_{\mathcal{F}} < +\infty$ and $\mathcal{W}$ satisfies hypothesis 3.3.1 with $J = \mathbb{R}^+$, then the solution of (3.22) is bounded for each initial condition $V_0 \in \mathcal{F}$. More precisely, the open ball B_ρ, centered at 0 with radius ρ in $\mathcal{F}$, is stable under the dynamics of (3.20). Moreover it is an attracting set for this dynamic and if $V_0 \notin B_\rho$ and $T = \inf\{t > 0 \text{ such that } V(t) \in B_\rho\}$ then:*

$$T \leq \log\left(\frac{2\|V_0\|_{\mathcal{F}} - \rho}{\rho}\right). \tag{3.23}$$

Proof. Let V be a solution defined on $\mathbb{R}^+$. Then we have for all $t \in \mathbb{R}_*^+$:

$$V(\Delta,z,t) = e^{-t}V_0(\Delta,z,t) + \int_0^t e^{-(t-u)}\left(f(V(\Delta,z,u)) + I_{ext}(\Delta,z,u)\right)du.$$

The following upperbound holds

$$\|V(t)\|_{\mathcal{F}} \leq e^{-t}\|V_0\|_{\mathcal{F}} + \left(S^m\mathcal{W}_0 + \sup_{t\in\mathbb{R}^+} \|I_{\text{ext}}(t)\|_{\mathcal{F}}\right)\left(1 - e^{-t}\right), \tag{3.24}$$

We can rewrite (3.24) as:

$$\|V(t)\|_{\mathcal{F}} \leq e^{-t}\left(\|V_0\|_{\mathcal{F}} - \frac{\rho}{2}\right) + \frac{\rho}{2}. \tag{3.25}$$

Let us now show that the open ball B_ρ centered at 0 with radius ρ in $\mathcal{F}$ is stable under the dynamics of (3.20). If $V_0 \in B_\rho$, this implies $\|V(t)\|_{\mathcal{F}} \leq \frac{\rho}{2}\left(1 + e^{-t}\right)$ for all

$t > 0$ and hence $\|V(t)\|_{\mathcal{F}} < \rho$ for all $t > 0$, proving that B_ρ is stable. Consider the case where $V_0 \in \complement B_\rho$. Now assume that $\|V(t)\|_{\mathcal{F}} > \rho$ for all $t \geq 0$. The inequality (3.25) shows that for t large enough this yields a contradiction. Therefore there exists $t_0 > 0$ such that $\|V(t_0)\|_{\mathcal{F}} = \rho$. At this time instant we have

$$\rho \leq e^{-t_0}\left(\|V_0\|_{\mathcal{F}} - \frac{\rho}{2}\right) + \frac{\rho}{2},$$

and hence

$$t_0 \leq \log\left(\frac{2\|V_0\|_{\mathcal{F}} - \rho}{\rho}\right).$$

□

3.3.2 Stationary solutions

We end this chapter with the study of the stationary solutions of equation (3.20). We suppose that $\mathcal{W}$ satisfies hypothesis 3.3.1 and the external input I_{ext} is independent of time. For convenience, we redefine the sigmoidal function to be of the form:

$$S(x) = \frac{1}{1 + e^{-x+\kappa}},$$

with κ a fixed threshold. We assume that the stationary states V_μ^0 of equation (3.20) depend upon μ the slope of the sigmoidal function in the following way

$$0 = -V_\mu^0(\Delta, z) + \int_{\mathbb{R}_*^+ \times \mathbb{D}} \mathcal{W}\left(\log\left(\frac{\Delta}{\Delta'}\right), d_{\mathbb{D}}(z, z')\right) S(\mu V_\mu^0(\Delta', z')) \frac{d\Delta'}{\Delta'} \mathrm{dm}(z') + I_{ext}(\Delta, z). \tag{3.26}$$

We define the nonlinear operator from $\mathcal{F}$ to $\mathcal{F}$, noted $\mathcal{G}_\mu$, to be the right-hand side of equation (3.26):

$$\mathcal{G}_\mu(V)(\Delta, z) = \int_{\mathbb{R}_*^+ \times \mathbb{D}} \mathcal{W}\left(\log\left(\frac{\Delta}{\Delta'}\right), d_{\mathbb{D}}(z, z')\right) S(\mu V(\Delta', z')) \frac{d\Delta'}{\Delta'} \mathrm{dm}(z'). \tag{3.27}$$

We recall that we have set for the Banach space $\mathcal{F} = L^\infty(\mathbb{R}_*^+ \times \mathbb{D})$ and proposition 3.3.1 shows that $\mathcal{G}_\mu : \mathcal{F} \to \mathcal{F}$. We have the further properties:

Proposition 3.3.3. *If we denote $S'_m = \sup_{x \in \mathbb{R}} S'(x)$, then $\mathcal{G}_\mu$ satisfies the following properties:*

- $\|\mathcal{G}_\mu(V_1) - \mathcal{G}_\mu(V_2)\|_{\mathcal{F}} \leq \mu \mathcal{W}_0 S'_m \|V_1 - V_2\|_{\mathcal{F}}$ *for all* $\mu \geq 0$,
- $\mu \to \mathcal{G}_\mu$ *is continuous on* $\mathbb{R}^+$,
- *for all* $\mu \geq 0$ *the nonlinear operator* $\mathcal{G}_\mu$ *is not compact.*

Proof. See [Faye 2011b]. □

Let $\mathcal{B}_\mu$ the set of the solutions of (3.26) for a given slope parameter μ:

$$\mathcal{B}_\mu = \{V \in \mathcal{F} | -V + \mathcal{G}_\mu(V) + I_{ext} = 0\}.$$

We have the following proposition.

Proposition 3.3.4. *If the input current I_{ext} is equal to a constant I^0_{ext}, i.e. does not depend upon the variables (Δ, z) then for all $\mu \in \mathbb{R}^+$, $\mathcal{B}_\mu \neq \emptyset$. In the general case $I_{ext} \in \mathcal{F}$, if the condition $\mu S'_m \mathcal{W}_0 < 1$ is satisfied, then $Card(\mathcal{B}_\mu) = 1$.*

Proof. Due to the properties of the sigmoid function, there always exists a constant solution in the case where I_{ext} is constant. In the general case where $I_{\text{ext}} \in \mathcal{F}$, the statement is a direct application of the Banach fixed point theorem, as in [Faugeras 2009b]. □

Remark 3.3.2. *If the external input does not depend upon the variables (Δ, z) and if the condition $\mu S'_m \mathcal{W}_0 < 1$ is satisfied, then there exists a unique stationary solution by application of proposition 3.3.4. Moreover, this stationary solution does not depend upon the variables (Δ, z) because there always exists one constant stationary solution when the external input does not depend upon the variables (Δ, z). Indeed equation (3.26) is then equivalent to:*

$$0 = -V^0 + \beta S(V^0)$$

where,

$$\beta = \int_{\mathbb{R}^+_* \times \mathbb{D}} \mathcal{W}\left(\log\left(\frac{\Delta}{\Delta'}\right), d_{\mathbb{D}}(z, z')\right) \frac{d\Delta'}{\Delta'} dm(z')$$

and β does not depend upon the variables (Δ, z). Because of the shape of the sigmoid function S equation $0 = -V^0 + \beta S(V^0)$ has always one solution.

If on the other hand the input current does depend upon these variables, is invariant under the action of a subgroup of $\boldsymbol{U}(1,1)$, the group of the isometries of $\mathbb{D}$ (see 3.2.3), and the condition $\mu S'_m \mathcal{W}_0 < 1$ is satisfied, then the unique stationary solution will also be invariant under the action of the same subgroup.

When the condition $\mu S'_m \mathcal{W}_0 < 1$ is satisfied we call trivial solution the unique homogeneous solution in $\mathcal{B}_\mu$.

We can now show that the condition $\mu S'_m \mathcal{W}_0 < 1$ guarantees the stability of the trivial solution to (3.4).

Theorem 3.3.2. *We suppose that $I_{ext} \in \mathcal{F}$ and that the condition $\mu S'_m \mathcal{W}_0 < 1$ is satisfied, then the associated trivial solution of (3.4) is asymptotically stable.*

Proof. Let V^0_μ be the primary stationary solution of (3.4), as $\mu S'_m \mathcal{W}_0 < 1$ is satisfied. Let also V_μ be the unique solution of the same equation with some initial condition $V_\mu(0) = \phi \in \mathcal{F}$. We introduce a new function $X = V_\mu - V^0_\mu$ which satisfies:

$$\left(\frac{d}{dt} + 1\right) X(\Delta, z, t) = \int_{\mathbb{R}^+_* \times \mathbb{D}} \mathcal{W}_m\left(\log\left(\frac{\Delta}{\Delta'}\right), d_{\mathbb{D}}(z, z')\right) \Theta(X(\Delta', z', t)) \frac{d\Delta'}{\Delta'} \mathrm{dm}(z')$$
$$\stackrel{def}{=} F_\Theta(X(\Delta, z, t)) \tag{3.28}$$

with initial condition $X(\Delta, z, 0) = \phi(\Delta, z) - V_\mu^0(\Delta, z)$. $\mathcal{W}_m$ is defined as

$$\mathcal{W}_m\left(\log\left(\frac{\Delta}{\Delta'}\right), d_{\mathbb{D}}(z, z')\right) = S'_m \mathcal{W}\left(\log\left(\frac{\Delta}{\Delta'}\right), d_{\mathbb{D}}(z, z')\right)$$

and the vector $\Theta(X(\Delta, z, t))$ is given by $\Theta(X(\Delta, z, t)) = \underline{S}(\mu V_\mu(\Delta, z, t)) - \underline{S}(\mu V_\mu^0(\Delta, z))$ with $\underline{S} = (S'_m)^{-1} S$. We note that, because of the definition of Θ and the mean value theorem $|\Theta(X(\Delta, z, t))| \leq \mu |X(\Delta, z, t)|$. This implies that $|\Theta(r)| \leq |r|$ for all $r \in \mathbb{R}$. We integrate over time equation (3.28) which gives

$$X(\Delta, z, t) = e^{-t} X(\Delta, z, 0) + \int_0^t e^{-(t-u)} F_\Theta(X(\Delta, z, u)) du.$$

We then obtain the following estimate

$$\Rightarrow \|X(t)\|_\infty \leq e^{-t} \|X(0)\|_\infty + \mu \mathcal{W}_0 S'_m \int_0^t e^{-(t-u)} \|X(u)\|_\infty du$$

If we set: $G(t) = e^t \|X(t)\|_\infty$, then we have:

$$G(t) \leq G(0) + \mu \mathcal{W}_0 S'_m \int_0^t G(u) du$$

and G is continuous for all $t \geq 0$. The Gronwall inequality implies that:

$$G(t) \leq G(0) e^{\mu \mathcal{W}_0 S'_m t}$$

$$\Rightarrow \|X(t)\|_\infty \leq e^{(\mu \mathcal{W}_0 S'_m - 1)t} \|X(0)\|_\infty,$$

and the conclusion follows.

□

3.4 Conclusion

In this chapter, we have introduced the structure tensor formalism developed by Chossat and Faugeras in [Chossat 2009] and derived the neural field equations set on the space of structure tensors $\mathbf{SPD}(2, \mathbb{R})$. We also presented the Riemannian structure of this space together with its relation to the Poincaré disk model. We gave arguments for a possible evidence of neurons selective to structure tensors in the visual cortical area V1. We ended this chapter by providing theoretical results of existence and uniqueness of a solution of the neural field equation (3.4) together with some properties of the stationary solutions.

Part II

Symmetry breaking mechanism in some neural field equations

Chapter 4

Introduction to bifurcation theory in infinite dimensional system

Contents

4.1 Elementary bifurcation 50
4.1.1 Saddle-node bifurcation 50
4.1.2 Pitchfork bifurcation 51
4.1.3 Transcritical bifurcation 52
4.2 Center manifold and normal form 52
4.2.1 Notations and definitions 52
4.2.2 Local center manifold 53
4.2.3 Parameter-dependent center manifold 55
4.2.4 Empty unstable spectrum 56
4.2.5 Normal forms 57
4.3 Equivariant bifurcation 58
4.3.1 Definitions 58
4.3.2 Equivariant center manifold 58
4.3.3 Equivariant Branching Lemma 59

The aim of this chapter is to introduce tools from bifurcation theory which are necessary for the study of neural field equations set in the primary visual cortex. In a first step, we deal with elementary bifurcations in low dimensions such as saddle-node, transcritical, pitchfork and Hopf bifurcations. Neural field equations are dynamical systems defined on Banach spaces and thus are infinite dimensional. Bifurcation analysis for infinite dimensional systems is subtle and can lead to difficult problems. Whenever it is possible, the idea is to locally reduce the problem to a finite dimensional one. This reduction is called the center manifold theory and it will be the main theoretical result of this chapter. We also present some extensions of the center manifold theorem for parameter-dependent and equivariant differential equations. Directly related to the center manifold theory is the normal form theory which is a canonical way to write differential equations. We conclude this chapter with an overview of bifurcations with symmetry and give as a result the Equivariant Branching Lemma. Most of the theorems of this chapter are taken from the book of

Haragus-Iooss [Haragus 2010] (center manifolds and normal forms). The last part on the Equivariant Branching Lemma is taken from the book of Chossat-Lauterbach [Chossat 2000].

4.1 Elementary bifurcation

Definition 4.1.1. *In dynamical systems, a bifurcation occurs when a small smooth change made to the parameter values (the bifurcation parameters) of a system causes a sudden "qualitative" or topological change in its behaviour. Generally, at a bifurcation, the local stability properties of equilibria, periodic orbits or other invariant sets changes.*

In this section, we consider scalar differential equations of the form

$$\frac{du}{dt} = f(u, \mu). \tag{4.1}$$

Here the unknown u is a real-valued function of the time t, and the vector field f is real-valued depending, besides u, upon a parameter μ. The parameter μ is the bifurcation parameter. We suppose that equation (4.1) is well-defined and satisfies the hypotheses of the Cauchy-Lipschitz theorem, such that for each initial condition there exists a unique solution of equation (4.1). Furthermore we assume that the vector field is of class $\mathcal{C}^k$, $k \geq 2$, in a neighborhood of $(0, 0)$ satisfying:

$$f(0, 0) = 0, \quad \frac{\partial f}{\partial u}(0, 0) = 0. \tag{4.2}$$

The first condition shows that $u = 0$ is an equilibrium of equation (4.1) at $\mu = 0$. We are interested in local bifurcations that occur in the neighborhood of this equilibrium when we vary the parameter μ. The second condition is a necessary, but not sufficient, condition for the appearance of local bifurcations at $\mu = 0$.

Remark 4.1.1. *Suppose that the second condition is not satified: $\partial f/\partial u(0, 0) \neq 0$. A direct application of the implicit function theorem shows that the equation $f(u, \mu) = 0$ possesses a unique solution $u = u(\mu)$ in a neighborhood of 0, for small enough μ. In particular $u = 0$ is the only equilibrium of equation (4.1) in a neighborhood of 0 when $\mu = 0$, and the same property holds for μ small enough. Furthermore, the dynamics of (4.1) in a neighborhood of 0 is qualitatively the same for all sufficiently small values of the parameter μ: no bifurcation occurs for small values of μ.*

4.1.1 Saddle-node bifurcation

Theorem 4.1.1 (Saddle-node bifurcation). *Assume that the vector field f is of class $\mathcal{C}^k$, $k \geq 2$, in a neighborhood of $(0, 0)$ and satisfies:*

$$\frac{\partial f}{\partial \mu}(0, 0) =: a \neq 0, \quad \frac{\partial^2 f}{\partial u^2}(0, 0) =: 2b \neq 0. \tag{4.3}$$

The following properties hold in neighborhood of 0 in $\mathbb{R}$ for small enough μ:

(i) if $ab < 0$ (resp. $ab > 0$) the differential equation has no equilibria for $\mu < 0$ (resp. for $\mu > 0$),

(ii) if $ab < 0$ (resp. $ab > 0$) the differential equation possesses two equilibria $u_\pm(\varepsilon)$, $\varepsilon = \sqrt{|\mu|}$ for $\mu > 0$ (resp. $\mu < 0$), with opposite stabilities. Furthermore, the map $\varepsilon \to u_\pm(\varepsilon)$ is of class $\mathcal{C}^{k-2}$ in a neighborhood of 0 in $\mathbb{R}$, and $u_\pm(\varepsilon) = O(\varepsilon)$.

Then for equation (4.1), a saddle-node bifurcation occurs at $\mu = 0$.

A direct consequence of conditions (4.3) is that f has the expansion:

$$f(u, \mu) = a\mu + bu^2 + o(|\mu| + u^2) \text{ as } (u, \mu) \to (0, 0).$$

The following bifurcation is an example where we impose some conditions on the vector field f such that the condition (4.3) is no longer satisfied.

4.1.2 Pitchfork bifurcation

Theorem 4.1.2 (Pitchfork bifurcation). *Assume that the vector field f is of class $\mathcal{C}^k$, $k \geq 3$, in a neighborhood of $(0, 0)$, that it is satisfies conditions (4.2), and that it is odd with respect to u:*

$$f(-u, \mu) = -f(u, \mu) \tag{4.4}$$

Furthermore assume that:

$$\frac{\partial^2 f}{\partial \mu \partial u}(0, 0) =: a \neq 0, \quad \frac{\partial^3 f}{\partial u^3}(0, 0) =: 6b \neq 0. \tag{4.5}$$

The following properties hold in neighborhood of 0 in $\mathbb{R}$ for small enough μ:

(i) if $ab < 0$ (resp. $ab > 0$) the differential equation has one trivial equilibrium $u = 0$ for $\mu < 0$ (resp. for $\mu > 0$). This equilibrium is stable when $b < 0$ and unstable when $b > 0$.

(ii) if $ab < 0$ (resp. $ab > 0$) the differential equation possesses the trivial equilibrium $u = 0$ and two nontrivial equilibria $u_\pm(\varepsilon)$, $\varepsilon = \sqrt{|\mu|}$ for $\mu > 0$ (resp. $\mu < 0$), which are symmetric, $u_+(\varepsilon) = -u_-(\varepsilon)$. The map $\varepsilon \to u_\pm(\varepsilon)$ is of class $\mathcal{C}^{k-3}$ in a neighborhood of 0 in $\mathbb{R}$, and $u_\pm(\varepsilon) = O(\varepsilon)$. The nontrivial equilibria are stable when $b < 0$ and unstable when $b > 0$, whereas the trivial equilibrium has opposite stability.

Then for equation (4.1), a pitchfork bifurcation occurs at $\mu = 0$.

A direct consequence of conditions (4.2), (4.4) and (4.5) is that f has the Taylor expansion:

$$f(u, \mu) = uh(u^2, \mu) \quad h(u^2, \mu) = a\mu + bu^2 + o(|\mu| + u^2) \text{ as } (u, \mu) \to (0, 0)$$

where h is of class $\mathcal{C}^{(k-1)/2}$ in a neighborhood of $(0, 0)$.

4.1.3 Transcritical bifurcation

Theorem 4.1.3 (Transcritical bifurcation). *Assume that the vector field f is of class $\mathcal{C}^k$, $k \geq 2$, in a neighborhood of $(0,0)$, that it is satisfies conditions (4.2), and also:*

$$\frac{\partial^2 f}{\partial \mu \partial u}(0,0) =: a \neq 0, \quad \frac{\partial^2 f}{\partial u^2}(0,0) =: 2b \neq 0. \tag{4.6}$$

The following properties hold in neighborhood of 0 in $\mathbb{R}$ for small enough μ:

(i) the differential equation possesses the trivial equilibrium $u = 0$ and the nontrivial equilibrium $u_0(\mu)$ where the map $\mu \to u_0(\mu)$ is of class $\mathcal{C}^{k-2}$ in a neighborhood of 0 in $\mathbb{R}$, and $u_0(\mu) = O(\mu)$.

(ii) if $a\mu < 0$ (resp. $a\mu > 0$) the trivial equilibrium $u = 0$ is stable (resp. unstable) whereas the nontrivial equilibrium $u_0(\mu)$ is unstable (resp. stable).

Then for equation (4.1), a transcritical bifurcation occurs at $\mu = 0$.

A direct consequence of conditions (4.2) and (4.6) is that f has the Taylor expansion:

$$f(u,\mu) = a\mu u + bu^2 + o(u|\mu| + u^2) \text{ as } (u,\mu) \to (0,0)$$

Remark 4.1.2. *In chapter 6, we will see the case of a transcritical bifurcation with triangular $\mathbf{D}_3$ symmetry in the plane (see figure 6.5 for the associated bifurcation diagram) where the solution $u_0(\mu)$ is unstable on both sides of the bifurcation point unless the subcritical branch bends back sufficiently near the bifurcation point.*

4.2 Center manifold and normal form

Center manifolds are fundamental for the study of dynamical systems near critical situations and in particular in bifurcation theory. Starting with an infinite-dimensional problem, the center manifold theorem will reduce the study of small solutions, staying sufficiently close to 0, to that of small solutions of a reduced system with finite dimension. The solutions on the center manifold are described by a finite-dimensional system of ordinary differential equations, also called the reduced system.

4.2.1 Notations and definitions

Consider two (complex or real) Banach spaces $\mathcal{X}$ and $\mathcal{Y}$. We shall use the following notations:

- $\mathcal{C}^k(\mathcal{Y}, \mathcal{X})$ is the Banach space of k-times continuously differentiable functions $F : \mathcal{Y} \to \mathcal{X}$ equiped with the norm on all derivatives up to order k,

$$\|F\|_{\mathcal{C}^k} = \max_{j=0,\dots,k} \left(\sup_{y \in \mathcal{Y}} \left(\|D^j F(y)\|_{\mathcal{L}(\mathcal{Y}^j, \mathcal{X})} \right) \right)$$

- $\mathcal{L}(\mathcal{Y}, \mathcal{X})$ is the Banach space of linear bounded operators $\mathbf{L} : \mathcal{Y} \to \mathcal{X}$, equiped with operator norm:

$$\|\mathbf{L}\|_{\mathcal{L}(\mathcal{Y},\mathcal{X})} = \sup_{\|u\|_{\mathcal{Y}}=1} (\|\mathbf{L}u\|_{\mathcal{X}})$$

  if $\mathcal{Y} = \mathcal{X}$, we write $\mathcal{L}(\mathcal{Y}) = \mathcal{L}(\mathcal{Y}, \mathcal{X})$.

- For a linear operator $\mathbf{L} : \mathcal{Y} \to \mathcal{X}$, we denote its range by im$\mathbf{L}$:

$$\text{im}\mathbf{L} = \{\mathbf{L}u \in \mathcal{X} \mid u \in \mathcal{Y}\} \subset \mathcal{X}$$

  and its kernel by ker$\mathbf{L}$:

$$\text{ker}\mathbf{L} = \{u \in \mathcal{Y} \mid \mathbf{L}u = 0\} \subset \mathcal{Y}$$

- Assume that $\mathcal{Y} \hookrightarrow \mathcal{X}$ with continuous embedding. For a linear operator $\mathbf{L} \in \mathcal{L}(\mathcal{Y}, \mathcal{X})$, we denote by $\rho(\mathbf{L})$, or simply ρ, the resolvent set of $\mathbf{L}$:

$$\rho = \{\lambda \in \mathbb{C} \mid \lambda Id - \mathbf{L} : \mathcal{Y} \to \mathcal{X} \text{ is bijective } \}.$$

  The complement of the resolvent set is the spectrum $\sigma(\mathbf{L})$, or simply σ,

$$\sigma = \mathbb{C} \setminus \{\rho\}.$$

Remark 4.2.1. *When $\mathbf{L}$ is real, both the resolvent set and the spectrum of $\mathbf{L}$ are symmetric with respect to the real axis in the complex plane.*

4.2.2 Local center manifold

Let $\mathcal{X}, \mathcal{Y}$ and $\mathcal{Z}$ be Banach spaces such that:

$$\mathcal{Z} \hookrightarrow \mathcal{Y} \hookrightarrow \mathcal{X}$$

with continuous embeddings. We consider a differential equation in $\mathcal{X}$ of the form:

$$\frac{du}{dt} = \mathbf{L}u + \mathbf{R}(u) \tag{4.7}$$

in which we assume that the linear part $\mathbf{L}$ and the nonlinear part $\mathbf{R}$ are such that the following holds.

Hypothesis 4.2.1 (Regularity). *We assume that $\mathbf{L}$ and $\mathbf{R}$ in (4.7) have the following properties:*

(i) $\mathbf{L} \in \mathcal{L}(\mathcal{Z}, \mathcal{X})$,

(ii) for some $k \geq 2$, there exists a neighborhood $\mathcal{V} \subset \mathcal{Z}$ of 0 such that $\mathbf{R} \in \mathcal{C}^k(\mathcal{V}, \mathcal{Y})$ and

$$\mathbf{R}(0) = 0, \quad D\mathbf{R}(0) = 0.$$

Hypothesis 4.2.2 (Spectral decomposition). *Consider the spectrum σ of the linear operator $\mathbf{L}$, and write:*

$$\sigma = \sigma_+ \cup \sigma_0 \cup \sigma_-$$

in which

$$\sigma_+ = \{\lambda \in \sigma \mid Re\lambda > 0\}, \quad \sigma_0 = \{\lambda \in \sigma \mid Re\lambda = 0\}, \quad \sigma_- = \{\lambda \in \sigma \mid Re\lambda < 0\}$$

We assume that:

(i) there exists a positive constant γ such that

$$\inf_{\lambda \in \sigma_+} (Re\lambda) > \gamma, \quad \sup_{\lambda \in \sigma_-} (Re\lambda) < -\gamma$$

(ii) the set σ_0 consists of a finite number of eigenvalues with finite algebraic multiplicities.

Hypothesis 4.2.3 (Resolvent estimates). *Assume that there exist positive constants $\omega_0 > 0$, $c > 0$ and $\alpha \in [0, 1)$ such that for all $\omega \in \mathbb{R}$ with $|\omega| \geq \omega_0$, we have that $i\omega$ belongs to the resolvent set of $\mathbf{L}$ and*

$$\begin{aligned} \|(i\omega Id - \mathbf{L})^{-1}\|_{\mathcal{L}(\mathcal{X})} &\leq \frac{c}{|\omega|} \\ \|(i\omega Id - \mathbf{L})^{-1}\|_{\mathcal{L}(\mathcal{Y},\mathcal{Z})} &\leq \frac{c}{|\omega|^{1-\alpha}} \end{aligned}$$

As a consequence of hypothesis 4.2.2 (ii), we can define the spectral projection $\mathcal{P}_0 \in \mathcal{L}(\mathcal{X})$, corresponding to σ_0, by the Dunford formula:

$$\mathcal{P}_0 = \frac{1}{2\pi i} \int_\Gamma (\lambda Id - \mathbf{L})^{-1} d\lambda \tag{4.8}$$

where Γ is a simple, oriented counterclockwise, Jordan curve surrounding σ_0 and lying entirely in $\{\lambda \in \mathbb{C} \mid |\mathrm{Re}\lambda| < \gamma\}$. Then

$$\mathcal{P}_0^2 = \mathcal{P}_0, \quad \mathcal{P}_0 \mathbf{L} u = \mathbf{L} \mathcal{P}_0 u \quad \forall u \in \mathcal{Z},$$

and $\mathrm{im}\mathcal{P}_0$ is finite-dimensional (σ_0 consists of a finite number of eigenvalues with finite algebraic multiplicities). In Particular, it satisfies $\mathrm{im}\mathcal{P}_0 \subset \mathcal{Z}$ and $\mathcal{P}_0 \in \mathcal{L}(\mathcal{X}, \mathcal{Z})$. We define a second projector $\mathcal{P}_h : \mathcal{X} \to \mathcal{X}$ by

$$\mathcal{P}_h = Id - \mathcal{P}_0$$

which also satisfies

$$\mathcal{P}_h^2 = \mathcal{P}_h, \quad \mathcal{P}_h \mathbf{L} u = \mathbf{L} \mathcal{P}_h u \quad \forall u \in \mathcal{Z},$$

and

$$\mathcal{P}_h \in \mathcal{L}(\mathcal{X}) \cap \mathcal{L}(\mathcal{Y}) \cap \mathcal{L}(\mathcal{Z}).$$

We consider the spectral subspaces associated with these two projections:

$$\mathcal{E}_0 = \mathrm{im}\mathcal{P}_0 = \ker \mathcal{P}_h \subset \mathcal{Z}, \quad \mathcal{X}_h = \mathrm{im}\mathcal{P}_h = \ker \mathcal{P}_0 \subset \mathcal{X}$$

which provides the decomposition:

$$\mathcal{X} = \mathcal{X}_h \oplus \mathcal{E}_0.$$

We also denote

$$\mathcal{Z}_h = \mathcal{P}_h\mathcal{Z} \subset \mathcal{Z}, \quad \mathcal{Y}_h = \mathcal{P}_h\mathcal{Y} \subset \mathcal{Y}$$

and denote by $\mathbf{L}_0 \in \mathcal{L}(\mathcal{E}_0)$ and $\mathbf{L}_h \in \mathcal{L}(\mathcal{Z}_h, \mathcal{X}_h)$ the restrictions of $\mathbf{L}$ to $\mathcal{E}_0$ and $\mathcal{Z}_h$. The spectrum of $\mathbf{L}_0$ is σ_0 and the spectrum of $\mathbf{L}_h$ is $\sigma_+ \cup \sigma_-$.

Theorem 4.2.1 (Center manifold theorem). *Assume that hypotheses 4.2.1, 4.2.2 and 4.2.3 hold. Then there exists a map $\Psi \in \mathcal{C}^k(\mathcal{E}_0, \mathcal{Z}_h)$, with*

$$\Psi(0) = 0, \quad D\Psi(0) = 0,$$

and a neighborhood $\mathcal{O}$ of 0 in $\mathcal{Z}$ such that the manifold:

$$\mathcal{M}_0 = \{u_0 + \Psi(u_0) \mid u_0 \in \mathcal{E}_0\} \subset \mathcal{Z}$$

has the following properties:

(i) $\mathcal{M}_0$ is locally invariant: if u is a solution of equation (4.7) satisfying $u(0) \in \mathcal{M}_0 \cap \mathcal{O}$ and $u(t) \in \mathcal{O}$ for all $t \in [0, T]$, then $u(t) \in \mathcal{M}_0$ for all $t \in [0, T]$.

(ii) $\mathcal{M}_0$ contains the set of bounded solutions of (4.7) staying in $\mathcal{O}$ for all $t \in \mathbb{R}$.

The manifold $\mathcal{M}_0$ is called a local center manifold of (4.7) and the map Ψ is referred to as the reduction function.

Let u be a solution of (4.7) which belongs to $\mathcal{M}_0$, then $u = u_0 + \Psi(u_0)$ and u_0 satisfies:

$$\frac{du_0}{dt} = \mathbf{L}_0 u_0 + \mathcal{P}_0\mathbf{R}(u_0 + \Psi(u_0)) \tag{4.9}$$

The reduction function Ψ satisfies:

$$D\Psi(u_0)(\mathbf{L}_0 u_0 + \mathcal{P}_0\mathbf{R}(u_0 + \Psi(u_0))) = \mathbf{L}_h\Psi(u_0) + \mathcal{P}_h\mathbf{R}(u_0 + \Psi(u_0)) \quad \forall u_0 \in \mathcal{E}_0$$

4.2.3 Parameter-dependent center manifold

We consider a parameter-dependent differential equation in $\mathcal{X}$ of the form

$$\frac{du}{dt} = \mathbf{L}u + \mathbf{R}(u, \mu) \tag{4.10}$$

where $\mathbf{L}$ is a linear operator as in the previous section, and the nonlinear part $\mathbf{R}$ is defined for (u, μ) in a neighborhood of $(0, 0) \in \mathcal{Z} \times \mathbb{R}^m$. Here $\mu \in \mathbb{R}^m$ is a parameter that we assume to be small. More precisely we keep hypotheses 4.2.2 and 4.2.3 and replace hypothesis 4.2.1 by the following:

Hypothesis 4.2.4 (Regularity). *We assume that $\mathbf{L}$ and $\mathbf{R}$ in (4.10) have the following properties:*

(i) $\mathbf{L} \in \mathcal{L}(\mathcal{Z}, \mathcal{X})$,

(ii) *for some* $k \geq 2$, *there exists a neighborhood* $\mathcal{V}_u \subset \mathcal{Z}$ *and* $\mathcal{V}_\mu \subset \mathbb{R}^m$ *of* 0 *such that* $\mathbf{R} \in \mathcal{C}^k(\mathcal{V}_u \times \mathcal{V}_\mu, \mathcal{Y})$ *and*

$$\mathbf{R}(0,0) = 0, \quad D_u\mathbf{R}(0,0) = 0.$$

Theorem 4.2.2 (Parameter-dependent center manifold theorem). *Assume that hypotheses 4.2.4, 4.2.2 and 4.2.3 hold. Then there exists a map* $\Psi \in \mathcal{C}^k(\mathcal{E}_0 \times \mathbb{R}^m, \mathcal{Z}_h)$, *with*

$$\Psi(0,0) = 0, \quad D_u\Psi(0,0) = 0,$$

and a neighborhood $\mathcal{O}_u \times \mathcal{O}_\mu$ *of* 0 *in* $\mathcal{Z} \times \mathbb{R}^m$ *such that for* $\mu \in \mathcal{O}_\mu$ *the manifold:*

$$\mathcal{M}_0(\mu) = \{u_0 + \Psi(u_0, \mu) \mid u_0 \in \mathcal{E}_0\} \subset \mathcal{Z}$$

has the following properties:

(i) $\mathcal{M}_0(\mu)$ *is locally invariant: if* u *is a solution of equation (4.10) satisfying* $u(0) \in \mathcal{M}_0(\mu) \cap \mathcal{O}_u$ *and* $u(t) \in \mathcal{O}_u$ *for all* $t \in [0,T]$, *then* $u(t) \in \mathcal{M}_0(\mu)$ *for all* $t \in [0,T]$.

(ii) $\mathcal{M}_0(\mu)$ *contains the set of bounded solutions of (4.10) staying in* $\mathcal{O}_u$ *for all* $t \in \mathbb{R}$.

Let u *be a solution of (4.10) which belongs to* $\mathcal{M}_0(\mu)$, *then* $u = u_0 + \Psi(u_0, \mu)$ *and* u_0 *satisfies:*

$$\frac{du_0}{dt} = \mathbf{L}_0 u_0 + \mathcal{P}_0\mathbf{R}(u_0 + \Psi(u_0,\mu), \mu) \stackrel{def}{=} f(u_0, \mu) \tag{4.11}$$

where we observe that $f(0,0) = 0$ *and* $D_{u_0}f(0,0) = \mathbf{L}_0$ *has spectrum* σ_0. *The reduction function* Ψ *satiafies:*

$$D_{u_0}\Psi(u_0,\mu)f(u_0,\mu) = \mathbf{L}_h\Psi(u_0,\mu) + \mathcal{P}_h\mathbf{R}(u_0 + \Psi(u_0,\mu),\mu) \quad \forall u_0 \in \mathcal{E}_0$$

4.2.4 Empty unstable spectrum

Theorem 4.2.3 (Center manifold for empty unstable spectrum). *Under the assumptions of theorem 4.2.1 and assume that* $\sigma_+ = \varnothing$. *Then in addition to properties of theorem 4.2.1, the local center manifold* $\mathcal{M}_0$ *is locally attracting: any solution of equation (4.7) that stays in* $\mathcal{O}$ *for all* $t > 0$ *tends exponentially towards a solution of (4.7) on* $\mathcal{M}_0$.

4.2.5 Normal forms

The normal forms theory aims at finding a polynomial change of variable which improves near a singularity a nonlinear system, in order to recognize more easily its dynamics.

We consider a parameter-dependent differential equations in $\mathbb{R}^n$ of the form

$$\frac{du}{dt} = \mathbf{L}u + \mathbf{R}(u, \mu) \tag{4.12}$$

in which we assume that $\mathbf{L}$ and $\mathbf{R}$ satisfy the following hypothesis.

Hypothesis 4.2.5 (Regularity). *Assume that* $\mathbf{L}$ *and* $\mathbf{R}$ *have the following properties:*

(i) $\mathbf{L}$ *is a linear map in* $\mathbb{R}^n$*;*

(ii) for some $k \geq 2$*, there exist neighborhoods* $\mathcal{V}_u \subset \mathbb{R}^n$ *and* $\mathcal{V}_\mu \subset \mathbb{R}^m$ *of* 0 *such that* $\mathbf{R} \in \mathcal{C}^k(\mathcal{V}_u \times \mathcal{V}_\mu, \mathbb{R}^n)$ *and*

$$\mathbf{R}(0,0) = 0, \quad D_u\mathbf{R}(0,0) = 0.$$

Theorem 4.2.4 (Normal form theorem). *Assume that hypothesis 4.2.5 holds. Then for any positive integer* p*,* $2 \leq p \leq k$*, there exist neighborhoods* $\mathcal{V}_1$ *and* $\mathcal{V}_2$ *of* 0 *in* $\mathbb{R}^n$ *and* $\mathbb{R}^m$ *such that for* $\mu \in \mathcal{V}_2$*, there is a polynomial map* $\Phi_\mu : \mathbb{R}^n \to \mathbb{R}^n$ *of degree* p *with the following properties:*

(i) the coefficients of the monomials of degree q *in* Φ_μ *are functions of* μ *of class* $\mathcal{C}^{k-q}$ *and*

$$\Phi_0(0) = 0, \quad D_u\Phi_0(0) = 0$$

(ii) for $v \in \mathcal{V}_1$*, the polynomial change of variable*

$$u = v + \Phi_\mu(v)$$

transforms equation (4.12) into the normal form:

$$\frac{dv}{dt} = \mathbf{L}v + \mathbf{N}_\mu(v) + \rho(v, \mu)$$

and the following properties hold:

(a) for any $\mu \in \mathcal{V}_2$*,* $\mathbf{N}_\mu$ *is a polynomial map* $\mathbb{R}^n \to \mathbb{R}^n$ *of degree* p*, with coefficients depending upon* μ*, such that the coefficients of the monomials of degree* q *are of class* $\mathcal{C}^{k-q}$ *and*

$$\mathbf{N}_0(0) = 0, \quad D_v\mathbf{N}_0(0) = 0$$

(b) the equality $\mathbf{N}_\mu(e^{t\mathbf{L}^*}v) = e^{t\mathbf{L}^*}\mathbf{N}_\mu(v)$ *holds for all* $(t, v) \in \mathbb{R} \times \mathbb{R}^n$ *and* $\mu \in \mathcal{V}_2$

(c) the map ρ *belongs to* $\mathcal{C}^k(\mathcal{V}_1 \times \mathcal{V}_2, \mathbb{R}^n)$ *and*

$$\rho(v, \mu) = o(\|v\|^p) \quad \forall \mu \in \mathcal{V}_2$$

4.3 Equivariant bifurcation

4.3.1 Definitions

Definition 4.3.1 (Representation). *A representation of a group G in a Banach space $\mathcal{X}$ is a continuous homomorphism $\tau : G \to GL(\mathcal{X})$ from G to the group of invertible linear maps in $\mathcal{X}$.*

Definition 4.3.2 (Irreducible representation). *A representation τ is irreducible if the only subspaces of $\mathcal{X}$ which are invariant by $\tau(g)$ for all $g \in G$ are $\{0\}$ and $\mathcal{X}$ itself.*

Definition 4.3.3 (Absolutely irreducible representation). *A representation τ of a compact group G in a (finite dimensional) space $\mathcal{X}$ is absolutely irreducible if all linear maps A which commute with τ are scalar multiple of the identity.*

Definition 4.3.4 (Equivariant map). *Let $\mathcal{X}$ and $\mathcal{Y}$ be two vector spaces with representations σ and τ of a group G. If $\mathcal{F} : \mathcal{X} \to \mathcal{Y}$ is a smooth operator (of class $\mathcal{C}^k$, $k \geq 2$), then $\mathcal{F}$ is G-equivariant if for every $g \in G$ and every $x \in \mathcal{X}$ we have*

$$\mathcal{F}(\sigma(g)x) = \tau(g)\mathcal{F}(x)$$

Definition 4.3.5.

(i) Let $x \in \mathcal{X}$, we define $H = G^x = \{g \in G \mid \tau(g)x = x\}$. H is the isotropy subgroup of x. Note that the isotropy subgroup of $\tau(g)x$ is gHg^{-1}, and when one talks about classification of isotropy subgroups (for a given action), it means "classification of conjugacy classes".

(ii) Given an isotropy subgroup H, let $Fix_H = \{x \in \mathcal{X} \mid \tau(h)x = x \text{ for all } h \in H\}$. This is a linear subspace of $\mathcal{X}$.

(iii) For $x \in \mathcal{X}$, the G-orbit of x is the set $G \cdot x = \{\tau(g)x, g \in G\}$: the image of x by the action of G.

Definition 4.3.6 (Normalizer). *Let $N(H)$ be the normalizer of H in G:*

$$N(H) = \{g \in G \mid gHg^{-1} = H\}.$$

4.3.2 Equivariant center manifold

Let $\mathcal{X}, \mathcal{Y}$ and $\mathcal{Z}$ be Banach spaces such that:

$$\mathcal{Z} \hookrightarrow \mathcal{Y} \hookrightarrow \mathcal{X}$$

with continuous embeddings. We consider a differential equation in $\mathcal{X}$ of the form:

$$\frac{du}{dt} = \mathbf{L}u + \mathbf{R}(u). \tag{4.13}$$

Hypothesis 4.3.1 (Equivariant equation). *We assume that there exists a linear operator* $\mathbf{T} \in \mathcal{L}(\mathcal{X}) \cap \mathcal{L}(\mathcal{Z})$*, which commutes with vector field in equation* (4.14)*:*

$$\mathbf{TL}u = \mathbf{LT}u, \quad \mathbf{TR}(u) = \mathbf{R}(\mathbf{T}u)$$

We also assume that the restriction $\mathbf{T}_0$ *of* $\mathbf{T}$ *to* $\mathcal{E}_0$ *is an isometry.*

Theorem 4.3.1 (Equivariant center manifold). *Under the assumption of theorem 4.2.1, we further assume that hypothesis 4.3.1 holds. Then one can find a reduction function* Ψ *which commutes with* $\mathbf{T}$*:*

$$\mathbf{T}\Psi u_0 = \Psi(\mathbf{T}_0 u_0), \quad \forall u_0 \in \mathcal{E}_0$$

and such that the vector field in the reduced equation (4.9) *commutes with* $\mathbf{T}_0$*.*

Remark 4.3.1. *Analogous results hold for the parameter-dependent equation* (4.10)*.*

4.3.3 Equivariant Branching Lemma

We consider a parameter-dependent differential equation in $\mathcal{X}$ of the form

$$\frac{du}{dt} = \mathbf{L}u + \mathbf{R}(u, \mu) = \mathcal{F}(u, \mu) \tag{4.14}$$

where $\mathbf{L}$ is a linear operator as in the previous section, and the nonlinear part $\mathbf{R}$ is defined for (u, μ) in a neighborhood of $(0, 0) \in \mathcal{Z} \times \mathbb{R}^m$. Here $\mu \in \mathbb{R}^m$ is a parameter that we assume to be small. We suppose that $\mathcal{F}$ is G-equivariant with respect to a representation τ of the group G. If we apply the parameter-dependent center manifold 4.3.1 theorem for equivariant differential equation (4.14), the reduced equation on $\mathcal{E}_0$ has the general form:

$$\frac{du_0}{dt} = \mathbf{L}_0 u_0 + \mathcal{P}_0 \mathbf{R}(u_0 + \Psi(u_0, \mu), \mu) \stackrel{def}{=} f(u_0, \mu)$$

with

$$\tau(g)\Psi(u_0, \mu) = \Psi(\tau(g)u_0, \mu), \quad \forall u_0 \in \mathcal{E}_0 \text{ and } \forall g \in G.$$

Since $\mathcal{E}_0$ is a real space of dimension n, we may regard f as a map $f : \mathbb{R}^n \times \mathbb{R}^m \to \mathbb{R}^n$. Moreover, G acts on $\mathbb{R}^n$ and f is equivariant for this action.

Suppose now that the action of G on $\mathbb{R}^n$ possesses an isotropy subgroup H with a one-dimensional fixed point space $\mathrm{Fix}(H)$. If we look for solutions in $\mathrm{Fix}(H)$, the reduced equation on the center manifold restricts to a scalar equation.

Hypothesis 4.3.2. *We suppose that* G *acts absolutely irreducibly on* $\mathcal{E}_0$*. As a consequence, the linearization of* f *at the origin is a multiple of the identity and we have* $D_u f(0, \mu) = c(\mu)Id$*.*

Theorem 4.3.2 (Steady-state Equivariant Branching Lemma).

We suppose that the assumptions of theorem 4.2.2 hold. Assume that the compact group G *acts linearly and that* $\mathcal{F}$ *is* G*-equivariant. We suppose that* G *acts absolutely irreducibly on* $\mathcal{E}_0$*. We also suppose that* $\mathbf{L}$ *has* 0 *as an isolated eigenvalue*

with finite multiplicity. If H is an isotropy subgroup of G with $\dim Fix(H) = 1$ *and if $c'(0) \neq 0$, then it exists a unique branch of solutions with symmetry H.*

Furthermore, for each isotropy subgroup H of G such that $\dim Fix(H) = 1$ *in $\mathcal{E}_0$, either one of the following situations occurs (where $f(u_0, \mu)$ is left hand side of equation (4.9) in $Fix(H)$):*

(i) $H = G$. *If $D_\mu f(0,0) \neq 0$, there exists one branch of solution $u(\mu)$. If in addition $D^2_{uu} f(0,0) \neq 0$, then $u^2 = O(\|\mu\|) \Rightarrow$ saddle-node bifurcation.*

(ii) $H < G$ *and the normalizer $N(H)$ acts trivially in $Fix(H)$. Then $f(u_0, \mu) = u_0 h(u_0, \mu)$ and if $D^2_{u\mu} f(0,0) \neq 0$ there exists a branch of solution $u(\mu)$. If in addition $D^2_{uu} f(0,0) \neq 0$, then $u = O(\|\mu\|) \Rightarrow$ transcritical bifurcation.*

(iii) $H < G$ *and the normalizer $N(H)/H$ acts as -1 in $Fix(H)$. Then $f(u_0, \mu) = u_0 h(u_0, \mu)$ with h an even function of u_0. If $D^2_{u\mu} f(0,0) \neq 0$ there exists a branch of solution $\pm u(\mu)$ such that if $D^3_{uuu} f(0,0) \neq 0$, then $u^2 = O(\|\mu\|) \Rightarrow$ pitchfork bifurcation.*

Remark 4.3.2.

- *If* $\dim Fix(H) = 1$, *then H is a maximal isotropy subgroup.*
- *When $H < G$, the bifurcating solutions in $Fix(H)$ have lower symmetry than the basic solution $u = 0$. This effect is called spontaneous symmetry breaking.*

Chapter 5

Pattern formation in the Euclidean case

Contents

5.1 Planforms on the Euclidean plane 63
5.1.1 Lattices and lattice patterns 63
5.1.2 Steady-state bifurcation on a lattice 64
5.2 Visual hallucination patterns of a square superlattice . . . 69
5.2.1 Simplified Ermentrout-Cowan model 69
5.2.2 Theoretical results 71
5.2.3 Network behaviour 73
5.3 Conclusion 75

The formation of steady patterns through Turing mechanism is a well-known phenomenon [Murray 2003, Hoyle 2006]. For example, it occurs when a homogeneous state of a system of reaction-diffusion equations defined on the Euclidean plane becomes neutrally stable when a bifurcation parameter reaches a critical value. For the analysis of this phenomenon, the assumption that the system is invariant under Euclidean transformations in the plane is essential. Any Fourier mode whose wave vector has critical length is a neutral stable mode and a consequence of the rotational symmetry of the system is that the kernel of the linearized problem at the bifurcation point is infinite dimensional. By looking at the class of $\mathcal{L}$-periodic states, $\mathcal{L}$ being a discrete translation subgroup of $\mathbb{R}^2$, or by looking at the system projected onto the torus $\mathbb{R}^2/\mathcal{L}$, one renders the spectrum of the linearized problem discrete: the critical wave vectors are finite in number, hence the critical eigenvalue has finite multiplicity and standard methods of equivariant bifurcation theory (see [Chossat 2000, Golubitsky 1988]) can be applied to compute bifurcated solutions within the class of $\mathcal{L}$-periodic states. Such solutions are called *planforms*.

The striking example of Turing mechanism in neuroscience is the Ermentrout and Cowan model [Ermentrout 1979] of visual hallucination patterns. Visual hallucinations can occur in a wide variety of situations such as with binocular deep pressure (see figure 5.1), migraine headaches, epilepsy or as the result of external stimulus by drugs such as LSD [Klüver 1966, Oster 1970, Tyler 1978]. Ermentrout and Cowan idealized the primary visual cortex to the Euclidean plane and analyzed neuronal activity in the neighborhood of an instability. Their equations, set on the visual cortex, inherit naturally the $\mathbf{E}(2)$-symmetry of the plane. By restricting the

solutions to doubly-periodic functions on some lattices, they demonstrated the existence of simple geometric patterns that are the cortical counterpart of the "forms" seen during visual hallucinosis. Bressloff *et al.* [Bressloff 2001b] revisited this theory and proposed a continuum model of the visual cortex defined on the space $\mathbb{R}^2 \times \mathbf{S}^1$ that takes into account the isotropic local and anisotropic lateral connections in V1. Neurons in each hypercolumn are all-to-all coupled, while the connections between hypercolumns couple only neurons sensitive to the same contour orientation that lie in the direction of the preferred orientation. This model has still the $\mathbf{E}(2)$-symmetry but its action differs from the model of Ermentrout and Cowan in the sense that there is a shift-twist symmetry of rotation due to the observation that if one rotates the whole visual cortex one has also to rotate each hypercolumn. Their model was able to produce new geometric visual hallucinations.

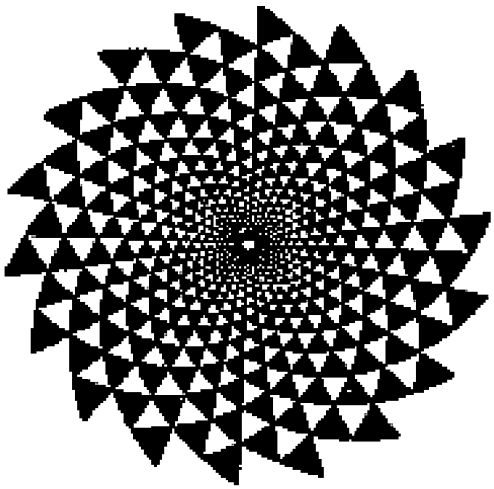

Figure 5.1: Typical observed binocular pressure phosphenes from Tyler's paper [Tyler 1978].

The aim of this chapter is to familiarize the reader to the notions of pattern formation on the Euclidean plane which will be essential for the understanding of the following chapter. Indeed, in the next chapter, we will treat an equivalent problem but in the context of hyperbolic geometry. In order to illustrate the theoretical results that we are going to present, we will present an elementary model of visual hallucination patterns. This toy model will emphasize on the different possible irreducible representations of a chosen lattice. To our knowledge, only the four-dimensional (resp. six-dimensional) representation of the square (resp. hexagonal) lattice has been studied in the context of visual hallucination patterns. In section 5.2, we treat the specific case of pattern formation on a square superlattice: the kernel of the linearized equation of the neural field equation, at the bifurcation point, consists of four complex Fourier modes.

5.1 Planforms on the Euclidean plane

5.1.1 Lattices and lattice patterns

The Euclidean group In the real 2-dimensional affine space R_2 we chose an origin O and a coordinate frame so that any point P is determined by its coordinates (x_1, x_2). The distance between P and Q is given by $d(P,Q) = \sqrt{\sum_{i=1}^{2}(x_i - y_i)^2}$. This gives R_2 a Euclidean structure. The Euclidean Group $\mathbf{E}(2)$ is the group of all linear or affine linear isometries acting on R_2: all linear transformations which preserve the distances. It can be shown that any such transformation is a composition of an orthogonal transformation $\mathcal{O}$, i.e. an isometry which keeps the origin O fixed, and a translation by a vector $\mathbf{e}$. $\mathbf{e}$ is a vector of $\mathbb{R}^2$. The group of isometries which keeps the origin O fixed is isomorphic to the real orthogonal group $\mathbf{O}(2)$. Given any $g \in \mathbf{E}(2)$ we write $g = (\mathcal{O}, \mathbf{e}) \in \mathbf{O}(2) \times \mathbb{R}^2$. The composition law is:

$$g \cdot g' = (\mathcal{O}\mathcal{O}', \mathcal{O}\mathbf{e} + \mathbf{e}').$$

This shows that $\mathbf{E}(2)$ is the semi-product $\mathbf{O}(2) \ltimes \mathbb{R}^2$.

Throughout this chapter, by "symmetry group" we will mean a closed subgroup of $\mathbf{E}(2)$.

Planar lattice Let ℓ_1, ℓ_2 be a basis of $\mathbb{R}^2$. The set $\mathcal{L} = \{m_1\ell_1 + m_2\ell_2 \mid (m_1, m_2) \in \mathbb{Z}^2\}$ is a discrete subgroup of $\mathbb{R}^2$. It is called a *lattice group* because the orbit of a point in R_2, under the action of $\mathcal{L}$ forms a *periodic lattice* of points in R_2. We set $\widetilde{\mathcal{L}} = \mathcal{L}(O)$. Denote by $\mathcal{H}$ the largest subgroup of $\mathbf{O}(2)$ which keeps $\widetilde{\mathcal{L}}$ invariant. Then the symmetry group of $\widetilde{\mathcal{L}}$ is generated by the semi-direct product $\mathcal{H} \ltimes \mathbb{T}^2$. The group $\mathcal{H}$ is called the *holohedry* of the lattice. We define the dual lattice of lattice $\mathcal{L}$ by $\mathcal{L}^* = \{m_1\mathbf{k}_1 + m_2\mathbf{k}_2 \mid (m_1, m_2) \in \mathbb{Z}^2\}$ with $\ell_i \cdot \mathbf{k}_j = 2\pi\delta_{i,j}$. We summerize in table 5.1 the different holohedries of the plane.

Name	Holohedry	Basis of $\mathcal{L}^*$
Hexagonal	$\mathbf{D}_6$	$\|\mathbf{k}_1\| = \|\mathbf{k}_2\| = k$ and $\langle \mathbf{k}_1, \mathbf{k}_2 \rangle = \pm k^2 \cos(2\pi/3)$
Square	$\mathbf{D}_4$	$\|\mathbf{k}_1\| = \|\mathbf{k}_2\|$ and $\langle \mathbf{k}_1, \mathbf{k}_2 \rangle = 0$
Rhombic	$\mathbf{D}_2$	$\|\mathbf{k}_1\| = \|\mathbf{k}_2\| = k$ and $\lvert\langle \mathbf{k}_1, \mathbf{k}_2 \rangle\rvert \neq 0, k^2 \cos(2\pi/3), k^2$
Rectangular	$\mathbf{D}_2$	$\|\mathbf{k}_1\| \neq \|\mathbf{k}_2\|$ and $\langle \mathbf{k}_1, \mathbf{k}_2 \rangle = 0$
Oblique	$\mathbf{C}_2$	$\mathbf{k}_1, \mathbf{k}_2$ not colinear, $\|\mathbf{k}_1\| \neq \|\mathbf{k}_2\|$ and $\langle \mathbf{k}_1, \mathbf{k}_2 \rangle \neq 0$

Table 5.1: Lattices and holohedries of the plane.

A planar lattice pattern or *planform* is a function $u(\mathbf{r}, t)$ of the spatial variable $\mathbf{r} \in \mathbb{R}^2$ and time t that is periodic on $\mathcal{L}$ so that

$$u(\mathbf{r} + \ell, t) = u(\mathbf{r}, t) \quad \forall \ell \in \mathcal{L}.$$

In general a $\mathcal{L}$-periodic function $u(\mathbf{r}, t)$ can be expressed as a sum of Fourier modes that lie on the dual lattice in the form:

$$u(\mathbf{r}, t) = \sum_{\mathbf{k} \in \mathcal{L}^*} z_{\mathbf{k}}(t) e^{i\mathbf{k}\cdot\mathbf{r}} + c.c.,$$

where *c.c.* stands for complex conjugate. From now on, we will only deal with dual lattices that have $\|\mathbf{k}_1\| = \|\mathbf{k}_2\|$.

5.1.2 Steady-state bifurcation on a lattice

Bifurcation problem We consider a general equation of the form

$$\frac{d}{dt} u(\mathbf{r}, t) = \mathcal{F}(u(\mathbf{r}, t), \mu), \tag{5.1}$$

where $\mathcal{F} : \mathcal{X} \times \mathbb{R} \to \mathcal{Y}$ is a smooth nonlinear operator between suitably chosen Banach spaces, $\mu \in \mathbb{R}$ is a bifurcation parameter and u is a function of the spatial variable $\mathbf{r} \in \mathbb{R}^2$ and time t. For simplicity, we assume that $u(\mathbf{r}, t) \in \mathbb{R}$. We assume that equation (5.1) has Euclidean symmetry and that the solutions evolve on the infinite plane. In this case, $\mathcal{F}$ is equivariant with respect to $\mathbf{E}(2)$, the Euclidean group, and we have

$$\gamma \mathcal{F}(u, \mu) = \mathcal{F}(\gamma u, \mu), \quad \forall \gamma \in \mathbf{E}(2). \tag{5.2}$$

Without loss of generality, we assume that for all values of μ the trivial state $u(\mathbf{r}, t) = 0$ is solution of (5.1) and thus invariant under the symmetries of the plane. We now assume that this trivial state undergoes a symmetry-breaking steady state bifurcation at $\mu = 0$, stable for $\mu < 0$ and unstable for $\mu > 0$. Consider Fourier mode perturbations $e^{i\mathbf{k}\cdot\mathbf{r}}$ to $u = 0$. We assume that at $\mu = 0$, the zero solution is neutrally stable to a circle of modes with $\|\mathbf{k}\| = k_c \neq 0$ and stable to all other modes, so that if a lattice pattern is selected from among that circle of modes it will be exactly periodic in space with well-defined period at onset.

At this point, we want to apply the centre manifold theorem (see chapter 4) to reduce the problem to a finite dimensional one. Unfortunately, there is an infinite number of neutral modes lying on the circle $\|\mathbf{k}\| = k_c$ and the hypothesis 4.2.2 of the spectral decomposition of the center manifold is not satisfied. However, we can restrict ourself to solutions that are doubly periodic with respect to a planar lattice. An important consequence of restricting the solution space to $\mathcal{L}$-periodic functions is that the spectrum of the linearized operator $\mathbf{L}_\mu = D_u \mathcal{F}(0, 0)$ is rendered discrete. This restriction ensures that there are only a finite number of zero eigenvalues at the bifurcation, with all other eigenvalues bounded away from the imaginary axis. The dimension of the bifurcation problem depends on the number of point $\mathbf{k} \in \mathcal{L}^*$ that lie one critical circle of radius k_c.

In what follows, it will be convenient to identify the kernel of the linear operator $\mathbf{L}_{\mu_c}$,

$$\ker \mathbf{L}_{\mu_c} = \{U = \sum_{j=1}^{m} z_j e^{i\mathbf{k}_j \cdot \mathbf{r}} U_j + \text{c.c.} \mid z_j \in \mathbb{C}, \|\mathbf{k}_j\| = k_c\}, \tag{5.3}$$

with the vector space

$$V = \{v = \sum_{j=1}^{m} z_j e^{i\mathbf{k}_j\cdot\mathbf{r}} + \text{c.c.} \mid z_j \in \mathbb{C}, \|\mathbf{k}_j\| = k_c\} \cong \mathbb{C}^m. \tag{5.4}$$

The isomorphism between V and $\mathbb{C}^m$ is defined by $v \to \mathbf{z} = (z_1, \ldots, z_m)$. Equation (5.1), restricted to the center manifold, lead to the following system of ordinary differential equations

$$\dot{\mathbf{z}} = f(\mathbf{z}, \mu), \quad f : \mathbb{C}^m \times \mathbb{R} \to \mathbb{C}^m. \tag{5.5}$$

In particular, if Γ is the symmetry group of the bifurcation problem (5.1), then f satisfies the usual equivariance condition

$$\gamma f(\mathbf{z}, \mu) = f(\gamma\mathbf{z}, \mu), \quad \forall\gamma \in \Gamma. \tag{5.6}$$

Irreducible representations For a given lattice $\mathcal{L}$, the vector space V is finite dimensional and is Γ-invariant if $\Gamma = \mathcal{H} \ltimes \mathbb{T}^2$. We enumerate in table 5.2 all the *translation free*[1] irreducible presentations of V under the action of Γ (see [Dionne 1992]).

Lattice	Dimension of representation
Hexagonal	6, 12
Square	4, 8
Rhombic	4

Table 5.2: Lattice groups: dimension of translation free irreducible representations.

We now give for each irreducible representation (only in the case of the square and hexagonal lattice) all the axial isotropy subgroups. Note that when the dimension of the irreducible representation is 8 (resp. 12) for the square (resp. hexagonal) lattice, we say that $\mathcal{L}$ is a *superlattice*.

Isotropy subgroups on a square and hexagonal lattice We consider a stationary bifurcation with Euclidean symmetry restricted to a square lattice. The symmetry group is then $\Gamma_s = \mathbf{D}_4 \ltimes \mathbb{T}^2$. We use the fundamental representation on the square lattice in which there are two critical orthogonal vectors $\mathbf{k}_1$ and $\mathbf{k}_2$, and to leading order a real scalar solution takes the form

$$u(\mathbf{r}, t) = \sum_{j=1}^{2} z_j(t) e^{i\mathbf{k}_j\cdot\mathbf{r}} + \text{c.c.}, \quad z_1, z_2 \in \mathbb{C}.$$

We consider the action of Γ_s on $\mathbb{C}^2$. The group Γ_s is generated by

[1] A representation is translation free if there are no (non-trivial) translations in Γ that acts trivially on V.

(i) ξ: a rotation through $\pi/2$ centered at the origin,

(ii) δ: a reflection which acts on $\mathbf{r} = (r_1, r_2) \in \mathbb{R}^2$ as $\delta \cdot (r_1, r_2) = (r_1, -r_2)$,

(iii) $\Theta \in \mathbb{T}^2$: a translation.

The action of Γ_s on $\mathbf{z} = (z_1, z_2)$ is given by:

$$\begin{cases} \xi(\mathbf{z}) &= (\bar{z}_2, z_1) \\ \delta(\mathbf{z}) &= (z_1, \bar{z}_2) \\ \Theta(\mathbf{z}) &= (e^{-i\theta_1} z_1, e^{-i\theta_2} z_2) \end{cases} \tag{5.7}$$

where $\Theta = \theta_1 \ell_1 + \theta_2 \ell_2$ with $\theta_1, \theta_2 \in [0, 2\pi[$.

The axial isotropy subgroups are given in table 5.3. We see that there exists two branches of one-dimensional fixed-point subspace: squares and rolls. The Equivariant Branching Lemma (see chapter 4) guarantees that they will be primary branches.

Branch	Isotropy subgroup H	Generators of H	dim Fix(H)
Squares	$\mathbf{D}_4$	ξ, δ	1
Rolls	$\mathbf{D}_2 \ltimes \mathbf{S}^1$	$\xi^2, \delta, [0, \theta_2]$	1

Table 5.3: The axial isotropy subgroups (up to conjugacy) for the steady bifurcation on a square lattice.

We now consider a stationary bifurcation with Euclidean symmetry restricted on a hexagonal lattice with symmetry group $\Gamma_h = \mathbf{D}_6 \ltimes \mathbb{T}^2$. We use the fundamental representation, writing a scalar solution to leading order as

$$u(\mathbf{r}, t) = \sum_{j=1}^{3} z_j(t) e^{i\mathbf{k}_j \cdot \mathbf{r}} + \text{c.c.}, \quad z_1, z_2, z_3 \in \mathbb{C}.$$

We consider the action of Γ_h on $\mathbb{C}^3$. For a hexagonal lattice, the wave vectors are at angles of $2\pi/3$ to each other and satisfy a resonance relation $\mathbf{k}_1 + \mathbf{k}_2 + \mathbf{k}_3 = 0$. The group Γ_h is generated by

(i) ξ: a rotation through $\pi/3$ centered at the origin,

(ii) δ: a reflection which acts on $\mathbf{r} = (r_1, r_2) \in \mathbb{R}^2$ as $\delta \cdot (r_1, r_2) = (r_1, -r_2)$,

(iii) $\Theta \in \mathbb{T}^2$: a translation.

The action of Γ_h on $\mathbf{z} = (z_1, z_2, z_3)$ is given by:

$$\begin{cases} \xi(\mathbf{z}) &= (\bar{z}_2, \bar{z}_3, \bar{z}_1) \\ \delta(\mathbf{z}) &= (z_1, z_3, z_2) \\ \Theta(\mathbf{z}) &= (e^{-i\theta_1} z_1, e^{-i\theta_2} z_2, e^{i(\theta_1+\theta_2)} z_3). \end{cases} \tag{5.8}$$

where $\Theta = \theta_1 \ell_1 + \theta_2 \ell_2$ with $\theta_1, \theta_2 \in [0, 2\pi[$.

The axial isotropy subgroups are given in table 5.4. We see that there exists two branches of one-dimensional fixed-point subspace: hexagons and rolls.

Branch	Isotropy subgroup H	Generators of H	dim Fix(H)
Hexagons	$\mathbf{D}_6$	ξ, δ	1
Rolls	$\mathbf{D}_2 \ltimes \mathbf{S}^1$	$\xi^3, \delta, [0, \theta_2]$	1

Table 5.4: The axial isotropy subgroups (up to conjugacy) for the steady bifurcation on a hexagonal lattice.

Isotropy subgroups on a square superlattice For the square lattice, we consider the case where the center manifold is 8-dimensional and define:

$$\left\{\begin{array}{lcl} \mathbf{K}_1 &=& \alpha\mathbf{k}_1 + \beta\mathbf{k}_2 = (\alpha, \beta) \\ \mathbf{K}_2 &=& -\beta\mathbf{k}_1 + \alpha\mathbf{k}_2 = (-\beta, \alpha) \\ \mathbf{K}_3 &=& \beta\mathbf{k}_1 + \alpha\mathbf{k}_2 = (\beta, \alpha) \\ \mathbf{K}_4 &=& -\alpha\mathbf{k}_1 + \beta\mathbf{k}_2 = (-\alpha, \beta) \end{array}\right. \tag{5.9}$$

where $\alpha, \beta \in \mathbb{Z}$, $\alpha > \beta > 0$, $\alpha \wedge \beta = 1$ and α, β are not both odd with $\|\mathbf{K}_j\| = k_c = \sqrt{\alpha^2 + \beta^2}$. Each eigenfunctions of V can be written:

$$u(\mathbf{r}, t) = \sum_{j=1}^{4} z_j(t) e^{i\mathbf{K}_j \cdot \mathbf{r}} + \text{c.c.}, \quad z_1, z_2, z_3, z_4 \in \mathbb{C}.$$

We identify each such eigenfunctions with the vector $(z_1, z_2, z_3, z_4) \in \mathbb{C}^4$. Let $\theta = \theta_1\ell_1 + \theta_2\ell_2 \cong [\theta_1, \theta_2] \in \mathbb{T}^2$, where $\theta_i \in [0, 2\pi[$ and the action of the torus $\mathbb{T}^2$ is given by

$$\theta \cdot (z_1, z_2, z_3, z_4) = (e^{-i(\alpha\theta_1+\beta\theta_2)}z_1, e^{-i(-\beta\theta_1+\alpha\theta_2)}z_2, e^{-i(\beta\theta_1+\alpha\theta_2)}z_3, e^{-i(-\alpha\theta_1+\beta\theta_2)}z_4). \tag{5.10}$$

If we denote ξ the counterclockwise rotation through angle $\frac{\pi}{2}$ and δ the reflection $(r_1, r_2) \to (r_1, -r_2)$, then the action of ξ and δ are:

$$\begin{array}{rcl} \xi \cdot (z_1, z_2, z_3, z_4) &=& (\bar{z}_2, z_1, \bar{z}_4, z_3) \\ \delta \cdot (z_1, z_2, z_3, z_4) &=& (\bar{z}_4, \bar{z}_3, \bar{z}_2, \bar{z}_1). \end{array} \tag{5.11}$$

Using standard notations for groups, we have listed in table 5.5 all the axial subgroups H (up to conjugacy) for 8-dimensional representation of Γ_s (see [Dionne 1997] for more details). The reflection δ_d is defined as $\delta_d = \delta\xi^3$ and is the reflection of axis $\ell_1 + \ell_2$. The groups $(\mathbf{s}_i)_{i=1\cdots4}$ are defined as follows: $\mathbf{s}_1 = \{(\beta s, -\alpha s) \in \mathbb{T}^2 \mid s \in \mathbb{R}\}$, $\mathbf{s}_2$ is generated by $\left(\frac{\alpha}{\alpha^2+\beta^2}, \frac{\beta}{\alpha^2+\beta^2}\right), \left(\frac{-\beta}{\alpha^2+\beta^2}, \frac{\alpha}{\alpha^2+\beta^2}\right) \in \mathbb{T}^2$, $\mathbf{s}_3$ is generated by $\left(\frac{1}{2\alpha}, \frac{1}{2\beta}\right), \left(\frac{-1}{2\alpha}, \frac{1}{2\beta}\right) \in \mathbb{T}^2$ and $\mathbf{s}_4$ is generated by $\left(\frac{\alpha}{\alpha^2-\beta^2}, \frac{-\beta}{\alpha^2-\beta^2}\right), \left(\frac{-\beta}{\alpha^2-\beta^2}, \frac{\alpha}{\alpha^2-\beta^2}\right) \in \mathbb{T}^2$.

Branch	H	Generators of H	Fixed vector	$\dim \mathrm{Fix}(H)$
Super squares	$\mathbf{D}_4$	ξ, δ	$(1,1,1,1)$	1
Anti-squares	$\mathbf{D}_4'$	$\xi, \delta\left[\frac{1}{2}, \frac{1}{2}\right]$	$(1,1,-1,-1)$	1
Rolls	$\mathbf{Z}_2 \ltimes \mathbf{s}_1$	$\xi^2, \mathbf{s}_1$	$(1,0,0,0)$	1
Simple squares	$\mathbf{Z}_4 \ltimes \mathbf{s}_2$	$\xi, \mathbf{s}_2$	$(1,1,0,0)$	1
Rhombs-1	$\mathbf{D}_2 \ltimes \mathbf{s}_3$	$\xi^2, \delta, \mathbf{s}_3$	$(1,0,0,1)$	1
Rhombs-2	$\mathbf{D}_{2,d} \ltimes \mathbf{s}_4$	$\xi^2, \delta_d, \mathbf{s}_4$	$(1,0,1,0)$	1

Table 5.5: Axial isotropy subgroups H (up to conjugacy) for 8-dimensional irreducible representation.

Isotropy subgroups on a hexagonal superlattice For the hexagonal lattice we define:

$$\begin{cases} \mathbf{K}_1 &= \alpha\mathbf{k}_1 + \beta\mathbf{k}_2 = (\alpha, \beta) \\ \mathbf{K}_2 &= (-\alpha+\beta)\mathbf{k}_1 + \alpha\mathbf{k}_2 = (-\alpha+\beta, -\alpha) \\ \mathbf{K}_3 &= -\beta\mathbf{k}_1 + (\alpha-\beta)\mathbf{k}_2 = (-\beta, \alpha-\beta) \\ \mathbf{K}_4 &= \alpha\mathbf{k}_1 + (\alpha-\beta)\mathbf{k}_2 = (\alpha, \alpha-\beta) \\ \mathbf{K}_5 &= -\beta\mathbf{k}_1 - \alpha\mathbf{k}_2 = (-\beta, -\alpha) \\ \mathbf{K}_6 &= (-\alpha+\beta)\mathbf{k}_1 + \beta\mathbf{k}_2 = (-\alpha+\beta, \beta) \end{cases} \tag{5.12}$$

where $\alpha, \beta \in \mathbb{Z}$, $\alpha > \beta > \alpha/2 > 0$, $\alpha \wedge \beta = 1$ and $3 \wedge \alpha + \beta = 1$ with $\|\mathbf{K}_j\| = k_c = \sqrt{\alpha^2 + \beta^2 - \alpha\beta}$.

Remark 5.1.1. *In the hexagonal case, the wave vectors $\mathbf{K}_2, \mathbf{K}_3$ are obtained by rotation $\mathbf{K}_1$ by $\pm\frac{2\pi}{3}$, $\mathbf{K}_5$ and $\mathbf{K}_6$ obtained from $\mathbf{K}_4$ in the same way.*

Then each eigenfunctions can be written:

$$u(\mathbf{r}, t) = \sum_{j=1}^{6} z_j(t) e^{i\mathbf{K}_j \cdot \mathbf{r}} + \text{c.c.}, \quad z_1, z_2, z_3, z_4, z_5, z_6 \in \mathbb{C}.$$

We identify each such eigenfunctions with the vector $(z_1, z_2, z_3, z_4, z_5, z_6) \in \mathbb{C}^6$. Let $\theta = \theta_1\ell_1 + \theta_2\ell_2 \cong [\theta_1, \theta_2] \in \mathbb{T}^2$, where $\theta_i \in [0, 2\pi[$ and the action of the torus $\mathbb{T}^2$ is given by

$$\begin{aligned} \theta \cdot (z_1, z_2, z_3, z_4) = (&e^{-i(\alpha\theta_1+\beta\theta_2)} z_1, e^{-i((-\alpha+\beta)\theta_1-\alpha\theta_2)} z_2, e^{-i(-\beta\theta_1+(\alpha-\beta)\theta_2)} z_3, \\ &e^{-i(\alpha\theta_1+(\alpha-\beta)\theta_2)} z_4, e^{-i(-\beta\theta_1-\alpha\theta_2)} z_5, e^{-i((-\alpha+\beta)\theta_1+\beta\theta_2)} z_6) \end{aligned}$$

If we denote ξ the counterclockwise rotation through angle $\frac{\pi}{3}$ and δ the reflection $(r_1, r_2) \to (r_1, -r_2)$, then the action of ξ and δ are:

$$\begin{aligned} \xi \cdot (z_1, z_2, z_3, z_4, z_5, z_6) &= (\bar{z}_2, \bar{z}_3, \bar{z}_1, \bar{z}_5, \bar{z}_6, \bar{z}_4) \\ \delta \cdot (z_1, z_2, z_3, z_4, z_5, z_6) &= \varepsilon(z_6, z_5, z_4, z_3, z_2, z_1). \end{aligned}$$

We have listed in table 5.6 all the axial subgroups H (up to conjugacy) for 12-dimensional representation. The reflection δ_n (resp. δ_m) is defined as $\delta_n = \xi\delta$

(resp. $\delta_m = \xi^5\delta$) and is the reflection through the axis $\ell_1 - 2\ell_2$ (resp. $\ell_1 + \ell_2$). The groups $(\mathbf{h}_i)_{i=1\cdots5}$ are defined as follows:
$\mathbf{h}_1 = \{(\beta s, -\alpha s) \in \mathbb{T}^2 \mid s \in \mathbb{R}\}$,
$\mathbf{h}_2$ is generated by $\left(\frac{\alpha-\beta}{\alpha^2-2\alpha\beta}, \frac{-1}{\alpha-2\beta}\right), \left(\frac{-\beta}{\alpha^2-2\alpha\beta}, \frac{1}{\alpha-2\beta}\right) \in \mathbb{T}^2$,
$\mathbf{h}_3$ is generated by $\left(\frac{\alpha}{\alpha^2-\beta^2}, \frac{-\beta}{\alpha^2-\beta^2}\right), \left(\frac{\beta}{\alpha^2-\beta^2}, \frac{-\alpha}{\alpha^2-\beta^2}\right) \in \mathbb{T}^2$,
$\mathbf{h}_4$ is generated by $\left(\frac{1}{2\alpha-\beta}, \frac{\alpha-\beta}{2\alpha\beta-\beta^2}\right), \left(\frac{-1}{2\alpha-\beta}, \frac{\alpha}{2\alpha\beta-\beta^2}\right) \in \mathbb{T}^2$
and $\mathbf{h}_5$ is generated by $\left(\frac{\alpha}{\alpha^2-\alpha\beta+\beta^2}, \frac{-\alpha+\beta}{\alpha^2-\alpha\beta+\beta^2}\right), \left(\frac{\beta}{\alpha^2-\alpha\beta+\beta^2}, \frac{-\alpha}{\alpha^2-\alpha\beta+\beta^2}\right) \in \mathbb{T}^2$.

Branch	H	Generators of H	Fixed vector	$\dim \mathrm{Fix}(H)$
Super hexagons	$\mathbf{D}_6$	ξ, δ	$(1,1,1,1,1,1)$	1
Rolls	$\mathbf{Z}_2 \ltimes \mathbf{h}_1$	$\xi^3, \mathbf{h}_1$	$(1,0,0,0,0,0)$	1
Rhombs-1	$\mathbf{D}_{2,n} \ltimes \mathbf{h}_2$	$\xi^3, \delta_n, \mathbf{h}_2$	$(1,0,0,1,0,0)$	1
Rhombs-2	$\mathbf{D}_{2,m} \ltimes \mathbf{h}_3$	$\xi^3, \delta_m, \mathbf{h}_3$	$(1,0,0,0,1,0)$	1
Rhombs-3	$\mathbf{D}_2 \ltimes \mathbf{h}_4$	$\xi^3, \delta, \mathbf{h}_4$	$(1,0,0,0,0,1)$	1
Simple hexagons	$\mathbf{Z}_6 \ltimes \mathbf{h}_5$	$\xi, \mathbf{h}_5$	$(1,1,1,0,0,0)$	1

Table 5.6: Axial isotropy subgroups H (up to conjugacy) for 12-dimensional irreducible representation.

5.2 Visual hallucination patterns of a square superlattice

5.2.1 Simplified Ermentrout-Cowan model

Following [Ermentrout 1979], we introduce the following neural field equation (see chapter 2) set on the visual cortex for a single population of neurons:

$$\tau \frac{d}{dt} V(\mathbf{r}, t) = -V(\mathbf{r}, t) + \int_{\mathbb{R}^2} W(\mathbf{r}|\mathbf{r}') S(\mu V(\mathbf{r}', t)) d\mathbf{r}' \tag{5.13}$$

where τ a synaptic constant. Without loss of generality we fix $\tau = 1ms$. $W(\mathbf{r}|\mathbf{r}') = W(\|\mathbf{r} - \mathbf{r}'\|)$ is an excitatory/inhibitory cortical connectivity function and S is a smooth function of sigmoidal type:

$$S(x) = \frac{1}{1 + \exp(-x + T)} - \frac{1}{1 + \exp(T)},$$

where T is a positive threshold. For the connectivity function, we take a local excitatory and lateral inhibitory function (see figure 5.2(a)) with a "Mexican hat" shape:

$$W(x) = A_1 e^{-\frac{x^2}{\sigma_1^2}} - A_2 e^{-\frac{x^2}{\sigma_2^2}}. \tag{5.14}$$

The stationary state $V = 0$ is solution of equation (5.13) and the linearized equation is given by:

$$\frac{\partial}{\partial t} U(\mathbf{r}, t) = -U(\mathbf{r}, t) + \mu s_1 \int_{\mathbb{R}^2} W(\|\mathbf{r} - \mathbf{r}'\|) U(\mathbf{r}', t) d\mathbf{r}' = \mathbf{L}_\mu(U(\mathbf{r}, t)) \tag{5.15}$$

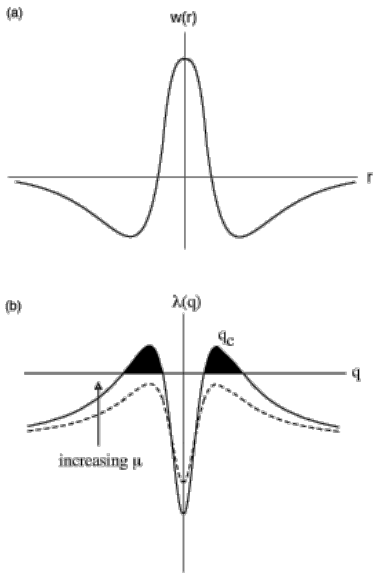

Figure 5.2: (a) "Mexican hat" shape connectivity function . (b) Dispersion curve. Increasing μ implies an upward translation of the dispersion curve which leads to Turing instabilities at the critical point $\mu_c = \left[s_1 \widehat{W}(q_c)\right]^{-1}$ with $\widehat{W}(q_c) = \max_q \left(\widehat{W}(q)\right)$. The stationary state $V = 0$ is unstable $\mu > \mu_c$.

where $s_1 = S'(0)$. We look for solutions of the form $U(\mathbf{r}, t) = U(\mathbf{r})e^{\lambda t}$, this gives:

$$\lambda U(\mathbf{r}) = -U(\mathbf{r}) + \mu s_1 \int_{\mathbb{R}^2} W(\|\mathbf{r} - \mathbf{r}'\|)U(\mathbf{r}')d\mathbf{r}'$$

then, applying Fourier transform on $\mathbb{R}^2$ we obtain the following spectral problem:

$$\lambda \widehat{U}_{\mathbf{k}} = \left[-1 + \mu s_1 \widehat{W}_{\mathbf{k}}\right] \widehat{U}_{\mathbf{k}}$$

with $\widehat{U}_{\mathbf{k}}$ et $\widehat{W}_{\mathbf{k}}$ are Fourier transforms of $U(\mathbf{r})$ and $W(\|\mathbf{r}\|)$. This yields a dispersion relation for λ as a function of $q = \|\mathbf{k}\|$:

$$\lambda(q) = -1 + \mu s_1 \widehat{W}(q). \tag{5.16}$$

Indeed, from the definition of W in equation (5.14) it is easy to obtain $\widehat{W}_{\mathbf{k}} = \widehat{W}(q)$:

$$\widehat{W}(q) = \widehat{W}_{\mathbf{k}} \overset{def}{=} \int_{\mathbb{R}^2} W(\|\mathbf{r}\|)e^{-\pi \mathbf{k}\cdot\mathbf{r}}d\mathbf{r} = A_1\pi\sigma_1^2 e^{-\sigma_1^2 q^2/4} - A_2\pi\sigma_2^2 e^{-\sigma_2^2 q^2/4}.$$

Now $\lambda(q)$ equals zero at the critical value $\mu_c = \left[s_1 \widehat{W}(q_c)\right]^{-1}$ with $\widehat{W}(q_c) = \max_q \left(\widehat{W}(q)\right)$ (see figure 5.2(b)). At the bifurcation point, there is a whole circle of critical eigenvectors which becomes unstable: $q_c = \|\mathbf{k}\|$. This is due to rotation symmetry of the system.

We restrict ourself to doubly periodic functions on the square lattice $\mathcal{L}$. We suppose that there are 8 points $\mathbf{k} \in \mathcal{L}^*$ that lie on the critical circle of radius q_c. These points are given by $\mathbf{K}_i$ in (5.9). The symmetry group acting on (5.13) is now $\Gamma_s = \mathbf{D}_4 \ltimes \mathbb{T}^2$ where $\mathbf{D}_4 =< \xi, \delta >$ with ξ the rotation of angle $\pi/2$ and δ the reflection of axis Ox. We suppose that $q_c = \sqrt{\alpha^2 + \beta^2}$ with α, β defined in (5.9). We identify the kernel of the linear operator $\mathbf{L}_{\mu_c}$,

$$\ker \mathbf{L}_{\mu_c} = \{U = \sum_{j=1}^{4} z_j e^{2i\pi \mathbf{K}_j \cdot \mathbf{r}} b_j + \text{c.c} \mid z_j \in \mathbb{C}, \|\mathbf{K}_j\| = q_c\}$$

with the vector space:

$$V = \{v = \sum_{j=1}^{4} z_j e^{2i\pi \mathbf{K}_j \cdot \mathbf{r}} + \text{c.c} \mid z_j \in \mathbb{C}, \|\mathbf{K}_j\| = q_c\} \cong \mathbb{C}^4$$

The isomorphism between V and $\mathbb{C}^4$ is given by $v \to \mathbf{z} = (z_1, z_2, z_3, z_4)$. The action of $\Gamma_s = \mathbf{D}_4 \ltimes \mathbb{T}^2$ on V is given by equations 5.10 and 5.11. The axial subgroups are given in table 5.5.

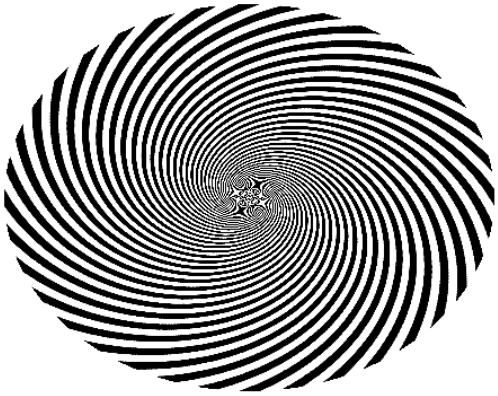

Figure 5.3: Rolls: $\mathbf{Z}_2 \ltimes \mathbf{s}_1$, in visual field coordinates.

5.2.2 Theoretical results

The normal form, with symmetry $\mathbf{D}_4$, for the eight-dimensional representation is given by (see [Dionne 1997]):

$$\begin{cases} \dot{z}_1 &= z_1 \left[\frac{\mu-\mu_c}{\mu_c} + a|z_1|^2 + b|z_2|^2 + c|z_3|^2 + d|z_4|^2\right] + \text{h.o.t} \\ \dot{z}_2 &= z_2 \left[\frac{\mu-\mu_c}{\mu_c} + a|z_2|^2 + b|z_1|^2 + c|z_4|^2 + d|z_3|^2\right] + \text{h.o.t} \\ \dot{z}_3 &= z_3 \left[\frac{\mu-\mu_c}{\mu_c} + a|z_3|^2 + b|z_4|^2 + c|z_1|^2 + d|z_2|^2\right] + \text{h.o.t} \\ \dot{z}_4 &= z_4 \left[\frac{\mu-\mu_c}{\mu_c} + a|z_4|^2 + b|z_3|^2 + c|z_2|^2 + d|z_1|^2\right] + \text{h.o.t} \end{cases} \tag{5.17}$$

Lemma 5.2.1. *The real coefficients a, b, c, d are given by:*

$$\left\{\begin{array}{rcl}
a\left(\mu_c^3\widehat{W}_{\mathbf{k}_c}\right)^{-1} & = & \dfrac{s_3}{2}+s_2^2\mu_c\left[\dfrac{\widehat{W}_0}{1-\widehat{W}_0\left(\widehat{W}_{\mathbf{k}_c}\right)^{-1}}+\dfrac{\widehat{W}_{2\mathbf{k}_c}}{2\left(1-\widehat{W}_{2\mathbf{k}_c}\left(\widehat{W}_{\mathbf{k}_c}\right)^{-1}\right)}\right]\\
b\left(\mu_c^3\widehat{W}_{\mathbf{k}_c}\right)^{-1} & = & s_3+s_2^2\mu_c\left[\dfrac{\widehat{W}_0}{1-\widehat{W}_0\left(\widehat{W}_{\mathbf{k}_c}\right)^{-1}}+2\dfrac{\widehat{W}_{\mathbf{K}_1+\mathbf{K}_2}}{1-\widehat{W}_{\mathbf{K}_1+\mathbf{K}_2}\left(\widehat{W}_{\mathbf{k}_c}\right)^{-1}}\right]\\
c\left(\mu_c^3\widehat{W}_{\mathbf{k}_c}\right)^{-1} & = & s_3+s_2^2\mu_c\left[\dfrac{\widehat{W}_0}{1-\widehat{W}_0\left(\widehat{W}_{\mathbf{k}_c}\right)^{-1}}+\dfrac{\widehat{W}_{\mathbf{K}_1+\mathbf{K}_3}}{1-\widehat{W}_{\mathbf{K}_1+\mathbf{K}_3}\left(\widehat{W}_{\mathbf{k}_c}\right)^{-1}}\right.\\
 & & \left.+\dfrac{\widehat{W}_{\mathbf{K}_1-\mathbf{K}_3}}{1-\widehat{W}_{\mathbf{K}_1-\mathbf{K}_3}\left(\widehat{W}_{\mathbf{k}_c}\right)^{-1}}\right]\\
d\left(\mu_c^3\widehat{W}_{\mathbf{k}_c}\right)^{-1} & = & s_3+s_2^2\mu_c\left[\dfrac{\widehat{W}_0}{1-\widehat{W}_0\left(\widehat{W}_{\mathbf{k}_c}\right)^{-1}}+\dfrac{\widehat{W}_{\mathbf{K}_1+\mathbf{K}_4}}{1-\widehat{W}_{\mathbf{K}_1+\mathbf{K}_4}\left(\widehat{W}_{\mathbf{k}_c}\right)^{-1}}\right.\\
 & & \left.+\dfrac{\widehat{W}_{\mathbf{K}_1-\mathbf{K}_4}}{1-\widehat{W}_{\mathbf{K}_1-\mathbf{K}_4}\left(\widehat{W}_{\mathbf{k}_c}\right)^{-1}}\right]
\end{array}\right. \tag{5.18}$$

where we have defined $s_k = S^{(k)}(0)$ and:

$$\left\{\begin{array}{ll}
\widehat{W}_0 & = \int_{\mathbb{R}^2} W(\|\mathbf{r}\|)d\mathbf{r}\\
\widehat{W}_{\mathbf{k}_c} & = \int_{\mathbb{R}^2} W(\|\mathbf{r}\|)e^{-i\mathbf{k}_c\cdot\mathbf{r}}d\mathbf{r} \text{ with } \mathbf{k}_c=\mathbf{K}_j\\
\widehat{W}_{2\mathbf{k}_c} & = \int_{\mathbb{R}^2} W(\|\mathbf{r}\|)e^{-2i\mathbf{k}_c\cdot\mathbf{r}}d\mathbf{r} \text{ with } \mathbf{k}_c=\mathbf{K}_j\\
\widehat{W}_{\mathbf{K}_m\pm\mathbf{K}_n} & = \int_{\mathbb{R}^2} W(\|\mathbf{r}\|)e^{-i(\mathbf{K}_m\pm\mathbf{K}_n)\cdot\mathbf{r}}d\mathbf{r}
\end{array}\right.$$

Remark 5.2.1. *Note that we have the following useful relations:*

$$\left\{\begin{array}{rcl}
\|\mathbf{K}_1+\mathbf{K}_2\| & = & \|\mathbf{K}_1-\mathbf{K}_2\|\\
\|\mathbf{K}_1+\mathbf{K}_4\| & = & \|\mathbf{K}_2-\mathbf{K}_3\|\\
\|\mathbf{K}_1-\mathbf{K}_4\| & = & \|\mathbf{K}_2+\mathbf{K}_3\|\\
\|\mathbf{K}_1+\mathbf{K}_3\| & = & \|\mathbf{K}_2+\mathbf{K}_4\|\\
\|\mathbf{K}_1-\mathbf{K}_3\| & = & \|\mathbf{K}_2+\mathbf{K}_4\|.
\end{array}\right.$$

The proof of the above lemma is a straightforward adaptation of the computations derived by Ermentrout in [Ermentrout 1991]. From the analysis conducted in [Dionne 1997], we have the following result.

Lemma 5.2.2. *The stability of the branches of solutions corresponding to the following isotropy subgroups is:*

(i) the $\mathbf{Z}_2 \ltimes \mathbf{s}_1$ branch (Rolls) is stable if and only if $a<0$, $b-a>0$, $c-a<0$ and $d-a<0$,

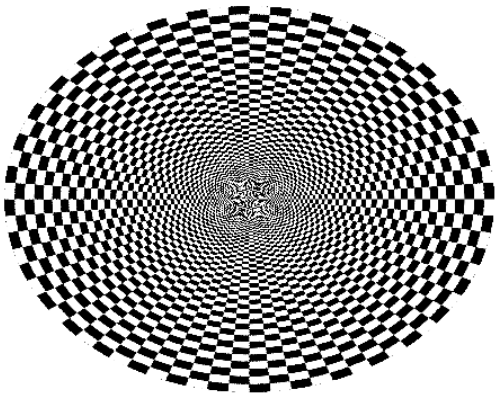

Figure 5.4: Rhombs-1: $\mathbf{D}_2 \ltimes \mathbf{s}_3$, in visual field coordinates.

(ii) the $\mathbf{Z}_4 \ltimes \mathbf{s}_2$ *branch (Simple squares) is stable if and only if* $a+b<0$, $a-b<0$ *and* $c+d-a-b<0$,

(iii) the $\mathbf{D}_2 \ltimes \mathbf{s}_3$ *branch (Rhombs-1) is stable if and only if* $a+c<0$, $a-b<0$ *and* $b+d-a-c<0$,

(iv) the $\mathbf{D}_{2,d} \ltimes \mathbf{s}_4$ *branch (Rhombs-2) is stable if and only if* $a+d<0$, $a-d<0$ *and* $b+c-a-d<0$.

The stability of the $\mathbf{D}_4$ *and* $\mathbf{D}_4'$ *branches require the computation of higher order terms in the normal form* (5.17).

5.2.3 Network behaviour

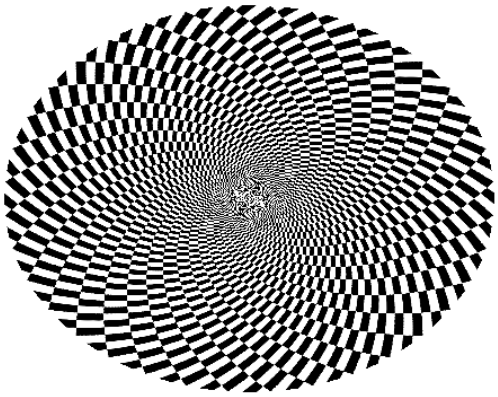

Figure 5.5: Rhombs-2: $\mathbf{D}_{2,d} \ltimes \mathbf{s}_4$, in visual field coordinates.

In order to restrict ourself to the space of solutions which are doubly periodic on a square superlattice we need to select a specific wave vector $\|\mathbf{k}_c\| = q_c = \sqrt{\alpha^2+\beta^2}$ with $\alpha > \beta > 0$, $\alpha \wedge \beta = 1$ and α, β not both odd. We have seen that k_c is determined as the maximum of the Fourier transform of the connectivity function W. This maximum occurs at

$$q_c = \frac{2}{\sigma_2^2 - \sigma_1^2}\sqrt{(\sigma_2^2 - \sigma_1^2)\ln\left(\frac{A_2\sigma_2^4}{A_1\sigma_1^4}\right)}.$$

From $q_c = \sqrt{\alpha^2+\beta^2}$, we find:

$$A_2 = A_1\left(\frac{\sigma_1}{\sigma_2}\right)^4 \exp\left(\frac{(\sigma_2^2 - \sigma_1^2)(\alpha^2+\beta^2)}{4}\right).$$

In order to describe completely the connectivity W with the only parameter σ_1, we impose that $\sigma_2 = 2\sigma_1$ and $A_1 = 4$. We plot in figure 5.6 the conditions given in lemma 5.2.2 as function of the threshold T of the sigmoidal function and the lateral extend of the connectivity σ_1 for $(\alpha, \beta) = (2, 1)$. We obtain exclusive regions where rolls, rhombs-1 and rhombs-2 can be stable patterns. We plot in figures 5.3, 5.4 and 5.5 the corresponding planforms in the visual field, using the retinotopic organization of the primary visual cortex as mentioned in chapter 1. We use a log-polar map [Ermentrout 1979, Bressloff 2001b] which transforms cortical coordinates (x, y) into polar coordinates (ρ, θ) on the retina by

$$\begin{aligned} \rho &= \omega \exp(\varepsilon x) \\ \theta &= \varepsilon y. \end{aligned}$$

In our retinal image, we take $\omega = \frac{30}{e^{2\pi}}$ and $\varepsilon = \frac{\pi}{18}$, as used in [Golubitsky 2003].

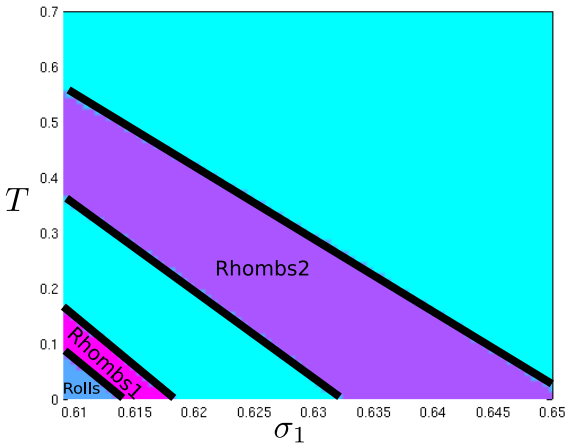

Figure 5.6: Regions in the (σ_1, T)-plane where Rolls, Rhombs-1 and Rhombs-2 planforms are stable for $(\alpha, \beta) = (2, 1)$.

5.3 Conclusion

In this introductory chapter, we have presented results of symmetry-breaking steady state bifurcation problems on planar lattices and illustrated it with a "toy model" leading to visual hallucination patterns on a square superlattice. We can now turn to the main results of part II that rely on the study of symmetry-breaking bifurcation problems for evolution equations set on the hyperbolic plane instead of the traditional Euclidean plane. The notion of dimension of irreducible representations will play a central role as it will be explained in chapters 7 and 8. The concept of Euclidean lattices will also be important for the last chapter of this part.

Chapter 6

Pattern formation in the Poincaré disk

Contents

6.1 Introduction to harmonic analysis in the Poincaré disk . . . 78
6.1.1 The Laplace-Beltrami operator on the Poincaré disk 78
6.1.2 Helgason-Fourier transform 80
6.1.3 Convolutional operator on the Poincaré disk 80
6.2 Spontaneous symmetry breaking in the Poincaré disk . . . 82
6.2.1 Periodic lattices 82
6.2.2 Periodic eigenfunctions of the Laplace-Beltrami operator . . . 84
6.2.3 Bifurcation of patterns in the Poincaré disk 86
6.3 A case study: the octagonal lattice 88
6.3.1 The octagonal lattice and its symmetris 89
6.3.2 Irreducible representation of the octagonal group 92
6.3.3 Octagonal H-planforms 95
6.4 Computation of hyperbolic planforms 99
6.4.1 Introduction 99
6.4.2 Desymmetrization of the octagon for the 1D case 100
6.4.3 Numerical experiments 101
6.5 Application to the structure tensor formalism 107
6.5.1 Bifurcation problem 108
6.5.2 Elementary results 110
6.6 Conclusion 110

Motivated by our structure tensor model for the perception of textures by the visual cortex in primates, we analyse in this chapter the bifurcation of periodic patterns for nonlinear equations describing the state of a system defined on the Poincaré disk $\mathbb{D}$, when these equations are further invariant with respect to the isometries of this space. We make use of the concept of periodic lattice in $\mathbb{D}$ to further reduce the problem to one on a compact Riemann surface $\mathbb{D}/\Gamma$, where Γ is a cocompact Fuchsian group. The knowledge of the symmetry group of this surface allows to carry out the machinery of equivariant bifurcation theory. Solutions which generically bifurcate are called "H-planforms", by analogy with the "planforms" introduced for pattern formation in Euclidean space. This concept is applied to the

case of an octagonal periodic pattern, where we are able to classify all possible H-planforms satisfying the hypotheses of the Equivariant Branching Lemma. These patterns are however not straightforward to compute, even numerically, and in section 6.4 we describe a method for computation illustrated with a selection of images of octagonal H-planforms. Finally, we show that this bifurcation analysis can be extended to the space of structure tensors $\mathbf{SPD}(2,\mathbb{R})$.

6.1 Introduction to harmonic analysis in the Poincaré disk

6.1.1 The Laplace-Beltrami operator on the Poincaré disk

The Laplace-Beltrami operator is the equivalent of the Laplacian for the Euclidean case. Writing the Riemannian structure in the general form

$$ds^2 = \sum_{k,l=1}^{2} g_{ij} dz_k dz_l \text{ where } g_{kl} = 4(1-|z|^2)^{-2}\delta_{kl} \text{ with } z = z_1 + iz_2$$

and putting $\bar{g} = |\det(g_{kl})|$, $g^{kl} = (g_{kl})^{-1}$ (inverse matrix), we recover the Riemannian measure (3.14) and the Laplace-beltrami operator:

$$L_{\mathbb{D}} : \Psi \to \frac{1}{\sqrt{\bar{g}}} \sum_k \partial_k \left(\sum_l g^{lk} \sqrt{\bar{g}} \partial_l \Psi \right)$$

becomes

$$L_{\mathbb{D}} = \frac{\left(1-|z|^2\right)^2}{4} \left(\frac{\partial^2}{\partial z_1^2} + \frac{\partial^2}{\partial z_2^2} \right). \tag{6.1}$$

Let b be a point on the circle $\partial\mathbb{D}$. For $z \in \mathbb{D}$, we define the "inner product" $\langle z, b\rangle$ as the algebraic distance to the origin of the (unique) horocycle based at b and passing through z. This distance is defined as the hyperbolic signed length of the segment $O\xi$ where ξ is the intersection point of the horocycle and the line (geodesic) Ob. This is illustrated in figure 6.1 in the case $b = b_1 = 1$. Note that $\langle z, b\rangle$ does not depend on the position of z on the horocycle. In other words, $\langle z, b\rangle$ is invariant under the action of the one-parameter group N (see definition 3.2.3).

In analogy to the Euclidean plane waves, we define the "hyperbolic plane waves" as the function

$$e_{\rho,b}(z) = e^{\left(i\rho+\frac{1}{2}\right)\langle z,b\rangle}, \quad \rho \in \mathbb{C}. \tag{6.2}$$

Lemma 6.1.1. *For the Laplace-Beltrami operator defined in equation (6.1), we have*

$$L_{\mathbb{D}}\ e_{\rho,b}(z) = -\left(\rho^2 + \frac{1}{4}\right) e_{\rho,b}(z), \quad \forall(\rho, z) \in \mathbb{C} \times \mathbb{D}. \tag{6.3}$$

Proof. See [Helgason 2000]. □

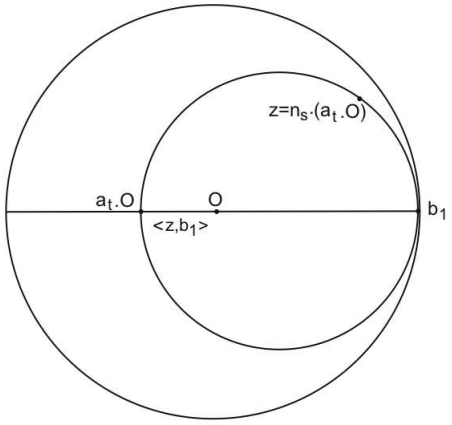

Figure 6.1: Each point z of $\mathbb{D}$ can be written in horocyclic coordinates $z = n_s \cdot (a_t \cdot O)$ (see 3.2.3). The horocycle through z is the circle tangent to $\partial\mathbb{D}$ at b_1 and going through z. $\langle z, b_1 \rangle$ is equal to the hyperbolic signed distance between the orgin O and the point $a_t \cdot O$. It is negative if O is inside the horocycle and positive otherwise.

These elementary eigenfunctions allow the construction of general eigenfunctions of $L_{\mathbb{D}}$. Let $\mathcal{A}(\partial\mathbb{D})$ denote the space of analytic functions on the boundary $\partial\mathbb{D}$ of the Poincaré disk, considered as an analytical manifold. Let U be an open annulus containing $\partial\mathbb{D}$, $\mathcal{H}(U)$ the space of holomorphic functions on U equipped with the topology of uniform convergence on compact subsets. We identify $\mathcal{A}(\partial\mathbb{D})$ with the union $\bigcup_U \mathcal{H}(U)$ and give it the limit topology. The element of the dual space $\mathcal{A}'(\partial\mathbb{D})$ are called *analytic functionals* or *hyperfunctions*. Since elements of $\mathcal{A}'(\partial\mathbb{D})$ generalize measures, it is convenient to write

$$T(f) = \int_{\partial\mathbb{D}} f(b) dT(b), \quad f \in \mathcal{A}(\partial\mathbb{D}) \text{ and } T \in \mathcal{A}'(\partial\mathbb{D}).$$

From Helgason's theory we have the following theorem.

Theorem 6.1.1. *The eigenfunctions of the Laplace-Beltrami operator on $\mathbb{D}$ are precisely the functions*

$$\Psi(z) = \int_{\partial\mathbb{D}} e_{\rho,b}(z) dT_\rho(b), \tag{6.4}$$

where $\rho \in \mathbb{C}$, $T_\rho \in \mathcal{A}'(\partial\mathbb{D})$ and the eigenvalue is $-(\rho^2 + 1)$.

Real eigenvalues $-\left(\rho^2 + \frac{1}{4}\right)$ of $L_{\mathbb{D}}$ correspond to taking ρ real or $\rho \in i\mathbb{R}$. The latter case is irrelevant for the following study as it corresponds to exponentially diverging eigenfunctions. Therefore the real spectrum of $L_{\mathbb{D}}$ is continuous and is bounded from above by $-\frac{1}{4}$.

6.1.2 Helgason-Fourier transform

Based on the elementary eigenfunctions 6.2, Helgason built a Fourier transform theory for the Poincaré disc, see [Helgason 2000] which we recall now.

Definition 6.1.1. *If f is a complex-valued function on $\mathbb{D}$, its Helgason-Fourier transform is defined by*

$$\tilde{f}(\rho, b) = \int_{\mathbb{D}} f(z) e^{\left(-i\rho+\frac{1}{2}\right)\langle z,b\rangle} dm(z) \tag{6.5}$$

for all $\rho \in \mathbb{C}$, $b \in \partial\mathbb{D}$ for which this integral exists.

If we denote $\mathcal{D}(\mathbb{D})$, the set of differentiable functions of compact support then the following inversion theorem holds.

Theorem 6.1.2. *If $f \in \mathcal{D}(\mathbb{D})$, then*

$$f(z) = \frac{1}{2\pi} \int_{\mathbb{R}} \int_{\partial\mathbb{D}} \tilde{f}(\rho, b) e^{\left(i\rho+\frac{1}{2}\right)\langle z,b\rangle} \rho \tanh(\pi\rho)\, d\rho db \tag{6.6}$$

where db is the circular measure on $\partial\mathbb{D}$ normalized by $\int_{\partial\mathbb{D}} db = 1$.

6.1.3 Convolutional operator on the Poincaré disk

In this subsection we want to show that the following linear operator is a convolutional operator on the Poincaré disk.

$$\mathcal{K}(V)(z) = \int_D W(d_{\mathbb{D}}(z, z'))V(z')\mathrm{dm}(z'). \tag{6.7}$$

If O is the center of the Poincaré disk, we denote dg the Haar measure on the group $\mathbf{SU}(1,1)$ (see [Helgason 2000]), normalized by:

$$\int_{\mathbf{SU}(1,1)} f(g \cdot O) dg \overset{def}{=} \int_{\mathbb{D}} f(z) dm(z), \tag{6.8}$$

for all functions of $\mathrm{L}^1(\mathbb{D})$. Given two functions f_1, f_2 in $\mathrm{L}^1(\mathbb{D})$ we define the convolution $*$ by:

$$(f_1 * f_2)(z) = \int_{\mathbf{SU}(1,1)} f_1(g \cdot O) f_2(g^{-1} \cdot z) dg \tag{6.9}$$

We recall the notation $\mathbf{W}(z) \overset{def}{=} W(d_{\mathbb{D}}(z, O))$, such that from equations (6.8) and (6.9) we have $\mathcal{K}(V) = \mathbf{W} * V$.

Lemma 6.1.2. *We suppose that the Helgason-Fourier $\widetilde{\boldsymbol{W}}$ of $\mathbf{W}$ is well defined. Then it does not depend upon the variable $b \in \partial\mathbb{D}$.*

Proof. For all $\rho \in \mathbb{R}$ and $b = e^{i\theta} \in \partial\mathbb{D}$, the Helgason-Fourier $\widetilde{\mathbf{W}}$ of $\mathbf{W}$ is given by

$$\widetilde{\mathbf{W}}(\rho, b) = \int_{\mathbb{D}} \mathbf{W}(z) e^{\left(-i\rho+\frac{1}{2}\right)<z,b>} dm(z).$$

We recall that for all $\phi \in \mathbb{R}$, r_ϕ is the rotation of angle ϕ. It is easy to see that we have:

$$\begin{aligned} \mathbf{W}(\mathrm{r}_\phi \cdot z) &= \mathbf{W}(z), \\ \mathrm{dm}(z) &= \mathrm{dm}(\mathrm{r}_\phi \cdot z), \\ \langle z, b\rangle &= \langle \mathrm{r}_\phi \cdot z, \mathrm{r}_\phi \cdot b\rangle, \end{aligned}$$

such that

$$\begin{aligned} \widetilde{\mathbf{W}}(\rho, b) &= \int_{\mathbb{D}} \mathbf{W}(\mathrm{r}_{-\theta} \cdot z) e^{\left(-i\rho+\frac{1}{2}\right)<\mathrm{r}_{-\theta}\cdot z, 1>} dm(z) \\ &= \int_{\mathbb{D}} \mathbf{W}(z) e^{\left(-i\rho+\frac{1}{2}\right)<z,1>} dm(z) \\ &\overset{def}{=} \widetilde{\mathbf{W}}(\rho). \end{aligned}$$

□

We can now state the following proposition about some eigenfunctions of the linear operator $\mathcal{K}$ which will be useful for our future studies.

Proposition 6.1.1. *Let* $\Phi_\rho(z) = \int_{\partial\mathbb{D}} e^{\left(i\rho+\frac{1}{2}\right)<z,b>} db$ *then:*

- $\mathcal{K}(e_{-\rho,b}) = \widetilde{\boldsymbol{W}}(\rho) e_{-\rho,b}$,
- $\mathcal{K}(\Phi_\rho) = \widetilde{\boldsymbol{W}}(\rho)\Phi_\rho$.

Proof. We begin with $b = 1 \in \partial\mathbb{D}$ and use the horocyclic coordinates $z = n_s a_\tau \cdot O$. The volume element $\mathrm{dm}(z)$ is changed in $e^{-\tau} d\tau ds$ in these coordinates and $e_{-\rho,1}(z)$ reduces to $e^{\left(-i\rho+\frac{1}{2}\right)\tau}$. We use the same changes of variables as in lemma

$$\begin{aligned} \mathcal{K}(e_{\rho,1})(n_s a_\tau . O) &= \int_{\mathbb{R}^2} W(d_{\mathbb{D}}(n_s a_\tau \cdot O, n_{s'} a_{\tau'} \cdot O)) e^{\left(-i\rho+\frac{1}{2}\right)\tau'} e^{-\tau'} d\tau' ds' \\ &= \int_{\mathbb{R}^2} W(d_{\mathbb{D}}(n_{s-s'} a_\tau \cdot O, a_{\tau'} \cdot O)) e^{\left(-i\rho-\frac{1}{2}\right)\tau'} d\tau' ds' \\ &= \int_{\mathbb{R}^2} W(d_{\mathbb{D}}(a_\tau n_{-x} \cdot O, a_{\tau'} \cdot O)) e^{\left(-i\rho-\frac{1}{2}\right)\tau'+\tau} d\tau' dx \\ &= \int_{\mathbb{R}^2} W(d_{\mathbb{D}}(O, n_x a_{\tau'-\tau} \cdot O)) e^{\left(-i\rho-\frac{1}{2}\right)\tau'+\tau} d\tau' dx \\ &= \int_{\mathbb{R}^2} W(d_{\mathbb{D}}(O, n_x a_y \cdot O)) e^{\left(-i\rho-\frac{1}{2}\right)(y+\tau)+\tau} dy dx \\ &= e^{\left(-i\rho+\frac{1}{2}\right)<n_s a_\tau \cdot O, 1>} \widetilde{\mathbf{W}}(\rho) \\ &= \widetilde{\mathbf{W}}(\rho) e_{-\rho,1}. \end{aligned}$$

The third equality comes from the change of variables $s' - s = xe^\tau$ and the relation $a_\tau n_x = n_{xe^\tau} a_\tau$ [Helgason 2000]. By rotation, we obtain the property for all $b \in \partial\mathbb{D}$.

For the second property [Helgason 2000, Lemma 4.7] shows that:

$$\mathbf{W} * \Phi_\rho(z) = \int_{\partial\mathbb{D}} e^{(i\rho+1)<z,b>} \widetilde{\mathbf{W}}(\rho) db = \widetilde{\mathbf{W}}(\rho)\Phi_\rho(z).$$

□

6.2 Spontaneous symmetry breaking in the Poincaré disk

6.2.1 Periodic lattices

A *Fuchsian group* is a discrete subgroup Γ of $\mathbf{SU}(1,1)$. We are going to be concerned with *fundamental regions* of Fuchsian groups.

Definition 6.2.1. *To any Fuchsian group we can associate a fundamental region which is the closure, noted F_Γ, of an open set $\overset{o}{F}_\Gamma \subset \mathbb{D}$ with the following properties:*

(i) *if $\gamma \neq Id \in \Gamma$, then $\gamma \cdot F_\Gamma \cap \overset{o}{F}_\Gamma = \emptyset$;*

(ii) $\bigcup_{\gamma\in\Gamma} \gamma \cdot F_\Gamma = \mathbb{D}$.

The familly $\{\gamma \cdot F_\Gamma \mid \gamma \in \Gamma\}$ is called the tesselation of $\mathbb{D}$.

Fundamental regions may be unnecessarily complicated, in particular they may not be connected. An alternative definition is that of a *Dirichlet region* of a Fuchsian group.

Definition 6.2.2. *Let Γ be a Fuchsian group and $z \in \mathbb{D}$ be not fixed by any element of $\Gamma \setminus Id$. We define the Dirichlet region for Γ centered at z to be the set:*

$$D_z(\Gamma) = \{z' \in \mathbb{D} \mid d_{\mathbb{D}}(z', z) \leq d_{\mathbb{D}}(z', \gamma \cdot z)\ \forall \gamma \in \Gamma\}.$$

From [Katok 1992], we have the following theorem.

Theorem 6.2.1. *If $z \in \mathbb{D}$ is not fixed by any element of $\Gamma\setminus Id$, then $D_z(\Gamma)$ is a connected fundamental region for Γ.*

Let Γ be a Fuchsian group acting on $\mathbb{D}$ with $\mu(\mathbb{D}/\Gamma) < \infty$, and F_γ be a fundamental region for this action. We write $\pi : \mathbb{D} \to \mathbb{D}/\Gamma$ the natural projection and the points of $\mathbb{D}/\Gamma$ are identified with the Γ-orbits. The restriction of π to F_Γ identifies the congruent points of F_Γ that necessarily belong to its boundary ∂F_Γ, and makes $\mathbb{D}/\Gamma$ into an oriented surface. Its topological type is determined by the number of *cusps* and by its *genus*: the number of handles if we view the surface as a sphere with handles. By choosing F_Γ to be Dirichlet region, we can find the topological type of $\mathbb{D}/\Gamma$ (in this case $\mathbb{D}/\Gamma$ is homeomorphic to F_Γ/Γ, see [Katok 1992]). Furthermore, if finite, the area of a fundamental region (with nice boundary) is a numerical invariant of the group Γ. Since the area of the quotient space $\mathbb{D}/\Gamma$ is induced by the hyperbolic area on $\mathbb{D}$, the hyperbolic area of $\mathbb{D}/\Gamma$, denoted by $\mu(\mathbb{D}/\Gamma)$, is well defined and equal to $\mu(F_\Gamma)$ for any fundamental region F_Γ. If Γ has a compact Dirichlet region F_Γ, then F_Γ has finitely many sides and the quotient space $\mathbb{D}/\Gamma$ is compact. If, in addition, Γ acts on $\mathbb{D}$ without fixed points, $\mathbb{D}/\Gamma$ is a compact Riemann surface and its fundamental group is isomorphic to Γ.

Definition 6.2.3. *A Fuchsian group is called cocompact if the quotient space $\mathbb{D}/\Gamma$ is compact.*

When a Fuchsian group is cocompact, then it contains no parabolic elements and its area is finite [Katok 1992]. Furthermore a fundamental region can always be

built as a polygon. The following definition is just a translation to the hyperbolic plane of the definition of an Euclidean lattice.

Definition 6.2.4. *A lattice group of $\mathbb{D}$ is a cocompact Fuchsian group which contains no elliptic element.*

The action of a lattice group has no fixed point, therefore the quotient surface $\mathbb{D}/\Gamma$ is a (compact) manifold and it is in fact a Riemann surface. A remarkable theorem states that any compact Riemann surface is isomorphic to a lattice fundamental domain of $\mathbb{D}$ if and only if it has genus $g \geq 2$ [Katok 1992]. The case $g = 1$ corresponds to lattices in the Euclidean plane (in this case there are three kinds of fundamental domains: rectangles, squares and hexagons). The simplest lattice in $\mathbb{D}$, with genus 2, is generated by an octagon and will be studied in detail in section 6.3.

Given a lattice, we may ask what is the symmetry group of the fundamental domain F_Γ, identified with the quotient surface $\mathbb{D}/\Gamma$. Indeed, this information will play a fundamental role in the subsequent bifurcation analysis. In the case of Euclidean lattice, the quotient $\mathbb{R}^2/\Gamma$ is a torus $\mathbb{T}$ (genus one surface), and the group of automorphisms is $\mathcal{H} \rtimes \mathbb{T}$ where $\mathcal{H}$ is the holohedry of the lattice: $\mathcal{H} = \mathbf{D}_2, \mathbf{D}_4$ or $\mathbf{D}_6$ for the rectangle, square and hexagonal lattices respectively. In the hyperbolic case the group of automorphisms of the surface is finite. In order to build this group we need first to introduce some additional definitions.

Tilings of the hyperbolic plane can be generated by reflections through the edges of a triangle τ with vertices P, Q, R and angles π/ℓ, π/m and π/n respectively, where ℓ, m, n are integers such that $1/\ell + 1/m + 1/n < 1$ [Katok 1992].

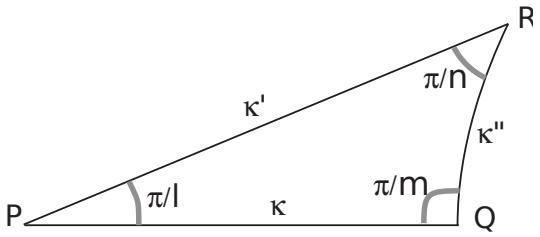

Figure 6.2: The triangle τ, also noted $T(2, 3, 8)$. The values of l, m, and n are $l = 8$, $m = 2$ and $n = 3$.

Remember that reflections are orientation-reversing isometries. We note κ, κ' and κ'' the reflections through the edges PQ, QR and RP respectively (figure 6.2). The group generated by these reflections contains an index 2 Fuchsian subgroup Λ called a triangle group, which always contains elliptic elements because the product of the reflections through two adjacent edges of a polygon is elliptic with fixed point at the corresponding vertex. One easily shows that Λ is generated by the rotations of angles $2\pi/l$, $2\pi/m$ and $2\pi/n$ around the vertices P, Q, R respectively. A fundamental domain of Λ is the "quadrangle" $F_\Lambda = \tau \cup \kappa\tau$ [Katok 1992]. Note that $F_\Lambda \simeq \mathbb{D}/\Lambda$ is a sphere (genus 0 surface) obtained by identifying the three edges of τ. The subgroup of hyperbolic translations in Λ is a lattice group Γ, normal in

Λ, whose fundamental domain is filled with copies of the basic tile τ. The group of orientation-preserving automorphisms of $F_\Gamma \simeq \mathbb{D}/\Gamma$ is therefore $G = \Lambda/\Gamma$. From the algebraic point of view, G is generated by three elements a, b, c satisfy the relations $a^\ell = b^m = c^n = 1$ and $a \cdot b \cdot c = 1$. We say that G is an (l, m, n) group. Taking account of orientation-reversing isometries, the full symmetry group of F_Γ is $G^* = G \cup \kappa G = G \rtimes \mathbb{Z}_2(\kappa)$. This is also a tiling group of F_Γ with tile τ: the orbit $G^*\tau$ fills F_Γ and its elements can only intersect at their edges.

Given a lattice, how to determine the groups G and G^*? The following theorem gives conditions for this, see [Hartshorne 1977].

Theorem 6.2.2. *An (l, m, n) group G is the tiling rotation group of a compact Riemann surface of genus g if and only if its order satisfies the Riemann-Hurwitz relation*

$$|G| = \frac{2g - 2}{1 - (\frac{1}{\ell} + \frac{1}{m} + \frac{1}{n})}.$$

Tables of triangle groups for surfaces of genus up to 13 can be found in [Broughton 2001].

6.2.2 Periodic eigenfunctions of the Laplace-Beltrami operator

Let us first recall the Euclidean setting for functions defined in $\mathbb{R}^2$. In this case every function of the form $e^{\lambda \mathbf{k}\cdot\mathbf{r}}$ where $\mathbf{k} \in \mathbb{R}^2$ is a unit vector, is an eigenfunction of the Laplace operator, denoted $\triangle$, in $\mathbb{R}^2$:

$$\triangle e^{\lambda \mathbf{k}\cdot\mathbf{r}} = -\lambda^2 e^{\lambda \mathbf{k}\cdot\mathbf{r}},\ \mathbf{r} \in \mathbb{R}^2.$$

The fact that the eigenvalues do not depend upon the direction of the wave vector $\mathbf{k}$ reflects the rotational invariance of the Laplace operator. Moreover if we take $\lambda = i\alpha$, $\alpha \in \mathbb{R}$, then $e^{\lambda \mathbf{k}\cdot\mathbf{r}}$ is invariant under translations in $\mathbb{R}^2$ by any vector $\mathbf{e}$ satisfying the condition $\mathbf{k} \cdot \mathbf{e} = 2n\pi$ where $n \in \mathbb{Z}$ (it clearly does not depend upon the coordinate along the axis orthogonal to $\mathbf{k}$). The functions $e^{i\alpha \mathbf{k}\cdot\mathbf{r}}$ are elementary spatial waves in $\mathbb{R}^2$.

Now, given $\alpha > 0$ and a basis of unit vectors $\{\mathbf{k}_1, \mathbf{k}_2\}$ of $\mathbb{R}^2$ we can define the translation group $\mathcal{L}$ spanned by $\mathbf{e}_i$, $i = 1, 2$, such that $\mathbf{k}_i \cdot \mathbf{e}_j = 2\pi/\alpha\delta_{ij}$. Hence $\mathcal{L}$ is a lattice group of $\mathbb{R}^2$. It defines a periodic tiling, the fundamental domain of which is a compact cell which we may identify with the quotient space $\mathbb{R}^2/\mathcal{L}$ and which we can identify with a 2-torus. Any smooth enough function in $\mathbb{R}^2$ which is invariant under the action of $\mathcal{L}$ can be expanded in a Fourier series of elementary spatial waves $e^{i\alpha(m\mathbf{k}_1 + n\mathbf{k}_2)\cdot\mathbf{r}}$, $m, n \in \mathbb{Z}$. The Laplace operator in the space of square-integrable functions in $\mathbb{R}^2/\mathcal{L}$ is self-adjoint and its spectrum consists of real isolated eigenvalues with finite multiplicities. The multiplicity depends upon the *holohedry* of the lattice, which we defined in the previous section (the largest subgroup of $\mathbf{O}(2)$ leaving invariant the lattice). There are five holohedries (see chapter 5). It follows from the above considerations that by restricting the analysis to classes of functions which are invariant under the action of a lattice group, one can apply standard techniques of equivariant bifurcation theory to assert the generic existence

of branches of solutions of Euclidean invariant bifurcation problems, which are spatially periodic with respect to lattice groups and whose properties are largely determined by the holohedry of the lattice [Golubitsky 1988],[Dionne 1992]. Note also this was the approach of [Bressloff 2002c] for the analysis of the occurence of visual hallucinations in the cortex.

We wish to apply the same idea to bifurcation problems defined in $\mathbb{D}$. For this we need to define elementary eigenfunctions of the Laplace-Beltrami operator such that spatially periodic functions (in a sense to be defined later) can be expanded in series of these elementary "waves" in $\mathbb{D}$. We have already seen that the "hyperbolic plane waves" are given by the function $e_{\rho,b}$ in equation (6.2). From theorem 6.1.1, any eigenfunction of $L_{\mathbb{D}}$ can be expressed as an integral over boundary elements.

In the following we will look for solutions of bifurcation problems in $\mathbb{D}$, which are invariant under the action of a lattice group: $\gamma \cdot u(z) = u(\gamma^{-1} z) = u(z)$ for $\gamma \in \Gamma$. This reduces to look at the problem restricted to a fundamental region with suitable boundary conditions imposed by the Γ-periodicity, or, equivalently, to looking for the solutions of the problem projected onto the orbit space $\mathbb{D}/\Gamma$ (which inherits a Riemannian structure from $\mathbb{D}$). Because the fundamental region is compact, it follows from general spectral theory that $L_{\mathbb{D}}$ is self-adjoint, non negative and has compact resolvent in $L^2(\mathbb{D}/\Gamma)$ [Buser 1992]. Hence its spectrum consists of real positive and isolated eigenvalues of finite multiplicity.

Coming back to theorem 6.1.1, we observe that those eigenvalues λ of $L_{\mathbb{D}}$ which correspond to Γ-invariant eigenfunctions, must have $\rho \in \mathbb{R}$ or $\rho \in i\mathbb{R}$. The case ρ real corresponds to the Euclidean situation of planar waves with a given wave number, the role of which is played by ρ in $\mathbb{D}$. In this case the eigenvalues of $L_{\mathbb{D}}$ satisfy $\frac{1}{4} < \lambda$. On the other hand there is no Euclidean equivalent of the case $\rho \in i\mathbb{R}$, for which the eigenvalues $0 < \lambda \leq \frac{1}{4}$ are in finite number. It turns out that such "exceptional" eigenvalues do not occur for "simple" groups such as the octagonal group to be considered in more details in the Section 6.3. This follows from formulas which give lower bounds for these eigenvalues. Let us give two examples of such estimates (derived by Buser [Buser 1992], see also [Iwaniec 2002]): (i) if g is the genus of the surface $\mathbb{D}/\Gamma$, there are at most $3g-2$ exceptional eigenvalues; (ii) if d is the diameter of the fundamental region, then the smallest (non zero) eigenvalue is bounded from below by $\left(4\pi \sinh \frac{d}{2}\right)^{-2}$.

Suppose now that the eigenfunction in theorem 6.1.1 is Γ-periodic. Then the distribution T_ρ satisfies the following equivariance relation [Pollicott 1989]. Let $\gamma(\theta)$ denote the image of $\theta \in \partial\mathbb{D}$ under the action of $\gamma \in \Gamma$. Then

$$T_\rho(\gamma \cdot \theta) = |\gamma'(\theta)|^{\frac{1}{2}+i\rho} T_\rho(\theta). \tag{6.10}$$

Remark 6.2.1. *As observed by [Series 1987], this condition is not compatible with T_ρ being a "nice" function. In fact, not only does there exist no explicit formula for these eigenfunctions, but their approximate computation is itself an uneasy task. We shall come back to this point in the next chapter.*

6.2.3 Bifurcation of patterns in the Poincaré disk

We consider equation (3.19). Assuming $I_{ext} = 0$ (no external input) and that the sigmoidal function is centered at the origin (such that $V = 0$ is a trivial solution of (3.19)), the equation (3.19) can be written

$$\frac{d}{dt}V(z,t) = -V(z,t) + \mu \mathbf{W}_{loc} * V(z,t) + \mathcal{R}(V(z,t)) \tag{6.11}$$

where:

- $\mu = S'(0)$,
- $\mathbf{W}_{loc} * V$ denotes the convolution product defined in equation (6.9) with the notation $\mathbf{W}_{loc}(z) = W_{loc}(d_{\mathbb{D}}(z, O))$,
- $\mathcal{R}(V)$ stands for the remainder terms in the integral part of equation (3.19),
- $\mathcal{R}(0) = D_V\mathcal{R}(0) = 0$.

Let us look at the linear stability of the trivial solution of (6.11) against perturbations in the form of hyperbolic waves (6.2) with $\rho \in \mathbb{R}$. Using lemma 6.1.2, this comes back to looking for σ's such that

$$\sigma(\rho) = -1 + \mu\widetilde{\mathbf{W}}_{loc}(\rho)$$

where $\widetilde{\mathbf{W}}_{loc}(\rho)$ is the Fourier-Helgason transform of $\mathbf{W}_{loc}$ as defined in (6.5). For a connectivity function $x \to W_{loc}(x)$ with a "Mexican hat" shape, the numerical calculation shows that for each value of ρ, there exists a value $\mu(\rho)$ such that if $\mu < \mu(\rho)$ then all σ's are negative, while $\sigma = 0$ at $\mu = \mu(\rho)$. The "neutral stability surface" defined by $\mu(\rho)$ is typically convex and reaches a minimum μ_c at some value ρ_c. Therefore when $\mu < \mu_c$ the trivial state $V = 0$ is stable against such perturbations while it becomes marginally stable when $\mu = \mu_c$ with critical modes $e_{\rho_c,b}$, for any $b \in S^1$ (rotational invariance). Therefore a bifurcation takes place at this critical value.

The situation is absolutely similar if instead of equation (6.11) we consider systems of PDEs in $\mathbb{D}$ with pattern selection behavior and with $\mathbf{U}(1,1)$ invariance. A paradigm for such systems is the "Laplace-Beltrami" version of Swift-Hohenberg equation

$$\frac{\partial u}{\partial t} = \mu u - (L_{\mathbb{D}} + \alpha)^2 u + u^2, \quad \alpha \in \mathbb{R}_*^+.$$

with $L_{\mathbb{D}}$ as in (6.1).

It is not possible to solve the bifurcation problem at this level of generality, because the fact that the spectrum is continuous plus that each eigenvalue σ has an infinite multiplicity (indifference to b) makes it impossible to use classical tools of bifurcation theory. As in the Euclidean case of pattern formation, we therefore want to look for solutions in a restricted class of patterns. In this chapter we look for periodic patterns, which means looking for bifurcating patterns which are invariant

under the action of a lattice group Γ in $\mathbf{SU}(1,1)$. There is however an immediate big difference with the Euclidean case. While in the latter any critical wave number α_c can be associated with a periodic lattice (of period $2\pi/\alpha_c$), in the hyperbolic case not every value of ρ_c can be associated with a lattice in $\mathbb{D}$. We can therefore look for the bifurcation of spatially periodic solutions associated with a given lattice, but these patterns will not in general correspond to the most unstable perturbations unless the parameters in the equations are tuned so that it happens this way. The question of the observability of such patterns is therefore completely open.

We henceforth look for patterns in $\mathbb{D}$ which are invariant under a lattice Γ in $\mathbb{D}$ and which are periodic. This reduces to look at solutions in the space $L^2(\mathbb{D}/\Gamma)$. With a suitable inner product this space admits an orthonormal Hilbert basis which is made of functions of the form

$$\Psi(z), \quad z \in \mathbb{D}$$

where Ψ are the eigenfunctions of $L_{\mathbb{D}}$ in $L^2(\mathbb{D}/\Gamma)$. As we mentioned in the previous section, these eigenfunctions are not known explicitly. By restricting the "neutral stability surface" $\mu(\rho)$ to those values which correspond to eigenfunctions with Γ periodicity, we obtain a discrete set of points on this surface with one minimum μ_0 associated with a value ρ_0 of ρ. In general this minimum is unique. Moreover the multiplicity of the 0 eigenvalue is now finite and this eigenvalue is semi-simple. Let us call X the eigenspace associated with the 0 eigenvalue (therefore X is the kernel of the critical linear operator).

The full symmetry group of $\mathbb{D}/\Gamma$ is equal to $\mathcal{G}$ where $\mathcal{G}$ is the (finite) group of automorphisms in $\mathbf{U}(1,1)$ of the Riemann surface $\mathbb{D}/\Gamma$. The equation restricted to this class of Γ-periodic patterns is invariant under the action of $\mathcal{G}$. We can therefore apply an equivariant Lyapunov-Schmidt reduction to this bifurcation problem [Chossat 2000], leading to a bifurcation equation in X

$$f(x,\mu) = 0, \quad x \in X \tag{6.12}$$

where $f : X \times \mathbb{R} \to X$ is smooth, $f(0,0) = 0$, $\partial_x f(0,0)$ is not invertible and $f(\cdot,\mu)$ commutes with the action of $\mathcal{G}$ in X.

Now the methods of equivariant bifurcation theory can be applied to (6.12). In particular we can apply the Equivariant Branching lemma (see chapter 4):

Theorem 6.2.3 (Equivariant Branching Lemma). *Suppose the action of $\mathcal{G}$ is absolutely irreducible in X (i.e. real equivariant linear maps in X are scalar multiple of the identity). Let H be an isotropy subgroup of $\mathcal{G}$ such that the subspace $X^H = \{x \in X \mid H \cdot x = x\}$ is one dimensional. Then generically a branch of solutions of (6.12) bifurcates in X^H. The conjugacy class of H (or isotropy type) is called "symmetry breaking".*

Let us briefly recall the meaning of this theorem. By equivariance of f, any subspace of X defined as X^H, H a (closed) subgroup of $\mathcal{G}$, is invariant under f. By the irreducibility assumption, if $H = \mathcal{G}$, then $\{x \in X \mid H \cdot x = x\} = \{0\}$. Therefore $f(0,\mu) = 0$ for all μ. Now the assumption of absolute irreducibility

implies that $\partial_x f(0,\mu) = a(\mu) Id_X$ where a is a smooth real function such that $a(0) = 0$ and generically $a'(0) \neq 0$. It follows that if now H is a subgroup such that $\dim X^H = 1$, then equation (6.12) restricted to this subspace reduces to a scalar equation $0 = a'(0)\mu x + x h(x,\mu)$ (with $h(0,0) = 0$), which has a branch of non trivial solutions by the implicit function theorem.

Remark 6.2.2. *The word "generically" can be interpreted as follows: the result is true unless additional degeneracies are introduced in the equations.*

Remark 6.2.3. *The assumption of absolute irreducibility is itself generic (in the above stated sense) for one-parameter steady-state bifurcation problems. A given irreducible representation of a compact or finite group need not be absolutely irreducible, this fact has to be proven.*

Remark 6.2.4. *Theorem 6.2.3 does not necessarily give an account of all possible branches of solutions of (6.12), see [Chossat 2000] and [Field 1989b]. It gives nevertheless a large set of generic ones. To go further it is necessary to compute the equivariant structure of f, or at least of its Taylor expansion to a sufficient order. The same is true if one wants to determine the stability of the bifurcated solutions, within the class of Γ periodic solutions of the initial evolution equation.*

This theorem, together with the knowledge of the lattices and the (absolutely) irreducible representations of the groups $\mathcal{G}$, gives us a mean to classify the periodic patterns which can occur in $\mathbb{D}$. By analogy with the Euclidean case (bifurcation of spatially periodic solutions in the Euclidean space), we call *H-planforms* the solutions of a $\mathbf{U}(1,1)$ invariant bifurcation problem in $\mathbb{D}$, which are invariant by a lattice group Γ.

Being interested in this chapter in the classification of solutions rather than in their actual computation for a specific equation, all remains to do is to determine the absolutely real irreducible representations of the group $\mathcal{G}$ and the computation of the dimensions of the subspaces X^H. Once the irreducible representations are known, this can be achieved by applying the "trace formula" [Golubitsky 1988, Chossat 2000]:

Proposition 6.2.1. *Let H be a subgroup of $\mathcal{G}$ acting in a space X by a representation $\rho : \mathcal{G} \to Aut(X)$, then*

$$\dim(V^H) = \frac{1}{|H|} \sum_{h \in H} \mathrm{tr}(\rho(h)). \tag{6.13}$$

Note that $\mathrm{tr}(\rho)$ is the character of the representation ρ (a homomorphism $\mathcal{G} \to \mathbb{C}$). What is really needed to apply the Equivaraint Branching Lemma is therefore the character table of the representations. In the next section we investigate this classification in the case when the lattice is the regular octagonal group.

6.3 A case study: the octagonal lattice

6.3.1 The octagonal lattice and its symmetris

Among all lattices in the hyperbolic plane, the octagonal lattice is the simplest one. As before we use the Poincaré disc representation of the hyperbolic plane. Then the octagonal lattice group Γ is generated by the following four hyperbolic translations (boosts), see [Balazs 1986]:

$$g_0 = \begin{pmatrix} 1+\sqrt{2} & \sqrt{2+2\sqrt{2}} \\ \sqrt{2+2\sqrt{2}} & 1+\sqrt{2} \end{pmatrix} \tag{6.14}$$

and $g_j = r_{j\pi/4} g_0 r_{-j\pi/4}$, $j = 1, 2, 3$, where r_φ indicates the rotation of angle φ around the origin in $\mathbb{D}$. A fundamental domain of the lattice is the regular octagon $\mathcal{O}$ as shown in Figure 6.3. The opposite sides of the octagon are identified by periodicity, so that the corresponding quotient surface $\mathbb{D}/\Gamma$ is isomorphic to a "double doughnut" (genus two surface) [Balazs 1986]. Note that the same octagon is also the fundamental domain of another group, not isomorphic to Γ, obtained by identifying not the opposite sides but pairs of sides as indicated in Figure. This is called the Gutzwiller octagon. A procedure of classification of the lattices using graphs is presented in [Sausset 2007]. For us however there is no difference between the two kinds of octagons because we are really interested in the full symmetry group of the pattern generated by Γ, which includes the rotations $r_{j\pi/4}$, $j = 1, \cdots, 8$, and therefore the boosts $r_{\pi/2} g_0^{-1}$, $g_1 r_{-\pi/2}$ and their conjugates by the rotation r_π, which are precisely the generators of the Gutzwiller lattice group.

We now determine what is the full symmetry group $\mathcal{G}$ of the octagonal lattice, or equivalently, of the surface $\mathbb{D}/\Gamma$. Clearly the symmetry group of the octagon itself is part of it. This is the dihedral group $\mathbf{D}_8$ generated by the rotation $r_{\pi/4}$ and by the reflection κ through the real axis, but there is more. We have seen in section 6.2.1 that $\mathcal{G} = \Lambda/\Gamma$, Λ being the "triangle group" generated by reflections through the edges of a triangle τ which tiles (by the action of Λ/Γ) the surface $\mathbb{D}/\Gamma$. The smallest triangle (up to symmetry) with these properties is the one shown in Figure 6.2. It has angles $\pi/8$, $\pi/2$ and $\pi/3$ at vertices $P = O$ (the center of $\mathbb{D}$), Q, R respectively, and its area is, by Gauss-Bonnet formula, equal to $\pi/24$. There are exactly 96 copies of τ filling the octagon, hence $|\mathcal{G}| = 96$. The index two subgroup G of orientation-preserving transformations in $\mathcal{G}$ has therefore 48 elements. In [Broughton 1991] it has been found that $G \simeq \mathbf{GL}(2,3)$, the group of invertible 2×2 matrices over the 3 elements field $\mathbb{Z}_3$. In summary:

Proposition 6.3.1. *The full symmetry group $\mathcal{G}$ of $\mathbb{D}/\Gamma$ is $G \cup \kappa G$ where $G \simeq \mathbf{GL}(2,3)$ has 48 elements.*

The isomorphism between $\mathbf{GL}(2,3)$ and G can be built as follows. We use the notation $\mathbb{Z}_3 = \{0, 1, 2\}$ and we call ρ the rotation by $\pi/4$ centered at P (mod Γ), σ the rotation by π centered at Q (mod Γ) and ε the rotation by $2\pi/3$ centered at R (mod Γ). In the notations of section 6.2.1, $a = \sigma$, $b = \varepsilon$, $c = \rho$, and $\rho\sigma\varepsilon = 1$. Then we can take

$$\rho = \begin{pmatrix} 0 & 2 \\ 2 & 2 \end{pmatrix}, \ \sigma = \begin{pmatrix} 2 & 0 \\ 0 & 1 \end{pmatrix}, \ \varepsilon = \begin{pmatrix} 2 & 1 \\ 2 & 0 \end{pmatrix}$$

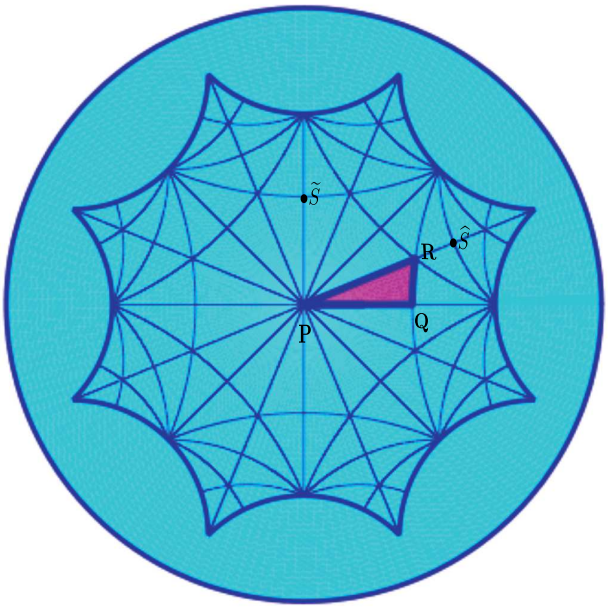

Figure 6.3: Tesselation of the hyperbolic octagon with the triangle $T(2,3,8)$, colored in purple in the plot. We define two points $\widehat{S}$ and $\widetilde{S}$. $\widehat{S}$ is the center of the rotation $\hat{\sigma}$ by π (mod Γ), see text in subsection 6.3.1. $\widetilde{S}$ is the center of the rotation $\tilde{\sigma}$ by π (mod Γ), see text in subsection 6.3.1.

since these matrices satisfy the conditions $\rho^8 = \sigma^2 = \varepsilon^3 = Id$ and $\rho\sigma\varepsilon = Id$. Note that $\rho^4 = -Id$ where Id is the identity matrix. We shall subsequently use this notation. The group $\mathbf{GL}(2,3)$, therefore the group G, is made of 8 conjugacy classes which we list in Table 6.1, indicating one representative, the number of elements in each class and their order. This result is classical and can be found, e.g., in [Lang 1993].

representative	Id	ρ	ρ^2	$-Id$	ρ^5	σ	ε	$-\varepsilon$
order	1	8	4	2	8	2	3	6
# elements	1	6	6	1	6	12	8	8

Table 6.1: Conjugacy classes of $G \simeq \mathbf{GL}(2,3)$.

We now turn to the full symmetry group $\mathcal{G}$ which is generated by G and κ, the reflection through the real axis in $\mathbb{D}$ and which maps the octagon $\mathcal{O}$ to itself. We write $\kappa' = \rho\kappa$ the reflection through the side PR of the triangle τ. Note that (i) κ' preserves also $\mathcal{O}$, (ii) $\kappa'' = \varepsilon\kappa' = \sigma\kappa$ is the reflection through the third side QR.

In what follows we rely on the group algebra software GAP (see [Schönert 1995]). For this we have first identified a presentation for $G \simeq \mathbf{GL}(2,3)$ considered as an abstract group, then a presentation for $\mathcal{G}$. The presentation for $\mathbf{GL}(2,3)$ can be obtained with the command "P := PresentationViaCosetTable(GL(2,3))" and the

class number	1	2	3	4	5	6	7
representative	Id	ρ	ρ^2	$-Id$	σ	ε	$-\varepsilon$
order	1	8	4	2	2	3	6
# elements	1	12	6	1	12	8	8

Table 6.2: Conjugacy classes of $\mathcal{G}$, orientation preserving transformations.

class number	8	9	10	11	12	13
representative	κ	κ'	$\widehat{\sigma}\kappa$	$\rho\widehat{\sigma}\kappa$	$\varepsilon\kappa$	$-\varepsilon\kappa$
order	2	2	8	4	12	12
# elements	6	12	12	2	8	8

Table 6.3: Conjugacy classes of $\mathcal{G}$, orientation reversing transformations

relations are shown with the command "TzPrintRelators(P)":

Lemma 6.3.1. *(i) As an abstract group, G is presented with two generators a and b and three relations $a^2 = 1$, $b^3 = 1$ and $(abab^{-1}ab^{-1})^2 = 1$. (ii) As an abstract group, $\mathcal{G}$ is presented with three generators a, b and c and six relations: the three relations for G plus the three relations $c^2 = 1$, $(ca)^2 = 1$ and $(cb)^2 = 1$.*
(iii) These abstract elements can be identified with automorphisms of $\mathbb{D}/\Gamma$ as follows: $a = \sigma$, $b = \varepsilon$ and $c = \kappa''$.

Applying the above lemma we find with GAP that the 96 elements group $\mathcal{G}$ has 13 conjugacy classes which are listed in table 6.2 for direct isometries and in table 6.3 for isometries which reverse orientation. GAP gives representatives of the conjugacy classes in the abstract presentation, which in general have complicated expressions. In some cases we have chosen other representatives, using in particular the 8-fold generator. To simplify some expressions in the tables 6.2 to 6.5 we also use the notations

$$\widehat{\sigma} = \varepsilon\sigma\varepsilon^{-1}, \quad \widetilde{\sigma} = \rho^2\sigma\rho^{-2},$$

where $\widehat{\sigma}$ is the rotation by π centered at $\widehat{S}$ (mod Γ) and $\widetilde{\sigma}$ is the rotation by π centered at $\widetilde{S}$ (mod Γ), see figure 6.3.

We shall also need in Section 6.3.3 the list of subgroups of $\mathcal{G}$ together with their decomposition in conjugacy classes (in $\mathcal{G}$) in order to apply the trace formula (6.13). Here again we rely on GAP to obtain the necessary informations.

Then representatives of each class are determined by inspection. These data are listed in tables 6.4 (subgroups of G) and 6.5 (subgroups containing orientation reversing elements). The subgroups are listed up to conjugacy in $\mathcal{G}$, the subgroups of order two are not listed. The rationale for the notations is as follows:

- G_0 is an index 2 subgroup of G. Seen as a subgroup of $\mathbf{GL}(2,3)$ it is $\mathbf{SL}(2,3)$, the subgroup of determinant 1 matrices. It contains no order 2 elements except $-Id$ and no order 8 elements.

- $\mathbf{C}_n$, $\widetilde{\mathbf{C}}_n$, $\mathbf{C}'_n$, denote order n cyclic groups. The notation $\mathbf{C}_n$ is standard for the n-fold rotation group centered at the origin.

- $\mathbf{D}_n$ denotes a group isomorphic to the dihedral group of order $2n$, generated by an n-fold rotation and a reflection. Hence $\mathbf{D}_8$ is the symmetry group of the octagon. The notation $\widetilde{\mathbf{D}}_n$ is used for a $2n$ element group which has an n-fold rotation and a 2-fold rotation as generators. For example $\widetilde{\mathbf{D}}_8 =< \rho,\ \widehat{\sigma} >$, and one can verify that $\widehat{\sigma}\rho\widehat{\sigma}^{-1} = \rho^3$, which makes $\widetilde{\mathbf{D}}_8$ a *quasidihedral group* (see [Gorenstein 1980]).

- $\mathbf{Q}_8$ is a usual notation for the 8 elements quaternionic group.

- The notation $H_{n\kappa}$ indicates a group generated by the group H_n and κ. Same thing if replacing κ by κ'. For example $\widetilde{\mathbf{C}}_{3\kappa'}$ is the 6 elements group generated by $\widetilde{\mathbf{C}}_3$ and κ'.

Subgroup	Order	Generators	Subclasses: representatives (# elements)
$G_0 \simeq \mathbf{SL}(2,3)$	24	$< \rho^2,\ \varepsilon >$	$\{Id\ (1),\ -Id\ (1),\ \rho^2\ (6),\ \varepsilon\ (8),\ -\varepsilon\ (8)\}$
$\widetilde{\mathbf{D}}_8$	16	$< \rho,\ \widehat{\sigma} >$	$\{Id\ (1),\ -Id\ (1),\ \rho\ (4),\ \rho^2\ (6),\ \widehat{\sigma}\ (4)\}$
$\widetilde{\mathbf{D}}_6$	12	$< -\varepsilon,\ \widetilde{\sigma} >$	$\{Id\ (1),\ -Id\ (1),\ \widetilde{\sigma}\ (6),\ \varepsilon\ (2),\ -\varepsilon\ (2)\}$
$\mathbf{C}_8$	8	$< \rho >$	$\{Id\ (1),\ -Id\ (1),\ \rho\ (4),\ \rho^2\ (2)\}$
$\mathbf{Q}_8$	8	$< \rho^2,\ \sigma\rho^2\sigma >$	$\{Id\ (1),\ -Id\ (1),\ \rho^2\ (6)\}$
$\widetilde{\mathbf{D}}_4$	8	$< \rho^2,\ \widehat{\sigma} >$	$\{Id\ (1),\ -Id\ (1),\ \rho^2\ (2),\ \widehat{\sigma}\ (4)\}$
$\widetilde{\mathbf{C}}_6$	6	$< -\varepsilon >$	$\{Id\ (1),\ -Id\ (1),\ \varepsilon\ (2),\ -\varepsilon\ (2)\}$
$\widetilde{\mathbf{D}}_3$	6	$< \varepsilon,\ \widetilde{\sigma} >$	$\{Id\ (1),\ \varepsilon\ (2),\ \widetilde{\sigma}\ (3)\}$
$\mathbf{C}_4$	4	$< \rho^2 >$	$\{Id\ (1),\ -Id\ (1),\ \rho^2\ (2)\}$
$\widetilde{\mathbf{D}}_2$	4	$< -Id, \sigma >$	$\{Id\ (1),\ -Id\ (1),\ \sigma\ (2)\}$
$\widetilde{\mathbf{C}}_3$	3	$< \varepsilon >$	$\{Id\ (1),\ \varepsilon\ (2)\}$
$\mathbf{C}_2$	2	$< -Id >$	$\{Id\ (1),\ -Id\ (1)\}$
$\widetilde{\mathbf{C}}_2$	2	$< \sigma >$	$\{Id\ (1),\ \sigma\ (1)\}$

Table 6.4: Subgroups of $G \subset \mathcal{G}$ (up to conjugacy). The last column provides datas about their conjugacy subclasses (in $\mathcal{G}$).

6.3.2 Irreducible representation of the octagonal group

There are 13 conjugacy classes and therefore we know there are 13 complex irreducible representations of $\mathcal{G}$, the characters of which will be denoted χ_j, $j = 1, ..., 13$. The character table, as computed by GAP, is shown in table 6.6.

The character of the identity is equal to the dimension of the corresponding representation. It follows from table 6.6 that there are 4 irreducible representations of dimension 1, 2 of dimension 2, 4 of dimension 3 and 3 of dimension 4. In the

Subgroup	Order	Generators	Subclasses: representatives (# elements)
$G_{0\kappa}$	48	$< G_0,\ \kappa >$	$G_0 \cup \{\kappa\ (6),\ \rho\widehat{\sigma}\kappa\ (2),\ \varepsilon\kappa\ (8),\ -\varepsilon\kappa\ (8)\}$
$G_{0\kappa'}$	48	$< G_0,\ \kappa' >$	$G_0 \cup \{\kappa'\ (12),\ \widehat{\sigma}\kappa\ (12)\}$
$\widetilde{\mathbf{D}}_{8\kappa}$	32	$< \widetilde{\mathbf{D}}_8,\ \kappa >$	$\widetilde{\mathbf{D}}_8 \cup \{\kappa\ (6),\ \kappa'\ (4),\ \widehat{\sigma}\kappa\ (4),\ \rho\widehat{\sigma}\kappa\ (2)\ \}$
$\widetilde{\mathbf{D}}_{6\kappa'}$	24	$< \widetilde{\mathbf{D}}_6,\ \kappa' >$	$\widetilde{\mathbf{D}}_6 \cup \{\kappa'\ (6),\ \varepsilon\kappa\ (2),\ -\varepsilon\kappa\ (2),\ \rho\widehat{\sigma}\kappa\ (2)\}$
$\mathbf{C}_{8\kappa}\ (=\mathbf{D}_8)$	16	$< \mathbf{C}_8,\ \kappa >$	$\mathbf{C}_8 \cup \{\kappa\ (4),\ \kappa'\ (4)\}$
$\mathbf{C}'_{8\kappa}$	16	$< \rho^2\sigma,\ \kappa >$	$\mathbf{C}_8 \cup \{\kappa\ (2),\ \rho\widehat{\sigma}\kappa\ (2),\ \widehat{\sigma}\kappa\ (4)\}$
$\mathbf{Q}_{8\kappa}$	16	$< \mathbf{Q}_8,\ \kappa >$	$\mathbf{Q}_8 \cup \{\kappa\ (6),\ \rho\widehat{\sigma}\kappa\ (2)\}$
$\mathbf{Q}_{8\kappa'}$	16	$< \mathbf{Q}_8,\ \kappa' >$	$\mathbf{Q}_8 \cup \{\kappa'\ (4),\ \widehat{\sigma}\kappa\ (4)\}$
$\widetilde{\mathbf{D}}_{4\kappa}$	16	$< \widetilde{\mathbf{D}}_4,\ \kappa >$	$\widetilde{\mathbf{D}}_4 \cup \{\kappa\ (4),\ \widehat{\sigma}\kappa\ (4)\}$
$\widetilde{\mathbf{D}}_{4\kappa'}$	16	$< \widetilde{\mathbf{D}}_4,\ \kappa' >$	$\widetilde{\mathbf{D}}_4 \cup \{\kappa\ (2),\ \kappa'\ (4),\ \rho\widehat{\sigma}\kappa\ (2)\}$
$\mathbf{C}'_{12}$	12	$< \varepsilon\kappa >$	$\widetilde{\mathbf{C}}_6 \cup \{\varepsilon\kappa\ (2),\ -\varepsilon\kappa\ (2),\ \rho\widehat{\sigma}\kappa\ (2)\}$
$\widetilde{\mathbf{C}}_{6\kappa'}$	12	$< \widetilde{\mathbf{C}}_6, \kappa' >$	$\widetilde{\mathbf{C}}_6 \cup \{\kappa'\ (6)\}$
$\mathbf{C}'_8$	8	$< \widehat{\sigma}\kappa >$	$\mathbf{C}_4 \cup \{\widehat{\sigma}\kappa\ (4)\}$
$\mathbf{C}_{4\kappa}\ (=\mathbf{D}_4)$	8	$< \mathbf{C}_4, \kappa >$	$\mathbf{C}_4 \cup \{\kappa\ (4)\}$
$\mathbf{C}_{4\kappa'}$	8	$< \mathbf{C}_4, \kappa' >$	$\mathbf{C}_4 \cup \{\kappa'\ (4)\}$
$\widetilde{\mathbf{D}}_{2\kappa}$	8	$< \widetilde{\mathbf{D}}_2, \kappa >$	$\widetilde{\mathbf{D}}_2 \cup \{\kappa\ (2),\ \kappa'\ (2)\}$
$\mathbf{C}'_{4\kappa}$	8	$< \mathbf{C}'_4, \kappa >$	$\mathbf{C}'_4 \cup \{\rho^2\ (2),\ \kappa\ (2)\}$
$\mathbf{C}'_{4\kappa'}$	8	$< \mathbf{C}'_4, \kappa' >$	$\mathbf{C}'_4 \cup \{\sigma\ (2),\ \kappa'\ (2)\}$
$\widetilde{\mathbf{C}}_{3\kappa'}$	6	$< \widetilde{\mathbf{C}}_3, \kappa' >$	$\widetilde{\mathbf{C}}_3 \cup \{\kappa'\ (3)\}$
$\mathbf{C}'_4$	4	$< \rho\widehat{\sigma}\kappa >$	$\{Id\ (1),\ -Id\ (1),\ \rho\widehat{\sigma}\kappa\ (2)\}$
$\mathbf{C}_{2\kappa}$	4	$< -Id, \kappa >$	$\{Id\ (1),\ -Id\ (1),\ \kappa\ (2)\}$
$\mathbf{C}_{2k'}$	4	$< -Id, \kappa' >$	$\{Id\ (1),\ -Id\ (1),\ \kappa'\ (2)\}$
$\widetilde{\mathbf{C}}_{2k}$	4	$< \sigma, \kappa >$	$\{Id\ (1),\ \sigma\ (1),\ \kappa\ (1),\ \kappa'\ (1)\}$
$\widetilde{\mathbf{C}}'_{2\kappa}$	4	$< \widetilde{\sigma}, \kappa >$	$\{Id\ (1),\ \widetilde{\sigma}\ (1),\ \kappa\ (1),\ \kappa'\ (1)\}$
$\mathbf{C}_{1\kappa}$	2	$< \kappa >$	$\{Id\ (1),\ \kappa\ (1)\}$
$\mathbf{C}_{1\kappa'}$	2	$< \kappa' >$	$\{Id\ (1),\ \kappa'\ (1)\}$

Table 6.5: Subgroups of $\mathcal{G}$, not in G (up to conjugacy). The last column provides datas about their conjugacy subclasses (in $\mathcal{G}$). $\widetilde{\mathbf{C}}_4$ is a subgroup conjugate to $\mathbf{C}_4$ with generator $(\rho^2\sigma)^2$.

Class #	1	2	3	4	5	6	7	8	9	10	11	12	13
Representative	Id	ρ	ρ^2	$-Id$	σ	ε	$-\varepsilon$	κ	κ'	$\widehat{\sigma}\kappa$	$\rho\widehat{\sigma}\kappa$	$\varepsilon\kappa$	$-\varepsilon\kappa$
χ_1	1	1	1	1	1	1	1	1	1	1	1	1	1
χ_2	1	-1	1	1	-1	1	1	1	-1	-1	1	1	1
χ_3	1	-1	1	1	-1	1	1	-1	1	1	-1	-1	-1
χ_4	1	1	1	1	1	1	1	-1	-1	-1	-1	-1	-1
χ_5	2	0	2	2	0	-1	-1	-2	0	0	-2	1	1
χ_6	2	0	2	2	0	-1	-1	2	0	0	2	-1	-1
χ_7	3	1	-1	3	-1	0	0	-1	-1	1	3	0	0
χ_8	3	1	-1	3	-1	0	0	1	1	-1	-3	0	0
χ_9	3	-1	-1	3	1	0	0	1	-1	1	-3	0	0
χ_{10}	3	-1	-1	3	1	0	0	-1	1	-1	3	0	0
χ_{11}	4	0	0	-4	0	-2	2	0	0	0	0	0	0
χ_{12}	4	0	0	-4	0	1	-1	0	0	0	0	$\sqrt{3}$	$-\sqrt{3}$
χ_{13}	4	0	0	-4	0	1	-1	0	0	0	0	$-\sqrt{3}$	$\sqrt{3}$

Table 6.6: Irreducible characters of $\mathcal{G}$

following we shall denote the irreducible representations by their character: χ_j is the representation with this character.

Lemma 6.3.2. *All irreducible representations of $\mathcal{G}$ listed in table 6.6 are real absolutely irreducible.*

Proof.

(i) This is clear for the one dimensional representations whose characters are real.

(ii) For the two dimensional representations, let us consider the dihedral subgroup $\mathbf{D}_3$ generated by the 3-fold symmetry ε and the reflection κ'. The representation of $\mathbf{D}_3$ in either representations planes of χ_5 and χ_6 have characters $\chi_j(\varepsilon) = -1$ and $\chi_j(\kappa') = 0$ ($j = 5$ or 6). These are the characters of the 2D irreducible representation of $\mathbf{D}_3$, which is absolutely irreducible, and therefore the representations χ_5 and χ_6 of $\mathcal{G}$ are also absolutely irreducible. Indeed if any real linear map which commutes with the elements of a subgroup is a scalar multiple of the identity, this is a fortiori true for the maps which commute with the full group.

(iii) For the three dimensional representations χ_7 to χ_{10}, let us first remark that if we write $\mathbf{C}_2 = \{Id, -Id\}$, then $G/\mathbf{C}_2 \simeq \mathbb{O}$, the octahedral group. Its subgroup $\mathbb{T}$ (tetrahedral group) can easily be identified with the 12 elements group generated by the "pairs" $\{Id, -Id\}$, $\{\varepsilon, -\varepsilon\}$ and $\{\rho^2, -\rho^2\}$. Now we consider the representation of G defined by the action of χ_j restricted to G (for each 3D χ_j). One can check easily from the character table that it projects onto a representation of $\mathcal{G}/\mathbf{C}_2$, the character of which is given by the value of χ_j on the corresponding conjugacy classes, and in particular the

character for the representation of the group $\mathbb{T}$ is given, for any $j = 7$ to 10, by $\chi_j(\{Id, -Id\}) = 3$, $\chi_j(\{\varepsilon, -\varepsilon\}) = 0$ and $\chi_j(\{\rho^2, -\rho^2\}) = -1$. But this is the character of the irreducible representation of $\mathbb{T}$ [Miller 1972], which is absolutely irreducible (natural action of $\mathbb{T}$ in $\mathbb{R}^3$). Hence the three dimensional representations of $\mathcal{G}$ are absolutely irreducible by the same argument as above.

(iv) It remains to prove the result for the four dimensional representations χ_{11}, χ_{12} and χ_{13}. For this we consider the action of the group $\mathbf{D}_8$ generated by ρ and κ, as defined by either one of these 4D irreducible representations of $\mathcal{G}$. We observe from the character table that in all cases, the character of this action is $\chi(\rho) = 0$, $\chi(\rho^2) = 0$, $\chi(-Id) = -4$, $\chi(\rho^3) = 0$ (ρ and ρ^3 are conjugate in $\mathcal{G}$), and $\chi(\kappa) = \chi(\kappa') = 0$. We can determine the isotypic decomposition for this action of $\mathbf{D}_8$ from these character values. The character tables of the four one dimensional and three two dimensional irreducible representations of $\mathbf{D}_8$ can be computed easily either by hand (see [Miller 1972] for the method) or using a computer group algebra software like GAP. For all one dimensional characters the value at $-Id$ is 1, while for all two dimensional characters, the value at $-Id$ is -2. Since $\chi(-Id) = -4$, it is therefore not possible to have one dimensional representations in this isotypic decomposition. It must therefore be the sum of two representations of dimension 2. Moreover, since $\chi(\rho) = \chi(\rho^2) = \chi(\rho^3) = 0$, it can't be twice the same representation. In fact it must be the sum of the representations whose character values at ρ are $\sqrt{2}$ and $-\sqrt{2}$ respectively. Now, these representations are absolutely irreducible (well-know fact which is straightforward to check), hence any $\mathbf{D}_8$-equivariant matrix which commutes with this action decomposes into a direct sum of two scalar 2×2 matrices λI_2 and μI_2 where λ and μ are real. But the representation of $\mathcal{G}$ is irreducible, hence $\lambda = \mu$, which proves that it is also absolutely irreducible.

□

6.3.3 Octagonal H-planforms

We can now apply Theorem 6.2.3 in order to determine the H-planforms for the octagonal lattice.

Theorem 6.3.1. *The irreducible representations of $\mathcal{G}$ admit H-planforms with the following isotropy types:*

- χ_1: $\mathcal{G}$;
- χ_2: $G_{0\kappa}$;
- χ_3: $G_{0\kappa'}$;
- χ_4: $G \simeq \mathbf{G}L(2,3)$;
- χ_5: $\widetilde{\mathbf{D}}_8$, $\mathbf{Q}_{8\kappa'}$;

- χ_6: $\widetilde{\mathbf{D}}_{8\kappa}$;
- χ_7: $\mathbf{C}'_{8\kappa}$, $\mathbf{C}'_{12}$, $\mathbf{C}_{4\kappa'}$;
- χ_8: $\mathbf{C}_{8\kappa}$, $\widetilde{\mathbf{C}}_{6\kappa'}$, $\widetilde{\mathbf{D}}_{2\kappa}$;
- χ_9: $\widetilde{\mathbf{D}}_6$, $\widetilde{\mathbf{D}}_{4\kappa}$;
- χ_{10}: $\widetilde{\mathbf{D}}_{6\kappa'}$, $\widetilde{\mathbf{D}}_{4\kappa'}$;
- χ_{11}: $\widetilde{\mathbf{C}}_{2\kappa}$, $\widetilde{\mathbf{C}}'_{2\kappa}$;
- χ_{12}: $\widetilde{\mathbf{D}}_3$, $\widetilde{\mathbf{C}}_{3\kappa'}$, $\widetilde{\mathbf{C}}_{2\kappa}$, $\widetilde{\mathbf{C}}'_{2\kappa}$;
- χ_{13}: $\widetilde{\mathbf{D}}_3$, $\widetilde{\mathbf{C}}_{3\kappa'}$, $\widetilde{\mathbf{C}}_{2\kappa}$, $\widetilde{\mathbf{C}}'_{2\kappa}$;

Proof.

For the one dimensional representations of $\mathcal{G}$ this is straightforward: each element whose character image is $+1$ belongs to the isotropy group. The result follows therefore directly from the character table and list of subgroups of $\mathcal{G}$. For the higher dimensional irreducible representations we need to find those isotropy subgroups H such that (see (6.13)):

$$1 = \dim(V^H) = \frac{1}{|H|}\sum_{h\in H}\chi_j(h)$$

where χ_j denotes the character of the j-th irreducible representation. This can be done in a systematic way by using the character table 6.6 and applying the datas on subgroups and their conjugacy classes listed in 6.4 and 6.5. The calculations are cumbersome but can be slightly simplified by noting that if $H \subset H'$ and $\dim(V^H) = 0$ (a case which occurs many times), then not only H is not symmetry breaking but also H', since $H \subset H' \Rightarrow V^{H'} \subset V^H$.

The following lemma is also useful as it eliminates most candidates in the case of 4D representations:

Lemma 6.3.3. *If a subgroup H contains $-Id$, then for $j = 11, 12$ or 13, one has $\sum_{h\in H}\chi_j(h) = 0$.* *Proof of the lemma.* In all three cases the result follows from the relations: (i) $\chi_j(-Id) = -\chi_j(Id)$, (ii) $\chi(-\varepsilon) = -\chi(\varepsilon)$ and $\chi(-\varepsilon\kappa) = -\chi(\varepsilon\kappa)$, (iii) $\chi_j(s) = 0$ for all s which is not conjugate to one in (i) or (ii). □

For the lower dimensional representations it is possible to reduce the problem to known situations and to provide bifurcation diagrams without any further calculations. The next theorem provides these informations. Stability of the solutions has to be understood here with respect to perturbations with the same octagonal periodicity in $\mathbb{D}$ and under the condition that, in $L^2(\mathbb{D}/\Gamma)$, the corresponding representation corresponds to the "most unstable" modes ("neutral modes" at bifurcation). We recall that the octahedral group $\mathbb{O}$, the direct symmetry group of the cube, possesses two irreducible representations of dimension three. In order to differentiate these two irreducible representations we adopt the convention "natural" and "non natural" as used in [Miller 1972].

Theorem 6.3.2. *For the one, two and three dimensional representations, the generic bifurcation diagrams have the following properties:*

(i) χ_1*: transcritical bifurcation (trivial symmetry, exchange of stability holds);*

(ii) χ_2, χ_3, χ_4*: pitchfork bifurcation (*$\mathbb{Z}_2$ *symmetry, exchange of stability holds);*

(iii) χ_5*: same as bifurcation with hexagonal* $\mathbf{D}_6$ *symmetry in the plane, see Figure 6.4;*

(iv) χ_6*: same as bifurcation with triangular* $\mathbf{D}_3$ *symmetry in the plane. In particular H-planforms are always unstable on both sides of the bifurcation point unless the subcritical branch bends back sufficiently near the bifurcation point (see Figure 6.5);*

(v) χ_7*: same as bifurcation with natural octahedral* $\mathbb{O}$ *symmetry in* $\mathbb{R}^3$*;*

(vi) χ_8*: same as bifurcation with natural full octahedral* $\mathbb{O} \ltimes \mathbb{Z}_2$ *symmetry in* $\mathbb{R}^3$*;*

(vii) χ_9*: same as bifurcation with the (unique) non natural full octahedral symmetry in* $\mathbb{R}^3$*;*

(viii) χ_{10}*: same as bifurcation with the (unique) non natural octahedral symmetry in* $\mathbb{R}^3$*.*

Proof.

(i) For the one dimensional representations, this follows from classical bifurcation theory: in χ_1 there is no symmetry breaking, hence generically the bifurcation is of transcritical type and the trivial and bifurcated solutions exchange stability at the bifurcation point. In the three other cases, a symmetry exists which acts by reversing direction on the axis as can be seen from Table 6.6. For example in χ_2 this can be taken as σ (but also κ' does the same thing). Hence the bifurcation is of pitchfork type and exchange of stability holds.

(ii) For χ_5, note that the subgroup $\mathbf{Q}_8$ acts trivially on any point of this plane ($\dim(V^{\mathbf{Q}_8}) = 2$). In fact $\mathbf{Q}_8$ is the isotropy group of the principal stratum in this group action. Now, $G \simeq \mathbf{GL}(2,3) = \mathbf{Q}_8 \ltimes \mathbf{D}_3$, hence $\mathcal{G}/\mathbf{Q}_8 \simeq \mathbf{D}_3 \ltimes \mathbb{Z}_2 \simeq \mathbf{D}_6$, the symmetry group of an hexagon. This group action is isomorphic to the natural action of $\mathbf{D}_6$ in the plane. It follows that the problem reduces in this case to a bifurcation problem with the action of $\mathbf{D}_6$ in the plane, see [Golubitsky 1988] for details.

(iii) In the case of χ_6, the maximal subgroup which keeps every point in the plane fixed is the 16 element group $\mathbf{Q}_{8\kappa}$. It follows that the problem reduces to a bifurcation problem in the plane with symmetry $\mathcal{G}/\mathbf{Q}_{8\kappa} \simeq \mathbf{D}_3$. Details on this bifurcation can be found in [Golubitsky 1988].

(iv) A similar reduction can be made with the 3 dimensional representations. Indeed it can be seen that the principal isotropy type (which keeps all points in the three dimensional representation space fixed) is $\mathbf{C}_4'$ for χ_7 and χ_{10}, and $\mathbf{C}_2$ for χ_8 and χ_9. In the first case, this leads to reducing the problem to one with $\mathcal{G}/\mathbf{C}_4' \simeq \mathbb{O}$ symmetry, where $\mathbb{O}$ is the 24 elements group of direct symmetries (rotations) of a cube. However there are two irreducible representations of dimension 3 of $\mathbb{O}$ [Miller 1972], and it turns out that χ_7 corresponds to one of them (the "natural" action of $\mathbb{O}$ in $\mathbb{R}^3$) while χ_{10} corresponds to the other representation. This explains why there are 3 types of H-planforms for χ_7 and only 2 for χ_{10}. Similarly, the principal isotropy type for χ_8 and χ_9 is the two element group $\mathbf{C}_2$, and $\mathcal{G}/\mathbf{C}_2 \simeq \mathbb{O} \ltimes \mathbb{Z}_2$. Then the same remark holds for these cases as for the previous ones. Note that the case of irreducible representation χ_8 will be studied in details in 8.3.2 and 8.3.3 and will rely on the singular theory with octahedral symmetry developed by Melbourne [Melbourne 1986].

□

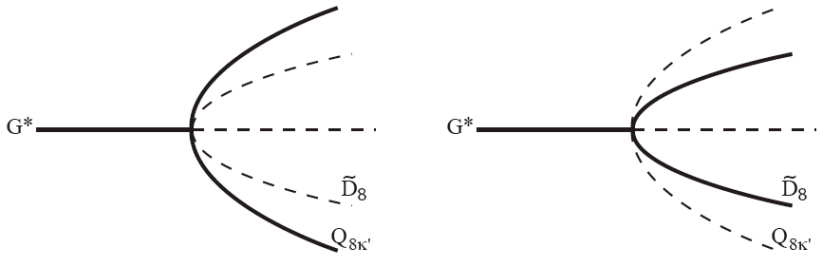

Figure 6.4: Bifurcation diagram for the case χ_5. Dotted lines: unstable branches.

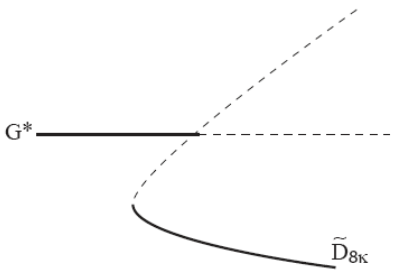

Figure 6.5: Bifurcation diagram for the case χ_6. Dotted lines: unstable branches.

Remark 6.3.1. *In the 4 dimensional cases, the principal isotropy type is the trivial group, hence no reduction can be made. Bifurcation in this case will be the subject of the next chapter 7.*

6.4 Computation of hyperbolic planforms

It follows from the definition that H-planforms are eigenfunctions of the Laplace-Beltrami operator in $\mathbb{D}$ which satisfy certain isotropy conditions: (i) being invariant under a lattice group Γ and (ii) being invariant under the action of an isotropy subgroup of the symmetry group of the fundamental domain $\mathbb{D}/\Gamma$ (mod Γ). Therefore in order to exhibit H-planforms, we need first to compute eigenvalues and eigenfunctions of $L_{\mathbb{D}}$ in $\mathbb{D}$, and second to find those eigenfunctions which satisfy the desired isotropy conditions. In this section we tackle this question in the case where the lattice has the regular octagon as a fundamental domain.

6.4.1 Introduction

Over the past decades, computing the eigenmodes of the Laplace-Beltrami operator on compact manifolds has received much interest from physicists. The main applications are certainly in quantum chaos [Balazs 1986, Aurich 1989, Aurich 1993, Schmit 1991, Cornish 1998] and in cosmology [Inoue 1999, Cornish 1999, Lehoucq 2002].

To our knowledge, the interest in such computation was sparkled by the study of classical and quantum mechanics on surfaces of constant negative curvature, and the connections between them (for an overview on the subject see [Balazs 1986]). To be more precise, *quantum chaology* can be defined as the study of the semiclassical behaviour characteristic of systems whose classical motion exhibits chaos, for example the classical free motion of a mass point on a compact surface of constant negative curvature (as it is the most chaotic possible). In [Balazs 1986, Aurich 1989, Cornish 1998], authors studied the time-independent Schroedinger equation on the compact Riemannian surface of constant curvature -1 and genus 2, which is topologically equivalent to the regular octagon with four periodic boundary conditions. This is the same as solving the eigenvalue problem for Γ invariant eigenmodes in $\mathbb{D}$. The first computations have been performed using the finite element method on "desymmetrised" domains of the hyperbolic octagon with a mixture of Dirichlet and Neumann boundary conditions [Balazs 1986, Schmit 1991]. We explain the procedure of desymmetrisation in the next subsection. Aurich and Steiner in [Aurich 1989] were the first to compute the eigenmodes on the whole octagon with periodic boundary conditions. They began with the finite element method of type $P2$ and were able to exhibit the first 100 eigenvalues. In [Aurich 1993], the same authors used the direct boundary-element method on an asymmetric octagon to reach the 20 000th eigenvalue.

There is also a strong interest of cosmologists for ringing the eigenmodes of the Laplace-Beltrami operator on compact surfaces. Indeed this is necessary in order to evaluate the cosmic microwave background anisotropy in multiply-connected compact cosmological models. For some models, this computation is performed on a compact hyperbolic 3-space called the Thurston manifold, and Inoue computed the first eigenmodes of Thurston space such that each corresponding eigenvalue

λ satisfies $\lambda \leq 10$ with the direct boundary-element method [Inoue 1999]. For 3-dimensional spherical spaces, several methods have been proposed: the "ghosts method" [Cornish 1999], the averaging method and the projection method. All these methods are explained and summarized in [Lehoucq 2002].

Our aim is different in that we do not want to compute all the eigenvalues of the Laplace-Beltrami operator, but instead to calculate the H-planforms with the isotropy types listed in theorem 6.3.1. The methods of numerical computation are however similar, and one question is to choose the method best suited to our goal. For the H-planforms associated to irreductible representations of dimension 1 (i.e. for $(\chi_i)_{i=1\cdots4}$), we use a desymmetrization of the octagon with a reformulation of the boundary conditions. For H-planforms associated with irreducible representations of dimension ≥ 2, the desymmetrization of the octagon is also possible but much more complicated as noticed by Balazs and Voros [Balazs 1986]. In the following chapter 7, we will treat the four-dimensional case in great details. Here we only identify some H-planforms of specific isotropy types. In order to find these H-planforms, we use the finite-element method with periodic boundary conditions. This choice is dictated by the fact that this method will allow us to compute all the first n eigenmodes and among all these we will identify those which correspond to a given isotropy group. As explained before, if we had used the direct boundary-element method, we would have reached any eigenmode but the search for H-planforms would also have became more random. Indeed, each iteration of this method gives only one eigenmode while the finite-element method provides n eigenmodes depending on the precision of the discretization. This is why we prefer to use this last method in order to find some H-planforms associated with irreducible representations of dimension ≥ 2, although it is quite more complicated to implement because of the periodic boundary conditions.

6.4.2 Desymmetrization of the octagon for the 1D case

We have already seen that the fundamental domain $T(2,3,8)$ of the group $\mathcal{G}$ generates a tiling of the octagon. Desymmetrization consists in separating the individual solutions according to the symmetry classes of $\mathcal{G}$. This entails solving the eigenvalue problem in certain irreducible subregions of the fundamental domain, such as $T(2,3,8)$, using special boundary conditions for these subregions. In effect the periodicity conditions in the original domain (octagon) may produce Dirichlet or Neumann conditions on the boundaries of these subregions. The symmetry group $\mathcal{G}$ has a smaller fundamental domain, the triangle $T(2,3,8)$ see figure 6.2, which is $\frac{1}{96}$th of the original octagon. The method of desymmetrization can be applied to many other techniques than finite element methods (see [Fässler 1992]).

We now focus on the four one-dimensional irreducible representations $(\chi_i)_{i=1\cdots4}$ acting upon the generators as indicated in table 6.6. One can find in the book of Fässler and Stiefel [Fässler 1992, Chapter 3] the principle of desymmetrization in the context of dihedral symmetry. We follow their method in the case of the symmetry group $\mathcal{G}$. The first step is to attribute one number (value) to each of the

96 triangles that tesselate the octagon under the action of $\mathcal{G}$ (see 6.3), according to the character values obtained from table 6.6, i.e. ± 1 depending on the conjugacy class (remember we restrict ourselves to the one dimensional representations χ_1 to χ_4).

Let us take the example of the first irreducible representation χ_1 and explain how we obtain the domain and the boundary conditions depicted in figure 6.6. Table 6.6 shows that all 96 triangles end up with the same value, 1. This means that the eigenfunction we are looking for is *even* under all the 96 elements in $\mathcal{G}$ and it follows that it must satisfy Neumann boundary conditions on all the edges of the tesselation of the hyperbolic octagon [Balazs 1986, Aurich 1989]. Finally, it is sufficient to solve the eigenproblem on the reduced domain $T(2,3,8)$ with Neumann boundary conditions on its three edges. For the four one-dimensional representations one has to choose the correct combination of Neumann and Dirichlet boundary conditions as shown in figure 6.6.

The representations of dimension ≥ 2 require the same number of values as their dimension. For example there are two basis vectors determining the function values in the case of an irreducible representation of dimension 2. The table 6.6 is then no longer sufficient to set the values of the function on each triangles and one has to explicitly write the matrices of the irreducible representation in order to obtain the suitable conditions.

6.4.3 Numerical experiments

As there exists an extensive literature on the finite element methods (see for an overview [Ciarlet 1991, Allaire 2005]) and as numerical analysis is not the main goal of this section, we do not detail the method itself but rather focus on the way to actually compute the eigenmodes of the Laplace-Beltrami operator.

Desymmetrized problem : For the four problems depicted in figure 6.6, we use the mesh generator *Mesh2D* from *Matlab* to tesselate the triangle $T(2,3,8)$ with 2995 nodes and we implement the finite element method of order 1. Our results are presented in figure 6.7 and are in a good agreement with those obtained by Balazs-Voros in [Balazs 1986] and Aurich-Steiner in [Aurich 1989]. Once we have computed the eigenfunction in $T(2,3,8)$, we extend it to the whole octagon by applying the generators of $\mathcal{G}$. We superimpose in figure 6.7(a) the tesselation of the octagon by the 96 triangles in order to allow the reader to see the symmetry class of $\mathcal{G}$.

Non desymmetrized problem : As discussed previously, we also present some H-planforms of higher dimension. We mesh the full octagon with 3641 nodes in such a way that the resulting mesh enjoys a $\mathbf{D}_8$-symmetry, see figure 6.8.

We implement, in the finite element method of order 1, the periodic boundary conditions of the eigenproblem and obtain the first 100 eigenvalues of the octagon. Our results are in agreement with those of Aurich and Steiner reported in

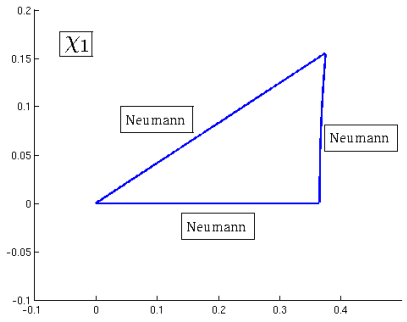

(a) $\chi_1 : \mathcal{G}$.

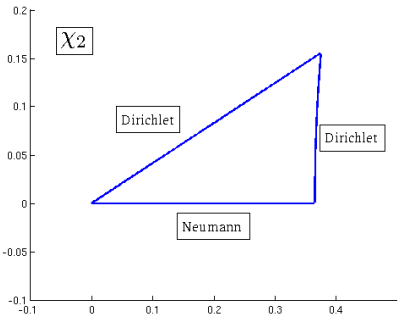

(b) $\chi_2 : G_{0\kappa}$.

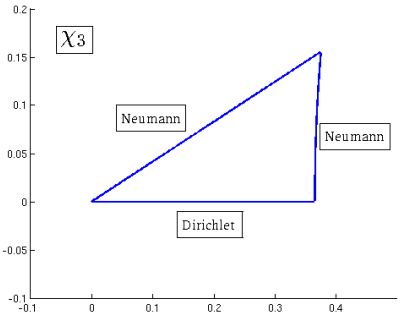

(c) $\chi_3 : G_{0\kappa'}$.

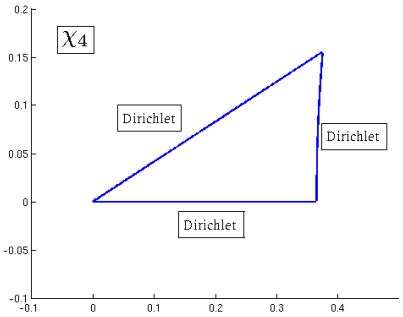

(d) $\chi_4 : G$.

Figure 6.6: Boundary conditions for the one-dimensional irreducible representations. Top left: boundary conditions for χ_1, corresponding to the isotropy group $\mathcal{G}$. Top right: boundary conditions for χ_2 corresponding to the isotropy group $G_{O\kappa}$. Bottom left: boundary conditions for χ_3 corresponding to the isotropy group $G_{0\kappa'}$. Bottom right: boundary conditions for χ_4 corresponding to the isotropy group G.

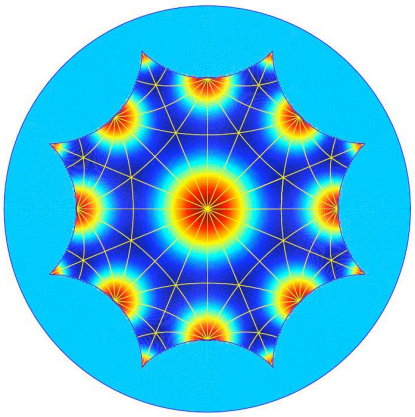

(a) $\chi_1 : \mathcal{G}$, the corresponding eigenvalue is $\lambda = 23.0790$.

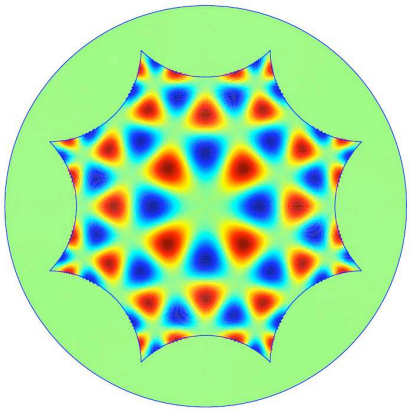

(b) $\chi_2 : G_{0\kappa}$, the corresponding eigenvalue is $\lambda = 91.4865$.

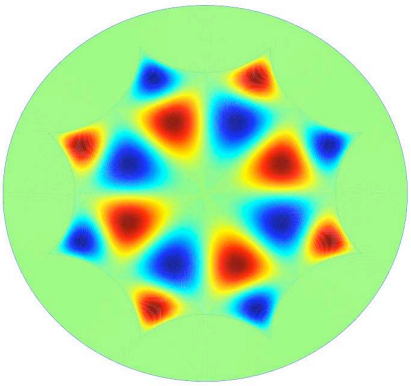

(c) $\chi_3 : G_{0\kappa'}$, the corresponding eigenvalue is $\lambda = 32.6757$.

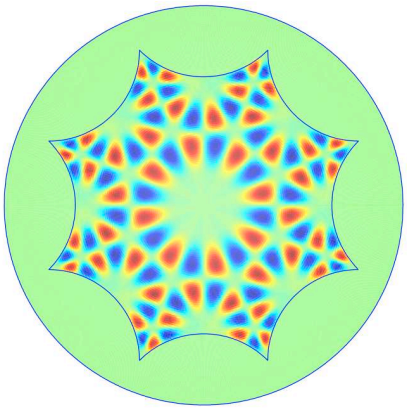

(d) $\chi_4 : G$, the corresponding eigenvalue is $\lambda = 222.5434$.

Figure 6.7: The four H-planforms with their corresponding eigenvalue associated with the four irreducible representations of dimension 1, see text.

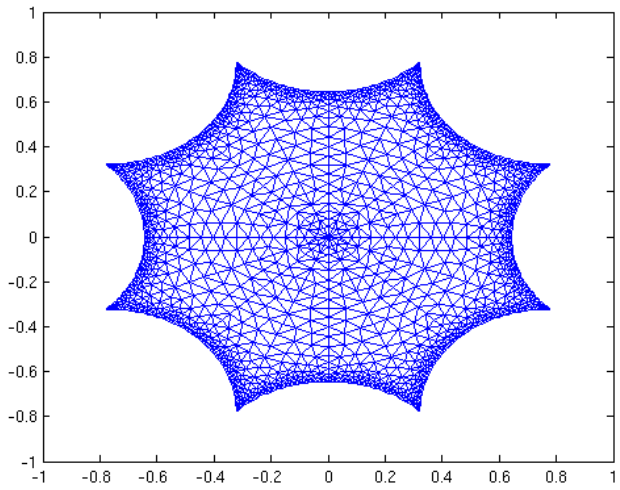

Figure 6.8: A mesh of the octagon with 3641 nodes which is used for the method of finite elements. It leads to matrices of dimension 3641×3641.

[Aurich 1989]. Instead of giving a table of all the eigenvalues, we prefer to plot the staircase function $N(\lambda) = \sharp\{\lambda_n | \lambda_n \leq \lambda\}$ for comparison with Weyl's law. Weyl's law is, in its simplest version, a statement on the asymptotic growth of the eigenvalues of the Laplace-Beltrami operator on bounded domains. If Ω is a given bounded domain of $\mathbb{R}^2$, then the staircase function has the following asymptotic behaviour: $N(\lambda) = \frac{|\Omega|}{4\pi}\lambda + o(\lambda)$ as $\lambda \to \infty$. We recall that in the case of the hyperbolic octagon, one has $|\Omega| = 4\pi$ and hence $N(\lambda) \sim \lambda$ as $\lambda \to \infty$. As can be seen in figure 6.9 the asymptotic law describes the staircase well down to the smallest eigenvalues, which confirms the validity of our numerical results.

We show in figure 6.10 two H-planforms, with $\widetilde{\mathbf{D}}_8$ and $\widetilde{\mathbf{D}}_{8\kappa}$ isotropy respectively. These two H-planforms belong to irreducible representations of dimension 2: χ_5 for 6.10(a) and χ_6 for 6.10(b) and 6.11(a).

We finally present in figure 6.11 three H-planforms, with $\mathbf{C}_{8\kappa}$, $\widetilde{\mathbf{D}}_{4\kappa}$ and $\widetilde{\mathbf{D}}_{4\kappa'}$ isotropy. These three H-planforms belong to irreducible representations of dimension 3: χ_8 for 6.11(a), χ_9 for 6.11(b) and χ_{10} for 6.11(c).

In figures 6.7,6.10 and 6.11, we have plotted, for convenience, the corresponding H-planforms in the octagon only. Nevertheless, H-planforms are periodic in the Poincaré disc, as stated before, and in figure 6.12, we plot the H-planform with $G_{0\kappa'}$ isotropy type of figure 6.7(c). We recall that the octagonal lattice group Γ is generated by the four boosts g_j of subsection 6.3.1. Then, once the H-planform is calculated, we report it periodically in the whole Poincaré disc by the actions of there four boosts and obtain figure 6.12. Note that it is arduous to tesselate the entire disc and this is why there remains some untesselated areas in the figure.

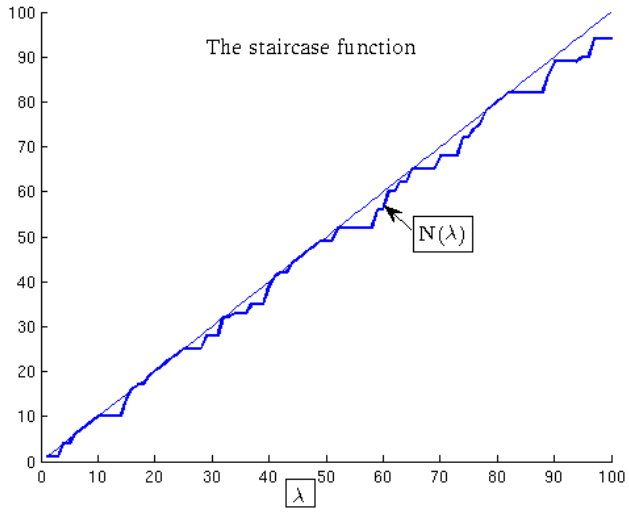

Figure 6.9: The staircase function $N(\lambda)$, in dark, is shown in comparison with Weyl's law $N(\lambda) \sim \lambda$ as $\lambda \to \infty$.

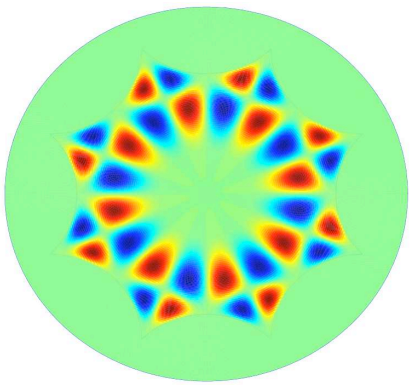

(a) χ_5 : $\widetilde{\mathbf{D}}_8$, the corresponding eigenvalue is $\lambda = 73.7323$.

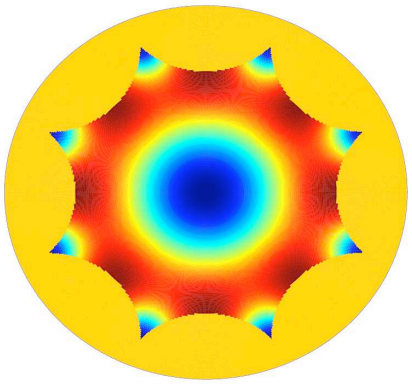

(b) χ_6 : $\widetilde{\mathbf{D}}_{8\kappa}$, the corresponding eigenvalue is $\lambda = 8.2501$.

Figure 6.10: Two H-planforms with their corresponding eigenvalue associated to the two irreducible representations of dimension 2, see text.

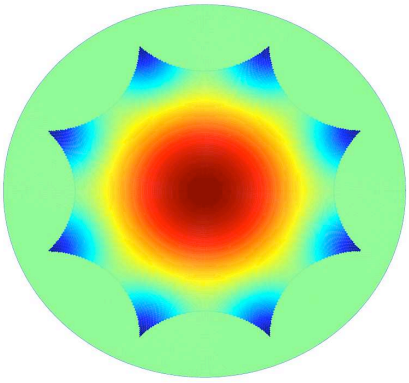

(a) χ_8 : $\mathbf{C}_{8\kappa}$, the corresponding eigenvalue is $\lambda = 3.8432$.

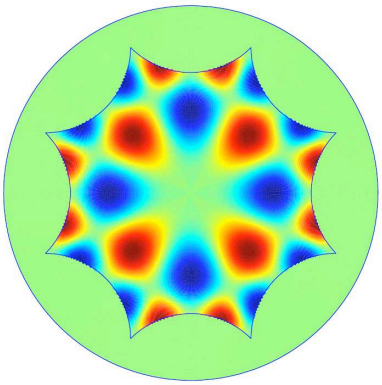

(b) χ_9 : $\widetilde{\mathbf{D}}_{4\kappa}$, the corresponding eigenvalue is $\lambda = 28.0888$.

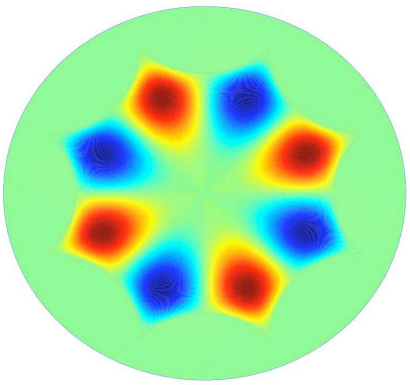

(c) χ_{10} : $\widetilde{\mathbf{D}}_{4\kappa'}$, the corresponding eigenvalue is $\lambda = 15.0518$.

Figure 6.11: Three H-planforms with their corresponding eigenvalue associated to three irreducible representations of dimension 3, see text.

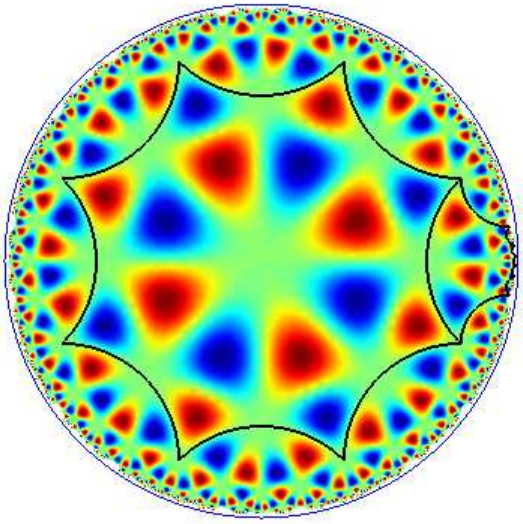

Figure 6.12: Extension of the $G_{0\kappa'}$ H-planform on the Poincaré disk.

Remark 6.4.1. *The finite element method relies on a variational principle and thus yields upper bounds for the eigenvalues. Note that it is not well-suited to compute high eigenvalues. Thus, if one wants to compute, for example, the first 125 eigenvalues, then the finite element method provides a very good approximation to the true eigenvalues. If however one wants to reach the 2000th eigenvalue by the finite element method we need to use matrices of size at least* $10^6 \times 10^6$ *which is impossible for desktop or laptop computers and requires going to more powerful architectures. This is why the direct boundary element method should be preferred for such computations (see [Aurich 1993]).*

6.5 Application to the structure tensor formalism

The aim of this section is to extend the results from the Poincaré disk to the set of structure tensors $\mathbf{SPD}(2,\mathbb{R})$. We can extend the definitions introduced in 6.2.1 to $\mathbf{SPD}(2,\mathbb{R}) = \mathbb{R}_*^+ \times \mathbb{D}$ as follows.

Definition 6.5.1. *A lattice group of* $\mathbb{R}^* \times \mathbb{D}$ *is a subgroup of the form* $\Xi \times \Gamma$ *where* Γ *is a lattice group acting in* $\mathbb{D}$ *and* Ξ *is a non trivial discrete subgroup of* $\mathbb{R}^*$.

Any discrete subgroup of $\mathbb{R}^*$ is generated by a positive number a and can be further identified with $\mathbb{Z}$: $\Xi = \{a^n,\ n \in \mathbb{Z}\}$. A fundamental domain for $\Xi \times \Gamma$ is a "box" $[1, a] \times F_\Gamma$.

The Laplace-Beltrami operator in $\mathbb{R}^* \times \mathbb{D}$ in (Δ, z_1, z_2) with $z = z_1 + iz_2$ coor-

dinates is

$$L_{\mathbf{SPD}(2,\mathbb{R})} = \Delta\frac{\partial}{\partial\Delta} + \Delta^2\frac{\partial^2}{\partial\Delta^2} + \frac{\left(1-|z|^2\right)^2}{4}\left(\frac{\partial^2}{\partial z_1^2} + \frac{\partial^2}{\partial z_2^2}\right). \tag{6.15}$$

By using (6.15) we extend Theorem 6.1.1 to $\mathbb{R}^* \times \mathbb{D}$:

Corollary 6.5.1.

(i) Let us note $\mathcal{T} = (\Delta, z_1, z_2) \in \boldsymbol{SPD}(2,\mathbb{R})$ and $z = z_1 + iz_2$. The function

$$\psi_{\rho,b,\beta}(\mathcal{T}) = e_{\rho,b}(z)\, e^{i\log\beta\log\Delta} \tag{6.16}$$

satisfies the relation $L_{\boldsymbol{SPD}(2,\mathbb{R})}\psi_{\rho,b,\beta} = -\left(\rho^2 + \frac{1}{4} + \log^2\beta\right)\psi_{\rho,b,\beta}$.

(ii) Any eigenfunction of $L_{\boldsymbol{SPD}(2,\mathbb{R})}$ admits a decomposition of the form

$$e^{i\log\beta\log\Delta}\int_{\partial\mathbb{D}} e_{\rho,b}(z)dT_\rho(b). \tag{6.17}$$

From there we can extend the definition (and properties) of the Helgason-Fourier transform in the Poincaré disk given by Helgason [Helgason 2000] to the space $\mathbf{SPD}(2,\mathbb{R})$. If we denote $\mathcal{T} = (\Delta, z) \in \mathbb{R}_*^+ \times \mathbb{D}$, then given a function f on $\mathbf{SPD}(2,\mathbb{R})$, its Fourier transform is defined by

$$\tilde{f}(\rho,b,\beta) = \int_{\mathbf{SPD}(2,\mathbb{R})} f(\Delta,z)e_{-\rho,b}(z)e^{-i\log\beta\log\Delta}\mathrm{dm}(z)\frac{d\Delta}{\Delta}. \tag{6.18}$$

In the following we will look for solutions of bifurcation problems in $\mathbf{SPD}(2,\mathbb{R})$, which are invariant under the action of a lattice group: $(\xi,\gamma)\cdot u(\Delta,z) = u(\xi^{-1}\Delta,\gamma^{-1}z) = u(\Delta,z)$ for $\xi\in\Xi$, $\gamma\in\Gamma$. This reduces to looking for the problem restricted to a fundamental domain with suitable boundary conditions imposed by the Γ-periodicity, or, equivalently, to looking for the solutions of the problem projected onto the orbit space $\mathbb{R}_*^+/\Xi\times\mathbb{D}/\Gamma$ (which inherits a Riemannian structure from $\mathbf{SPD}(2,\mathbb{R})$). Because the fundamental domain is compact, it follows from general spectral theory that $-L_{\mathbf{SPD}(2,\mathbb{R})}$ is self-adjoint, non negative and has compact resolvent in $L^2(\mathbb{R}_*^+/\Xi\times\mathbb{D}/\Gamma)$. Hence its spectrum consists of real positive and isolated eigenvalues of finite multiplicity.

6.5.1 Bifurcation problem

We now consider equation (3.4). Assuming again $I_{ext} = 0$ (no external input) and that the sigmoidal function is centered at the origin (such that $V = 0$ is a trivial solution of (3.19)), the equation (3.4) can be written

$$\frac{d}{dt}V(\mathcal{T},t) = -V(\mathcal{T},t) + \mu W_{loc} *_{\mathbf{SPD}(2,\mathbb{R})} V(\mathcal{T},t) + \mathcal{R}(V(\mathcal{T},t)) \tag{6.19}$$

where:

- $\mu = S'(0)$,
- $W_{loc} *_{\mathbf{SPD}(2,\mathbb{R})} V$ denotes the convolution product

$$W_{loc} *_{\mathbf{SPD}(2,\mathbb{R})} V(\mathcal{T}) = \int_{\mathbf{SPD}(2,\mathbb{R})} W_{loc}(d_{\mathbf{SPD}(2,\mathbb{R})}(\mathcal{T}, \mathcal{T}'))V(\mathcal{T}')d\mathcal{T}'$$

  defined on $\mathbf{SPD}(2,\mathbb{R})$,
- $\mathcal{R}(V)$ stands for the remainder terms in the integral part of equation (3.4),
- $\mathcal{R}(0) = D_V\mathcal{R}(0) = 0$.

Following the same lines as in the previous section, we look at the linear stability of the trivial solution of against perturbations in the form of hyperbolic waves (6.16) with $\rho \in \mathbb{R}$. This comes back to looking for σ's such that

$$\sigma(\rho, \beta) = -1 + \mu\widetilde{W}_{loc}(\rho, \beta)$$

where $\widetilde{W}_{loc}(\rho, \beta)$ is the hyperbolic Fourier transform of W_{loc} as defined in (6.18). The numerical calculation shows that for each value of ρ and β, there exists a value $\mu(\rho, \beta)$ such that if $\mu < \mu(\rho, \beta)$ then all σ's are negative, while $\sigma = 0$ at $\mu = \mu(\rho, \beta)$. The "neutral stability surface" defined by $\mu(\rho, \beta)$ is typically convex and reaches a minimum μ_c at some values ρ_c, β_c. Therefore when $\mu < \mu_c$ the trivial state $V = 0$ is stable against such perturbations while it becomes marginally stable when $\mu = \mu_c$ with critical modes ψ_{ρ_c,b,β_c}, for any $b \in \mathbf{S}^1$ (rotational invariance). Therefore a bifurcation takes place at this critical value.

In this section, we restrict ourself to bifurcating patterns in $\mathbf{SPD}(2,\mathbb{R})$ which are invariant under a lattice Γ in $\mathbb{D}$ and which are periodic, with period $2\pi/\beta_c$, in $\mathbb{R}_*^+$. This reduces to look for solutions in the space $L^2(\mathbb{R}_*^+/\beta_c\mathbb{Z}_*^+ \times \mathbb{D}/\Gamma)$. Note that $\mathbb{R}_*^+/\beta_c\mathbb{Z}_*^+ \simeq \mathbf{S}^1$. With a suitable inner product this space admits an orthonormal Hilbert basis which is made of functions of the form

$$\Psi(z)e^{ni\log(\beta_c)\log(\Delta)}, \quad z \in \mathbb{D}, \quad n \in \mathbb{N}$$

where Ψ are the eigenfunctions of $L_{\mathbb{D}}$ in $L^2(\mathbb{D}/\Gamma)$. As we mentioned in the previous section, these eigenfunctions are not known explicitly. By restricting the "neutral stability surface" $\mu(\rho, \beta)$ to those values which correspond to eigenfunctions with $\beta_c\mathbb{Z}_*^+ \times \Gamma$ periodicity, we obtain a discrete set of points on this surface with one minimum μ_0 associated with a value ρ_0 of ρ and β_0 of β. In general this minimum is unique. Moreover the multiplicity of the 0 eigenvalue is now finite and this eigenvalue is semi-simple. Let us call X the eigenspace associated with the 0 eigenvalue.

The full symmetry group of $\mathbf{S}^1 \times \mathbb{D}/\Gamma$ is equal to $\mathbf{O}(2) \times \mathcal{G}$ where $\mathcal{G}$ as been introduced in the previous section and $\mathbf{O}(2)$ is the symmetry group of the circle (generated by $\mathbf{S}^1$ and by reflection across a diameter).

6.5.2 Elementary results

The Equivariant Branching Lemma (6.2.3), together with the knowledge of the lattices and the (absolutely) irreducible representations of the group $\mathcal{G}$, gives us a mean to classify the periodic patterns which can occur in $\mathbb{R}_*^+ \times \mathbb{D}$. Again, being interested here in the classification of solutions rather than in their actual computation for a specific equation, all remains to do is to determine the absolutely real irreducible representations of the group $\mathbf{O}(2) \times \mathcal{G}$ and the computation of the dimensions of the subspaces X^H.

It only remains to deal with the $\mathbf{S}^1$ component of the domain of periodicity, the $\mathcal{G}$ component has been done in the previous section. Let $H = H_1 \times H_2$ be an isotropy subgroup for the representation R of $\mathbf{O}(2) \times \mathcal{G}$ acting in X. Then $X = V \otimes W$ and $R = S \otimes T$, where S is an irreducible representation $\mathcal{G}$ in V and T is an irreducible representation of $\mathbf{O}(2)$ in W [Serre 1978], and therefore H_1 acts in V and H_2 acts in W. Now we have the following lemma, the proof of which is straightforward:

Lemma 6.5.1. $\dim(X^H) = 1$ *if and only if* $\dim(V^{H_1}) = \dim(W^{H_2}) = 1$.

Now, the irreducible real representations of $\mathbf{O}(2)$ are well-known: they are either one dimensional (in which case every point is rotationally invariant) or two-dimensional, and in the latter case the only possible one dimensional subspaces W^{H_2} are the reflection symmetry axes in $\mathbb{R}^2$ (which are all equivalent under rotations in $\mathbf{O}(2)$). Then the classification follows straightforwardly from the classification of the isotropy subgroups H_1 of the irreducible representations of $\mathcal{G}$ which has been done in 6.3.2.

6.6 Conclusion

In this chapter, we have analyzed the bifurcation of periodic patterns for nonlinear equations describing the state of a system defined on the Poincaré disk, when these equations are further invariant under the isometries in this space. We have made use of the concept of periodic lattice in $\mathbb{D}$ to further reduce the problem to one on a compact Riemann surface $\mathbb{D}/\Gamma$, where Γ is a cocompact Fuchsian group. We have applied the machinery of equivariant bifurcation theory in the case of an octagonal periodic pattern, where we have been able to classify all possible H-planforms satisfying the hypotheses of the Equivariant Branching Lemma. We have also described a method to compute these patterns and illustrated it with a selection of images of octagonal H-planforms. In the last section, we have described how these results can be transferred to the case of bifurcating patterns in $\mathbf{SPD}(2, \mathbb{R})$.

There are three main questions which are raised by this analysis.

(i) The first one is that of the interpretation of these H-planforms for the modeling of the visual cortex. At this moment we believe that they could be involved in the process of defining texture tuning curves in a way that would resemble the definition of orientation tuning curves in the related ring model of orientation selectivity [Hansel 1997, Shriki 2003, Ermentrout 1998, Dayan 2001,

Bressloff 2000, Bressloff 2001b, Veltz 2010b]. Another fascinating possibility is that they could be related to neural illusions caused by the existence of several stable stationary solutions to (6.11) when, e.g., the slope of the sigmoid at the origin becomes larger than that at which several branches of solutions bifurcate from the trivial one. These neural illusions would be functions of membrane potential values that would not correspond to the actual thalamic input and could be expressed as combinations of these H-planforms. This is of course still very speculative but very much worth investigating.

(ii) The second one is about the observability of such patterns in a natural system or under direct simulation of the evolution equations. Indeed, not only there is a high degeneracy of the bifurcation problem if one removes the assumption that all perturbations respect the periodicity of the pattern, which is also the case for patterns in Euclidean space, but in addition the fact that such patterns would be neutral modes for the bifurcation problem posed in full generality in $\mathbb{D}$ is non generic. We may however imagine mechanisms such as "spatial frequency locking" by which periodic patterns could become "robust", hence observable.

(iii) The third one is that of a more effective computation of H-planforms for a given isotropy type. As we have seen in section 6.4, a desymmetrization of the domain allowed us to calculate all the H-planforms with isotropy types associated to irreducible representations of dimension 1. For irreducible representations of dimension ≥ 2 the computation becomes more intricate as the desymmetrization method is no longer straightforward and remains misunderstood. Naturally, one solution would be to elaborate a general algorithm which, for a given isotropy type, computes systematically the associated H-planform. We think that such an algorithm would be of interests for quantum physicists and cosmologists.

Chapter 7

Study of the four-dimensional representations

Contents

7.1 Basic facts and results 114
7.1.1 Steady-state bifurcations with $\mathcal{G}$ symmetry 114
7.1.2 Octagonal H-planforms in the 4D case 116
7.1.3 Bifurcation with submaximal isotropy 118
7.1.4 Presentation with biquaternions 122
7.1.5 Molien series 124
7.2 Bifurcation diagrams in the case of the representation χ_{12} 126
7.2.1 Equivariant structure of the equations on the center manifold 126
7.2.2 Isotropy types and fixed points subspaces 127
7.2.3 Bifurcation analysis 128
7.3 Bifurcation diagrams in the case of the representation χ_{11} 131
7.3.1 Equivariant structure of the equations on the center manifold 131
7.3.2 Isotropy types and fixed points subspaces 132
7.3.3 Bifurcation analysis 133
7.4 Bifurcation of a heteroclinic network in the χ_{11} case 140
7.4.1 Existence 140
7.4.2 Quotient network 141
7.4.3 Asymptotic stability 142
7.4.4 Computation of the stability conditions 147
7.5 Conclusion 148

This chapter completes the classification of bifurcation diagrams for H-planforms in the Poincaré disc $\mathbb{D}$ whose fundamental domain is a regular octagon. An H-planform is a steady solution of a PDE or integro-differential equation in $\mathbb{D}$, which is invariant under the action of a lattice subgroup Γ of $\mathbf{U}(1,1)$, the group of isometries of $\mathbb{D}$. In our case Γ generates a tiling of $\mathbb{D}$ with regular octagons. Under "generic" assumptions the bifurcation problem reduces to an ODE which is invariant by an irreducible representation of the group of automorphisms $\mathcal{G}$ of the compact Riemann surface $\mathbb{D}/\Gamma$. The irreducible representations of $\mathcal{G}$ have dimension one, two, three and four. The bifurcation diagrams for the representations of dimension less than four have already been described in the previous chapter and correspond to already

well known group actions. In the present chapter we compute the bifurcation diagrams for the remaining three irreducible representations of dimension four, thus completing the classification. In one of these cases, there is generic bifurcation of a heteroclinic network connecting equilibria with two different orbit types.

7.1 Basic facts and results

In this section we summarize results for chapter 6 which will be useful in subsequent analysis.

7.1.1 Steady-state bifurcations with $\mathcal{G}$ symmetry

We shall assume throughout this chapter that a center manifold reduction has been performed for a steady-state bifurcation problem with $\mathcal{G}$ symmetry as can arise from Equation (6.11) restricted to Γ-periodic patterns in $\mathbb{D}$. This means that a linear stability analysis of the trivial solution has led to finding a critical parameter value μ_c at which, in the class of Γ-periodic functions, 0 is an eigenvalue of the linear part. It is a generic fact that the corresponding eigenspace X be an irreducible representation space of $\mathcal{G}$, and any irreducible representation can be involved, depending on the form of the function W_{loc} defined in equation (6.11). Then the center manifold theorem reduces the initial problem to an ODE posed in X, which is invariant under the action of the irreducible representation of $\mathcal{G}$ in X. See [Haragus 2010] for a complete and rigorous exposition of the method and [Chossat 2000] for an exposition in the context of equivariant bifurcations.

Here it may be useful to recall some basic facts about bifurcations with symmetry. We write the bifurcation equation in X

$$\frac{dx}{dt} = \alpha(\lambda)\ x + f(x,\lambda) \tag{7.1}$$

where $\lambda = \mu - \mu_c$ and α is a real C^k function ($k \geq 1$) with $\alpha(0) = 0$, $f : X \times \mathbb{R} \to X$ has order $\|x\|o(\|x\|)$ and commutes with the action of $\mathcal{G}$ in X: if we denote by $(g,x) \mapsto g{\cdot}x$ the action (representation) of the group in X, then $f(g{\cdot}x,\lambda) = g{\cdot}f(x,\lambda)$ for all triples (g,x,λ). Moreover the property $\alpha'(0) \neq 0$ is generic and in our neural field model $\alpha'(0) = \mu_c^{-1} > 0$ (see [Veltz 2010b]) so that the trivial solution looses stability when $\lambda > 0$. This implies that after a suitable change of variable we have $\alpha(\lambda) = \lambda$ in (7.1).

The problem is now to find the non trivial solutions $(x(\lambda),\lambda)$ of (7.1) such that $x(0) = 0$ and to analyze the local dynamics. Let H be an isotropy subgroup of $\mathcal{G}$: $H = \{g \in \mathcal{G} \mid g \cdot x = x\}$ for some point $x \in X$. We define the fixed point subspace of H, or subspace of H symmetry, as

$$X^H = \{x \in X \mid H \cdot x = x\}.$$

Then for all $h \in H$ we have that $h \cdot f(x,\lambda) = f(h \cdot x,\lambda) = f(x,\lambda)$. Hence X^H is invariant under the flow generated by (7.1): if $x(0) \in X^H$, then $x(t) \in X^H$ for all

t. We shall later use the notation $\mathrm{Fix}(H)$ instead of X^H for convenience. It follows that by restricting ourselves to the search of solutions with a given isotropy H, we just need to solve (7.1) in the fixed point subspace X^H. The case when $\dim X^H = 1$ is of particular interest. In this case looking for solutions with isotropy H reduces to solving a *scalar bifurcation equation*. Under the above assumptions, this equation always has a branch of non trivial, bifurcated equilibria. By group equivariance of the problem any solution generates new solutions by letting $\mathcal{G}$ act on it. There is a one to one correspondance between the number of elements in this $\mathcal{G}$-orbit of solutions and the number of elements in the quotient $\mathcal{G}/H$ (number of subgroups conjugate to H in $\mathcal{G}$). We call the conjugacy class of an isotropy subgroup H the *isotropy type* of H.

Note that, when restricted to the invariant axis X^H as above, the *exchange of stability principle* holds for these solutions. Indeed let the axis of symmetry be parametrized by a real coordinate u, the equation on this axis at leading order has the form $\dot{u} = \lambda u + Cu^k$ where C is a real coefficient and $k \geq 2$. The bifurcated branch is parametrized (at leading order) by $\lambda = -Cu^{k-1}$, so that the radial eigenvalue is $(k-1)Cu^{k-1} = -(k-1)\lambda$ (at leading order). It therefore changes sign with λ. This eigenvalue is called *radial*. The other eigenvalues for the Jacobian matrix J of (7.1) evaluated at the solutions are *transverse* (the eigenvectors point orthogonally to the axis of symmetry). The bifurcated equilibria are stable in X if the eigenvalues of J all have a negative real part. The exchange of stability principle does not hold in general when considering stability in the full space X.

Equilibria with isotropy not satisfying the condition $\dim X^H = 1$ or other types of bounded solutions may also exist. However their analysis requires knowledge of the *equivariant structure* of the vector field f or at least of its Taylor expansion up to an order large enough to fully determine the bifurcation diagram. We shall see in the next sections that solving the bifurcation equation (7.1) when $\dim X = 4$ requires computing the equivariant terms in the expansion of $f(\cdot, \lambda)$ up to order 3, 5 or 7 depending on the problem treated.

We now come back to our specific problem with $\mathcal{G}$ symmetry. We can see from the character table 6.6 that there are 13 possible cases for the irreducible representations. The dimension of X for each representation χ_j $(j = 1, \ldots, 13)$ is given by the corresponding character evaluated at the identity. We see that $\dim(X) = 1$ for $\chi_1, \ldots, \chi_4$, $\dim(X) = 2$ for χ_5, χ_6, $\dim(X) = 3$ for $\chi_7, \ldots, \chi_{10}$ and $\dim(X) = 4$ for χ_{11}, χ_{12} and χ_{13}.

For the representations χ_1 to χ_{10} in Table 6.6, we have established that the bifurcation diagrams are identical to those of classical bifurcation problems with symmetry in $\mathbb{R}$, $\mathbb{R}^2$ or $\mathbb{R}^3$. Theorem 6.3.1 gives also the isotropy types of representations χ_{11}, χ_{12} and χ_{13} which have one dimensional fixed-point subspace. Hence by application of the Equivariant Branching Lemma, we know that branches of solutions with these isotropies exist (in a generic sense). However bifurcation diagrams cannot be deduced from already known bifurcation problems. Our aim in the remainder of this chapter is to fill this gap. In the next proposition we list these isotropy subgroups which give bifurcated solutions by the Equivariant Branching

Lemma. We introduce the following subgroups which will be relevant in the remainder of the paper. We use the notation $\widetilde{\sigma} = \rho^2\sigma\rho^{-2}$ (see Table 6.2).

Definition 7.1.1.

$$\begin{aligned}
\widetilde{\mathbf{C}}_{2\kappa} &= \langle\sigma,\kappa\rangle = \{Id,\sigma,\kappa,\kappa''\}\\
\widetilde{\mathbf{C}}'_{2\kappa} &= \langle\widetilde{\sigma},\kappa\rangle = \{Id,\tilde{\sigma},\kappa,-\rho^2\kappa''\rho^{-2}\}\\
\widetilde{\mathbf{C}}_{3\kappa'} &= \langle\varepsilon,\kappa'\rangle = \{Id,\varepsilon,\varepsilon^2,\kappa',\varepsilon\kappa'\varepsilon^2,\varepsilon^2\kappa'\varepsilon\}\\
\widetilde{\mathbf{D}}_3 &= \langle\widetilde{\sigma},\varepsilon\rangle = \{Id,\varepsilon,\varepsilon^2,\widetilde{\sigma},\varepsilon\widetilde{\sigma}\varepsilon^2,\varepsilon^2\widetilde{\sigma}\varepsilon\}
\end{aligned}$$

Proposition 7.1.1. *For the 4D representations of $\mathcal{G}$, the isotropy subgroups with one dimensional fixed point subspace are the following:*

- χ_{11}: $\widetilde{\mathbf{C}}_{2\kappa}$, $\widetilde{\mathbf{C}}'_{2\kappa}$;
- χ_{12}: $\widetilde{\mathbf{D}}_3$, $\widetilde{\mathbf{C}}_{3\kappa'}$, $\widetilde{\mathbf{C}}_{2\kappa}$, $\widetilde{\mathbf{C}}'_{2\kappa}$;
- χ_{13}: $\widetilde{\mathbf{D}}_3$, $\widetilde{\mathbf{C}}_{3\kappa'}$, $\widetilde{\mathbf{C}}_{2\kappa}$, $\widetilde{\mathbf{C}}'_{2\kappa}$.

These isotropy types are therefore symmetry-breaking.

7.1.2 Octagonal H-planforms in the 4D case

In order to illustrate our purposes, we numerically compute the octagonal H-planforms associated to the isotropy groups given in proposition 7.1.1. We recall that these planforms are eigenfunctions of the Laplace-Beltrami operator in $\mathbb{D}$ which satisfy certain isotropy conditions: (i) being invariant under a lattice group Γ and (ii) being invariant under the action of an isotropy subgroup of the symmetry group of the fundamental domain $\mathbb{D}/\Gamma$ (mod Γ). In section 6.4 of chapter 6, we tackled the problem of computing octagonal H-planforms and we described the required numerical and geometrical methods. In this subsection, we complete this study for the four-dimensional case and we illustrate it with a selection of images of octagonal H-planforms.

We first explain how to recover the desymmetrized domain and the associated boundary conditions for isotropy group $\widetilde{\mathbf{C}}_{3\kappa'}$ in Figure 7.1(a). The group $\widetilde{\mathbf{C}}_{3\kappa'}$ has six elements among them are ε the rotation by $2\pi/3$ centered at R and the reflections κ', κ''through the side PR and QR respectively, where P, Q and R are the vertices of the purple triangle in Figure 6.3. Each reflection implies Neumann boundary conditions on their respective edges. The Dirichlet boundary conditions prevent an additional 3-fold rotation. The last Neumann boundary condition is obtained by translating the desymmetrized domain with the four boosts (6.14).

In order to better illustrate the intrinsic differences of planforms with isotropy types $\widetilde{\mathbf{C}}_{2\kappa}$ and $\widetilde{\mathbf{C}}'_{2\kappa}$, we decide to work with $\overline{\mathbf{C}}'_{2\kappa} = \{Id,-\sigma,-\kappa,\kappa''\}$, a conjugate of $\widetilde{\mathbf{C}}'_{2\kappa}$. Indeed, isotropy groups $\widetilde{\mathbf{C}}_{2\kappa}$ and $\overline{\mathbf{C}}'_{2\kappa}$ share the same desymmetrized domain but have different boundary conditions depending on their symmetries, see Figure 7.1(b) and 7.1(c). As we apply finite element method to compute the eigenvalues

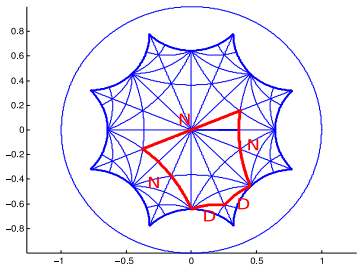

(a) $\widetilde{\mathbf{C}}_{3\kappa'}$

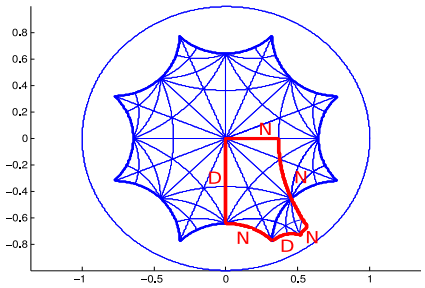

(b) $\widetilde{\mathbf{C}}_{2\kappa}$

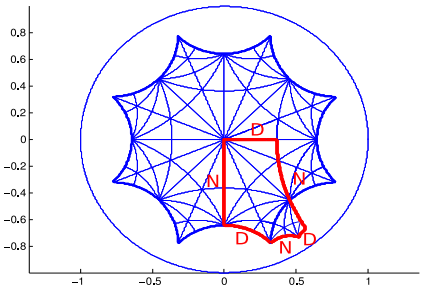

(c) $\overline{\mathbf{C}}'_{2\kappa}$

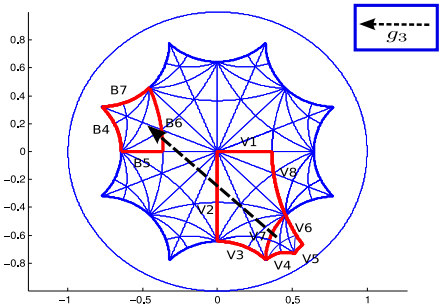

(d) Action of the boost g_3 on the desymmetrized domain corresponding to isotropy groups $\widetilde{\mathbf{C}}_{2\kappa}$ and $\overline{\mathbf{C}}'_{2\kappa}$, see text.

Figure 7.1: Desymmetrized domain in red and associated boundary conditions corresponding to isotropy groups $\widetilde{\mathbf{C}}_{3\kappa'}$, $\widetilde{\mathbf{C}}_{2\kappa}$ and $\overline{\mathbf{C}}'_{2\kappa}$. Letters N and D mean respectively Neumann and Dirichlet boundary conditions.

and eigenvectors of the Laplace-Beltrami operator, it is more convenient to work with a connected domain. This is why the desymmetrized domain of isotropy groups $\widetilde{\mathbf{C}}_{2\kappa}$ and $\overline{\mathbf{C}}'_{2\kappa}$ has the particularity of a part outside the octagon, however by the action of the boost g_3 one can translate this part inside the octagon, see Figure 7.1(d). Indeed, domain delimited by edges $V4 - V5 - V6 - V7$ is translated into the domain delimited by edges $B4 - B5 - B6 - B7$ by the boost g_3. For isotropy group $\widetilde{\mathbf{C}}_{2\kappa}$, the reflection κ imposes Neumann boundary condition on edges $V1, B5$ and κ'' on $V8, V6$. The action of g_3^{-1} implies Neumann boundary condition on edge $V5 = g_3^{-1}(B5)$. We have to impose Dirichlet boundary condition on edge $V2$ to prevent the action of $-\kappa$, which does not belong to $\widetilde{\mathbf{C}}_{2\kappa}$ and further implies Dirichlet condition on $B4$ and thus on $V4$. Finally, reflection κ combined with boost g_2 which translates edge $V3$ to the opposite side of the octagon, gives Neumann boundary condition on edge $V3$. The same method applies to isotropy group $\overline{\mathbf{C}}'_{2\kappa}$ and we find the boundary conditions presented in Figure 7.1(c). For isotropy group $\widetilde{\mathbf{D}}_3$, we do not find any simple desymmetrized domain as in the other cases and we use the finite element method on the full octagon with periodic boundary conditions: opposite sides of the octagon are identified by periodicity. To identify planforms with isotropy group $\widetilde{\mathbf{D}}_3$, we first select eigenvectors with eigenfunctions of multiplicity 4 and then check the symmetries.

We show in Figure 7.2 four H-planforms with isotropy groups $\widetilde{\mathbf{C}}_{2\kappa}$, $\overline{\mathbf{C}}'_{2\kappa}$, $\widetilde{\mathbf{C}}_{3\kappa'}$ and $\widetilde{\mathbf{D}}_3$ with eigenvalue $\lambda = 5.3537$ and in Figure 7.3 two H-planforms with isotropy groups $\widetilde{\mathbf{C}}_{2\kappa}$, $\overline{\mathbf{C}}'_{2\kappa}$. Planform with isotropy group $\widetilde{\mathbf{D}}_3$ is the only one which does not possess any reflection, it is then easy to distinguish it from other planforms, see Figure 7.2(d). We notice that patterns of planforms with isotropy $\widetilde{\mathbf{C}}_{2\kappa}$ (in Figure 7.2(a)) and $\widetilde{\mathbf{C}}_{3\kappa'}$ (in Figure 7.2(c)) appear to be similar up to a rotation, despite the fact that the two cooresponding groups are different. On the contrary, it is easy to distinguish patterns of groups $\widetilde{\mathbf{C}}_{2\kappa}$, Figures 7.2(a) and 7.3(a), and $\overline{\mathbf{C}}'_{2\kappa}$, Figures 7.2(b) and 7.3(b).

In Figures 7.2 and 7.3, we have plotted for convenience, the corresponding H-planforms in the octagon only. Nevertheless, H-planforms are periodic in the Poincaré disc and in Figure 7.4, we plot the H-planform with $\widetilde{\mathbf{C}}_{3\kappa'}$ isotropy type of Figure 7.2(c). As the octagonal lattice group Γ is generated by the four boosts of Equation (6.14), then once an H-planform is computed, we report it periodically in the whole Poincaré disc by the action of these boosts and obtain Figure 7.4.

7.1.3 Bifurcation with submaximal isotropy

We briefly recall some basic results on bifurcation with submaximal isotropy which will be used in sections 7.2 and 7.3. The condition $\dim X^H = 1$, required by the Equivariant Branching Lemma, implies that H is *maximal* (there no isotropy subgroup between H and $\mathcal{G}$) and moreover in the case of representations χ_{11}, χ_{12} and χ_{13} there are no maximal isotropy subgroups with fixed-point subspaces of dimension greater than 1. However it is well-known that solutions with non maximal isotropy can occur in generic bifurcation problems. It follows that the Equivariant

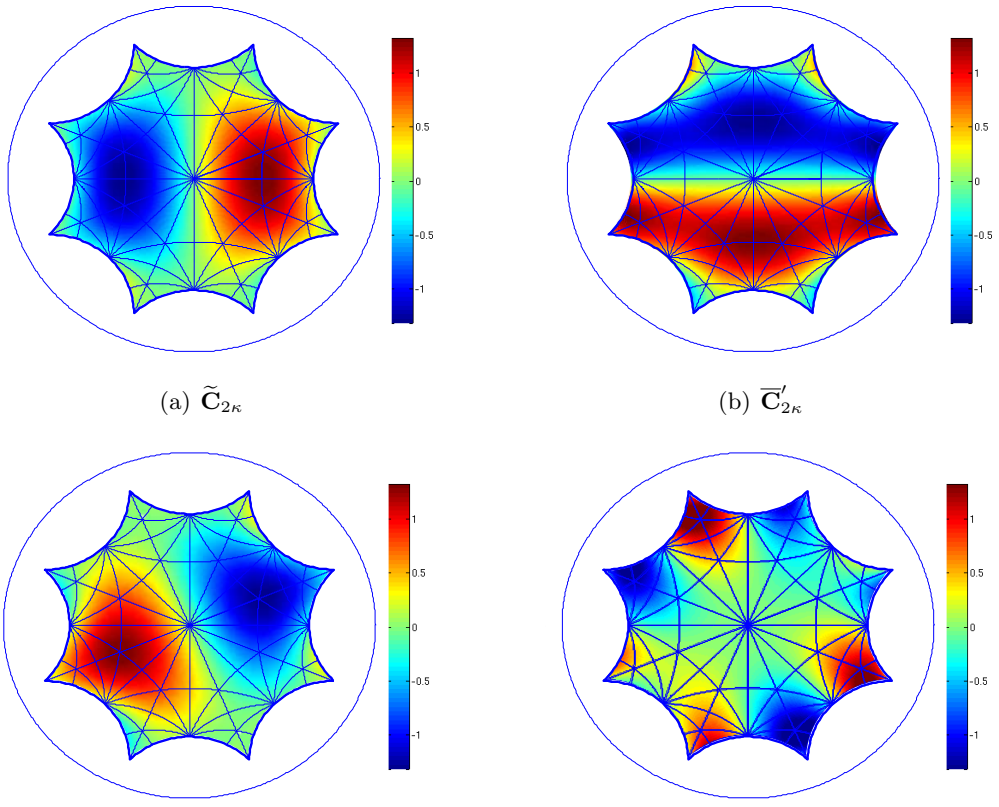

(a) $\widetilde{\mathbf{C}}_{2\kappa}$ (b) $\overline{\mathbf{C}}'_{2\kappa}$

(c) $\widetilde{\mathbf{C}}_{3\kappa'}$ (d) $\widetilde{\mathbf{D}}_3$

Figure 7.2: The four H-planforms associated to the eigenvalue $\lambda = 5.3537$.

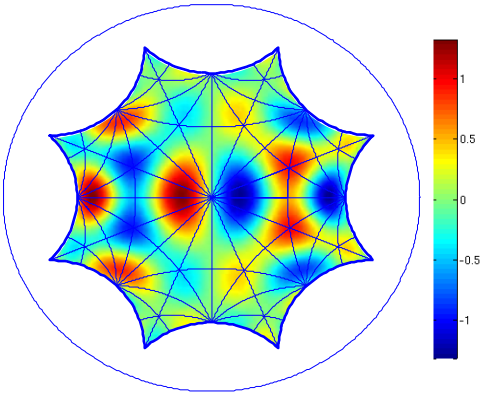

(a) $\widetilde{\mathbf{C}}_{2\kappa}$

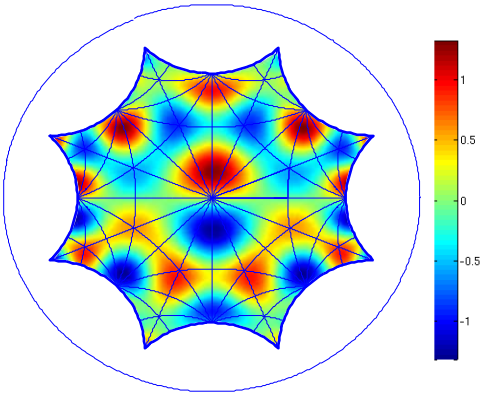

(b) $\overline{\mathbf{C}}'_{2\kappa}$

Figure 7.3: Two H-planforms corresponding to isotropy group $\widetilde{\mathbf{C}}_{2\kappa}$ right and $\overline{\mathbf{C}}'_{2\kappa}$ left for eigenvalue $\lambda = 42.3695$.

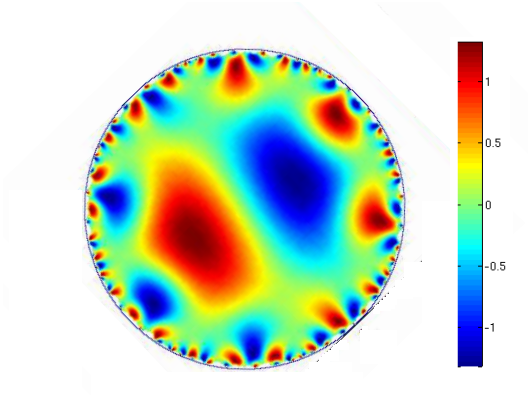

Figure 7.4: Extension of the $\widetilde{\mathbf{C}}_{3\kappa'}$ H-planform on the Poincaré disc of Figure 7.2(c).

Branching Lemma does not account for all the bifurcating equilibria and that the study of bifurcation with *submaximal* isotropy is an important issue. Here we adopt the approach of [Chossat 1990], see also [Chossat 2000].

The key for the analysis of bifurcation with submaximal isotropy is the determination of the number of copies in $\mathrm{Fix}(\Sigma)$ of subspaces $\mathrm{Fix}(\Delta)$ for the isotropy subgroups Δ containing Σ. Let $[\Sigma]$ be the conjugacy class of Σ and write $[\Sigma] < [\Delta]$ if only if $[\Sigma] \neq [\Delta]$ and $\gamma^{-1}\Sigma\gamma \subset \Delta$ for some $\gamma \in \mathcal{G}$. We call *isotropy type* the conjugacy class of an isotropy subgroup. Let $[\Delta_1], \ldots, [\Delta_r]$ be the isotropy types which satisfy the former condition. Let a_j the number of solution branches with isotropy Δ_j (a_j may be equal to 0). Then the total number of nontrivial solution branches in $\mathrm{Fix}(\Sigma)$ with higher isotropy is

$$N^{\Sigma} = \sum_{j=1}^{r} a_j n(\Sigma, \Delta_j)$$

where $n(\Sigma, \Delta_j)$ is the number of conjugate copies of $\mathrm{Fix}(\Delta)$ inside $\mathrm{Fix}(\Sigma)$.

We denote f^{Σ} the restriction to $\mathrm{Fix}(\Sigma)$ of f given in Eq. (7.1). Then, if f^{Σ} has N^0 zeroes in a neighborhood of the origin, there are precisely $N^0 - N^{\Sigma} - 1$ branches of equilibria with isotropy Σ.

If we set $N(\Sigma) = \{g \in \mathcal{G} \mid g^{-1}\Sigma g = \Sigma\}$ (normalizer of Σ in $\mathcal{G}$) and $N(\Sigma, \Delta) = \{g \in \mathcal{G} \mid \Sigma \subset g\Delta g^{-1}\}$, the quotient set $\dfrac{N(\Sigma, \Delta)}{N(\Delta)}$ is well-defined even though $N(\Sigma, \Delta)$ is not a group in general [Chossat 1990]. Moreover we have that

$$n(\Sigma, \Delta) = \left| \frac{N(\Sigma, \Delta)}{N(\Delta)} \right|$$

This formula allow us to compute the numbers $n(\Sigma, \Delta)$, hence to determine the number of solutions with isotropy Δ in $\mathrm{Fix}(\Sigma)$.

Now note that the maximal isotropy subgroups for the representations χ_{11}, χ_{12} and χ_{13} which are listed in Definition 7.1.1, have only cyclic subgroups generated by elements σ, ε, κ or κ' (or conjugates). The following lemmas give the informations when Δ is maximal.

Lemma 7.1.1. *The normalizers of the isotropy subgroups of proposition 7.1.1 are listed in table 7.1.*

Δ	$N(\Delta)$	$\lvert N(\Delta)\rvert$
$\widetilde{\mathbf{D}}_3$	$\langle \widetilde{\mathbf{D}}_3, -Id \rangle$	12
$\widetilde{\mathbf{C}}_{3\kappa'}$	$\langle \widetilde{\mathbf{C}}_{3\kappa'}, -Id \rangle$	12
$\widetilde{\mathbf{C}}_{2k}$	$\langle \widetilde{\mathbf{C}}_{2k}, -Id \rangle$	8
$\widetilde{\mathbf{C}}'_{2\kappa}$	$\langle \widetilde{\mathbf{C}}'_{2\kappa}, -Id \rangle$	8

Table 7.1: Isotropy subgroups of $\mathcal{G}$ and their normalizer. The last column provides the cardinal of the normalizer.

Proof. Let us consider, for example, $\Sigma = \widetilde{\mathbf{C}}_{2k} = \langle \sigma, \kappa \rangle$. The only conjugate of κ in $\widetilde{\mathbf{C}}_{2k}$ is κ itself, and the same holds for σ and $\sigma\kappa = \kappa'$. Therefore $N(\widetilde{\mathbf{C}}_{2k}) = N(\langle\kappa\rangle) \cap N(\langle\sigma\rangle) \cap N(\langle\sigma\kappa\rangle)$. Now for any element $h \in \mathcal{G}$, we have that $|N(\langle h \rangle)| = \frac{96}{|[h]|}$. Tables 6.2 and 6.3 show that $|[\kappa]| = 6$ while $|[\sigma]| = |[\kappa']| = 12$. It follows that $|N(\langle\kappa\rangle)| = 16$ while $|N(\langle\sigma\rangle)| = |N(\langle\kappa'\rangle)| = 8$. Hence $|N(\Sigma)| \leq 8$. But $\Sigma \subset N(\Sigma)$ and $|\Sigma| = 4$, moreover $-Id$ commutes with any element in $\mathcal{G}$ and therefore belongs to $N(\Sigma)$. It follows that the group $\langle \Sigma, -Id \rangle = N(\Sigma)$. The same rationale applies to the other isotropy subgroups. □

Lemma 7.1.2. *The values of $n(\Sigma, \Delta)$ for the maximal isotropy subgroups Δ (see Definition 7.1.1) are given in table 7.2.*

$[\Sigma]$	$[\Delta]$	$n(\Sigma, \Delta)$
$\langle\sigma\rangle$	$\widetilde{\mathbf{C}}_{2k}$	1
$\langle\sigma\rangle$	$\widetilde{\mathbf{C}}'_{2k}$	1
$\langle\sigma\rangle$	$\widetilde{\mathbf{D}}_3$	2
$\langle\varepsilon\rangle$	$\widetilde{\mathbf{D}}_3$	2
$\langle\varepsilon\rangle$	$\widetilde{\mathbf{C}}_{3\kappa'}$	2
$\langle\kappa\rangle$	$\widetilde{\mathbf{C}}_{2k}$	2
$\langle\kappa\rangle$	$\widetilde{\mathbf{C}}'_{2\kappa}$	2
$\langle\kappa'\rangle$	$\widetilde{\mathbf{C}}_{2\kappa}$	1
$\langle\kappa'\rangle$	$\widetilde{\mathbf{C}}'_{2\kappa}$	1
$\langle\kappa'\rangle$	$\widetilde{\mathbf{C}}_{3\kappa'}$	2

Table 7.2: Values of $n(\Sigma, \Delta)$.

Proof.

- Case $\Sigma = \langle\kappa\rangle$: we have $N(\Sigma, \widetilde{\mathbf{C}}_{2k}) = N(\Sigma, \widetilde{\mathbf{C}}'_{2k}) = N(\Sigma)$ as κ is not conjugate to σ nor to $\sigma\kappa$. Moreover, $|N(\Sigma)| = 16$ (see proof of Lemma 7.1.1) and $|N(\widetilde{\mathbf{C}}_{2k})| = |N(\widetilde{\mathbf{C}}'_{2k})| = 8$, hence $n(\Sigma, \widetilde{\mathbf{C}}_{2k}) = n(\Sigma, \widetilde{\mathbf{C}}'_{2k}) = 2$.
- Case $\Sigma = \langle\sigma\rangle$: we have $N(\Sigma, \widehat{\mathbf{C}}_{2k}) = N(\Sigma, \widetilde{\mathbf{C}}'_{2k}) = N(\Sigma)$ with $|N(\Sigma)| = 8$ (see proof of Lemma 7.1.1), hence $n(\Sigma, \widehat{\mathbf{C}}_{2k}) = n(\Sigma, \widetilde{\mathbf{C}}'_{2k}) = 1$. By definition $N(\Sigma, \widetilde{\mathbf{D}}_3) = \{g \in \mathcal{G} \mid g\Sigma g^{-1} \subset \widetilde{\mathbf{D}}_3\} = \{g \in \mathcal{G} \mid g\widetilde{\sigma}g^{-1} \in \mathbf{D}_3\}$. There are three conjugates of $\widetilde{\sigma}$ in $\widetilde{\mathbf{D}}_3$. Therefore $|N(\Sigma, \widetilde{\mathbf{D}}_3)| = 3|N(\langle\sigma\rangle)|$. As shown in the proof of Lemma 7.1.1), $|N(\langle\sigma\rangle)| = 8$, hence $N(\Sigma, \widetilde{\mathbf{D}}_3) = 24$ and $n(\Sigma, \widetilde{\mathbf{D}}_3) = 2$.
- The proof for the other cases uses the same arguments as above.

□

7.1.4 Presentation with biquaternions

It is natural to identify the finite group $\mathcal{G}$ to a group of 4×4 real matrices as $\dim(\chi_{12}) = 4$. Lauterbach and Matthews [Lauterbach 2010] have successfuly introduced biquaternions to study equivariant dynamical systems with $\mathbf{SO}(4)$ symmetry.

Here we also use biquaterions to give a geometric way to describe the group $\mathcal{G}$. We denote by $\mathcal{Q}$ the set of unit quaternions. The set of pairs of such quaternions forms a group, called the spinor group and denoted by Spin_4. We get a map [Conway 2003]:

$$\mathrm{Spin}_4 \to \mathbf{SO}(4) : (l, r) \mapsto [l, r] = \{x \mapsto \bar{l}xr\}$$

where a vector $\mathbf{x} \in \mathbb{R}^4$ is identified with a quaternion $x \in \mathbb{H}$ via

$$\mathbf{x} = \begin{pmatrix} x_1 \\ x_2 \\ x_3 \\ x_4 \end{pmatrix} \Leftrightarrow x = ex_1 + ix_2 + jx_3 + kx_4.$$

The two following propositions hold.

Proposition 7.1.2. *For the irreducible representations χ_{12}, χ_{13}, the group $\mathcal{G}$ admits the following presentation with biquaternions:*

$$\mathcal{G} = \langle [j, e], \left[\frac{\sqrt{2}}{2}(j+k), j\right], [e, i], [i, e], \left[\frac{1}{2}(-e+i+j+k), \frac{1}{2}(\sqrt{3}e+i)\right]\rangle.$$

It is also possible to identify the generators of $\mathcal{G}$ in matrix form:

$$\begin{aligned} \kappa &= \begin{bmatrix} 0 & 0 & 0 & -1 \\ 0 & 0 & -1 & 0 \\ 0 & -1 & 0 & 0 \\ -1 & 0 & 0 & 0 \end{bmatrix}, \quad \rho = \frac{\sqrt{2}}{2}\begin{bmatrix} 0 & 0 & -1 & -1 \\ 0 & 0 & 1 & -1 \\ -1 & -1 & 0 & 0 \\ 1 & -1 & 0 & 0 \end{bmatrix}, \\ \sigma &= \frac{\sqrt{2}}{4}\begin{bmatrix} 1 & \sqrt{3} & -1 & \sqrt{3} \\ \sqrt{3} & -1 & -\sqrt{3} & -1 \\ -1 & -\sqrt{3} & -1 & \sqrt{3} \\ \sqrt{3} & -1 & \sqrt{3} & 1 \end{bmatrix}. \end{aligned} \tag{7.2}$$

Proof. The computer algebra program GAP gives the presentation of $\mathcal{G}$ as $\mathcal{G} = \langle m_1, m_2, m_3, m_4, m_5\rangle$ with:

$$\begin{aligned} m_1 &= [j, e], \\ m_2 &= \left[\frac{\sqrt{2}}{2}(j+k), j\right], \\ m_3 &= [e, i], \\ m_4 &= [i, e], \\ m_5 &= \left[\frac{1}{2}(-e+i+j+k), \frac{1}{2}(\sqrt{3}e+i)\right]. \end{aligned}$$

We express each endomorphisms $(m_l)_{l=1\ldots5}$ of $\mathcal{G}$ in the canonical basis $\mathcal{B} = (e, i, j, k)$ and form the corresponding matrices $M_l = \mathcal{M}at_{\mathcal{B},\mathcal{B}}(m_l)$ for $l = 1 \ldots 5$. A direct calculation shows that $\mathrm{trace}(M_5) = -\sqrt{3}$ and M_5 is of order 12, such that we can

write with our notations that (up to a conjugate) $M_5 = -\varepsilon\kappa$. Matrices M_1, M_3, M_4 are of order 4 and M_2 of order 2. We set $\kappa = -M_1M_3$, such that $\varepsilon = M_5M_1M_3$. We recognize that $M_2 = \kappa' = \rho\kappa$ then $\rho = -M_2M_1M_3$ and we verify that ρ is of order 8. A straightforward calculation shows that $\rho^2 = -M_4$ and we finally note $\sigma = \rho^{-1}\varepsilon^{-1}$. The expression of the matrices of generators of $\mathcal{G}$ are given in Eq. (7.2). □

Proposition 7.1.3. *For the irreducible representation χ_{11}, the group $\mathcal{G}$ admits the following presentation with biquaternions:*

$$\mathcal{G} = \langle \left[\frac{1}{2}(-e+i+j+k), e\right], [e,j], [e,-e], [i,e], \left[\frac{\sqrt{2}}{2}(j+k), i\right] \rangle.$$

It is also possible to identify the generators of $\mathcal{G}$ in matrix form:

$$\kappa = \begin{bmatrix} 0 & 0 & 0 & -1 \\ 0 & 0 & 1 & 0 \\ 0 & 1 & 0 & 0 \\ -1 & 0 & 0 & 0 \end{bmatrix}, \quad \rho = \frac{\sqrt{2}}{2}\begin{bmatrix} 0 & 1 & 1 & 0 \\ -1 & 0 & 0 & -1 \\ 1 & 0 & 0 & -1 \\ 0 & -1 & 1 & 0 \end{bmatrix}, \quad \sigma = \frac{\sqrt{2}}{2}\begin{bmatrix} 0 & 0 & -1 & 1 \\ 0 & 0 & 1 & 1 \\ -1 & 1 & 0 & 0 \\ 1 & 1 & 0 & 0 \end{bmatrix}. \tag{7.3}$$

Proof. The proof is exactly the same as the previous one. □

7.1.5 Molien series

In [Chossat 2000] we find theorems which allow to compute the vector space dimensions of the space of equivariant and invariant polynomial maps for a group action of a given degree. We recall that the set of $\mathcal{G}$-equivariant polynomial maps forms a module $\mathcal{M}$ over the ring $\mathcal{R}_\mathcal{G}$ of $\mathcal{G}$-invariant polynomial maps. We denote by $r_d = \dim \overrightarrow{\mathcal{P}}^d(\mathcal{G})$ the dimension of the polynomial equivariants of degree d.

Theorem 7.1.1 (Equivariant Molien's theorem). *Consider the formal power series*

$$\Phi^\rho_\mathcal{M}(z) = \sum_{d=0}^{\infty} r_d z^d.$$

It has a representation

$$\Phi^\rho_\mathcal{M}(z) = \int_\mathcal{G} \frac{Tr(g)}{\det(\mathbf{1} - z\rho(g))} dg.$$

In our case, $\mathcal{G}$ is a finite group, and we can directly apply this theorem together with table 6.6 to find:

- for χ_{12}:

$$\Phi^{\chi_{12}}_\mathcal{M}(z) = \frac{1}{96}\left[\frac{4}{(1-z)^4} - \frac{4}{(1+z)^4} + \frac{8}{1-z-z^3+z^4} - \frac{8}{1+z+z^3+z^4} + \frac{8\sqrt{3}}{1-z\sqrt{3}+2z^2-z^3\sqrt{3}+z^4} - \frac{8\sqrt{3}}{1+z\sqrt{3}+2z^2+z^3\sqrt{3}+z^4}\right]$$

and $\Phi_{\mathcal{M}}^{\chi_{12}}(z) = z + 2z^3 + 5z^5 + 10z^7 + O(z^7)$.

- for χ_{11}:

$$\Phi_{\mathcal{M}}^{\chi_{11}}(z) = \frac{1}{96}\left[\frac{4}{(1-z)^4} - \frac{4}{(1+z)^4} - \frac{16}{(1+z+z^2)^2} + \frac{16}{(1-z+z^2)^2}\right]$$

and $\Phi_{\mathcal{M}}^{\chi_{11}}(z) = z + z^3 + 4z^5 + 12z^7 + O(z^7)$.

An analog of the Equivariant Molien's theorem holds for invariant polynomial maps and we denote $c_d = \dim \mathcal{R}^d$ the dimension of invariants polynomials of degree d.

Theorem 7.1.2 (Invariant Molien's theorem). *Consider the formal power series*

$$P_{\mathcal{R}_\mathcal{G}}^{\rho}(z) = \sum_{d=0}^{\infty} c_d z^d.$$

It has a representation

$$P_{\mathcal{R}_\mathcal{G}}^{\rho}(z) = \int_{\mathcal{G}} \frac{1}{\det(\mathbf{1} - z\rho(g))} dg.$$

Applying this theorem together with tables 6.2 and 6.3 yields

- for χ_{12}:

$$P_{\mathcal{R}_\mathcal{G}}^{\chi_{12}}(z) = z^2 + 2z^4 + 3z^6 + O(z^6)$$

- for χ_{11}:

$$P_{\mathcal{R}_\mathcal{G}}^{\chi_{11}}(z) = z^2 + z^4 + 3z^6 + O(z^6).$$

These results are summerized in the following table:

Character	e3	i4	e5	i6	e7
χ_{11}	1	1	4	3	12
χ_{12}	2	2	5	3	10
χ_{13}	2	2	5	3	10

Table 7.3: The information on the number of invariant/equivariant polynomial maps for the irreducible representations χ_{11}, χ_{12} and χ_{13}. Here e stands for equivariant, i for invariant and the number behind these letters for the degree of the polynomial map. The number in the table gives the dimension of the space of equivariant/invariant polynomial maps in the given degrees.

7.2 Bifurcation diagrams in the case of the representation χ_{12}

The character table 6.6 shows that the two 4D representations χ_{12} and χ_{13} are almost identical, the only difference coming from the fact that the characters of the group elements $\varepsilon\kappa$ and $-\varepsilon\kappa$ have opposite signs. It follows that the general bifurcation analysis in the case of χ_{13} is identical to the case of χ_{12} and does not introduce any novelty. In the following we shall therefore only describe the χ_{12} case.

7.2.1 Equivariant structure of the equations on the center manifold

We need to know the form of the asymptotic expansion of the $\mathcal{G}$ equivariant map $f(\cdot,\lambda)$ in Equation (7.1). Table 7.3 tells us that there are two independent equivariant homogeneous polynomial maps of order 3. The computation of these terms will prove to be sufficient to fully determine the bifurcation diagram under generic conditions.

We first need to choose a system of coordinates in $\mathbb{R}^4$. In the remaining part of this paper we shall use the same notation for an element in $\mathcal{G}$ and for its representation when there is no ambiguity. The following lemma is proved in Appendix A.1.1.

Lemma 7.2.1. *For the representation χ_{12} the diagonalization of the 8-fold symmetry matrix ρ has the form*

$$\rho = \begin{bmatrix} \exp(\frac{\mathbf{i}\pi}{4}) & 0 & 0 & 0 \\ 0 & \exp(-\frac{\mathbf{i}\pi}{4}) & 0 & 0 \\ 0 & 0 & \exp(\frac{3\mathbf{i}\pi}{4}) & 0 \\ 0 & 0 & 0 & \exp(-\frac{3\mathbf{i}\pi}{4}) \end{bmatrix}.$$

We note $(z_1, \bar{z}_1, z_2, \bar{z}_2)$ the complex coordinates in the corresponding basis.

The following theorem gives the form of the bifurcation equations on the center manifold .

Theorem 7.2.1. *For the representation χ_{12}, Equation (7.1) expressed in the coordinates $(z_1, \bar{z}_1, z_2, \bar{z}_2)$ admits the following expansion*

$$\dot{z}_1 = \left[\lambda + a(|z_1|^2 + |z_2|^2)\right] z_1 + b\left[\sqrt{3}\left(3z_1^2 + \bar{z}_2^2\right)\bar{z}_1 - \mathbf{i}\left(z_2^2 + 3\bar{z}_1^2\right) z_2\right] + h.o.t. \quad (7.4)$$

$$\dot{z}_2 = \left[\lambda + a(|z_1|^2 + |z_2|^2)\right] z_2 + b\left[\sqrt{3}\left(3z_2^2 + \bar{z}_1^2\right)\bar{z}_2 + \mathbf{i}\left(z_1^2 + 3\bar{z}_2^2\right) z_1\right] + h.o.t. \quad (7.5)$$

where $(a, b) \in \mathbb{R}^2$. Moreover the cubic part is the gradient of the $\mathcal{G}$ invariant real polynomial function

$$\frac{a}{2}\left[\left(|z_1|^2 + |z_2|^2\right)^2\right] + b\cdot\left[\frac{\sqrt{3}}{2}\left(3\left(z_1^2\bar{z}_1^2 + z_2^2\bar{z}_2^2\right) + z_1^2 z_2^2 + \bar{z}_1^2\bar{z}_2^2\right) + \mathbf{i}\left(z_1^3\bar{z}_2 + \bar{z}_2^3 z_1 - z_2^3\bar{z}_1 - z_2\bar{z}_1^3\right)\right].$$

Proof. We postpone to appendix A.1.1 the computation of the two cubic equivariant maps. The check of the gradient form is straightforward. □

7.2.2 Isotropy types and fixed points subspaces

Lemma 7.2.2. *The lattice of isotropy types for the representation χ_{12} is shown in Figure 7.5. The numbers in parentheses indicate the dimension of corresponding fixed-point subspaces.*

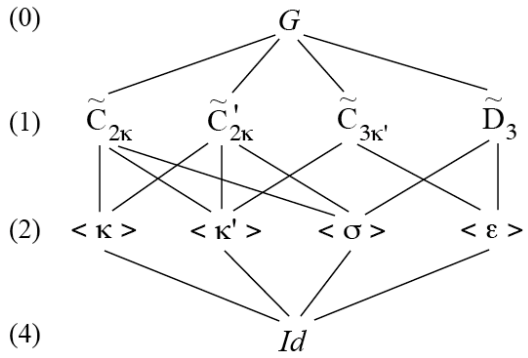

Figure 7.5: The lattice of isotropy types for the representation χ_{12}.

Proof. We recall the trace formula given in equation (6.13): if H is a subgroup and χ is the character of the representation, then

$$\dim(X^H) = \frac{1}{|H|}\sum_{h\in H}\chi(h).$$

By applying this formula for χ_{12} (see Table 6.6), one finds that the only cyclic subgroups of $\mathcal{G}$ (subgroups generated by one element) with a fixed-point subspace of positive dimension are those listed in the diagram of Figure 7.5, and this dimension is equal to 2. The result follows. □

The next lemma gives expressions for the fixed-point subspaces of two-element groups in the $(z_1, \bar{z}_1, z_2, \bar{z}_2)$ coordinates, which will be useful for the bifurcation analysis of (7.1) in the planes of symmetry. There are four types of these planes but we express the fixed-point planes for the conjugates $\tilde{\sigma}$ of σ and κ'' of κ' for later convenience.

Lemma 7.2.3. *Fixed-point subspaces associated with the isotropy groups in the diagram 7.5 have the following equations.*

- $Fix(\sigma) = \{(z_1, \bar{z}_1, z_2, \bar{z}_2) \mid z_2 = (\sqrt{2}-1)(\sqrt{2}z_1 - \mathbf{i}\sqrt{3}\bar{z}_1)\}$;
- $Fix(\tilde{\sigma}) = \rho^2 Fix(\sigma) = \{(z_1, \bar{z}_1, z_2, \bar{z}_2) \mid z_2 = (1-\sqrt{2})(\sqrt{2}z_1 + \mathbf{i}\sqrt{3}\bar{z}_1)\}$;
- $Fix(\varepsilon) = \{(z_1, \bar{z}_1, z_2, \bar{z}_2) \mid z_2 = (1+\mathbf{i})z_1 + \sqrt{3}\bar{z}_1\}$;
- $Fix(\kappa) = \{(z_1, \bar{z}_1, z_2, \bar{z}_2) \mid z_1 = \mathbf{i}\bar{z}_1 \text{ and } z_2 = \mathbf{i}\bar{z}_2\}$;
- $Fix(\kappa') = \{(z_1, \bar{z}_1, z_2, \bar{z}_2) \mid \sqrt{2}z_1 = (-1+\mathbf{i})\bar{z}_1)\} \text{ and } \sqrt{2}z_2 = -(1+\mathbf{i})\bar{z}_2)\}$.
- $Fix(\kappa'') = \{(z_1, \bar{z}_1, z_2, \bar{z}_2) \mid z_2 = (\sqrt{3}-\sqrt{2})(-\sqrt{2}z_1 + \mathbf{i}\bar{z}_1)\}$.

Proof. Given in Appendix A.2.1. □

The one dimensional fixed point subspaces are the intersections of planes of symmetry. This allows to easily obtain expressions for these axes from the expressions listed in Lemma 7.2.3. For example we can write

$$\mathrm{Fix}(\widetilde{\mathbf{C}}_{2\kappa}) = \{(z_1, z_2) \in \mathbb{C}^2 \mid z_1 = \mathbf{i}\bar{z}_1 \text{ and } z_2 = (\sqrt{2}-1)(\sqrt{2}-\sqrt{3})z_1\}.$$

7.2.3 Bifurcation analysis

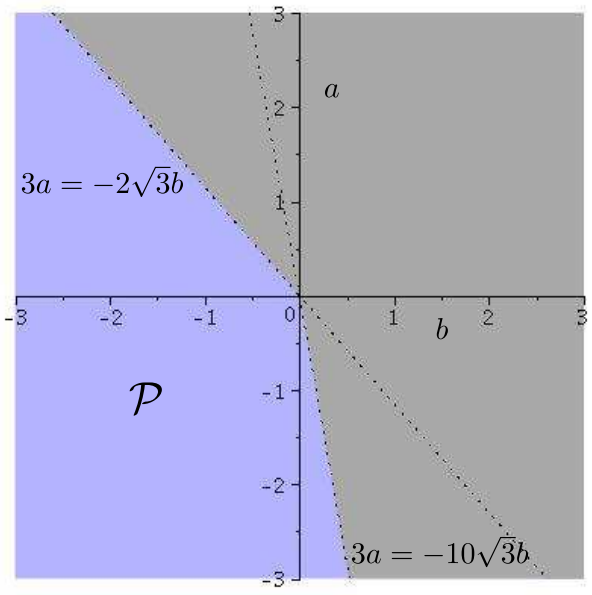

Figure 7.6: Region $\mathcal{P} = \{(a,b) \in \mathbb{R}^2 \mid 3a + 2b\sqrt{3} < 0 \text{ and } 3a + 10b\sqrt{3} < 0\}$ for the value of the parameters (a,b) is colored in blue.

Theorem 7.2.2. *Provided that* $(a,b) \in \mathcal{P} = \{(a,b) \in \mathbb{R}^2 \mid 3a+2b\sqrt{3} < 0$ *and* $3a+10b\sqrt{3} < 0\}$ *(see Figure 7.6), the following holds for Equations* (7.4)-(7.5).

(i) No solution with submaximal isotropy bifurcates in the planes of symmetry.

(ii) The branches of equilibria with maximal isotropy (as listed in Proposition 7.1.1) are pitchfork and supercritical.

(iii) If $b > 0$ *(resp.* $b < 0$*), the equilibria with isotropy type* $\widetilde{\mathbf{C}}_{3\kappa'}$ *(resp.* $\widetilde{\mathbf{D}}_3$*) are stable in* $\mathbb{R}^4$*. Branches with isotropy* $\widetilde{\mathbf{C}}_{2\kappa}$ *and* $\widetilde{\mathbf{C}}'_{2\kappa}$ *are always saddles.*

Remark 7.2.1. *We have numerically checked that the domain* $\mathcal{P}$ *coincides with the existence of an attracting, flow invariant sphere homeomorphic to* S^3 *in* $\mathbb{R}^4$*. By a theorem due to Field [Field 1989a, Chossat 2000], a condition for the existence of such a sphere is that* $\langle q(\xi), \xi\rangle < 0$ *for all* $\xi \neq 0$*, where* $\xi = (z_1, \bar{z}_1, z_2, \bar{z}_2)$*,* q *is the cubic part in the equations* (7.4), (7.5) *and* $\langle\ ,\ \rangle$ *denotes the inner product*

$\Re(z_1\bar{z}_1' + z_2\bar{z}_2')$. *Since q is an homogeneous polynomial map, it is sufficient to check the condition for $(z_1, z_2) \in S^3$, which does not present any difficulty.*

Remark 7.2.2. *The theorem doesn't rule out the possibility that equilibria with trivial isotropy could bifurcate. We conjecture this is not the case. This is supported by the fact that under the "generic" hypotheses of the theorem: (i) no other solution than those with maximal isotropy bifurcates in the planes of symmetry, (ii) the stability of these solutions is determined at cubic order and one of these types is always stable, (iii) the system is gradient at cubic order, (iv) admitting the existence of an invariant sphere (previous remark), the conjecture doesn't contradict Poincaré-Hopf formula [Guillemin 2010]: one can check that the sum of indices of equilibria with maximal isotropy is equal to 0, the Euler characteristic of S^3.*

Proof. We first compute the branches with maximal isotropy, then we examine bifurcation in the invariant planes and finally we provide the eigenvalues of the bifurcated equilibria to complete the stability diagrams.

1. Branches with maximal isotropy. Notice that, since $-Id$ acts non trivially in $\mathbb{R}^4 - \{0\}$ for χ_{12}, equilibria have to occur via pitchfork bifurcations. The maximal isotropy subgroups are $\widetilde{\mathbf{C}}_{2\kappa}$, $\widetilde{\mathbf{C}}'_{2\kappa}$, $\widetilde{\mathbf{C}}_{3\kappa'}$ and $\widetilde{\mathbf{D}}_3$. By Lemma 7.2.3 one can easily find the following parametrizations. Plugging this into the system (7.4)-(7.5) we obtain scalar equations which we solve for the bifurcated branches:

- $\mathrm{Fix}(\widetilde{\mathbf{C}}_{2\kappa}) = \{z_1 = (1+\mathbf{i})x,\ z_2 = (\sqrt{2}-1)(\sqrt{2}z_1 - \mathbf{i}\sqrt{3}\bar{z}_1)\}$.
  Bifurcated branch: $\lambda = -4K_1\left(a + 2b(1+\sqrt{3})\right)x^2 + O(x^4)$, where $K_1 = 8 - 3\sqrt{6} - 5\sqrt{2} + 4\sqrt{3} > 0$.

- $\mathrm{Fix}(\widetilde{\mathbf{C}}'_{2\kappa}) = \{z_1 = (1+\mathbf{i})x,\ z_2 = (1-\sqrt{2})(\sqrt{2}z_1 + \mathbf{i}\sqrt{3}\bar{z}_1)\}$.
  Bifurcated branch: $\lambda = -4K_2\left(a + 2b(\sqrt{3}-1)\right)x^2 + O(x^4)$, where $K_2 = 8 + 3\sqrt{6} - 5\sqrt{2} - 4\sqrt{3} > 0$.

- $\mathrm{Fix}(\widetilde{\mathbf{C}}_{3\kappa'}) = \{z_1 = (1+\mathbf{i}(1+\sqrt{2}))x,\ z_2 = (1+\mathbf{i})z_1 + \sqrt{3}\bar{z}_1\}$.
  Bifurcated branch: $\lambda = -4K_3\left(a\sqrt{3} + 10b\right)x^2 + O(x^4)$, where $K_3 = -2 + \sqrt{6} - 2\sqrt{2} + 2\sqrt{3} > 0$.

- $\mathrm{Fix}(\widetilde{\mathbf{D}}_3) = \{z_1 = \left(1 + \mathbf{i}\frac{1+\sqrt{6}-\sqrt{3}}{-3+\sqrt{2}+\sqrt{3}}\right)x,\ z_2 = (1+\mathbf{i})z_1 + \sqrt{3}\bar{z}_1\}$.
  Bifurcated branch: $\lambda = -4K_4\left(a\sqrt{3} + 2b\right)x^2 + O(x^4)$, where $K_4 = 6\sqrt{3} + 4\sqrt{6} + 10 + 7\sqrt{2} > 0$.

From the formulas for the branches we deduce the direction of branching of the equilibria, hence their stability *along their axes of symmetry.* For example the equilibria with $\widetilde{\mathbf{C}}_{2\kappa}$ isotropy bifurcate supercriticaly if $a + 2b(1+\sqrt{3}) < 0$, and therefore the principle of exchange of stability (between the trivial state and the bifurcated one) holds against perturbations with the same isotropy.

2. Bifurcation in the planes of symmetry. In each of the planes of symmetry there are precisely 4 axes of symmetry. This immediately follows from Table 7.2. For example $\mathrm{Fix}(\langle\sigma\rangle)$ contains one copy of $\mathrm{Fix}(\widetilde{\mathbf{C}}_{2\kappa})$, one copy of $\mathrm{Fix}(\widetilde{\mathbf{C}}'_{2\kappa})$ and two

copies of Fix($\widetilde{\mathbf{D}}_3$). Let us choose real coordinates (x, y) in a plane of symmetry P and write the equations in P

$$\dot{x} = \lambda x + q_1(x, y) + h.o.t. \tag{7.6}$$
$$\dot{y} = \lambda y + q_2(x, y) + h.o.t. \tag{7.7}$$

where q_1 and q_2 are the components of the cubic part in the Taylor expansion of f restricted to P. If $(x(\lambda), y(\lambda))$ is a branch of equilibria of this system, then the equation

$$Q(x, y) = yq_1(x, y) - xq_2(x, y) = 0 \tag{7.8}$$

admits an axis of solutions $\varepsilon(x_0, y_0)$ where (x_0, y_0) represents the leading order in the Taylor expansion of the solution. If Q is not degenerate the number of such axes is bounded by the degree of Q which is equal to 4. Now, there are 4 axes of symmetry in P and each of them corresponds to an axis of solutions of the above equation. Therefore if Q is not degenerate, there are no other invariant axes for Equation (7.8). To prove that there are no submaximal branches of solutions in the planes of symmetry it remains to check the non degeneracy of Q.
Calculations with Maple have shown that in all cases the form Q in non degenerate, hence there are no generic bifurcations of solutions with submaximal isotropy in these planes.

Remark. The stability of the bifurcated equilibria in the planes of symmetry is determined by the sign of the eigenvalues of the Jacobian matrix $\begin{pmatrix} \partial_x\dot{x} & \partial_y\dot{x} \\ \partial_x\dot{y} & \partial_y\dot{y} \end{pmatrix}$ evaluated at the equilibria. One eigenvalue is radial with leading part -2λ (since q_1 and q_2 are cubic), the other one is transverse (see subsection 7.1.1). Calculations lead to the Table 7.4 for the transverse eigenvalues.

3. Stability in $\mathbb{R}^4$.

Table 7.4 shows the leading part of the transverse eigenvalues for the two types of bifurcated equilibria. Each equilibrium lies at the intersection of three planes. The four constants $(C_i)_{i=1\ldots4}$ in Table 7.4 are given by:

$$\begin{array}{lllllll} C_1 & = & 10 + 6\sqrt{3} - 4\sqrt{6} - 7\sqrt{2} > 0 & C_2 & = & -10 + 6\sqrt{3} - 4\sqrt{6} + 7\sqrt{2} > 0 \\ C_3 & = & 2 + 2\sqrt{3} - 2\sqrt{2} - \sqrt{6} > 0 & C_4 & = & -2 + 2\sqrt{3} + 2\sqrt{2} - \sqrt{6} > 0. \end{array}$$

For those with $\widetilde{\mathbf{C}}_{2\kappa}$ and $\widetilde{\mathbf{C}}'_{2\kappa}$ isotropy, the planes are Fix(κ), Fix(σ) and Fix(κ'). The equilibria with $\widetilde{\mathbf{C}}_{3\kappa'}$ isotropy lie in Fix(ε) and Fix(κ'). The action of ε "rotates" Fix(κ') by an angle $2\pi/3$ around the axis Fix($\widetilde{\mathbf{C}}_{3\kappa'}$), hence a transverse eigenvalue is double and has eigenvectors in Fix(κ') and its copies by ε and ε^2. Similarly, equilibria with $\widetilde{\mathbf{D}}_3$ isotropy have a double transverse eigenvalue with eigenvectors in Fix(σ) and its copies by ε and ε^2.

Now, Table 7.4 shows that equilibria with isotropies $\widetilde{\mathbf{C}}_{2\kappa}$ and $\widetilde{\mathbf{C}}'_{2\kappa}$ are never stable. Indeed their transverse eigenvalues in the planes Fix(σ) and Fix(κ') have opposite signs (we assume the generic condition $b \neq 0$ to be true). Now suppose

	$\widetilde{\mathbf{C}}_{2\kappa}$	$\widetilde{\mathbf{C}}'_{2\kappa}$	$\widetilde{\mathbf{C}}_{3\kappa'}$	$\widetilde{\mathbf{D}}_3$
$\mathrm{Fix}(\kappa)$	$-32K_1bX^2$	$32K_2bX^2$	no	no
$\mathrm{Fix}(\varepsilon)$	no	no	$-64K_3bX^2$	$64K_4bX^2$
$\mathrm{Fix}(\sigma)$	$-16C_1bX^2$	$-16C_2bX^2$	no	$16K_4bX^2$ (2)
$\mathrm{Fix}(\kappa')$	$16C_3bX^2$	$16C_4bX^2$	$-16K_3bX^2$ (2)	no

Table 7.4: Transverse eigenvalues of bifurcated equilibria in $\mathbb{R}^4$.

that the solutions with isotropy $\widetilde{\mathbf{D}}_3$ are supercritical, a condition which is fulfilled if $a\sqrt{3}+2b<0$. Their transverse eigenvalues have the same sign as b. It follows that if $b<0$ these solutions are stable (while all other equilibria are unstable).
The same argument applies to solutions with isotropy $\widetilde{\mathbf{C}}_{3\kappa'}$: if $a\sqrt{3}+10b<0$ (supercritical branch) and $b>0$, these solutions are stable in $\mathbb{R}^4$ while all other equilibria are unstable.
It remains to check the domain $\mathcal{P}$ in the theorem. One can easily show that all bifurcated branches are supercritical if the inequalities $a\sqrt{3}+2b<0$ and $a\sqrt{3}+10b<0$ are satisfied. This finishes the proof. □

7.3 Bifurcation diagrams in the case of the representation χ_{11}

7.3.1 Equivariant structure of the equations on the center manifold

As for representation χ_{12}, we also need to know the form of the asymptotic expansion of $f(\cdot,\lambda)$ in equation (7.1). Table 7.3, given by the computation of Molien series, shows that there are only one equivariant homogeneous polynomial map of order 3 and four linearly independent equivariant maps of order 5. The bifurcation diagrams are fully determined, under generic conditions, by the computations of these terms. However, it turns out that these computations are not anymore sufficient if one wants to study some specific dynamics of equation (7.1) as depicted in section 7.4.

We first need to choose a system of coordinates in $\mathbb{R}^4$. The following lemma is proved in Appendix A.1.2.

Lemma 7.3.1. *For the representation χ_{11} the diagonalization of the 8-fold symmetry matrix ρ has the form*

$$\rho=\begin{bmatrix}\exp(\frac{\mathbf{i}\pi}{4}) & 0 & 0 & 0\\ 0 & \exp(-\frac{\mathbf{i}\pi}{4}) & 0 & 0\\ 0 & 0 & \exp(\frac{3\mathbf{i}\pi}{4}) & 0\\ 0 & 0 & 0 & \exp(-\frac{3\mathbf{i}\pi}{4})\end{bmatrix}.$$

We note $(z_1,\bar{z}_1,z_2,\bar{z}_2)$ the complex coordinates in the corresponding basis.

Remark 7.3.1. *The diagonal matrix is the same as in Lemma 7.2.1, however the corresponding bases differ for the two representations χ_{12}, χ_{11}. Indeed, from Propo-*

sitions 7.1.2 and 7.1.3, one can check that the presentation given by biquaternions of ρ for representation χ_{12} and χ_{11} are different.

The bifurcation equations of the center manifold is given by the following theorem.

Theorem 7.3.1. *For the representation χ_{11}, Equation (7.1) expressed in the coordinates $(z_1, \bar{z}_1, z_2, \bar{z}_2)$ admits the following expansion*

$$\dot{z}_1 = \lambda z_1 + A z_1 \left(|z_1|^2 + |z_2|^2\right) + a z_1 \left(|z_1|^2 + |z_2|^2\right)^2 + b\left(z_1^4 \bar{z}_2 + 4 z_2^3 |z_1|^2 - z_2^3 |z_2|^2\right) + c\left(3\bar{z}_1^2 z_2 |z_2|^2 - z_1^2 \bar{z}_2^3 - 2\bar{z}_1^2 |z_1|^2 z_2\right) + d\left(-5\bar{z}_1^4 \bar{z}_2 + \bar{z}_2^5\right) + h.o.t \quad (7.9)$$

$$\dot{z}_2 = \lambda z_2 + A z_2 \left(|z_1|^2 + |z_2|^2\right) + a z_2 \left(|z_1|^2 + |z_2|^2\right)^2 + b\left(-\bar{z}_1 z_2^4 - 4 z_1^3 |z_2|^2 + z_1^3 |z_1|^2\right) + c\left(-3 z_1 \bar{z}_2^2 |z_1|^2 + \bar{z}_1^3 z_2^2 + 2 z_1 \bar{z}_2^2 |z_2|^2\right) + d\left(5\bar{z}_1 \bar{z}_2^4 - \bar{z}_1^5\right) + h.o.t \quad (7.10)$$

where $(A, a, b, c, d) \in \mathbb{R}^5$.

Proof. There is one $\mathcal{G}$-equivariant cubic map, hence necessarily equals to $E_3(\mathbf{z}) = \mathbf{z}\|\mathbf{z}\|^2$ with $\mathbf{z} = (z_1, \bar{z}_1, z_2, \bar{z}_2)$. We postpone to Appendix A.1.2 the computation of the four quintic equivariant maps. □

7.3.2 Isotropy types and fixed points subspaces

Lemma 7.3.2. *The lattice of isotropy types for the representation χ_{11} is shown in Figure 7.7. The numbers in parentheses indicate the dimension of corresponding fixed-point subspaces.*

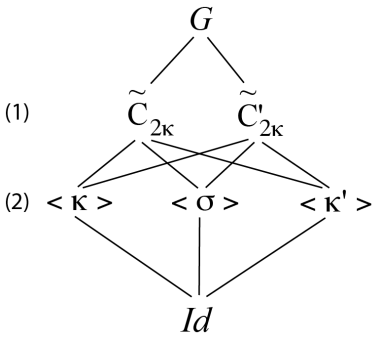

Figure 7.7: The lattice of isotropy types for the representation χ_{11}.

Proof. The only cyclic subgroups of $\mathcal{G}$ with a fixed-point subspace of positive dimension are given in the diagram of Figure 7.7 and determined by applying (6.13) for χ_{11} (see Table 6.6). □

The next lemma gives expressions for the fixed-point subspaces of two-element groups in the $(z_1, \bar{z}_1, z_2, \bar{z}_2)$ coordinates, which will be useful for the bifurcation analysis of (7.1) in the planes of symmetry. There are three types of these planes. We also express the fixed-point plane for the conjugate κ'' of κ' for later convenience.

Lemma 7.3.3. *Fixed-point subspaces associated with the isotropy groups in the diagram 7.7 have the following equations.*

- $Fix(\sigma) = \{(z_1, \bar{z}_1, z_2, \bar{z}_2) \mid z_2 = \mathbf{i}(1+\sqrt{2})z_1\}$;
- $Fix(\kappa) = \{(z_1, \bar{z}_1, z_2, \bar{z}_2) \mid z_1 = \mathbf{i}\bar{z}_1 \text{ and } z_2 = -\mathbf{i}\bar{z}_2\}$;
- $Fix(\kappa') = \{(z_1, \bar{z}_1, z_2, \bar{z}_2) \mid z_1 = \frac{\sqrt{2}}{2}(\mathbf{i}-1)\bar{z}_1 \text{ and } z_2 = \frac{\sqrt{2}}{2}(\mathbf{i}+1)\bar{z}_2\}$;
- $Fix(\kappa'') = \{(z_1, \bar{z}_1, z_2, \bar{z}_2) \mid z_2 = \mathbf{i}z_1 - \sqrt{2}\bar{z}_1\}$.

Proof. Given in Appendix A.2.2. □

The one dimensional fixed point subspaces are the intersections of planes of symmetry. This allows to easily obtain expressions for these axes from the expressions listed in Lemma 7.3.3. For example we can write

$$\mathrm{Fix}(\widetilde{C}_{2\kappa}) = \{(z_1, z_2) \in \mathbb{C}^2 \mid z_1 = \mathbf{i}\bar{z}_1 \text{ and } z_2 = \mathbf{i}(1+\sqrt{2})z_1\}.$$

7.3.3 Bifurcation analysis

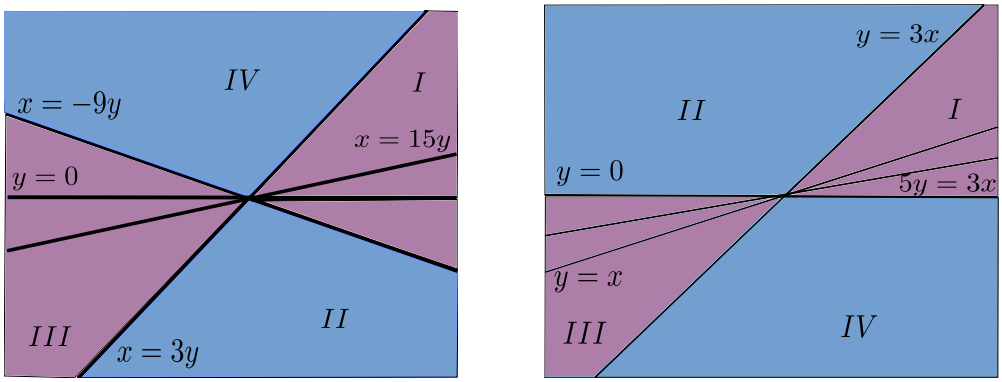

(a) In $\mathrm{Fix}(\sigma)$, bifurcation of submaximal solutions occur for values of coefficients (b, c, d) in the blue regions II and IV. We have set $x = b + c$ and $y = d$.

(b) In $\mathrm{Fix}(\kappa')$, bifurcation of submaximal solutions occur for values of coefficients (b, c, d) in the regions II and IV. We have set $x = c$ and $y = b + d$.

Figure 7.8: Conditions on coefficients (b, c, d) of existence of submaximal solutions in the planes $\mathrm{Fix}(\sigma)$ and $\mathrm{Fix}(\kappa'')$ (in blue).

Theorem 7.3.2. *Provided that $A < 0$, there exists an attracting, flow invariant, sphere homeomorphic to S^3 in $\mathbb{R}^4$ and branches of equilibria with maximal isotropy (as listed in Proposition 7.1.1) are pitchfork and supercritical. The bifurcation diagrams in each fixed-point planes are as follows.*

(i) $Fix(\kappa)$ contains two copies of each type of isotropy axes. Moreover,

- *No solution with submaximal isotropy bifurcates in $Fix(\kappa)$.*

- *If $b < d$ (resp. $b > d$) the equilibria with isotropy $\widetilde{\mathbf{C}}_{2\kappa}$ are stable (resp. saddles) and $\widetilde{\mathbf{C}}'_{2\kappa}$ are saddles (resp. stable).*

(ii) Fix(σ) contains one copy of each type of isotropy axes. Moreover,

- *If $b + c + 9d > 0$ (resp. $b + c + 9d < 0$) equilibria with isotropy $\widetilde{\mathbf{C}}_{2\kappa}$ are stable (resp. saddles) and $\widetilde{\mathbf{C}}'_{2\kappa}$ are saddles (resp. stable), see regions I and IV (resp. II and III) in Figure 7.8(a).*
- *If $d(3d - b - c) < 0$ or $(b + c - 15d)(b + c + 9d) > 0$, no solution with submaximal isotropy bifurcates in fixed-point plane Fix(σ), see regions I and III in Figure 7.8(a).*
- *If $d(3d - b - c) > 0$ and $(b + c - 15d)(b + c + 9d) < 0$, regions II and IV in Figure 7.8(a), solutions with submaximal isotropy bifurcate form equilibria $\widetilde{\mathbf{C}}_{2\kappa}$ and $\widetilde{\mathbf{C}}'_{2\kappa}$ in Fix(σ). The corresponding phase diagram is shown in Figure 7.9.*

(iii) Fix(κ') contains one copy of each type of isotropy axes. Moreover,

- *If $d + b - 3c < 0$ (resp. $d + b - 3c > 0$) equilibria with isotropy $\widetilde{\mathbf{C}}_{2\kappa}$ are stable (resp. saddles) and $\widetilde{\mathbf{C}}'_{2\kappa}$ are saddles (resp. stable), see regions II and III (resp. I and IV) in Figure 7.8(b).*
- *If $(b+d)(b+d-c) < 0$ or $(5d-3c+5b)(d+b-3c) < 0$, no solution with submaximal isotropy bifurcates in fixed-point plane Fix(κ'), see regions I and III in Figure 7.8(b).*
- *If $(b+d)(b+d-c) > 0$ or $(5d-3c+5b)(d+b-3c) > 0$, regions II and IV in Figure 7.8(b), solutions with submaximal isotropy bifurcate form equilibria $\widetilde{\mathbf{C}}_{2\kappa}$ and $\widetilde{\mathbf{C}}'_{2\kappa}$ in fixed-point plane Fix(κ'). The corresponding phase diagram is given in Figure 7.9.*

Proof. The assumption $A < 0$ ensures that $\langle q(\xi), \xi\rangle = A\|\xi\|^4 < 0$ for all $\xi \neq 0$, where $\xi = (z_1, \bar{z}_1, z_2, \bar{z}_2)$, q is the cubic part in the equations (7.9), (7.10) and $\langle\ ,\ \rangle$ denotes the inner product $\Re(z_1\bar{z}'_1 + z_2\bar{z}'_2)$ and $\|\ \|$ the associated norm. This implies the existence of the invariant sphere homeomorphic to S^3 in $\mathbb{R}^4$. We now examine bifurcation in the invariant planes. We can already note that, since $-Id$ acts non trivially in $\mathbb{R}^4 - \{0\}$ for χ_{12}, equilibria have to occur via pitchfork bifurcations. We proceed as in section 7.2 for the case with representation χ_{12}.

1. *Branches with maximal isotropy.* Since $A < 0$ branches of solutions along the axis of symmetry exist for $\lambda > 0$ with leading part $\lambda = -A\|X\|^2$ where X belongs to the corresponding axis.

2. *Bifurcation and stability in* Fix(κ). By Lemma 7.3.3,

$$\mathrm{Fix}(\kappa) = \{(z_1, z_2) \in \mathbb{C}^2 | z_1 = (1 + \mathbf{i})x \text{ and } z_2 = (1 - \mathbf{i})y, \quad (x, y) \in \mathbb{R}^2\}\ .$$

   By Table 7.2 this plane contains two axes with isotropy type $\widetilde{\mathbf{C}}_{2\kappa}$ and two axes with isotropy type $\widetilde{\mathbf{C}}'_{2\kappa}$. We can choose as representative $\mathrm{Fix}(\widetilde{\mathbf{C}}_{2\kappa}) =$

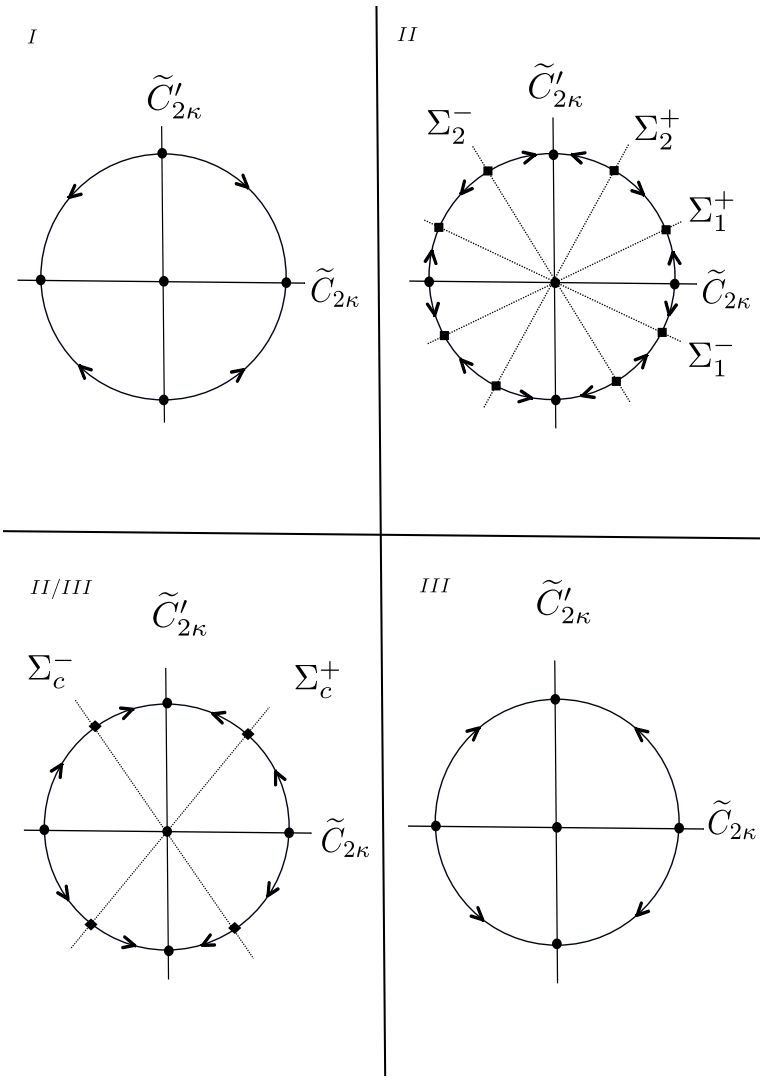

Figure 7.9: Changes of phase diagram in Fix(σ) and Fix(κ') as the coefficients (b, c, d) pass from regions $I - II - III$ in Figure 7.8(a) (for Fix(σ)) and in Figure 7.8(b) (for Fix(κ')). $\Sigma_1^{\pm}$ and $\Sigma_2^{\pm}$ indicate solutions with submaximal isotropy. The case II/III corresponds to coefficient values at the boundary between region II and III (saddle-node bifurcation of equilibria with submaximal isotropy).

$\{y = -(1+\sqrt{2})x\}$ and $\mathrm{Fix}(\widetilde{\mathbf{C}}'_{2\kappa}) = \{y = (1+\sqrt{2})x\}$. We change coordinates so that $\mathrm{Fix}(\widetilde{\mathbf{C}}_{2\kappa})$ is the real axis. With the following choice:

$$\begin{pmatrix} x \\ y \end{pmatrix} = \begin{bmatrix} \alpha^{-1} & \beta^{-1} \\ -\alpha^{-1}(1+\sqrt{2}) & \beta^{-1}(\sqrt{2}-1) \end{bmatrix} \begin{pmatrix} X \\ Y \end{pmatrix}$$

where $\alpha = \sqrt{4+2\sqrt{2}}$ and $\beta = \sqrt{4-2\sqrt{2}}$, the equations (7.9) and (7.10) read

$$\begin{aligned} \dot{X} = \lambda X + 2AX(X^2+Y^2) + 4aX(X^2+Y^2)^2 + 2bX(-X^4 - 2X^2Y^2 + 7Y^4) \\ + 2cX(X^4 - 6X^2Y^2 + Y^4) + 2dX(3X^4 - 10X^2Y^2 - 5Y^4) \end{aligned}$$

$$\begin{aligned} \dot{Y} = \lambda Y + 2AY(X^2+Y^2) + 4aY(X^2+Y^2)^2 - 2bY(-7X^4 + 2X^2Y^2 + Y^4) \\ + 2cY(X^4 - 6X^2Y^2 + Y^4) - 2dY(5X^4 + 10X^2Y^2 - 3Y^4) \end{aligned}$$

and the polynomial map Q defined in Equation (7.8) is $Q(X,Y) = -16(X-Y)(X+Y)(X^2+Y^2)XY(b-d)$. The axes $Y=0$ and $X=0$ correspond to $\widetilde{\mathbf{C}}_{2\kappa}$ isotropy type and the axes $X = \pm Y$ correspond to $\widetilde{\mathbf{C}}'_{2\kappa}$ isotropy type. Therefore if $b \neq d$ there are no submaximal solutions in $\mathrm{Fix}(\kappa)$.

Stability of the solutions. The transverse eigenvalues are computed from these equations and are summarized in Table 7.5.

Isotropy type	$\widetilde{\mathbf{C}}_{2\kappa}$	$\widetilde{\mathbf{C}}'_{2\kappa}$
Tranverse eigenvalue	$16(b-d)X^4$	$-64(b-d)X^4$

Table 7.5: Transverse eigenvalues (leading order) of bifurcated equilibria in $\mathrm{Fix}(\kappa)$.

3. *Bifurcation and stability in* $\mathrm{Fix}(\sigma)$. By Lemma 7.3.3,

$$\mathrm{Fix}(\sigma) = \{(z_1, z_2) \in \mathbb{C}^2 \mid z_2 = \mathbf{i}(1+\sqrt{2})z_1\} .$$

By Table 7.2 there are two axes of symmetry in this plane: one of type $\widetilde{\mathbf{C}}_{2\kappa}$ and one of type $\widetilde{\mathbf{C}}'_{2\kappa}$. From Definition 7.1.1, a conjugate of $\widetilde{\mathbf{C}}'_{2\kappa}$ containing σ is $\widetilde{\mathbf{C}}''_{2\kappa} = \rho^{-2}\widetilde{\mathbf{C}}'_{2\kappa}\rho^2 = \{Id, \sigma, -\kappa, -\kappa''\}$.

Let us write $z_1 = x + \mathbf{i}y$. In the (x,y) coordinates, $\mathrm{Fix}(\widetilde{\mathbf{C}}_{2\kappa}) = \{y = x\}$, $\mathrm{Fix}(\widetilde{\mathbf{C}}''_{2\kappa}) = \{y = -x\}$. We change coordinates such that $x = \sqrt{2}/2(X+Y)$, $x = \sqrt{2}/2(X-Y)$. Hence $Y=0$ is the equation of $\mathrm{Fix}(\widetilde{\mathbf{C}}_{2\kappa})$ and $X=0$ is the equation of $\mathrm{Fix}(\widetilde{\mathbf{C}}''_{2\kappa})$. Then

$$\begin{aligned} \dot{X} = \lambda X + 2E_1AX(X^2+Y^2) + 8E_2aX(X^2+Y^2)^2 - 4E_2bX(X^2+Y^2)(X^2-3Y^2) \\ + 4E_2cX(X^2+Y^2)^2 + 12E_2dX(X^4 - 10X^2Y^2 + 5Y^4) \end{aligned}$$

$$\begin{aligned} \dot{Y} = \lambda Y + 2E_1AY(X^2+Y^2) + 8E_2aY(X^2+Y^2)^2 - 4E_2bY(X^2+Y^2)(3X^2-Y^2) \\ - 4E_2cY(X^2+Y^2)^2 - 12E_2dX(5X^4 - 10X^2Y^2 + Y^4) \end{aligned}$$

where $E_1 = 2+\sqrt{2}$ and $E_2 = 3+2\sqrt{2}$. For this system we obtain

$$Q(X,Y) = 8E_2XY\left[(b+c+9d)X^4 + 2(b+c-15d)X^2Y^2 + (b+c+9d)Y^4\right]$$

We denote $H(X,Y) = (b+c+9d)X^4 + 2(b+c-15d)X^2Y^2 + (b+c+9d)Y^4$.

Study of the polynomial map $H(X,Y)$. We consider H as a polynomial map of degree two in X^2. When $b+c-15d = 0$, then H is simplified as $H(X,Y) = (b+c+9d)(X^4+Y^4)$, and there is no submaximal bifurcation in $\mathrm{Fix}(\sigma)$. In the remaining part of this paragraph, we suppose that $b+c-15d \neq 0$.

- Suppose that $d(3d-b-c) > 0$ then $X^2 = \nu_\pm Y^2$ with

$$\nu_\pm = \frac{-(b+c-15d) \pm \sqrt{48d(3d-b-c)}}{(b+c+9d)}$$

  and $\nu_+\nu_- = 1$, $\nu_+ + \nu_- = -2\frac{b+c-15d}{b+c+9d}$. Hence if $\frac{b+c-15d}{b+c+9d} < 0$, there are four axes $X = \pm\sqrt{\nu_\pm}Y$ which correspond to bifurcated submaximal solutions in $\mathrm{Fix}(\sigma)$. If $\frac{b+c-15d}{b+c+9d} > 0$ no submaximal bifurcation can bifurcate in $\mathrm{Fix}(\sigma)$.
- Suppose that $d = 0$ and $b+c \neq 0$ then $H(X,Y) = (b+c)(X^2+Y^2)^2$. This implies that no submaximal bifurcation can bifurcate in $\mathrm{Fix}(\sigma)$ if $d = 0$ and $b+c \neq 0$.
- If $3d = b+c \neq 0$ then $H(X,Y) = 12d(X-Y)^2(X+Y)^2$ and the axes $X = \pm Y$ correspond to bifurcated submaximal solutions in $\mathrm{Fix}(\sigma)$.
- If $d(3d-b-c) < 0$ then H has no other root than $(0,0)$. By the same argument as before, this shows that no submaximal solution can bifurcate in $\mathrm{Fix}(\sigma)$ in this case.

Stability of the solutions. The transverse eigenvalues for isotropy types $\widetilde{\mathbf{C}}_{2\kappa}$ and $\widetilde{\mathbf{C}}'_{2\kappa}$ are computed from the above equations and are summarized in Table 7.6.

Isotropy type	$\widetilde{\mathbf{C}}_{2\kappa}$	$\widetilde{\mathbf{C}}'_{2\kappa}$
Transverse eigenvalue	$-8(3+2\sqrt{2})(b+c+9d)X^4$	$8(3+2\sqrt{2})(b+c+9d)X^4$

Table 7.6: Transverse eigenvalues (leading order) of equilibria with maximal isotropy in $\mathrm{Fix}(\sigma)$.

We now discuss the stability of the bifurcated submaximal solutions found for $d(3d-b-c) > 0$ and $(b+c-15d)(b+c+9d) < 0$, i.e regions II and IV of Figure 7.8(a). We denote Σ_1^+ (resp. Σ_1^-) the branch of solutions with axis $X = \sqrt{\nu_+}Y$ (resp. $X = -\sqrt{\nu_+}Y$) and Σ_2^+ (resp. Σ_2^-) the branch of solutions with axis

$X = \sqrt{\nu_-}Y$ (resp. $X = -\sqrt{\nu_-}Y$). When parameters pass from region I to region II in Figure 7.8(a), pitchfork bifurcation with submaximal isotropy occurs and two equilibria $\Sigma_1^{\pm}$ emerge from equilibria with isotropy type $\widetilde{\mathbf{C}}_{2\kappa}$ and two equilibria $\Sigma_2^{\pm}$ emerge from equilibria with isotropy type $\widetilde{\mathbf{C}}'_{2\kappa}$ with exchange of stability: $\widetilde{\mathbf{C}}_{2\kappa}$ becomes unstable and $\widetilde{\mathbf{C}}'_{2\kappa}$ stable, which implies that $\Sigma_1^{\pm}$ are stable and $\Sigma_2^{\pm}$ are saddles, see Figure 7.9 (upper right). At the boundary between region II and III, equilibria Σ_1^+ (resp. Σ_1^-) and Σ_2^+ (resp. Σ_2^-) collide and form only one equilibrium denoted Σ_c^+ (resp. Σ_c^-), which no longer exists in region III: saddle-node bifurcation. These two equilibria $\Sigma_c^{\pm}$ are saddles, see Figure 7.9 (lower left). In region III, equilibria with isotropy type $\widetilde{\mathbf{C}}_{2\kappa}$ are now unstable whereas equilibria with isotropy type $\widetilde{\mathbf{C}}'_{2\kappa}$ are stable, see Figure 7.9 (lower right). Same phenomena occur when values of the parameters pass from region III to region I through region IV in Figure 7.8(a). We summerize the positive section of the bifurcation diagrams of Figure 7.9 in Figure 7.10.

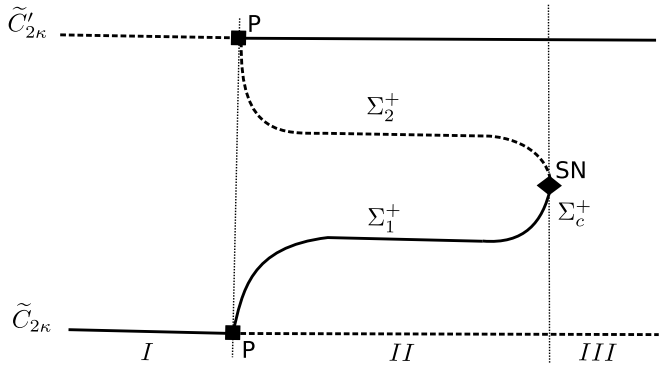

Figure 7.10: Positive section of the bifurcation diagrams of Figure 7.9 when parameters pass from regions $I - II - III$. Dashed lines represent unstable branches and continuous lines represent stable branches. ■-P stands for pitchfork bifurcation and ⧫-SN for saddle-node bifurcation, see text for notations.

4. *Bifurcation and stability in* $\mathrm{Fix}(\kappa')$. We consider instead $\mathrm{Fix}(\kappa'')$. By Lemma 7.3.3,

$$\mathrm{Fix}(\kappa'') = \{(z_1, \bar{z}_1, z_2, \bar{z}_2) \mid z_2 = \mathbf{i}z_1 - \sqrt{2}\bar{z}_1\} \ .$$

By Table 7.2 there are two axes of symmetry in this plane: one of type $\widetilde{\mathbf{C}}_{2\kappa}$ and one of type $\widetilde{\mathbf{C}}'_{2\kappa}$. We have already noticed that a conjugate of $\widetilde{\mathbf{C}}'_{2\kappa}$ which contains κ'' is $\widehat{\mathbf{C}}'_{2\kappa} = \{Id, -\sigma, -\kappa, \kappa''\}$. Setting $z_1 = x + \mathbf{i}y$, the equations for $\mathrm{Fix}(\widetilde{\mathbf{C}}_{2\kappa})$ and $\mathrm{Fix}(\widehat{\mathbf{C}}'_{2\kappa})$ are respectively $y = x$ and $y = -x$. With the change of coordinates $x = \sqrt{2}/2(X + Y)$, $x = \sqrt{2}/2(X - Y)$ the equations become:

$$\dot{X} = \lambda X + 2E_1AX(X^2 + E_3^2Y^2) + 8E_2aX(X^2 + E_3^2Y^2)^2 \\ + 4E_2bX(-X^2 + 2\sqrt{2}E_3XY + E_3^2Y^2)(X^2 + 2\sqrt{2}E_3XY - E_3^2Y^2) \\ +4E_2cX(X^2-5E_3^2Y^2)(X-E_3Y)(X+E_3Y)+4E_2dX(3X^4+10E_3^2X^2Y^2-5E_3^4Y^4)$$

$$\dot{Y} = \lambda Y + 2E_1AY(X^2 + E_3^2Y^2) + 8E_2aY(X^2 + E_3^2Y^2)^2 \\ - 4E_2bY(-X^2 + 2\sqrt{2}E_3XY + E_3^2Y^2)(X^2 + 2\sqrt{2}E_3XY - E_3^2Y^2) \\ -4E_2cY(5X^2-E_3^2Y^2)(X-E_3Y)(X+E_3Y)+4E_2dY(5X^4-10E_3^2X^2Y^2-3E_3^4Y^4)$$

where $E_3 = 1 - \sqrt{2}$. Then

$$Q(X,Y) = -8E_2XY\left[(b+d-3c)X^4 - 2E_3^2(5d+5b-3c)X^2Y^2 \right. \\ \left. +E_3^4(b+d-3c)Y^4\right].$$

We set $K(X,Y) = (b+d-3c)X^4 - 2E_3^2(5d+5b-3c)X^2Y^2 + E_3^4(b+d-3c)Y^4$.

Study of the polynomial map $K(X,Y)$. We consider K as a polynomial of degree two in X^2. If $5d+5b-3c=0$, then $K(X,Y) = (b+d-3c)(X^4+E_3^4Y^4)$, and no submaximal bifurcation can occur in fixed-point plane $\mathrm{Fix}(\kappa'')$. We now suppose that $5d+5b-3c \neq 0$.

- If $(b+d)(b+d-c) > 0$ then $X^2 = \nu_\pm Y^2$ with
$$\nu_\pm = E_3^2\frac{5d-3c+5b \pm 2\sqrt{6(b+d)(b+d-c)}}{(d+b-3c)}Y^2$$
where $\nu_+\nu_- = C^2$ and $\nu_+ + \nu_- = 2E_3^2\frac{5d-3c+5b}{d+b-3c}$. This implies that if $(5d-3c+5b)(d+b-3c) > 0$ there are four axes $X = \pm\sqrt{\nu_\pm}Y$ which correspond to bifurcated submaximal solutions in $\mathrm{Fix}(\kappa'')$. And if $(5d-3c+5b)(d+b-3c) < 0$, no submaximal solution can bifurcate in this plane.
- If $b+d=c$ and $c \neq 0$, then $K(X,Y) = -2c(X^2+E_3^2Y^2)^4$. There is no bifurcated submaximal solution in $\mathrm{Fix}(\kappa'')$.
- Suppose that $d+b=0$ and $c \neq 0$, then $K(X,Y) = -3c(X^2-E_3^2Y^2)^2$ and the axes $X = \pm E_3Y$ correspond to bifurcated submaximal solutions in $\mathrm{Fix}(\kappa'')$.
- Finally, if $(b+d)(b+d-c) < 0$, then K has no other root than $(0,0)$. By the same argument as before, this shows that no submaximal solution can bifurcate in fixed-point plane $\mathrm{Fix}(\kappa'')$.

Stability of the solutions. The transverse eigenvalues for isotropy type $\widetilde{\mathbf{C}}_{2\kappa}$ and $\widetilde{\mathbf{C}}'_{2\kappa}$ are summarized in Table 7.7.

The bifurcation analysis of submaximal solutions is the same as in fixed-point plane $\mathrm{Fix}(\sigma)$ and presents no difficulty.

Isotropy type	$\widetilde{\mathbf{C}}_{2\kappa}$	$\widetilde{\mathbf{C}}'_{2\kappa}$
Transverse eigenvalue	$8(3+2\sqrt{2})(d+b-3c)X^4$	$-8(3-2\sqrt{2})(d+b-3c)X^4$

Table 7.7: Transverse eigenvalues (leading order) of equilibria with maximal isotropy in Fix(κ'').

□

Remark 7.3.2. *From tables 7.5, 7.6 and 7.7, we deduce that there always exists a range of parameters such that equilibria with isotropy type $\widetilde{\mathbf{C}}_{2\kappa}$ and $\widetilde{\mathbf{C}}'_{2\kappa}$ are unstable. We also point out that, to leading order, the sign of transverse eigenvalues for isotropy type $\widetilde{\mathbf{C}}_{2\kappa}$ is the opposite of the sign of transverse eigenvalues for isotropy type $\widetilde{\mathbf{C}}'_{2\kappa}$.*

We can choose coordinates to express fixed-point lines Fix($\widetilde{\mathbf{C}}_{2\kappa}$) and Fix($\widetilde{\mathbf{C}}'_{2\kappa}$) in $\mathbb{R}^4$ as Fix($\widetilde{\mathbf{C}}_{2\kappa}$) $= \{(x, x, -(1+\sqrt{2})x, (1+\sqrt{2})x) \mid x \in \mathbb{R}\}$ and Fix($\widetilde{\mathbf{C}}'_{2\kappa}$) $= \{(x, -x, (1+\sqrt{2})x, (1+\sqrt{2})x) \mid x \in \mathbb{R}\}$. We summerize in table 7.8, to leading order, radial and transverse eigenvalues (denoted t_k, $k = 1 \dots 3$) of bifurcated branches $\widetilde{\mathbf{C}}_{2\kappa}$ and $\widetilde{\mathbf{C}}'_{2\kappa}$ in $\mathbb{R}^4$.

Isotropy type	$\widetilde{\mathbf{C}}_{2\kappa}$	$\widetilde{\mathbf{C}}'_{2\kappa}$
Radial eigenvalue	$8(2+\sqrt{2})Ax^2$	$8(2+2\sqrt{2})Ax^2$
t_1	$128(3+2\sqrt{2})(b-d)x^4$	$-128(3+2\sqrt{2})(b-d)x^4$
t_2	$-32(3+2\sqrt{2})(b+c+9d)x^4$	$32(3+2\sqrt{2})(b+c+9d)x^4$
t_3	$32(3+2\sqrt{2})(b+d-3c)x^4$	$-32(3+2\sqrt{2})(b+d-3c)x^4$

Table 7.8: Radial and transverse eigenvalues (leading order) of bifurcated branches in $\mathbb{R}^4$.

7.4 Bifurcation of a heteroclinic network in the χ_{11} case

7.4.1 Existence

We suppose now that the cubic term coefficient $A < 0$, and by a suitable change of time scale we can take $A = -1$. This implies, as shown in Theorem 7.3.2, that a flow-invariant S^3 sphere bifurcates for Equations (7.9) and (7.10). The system reads:

$$\begin{cases} \dot{z}_1 &= \lambda z_1 - z_1\left(|z_1|^2+|z_2|^2\right) + a z_1\left(|z_1|^2+|z_2|^2\right)^2 + b\left(z_1^4\bar{z}_2 + 4z_2^3|z_1|^2 - z_2^3|z_2|^2\right) \\ &\quad +c\left(3\bar{z}_1^2 z_2|z_2|^2 - z_1^2\bar{z}_2^3 - 2\bar{z}_1^2|z_1|^2 z_2\right) + d\left(-5\bar{z}_1^4\bar{z}_2 + \bar{z}_2^5\right) + h.o.t. \\ \dot{z}_2 &= \lambda z_2 - z_2\left(|z_1|^2+|z_2|^2\right) + a z_2\left(|z_1|^2+|z_2|^2\right)^2 + b\left(-\bar{z}_1 z_2^4 - 4z_1^3|z_2|^2 + z_1^3|z_1|^2\right) \\ &\quad +c\left(-3z_1\bar{z}_2^2|z_1|^2 + \bar{z}_1^3 z_2^2 + 2z_1\bar{z}_2^2|z_2|^2\right) + d\left(5\bar{z}_1\bar{z}_2^4 - \bar{z}_1^5\right) + h.o.t. \end{cases} \tag{7.11}$$

In the sequel we also suppose that coefficients (b, c, d) satisfy the following conditions:

- **C1**: $b - d > 0$,
- **C2**: $d(3d - b - c) < 0$ and $b + c + 9d > 0$,
- **C3**: $(b + d)(b + d - c) < 0$ and $b + d - 3c < 0$.

Under these conditions all bifurcated equilibria have maximal isotropy and moreover, according to remark 7.3.2, none of them is stable. More precisely, condition **C1** implies that saddle-sink heteroclinic orbits connect in the plane $\mathrm{Fix}(\kappa)$ equilibria of isotropy type $\widetilde{\mathbf{C}}_{2\kappa}$ to equilibria with isotropy type $\widetilde{\mathbf{C}}'_{2\kappa}$. Condition **C2** implies that saddle-sink heteroclinic orbits connect in the plane $\mathrm{Fix}(\sigma)$ equilibria with isotropy type $\widetilde{\mathbf{C}}'_{2\kappa}$ to equilibria with isotropy type $\widetilde{\mathbf{C}}_{2\kappa}$ (case I in figure 7.9). In the same fashion, saddle-sink heteroclinic orbits connect in the plane $\mathrm{Fix}(\kappa'')$ equilibria with isotropy type $\widetilde{\mathbf{C}}_{2\kappa}$ to equilibria with isotropy type $\widetilde{\mathbf{C}}'_{2\kappa}$ when condition **C3** is satisfied.

These heteroclinic orbits are robust against $\mathcal{G}$-equivariant perturbations. Their $\mathcal{G}$-orbit realizes a *heteroclinic network* between the $\mathcal{G}$-orbits of equilibria of types $\widetilde{\mathbf{C}}_{2\kappa}$ and $\widetilde{\mathbf{C}}'_{2\kappa}$.

Notice that under the above hypotheses the equilibria of type $\widetilde{\mathbf{C}}_{2\kappa}$ have a one dimensional unstable manifold, while equilibria of type $\widetilde{\mathbf{C}}'_{2\kappa}$ have a two dimensional unstable manifold which contains the heteroclinic orbits lying in the planes of type $\mathrm{Fix}(\sigma)$ and $\mathrm{Fix}(\kappa'')$.

The existence of a heteroclinic network can lead to interesting non trivial dynamics characterized by long periods of quasi-static state (trajectory approaches an equilibrium of the cycle) followed by a fast excursion far from equilibrium and relaxation to another quasi-static state, the process being repeated in an aperiodic way [Chossat 2000, Armbruster 1988, Guckenheimer 1987]. This point will be considered in subsection 7.4.3, but we first simplify the problem by proceeding to a suitable orbit space reduction.

7.4.2 Quotient network

The heteroclinic network introduced above has 48 nodes (equilibria) and 144 edges (heteroclinic orbits). Indeed the isotropy subgroups $\widetilde{\mathbf{C}}_{2\kappa}$ and $\widetilde{\mathbf{C}}'_{2\kappa}$ have order 4, hence the orbits of equilibria with these isotropies have $|\mathcal{G}|/4 = 24$ elements each. To each node of type $\widetilde{\mathbf{C}}_{2\kappa}$ are associated 2 "outgoing" edges and 4 "incoming" edges. There are 48 nodes but each edge has two ends, hence the result. We can simplify this structure by projecting the system onto the quotient space (orbit space) $S^3/\mathcal{G}$ where S^3 is the flow-invariant sphere. This procedure would project the network onto a simpler one in which there are only two nodes. Moreover the trajectories of the equivariant vector field in S^3 project on trajectories for a smooth vector field defined on the orbit space [Chossat 2000]. However this orbit space is not a manifold (it would be if the action of $\mathcal{G}$ were free) and its geometric, stratified structure is too difficult to compute to make this method useful in our case. We can however proceed as [Aguiar 2005] by identifying a subgroup H of $\mathcal{G}$ with a free

action on S^3 and large enough to allow for a substantial reduction of the number of equilibria on the 3-dimensional manifold S^3/H. This is the aim of the next lemma.

Lemma 7.4.1. *The group $G_0 \simeq \mathbf{SL}(2,3)$ generated by the elements ρ^2 and ε has 24 elements (see table 6.4). It acts fixed-point free on S^3 and the two $\mathcal{G}$-orbits of equilibria on S^3 reduce to a pair of equilibria in the manifold S_3/G_0 for the projected dynamics.*

Proof. In subsection 6.3.1 of the previous chapter, G_0 has already been identified with the 24 element group $\mathbf{SL}(2,3)$, the group of 2×2 matrices over the field $\mathbb{Z}_3$. Since none of its elements appears in the isotropy subgroups of $\mathcal{G}$ for the representation χ_{11}, its elements only fix the origin. For the same reason G_0 acts fixed point free on the 24 elements orbits of equilibria and by taking the quotient by this action these orbits reduce to single equilibria. □

It follows that the heteroclinic network "drops down" to a quotient heteroclinic network between the two equilibria which we denote by A ($\widetilde{\mathbf{C}}_{2\kappa}$ type) and B ($\widetilde{\mathbf{C}}'_{2\kappa}$ type) in S^3/G_0. There are two connections from A to B and four connections from B to A, as it can be seen in figure 7.11. This projected heteroclinic network can be seen as the union of eight *heteroclinic cycles* which however belong to two symmetry classes only: the cycles $1 \to 5$, $2 \to 5$, $1 \to 6$, $2 \to 6$ are exchanged by reflection symmetries (projected on S^3/G_0), same thing for the cycles $3 \to 5$, $4 \to 5$, $3 \to 6$, $4 \to 6$. We call ν-cycle (resp. μ-cycle) the cycle $1 \to 5$ (resp. $4 \to 5$). We denote ν_A, ν_B (resp. μ_A, μ_B) the eigenvalues at A and B along the connection $1-2$ (resp. $3-4$).

7.4.3 Asymptotic stability

The asymptotic stability of heteroclinic cycles has been studied by several authors [Krupa 1992, Krupa 1995, Ashwin 1999, Krupa 2004] and sufficient conditions on the ratio of eigenvalues "along" the cycle have been provided to ensure this property generically. Roughly speaking, the attractiveness property of a heteroclinic cycle is determined by the relative strength of the contracting and expanding eigenvalues along the cycle, computed at the equilibria in the cycle. If at an equilibrium in the cycle the unstable manifold has dimension > 1 and does not realize a saddle-sink connection to other equilibria in some fixed-point subspace, the heteroclinic cycle can not be asymptotically stable in the usual sense, that is asymptotically attracting for initial conditions in an open tubular neighborhood of the cycle. As shown by Krupa and Melbourne in [Krupa 1992], it can still have a weaker attractiveness property which they called essential stability: under certain conditions on the eigenvalues the heteroclinic cycle is attracting for initial conditions belonging to the complement of a cuspidal region in a tubular neighborhood of the cycle.

A heteroclinic network is a union of cycles. As observed by Kirk and Silber [Kirk 1994] those cycles can not be simultaneously essentially stable but conditions can be derived to determine which one is. In this subsection we derive sufficient conditions for the essential stability of the two cycles in our heteroclinic network projected on the orbit space S^3/G_0.

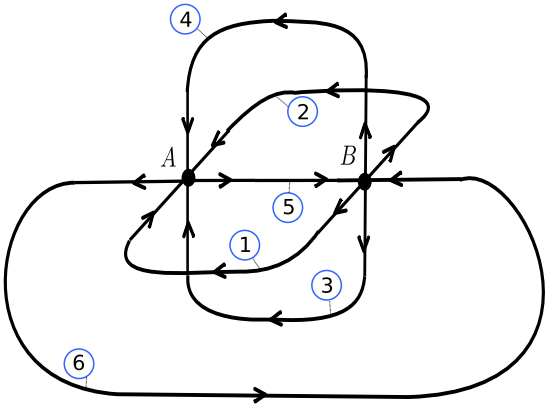

Figure 7.11: Representation of the quotient heteroclinic network between equilibria A ($\widetilde{\mathbf{C}}_{2\kappa}$ type) and B ($\widetilde{\mathbf{C}}'_{2\kappa}$ type) in S^3/G_0. Heteroclinic connections denoted $1, 2$, which link B to A, result of the quotient in S^3/G_0 of the heteroclinic connections which connect $\widetilde{\mathbf{C}}''_{2\kappa}$ to $\widetilde{\mathbf{C}}_{2\kappa}$ in $\mathrm{Fix}(\sigma)$. Heteroclinic connections denoted $3, 4$, which link B to A, result of the quotient in S^3/G_0 of the heteroclinic connections which connect $\widehat{\mathbf{C}}_{2\kappa}$ to $\widetilde{\mathbf{C}}'_{2\kappa}$ in $\mathrm{Fix}(\kappa'')$. Heteroclinic connections denoted $5, 6$, which link A to B, result of the quotient in S^3/G_0 of the heteroclinic connections which connect $\widetilde{\mathbf{C}}_{2\kappa}$ to $\widetilde{\mathbf{C}}'_{2\kappa}$ in $\mathrm{Fix}(\kappa)$.

First we simplify notation by denoting $(\lambda_A, -\nu_A, -\mu_A)$ the eigenvalues at equilibrium A and $(-\lambda_B, \nu_B, \mu_B)$ the eigenvalues at equilibrium B. We consider:

$$\lambda_e > 0, \quad \nu_e > 0, \quad \mu_e > 0 \quad e = A, B$$

The hypotheses of [Krupa 1992] do not apply but we will proceed in the same fashion as in [Kirk 1994]. In the following, we suppose without loss of generality that:

$$\nu_B > \mu_B \tag{7.12}$$

We define:

$$\rho_\mu = \frac{\mu_A \lambda_B}{\lambda_A \mu_B}, \quad \sigma_\mu = \frac{\mu_A}{\lambda_A}\left[\frac{\nu_B}{\mu_B} - \frac{\nu_A}{\mu_A}\right], \quad \rho_\nu = \frac{\nu_A \lambda_B}{\lambda_A \nu_B}, \quad \sigma_\nu = \frac{\nu_A}{\lambda_A}\left[\frac{\mu_B}{\nu_B} - \frac{\mu_A}{\nu_A}\right]$$

Theorem 7.4.1. *(i) Suppose that $\rho_\mu > 1$ and $\rho_\nu > 1$.*

1. *If $\sigma_\nu < 0$ and $\sigma_\mu > 0$, almost all orbits passing through a tubular neighborhood of the μ-cycle escape this neighborhood in finite time, exceptions being those orbits that lie in the stable manifolds of A or B. The ν-cycle is* essentially asymptotically stable*: it attracts almost all trajectories starting in a small enough tubular neighborhood of it, the only possible exceptions being those orbits that pass through a cuspoidal region abutting the heteroclinic connection from A to B.*

2. *If $\sigma_\nu > 0$ and $\sigma_\mu < 0$, almost all orbits passing through a tubular neighborhood of the ν-cycle escape this neighborhood in finite time, exceptions being those orbits that lie in the stable manifolds of A or B. The μ-cycle is* essentially asymptotically stable*: it attracts almost all trajectories starting in a small enough tubular neighborhood of it, the only possible exceptions being those orbits that pass through a cuspoidal region abutting the heteroclinic connection from A to B.*

(ii) Suppose that $0 < \rho_\mu < 1$ (resp. $0 < \rho_\nu < 1$). Then the μ-cycle (resp. ν-cycle) repels almost all orbits and the attractivity properties of the ν-cycle (esp. μ-cycle) are determined by σ_ν (resp. σ_μ) as above.

Proof.

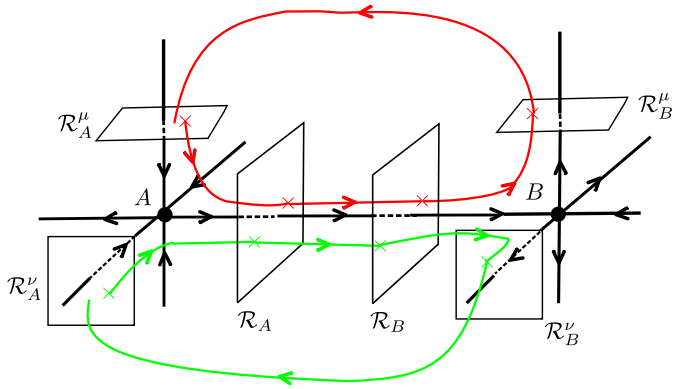

Figure 7.12: First return map in S^3.

We apply the method for stability analysis of heteroclinic cycles as exposed in [Krupa 1992] and [Krupa 1995], to which we refer for justifications. We first linearize the flow in neighborhoods of A and B by a $\mathcal{C}^1$ and equivariant change of variables. This requires that a finite set of nonresonance conditions between the eigenvalues at A and B be satisfied. Such conditions are generic and can be verified numerically in our case. In fact they can also be removed as shown for example in [Field 1991]. We can further choose local coordinates such that the local stable and unstable manifolds of A and B are either the horizontal axis or the vertical plane. Using Euclidean coordinates (v, w) in the vertical plane and u for the horizontal axis, we have for A:

$$W^u_{loc}(A) = \{(u, 0, 0) \mid u \in \mathbb{R}\} \quad W^s_{loc}(A) = \{(0, v, w) \mid (v, w) \in \mathbb{R}^2\}$$

and for B:

$$W^s_{loc}(B) = \{(u,0,0) \mid u \in \mathbb{R}\} \quad W^u_{loc}(B) = \{(0,v,w) \mid (v,w) \in \mathbb{R}^2\}.$$

The linearized vector field about A is

$$\begin{aligned} \dot{u} &= \lambda_A u \\ \dot{v} &= -\nu_A v \\ \dot{w} &= -\mu_A w \end{aligned}$$

and about B:

$$\begin{aligned} \dot{u} &= -\lambda_B u \\ \dot{v} &= \nu_B v \\ \dot{w} &= \mu_B w. \end{aligned}$$

We now define rectangular cross sections in neighborhoods of e, $e = A, B$ (see figure 7.12):

$$\begin{aligned} \mathcal{R}_e &= \{(u,v,w) \mid u = 1, \quad -v_e \le v \le v_e, \quad -w_e \le w \le w_e\}, \\ \mathcal{R}^\mu_e &= \{(u,v,w) \mid w = 1, \quad -u_e \le u \le u_e, \quad -v_e \le v \le v_e\}, \\ \mathcal{R}^\nu_e &= \{(u,v,w) \mid v = 1, \quad -u_e \le u \le u_e, \quad -w_e \le w \le w_e\}. \end{aligned}$$

We can then build two first return maps $\Psi^\mu : \mathcal{R}^\mu_A \to \mathcal{R}^\mu_A$ and $\Psi^\nu : \mathcal{R}^\nu_A \to \mathcal{R}^\nu_A$ as follows:
$\Psi^\mu = \Psi^\mu_{BA} \circ \Phi^\mu_B \circ \Psi_{AB} \circ \Phi^\mu_A$ and $\Psi^\nu = \Psi^\nu_{BA} \circ \Phi^\nu_B \circ \Psi_{AB} \circ \Phi^\nu_A$ where

$$\Phi^\mu_A : \mathcal{R}^\mu_A \to \mathcal{R}_A \quad \Phi^\mu_B : \mathcal{R}_B \to \mathcal{R}^\mu_B \quad \Phi^\nu_A : \mathcal{R}^\nu_A \to \mathcal{R}_A \quad \Phi^\nu_B : \mathcal{R}_B \to \mathcal{R}^\nu_B$$

$$\Psi_{AB} : \mathcal{R}_A \to \mathcal{R}_B \quad \Psi^\mu_{BA} : \mathcal{R}^\mu_B \to \mathcal{R}^\mu_A \quad \Psi^\nu_{BA} : \mathcal{R}^\nu_B \to \mathcal{R}^\nu_A.$$

The local maps Φ^μ_A and Φ^ν_A are obtained by integrating the equations for the flow linearized about A:

$$\Phi^\mu_A(u,v,1) = (1, vu^{\frac{\nu_A}{\lambda_A}}, u^{\frac{\mu_A}{\lambda_A}}) \text{ with } u \neq 0,$$

$$\Phi^\nu_A(u,1,w) = (1, u^{\frac{\nu_A}{\lambda_A}}, wu^{\frac{\mu_A}{\lambda_A}}) \text{ with } u \neq 0.$$

Same thing for the maps Φ^μ_B and Φ^ν_B:

$$\Phi^\mu_B(1,v,w) = (w^{\frac{\lambda_B}{\mu_B}}, vw^{-\frac{\nu_B}{\mu_B}}, 1) \text{ with } w^{\frac{\nu_B}{\mu_B}} > v \ge 0,$$

$$\Phi^\nu_B(1,v,w) = (v^{\frac{\lambda_B}{\nu_B}}, 1, wv^{-\frac{\mu_B}{\nu_B}}) \text{ with } v > w^{\frac{\nu_B}{\mu_B}} \ge 0$$

where $\mathcal{C}^\mu_B = \{(v,w) \in \mathcal{R}_B \mid w^{\frac{\nu_B}{\mu_B}} > v \ge 0\}$ and $\mathcal{C}^\nu_B = \{(v,w) \in \mathcal{R}_B \mid v > w^{\frac{\nu_B}{\mu_B}} \ge 0\}$ are complementary domains in $\mathcal{R}_B$ of the maps Φ^μ_B and Φ^ν_B. Note that the point at which a trajectory intersects $\mathcal{R}_B$ determines whether the trajectory leaves the vicinity of B in the direction of A through $\mathcal{R}^\mu_B$ or $\mathcal{R}^\nu_B$. Condition (7.12) implies that $\mathcal{C}^\mu_B$ is a cuspoidal region of $\mathcal{R}^\mu_B$.

By exploiting the equivariance of the vector field, we obtain for the "global" maps Ψ_{AB}, Ψ^{μ}_{BA} : and Ψ^{ν}_{BA}:

$$\Psi_{AB}(1, v, w) = (1, \alpha_{AB} v, \beta_{AB} w) + \text{h.o.t}$$
$$\Psi^{\mu}_{BA}(u, v, 1) = (\alpha^{\mu}_{BA} u, \beta^{\mu}_{BA} v, 1) + \text{h.o.t}$$
$$\Psi^{\nu}_{BA}(u, 1, w) = (\alpha^{\nu}_{BA} u, 1, \beta^{\nu}_{BA} w) + \text{h.o.t}$$

where the α's and β's are real coefficients.

- Study of the μ-cycle. We consider trajectories that pass through $\mathcal{R}^{\mu}_{A}$ and then travel through a tubular neighborhood of the μ-cycle before returning to $\mathcal{R}^{\mu}_{A}$. The behaviour of these trajectories is modelled by the return map Ψ^{μ} and we find to leading order:

  $$\Psi^{\mu}(u, v, 1) = (c_1 u^{\rho_\mu}, c_2 v u^{-\sigma_\mu}, 1) \text{ with } 0 \leq v < c_3 u^{\sigma_\mu}.$$

  The domain of the return map is then defined as $\mathcal{D}^{\mu}_{A} = \{(u, v) \in \mathcal{R}^{\mu}_{A} \mid 0 \leq v < c_3 u^{\sigma_\mu}\}$. A sufficient condition for $\mathcal{D}^{\mu}_{A}$ to be mapped into itself is $\sigma_\mu < 0$. This follows from the observation that the image under Ψ^{μ} of the bounding surface defined by the equation $v = c_3 u^{\sigma_\mu}$ is the boundary defined by $U = c_4$, where $c_4 > 0$ is some constant. Finally, if $\rho_\mu > 1$ and $\sigma_\mu < 0$ then Ψ^{μ} is a contraction on $\mathcal{D}^{\mu}_{A}$.

- Study of the ν-cycle. We consider trajectories that pass through $\mathcal{R}^{\nu}_{A}$ and then travel once through a tubular neighborhood of the ν-cycle before returning to $\mathcal{R}^{\nu}_{A}$. The behaviour of these trajectories is modelled by the return map Ψ^{ν} and we find to leading order:

  $$\Psi^{\nu}(u, 1, w) = (c_4 u^{\rho_\nu}, 1, c_5 w u^{-\sigma_\nu}, 1) \text{ with } 0 \leq w < c_6 u^{\sigma_\nu}.$$

  The study is analogous to that for the μ-cycle. If $\rho_\nu > 1$ and $\sigma_\nu < 0$ then the ν-cycle attracts all trajectories that cross $\mathcal{R}^{\nu}_{A}$ sufficiently close to the origin.

The main difference between the results obtained for the μ-cycle and the ν-cycle comes from the condition (7.12). If $\rho_\nu > 1$ and $\sigma_\nu < 0$ the ν-cycle attracts almost all trajectories that lie near the heteroclinic connection from A to B, while, if $\rho_\mu > 1$ and $\sigma_\mu < 0$ the μ-cycle attracts just trajectories in a cuspoidal region emananting from the heteroclinic connection.

It is not possible that both σ_μ and σ_ν be simultaneously positive:

$$\sigma_\mu = -\frac{\nu_B}{\mu_B} \sigma_\nu.$$

Note that if $\sigma_\mu > 0$ when $\rho_\nu, \rho_\mu > 1$, then almost all trajectories near the μ-cycle eventually leave it in the direction of the ν-cycle. However, since $\sigma_\nu < 0$ in this case, the trajectories that switch to the ν-cycle can not at a later time switch back to the μ-cycle.

□

7.4.4 Computation of the stability conditions

In principle the stability conditions stated in Theorem 7.4.1 are easy to compute. In our case however there is a difficulty which comes from the fact that for the system (7.11), which is truncated at order 5, the expanding and contracting eigenvalues along a given connection have exactly the same magnitude (see table 7.8). It is interesting to observe that this follows from a property of reversibility of the vector field on the invariant sphere, as the next lemma shows (proof of the lemma is straightforward).

Lemma 7.4.2. *Let* $\mathbf{s}$ *be the transformation in* $\mathbb{R}^4$ *defined by* $\mathbf{s}(z_1, \bar{z}_1, z_2, \bar{z}_2) = (z_2, \bar{z}_2, z_1, \bar{z}_1)$. *Let us rewrite* $X = (z_1, \bar{z}_1, z_2, \bar{z}_2)$ *and equation* (7.11) *in the form*

$$\dot{X} = (\lambda - \|X\|^2 + b\|X\|^4)X + E_{c,d}(X) \tag{7.13}$$

with $E_{c,d}(X) = cE_{5,3}(X) + dE_{5,4}(X)$.

Then $E_{c,d}(\mathbf{s}X) = -\mathbf{s}E_{c,d}(X)$ *for all* X. *Moreover,* $Fix(\widetilde{\mathbf{C}}'_{2\kappa}) = \mathbf{s}Fix(\widetilde{\mathbf{C}}_{2\kappa})$.

Remark 7.4.1. *We recall that* $E_{5,3}$ *(resp.* $E_{5,4}$*) is the quintic equivariant map in factor of* c *(resp.* d*) in equations* (7.9) *and* (7.10) *of Theorem 7.3.1, see Appendix A.1.2 for the computations.*

Now let $X = rU$, $U \in S^3$. The system (7.11) decouples in a radial part and tangential part:

$$\dot{r} = (\lambda - r^2 + br^4)r + r^5\langle E_{c,d}(U), U\rangle \tag{7.14}$$

$$\dot{U} = r^4[E_{c,d}(U) - \langle E_{c,d}(U), U\rangle U] = r^4 H(U). \tag{7.15}$$

By lemma 7.4.2 the tangential part is a reversible vector field. Let $X_0 = r_0U_0$ be an equilibrium on $\mathrm{Fix}(\widetilde{\mathbf{C}}_{2\kappa})$ and $X'_0 = \mathbf{s}X_0 = r_0\mathbf{s}U_0$. Then X'_0 is also an equilibrium, moreover $DH(\mathbf{s}U_0) = -\mathbf{s}DH(U_0)\mathbf{s}$, which implies that the transverse eigenvalues at X'_0 are exactly opposite to the transverse eigenvalues at X_0. This property is conserved by projection of the system on the orbit space S^3/G_0.

It is therefore necessary to consider the 7th order expansion of the system in order to remove this degeneracy. There are 12 equivariant terms of order 7 (see table 7.3). We have checked that some of these terms are not reversible, for example the following vector field which we note E_7:

$$\begin{aligned} \dot{z}_1 &= \bar{z}_1^7 + 7\bar{z}_1^3\bar{z}_2^4 \\ \dot{z}_2 &= \bar{z}_2^7 + 7\bar{z}_2^3\bar{z}_1^4 \end{aligned}$$

Numerical simulations have been carried out with Matlab by introducing the term E_7 in the system:

$$\dot{X} = (\lambda - \|X\|^2 + b\|X\|^4)X + E_{c,d}(X) + eE_7(X) \tag{7.16}$$

We give in tables 7.9 and 7.10, to leading order, the transverse eigenvalues of bifurcated branches in $\mathbb{R}^4$ depending upon the parameter e of equation 7.16. These transverse eigenvalues allow us to compute the stability conditions of Theorem 7.4.1.

For the numerical simulations, the coefficient values are $\lambda = 0.1$, $a = 0$, $b = 0.6$, $c = 1.2$ $d = 0.55$. We set $e = -1$ and we obtain:

$$\lambda_A = 0.0011 \quad \nu_A = 0.0745 \quad \mu_A = 0.0266$$

$$\lambda_B = 0.0023 \quad \nu_B = 0.0585 \quad \mu_B = 0.0215$$

which implies that:

$$\rho_\mu = 2.6336 > 1 \quad \sigma_\mu = -1.8221 < 0 \quad \rho_\nu = 2.7060 > 1 \quad \sigma_\nu = 0.6686 > 0$$

Then we are in the second case of Theorem 7.4.1. Figure 7.13 shows one hour runs with an initial condition close to an equilibrium with isotropy $\widetilde{\mathbf{C}}_{2\kappa}$. For the value $e = -1$ the solution converges to a heteroclinic cycle of type μ-cycle, while for $e = 3$ none of the heteroclinic cycles are stable.

Isotropy type	$\widetilde{\mathbf{C}}_{2\kappa}$
$t_1(e)$	$128(3+2\sqrt{2})(b-d+(2+\sqrt{2})ex^2)x^4$
$t_2(e)$	$-32(3+2\sqrt{2})(b+c+9d+24(2+\sqrt{2})ex^2)x^4$
$t_3(e)$	$32(3+2\sqrt{2})(b+d-3c-10(2+\sqrt{2})ex^2)x^4$

Table 7.9: Transverse eigenvalues (leading order) of bifurcated branch $\widetilde{\mathbf{C}}_{2\kappa}$ in $\mathbb{R}^4$ depending upon the parameter e of equation 7.16.

Isotropy type	$\widetilde{\mathbf{C}}'_{2\kappa}$
$t_1(e)$	$-128(3+2\sqrt{2})(b-d-(2+\sqrt{2})ex^2)x^4$
$t_2(e)$	$32(3+2\sqrt{2})(b+c+9d-24(2+\sqrt{2})ex^2)x^4$
$t_3(e)$	$-32(3+2\sqrt{2})(b+d-3c+10(2+\sqrt{2})ex^2)x^4$

Table 7.10: Transverse eigenvalues (leading order) of bifurcated branch $\widetilde{\mathbf{C}}'_{2\kappa}$ in $\mathbb{R}^4$ depending upon the parameter e of equation 7.16.

7.5 Conclusion

In this chapter we have completed the bifurcation analysis of periodic patterns, started in chapter 6, for neural field equations defined on the Poincaré disk $\mathbb{D}$. These equations are assumed invariant under the action of the lattice group Γ of $\mathbf{U}(1,1)$ whose fundamental domain is the regular octagon. We have computed the bifurcation diagrams for the three irreducible representations of dimension four. We have proved that for two of the four-dimensional irreducible representations, generically, there always exist stable equilibria with a given isotropy type. For the third representation we have presented bifurcation diagrams in fixed-point planes

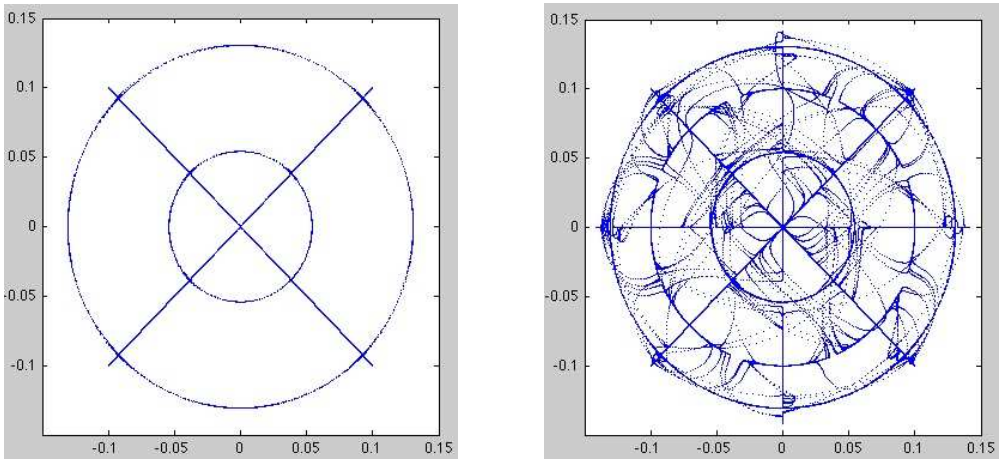

(a) $e = -1$. (b) $e = 3$.

Figure 7.13: Projection on the plane (x_1, y_1) of a trajectory of (7.16) with initial condition near an equilibrium of type $\widetilde{\mathbf{C}}_{2\kappa}$. Coefficient values in both cases are $\lambda = 0.1$, $a = 0$, $b = 0.6$, $c = 1.2$ $d = 0.55$.

and also shown that: (i) bifurcation of submaximal solutions can be generic, (ii) bifurcation of a heteroclinic network connecting the equilibria with maximal isotropy type can also occur generically. In the final section, a stability analysis of this heteroclinic network was presented.

The existence of the heteroclinic network raises many interesting questions from the neuroscience point of view. Metastability in neuronal network has been observed in the brains of anaesthetized animals where the cortex seems to show an intrinsic pattern of activity that evolves over time by switching among a specific set of states [Kenet 2003, Ringach 2003, Goldberg 2004]. It has also been shown that metastable states play a key role in the execution of cognitive functions. Indeed, experimental and modeling studies suggest that most of these functions are the result of transient activity of large-scale brain networks in the presence of noise [Rabinovich 2008, Rabinovich 2010]. In our case the spontaneous activity represented by the heteroclinic network corresponds to switches between multiple states where each state is a specific textural feature. Despite the fact that it seems unrealistic to investigate experimentally the predicted behaviour, the presence of the heteroclinic network is nonetheless an interesting mechanism which should be taken into account for the validation of our texture model.

Chapter 8

Application to spontaneous pattern formation in V1 using structure tensor formalism

Contents

8.1 The continuum models of V1 and their symmetries 152
8.1.1 The model equations 153
8.1.2 Symmetries of the model 153
8.1.3 The Poincaré disk model 154
8.1.4 Two complementary approaches 155
8.2 Problem 1: weak anisotropic coupling on a bounded structure tensor space 156
8.2.1 Eigenfunctions of the Laplace-Beltrami operator on Ω 156
8.2.2 Study of an isolated hypercolumn 159
8.2.3 Weak lateral interactions 162
8.3 Problem 2: bifurcation of doubly periodic planforms in both $\mathbb{R}^2$ and $\mathbb{D}$ 166
8.3.1 Bifurcation problem 167
8.3.2 Bifurcations of octagonal H-planforms 168
8.3.3 Bifurcation diagrams for one hypercolumn 172
8.3.4 Symmetry-breaking bifurcations on lattices 177
8.3.5 Group actions 178
8.3.6 Selection and stability of patterns 180
8.3.7 Pictures of axial planforms Σ_1 and Σ_2 181
8.3.8 Forced symmetry breaking 184
8.4 Conclusion 186

Ermentrout and Cowan [Ermentrout 1979] were first to propose a mathematical theory of visual patterns seen during hallucinations. Hallucinations can occur in a wide variety of situations such as with migraine headaches, epilepsy or as the result of external stimulus by drugs such as LSD [Klüver 1966, Oster 1970]. In their model, the visual cortex is idealized by the Euclidean plane and it is assumed that the effect of drugs is to cause instabilities, by spontaneous symmetry- breaking, in the neural activity and these instabilities result in the visual patterns experienced

by the subjects. This model is simple as that it assumes that neurons in the visual cortex are not sensitive to features such as orientation, texture, color etc.

However we have seen in the first chapter of this Thesis that neurons in the primary visual cortex respond preferentially to visual stimuli that have a specific orientation. Subgroups of inhibitory and excitatory neurons are tuned to a particular orientation of an external stimulus; they form what we have called a hypercolumn. Two cortical circuits have been characterised which further manifest the functional structure of V1. A local circuit, operating at sub-hypercolumn dimensions, consists of a mixture of intra-cortical excitation and inhibition and a lateral circuit, operating between hypercolumns, anisotropically connects cells with similar functional properties: cells in different hypercolumns tend to connect in directions parallel to their common preferred orientation (see figures 1.11 and 3.4). Based on these anatomical structures, Bressloff *et al.* [Bressloff 2001b, Bressloff 2002b] took into account the orientation of cortical neurons and abstracted the visual cortex as $\mathbb{R}^2 \times \mathbf{S}^1$. Their analysis recovered thin line hallucinations such as cobwebs and honeycombs. However, the anisotropic nature of cortical long-range connections can be weak upon species. For macaques (see figure 3.4) anisotropy tends to be weaker than for tree shrews (see figure 1.11). Following this idea, Golubitsky *et al.* [Golubitsky 2003] revisited the model of Bressloff *et al.* [Bressloff 2001b, Bressloff 2002b] by determining solutions obtained from symmetry-breaking bifurcations in the case of isotropic lateral coupling and then studying how these solutions may change when anisotropy is introduced as a forced symmetry-breaking parameter.

Our aim is now at (i) analyzing the spontaneous bifurcation of patterns for our spatialized model of the primary visual cortex using structure tensor formalism introduced in chapter 3 and (ii) at comparing our results with those found by Bressloff and Golubitsky. The visual cortex is now abstracted as $\mathbb{R}^2 \times \mathbf{SPD}(2, \mathbb{R})$, where the feature space $\mathbf{SPD}(2, \mathbb{R})$ is the set of all structure tensors. This introduces an important complication compared to the ring model of orientation preferences for the bifurcation analysis. We shall see in section 8.1 that two different approaches can be followed in order to overcome this difficulty. One is to remark that in a "real" cortex an upper bound must exist to the norm of effectively detectable structure tensors, and therefore consider a suitably chosen bounded domain in $\mathbf{SPD}(2, \mathbb{R})$ instead of $\mathbf{SPD}(2, \mathbb{R})$ itself. The other is to take advantage of the previous analysis presented in chapter 6 where the bifurcation of periodic patterns in $\mathbf{SPD}(2, \mathbb{R})$ was investigated. Periodic means here that the patterns are invariant under the action of a discrete subgroup H of $\mathbf{GL}(2, \mathbb{R})$ which tiles the space $\mathbf{SPD}(2, \mathbb{R})$ with a compact fundamental domain (the octagonal group in our case). This method allows to reduce the domain to the quotient space $\mathbf{SPD}(2, \mathbb{R})/H$, which is a compact manifold. These two approaches are investigated respectively in sections 8.2 and 8.3.

8.1 The continuum models of V1 and their symmetries

8.1.1 The model equations

We now recall the model that we have introduced in chapter 3. The average membrane potential of a population of neurons at a cortical position $\mathbf{r} \in \mathbb{R}^2$ at time t is characterized by the real valued function $V(\mathbf{r}, \mathcal{T}, t)$, where $\mathbf{r}$ labels a point in the visual cortex and $\mathcal{T}$ is a structure tensor. All possible textures are represented at every position: $\mathbf{r}$ and $\mathcal{T}$ are independent variables. The average membrane potential evolves according to equation (3.5):

$$\frac{\partial V(\mathbf{r}, \mathcal{T}, t)}{\partial t} = -V(\mathbf{r}, \mathcal{T}, t) + \int_{\mathbb{R}^2} \int_{\mathbf{SPD}(2,\mathbb{R})} W(\mathbf{r}, \mathcal{T} \mid \mathbf{r}', \mathcal{T}') S(\mu V(\mathbf{r}', \mathcal{T}', t)) d\mathcal{T}' d\mathbf{r}'. \tag{8.1}$$

Note that we put no external input in this equation, meaning that we look at *spontaneous pattern formation*. The nonlinearity S is a smooth sigmoidal function which saturates at $\pm\infty$ with $S(0) = 0$. In order to fix ideas we work with the following sigmoidal function:

$$S(x) = \frac{1}{1 + e^{-x+T}} - \frac{1}{1 + e^{T}}, \tag{8.2}$$

where T is a positive threshold. The parameter μ describes the stiffness of the sigmoid.
With this nonlinearity, $V = 0$ is always a solution.

The associated weight distribution is decomposed into local (within the hypercolumns) and long-range parts according to equation (3.6):

$$W(\mathbf{r}, \mathcal{T} \mid \mathbf{r}', \mathcal{T}') = W_{loc}(d_{\mathbf{SPD}(2,\mathbb{R})}(\mathcal{T}, \mathcal{T}'))\delta_{\mathbf{r},\mathbf{r}'} + \beta(1 - \delta_{\mathbf{r},\mathbf{r}'}) W^{\varepsilon}_{lat}(\mathbf{r}, \mathcal{T} \mid \mathbf{r}', \mathcal{T}'). \tag{8.3}$$

Microelectrode recordings suggest that β is small and therefore that the lateral connections modulate rather than drive the cortical activity. The sign of β will determine whether the lateral connections have a net excitatory or inhibitory effect. The rules of long-range connections are given by equation (3.7):

$$W^{\varepsilon}_{lat}(\mathbf{r}, \mathcal{T} \mid \mathbf{r}', \mathcal{T}') = \mathcal{J}\left(\sqrt{(\mathbf{r} - \mathbf{r}')^{\mathbf{T}}(\mathbf{I}_2 + \varepsilon\mathcal{T})(\mathbf{r} - \mathbf{r}')}\right) \mathcal{K}\left(d\left(\mathcal{T}, \mathcal{T}'\right)\right) \tag{8.4}$$

The factors $\mathcal{J}$ and $\mathcal{K}$ have been explained in details in subsection 3.1.4 of chapter 3. We recall that the parameter ε controls the degree of anisotropy.

8.1.2 Symmetries of the model

The Euclidean group $\mathbf{E}(2)$ is crucial to the analyses in [Bressloff 2001b, Bressloff 2001a] where it acts on $\mathbb{R}^2 \times \mathbf{S}^1$ by the so-called "shift-twist" representation due to the anisotropic nature of the lateral connections. In our model, the action of $\mathbf{E}(2)$ on $\mathbb{R}^2 \times \mathbf{SPD}(2,\mathbb{R})$ that preserves the structure of the long-range connections in equation (8.4) is given by

$$\begin{aligned} a \cdot (\mathbf{r}, \mathcal{T}) &= (\mathbf{r} + a, \mathcal{T}) \quad a \in \mathbb{R}^2 \\ \mathcal{R}_\theta \cdot (\mathbf{r}, \mathcal{T}) &= \left(\mathcal{R}_\theta \mathbf{r}, \mathcal{R}_\theta \mathcal{T} \mathcal{R}_\theta^{\mathbf{T}}\right) \quad \theta \in \mathbf{S}^1 \\ \mathcal{M}_\kappa \cdot (\mathbf{r}, \mathcal{T}) &= (\mathcal{M}_\kappa \mathbf{r}, \mathcal{M}_\kappa \mathcal{T} \mathcal{M}_\kappa^{\mathbf{T}}) \end{aligned} \tag{8.5}$$

where $\mathcal{M}_\kappa$ is the matrix representation of the reflection $\kappa : (r_1, r_2) \to (r_1, -r_2)$ and $\mathcal{R}_\theta$ is a matrix rotation of angle θ.

The corresponding group action on a function $V : \mathbb{R}^2 \times \mathbf{SPD}(2,\mathbb{R}) \to \mathbb{R}$ is given by:

$$\gamma \cdot V(\mathbf{r}, \mathcal{T}) = V\left(\gamma^{-1} \cdot (\mathbf{r}, \mathcal{T})\right)$$

for all $\gamma \in \mathbf{E}(2)$ and the action on the weight distribution $W(\mathbf{r}, \mathcal{T} \mid \mathbf{r}', \mathcal{T}')$ is

$$\gamma \cdot W(\mathbf{r}, \mathcal{T} \mid \mathbf{r}', \mathcal{T}') = W\left(\gamma^{-1} \cdot (\mathbf{r}, \mathcal{T}) \mid \gamma^{-1} \cdot (\mathbf{r}', \mathcal{T}')\right).$$

It follows that W given by (8.3) and (8.4) is invariant under the action of the Euclidean group defined by equations (8.5). As a consequence, equation (8.1) is equivariant with respect to the symmetry group.

In the limit $\varepsilon = 0$, the lateral connectivity function defined in equation (8.4) is called *isotropic* and reduces to

$$W^0_{lat}(\mathbf{r}, \mathcal{T} \mid \mathbf{r}', \mathcal{T}') = \mathcal{J}\left(\|\mathbf{r} - \mathbf{r}'\|\right) \mathcal{K}\left(d\left(\mathcal{T}, \mathcal{T}'\right)\right). \tag{8.6}$$

In that particular case, in addition to Euclidean symmetry, equation (8.1) admits a $\mathbf{GL}(2,\mathbb{R})$-symmetry,. The two actions decouple and are given by:

$$\begin{aligned} \gamma \cdot (\mathbf{r}, \mathcal{T}) &= (\gamma\mathbf{r}, \mathcal{T}) \quad \gamma \in \mathbf{E}(2) \\ M \cdot (\mathbf{r}, \mathcal{T}) &= (\mathbf{r}, M\mathcal{T}M^{\mathbf{T}}) \quad M \in \mathbf{GL}(2,\mathbb{R}). \end{aligned} \tag{8.7}$$

8.1.3 The Poincaré disk model

The feature space $\mathbf{SPD}(2,\mathbb{R})$ of structure tensors is the set of 2×2 symmetric positive definite matrices. We have already seen that $\mathbf{SPD}(2,\mathbb{R}) \simeq \mathbb{R}^+_* \times \mathbb{D}$ in chapter 3 with the coordinates $\mathcal{T} = (\Delta, z) \in \mathbb{R}^+_* \times \mathbb{D}$ for a given structure tensor $\mathcal{T} \in \mathbf{SPD}(2,\mathbb{R})$. For mathematical convenience, we cancel out the dependence on $\Delta \in \mathbb{R}^+_*$ as it would not play a significant role in the analysis that follows.

Hypothesis 8.1.1. *Equation (8.1) is posed on $\mathbb{R}^2 \times \mathbb{D}$ from now on.*

The group of isometries of $\mathbb{D}$ is the unitary group $\mathbf{U}(1,1)$, see subsection 3.2.3 of chapter 3 for definitions.

One can transcribe the group actions of $\mathbf{E}(2)$ and $\mathbf{U}(1,1)$ defined in equations (8.5) and (8.7) respectively on the space $\mathbb{R}^2 \times \mathbb{D}$. In the anisotropic case we have:

$$\begin{aligned} a \cdot (\mathbf{r}, z) &= (\mathbf{r} + a, z) \quad a \in \mathbb{R}^2 \\ \mathcal{R}_\theta \cdot (\mathbf{r}, z) &= \left(\mathcal{R}_\theta \mathbf{r}, e^{2i\theta} z\right) \quad \theta \in \mathbf{S}^1 \\ \mathcal{M}_\kappa \cdot (\mathbf{r}, z) &= (\kappa\mathbf{r}, \bar{z}). \end{aligned} \tag{8.8}$$

and in the isotropic case ($\varepsilon = 0$):

$$\begin{aligned} \gamma \cdot (\mathbf{r}, z) &= (\gamma\mathbf{r}, z) \quad \gamma \in \mathbf{E}(2) \\ g \cdot (\mathbf{r}, z) &= (\mathbf{r}, g \cdot z) \quad g \in \mathbf{U}(1,1) \end{aligned} \tag{8.9}$$

where the action of $g \in \mathbf{U}(1,1)$ on $z \in \mathbb{D}$ is defined in equation (3.16).

If we now write equation (8.1) as an abstract problem of the form:

$$\frac{dV(t)}{dt} = \mathbf{F}(V(t), \mu, \beta, \varepsilon) = 0 \tag{8.10}$$

then we can summarize the previous discussion as follows:

1. for all $(\mu, \beta, \varepsilon)$, $\mathbf{F}(\cdot, \mu, \beta, \varepsilon)$ is equivariant with respect to $\mathbf{E}(2)$ with shift-twist action;
2. $\mathbf{F}(\cdot, \mu, \beta, 0)$ is equivariant with respect to $\mathbf{E}(2) \times \mathbf{U}(1,1)$ (isotropic case);
3. $\mathbf{F}(\cdot, \mu, 0, 0)$ is equivariant with respect to $\mathbf{U}(1,1)$ (no lateral connections).

8.1.4 Two complementary approaches

We are interested in the bifurcations from the trivial state $V = 0$ of equation (8.10) where μ is the bifurcation parameter. Previous works like [Ermentrout 1979] and [Golubitsky 2003] have assumed that the pattern arising in the V1 plane was doubly periodic, ocuring either on a square or hexagonal lattice. This assumption allows to reduce the bifurcation problem to a finite dimensional center manifold and we shall keep this framework in the present chapter. We have however an additional complication, of similar type, due to the fact that the feature space of structure tensors, which we assimilate to the Poincaré disc $\mathbb{D}$, is unbounded and has non compact isometry group $\mathbf{U}(1,1)$, which puts a strong obstruction to apply the standard tools of bifurcation theory. To overcome this difficulty we can take two different approaches which we now define.

Problem 8.1.1. *Observe that natural images can only produce a bounded set of structure tensors with determinant equal to one. This suggests to restrict ourselves to a bounded domain of the Poincaré disc for the feature space. It is convenient to choose a domain which still preserves the rotational invariance of (8.8). We therefore choose a disc $\Omega \subset \mathbb{D}$ of radius r_ω such that $r_\omega = \tanh(\omega/2) < 1$.*
As suggested by microelectrode recordings, β is small and therefore the lateral connections modulate rather than drive the cortical activity. This suggests to begin to study the case of no lateral coupling: $\beta = 0$ (model of a single hypercolumn defined on Ω) and then use perturbation analysis when anisotropic coupling is switched on: $0 < \beta \ll 1$. Problem 8.1.1 is closely linked to the analysis of [Bressloff 2001b, Bressloff 2002b] for the ring model (the feature space is $\mathbf{S}^1$) and [Bressloff 2003b, Bressloff 2003a] for the spherical model (the feature space is the sphere S^2 which accounts for orientations and spatial frequency), where perturbation theory is used to calculate the eigenvalues and eigenfunctions of the "spatialized" cortical dynamics. Our aim is to use a similar approach in the case of a bounded domain Ω, with lateral coupling given by equations (8.3) and (8.4). This problem is treated in section 8.2.

Problem 8.1.2. *We consider again the full feature space $\mathbb{D}$ and we rely on the following remark. The anisotropy in lateral connections can be small depending on*

the animal studied [Lund 2003] and in that case we can assume $\varepsilon \approx 0$. *This suggests to study first the isotropic case:* $\varepsilon = 0$, *which has symmetry group* $\mathbf{E}(2) \times \boldsymbol{U}(1,1)$, *for patterns which are periodic both spatially in* $\mathbb{R}^2$ *and in the feature space* $\mathbb{D}$. *Then we break the symmetry by switching on* $0 < \varepsilon \ll 1$, *so that it is reduced to* $\mathbf{E}(2)$. *This forced symmetry breaking is treated as a perturbation of the isotropic case.* Section 8.3 is devoted to this problem. This approach was initiated by Golubitsky et al in [Golubitsky 2003] for the ring model. There is however an important difference: in [Golubitsky 2003], the symmetry group for one (isolated) hypercolumn is S^1 and it does not take account of the reflections which should naturally occur if the connectivity function W_{loc} did only depend on the distance between angles. In their case the "isotropic" symmetry group is $\mathbf{E}(2) \ltimes S^1$. However if reflections are included in the symmetries, the group becomes the direct product $\mathbf{E}(2) \times \mathbf{O}(2)$. In our case, because we use an explicit expression for W_{loc}, the "isotropic" symmetry group is $\mathbf{E}(2) \times \mathbf{U}(1,1)$.

8.2 Problem 1: weak anisotropic coupling on a bounded structure tensor space

8.2.1 Eigenfunctions of the Laplace-Beltrami operator on Ω

This section is devoted to the study of the eigenfunctions of the Laplace-Beltrami operator on Ω which will be needed for the spectral analysis of the following parts. We impose Dirichlet conditions on the boundary of the disk. From a physic point of view, this problem is analog to finding the modes of a vibrating membrane in hyperbolic geometry. The Laplace-Beltrami operator $L_{\mathbb{D}}$ on $\mathbb{D}$ in hyperbolic polar coordinates (τ, θ) with $z = \tanh(\tau/2)e^{i\theta}$ is defined by:

$$L_{\mathbb{D}} = \frac{\partial^2}{\partial \tau^2} + \coth(\tau)\frac{\partial}{\partial \tau} + \sinh(\tau)^{-2}\frac{\partial^2}{\partial \theta^2}. \tag{8.11}$$

We are looking for eigensolutions of

$$\begin{cases} -L_{\mathbb{D}}V(z) = \lambda V(z), \quad \forall z \in \Omega, \quad \lambda \in \mathbb{R}^+ \\ \qquad V(z) = 0 \quad \forall z \in \partial\Omega \end{cases} \tag{8.12}$$

which can be written $V_m(z) = e^{im\theta}U_m(\cosh(\tau))$. Replacing the expression of $V_m(z)$ into equation (8.12) and setting $y = \cosh(\tau)$ yields

$$(y^2-1)\ddot{U}_m(y) + 2y\dot{U}_m(y) + \left(\lambda - \frac{m^2}{y^2-1}\right)U_m(y) = 0.$$

We set $-\lambda = l(l+1)$ with $l = -\frac{1}{2} + i\rho$ such that $\lambda = \rho^2 + \frac{1}{4}$. The Legendre functions $\mathcal{P}_l^m$ of the first kind and $\mathcal{Q}_l^m$ of the second kind form a basis of the space of solutions. Solutions $\mathcal{Q}_l^m$ are not physically relevent as they blow up at $\tau = 0$. We write $V_m(z) = e^{im\theta}\mathcal{P}_l^m(\cosh(\tau))$ for the other solutions. Finally the solutions of (8.12) which further satisfy $V_m(z) = 0$ for all $z \in \partial\Omega$ can be expressed

as $V_m(z) = e^{im\theta}\mathcal{P}_l^m(\cosh(\tau))$ with $\mathcal{P}_l^m(\cosh(\omega)) = 0$. Then for each $m \in \mathbb{Z}$, one has to impose that $l_{m,n} = -\frac{1}{2} + i\lambda_{m,n}$, where $\lambda_{m,n}$ is the nth root of the function $\lambda \to \mathcal{P}^m_{-\frac{1}{2}+i\lambda}(\cosh(\omega))$. As a consequence, each solution of (8.12) V can be written:

$$\begin{aligned} V(z) &= \sum_{m\in\mathbb{Z}}\sum_{n\in\mathbb{N}^*} a_{m,n}\mathcal{P}^m_{l_{m,n}}(\cosh(\tau))e^{im\theta} \quad \forall z \in \Omega \text{ and } a_{m,n} \in \mathbb{C} \\ &= \sum_{n=1}^{+\infty} A_{0,n}\mathcal{P}_{l_{m,n}}(\cosh(\tau)) + \sum_{m=1}^{+\infty}\sum_{n=1}^{+\infty} A_{m,n}\mathcal{P}^m_{l_{m,n}}(\cosh(\tau))\cos(m\theta) \\ &\quad + \sum_{m=1}^{+\infty}\sum_{n=1}^{+\infty} B_{m,n}\mathcal{P}^m_{l_{m,n}}(\cosh(\tau))\sin(m\theta) \end{aligned}$$

where $A_{0,n}, A_{m,n}$ and $B_{m,n}$ are real.

From the properties [Erdelyi 1985]:

$$\mathcal{P}_l^m = \mathcal{P}^m_{-l-1} \text{ and } \mathcal{P}_l^m = \frac{\Gamma(l+m+1)}{\Gamma(l-m+1)}\mathcal{P}_l^{-m},$$

where Γ is the Gamma function, we can deduce that:

$$\begin{aligned} A_{m,n} &= a_{m,n} + \frac{\Gamma(l_{m,n}-m+1)}{\Gamma(l_{m,n}+m+1)}a_{-m,n} \\ B_{m,n} &= i\left(a_{m,n} - \frac{\Gamma(l_{m,n}-m+1)}{\Gamma(l_{m,n}+m+1)}a_{-m,n}\right). \end{aligned}$$

Proposition 8.2.1. *For fixed m and ω, the function $\lambda \to \mathcal{P}^m_{-\frac{1}{2}+i\lambda}(\cosh(\omega))$ possesses only isolated simple zeros which satisfy:*

$$0 < \lambda_{m,1} < \lambda_{m,2} < \cdots < \lambda_{m,n} < \ldots \text{ with } \lim_{n\to+\infty}\lambda_{m,n} = +\infty.$$

If we normalize associated Legendre functions such that

$$\begin{aligned} \mathcal{Y}_n^m(\tau) &\overset{def}{=} \mathcal{Y}^m_{l_{m,n}}(\tau) = \frac{\mathcal{P}^m_{-1/2+i\rho_{m,n}}(\cosh\tau)}{p_{m,n}} \\ \text{with } p^2_{m,n} &\overset{def}{=} \int_0^\omega \left[\mathcal{P}^m_{-1/2+i\rho_{m,n}}(\cosh\tau)\right]^2 \sinh\tau d\tau \end{aligned}$$

then

$$< \mathcal{Y}_n^m, \mathcal{Y}_{n'}^m >= \int_0^\omega \mathcal{Y}_n^m(\tau)\mathcal{Y}_{n'}^m(\tau)\sinh\tau d\tau = \delta_{n,n'}.$$

Proof.

Multiplying equation (8.12) by $\sinh(\tau)$ we can rewrite the eigenvalue problem as a Sturm Liouville problem:

$$\frac{d}{d\tau}\left(\sinh(\tau)\frac{dV}{d\tau}(\tau)\right) - \frac{m^2}{\sinh(\tau)}V(\tau) = -\lambda\sinh(\tau)V(\tau), \quad \forall\tau \in]0,\omega] \tag{8.13}$$

with the boundary conditions: $V(\omega) = 0$ and $\lim_{\tau\to 0} V(\tau) < +\infty$. We look for eigenvalues of the form $\lambda = \rho^2 + \frac{1}{4}$.

We first assume that $m = 0$ such that equation (8.13) is now defined on $[0, \omega]$ and is a regular Sturm Liouville problem. Sturm Liouville theorem for regular problem [Zettl 2005, Chavel 1984] ensures that the eigenvalues of (8.13) are non-negative, real and simple such that:

$$0 < \lambda_{0,1} < \lambda_{0,2} < \cdots < \lambda_{0,n} < \ldots \text{ with } \lim_{n\to+\infty} \lambda_{0,n} = +\infty.$$

On the other hand, equation (8.13) is a second order differential equation which admits two real linearily independant solutions $\tau \to \mathcal{P}_\nu(\cosh(\tau))$ and $\tau \to \mathcal{Q}_\nu(\cosh(\tau))$ with $\nu = -\frac{1}{2} + i\rho$. As we impose the boundary condition $\lim_{\tau\to 0} V(\tau) < +\infty$, we only keep the solution $\tau \to \mathcal{P}_\nu(\cosh(\tau))$. The other boundary condition imposes that $\mathcal{P}_{-\frac{1}{2}+i\rho}(\cosh(\omega)) = 0$, and if $\rho_{0,n}$ is the nth zero of the analytic function $\rho \to \mathcal{P}_{-\frac{1}{2}+i\rho}(\cosh(\omega))$ we have $\lambda_{0,n} = \rho_{0,n}^2 + \frac{1}{4}$. Finally $(\lambda_{0,n}, \mathcal{P}_{-\frac{1}{2}+i\rho_{0,n}}(\cosh(\cdot))$ is the solution of the eigenvalue problem (8.13). The orthogonality property is a consequence of the simplicity of each eigenvalue and the form of equation (8.13). Take $(\lambda_{0,n}, V_n = \mathcal{P}_{-\frac{1}{2}+i\rho_{0,n}}(\cosh(\cdot))$ and $(\lambda_{0,n'}, V_{n'} = \mathcal{P}_{-\frac{1}{2}+i\rho_{0,n'}}(\cosh(\cdot))$ two solutions of equation (8.13) then:

$$\begin{aligned}
\int_0^\omega V_n(\tau)V_{n'}(\tau)\sinh(\tau)d\tau &= -\frac{1}{\lambda_{0,n}}\int_0^\omega \frac{d}{d\tau}\left(\sinh(\tau)\frac{dV_n}{d\tau}(\tau)\right)V_{n'}(\tau)d\tau \\
&= \frac{1}{\lambda_{0,n}}\int_0^\omega \sinh(\tau)\frac{dV_n}{d\tau}(\tau)\frac{dV_{n'}}{d\tau}(\tau)d\tau \\
&= \frac{\lambda_{0,n'}}{\lambda_{0,n}}\int_0^\omega V_n(\tau)V_{n'}(\tau)\sinh(\tau)d\tau.
\end{aligned}$$

This implies that for $n \neq n'$, $\int_0^\omega V_n(\tau)V_{n'}(\tau)\sinh(\tau)d\tau = 0$.

Next, suppose $m \geq 1$. The eigenvalue problem (8.13) is now a singular Sturm-Liouville problem because of the singularity at $\tau = 0$. Nevertheless, it is still possible to prove the existence of real non-negative and simple eigenvalues of (8.13) ([Zettl 2005, Chavel 1984]):

$$0 < \lambda_{m,1} < \lambda_{m,2} < \cdots < \lambda_{m,n} < \ldots \text{ with } \lim_{n\to+\infty} \lambda_{m,n} = +\infty.$$

It is straightforward to see that $(\lambda_{m,n}, \mathcal{P}^m_{-\frac{1}{2}+i\rho_{m,n}}(\cosh(\cdot))$ is a solution of the eigenvalue problem. The proof of the orthogonality property follows the same lines as for the case $m = 0$, with the additional remark that for all $m \geq 1$ the function

$$\tau \to \sinh(\tau)^{-1}\mathcal{P}^m_{-\frac{1}{2}+i\rho_{m,n}}(\cosh(\tau))\mathcal{P}^m_{-\frac{1}{2}+i\rho_{m,n'}}(\cosh(\tau))$$

is integrable on $]0, \omega]$ for all $n, n' \in \mathbb{N}^*$. □

The multiplicity of the eigenvalues of the Laplace-Beltrami operator is a complex problem. As for the zeros of Bessel functions [Watson 1995], between two consecutive zeros of $\lambda \to \mathcal{P}^m_{-\frac{1}{2}+i\lambda}(\cosh(\omega))$ there exists one zero of $\lambda \to \mathcal{P}^{m+1}_{-\frac{1}{2}+i\lambda}(\cosh(\omega))$ [Lebedev 1972]. This implies that the multiplicity of $\lambda_{0,1}$ is one and the multiplicity of $\lambda_{1,1}$ is two. We further have $0 < \lambda_{0,1} < \lambda_{1,1} < \cdots$.

8.2.2 Study of an isolated hypercolumn

8.2.2.1 Linear stability analysis

We rewrite equation (8.1) for $\beta = 0$ in the lateral coupling function in (τ, θ)-coordinates.

$$\frac{\partial V(\mathbf{r},\tau,\theta,t)}{\partial t} = -V(\mathbf{r},\tau,\theta,t) + \int_0^{\omega}\int_0^{2\pi} W_{loc}\left(d_{\mathbb{D}}\left(\tanh(\tau/2)e^{i\theta}, \tanh(\tau'/2)e^{i\theta'}\right)\right) \times S(\mu V(\mathbf{r},\tau',\theta',t))\sinh(\tau')d\tau' d\theta' \tag{8.14}$$

The local connectivity function can be expressed in a compact form as

$$W_{loc}(\tau,\tau' \mid \theta-\theta') \stackrel{def}{=} W_{loc}\left(d_{\mathbb{D}}\left(\tanh(\tau/2)e^{i\theta}, \tanh(\tau'/2)e^{i\theta'}\right)\right) = \sum_{m=0}^{+\infty}\sum_{n\in\mathbb{N}^*} \widehat{W}_{m,n}\mathcal{Y}_n^m(\tau)\mathcal{Y}_n^m(\tau')\cos(m(\theta-\theta')). \tag{8.15}$$

Equation (8.14) presents an $\mathbf{O}(2)$ symmetry with action:

$$\varphi\cdot(\tau,\theta) = (\tau,\theta+\varphi) \quad \varphi\in[0,2\pi]$$
$$s\cdot(\tau,\theta) = (\tau,-\theta).$$

With the fact that $S(0) = 0$ in the definition of the sigmoidal function S, the fully symmetric state $V = 0$ is always a solution of (8.14) for all values of the parameter μ. To study the linear stability of the trivial state $V = 0$, we have to look at solutions of the linearized equation

$$\frac{\partial V(\mathbf{r},\tau,\theta,t)}{\partial t} = -V(\mathbf{r},\tau,\theta,t) + \mu s_1\int_0^{\omega}\int_0^{2\pi} W_{loc}\left(\tau,\tau' \mid \theta-\theta'\right) \times V(\mathbf{r},\tau',\theta',t)\sinh(\tau')d\tau' d\theta'. \tag{8.16}$$

with $s_1 = S'(0)$, of the form $e^{\sigma t}U(\mathbf{r},\tau,\theta)$. Substituting the distribution (8.15) for W_{loc} and using orthogonality relation shows that the dispersion relation is given by:

$$\sigma_{n,m} = -1 + \mu s_1\widehat{W}_{m,n}$$

with corresponding eigenvectors $\mathcal{Y}_n^m(\tau)\cos(m\theta)$ and $\mathcal{Y}_n^m(\tau)\sin(m\theta)$ if $m \geq 1$, $\mathcal{Y}_n^0(\tau)$ if $m = 0$. Thus the eigenvalue $\sigma_{n,m}$ is at least 2-fold degenerate for $m \geq 1$. If we denote

$$\widehat{W}_{M,N} = \max\{\widehat{W}_{m,n} \mid (m,n)\in\mathbb{N}\times\mathbb{N}^*\}$$

then $V = 0$ becomes unstable at a critical value $\mu_c = \left(s_1\widehat{W}_{M,N}\right)^{-1}$.

The cases $(M = 0, N = 1)$ and $(M = 1, N = 1)$ are relevant from a biological point of view. If $M = 0$ and $N = 1$, sufficiently close to the bifurcation point, the resulting activity profile satisfies

$$V(\mathbf{r},\tau,\theta) = a(\mathbf{r})\mathcal{Y}_1(\tau)$$

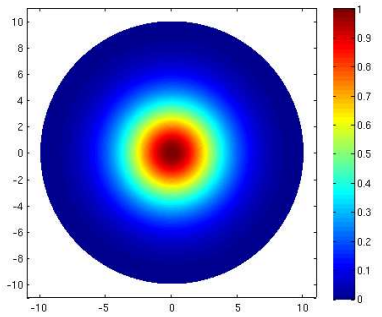

(a) Mode $(0,1)$ with $\lambda_{0,1} = 0.2798$.

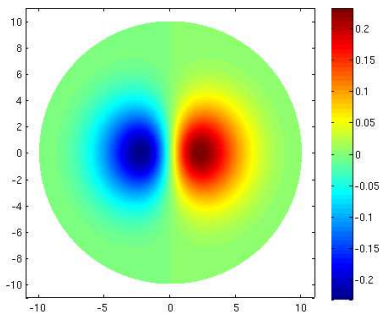

(b) Mode $(1,1)$ with $\lambda_{1,1} = 0.334$.

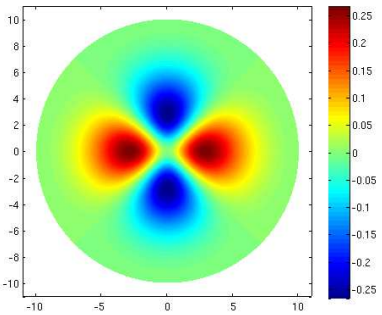

(c) Mode $(2,1)$ with $\lambda_{2,1} = 0.3585$.

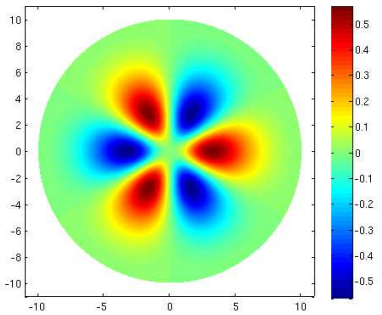

(d) Mode $(3,1)$ with $\lambda_{3,1} = 0.3753$.

Figure 8.1: Plot of solution of the form $\mathcal{P}^m_{l_{m,n}}(\cosh(\tau))\cos(m\theta)$ with $(\tau,\theta) \in [0,\omega] \times [0,2\pi]$ and $l_{m,n} = -\frac{1}{2} + i\lambda_{m,n}$.

and if $M = 1$ and $N = 1$ we have:

$$V(\mathbf{r}, \tau, \theta) \quad = \quad \alpha(\mathbf{r}) \mathcal{Y}_1^1(\tau) \cos\left(\theta - \phi(\mathbf{r})\right).$$

In the first case, the new steady state shows no orientation preference as it can be seen in figure 8.1(a) where the region of high activity is centered at $z = 0$. In the second case, the response is both unimodal with respect to τ and θ, see figure 8.1(b). The ocurence of a tuned surface peaked at some angle $\phi(\mathbf{r})$ corresponds to the presence of local contour there. The angle $\phi(\mathbf{r})$ for each tuning surface is arbitrary which reflects the $\mathbf{O}(2)$ equivariance of equation (8.14). Without any lateral connections, the overall tuned response is uncorrelated across the cortex. As explained in [Bressloff 2001b], the presence of anisotropy has for consequence to correlate the peaks of the tuning surfaces at different locations.

8.2.2.2 Steady-state bifurcation with $\mathbf{O}(2)$ symmetry

From the linear stability analysis and the symmetries of the system, we have a steady-state bifurcation with $\mathbf{O}(2)$ symmetry at the critical point $\mu = \mu_c$. In order to be able to compare our results with those obtained in the Ring Model of orientation, we select unimodal solution in the θ variable: $M = 1$ and the τ variable $N = 1$. Close to the bifurcation point $(V = 0, \mu = \mu_c)$ there exists a polynomial change of variables of the form

$$V(\mathbf{r}, \tau, \theta, t) = A(\mathbf{r}, t)\zeta_1(\tau, \theta) + B(\mathbf{r}, t)\zeta_2(\tau, \theta) + \Psi(A(\mathbf{r}, t), B(\mathbf{r}, t), \mu - \mu_c)$$

with

$$\zeta_1(\tau, \theta) = \mathcal{Y}_1^1(\tau)\cos(\theta) \text{ and } \zeta_2(\tau, \theta) = \mathcal{Y}_1^1(\tau)\sin(\theta)$$

which transforms equation (8.14) into the normal form

$$\begin{aligned} \frac{dA}{dt} &= \left[\frac{\mu - \mu_c}{\mu_c} + \varpi(A^2 + B^2)\right] A + \text{h.o.t.} \\ \frac{dB}{dt} &= \left[\frac{\mu - \mu_c}{\mu_c} + \varpi(A^2 + B^2)\right] B + \text{h.o.t.} \end{aligned} \tag{8.17}$$

and ϖ can be expressed as

$$\varpi = \frac{\mu_c^3 \pi \widehat{W}_{1,1}}{4} \left(\frac{s_3 \Lambda}{2} + \mu_c s_2^2 \sum_{n \in \mathbb{N}^*} \left[\frac{\pi \widehat{W}_{0,n} \left(\gamma_{0,n}\right)^2}{\left(1 - \mu_c s_1 2\pi \widehat{W}_{0,n}\right)} + \frac{\pi \widehat{W}_{2,n} \left(\gamma_{2,n}\right)^2}{4\left(1 - \mu_c s_1 \pi \widehat{W}_{2,n}\right)} \right] \right) \tag{8.18}$$

with $s_2 = S''(0), s_3 = S'''(0)$ and

$$\begin{aligned} \Lambda &= \int_0^\omega \left(\mathcal{Y}_1^1(\tau)\right)^4 \sinh(\tau) d\tau \\ \gamma_{k,n} &= \int_0^\omega \mathcal{Y}_n^k(\tau') \left(\mathcal{Y}_1^1(\tau')\right)^2 \sinh(\tau') d\tau'. \end{aligned}$$

Proof. These formulas are derived in appendix B.1. □

The sign of ϖ determines if the bifurcation is subcritical or supercritical. If $\varpi < 0$, the Pitchfork is oriented towards the increasing μ (supercritical) otherwise it points towards the decreasing μ (subcritical). In this latter case, it can be shown [Veltz 2010b] that the bifurcated branch has to "turn around", which produces two additional solutions on each branch. As it has been noticed in [Veltz 2010a] in the case of the ring model of orientation, the condition $\varpi > 0$ does not give a biological plausible behaviour of the network. This is why we impose the condition $\varpi < 0$, which gives a constrain on the threshold T of the sigmoidal function defined in equation (8.2) and the coefficients $\widehat{W}_{m,n}$ of the coupling function W_{loc}. In the simplified case where $\widehat{W}_{0,1} = -1$ and $\widehat{W}_{m,n} = 0$ for all $(m,n) \in \mathbb{N} \times \mathbb{N}^* \setminus \{(0,1),(1,1)\}$, we plot in figure 8.2 the sign of ϖ as a function of T and $\widehat{W}_{1,1}$.

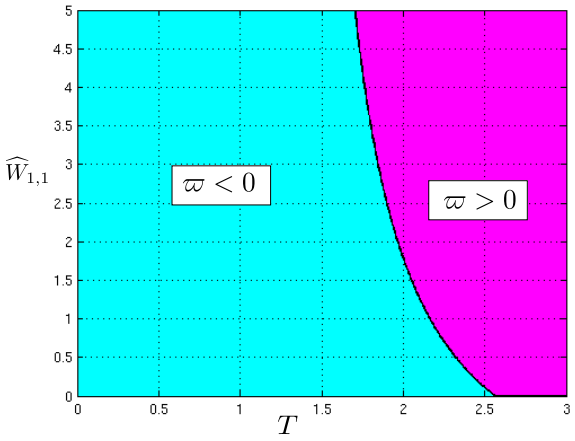

Figure 8.2: Plot of the sign of ϖ as a function of T and $\widehat{W}_{1,1}$.

8.2.3 Weak lateral interactions

We now turn on the lateral interactions: $\beta \neq 0$. We have already mentioned in Problem 8.1.1 that the lateral connections modulate rather than drive the cortical activity. This is why we will work in the regime where $0 < \beta \ll 1$. In order to be able to present some analytic results, we select a simplified version of the function $\mathcal{K}$ (this is the limit case $k_c \to 0$ in the definition of $\mathcal{K}$ in equation (8.4)):

$$\mathcal{K}(\tau,\theta \mid \tau',\theta') = \frac{1}{\sinh(\tau)}\delta_{\tau,\tau'}\delta_{\theta,\theta'}.$$

8.2.3.1 Eigenvalues and eigenfunctions of the linear problem

We first linearize equation (8.1) close to the fully symmetric state $V(\mathbf{r},\tau,\theta,t) = 0$.

$$\frac{\partial V(\mathbf{r},\tau,\theta,t)}{\partial t} = -V(\mathbf{r},\tau,\theta,t) + \mu s_1 \left[\int_0^{\omega} \int_0^{2\pi} W_{loc}\left(\tau,\tau' \mid \theta-\theta'\right) \right.$$
$$\left. \times V(\mathbf{r},\tau',\theta',t)\sinh(\tau')d\tau' d\theta' + \beta \int_{\mathbb{R}^2} \mathcal{J}(\mathbf{r}-\mathbf{r}',\tau,\theta)V(\mathbf{r}',\tau,\theta)d\mathbf{r}' \right], \tag{8.19}$$

where we have set:

$$\mathcal{J}(\mathbf{r}-\mathbf{r}',\tau,\theta) \overset{def}{=} \mathcal{J}\left(\sqrt{(\mathbf{r}-\mathbf{r}')^{\mathbf{T}}(\mathbf{I}_2+\varepsilon\mathcal{T}(\tau,\theta))(\mathbf{r}-\mathbf{r}')}\right)$$

with $\mathcal{T}(\tau,\theta)$ given through the "$\mathbb{D}$ to $\mathbf{SSPD}(2,\mathbb{R})$" dictionary in subsection 3.2.2 of chapter 3 by

$$\mathcal{T}(\tau,\theta) = \begin{pmatrix} a(\tau,\theta) & c(\tau,\theta) \\ c(\tau,\theta) & b(\tau,\theta) \end{pmatrix}$$

and

$$a(\tau,\theta) = \frac{1+\tanh(\tau/2)^2+2\tanh(\tau/2)\cos(\theta)}{1-\tanh(\tau/2)^2}$$
$$b(\tau,\theta) = \frac{1+\tanh(\tau/2)^2-2\tanh(\tau/2)\cos(\theta)}{1-\tanh(\tau/2)^2}$$
$$c(\tau,\theta) = \frac{2\tanh(\tau/2)\sin(\theta)}{1-\tanh(\tau/2)^2}.$$

We look for perturbations of the form $e^{\sigma t}u_{\mathbf{k}}(\tau,\theta)e^{i\mathbf{k}\cdot\mathbf{r}} + \text{cc}$ with $\mathbf{k} = q(\cos\varphi,\sin\varphi)$ and $u_{\mathbf{k}}(\tau,\theta) = u(\tau,\theta-2\varphi)$. Equation (8.19) leads to the eigenvalue problem for $(\sigma,u(\tau,\theta))$:

$$\sigma u(\tau,\theta) = -u(\tau,\theta) + \mu s_1 \beta \widetilde{\mathcal{J}}_{\mathbf{k}}(\tau,\theta+2\varphi)u(\tau,\theta)$$
$$+ \mu s_1 \int_0^{\omega}\int_0^{2\pi} W_{loc}\left(\tau,\tau' \mid \theta-\theta'\right) u(\tau',\theta')\sinh(\tau')d\tau' d\theta' \tag{8.20}$$

with

$$\widetilde{\mathcal{J}}_{\mathbf{k}}(\tau,\theta+2\varphi) = \int_{\mathbb{R}^2} \mathcal{J}(\mathbf{r}-\mathbf{r}',\tau,\theta+2\varphi)e^{i\mathbf{k}\cdot(\mathbf{r}-\mathbf{r}')}d\mathbf{r}'.$$

Due to the rotational invariance of the lateral coupling (8.4) with shift-twist action, the function $\widetilde{\mathcal{J}}_{\mathbf{k}}(\tau,\theta+2\varphi)$ only depends upon q the magnitude of vector $\mathbf{k}\in\mathbb{R}^2$. This is why $(\sigma,u(\tau,\theta))$ given by equation (8.20) also only depends upon q. Expanding $u(\tau,\theta)$ on the basis $(\mathcal{Y}_n^m(\tau)\cos(m\theta),\mathcal{Y}_n^m(\tau)\sin(m\theta))_{m\in\mathbb{Z},n\geq 1}$ we obtain:

$$u(\tau,\theta) = \sum_{n=1}^{+\infty} A_{0,n}(q)\mathcal{Y}_n(\tau) + \sum_{m=1}^{+\infty}\sum_{n=1}^{+\infty} \mathcal{Y}_n^m(\tau)\left(A_{m,n}(q)\cos(m\theta)+B_{m,n}(q)\sin(m\theta)\right).$$

Taking the scalar product of equation (8.20) with $\mathcal{Y}_n, \mathcal{Y}_n^m\cos(m\theta)$ and $\mathcal{Y}_n^m\sin(m\theta')$ gives respectively:

$$\left[\frac{\sigma+1}{\mu s_1}-\widehat{W}_{0,n}\right]A_{0,n}(q)=\beta\sum_{m'\in\mathbb{N}}\sum_{n'\in\mathbb{N}^*}\widetilde{\mathcal{J}}^{0}_{0n,m'n'}(q)A_{m',n'}(q)$$
$$\left[\frac{\sigma+1}{\mu s_1}-\widehat{W}_{m,n}\right]A_{m,n}(q)=\beta\sum_{m'\in\mathbb{N}}\sum_{n'\in\mathbb{N}^*}\widetilde{\mathcal{J}}^{+}_{mn,m'n'}(q)A_{m',n'}(q)$$
$$\left[\frac{\sigma+1}{\mu s_1}-\widehat{W}_{m,n}\right]B_{m,n}(q)=\beta\sum_{m'\in\mathbb{N}^*}\sum_{n'\in\mathbb{N}^*}\widetilde{\mathcal{J}}^{-}_{mn,m'n'}(q)B_{m',n'}(q)$$

where

$$\widetilde{\mathcal{J}}^{0}_{0n,m'n'}(q)=\frac{1}{2\pi}\int_0^{\omega}\int_0^{2\pi}\widetilde{\mathcal{J}}_{\mathbf{k}}(\tau,\theta+2\varphi)\mathcal{Y}_n(\tau)\mathcal{Y}^{m'}_{n'}(\tau)\cos(m'\theta)\sinh(\tau)d\tau d\theta$$
$$\widetilde{\mathcal{J}}^{+}_{mn,m'n'}(q)=\frac{1}{\pi}\int_0^{\omega}\int_0^{2\pi}\widetilde{\mathcal{J}}_{\mathbf{k}}(\tau,\theta+2\varphi)\mathcal{Y}^{m}_{n}(\tau)\mathcal{Y}^{m'}_{n'}(\tau)\cos(m\theta)\cos(m'\theta)\sinh(\tau)d\tau d\theta$$
$$\widetilde{\mathcal{J}}^{-}_{mn,m'n'}(q)=\frac{1}{\pi}\int_0^{\omega}\int_0^{2\pi}\widetilde{\mathcal{J}}_{\mathbf{k}}(\tau,\theta+2\varphi)\mathcal{Y}^{m}_{n}(\tau)\mathcal{Y}^{m'}_{n'}(\tau)\sin(m\theta)\sin(m'\theta)\sinh(\tau)d\tau d\theta.$$

Based on the analysis made for $\beta=0$, we assume that

$$\widehat{W}_{1,1}=\max\{\widehat{W}_{m,n}\mid(m,n)\in\mathbb{N}\times\mathbb{N}^*\}.$$

There is a $\mathbf{k}$-dependent splitting of the degenerate eigenvalue σ associated to the mode $(1,1)$ and denoting the characteristic size of such a splitting by $\delta\sigma=\mathcal{O}(\beta)$, we impose the condition that $\delta\sigma\ll\mu\Delta\widehat{W}$, where $\Delta\widehat{W}=\min\{\widehat{W}_{1,1}-\widehat{W}_{m,n},m\neq 1\text{ and }n\neq 1\}$. We can introduce the following perturbation expansions and solve the resulting hierarchy of equations to successive orders in β:

$$\frac{\sigma_\pm+1}{\mu}=\widehat{W}_{1,1}+\beta\sigma^{(1)}_\pm+\beta^2\sigma^{(2)}_\pm+\dots$$
$$A_{m,n}(q)=A(q)\delta_{m,1}\delta_{n,1}+\beta A^{(1)}_{m,n}(q)+\beta^2A^{(2)}_{m,n}(q)+\dots$$
$$B_{m,n}(q)=B(q)\delta_{m,1}\delta_{n,1}+\beta B^{(1)}_{m,n}(q)+\beta^2B^{(2)}_{m,n}(q)+\dots$$

Setting $m=1$ and $n=1$ we can collect the $\mathcal{O}(\beta)$ terms and get:

$$\sigma^{(1)}_\pm=\widetilde{\mathcal{J}}^{\pm}_{11,11}(q)$$
$$A^{(1)}_{m,n}(q)=\frac{\widetilde{\mathcal{J}}^{+}_{mn,11}(q)A(q)}{\widehat{W}_{1,1}-\widehat{W}_{m,n}}$$
$$B^{(1)}_{m,n}(q)=\frac{\widetilde{\mathcal{J}}^{-}_{mn,11}(q)B(q)}{\widehat{W}_{1,1}-\widehat{W}_{m,n}}.$$

For the $\mathcal{O}(\beta^2)$ terms we obtain two equations:

$$\left[\sigma_+^{(1)} - \widetilde{\mathcal{J}}^+_{11,11}(q)\right] A^{(1)}_{1,1}(q) + \sigma_+^{(2)} A(q) = \sum_{(m',n')\neq(1,1)} \widetilde{\mathcal{J}}^+_{11,m'n'}(q) A^{(1)}_{m',n'}(q)$$
$$\left[\sigma_-^{(1)} - \widetilde{\mathcal{J}}^-_{11,11}(q)\right] B^{(1)}_{1,1}(q) + \sigma_-^{(2)} B(q) = \sum_{(m',n')\neq(1,1)} \widetilde{\mathcal{J}}^-_{11,m'n'}(q) B^{(1)}_{m',n'}(q)$$

which give:

$$\Rightarrow \lambda^{(2)}_{\pm} = \sum_{(m',n')\neq(1,1)} \frac{\left(\widetilde{\mathcal{J}}^{\pm}_{11,m'n'}(q)\right)^2}{\widehat{W}_{1,1} - \widehat{W}_{m',n'}}.$$

Finally we have the following proposition.

Proposition 8.2.2. *The two dispersion relations are given by:*

$$\sigma_{\pm} = -1 + \mu s_1 \left[\widehat{W}_{1,1} + \beta \widetilde{\mathcal{J}}^{\pm}_{11,11}(q) + \beta^2 \sum_{(m',n')\neq(1,1)} \frac{\left(\widetilde{\mathcal{J}}^{\pm}_{11,m'n'}(q)\right)^2}{\widehat{W}_{1,1} - \widehat{W}_{m',n'}} + \mathcal{O}(\beta^2)\right] \tag{8.21}$$

and $u_{\mathbf{k}}(\tau,\theta) = u^{\pm}_{\mathbf{k}}(\tau,\theta)$ *where to* $\mathcal{O}(\beta)$*:*

$$u^+_{\mathbf{k}}(\tau,\theta) = \mathcal{Y}^1_1(\tau)\cos(\theta - 2\varphi) + \beta \sum_{(m,n)\neq(1,1)} \mathcal{Y}^m_n(\tau) \frac{\widetilde{\mathcal{J}}^+_{mn,11}(q)}{\widehat{W}_{1,1} - \widehat{W}_{m,n}} \cos(m(\theta - 2\varphi)) \tag{8.22}$$

$$u^-_{\mathbf{k}}(\tau,\theta) = \mathcal{Y}^1_1(\tau)\sin(\theta - 2\varphi) + \beta \sum_{(m,n)\neq(1,1)} \mathcal{Y}^m_n(\tau) \frac{\widetilde{\mathcal{J}}^-_{mn,11}(q)}{\widehat{W}_{1,1} - \widehat{W}_{m,n}} \sin(m(\theta - 2\varphi)). \tag{8.23}$$

8.2.3.2 Discussion

We suppose that $\mathcal{H}_{\pm}(q) = \widehat{W}_{1,1} + \beta \widetilde{\mathcal{J}}^{\pm}_{11,11}(q)$ has a unique maximum at $q = q_{\pm} \neq 0$. We define $q_c = q_+$ if $\mathcal{H}_+(q_+) > \mathcal{H}_-(q_-)$ and $q_c = q_-$ if $\mathcal{H}_+(q_+) < \mathcal{H}_-(q_-)$, then the homogeneous state $a(\mathbf{r},\tau,\theta) = 0$ is marginally stable at $\mu_c = (s_1\mathcal{H}_+(q_c))^{-1}$ if $q_c = q_+$ and at $\mu_c = (s_1\mathcal{H}_-(q_c))^{-1}$ if $q_c = q_-$. From the rotation invariance, all modes lying on the critical circle $\|\mathbf{k}\| = q_c$ become neutrally stable at $\mu = \mu_c$. The question of the ocurence of even or odd patterns depends of the specific form of the lateral connection $\mathcal{J}$ in equation (8.4).

The infinite degeneracy of the modes on the critical circle can be reduced to a finite set of modes by restricting solutions to be doubly periodic functions on the Euclidean plane, for which we recall some basic properties. Let ℓ_1, ℓ_2 be a basis of $\mathbb{R}^2$ and $\mathcal{L}$ be a planar lattice of $\mathbb{R}^2$: $\mathcal{L} = \{2\pi m_1\ell_1 + 2\pi m_2\ell_2 \mid (m_1,m_2) \in \mathbb{Z}^2\}$.. If we

denote by $\mathcal{H}$ the holohedry of the lattice, then the symmetry group $\Gamma_{\mathcal{L}}$ of the lattice is generated by the semi-direct product $\Gamma_{\mathcal{L}} = \mathcal{H} \ltimes \mathbb{T}^2$, where $\mathbb{T}^2$ is the 2-torus. We also define the dual lattice of $\mathcal{L}$ by $\mathcal{L}^* = \{2\pi m_1 \mathbf{k}_1 + 2\pi m_2 \mathbf{k}_2 \mid (m_1, m_2) \in \mathbb{Z}^2\}$ with $\ell_i \cdot \mathbf{k}_j = \delta_{i,j}$. The action of $\Gamma_{\mathcal{L}}$ on the space of doubly periodic functions is the one induced from the action of $\mathbf{E}(2)$ on $\mathbb{R}^2 \times \Omega$ given in (8.8). We consider only bifurcations based on dual wave vectors of shortest (unit) length and assume that the critical eigenspace $V_{\mathbf{k}}$ consists of functions of the form:

$$a(\mathbf{r}, \tau, \theta) = \sum_{j=1}^{s} z_j u_{\mathbf{k}_j}(\tau, \theta) e^{i\mathbf{k}_j \cdot \mathbf{r}} + \text{c.c.} \tag{8.24}$$

where $(z_1, \ldots, z_s) \in \mathbb{C}^s$ with $s = 2$ for square or rhombic lattices and $s = 3$ for hexagonal lattices. It was shown in [Bressloff 2001a] that the subspace $V_{\mathbf{k}}$ decomposes into two nonisomorphic absolutely irreducible representations of $\Gamma_{\mathcal{L}}$: $V_{\mathbf{k}} = V_{\mathbf{k}}^+ \oplus V_{\mathbf{k}}^-$, where $V_{\mathbf{k}}^+$ is the space of even eigenfunctions and $V_{\mathbf{k}}^-$ is the space of odd eigenfunctions in θ. The actions of the group $\Gamma_{\mathcal{L}}$ on $V_{\mathbf{k}}^+$ and $V_{\mathbf{k}}^-$ can be explicitely written down for both the square or rhombic and hexagonal lattices and are given in [Bressloff 2001b].

Finally, by applying the Equivariant Branching Lemma [Golubitsky 1988, Chossat 2000], we can show the existence of branches of solution for each of the axial subgroups of $\Gamma_{\mathcal{L}}$. All these axial subgroups have been calculated in [Bressloff 2001a, Bressloff 2001b] and lead to even and odd planforms. In particular, the perturbation analysis made in the previous part shows that $u_{\mathbf{k}}(\tau, \theta)$ in equation (8.24) can take the forms:

(i) $u_{\mathbf{k}}(\tau, \theta) \approx \mathcal{Y}_1^1(\tau) \cos(\theta - 2\varphi)$ for even planforms (equation (8.22)),

(ii) $u_{\mathbf{k}}(\tau, \theta) \approx \mathcal{Y}_1^1(\tau) \sin(\theta - 2\varphi)$ for odd planforms (equation (8.23)).

The reduced feature space model for structure tensors is then a direct generalization of the model developed by Bressloff et al in [Bressloff 2001a, Bressloff 2001b] but it does not predict new planforms.

8.3 Problem 2: bifurcation of doubly periodic planforms in both $\mathbb{R}^2$ and $\mathbb{D}$

In this section, we adopt the strategy developed in [Golubitsky 2003]. We will determine solutions to symmetry-breaking bifurcations in the isotropic case ($\varepsilon = 0$), with symmetry group $\mathbf{E}(2) \times \mathbf{U}(1,1)$, and then study how these solutions change when anisotropy is introduced as a forced symmetry-breaking parameter ($0 < \varepsilon \ll 1$).

8.3.1 Bifurcation problem

First of all we rewrite equation (8.5) on $\mathbb{R}^2 \times \mathbb{D}$ with W_{lat}^0 in the definition of (8.3), which gives

$$\begin{aligned}\frac{\partial V(\mathbf{r},z,t)}{\partial t} &= -V(\mathbf{r},z,t) + \int_{\mathbb{D}} W_{loc}\left(d_{\mathbb{D}}(z,z')\right) S(\mu V(\mathbf{r},z',t))\mathrm{dm}(z') \\ &\quad + \beta \int_{\mathbb{D}}\int_{\mathbb{R}^2} \mathcal{J}(\|\mathbf{r}-\mathbf{r}'\|)\mathcal{K}\left(d_{\mathbb{D}}(z,z')\right) S(\mu V(\mathbf{r}',z',t))\mathrm{dm}(z')d\mathbf{r}'.\end{aligned} \tag{8.25}$$

With the fact that $S(0) = 0$ in the definition of the sigmoidal function S, the fully symmetric state $V = 0$ is always a solution of (8.25) for all values of the parameter μ. To study the linear stability of the trivial state $V = 0$, we have to look at solutions of the linearized equation

$$\begin{aligned}\frac{\partial V(\mathbf{r},z,t)}{\partial t} &= -V(\mathbf{r},z,t) + \mu s_1 \int_{\mathbb{D}} W_{loc}\left(d_{\mathbb{D}}(z,z')\right) V(\mathbf{r},z',t)\mathrm{dm}(z') \\ &\quad + \beta\mu s_1 \int_{\mathbb{D}}\int_{\mathbb{R}^2} \mathcal{J}(\|\mathbf{r}-\mathbf{r}'\|)\mathcal{K}\left(d_{\mathbb{D}}(z,z')\right) V(\mathbf{r}',z',t)\mathrm{dm}(z')d\mathbf{r}'.\end{aligned} \tag{8.26}$$

with $s_1 = S'(0)$ of the form $e^{\sigma t}U(\mathbf{r},z)$. Solutions must satisfy the eigenvalue problem:

$$\begin{aligned}(\sigma+1)U(\mathbf{r},z) &= \mu s_1 \int_{\mathbb{D}} W_{loc}\left(d_{\mathbb{D}}(z,z')\right) U(\mathbf{r},z')\mathrm{dm}(z') \\ &\quad + \beta\mu s_1 \int_{\mathbb{D}}\int_{\mathbb{R}^2} \mathcal{J}(\|\mathbf{r}-\mathbf{r}'\|)\mathcal{K}\left(d_{\mathbb{D}}(z,z')\right) U(\mathbf{r}',z')\mathrm{dm}(z')d\mathbf{r}'.\end{aligned} \tag{8.27}$$

Because of the $\mathbf{E}(2)\times\mathbf{U}(1,1)$ equivariance of equation (8.25), solutions of (8.27) are plane waves in $\mathbb{R}^2 \times \mathbb{D}$. Assuming that $U(\mathbf{r},z) = e^{i\mathbf{k}\cdot\mathbf{r}}e_{\rho,b}(z)$ we obtain the following relation

$$\sigma = -1 + \mu s_1\left(\widetilde{W}_{loc}(\rho) + \beta\widehat{\mathcal{J}}(q)\widetilde{\mathcal{K}}(\rho)\right) \tag{8.28}$$

where $\widehat{\mathcal{J}}(q)$ is the Hankel transform of $\mathcal{J}(\|\cdot\|)$ with $q = \|\mathbf{k}\|$ and $\widetilde{W}_{loc}(\rho)$ (resp. $\widetilde{\mathcal{K}}(\rho)$) is the Helgason-Fourier transform of $W_{loc}(d_{\mathbb{D}}(\cdot,0))$ (resp. $\mathcal{K}(d_{\mathbb{D}}(\cdot,0))$). The fact that Helgason-Fourier transform of $W_{loc}(d_{\mathbb{D}}(\cdot,0))$ and $\mathcal{K}(d_{\mathbb{D}}(\cdot,0))$ does not depend upon $b \in \partial\mathbb{D}$ was already proved in lemma 6.1.2 of chapter 6. It follows that the neutral stability curve

$$\mu(q,\rho) = \left(s_1\left(\widetilde{W}_{loc}(\rho) + \beta\widehat{\mathcal{J}}(q)\widetilde{\mathcal{K}}(\rho)\right)\right)^{-1}$$

attains its minimum at $\mu_c = \left(s_1\left(\widetilde{W}_{loc}(\rho_c) + \beta\widehat{\mathcal{J}}(q_c)\widetilde{\mathcal{K}}(\rho_c)\right)\right)^{-1}$ with (q_c,ρ_c) defined by $(q_c,\rho_c) = \max_{(q,\rho)\in\mathbb{R}^+\times\mathbb{R}}\left[\widetilde{W}_{loc}(\rho) + \beta\widehat{\mathcal{J}}(q)\widetilde{\mathcal{K}}(\rho)\right]$.

A consequence of the $\mathbf{E}(2)\times\mathbf{U}(1,1)$ symmetry is that the kernel of the linearized equation (8.26), at the critical point $\mu = \mu_c$ is infinite dimensional (indifference to b and all $\mathbf{k}$ such that $\|\mathbf{k}\| = q_c$). As in the Euclidean case of pattern formation, we want to look for solutions in the restricted class of patterns which are doubly

periodic in the $\mathbf{r}$ variable and spatially periodic in the z variable. Doubly-periodic functions on the Euclidean plane correspond to rectangular, square and hexagonal tilings of $\mathbb{R}^2$. Functions which are periodic in the Poincaré disk $\mathbb{D}$ are, by definition, invariant under the action of a discrete subgroup $\mathbf{G}$ of $\mathbf{U}(1,1)$ whose fundamental domain is a polygon (see chapter 6).

Tilings of the Poincaré disc have very different properties from tilings of the Euclidean plane. In particular tilings exist with polygons having an arbitrary number of sides, while in $\mathbb{R}^2$ only rectangular, square and hexagonal periodic tilings exist. But the size of a regular polygon with a given number of vertices is fixed in hyperbolic geometry, a consequence of the Gauss-Bonnet formula [Katok 1992]. This has for consequence to render discrete the set of values of the wave number ρ_c and hence μ_c. It follows that, although we can look for the bifurcation of spatially periodic solutions associated with a given tesselation in $\mathbb{D}$, these patterns will not in general correspond to the most unstable perturbations unless the parameters in the equation are tuned so that it happens this way. In section 8.3.3, we will tune the parameters of the local connectivity function W_{loc}, such that the most unstable mode is associated to the tiling that we have choosen.

8.3.2 Bifurcations of octagonal H-planforms

Irreducible representation χ_8 For each representations χ_1 to χ_{13}, we have given in chapter 6 the isotropy types of each representations which have on dimensional fixed-point subspace and presented the corresponding bifurcation diagrams (see chapter 7 for the four-dimensional representation case). In this chapter, we focus on the case of the irreducible representation χ_8. The choice of χ_8 is arbitrary for the moment but will be explained in the last paragraph of this subsection. In that case, from Theorem 6.3.1, we have the following proposition. We recall that the octahedral group $\mathbb{O}$, the direct symmetry group of the cube, possesses two irreducible representations of dimension three. In order to differentiate these two irreducible representations we adopt the convention "natural" as used in [Miller 1972].

Proposition 8.3.1. *For the three dimensional irreducible representation χ_8 of $\mathcal{G}$, the isotropy subgroups with one dimensional fixed point subspace are the following:*

$$\begin{aligned}\mathbf{D}_8 &= \langle \rho, \kappa \rangle \\ \widetilde{\mathbf{C}}_{6\kappa'} &= \langle -\varepsilon, \kappa' \rangle \\ \widetilde{\mathbf{D}}_{2\kappa} &= \langle -Id, \sigma, \kappa \rangle.\end{aligned}$$

The bifurcation diagram is the same as the bifurcation diagram with "natural" full octahedral $\mathbb{O} \ltimes \mathbb{Z}_2$ symmetry in $\mathbb{R}^3$.

Associated octagonal H-planforms In order to illustrate our purpose, we numerically compute the octagonal H-planforms associated to the irreducible representation χ_8 of $\mathcal{G}$ (see section 6.4 of chapter 6). We recall that these planforms are eigenfunctions of the Laplace-Beltrami operator in $\mathbb{D}$. In figure 8.4, we plot the

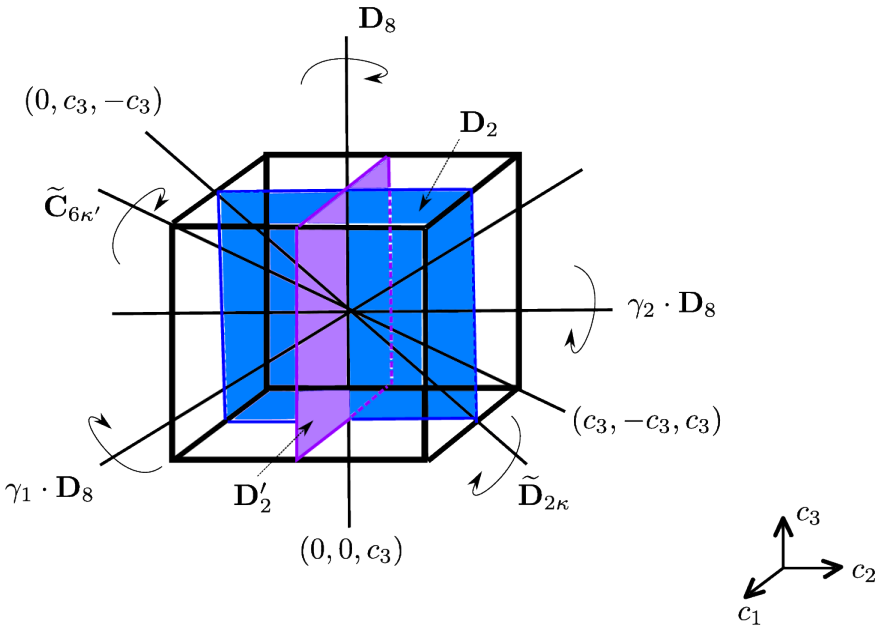

Figure 8.3: Maximal isotropy subgroups $\mathbf{D}_8, \widetilde{\mathbf{C}}_{6\kappa'}$ and $\widetilde{\mathbf{D}}_{2\kappa}$ of $\mathbb{O} \ltimes \mathbb{Z}_2$. The axes $\gamma_1 \cdot \mathbf{D}_8$ and $\gamma_2 \cdot \mathbf{D}_8$ are copies of $\mathbf{D}_8$ by the elements $\gamma_1, \gamma_2 \in \mathcal{G}$ (see 8.3.2). The plane $(0, c_2, c_3)$ (resp. $(c_1, 0, c_3)$) has symmetry $\mathbf{D}_2$ (resp. $\mathbf{D}_2'$).

corresponding eigenfunctions of the Laplace-Beltrami operator associated to the lowest non-negative eigenvalue $\lambda = 3.8432$ with multiplicity 3. We identify each solution by its symmetry group. Note that the solution in figure 8.4(a) corresponds to an axis of symmetry in the sense that its symmetry group is an isotropy subgroup with one dimensional fixed point subspace. In figure 8.5, we plot each eigenfunction in the Poincaré disk. It becomes now clear that 8.5(b) and 8.5(c) can be obtained from 8.5(a) by hyperbolic transformations. From subsection 6.3.1 of chapter 6 and the definition of g_0 in equation (6.14), we see that $g_0 = a_{r_0}$ with $r_0 = \ln\left(1+\sqrt{2}+\sqrt{2+\sqrt{2}}\right)$. If we define $\gamma_k \in \mathcal{G}$ by:

$$\gamma_k = \mathrm{rot}_{k\pi/4} a_{r_0/2} \mathrm{rot}_{-k\pi/4}$$

then figure 8.5(b) (resp. 8.5(c)) is obtained from 8.5(a) by applying γ_1 (resp. γ_2). Planforms in figure 8.5 correspond the three coordinate axes of the cube in figure 8.3.

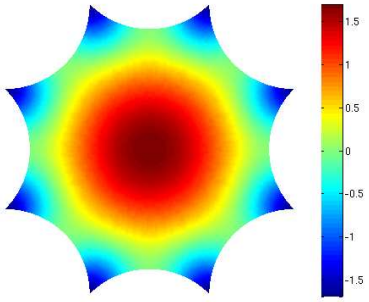

(a) Symmetry $\mathbf{D}_8 =< \rho, \kappa >$.

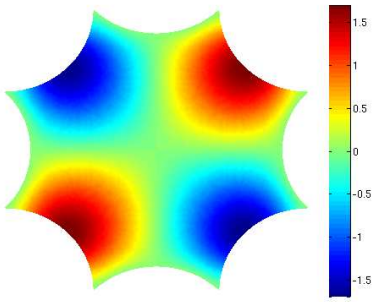

(b) Symmetry $\mathbf{D}'_2 =< -Id, \rho^2\kappa >$.

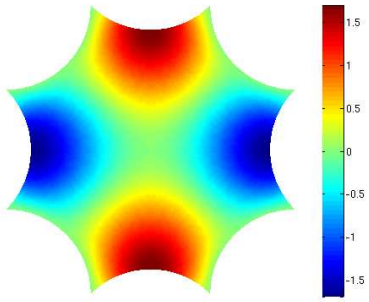

(c) Symmetry $\mathbf{D}_2 =< -Id, \kappa >$.

Figure 8.4: Plot of the eigenfunctions of the Laplace-Beltrami operator in the octagon $\mathcal{O}$ associated to the lowest non-negative eigenvalue $\lambda = 3.8432$ corresponding to the irreducible representation χ_8.

Choice of χ_8 The choice of irreducible representation χ_8 comes from the direct interpretation of H-planforms ploted in figures 8.4(b), 8.4(c) and 8.4(a) in terms of

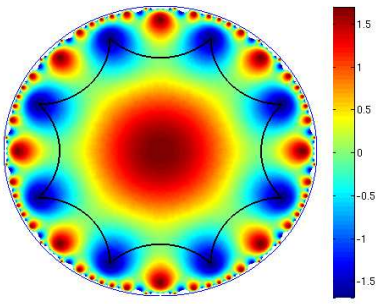

(a) H-planform Ψ_3 with symmetry $\mathbf{D}_8$.

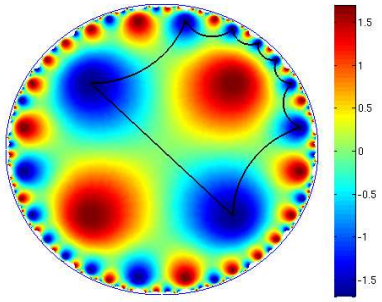

(b) H-planform Ψ_1 with symmetry $\gamma_1 \cdot \mathbf{D}_8$.

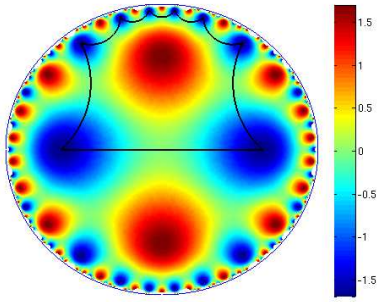

(c) H-planform Ψ_2 with symmetry $\gamma_2 \cdot \mathbf{D}_8$.

Figure 8.5: Plot of the eigenfunctions of the Laplace-Beltrami operator in the Poincaré disk $\mathbb{D}$ associated to the lowest non-negative eigenvalue $\lambda = 3.8432$ corresponding to the irreducible representation χ_8. In (a) we also plot the octagon (black line) and in (b),(c) its image by γ_1, γ_2 respectively.

preferred orientation. For example, in figure 8.4(a), the high region of activity near the center of the Poincaré disk traduces the fact the point $z = 0$ is preferred, this means that the selectivity is low and all orientations are represented. On the other hand, in figure 8.4(b), two points on the boundary of the octagon correspond to high activity of the eigenfunction. Due to the periodicity (opposite faces of the octagon are identified), these two points are the same and thus there is a preferred orientation at $\frac{\pi}{4}$. With a similar argument, in figure 8.4(c), there is a preferred orientation at $\frac{\pi}{2}$. As surprising as it can be, solutions in figures 8.4(b), 8.4(c) and 8.4(a) have to be thought as unimodal solution of the z variable due to the periodicity. These solutions are the counterpart, in the hyperbolic disk, to the tuning curves found in the ring model of orientations [Ben-Yishai 1995, Hansel 1997].

8.3.3 Bifurcation diagrams for one hypercolumn

In this paragraph, we consider the case $\beta = 0$ and deal with the following equation:

$$\frac{\partial V(z,t)}{\partial t} = -V(z,t) + \int_{\mathbb{D}} W_{loc}\left(d_{\mathbb{D}}(z,z')\right) S(\mu V(z',t))\mathrm{dm}(z'). \tag{8.29}$$

For $S(0) = 0$, the fully symmetric state $V = 0$ is always solution of (8.29) and the associated linear equation is given by

$$\frac{\partial V(z,t)}{\partial t} = -V(z,t) + \mu s_1 \int_{\mathbb{D}} W_{loc}\left(d_{\mathbb{D}}(z,z')\right) V(z',t)\mathrm{dm}(z'). \tag{8.30}$$

If we denote Ψ_1 the H-planform in figure 8.4(b), Ψ_2 the H-planform in figure 8.4(c) and Ψ_3 the H-planform corresponding to the symmetry group $\mathbf{D}_8$ in figure 8.4(a), then (Ψ_1, Ψ_2, Ψ_3) is a basis for the irreducible representation χ_8. This can be easily seen through the identification of each H-planform to the three coordinate axes of the cube in figure 8.3. Then if we define:

$$\frac{1}{4\pi}\int_{\mathcal{O}}\int_{\mathbb{D}} W_{loc}\left(d_{\mathbb{D}}(z,z')\right)\Psi_i(z)\Psi_i(z')\mathrm{dm}(z')\mathrm{dm}(z) = \widetilde{W}^c_{loc} \quad \forall i = 1\ldots 3$$

there is a bifurcation at $\mu_c = \left(s_1\widetilde{W}^c_{loc}\right)^{-1}$ such that for $\mu < \mu_c$ the state $V = 0$ is stable. Note that we have normalized planforms such that:

$$\langle \Psi_i, \Psi_j \rangle = \frac{1}{4\pi}\int_{\mathcal{O}} \Psi_i(z)\Psi_j(z)\mathrm{dm}(z) = \delta_{i,j}.$$

If we rewrite equation (8.29) as

$$V' = \mathbf{L}V + \mathcal{R}(V,\lambda)$$

with $\lambda = \mu - \mu_c$ and

$$\begin{aligned}\mathbf{L}V &= -V + \mu_c s_1 W_{loc} \star V \\ \mathcal{R}(V,\lambda) &= W_{loc} \star \left(S((\lambda+\mu_c)V) - \mu_c s_1 V\right).\end{aligned}$$

Close to the bifurcation point, there exists a polynomial map $\Phi(\cdot,\lambda)$ such that the change of variable:

$$V(z) = c_1\Psi_1 + c_2\Psi_2 + c_3\Psi_3 + \Phi(c_1,c_2,c_3,\lambda) + \text{h.o.t.}$$

transforms equation (8.29) into the normal form (see [Melbourne 1986] for a review on bifurcation problems with octahedral symmetry):

$$\left\{\begin{array}{rcl} \frac{dc_1}{dt} &=& \frac{\lambda}{\mu_c}c_1 + \left[a(c_2^2+c_3^2)+bc_1^2\right]c_1 + \text{h.o.t.} \\ \frac{dc_2}{dt} &=& \frac{\lambda}{\mu_c}c_2 + \left[a(c_1^2+c_3^2)+bc_2^2\right]c_2 + \text{h.o.t.} \\ \frac{dc_3}{dt} &=& \frac{\lambda}{\mu_c}c_3 + \left[a(c_1^2+c_2^2)+bc_3^2\right]c_3 + \text{h.o.t.} \end{array}\right. \tag{8.31}$$

Taylor expanding the map Φ:

$$\Phi(c_1,c_2,c_3,\lambda) = \sum_{1\le r+s+l+m\le 3} c_1^r c_2^s c_3^l \lambda^m \Phi_{rslm}$$

and $\mathcal{R}$:

$$\mathcal{R}(V,\lambda) = \mathcal{R}_{11}(V,\lambda) + \mathcal{R}_{20}(V,V) + \mathcal{R}_{30}(V,V,V) + \text{h.o.t.}$$

with

$$\begin{aligned} \mathcal{R}_{11}(V,\lambda) &= \lambda s_1 W_{loc} \star V \\ \mathcal{R}_{20}(U,V) &= \frac{\mu_c^2 s_2}{2} W_{loc} \star (UV) \\ \mathcal{R}_{300}(U,V,W) &= \frac{\mu_c^3 s_3}{6} W_{loc} \star (UVW) \end{aligned}$$

where $s_2 = S''(0)$ and $s_3 = S'''(0)$ we obtain the following system of equations:

$$\begin{aligned} 0 &= -\mathbf{L}\Phi_{0020} - \mathcal{R}_{20}(\Psi_3,\Psi_3) \\ 0 &= -\mathbf{L}\Phi_{1010} - 2\mathcal{R}_{20}(\Psi_1,\Psi_3) \\ a &= \langle 2\mathcal{R}_{20}(\Phi_{0020},\Psi_1) + 2\mathcal{R}_{20}(\Phi_{1010},\Psi_3) + 3\mathcal{R}_{30}(\Psi_1,\Psi_3,\Psi_3),\Psi_1\rangle \\ b &= \langle 2\mathcal{R}_{20}(\Psi_3,\Phi_{0020}) + \mathcal{R}_{30}(\Psi_3,\Psi_3,\Psi_3),\Psi_3\rangle. \end{aligned} \tag{8.32}$$

In order to solve the two first equations of the previous system, we need to know the functions $\Psi_3(z)\Psi_3(z)$ and $\Psi_1(z)\Psi_3(z)$ can be expressed as a linear combination of eigenfunctions of the Laplace-Beltrami operator on $\mathcal{O}$. In general, it is very difficult to obtain these expressions because the eigenfunctions are only know numerically and one needs the computation of the associated Clebsch-Gordan coefficients. It turns out that in our case we have been able to conjecture and numerically verify the following relations:

$$\begin{aligned} \Psi_1(z)\Psi_3(z) &= \frac{1}{\sqrt{3}}\Psi_{\chi_{10}}^{\mathbf{D}'_{2\kappa}}(z) \\ \Psi_3^2(z) &= \frac{6}{5}\Psi_{\chi_6}^{\widetilde{\mathbf{D}}_{8\kappa}}(z) + 1 \end{aligned}$$

where the corresponding isotropy subgroups are given by:

$$\mathbf{D}'_{2\kappa} =< -Id, \rho^2\kappa, \rho^2\sigma > \text{ and } \widetilde{\mathbf{D}}_{8\kappa} =< \rho, \rho^2\sigma\rho^{-2}, \kappa > .$$

Furthermore we have normalized $\Psi_{\chi_{10}}^{\mathbf{D}'_{2\kappa}}$ and $\Psi_{\chi_6}^{\widetilde{\mathbf{D}}_{8\kappa}}$ such that:

$$\langle \Psi_{\chi_{10}}^{\mathbf{D}'_{2\kappa}}, \Psi_{\chi_{10}}^{\mathbf{D}'_{2\kappa}} \rangle = \langle \Psi_{\chi_6}^{\widetilde{\mathbf{D}}_{8\kappa}}, \Psi_{\chi_6}^{\widetilde{\mathbf{D}}_{8\kappa}} \rangle = 1.$$

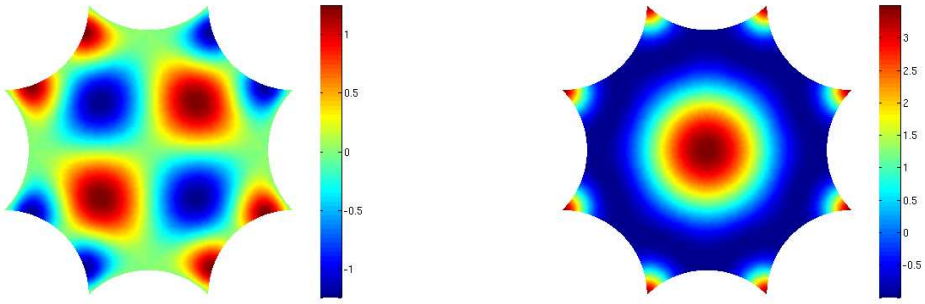

(a) Plot of $\Psi_{\chi_{10}}^{\mathbf{D}'_{2\kappa}}$. (b) Plot of $\Psi_{\chi_6}^{\widetilde{\mathbf{D}}_{8\kappa}}$.

Figure 8.6: Plot of the eigenfunctions of the Laplace-Beltrami operator in the octagon $\mathcal{O}$ corresponding to the irreducible representations χ_{10} with eigenvalue $\lambda = 15.0518$ (left) and χ_6 with eigenvalue $\lambda = 8.2501$ (right).

In figure 8.6, we plot the eigenfunctions $\Psi_{\chi_{10}}^{\mathbf{D}'_{2\kappa}}$ and $\Psi_{\chi_6}^{\widetilde{\mathbf{D}}_{8\kappa}}$ of the Laplace-Beltrami operator in the octagon $\mathcal{O}$. One interesting remark is that the product $\Psi_1\Psi_3$ corresponding to the three dimensional irreducible representation χ_8 produces an eigenfunction associated to another three dimensional irreducible representation: χ_{10} whereas Ψ_3^2 is the linear combination of the constant function which has $\mathcal{G}$ as isotropy subgroup and thus corresponds to χ_1 and the eigenfunction $\Psi_{\chi_6}^{\widetilde{\mathbf{D}}_{8\kappa}}$ which is associated to two dimensional irreducible representation χ_6.

If we define

$$\widetilde{W}_{loc}^{\chi_{10},\mathbf{D}'_{2\kappa}} = \frac{1}{4\pi}\int_{\mathcal{O}}\int_{\mathbb{D}} W_{loc}\left(d_{\mathbb{D}}(z,z')\right)\Psi_{\chi_{10}}^{\mathbf{D}'_{2\kappa}}(z)\Psi_{\chi_{10}}^{\mathbf{D}'_{2\kappa}}(z')\mathrm{dm}(z')\mathrm{dm}(z)$$
$$\widetilde{W}_{loc}^{\chi_6,\widetilde{\mathbf{D}}_{8\kappa}} = \frac{1}{4\pi}\int_{\mathcal{O}}\int_{\mathbb{D}} W_{loc}\left(d_{\mathbb{D}}(z,z')\right)\Psi_{\chi_6}^{\widetilde{\mathbf{D}}_{8\kappa}}(z)\Psi_{\chi_6}^{\widetilde{\mathbf{D}}_{8\kappa}}(z')\mathrm{dm}(z')\mathrm{dm}(z)$$
$$\widetilde{W}_{loc}^{\chi_1} = \int_{\mathbb{D}} W_{loc}\left(d_{\mathbb{D}}(z,z')\right)\mathrm{dm}(z')$$

then the two first equations of system (8.32) give

$$\Phi_{0020} = \text{Span}\,(\Psi_1, \Psi_2, \Psi_3) + \frac{\mu_c^2 s_2}{2}\left[\frac{\widetilde{W}_{loc}^{\chi_1}}{1-\widetilde{W}_{loc}^{\chi_1}/\widetilde{W}_{loc}^{c}} + \frac{6}{5}\frac{\widetilde{W}_{loc}^{\chi_6,\widetilde{\mathbf{D}}_{8\kappa}}}{1-\widetilde{W}_{loc}^{\chi_6,\widetilde{\mathbf{D}}_{8\kappa}}/\widetilde{W}_{loc}^{c}}\Psi_{\chi_6}^{\widetilde{\mathbf{D}}_{8\kappa}}\right]$$

$$\Phi_{1010} = \text{Span}\,(\Psi_1, \Psi_2, \Psi_3) + \frac{\mu_c^2 s_2}{\sqrt{3}}\frac{\widetilde{W}_{loc}^{\chi_{10},\mathbf{D}'_{2\kappa}}}{1-\widetilde{W}_{loc}^{\chi_{10},\mathbf{D}'_{2\kappa}}/\widetilde{W}_{loc}^{c}}\Psi_{\chi_{10}}^{\mathbf{D}'_{2\kappa}}.$$

We can now obtain the expression of the coefficients a and b in the reduced equation (8.31).

Lemma 8.3.1.

$$a = \mu_c^3 W_{loc}^c\left(\frac{s_3}{6} + \frac{\mu_c s_2^2}{2}\left[\frac{\widetilde{W}_{loc}^{\chi_1}}{1-\widetilde{W}_{loc}^{\chi_1}/\widetilde{W}_{loc}^{c}} - \frac{2}{3}\frac{\widetilde{W}_{loc}^{\chi_6,\widetilde{\mathbf{D}}_{8\kappa}}}{1-\widetilde{W}_{loc}^{\chi_6,\widetilde{\mathbf{D}}_{8\kappa}}/\widetilde{W}_{loc}^{c}} + \frac{1}{3}\frac{\widetilde{W}_{loc}^{\chi_{10},\mathbf{D}'_{2\kappa}}}{1-\widetilde{W}_{loc}^{\chi_{10},\mathbf{D}'_{2\kappa}}/\widetilde{W}_{loc}^{c}}\right]\right) \tag{8.33}$$

$$b = \mu_c^3 W_{loc}^c\left(\frac{61 s_3}{150} + \frac{\mu_c s_2^2}{2}\left[\frac{\widetilde{W}_{loc}^{\chi_1}}{1-\widetilde{W}_{loc}^{\chi_1}/\widetilde{W}_{loc}^{c}} + \frac{36}{25}\frac{\widetilde{W}_{loc}^{\chi_6,\widetilde{\mathbf{D}}_{8\kappa}}}{1-\widetilde{W}_{loc}^{\chi_6,\widetilde{\mathbf{D}}_{8\kappa}}/\widetilde{W}_{loc}^{c}}\right]\right). \tag{8.34}$$

Proof. See appendix B.2. □

From the analysis derived in [Melbourne 1986], we have the following result.

Lemma 8.3.2. *The stability of the branches of solutions corresponding to the three maximal isotropy subgroups given in proposition 8.3.1 is:*

(i) the $\mathbf{D}_8$ *branch is stable if and only if* $a < b < 0$,

(ii) the $\widetilde{\mathbf{C}}_{6\kappa'}$ *branch is stable if and only if* $2a + b < 0$ *and* $b - a < 0$,

(iii) the $\widetilde{\mathbf{D}}_{2\kappa}$ *branch is never stable.*

The corresponding bifurcation diagram is given in figure 8.7 for $a < b < 0$.

We want that our hypercolumn produces tuning surfaces close the bifurcation point $\mu = \mu_c$. From the discussion on the interpretation of H-planforms, we impose that the condition $a < b < 0$ is satisfied such that the $\mathbf{D}_8$ branch is the only stable branch. Depending on the initial condition in the (c_1, c_2, c_3)-space, the solution will converge to one of three axis of coordinates: $\mathbf{D}_8, \gamma_1 \cdot \mathbf{D}_8$ or $\gamma_2 \cdot \mathbf{D}_8$. The condition $a < b < 0$ gives a constrain on the threshold T of the sigmoidal function defined in equation (8.2) and the different coefficients $\widetilde{W}_{loc}$ of the coupling function W_{loc}.

In order to illustrate this constrain on the parameters, we present a specific example. The local coupling function is given by:

$$W_{loc}(x) = A\cosh(2x)^{-\sigma_0} - \cosh(2x)^{-\sigma} \tag{8.35}$$

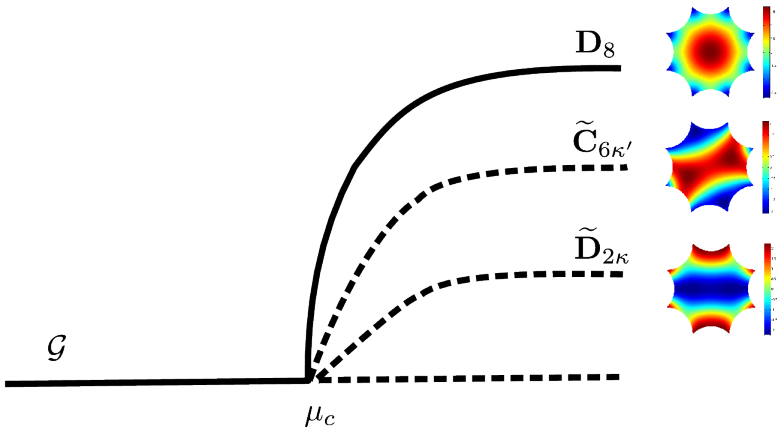

Figure 8.7: Bifurcation diagram in the case $a < b < 0$. Solid lines correspond to stable branches, dotted ones to unstable branches. For each maximal isotropy subgroups, we plot the corresponding planform.

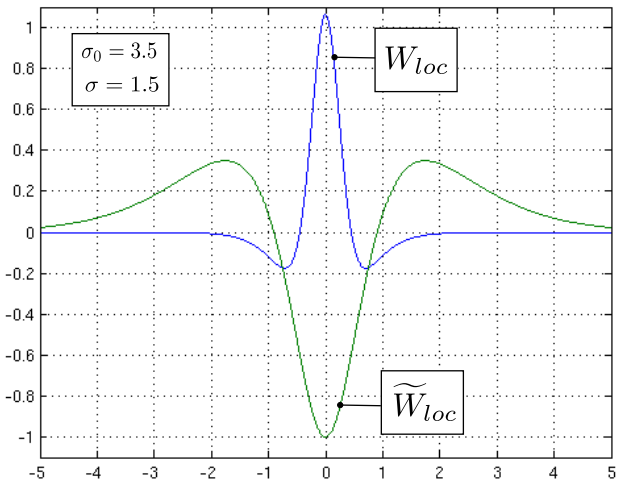

Figure 8.8: Plot of the local coupling function W_{loc} given in equation (8.35) and its Helgason-Fourier transform $\widetilde{W}_{loc}$ given in equation (8.35) with $\sigma_0 = 3.5$ and $\sigma = 1.5$. For the choice of A, see text.

with $A > 1$ and $\sigma_0 > \sigma > \frac{1}{2}$. The Helgason-Fourier transform of $z \to W_{loc}(d_{\mathbb{D}}(z,0))$ can be computed analytically [Terras 1988] and we have shown that it only depends upon $\rho \in \mathbb{R}$:

$$\widetilde{W}_{loc}(\rho) = \sqrt{\pi}\left[A\frac{2^{\sigma_0-3}}{\Gamma(\sigma_0)}\left|\Gamma\left(\frac{\sigma_0+i\rho-\frac{1}{2}}{2}\right)\right|^2 - \frac{2^{\sigma-3}}{\Gamma(\sigma)}\left|\Gamma\left(\frac{\sigma+i\rho-\frac{1}{2}}{2}\right)\right|^2\right]. \quad (8.36)$$

Firstly, we fix the value of $\sigma_0 = 3.5$. Then, we tune the value of A such that the most unstable mode $\rho_c = \max_{\rho\in\mathbb{R}} \widetilde{W}_{loc}(\rho)$ corresponds to the irreducible representation χ_8. Note that A depends upon (σ_0, σ). In figure 8.8, we plot both the local connectivity function and its Helgason-Fourier transform for $\sigma = 1.5$. For each

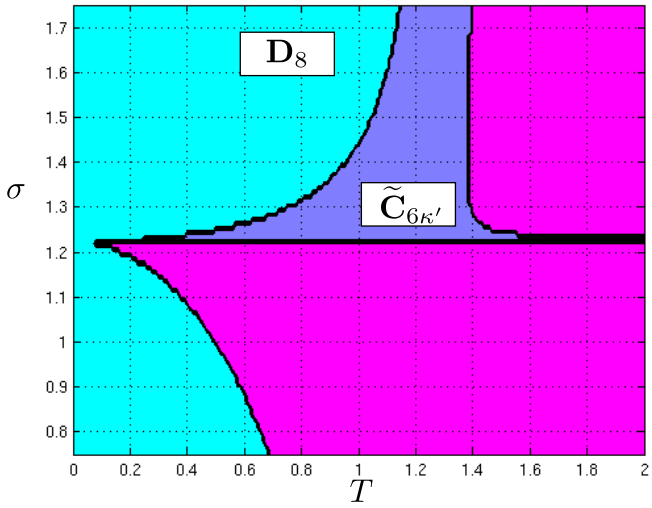

Figure 8.9: Regions of the plane (T, σ) where the branches $\mathbf{D}_8$ and $\widetilde{\mathbf{C}}_{6\kappa'}$ are stable with $\sigma_0 = 3.5$.

value of (T, σ) in $[0, 2] \times [0.75, 1.75]$ we have numerically computed the coefficients a and b given in lemma 8.3.1 and then checked if the stability conditions in lemma 8.3.2 are satisfied. Our results are ploted in figure 8.9. We can see the different regions of the plane (T, σ) where the branches $\mathbf{D}_8$ and $\widetilde{\mathbf{C}}_{6\kappa'}$ are stable: in blue the region where $\mathbf{D}_8$ is stable and in purple the region where $\widetilde{\mathbf{C}}_{6\kappa'}$ is stable.

8.3.4 Symmetry-breaking bifurcations on lattices

Knowing the behaviour of our network at the hypercolumnar level, we can come back to the fully isotropically connected model and we restrict ourselves to doubly periodic functions on a square lattice for the $\mathbf{r}$ variable and periodic on the octagon $\mathcal{O}$ in the z variable. The choice of the square lattice is dictated by the fact that the rotations by $\pi/2$ centered at 0 in the Euclidean square and of π at 0 in the hyperbolic octagon can be identified. Indeed, for anisotropic coupling, the action

of a rotation on $(\mathbf{r}, z)$ is given by (see equation (8.8))

$$\mathcal{R}_\theta \cdot (\mathbf{r}, z) = \left(\mathcal{R}_\theta \mathbf{r}, e^{2i\theta} z\right)$$

so that if $\mathcal{O}$ is the feature space, only rotations with angle $\theta = k\frac{\pi}{4}$ are allowed. Hence the hexagonal lattice is not compatible with the octagonal tiling whereas both rhombic and square lattices are compatible.

By restricting the bifurcation problem to a direct product of lattices, the group of symmetries $\mathbf{E}(2) \times \mathbf{U}(1,1)$ is transformed to the compact group $\Gamma \stackrel{def}{=} (\mathbf{D}_4 \ltimes \mathbb{T}^2) \times \mathcal{G}$, where $\mathbf{D}_4$ is the holohedry of the square lattice, $\mathbb{T}^2$ is the 2-torus (see paragraph 8.2.3.2) and $\mathcal{G}$ is the group of automorphisms of the octagon $\mathcal{O}$. The kernel of the linearized equation (8.26), at the critical point $\mu = \mu_c$ is now finite dimensional and tools from equivariant bifurcation theory can be applied. Namely, the Equivariant Branching Lemma [Golubitsky 1988, Chossat 2000] ensures the existence of branches of equilibria for every axial subgroup of Γ and the remaining paragraphs will be dedicated to this study. There have been previous results on visual pattern formation on the square lattice. In the Ermentrout-Cowan formalism [Ermentrout 1979], the visual cortex is modeled by the Euclidean plane and translation symmetry leads to doubly periodic solutions on the square lattice: stripes and spots. In Bressloff et al. [Bressloff 2001b, Bressloff 2001a], the visual cortex is idealized by $\mathbb{R}^2 \times \mathbf{S}^1$ and their model is able to produce a large variety of geometric visual hallucinations recorder by experimentalists. Finally, Golubistky et al. [Golubitsky 2003] worked with a model similar to those of Bressloff et al. but considered weak anisotropy in the lateral coupling which leads to rotating planforms.

8.3.5 Group actions

As the principal isotropy subgroup for χ_8 is $\mathbf{C}_2 =< Id, -Id >$ we get a faithfull action by taking $\mathcal{G}/\mathbf{C}_2 \cong \mathbb{O} \times \mathbb{Z}_2$, where $\mathbb{O}$ is the octahedral group. By identifying elements of $\mathcal{G}$ with elements of the octahedral group $\mathbb{O}$ it is possible to construct action on the eigenspace spanned by Ψ_1, Ψ_2, Ψ_3. If we have:

$$u(z) = c_1\Psi_1(z) + c_2\Psi_2(z) + c_3\Psi_3(z)$$

we identify the eigenspace with $(c_1, c_2, c_3) \in \mathbb{R}^3$ and we have

$$\begin{cases} \rho \cdot (c_1, c_2, c_3) &= (-c_2, c_1, c_3) \\ \kappa \cdot (c_1, c_2, c_3) &= (-c_1, c_2, c_3) \\ \sigma \cdot (c_1, c_2, c_3) &= (-c_1, -c_3, -c_2) \\ \varepsilon \cdot (c_1, c_2, c_3) &= (-c_2, -c_3, c_1) \end{cases}$$

where ρ, κ, σ and ε have been defined in 6.3.1.

We denote ξ the rotation of angle $\pi/2$ centered at 0 of the square, δ the reflection along the horizontal axis and

$$\Theta = \theta_1\ell_1 + \theta_2\ell_2 \stackrel{def}{=} [\theta_1, \theta_2] \tag{8.37}$$

with $(\theta_1, \theta_2) \in [0, 2\pi[^2$. We suppose that the critical eigenspace $\mathcal{W}$ consists of functions of the form:

$$\begin{aligned} a(\mathbf{r}, z) = &\left(c_1\Psi_1(z) + c_2\Psi_2(z) + c_3\Psi_3(z)\right) e^{i\mathbf{k}_1\cdot\mathbf{r}} \\ &+ \left(d_1\Psi_1(z) + d_2\Psi_2(z) + d_3\Psi_3(z)\right) e^{i\mathbf{k}_2\cdot\mathbf{r}} + \text{c.c} \end{aligned} \tag{8.38}$$

where $(c_1, c_2, c_3, d_1, d_2, d_3) \in \mathbb{C}^6$. We will identify $\mathcal{W}$ with $\mathbb{C}^6$ through 8.38.

The action of ξ on $a(\mathbf{r}, z)$ can be expressed as:

$$\begin{aligned} \xi \cdot a(\mathbf{r}, z) &= a(\xi^{-1}\mathbf{r}, z) \\ &= \left(c_1\Psi_1(z) + c_2\Psi_2(z) + c_3\Psi_3(z)\right) e^{i\mathbf{k}_1\cdot\xi^{-1}\mathbf{r}} \\ &\quad + \left(d_1\Psi_1(z) + d_2\Psi_2(z) + d_3\Psi_3(z)\right) e^{i\mathbf{k}_2\cdot\xi^{-1}\mathbf{r}} + \text{c.c} \\ &= \left(\bar{d}_1\Psi_1(z) + \bar{d}_2\Psi_2(z) + \bar{d}_3\Psi_3(z)\right) e^{i\mathbf{k}_1\cdot\mathbf{r}} \\ &\quad + \left(c_1\Psi_1(z) + c_2\Psi_2(z) + c_3\Psi_3(z)\right) e^{i\mathbf{k}_2\cdot\mathbf{r}} + \text{c.c}\ . \end{aligned}$$

Then we have $\xi \cdot (c_1, c_2, c_3, d_1, d_2, d_3) = (\bar{d}_1, \bar{d}_2, \bar{d}_3, c_1, c_2, c_3)$ and the action of each elements on $(c_1, c_2, c_3, d_1, d_2, d_3)$ is given by

$$\left\{\begin{array}{lcl} \xi \cdot (c_1, c_2, c_3, d_1, d_2, d_3) & = & (\bar{d}_1, \bar{d}_2, \bar{d}_3, c_1, c_2, c_3) \\ \delta \cdot (\quad'' \quad) & = & (c_1, c_2, c_3, \bar{d}_1, \bar{d}_2, \bar{d}_3,) \\ \Theta \cdot (\quad'' \quad) & = & (e^{-i2\pi\theta_1}(c_1, c_2, c_3), e^{-i2\pi\theta_2}(d_1, d_2, d_3)) \\ \rho \cdot (\quad'' \quad) & = & (-c_2, c_1, c_3, -d_2, d_1, d_3) \\ \kappa \cdot (\quad'' \quad) & = & (-c_1, c_2, c_3, -d_1, d_2, d_3) \\ \sigma \cdot (\quad'' \quad) & = & (-c_1, -c_3, -c_2, -d_1, -d_3, -d_2) \\ \varepsilon \cdot (\quad'' \quad) & = & (-c_2, -c_3, c_1, -d_2, -d_3, d_1). \end{array}\right. \tag{8.39}$$

Lemma 8.3.3. *The action of Γ on $\mathbb{C}^6$, given in 8.39, is absolutely irreducible.*

Proof. Any 6×6 complex matrix which commutes with the action $\mathbf{D}_4 \ltimes \mathbb{T}^2$ decomposes into a direct sum of two 3×3 identical diagonal matrices with real entries. Indeed the action of translations forces any 6×6 complex matrix to be diagonal with real entries and the action of $\mathbf{D}_4$ decomposes this matrix into two 3×3 identical diagonal matrices. The action of $\mathcal{G}$ renders each diagonal matrix equal to a scalar multiple of the identity matrix $\mathbb{I}_3$, which proves that the action of Γ is absolutely irreducible. Note that we could also directly apply the general result of lemma 8.3.4 in order to prove this lemma. □

Our aim is now to apply the Equivariant Branching Lemma (see [Golubitsky 1988]). For this, we need to compute each axial isotropy subgroup Σ of Γ such that the subspace $\mathcal{W}^\Sigma = \{x \in \mathcal{W} \mid \Sigma \cdot x = x\}$ is one dimensional. We recall the following lemma 6.5.1.

Lemma 8.3.4. *Let $H = H_1 \times H_2$ be an isotropy subgroup for the irreducible representation R of $G_1 \times G_2$ acting in X. Then $X = X_1 \otimes X_2$ and $R = R_1 \otimes R_2$ where R_1 is an irreducible representation of G_1 in V_1 and R_2 is an irreducible representation of G_2 in V_2 and therefore H_1 acts in V_1 and H_2 acts in V_2. Furthermore we have:*

$$dim\left(X^H\right) = 1 \text{ if and only if } dim\left(V_1^{H_1}\right) = dim\left(V_2^{H_2}\right) = 1.$$

It is then possible to determine the maximal isotropy subgroups of Γ that satisfy the hypotheses of the Equivariant Branching Lemma.

Theorem 8.3.1. *The axial subgroups are (up to conjugacy):*

- $\Sigma_1 = \mathbf{D}_4(\xi, \delta) \times \mathbf{D}_8$
- $\Sigma_2 = \left[\mathbf{O}_2(\xi^2, [0, \theta_2]) \times \mathbf{Z}_2(\delta)\right] \times \mathbf{D}_8$
- $\Sigma_3 = \mathbf{D}_4(\xi, \delta) \times \widetilde{\mathbf{C}}_{6\kappa'}$
- $\Sigma_4 = \left[\mathbf{O}_2(\xi^2, [0, \theta_2]) \times \mathbf{Z}_2(\delta)\right] \times \widetilde{\mathbf{C}}_{6\kappa'}$
- $\Sigma_5 = \mathbf{D}_4(\xi, \delta) \times \widetilde{\mathbf{D}}_{2\kappa}$
- $\Sigma_6 = \left[\mathbf{O}_2(\xi^2, [0, \theta_2]) \times \mathbf{Z}_2(\delta)\right] \times \widetilde{\mathbf{D}}_{2\kappa}$.

The corresponding fixed subspaces are listed in table 8.1.

Proof. We have already seen that $\mathbf{D}_8, \widetilde{\mathbf{C}}_{6\kappa'}$ and $\widetilde{\mathbf{D}}_{2\kappa}$ are the three axial isotropy subgroups for the irreducible representation χ_8 of $\mathcal{G}$. $\mathbf{D}_4(\xi, \delta)$ and $\mathbf{O}_2(\xi^2, [0, \theta_2]) \times \mathbf{Z}_2(\delta)$ are the two axial subgroups for the irreducible action of $\mathbf{D}_4 \ltimes \mathbb{T}^2$ on $\mathbb{C}^2$ [Golubitsky 1988, Hoyle 2006]. Lemma 8.3.4 gives the result. □

Axial subgroup	Fixed subspace
Σ_1	$\mathbb{R}\{(0,0,1,0,0,1)\}$
Σ_2	$\mathbb{R}\{(0,0,1,0,0,0)\}$
Σ_3	$\mathbb{R}\{(1,-1,1,1,-1,1)\}$
Σ_4	$\mathbb{R}\{(1,-1,1,0,0,0)\}$
Σ_5	$\mathbb{R}\{(0,1,-1,0,1,-1)\}$
Σ_6	$\mathbb{R}\{(0,1,-1,0,0,0)\}$

Table 8.1: Fixed subspaces of $\mathbb{C}^6$ for each axial subgroups.

8.3.6 Selection and stability of patterns

Close to the bifurcation point, there exists a polynomial map $\Phi(\cdot, \lambda)$ such that the change of variable:

$$V(\mathbf{r}, z) = \sum_{l=1}^{3} \left[c_l \Psi_l(z) e^{i\mathbf{k}_1 \cdot \mathbf{r}} + d_l \Psi_l(z) e^{i\mathbf{k}_2 \cdot \mathbf{r}}\right] + \sum_{l=1}^{3} \left[\bar{c}_l \Psi_l(z) e^{-i\mathbf{k}_1 \cdot \mathbf{r}} + \bar{d}_l \Psi_l(z) e^{-i\mathbf{k}_2 \cdot \mathbf{r}}\right] + \Phi(c_1, c_2, c_3, d_1, d_2, d_3, \bar{c}_1, \bar{c}_2, \bar{c}_3, \bar{d}_1, \bar{d}_2, \bar{d}_3, \lambda) + \text{h.o.t.}$$

transforms equation (8.25) into

$$\begin{cases} \dot{c}_1 &= \lambda c_1 + c_1 \left[\alpha_1 |c_1|^2 + \alpha_2 \left(|c_2|^2 + |c_3|^2\right) + \alpha_3 |d_1|^2 + \alpha_4 \left(|d_2|^2 + |d_3|^2\right)\right] + \text{h.o.t.} \\ \dot{d}_1 &= \lambda d_1 + d_1 \left[\alpha_1 |d_1|^2 + \alpha_2 \left(|d_2|^2 + |d_3|^2\right) + \alpha_3 |c_1|^2 + \alpha_4 \left(|c_2|^2 + |c_3|^2\right)\right] + \text{h.o.t.} \end{cases} \tag{8.40}$$

with $(\alpha_1, \alpha_2, \alpha_3, \alpha_4) \in \mathbb{R}^4$. Equations for $\dot{c}_j, \dot{d}_j$, $j = 2, 3$, are obtained by cyclic permutation.

Proof. See appendix B.3 for the computation of cubic equivariants. □

Remark 8.3.1. *In order to simplify notations, we have normalized the normal form equation (8.40) such that λ is the coefficient of the linear terms and not $\frac{\lambda}{\mu_c}$ as for normal form (8.31).*

Theorem 8.3.2. *The branches of solutions corresponding to the six maximal isotropy subgroups satisfy the following equations:*

- Σ_1 : $\lambda = -(\alpha_1 + \alpha_3)x^2 + o(x^4)$,
- Σ_2 : $\lambda = -\alpha_1 x^2 + o(x^4)$,
- Σ_3 : $\lambda = -(\alpha_1 + 2\alpha_2 + \alpha_3 + 2\alpha_4)x^2 + o(x^4)$,
- Σ_4 : $\lambda = -(\alpha_1 + 2\alpha_2)x^2 + o(x^4)$,
- Σ_5 : $\lambda = -(\alpha_1 + \alpha_2 + \alpha_3 + \alpha_4)x^2 + o(x^4)$,
- Σ_6 : $\lambda = -(\alpha_1 + \alpha_2)x^2 + o(x^4)$.

The Σ_1 branch is stable if and only if $\alpha_2 + \alpha_4 < \alpha_1 + \alpha_3$ and $\alpha_1 < -|\alpha_3|$. The Σ_2 branch is stable if and only if $\alpha_1 < 0$, $\alpha_2 < \alpha_1$, $\alpha_3 < \alpha_1$ and $\alpha_4 < \alpha_1$. The Σ_3 branch is stable if and only if $\alpha_1 + 2\alpha_2 < -|\alpha_3 + 2\alpha_4|$ and $\alpha_1 - \alpha_2 < -|\alpha_3 - \alpha_4|$. The Σ_4 branch is stable if and only $\alpha_1 + 2\alpha_2 < 0$, $\alpha_1 < \alpha_2$ and $\alpha_3 + 2\alpha_4 < \alpha_1 + 2\alpha_2$. Branches Σ_5 and Σ_6 are never stable.

Proof. The equation of each branch of solutions comes directly from table 8.1 and the amplitude equations (8.40). The stability of a branch requires the computation of the Jacobian matrix of (8.40) evaluated on the branch and the study of the corresponding eigenvalues. It is always possible to set the imaginary parts of any solution $(c_1, c_2, c_3, d_1, d_2, d_3)$ to zero, by moving the origin, and then choose $(c_1, c_2, c_3, d_1, d_2, d_3)$ to be real.

For the Σ_1 branch for example, a straightforward calculation shows that the eigenvalues of the Jacobian matrix evaluated at $(0, 0, x, 0, 0, x)$ are:

$$\begin{aligned}
\mu_1 &= \lambda + 3(\alpha_1 + \alpha_3)x^2 = 2(\alpha_1 + \alpha_3)x^2 + o(x^4) \\
\mu_2 &= \lambda + (3\alpha_1 - \alpha_3)x^2 = 2(\alpha_1 - \alpha_3)x^2 + o(x^4) \\
\mu_3 &= \mu_4 = \mu_5 = \mu_6 = \lambda + (\alpha_2 + \alpha_4)x^2 = (\alpha_2 + \alpha_4 - \alpha_1 - \alpha_3)x^2 + o(x^4).
\end{aligned}$$

And the stability result automatically follows. □

8.3.7 Pictures of axial planforms Σ_1 and Σ_2

We have already explained that it is possible to interpret, in term of tuning surface, planforms with $\mathbf{D}_8$-symmetry in the case of an isolated hypercolumn. This is why,

(a) (b)

Figure 8.10: Axial planforms on the square lattice associated with $\mathbf{D}_8$-symmetry: (a) square, (b) roll.

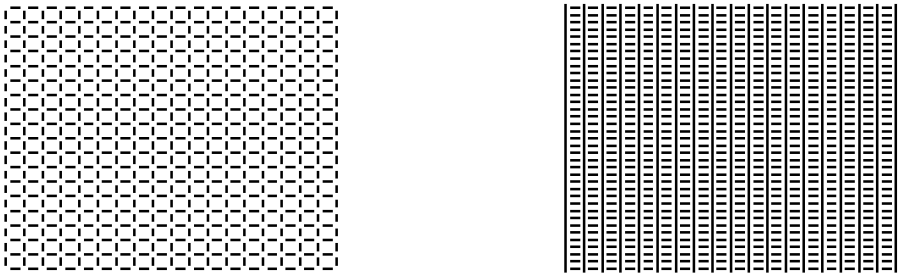

(a) (b)

Figure 8.11: Axial planforms on the square lattice associated with $\gamma_1 \cdot \mathbf{D}_8$-symmetry: (a) square, (b) roll.

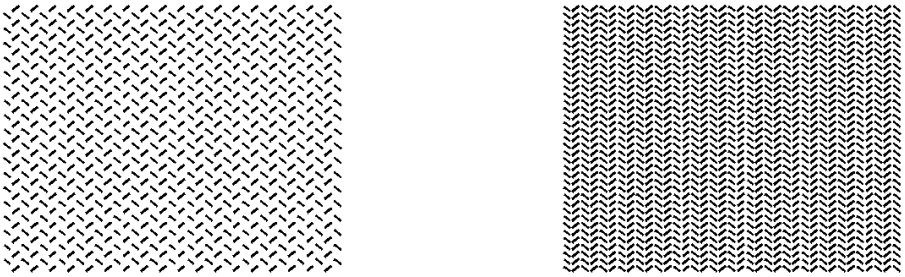

(a) (b)

Figure 8.12: Axial planforms on the square lattice associated with $\gamma_2 \cdot \mathbf{D}_8$-symmetry: (a) square, (b) roll.

(a) (b)

Figure 8.13: Axial planforms on the square lattice associated with $\mathbf{D}_8$-symmetry in the visual field: (a) square, (b) roll.

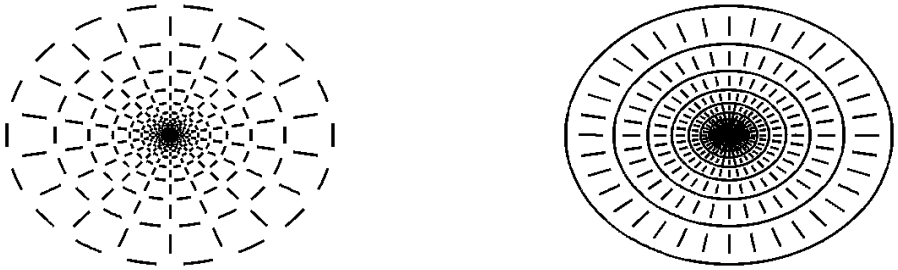

(a) (b)

Figure 8.14: Axial planforms on the square lattice associated with $\gamma_1 \cdot \mathbf{D}_8$-symmetry in the visual field: (a) square, (b) roll.

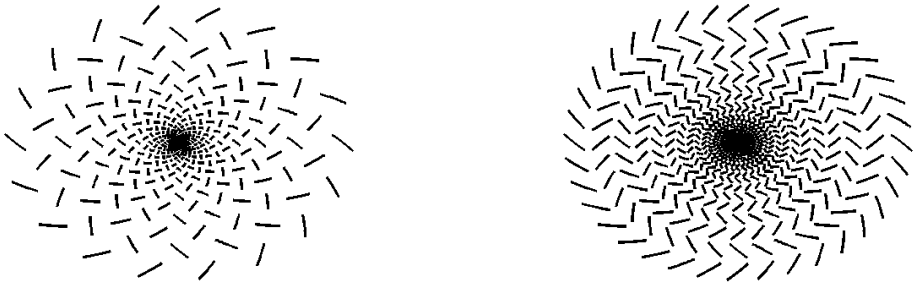

(a) (b)

Figure 8.15: Axial planforms on the square lattice associated with $\gamma_1 \cdot \mathbf{D}_8$-symmetry in the visual field: (a) square, (b) roll.

we will focus only on axial planforms Σ_1 and Σ_2 of theorem 8.3.1. For example, in the case of Σ_1, the corresponding planform can be written as:

$$a(\mathbf{r}, z) = c\Psi_3(z)\,(\cos(r_1) + \sin(r_2))$$

with $\mathbf{r} = (r_1, r_2)$ and c a real constant. Planform $\Psi_3(z)$ has $z = 0$ as preferred point in the Poincaré disk such that if we further have $\cos(r_1) + \sin(r_2) > 0$ then we represent a dark region at $\mathbf{r}$ in terms of activity profile in V1 . On the other side, planform $-\Psi_3(z)$ has $z = \pm(2k+1)\pi/8$ with $k = 0 \dots 3$ as preferred points in the Poincaré disk such that when $\cos(r_1) + \sin(r_2) < 0$ we draw a star shape indicating the presence of multiple orientations at $\mathbf{r}$. In figure 8.10, we plot the axial planforms corresponding to square and roll solutions on the plane and $\mathbf{D}_8$ solutions on the Poincaré disk. In figures 8.11 and 8.12 we plot the planforms corresponding to branches of solution with symmetry $\gamma_1 \cdot \mathbf{D}_8$ and $\gamma_2 \cdot \mathbf{D}_8$. Note that these planforms are now contoured planforms as they only have one preferred orientation. In figures 8.13, 8.14 and 8.15 we plot the same planforms in the visual field coordinates, with methods developped in [Bressloff 2001b]. Planforms in figures 8.11 and 8.12 have already been found by Bressloff et al in [Bressloff 2001a, Bressloff 2001b], whereas to our best knowledge it is the first time that planform of type 8.10 is found. Planform in figure 8.10 is a combination of both contoured and non-contoured regions, contoured regions having multiple orientations. In [Bressloff 2001a, Bressloff 2001b], contoured planforms with multiple orientations have been found only in the case of an hexagonal lattice.

8.3.8 Forced symmetry breaking

In this section we study the effect of taking $\varepsilon \neq 0$ in the bifurcation problem analyzed in the previous sections. We therefore assume a square lattice in the plane and the octagonal lattice in $\mathbb{D}$. We wish to treat the problem as a weak perturbation of the isotropic case. The symmetry group when $\varepsilon = 0$ is Γ and it acts as defined in (8.39). The $\mathcal{G}$ symmetry of individual hypercolumns disappears when $\varepsilon \neq 0$ but something remains of it through the "shift-twist" symmetries (8.8) which act simultaneously on the "spatial" and "structure tensor" components. The action of square symmetries ξ and δ introduced in (8.39) have therefore to be replaced by the transformations $R = \xi\rho$ and $K = \delta\kappa$, which act on $(c_1, c_2, c_3, d_1, d_2, d_3)$ as follows

$$\begin{array}{rcl} R(c_1, c_2, c_3, d_1, d_2, d_3) & = & (-\bar{d}_2, \bar{d}_1, \bar{d}_3, -c_2, c_1, c_3) \\ K(c_1, c_2, c_3, d_1, d_2, d_3) & = & (-c_1, c_2, c_3, -\bar{d}_1, \bar{d}_2, \bar{d}_3) \end{array} \tag{8.41}$$

The continuous part Θ of the action in (8.39) remains unchanged. R, K and Θ define a new action of $\mathbf{D}_4 \ltimes \mathbb{T}^2$ in $\mathbb{R}^{12} \simeq \mathbb{C}^6$.

What is the effect of this perturbation on the bifurcation problem? In order to give a full description of the perturbed bifurcation diagram one should consider the codimension two bifurcation problem in the limit when both $\mu \to \mu_c$ and $\varepsilon \to 0$, which requires first to compute the eigenvalues of the linear operator $\mathbf{L}_{\mu,\beta,\varepsilon} =$

$D_V\mathbf{F}(0,\mu,\beta,\varepsilon)$ (see equation (8.10) when $(\mu,\varepsilon)\sim(\mu_C,0)$. For this we need to know how the representation of $D_4\ltimes\mathbb{T}^2$ we just defined above decomposes into irreducible components. There are two 4 dimensional irreducible representations of this group which are called scalar and pseudoscalar because the former occur naturally in the bifurcation analysis for scalar fields while the latter occur naturally in the analysis of pseudoscalar fields[1].

Lemma 8.3.5. *The representation of $\mathbf{D}_4\ltimes\mathbb{T}^2$ in $\mathbb{R}^{12}$ defined by Θ and (8.41) is the sum of three real absolutely irreducible representations T_1, T_2, T_3, each of dimension 4, which act respectively on the subspaces $E_1=\{(c_1,d_2,\bar{c}_1,\bar{d}_2)\}$, $E_2=\{(c_2,d_1,\bar{c}_2,\bar{d}_1)\}$ and $E_3=\{(c_3,d_3,\bar{c}_3,\bar{d}_3)\}$. The representation T_1 is pseudoscalar while T_2 and T_3 are scalar (therefore equivalent).*

Proof. The subspaces are clearly invariant by $\Theta=[\theta_1,\theta_2]$, R and K. We note R_j and K_j the restrictions of R and K on E_j for $j=1,2,3$. Then a simple computation using (8.41) shows that

$$[\pi/2,-\pi/2]\,R_2\,[-\pi/2,\pi/2]=R_3 \text{ and } [\pi/2,-\pi/2]\,K_2\,[-\pi/2,\pi/2]=K_3.$$

This implies the equivalence of T_2 and T_3. Now, T_3 is the "standard" scalar absolutely irreducible representation of dimension 4. There is however no such equivalence with T_1. Hence T_1 is the pseudoscalar irreducible representation of dimension 4. □

This lemma provides the isotypic decomposition of the representation and it implies that $\mathbf{L}_{\mu,\beta,\varepsilon}$ admits a bloc diagonal decomposition with one 4×4 bloc $\mathbf{L}^1_{\mu,\varepsilon}=\lambda(\mu,\varepsilon)\mathbf{I}_4$, $\lambda\in\mathbb{R}$ and $\lambda(0,0)=0$, corresponding to T_1 and another 8×8 bloc $\mathbf{L}^2_{\mu,\varepsilon}$ corresponding to the sum T_2+T_3. We shall however not go further in this bifurcation analysis here, it will be the subject of a forthcoming work.

We can instead look at the perturbation of the branches of equilibria listed in Theorem 8.3.1 "far" from the bifurcation. Given such an equilibrium P, its orbit under the action of Γ consists in a disjoint union of tori which are isomorphic to $\mathbb{T}^2$, resp. $\mathbb{T}$, depending on whether its isotropy subgroup is finite, resp. contains $\mathbb{T}$. The number of connected components in the orbit is given by the action of $\mathcal{G}$, more precisely it is equal to $n_H=|\mathcal{G}|/|H|$ where H is the part in $\mathcal{G}$ of the isotropy subgroup of P. If this orbit is hyperbolic, in particular if the equilibrium is orbitally stable, it persists as an invariant set for the equation when $\varepsilon\neq0$ (small enough). Moreover this invariant set is still filled with equilibria because the torus action is not destroyed by the perturbation. However the n_H tori are not anymore in the same group orbit and therefore they correspond to different solutions.

Let us concentrate on the solutions of types Σ_1 and Σ_2. Note that $\Gamma\cap\Sigma_1=\Gamma\cap\Sigma_2=\mathbf{D}_8$, hence $n_{\Sigma_1}=n_{\Sigma_2}=96/16=6$. These six components correspond to the hyperbolic planforms $\pm\Psi_1(z)$, $\pm\Psi_2(z)$ and $\pm\Psi_3(z)$. These orientations persist at leading order for the perturbed equilibria.

[1] A field $u:\ \mathbb{R}^2\to\mathbb{R}$ is pseudoscalar if a reflection S in the plane acts by $S\cdot u(x)=-u(Sx)$), see [Bosch Vivancos 1995]. The importance of this distinction in the context of neural fields was first noticed by [Golubitsky 2003] in the ring model.

One can say a little more. Looking for $\lambda(\mu, \varepsilon) = 0$ and assuming that we have $\lambda'_\mu(0,0) \neq 0$, we have a curve of solutions $\mu_c(\varepsilon)$. For a fixed value of ε, a bifurcation occurs at $\mu = \mu_c(\varepsilon)$, with kernel E_1 and invariance by the pseudoscalar representation T_1. Therefore we expect branches of "anti-rolls" and "anti-squares" to bifurcate [Bosch Vivancos 1995]. We recall that these planforms have isotropies $[\pi, 0]\mathbf{O}(2)$ and $[\pi, 0]\mathbf{D}_4$ respectively. Here $\mathbf{O}(2)$ is generated by the translations $[0, \theta_2]$, $\theta_2 \in \mathbf{S}^1$, and K, while $\mathbf{D}_4$ is generated by R and K. A simple computation shows that indeed, $\dim \mathbf{Fix}([\pi, 0]\mathbf{O}(2)) = 1$ and $\dim \mathbf{Fix}([\pi, 0]\mathbf{D}_4) = 1$ (the Equivariant Branching Lemma can be applied), these axes belonging to the subspace E_1, while $\dim \mathbf{Fix}(\mathbf{O}(2)) = \dim \mathbf{Fix}(\mathbf{D}_4) = 2$ and these planes are in $E_2 + E_3$.

8.4 Conclusion

In this chapter, we have analysed the spatialized network of interacting hypercolumns introduced in chapter 3. Such a network is described by Wilson-Cowan neural field equations set on an abstracted cortex $\mathbb{R}^2 \times \mathbf{SPD}(2, \mathbb{R})$, where the feature space $\mathbf{SPD}(2, \mathbb{R})$ is the set of structure tensors. The coupling function of the network is charaterized by local and long-range connections and can explicitly be written down. Long-range connections modulate rather than drive the cortical activity and can have an isotropic or anisotropic nature. We have only considered structure tensors with determinant equal one for mathematical convenience and identified the feature space to the Poincaré disk $\mathbb{D}$. We addressed two complementary problems. The first one was to study the effect of weak anisotropic lateral coupling on the cortical activity when the feature space is reduced to a bounded compact disk Ω of the Poincaré disk. We have generalized the results obtained by Bressloff *et al.* [Bressloff 2001a, Bressloff 2001b] for orientation to the context of structure tensors. The second problem that we addressed in this chapter was the spontaneous pattern formation for a model with $\mathbf{E}(2) \times \mathbf{U}(1,1)$ symmetry. We have restricted our study to solutions which are doubly periodic on the Euclidean plane and periodic on the Poincaré disk. The visual planforms generated by our spatialized network are correlated tuning surfaces across the visual cortex and are the counterpart of the visual geometric hallucinations for orientation in the context of textures.

An extension of this work would be to include external stimuli and see how long-range connections modulate its effects. We think that our framework (center manifold reduction close to the point of instability) is applicable if we further suppose that the external input is sufficiently weak: amplitude of order $O(\beta)$ if β is the strength of the lateral coupling function. Of course it could be interesting to include the effects of noise in our model and one approach would consist to add space-dependent noise term to the external stimuli.

Another approach to the modelling of the primary visual cortex is to consider model with no feature space [Bressloff 2003c, Blumenfeld 2006, Baker 2009, Veltz 2011] where cortical maps are included into the equations. This re-

quires understanding the mechanism of their formation. Wolf *et al.* [Wolf 1998, Kaschube 2008, Kaschube 2010] have designed equations for the development of cortical map of orientations and Bressloff-Oster [Oster 2006, Bressloff 2010] for ocular dominance map. One can ask the question of formation of cortical map of structure tensors during development. Then it would be very interesting to model a structure tensor map embedded in the Riemannian manifold $\mathbf{SPD}(2, \mathbb{R})$ on a growing cortex with different topology (disk, square and sphere) using an evolution equation similar to those proposed in [Kaschube 2008, Bressloff 2010]. The maps obtained from the model could be then compared to those obtained experimentally by optical imaging technics and incorporated into a model of V1 with no feature space.

Part III

Localized states on unbounded neural field equations

Chapter 9

General introduction

We arrive at the last part of the Thesis, the one concerned with localized solutions of unbounded neural field equations. Localized patterns arise everywhere in nature: spots bundle magnetic field lines in ferromagnetic fluids, grass spots and rings develop in deserts where resources are scarce or hexagon patches in cooling lava fields (see figure 9.1). Spatially localized structures have also be found in some cortical activity recordings (see figure 9.2).

Figure 9.1: Examples of natural patterns: desert grass spots and rings, hexagon patches form in cooling lava fields and ferrosolitions.

In the past decades there has been a great deal of interest in the origin and properties of these spatially localized structures in differential equations [Amari 1977, Champneys 1998, Pinto 2001b, Laing 2002, Coombes 2005b, Guo 2005b, Burke 2006]. The equation that is the most studied in pattern formation is the well-known generalized Swift-Hohenberg equation

$$\partial_t u(\mathbf{r},t) = -(1+\triangle)^2 u(\mathbf{r},t) - \mu u + f(u(\mathbf{r},t)), \quad \forall \mathbf{r} \in \mathbb{R}^n \tag{9.1}$$

with either cubic/quintic or quadratic/cubic nonlinearities f. For this particular example, the presence of localized steady states is a dynamical property: a bifurcation from the trivial state occurs for some value of the control parameter μ. These localized solutions are then viewed as homoclinic orbits to the trivial state.

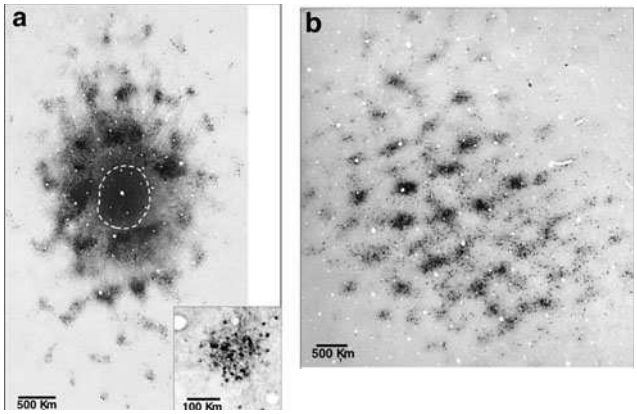

Figure 9.2: Cortical activity in the primary visual cortex, redrawn from [Angelucci 2002, Lund 2003].

In the neuroscience community, the canonical example is the unbounded Wilson-Cowan neural field equation (see chapter 2):

$$\tau \frac{d}{dt} V(\mathbf{r}, t) = -V(\mathbf{r}, t) + \int_{\mathbb{R}^n} W(\mathbf{r}, \mathbf{r}') S(V(\mathbf{r}', t)) d\mathbf{r}'. \tag{9.2}$$

The study of localized solutions of equation (9.2) is an old and recurrent topic in the mathematical neuroscience community, where a number of different coupling functions W and firing-rate functions S have been used. The firing rate function can be an Heaviside step function [Amari 1977, Pinto 2001b, Coombes 2005b], a piecewise linear function [Guo 2005b, Guo 2005a] or a smooth function of sigmoidal type [Laing 2002, Coombes 2003, Faugeras 2008, Elvin 2010]. The connectivity function is always assumed to have a so-called "Mexican hat" or so-called "wizard hat" shape. Partial differential equation (PDE) methods [Laing 2002, Laing 2003a] can be employed to transform the neural field equation (9.2) into a partial differential equation involving high-order spatial derivatives. Interestingly spatially localized solutions of persistent activity have been linked to working memory (the temporary storage of information within the brain). In many models of working memory, transient stimuli are encoded by feature-selective persistent neural activity. Such stimuli are imagined to induce the formation of a spatially localized state of persistent activity (which coexists with a stable uniform state).

For $n = 1$, Laing *et al.* [Laing 2002] numerically investigated the integro-differential equation (9.2) with

$$S(x) = 2 \exp\left(-r/(x-\theta)^2\right) H(x-\theta) \tag{9.3}$$

where H is the Heaviside step function and

$$W(x) = e^{-b|x|}(b \sin |x| + \cos x). \tag{9.4}$$

The parameter b governs the rate at which oscillations in W decay with distance from $x = 0$, the firing rate function S has threshold θ and slope r. In [Laing 2002], numerical simulations of (9.2) show the existence of spatially localized states. Numerical continuation techniques were used to follow, as the parameter b is varied, branches of localized solutions of (9.2) and so-called "snaking" behaviour was found. This remarkable phenomenon, in which a series of fold bifurcations give rise to a hierarchy of localized solution branches with increasing number of bumps, has been studied extensively for the canonical Swift-Hohenberg equation [Woods 1999, Burke 2007a, Burke 2007b, McCalla 2010]. Numerical investigations of [Laing 2002] indicate that localized solutions of equation (9.2) do not come into existence through a reversible-Hopf bifurcation from a constant solution as is the case for the Swift-Hohenberg equation. Although their system is reversible, the shape of the nonlinearity function S in equation (9.3) (S is not analytical at $x = 0$) renders impossible the application of tools from bifurcation theory. More recently, Elvin et al [Elvin 2010] used the Hamiltonian structure of equation (9.2) and developed numerical techniques to find all homoclinic orbits of the system.

In this final part, we will study equation (9.2) for $n = 1$ and $n = 2$ with a sigmoidal firing-rate function for specific type of connectivity function. The case $n = 1$ will be the subject of chapter 10 and $n = 2$ of chapter 11. The shape of the solutions in the scalar case is given in figures 10.4 and 10.5. For two dimensional patterns, things can get more interesting. There are spots as seen in figures 9.1 and 9.3(a), rings (figure 9.1). Spots can also be concentrated on a hexagonal lattice to produce hexagon patches as seen in figure 9.3(b).

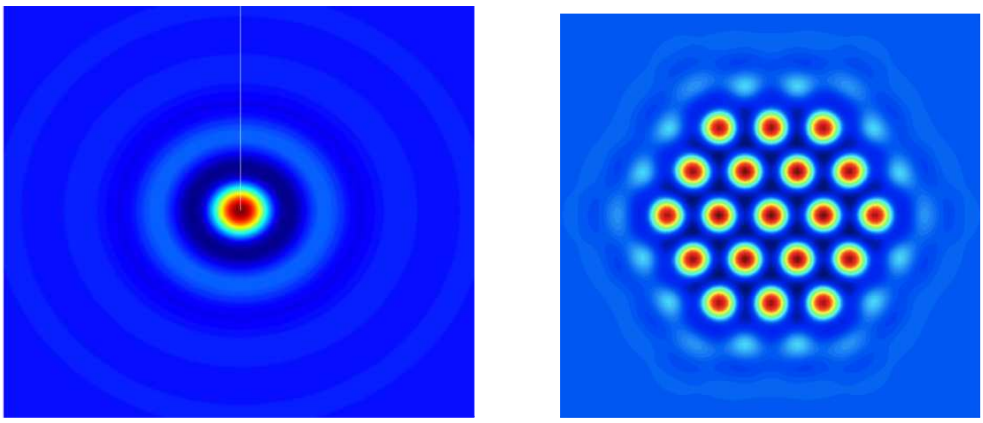

(a) Redrawn from Lloyd and Sandstede [Lloyd 2009].

(b) Redrawn from Lloyd *et al.* [Lloyd 2008].

Figure 9.3: Left: spot. Right: patch of hexagons.

In chapter 11, we will be only interested in radially symmetric solutions of equation (9.2) and let the analysis of localized solutions concentrated on a hexagonal

lattice for future research. Note that spot solution in planar neural field equations has been studied in [Laing 2003a, Laing 2003b, Folias 2004, Owen 2007] with an Heaviside firing-rate function. The aim of chapter 11 is to extend some results [Scheel 2003, Lloyd 2009, McCalla 2010] that have been obtained for the planar Swift-Hohenberg equation to neural field equation set on the Euclidean plane. At the end of chapter 11, we further extend the results in the case where the neural field equation is set on the Poincaré disk.

Chapter 10

Localized states of NFEs on the real line

Contents

10.1 Wizard hat model 196
10.1.1 Connectivity function 197
10.1.2 Linear stability analysis of the trivial state 198
10.1.3 Bifurcation of the trivial state for the full system 199
10.2 Reversible Hopf bifurcation with 1:1 resonance 200
10.2.1 PDE methods 200
10.2.2 Reversible-Hopf bifurcation 202
10.2.3 Normal form theory 202
10.2.4 Existence of homoclinic orbits 204
10.3 Stability of localized solutions 205
10.3.1 Asymptotic stability 205
10.3.2 Stability against perturbations in the connectivity function . 209
10.4 Numerical results 211
10.4.1 Tuning the parameters 211
10.4.2 Numerical computation of the stability of localized solutions 211
10.4.3 Snaking behaviour and localized solutions varying μ 212
10.4.4 Regions of localized solutions in the parameter plane 214
10.5 Conclusion 216

The main motivation of this chapter is to complete the study of localized states of neural field equations on the unbounded real line initiated in [Laing 2002, Elvin 2010] by showing that these states are bifurcated branches of solutions emerging from the trivial state of equation (9.2) through reversible Hopf bifurcation with 1:1 resonance when the slope of the sigmoidal function is increased. To achieve this goal, we work with a wizard hat coupling function $w(x)$ (difference of exponential functions) and a smooth firing rate function which has non-vanishing derivatives at the fixed point of equation (9.2). As previously shown for the Swift-Hohenberg equation on the real line in [Burke 2007b], we calculate the normal form coefficients [Iooss 1993, Haragus 2010] for the reversible 1:1 Hopf bifurcation and find a condition on the different parameters which ensures the existence of a pair of homoclinic branches. We present results on the stability of the bifurcating branches.

We use numerical continuation in order to extend the study with an investigation of snaking behaviour; these methods have been applied extensively for the Swift-Hohenberg equation [Burke 2006, Burke 2007a, Champneys 1998, Lloyd 2009, McCalla 2010, Woods 1999] and, in a few isolated cases for the neural field equation [Laing 2002, Laing 2003a, Coombes 2003]. Here, we use the continuation package AUTO [Doedel 1997] with the extension HOMCONT to follow homoclinic cycles corresponding to localized solutions under variation of system parameters. We confirm the solution structure determined analytically in this paper and reproduce previously observed snaking behaviour. Further, we identify the exact regions of parameter space for which localized solutions persist in terms of two parameters governing the shape of the nonlinearity S and a third parameter governing the shape of the connectivity function w.

This chapter is organized as follows. In section 10.1 our model and notations are introduced. We explain in section 10.2 how stationary solutions of the neural field equation are equivalent to homoclinic orbits in a related fourth order ordinary differential equation and we show the existence of branches of localized solutions using normal form theory. Section 10.3 focuses on the stability of these branches of solutions. Finally, in section 10.4 we build on the theoretical results with a numerical investigation of localized solutions under the variation of three parameters.

10.1 Wizard hat model

We introduce a bifurcation parameter $\mu > 0$ in the neural field equation (9.2)

$$\begin{aligned} \frac{d}{dt}v(x,t) &= -v(x,t) + \int_{-\infty}^{+\infty} w(x-y)S(\mu v(y,t))dy, \\ &= \mathcal{F}(v(x,t),\mu). \end{aligned} \tag{10.1}$$

The firing rate function is either taken to be the sigmoidal function

$$S(x) = \frac{1}{1+e^{-x+\theta}} \text{ with } \theta > 0 \tag{10.2}$$

or its shifted version via:

$$S_0(x) = \frac{1}{1+e^{-x+\theta}} - \frac{1}{1+e^{\theta}}. \tag{10.3}$$

We define a stationary solution to be time independent solution of (10.1), thus satisfies the equation:

$$v(x) = \int_{-\infty}^{+\infty} w(x-y)S(\mu v(y))dy. \tag{10.4}$$

For a solution of (10.4), we define its region of excitation to be the set:

$$R_\mu^\theta(v) = \{x \in \mathbb{R} \mid \mu v(x) > \theta\}.$$

Following Amari's definition [Amari 1977], a *localized solution* of (10.4) is a pattern $v(x)$ whose region of excitation consists of a finite disjoint union of bounded connected intervals and which decays to zero as x goes to infinity.

10.1.1 Connectivity function

In order to well define the convolutional part of the right hand side of equation (10.1), we have to take a connectivity function at least integrable over the real line. If w belongs to $\mathrm{L}^1(\mathbb{R})$, the space of integrable functions on $\mathbb{R}$, we can define its Fourier transform $\widehat{w}$ as:

$$\widehat{w}(\xi) = \int_{\mathbb{R}} w(x) e^{-i\xi x} dx.$$

If we further suppose that $\widehat{w} \in \mathrm{L}^1(\mathbb{R})$, then the inversion formula applies and we have:

$$w(x) = \frac{1}{2\pi} \int_{\mathbb{R}} \widehat{w}(\xi) e^{i\xi x} d\xi.$$

We now introduce some conditions on the connectivity function.

Hypothesis 10.1.1. *We suppose that the following conditions are satisfied:*

(i) $w, \widehat{w} \in L^1(\mathbb{R})$,

(ii) $w(0) > 0$,

(iii) $\widehat{w}_0 \overset{def}{=} \widehat{w}(0) < 0$,

(iv) there exists $\xi_c > 0$ *such that* $\widehat{w}_c \overset{def}{=} \widehat{w}(\pm\xi_c) = \max_{\xi \in \mathbb{R}} \widehat{w}(\xi) > 0$,

(v) $\widehat{w}(\xi) = \frac{R(\xi^2)}{Q(\xi^2)}$ *with* R, Q *polynomial in* ξ^2 *satisfying* $\deg R < \deg Q$.

The first condition tells us that the connectivity function and its Fourier transform are integrable over the real line such that we can apply the inversion formula for Fourier transform. The second condition ensures that the connectivity function is locally excitatory and the third condition that it is laterally inhibitory. The fourth condition says that $\widehat{w}(\xi)$ has two global maxima at $\pm\xi_c$. The condition $\widehat{w}_c > 0$ is necessary for the stability analysis developed in 10.1.2. Finally, the last condition ensures that the partial differential equation (PDE) method conducted in 10.2.1 can be applied.

In order to fix ideas, from now on, we will work with the following connectivity function (as used in [Guo 2005b, Guo 2005a]):

$$w(x) = b_1 e^{-\sigma_1 |x|} - b_2 e^{-\sigma_2 |x|}, \tag{10.5}$$

with Fourier transform given by

$$\widehat{w}(\xi) = \int_{\mathbb{R}} w(x) e^{-i\xi x} dx = 2 \left(\frac{b_1 \sigma_1}{\sigma_1^2 + \xi^2} - \frac{b_2 \sigma_2}{\sigma_2^2 + \xi^2} \right). \tag{10.6}$$

The real constants $(b_1, b_2, \sigma_1, \sigma_2)$ are chosen such that all the conditions in Hypothesis 10.1.1 are satisfied.

Hypothesis 10.1.2. *We assume that* $\xi_c = 1$. We impose this condition in order to fix the period to 2π of the critical modes which will bifurcate from the trivial state (see 10.1.2). Now, if we define

$$\begin{aligned} \Gamma_1 &= 2\sigma_1\sigma_2(b_1\sigma_2 - b_2\sigma_1), \\ \Gamma_2 &= 2(b_1\sigma_1 - b_2\sigma_2), \end{aligned} \tag{10.7}$$

then $\widehat{w}_c$ can be written:

$$\widehat{w}_c = \frac{\Gamma_1 + \Gamma_2}{1 + \sigma_1^2 + \sigma_2^2 + \sigma_1^2\sigma_2^2}. \tag{10.8}$$

The condition $\xi_c = 1$, which is equivalent to $\frac{d}{d\xi}\widehat{w}(\xi)|_{\xi=1} = 0$, reduces to

$$\Gamma_1(\sigma_1^2 + \sigma_2^2 + 2) + \Gamma_2(1 - \sigma_1^2\sigma_2^2) = 0. \tag{10.9}$$

It is a straightforward computation to see that equations (10.8) and (10.9) imply that:

$$\begin{aligned} \sigma_1^2\sigma_2^2 - \frac{\Gamma_1}{\widehat{w}_c} &= 1 \\ \sigma_1^2 + \sigma_2^2 - \frac{\Gamma_2}{\widehat{w}_c} &= -2. \end{aligned} \tag{10.10}$$

10.1.2 Linear stability analysis of the trivial state

The aim of this subsection is to show that equation (10.1) has always a unique trivial state that undergoes a bifurcation when increasing the slope μ of the sigmoidal function. We present the results for both shifted and unshifted sigmoidal function.

10.1.2.1 Unshifted sigmoidal function S

Equation (10.1) has the trivial solution $v_0(\mu)$ independent of time and space that satisfies:

$$v_0(\mu) = \widehat{w}_0 S(\mu v_0(\mu)) \text{ for all } \mu > 0.$$

The linearized equation around this trivial solution is:

$$\partial_t u(x,t) = -u(x,t) + \mu S'(\mu v_0(\mu)) \int_{\mathbb{R}} w(x-y)u(y,t)dy. \tag{10.11}$$

Looking at perturbation of the form $u(x,t) = e^{\sigma t}e^{i\xi x}$, we obtain the following dispersion relation:

$$\sigma(\xi) = -1 + \mu S'(\mu a_0(\mu))\widehat{w}(\xi). \tag{10.12}$$

Lemma 10.1.1. *There exists a unique solution* $(\mu_c, v_c = v_0(\mu_c))$ *of:*

$$\begin{cases} v_c &= \widehat{w}_0 S(\mu_c v_c) \\ 1 &= \mu_c S'(\mu_c v_c)\widehat{w}_c. \end{cases} \tag{10.13}$$

It is possible to express (μ_c, v_c) *with the following analytic formulas:*

$$\begin{aligned} \mu_c &= \frac{\widehat{w}_0^2}{v_c\widehat{w}_c(\widehat{w}_0 - v_c)}, \\ v_c &= \frac{\widehat{w}_0\widehat{w}_c W\left(-\widehat{w}_0 e^{-\frac{-\widehat{w}_0+\theta\widehat{w}_c}{\widehat{w}_c}}/\widehat{w}_c\right)}{\widehat{w}_c W\left(-\widehat{w}_0 e^{-\frac{-\widehat{w}_0+\theta\widehat{w}_c}{\widehat{w}_c}}/\widehat{w}_c\right) - \widehat{w}_0}. \end{aligned} \tag{10.14}$$

W *is the Lambert function which satisfies* $W(x)e^{W(x)} = x$.

Proof. The proof is given in appendix C.1. □

From this Lemma, we deduce that for all $\mu < \mu_c$ the trivial solution $v_0(\mu)$ is stable.

10.1.2.2 Shifted sigmoidal function S_0

In the case of the shifted sigmoidal function defined in equation (10.3), the null solution $v_0 = 0$ is clearly a solution of (10.4) for all $\mu > 0$. Under the condition $\widehat{w}_0 < 0$ it is the unique solution independent of time and space of (10.4). Following the same lines as for the unshifted sigmoidal function, for perturbation of the form $u(x,t) = e^{\sigma t}e^{i\xi x}$, we obtain for the dispersion relation:

$$\sigma(\xi) = -1 + \mu S_0'(0)\widehat{w}(\xi). \tag{10.15}$$

Then the critical value μ_c is given by:

$$\mu_c = \frac{1}{S_0'(0)\widehat{w}_c}, \tag{10.16}$$

and for all $\mu < \mu_c$ the null solution is stable.

10.1.2.3 Choice of the sigmoidal function

In order to simplify our notations, from now on, we work with the shifted sigmoidal function S_0 and denote for all $k \geq 1$, $S_0^{(k)}(0) = s_k$. Of course, all the results that we are going to present in the following sections are easily transportable to the unshifted case.

10.1.3 Bifurcation of the trivial state for the full system

The trivial state $v_0 = 0$ undergoes a bifurcation at the critical value $\mu = \mu_c$. Furthermore, as equation (10.1) is equivariant with respect to the translations and the symmetry $(x \to -x, v \to v)$, the bifurcation is a steady bifurcation with $\mathbf{O}(2)$-symmetry [Chossat 2000, Haragus 2010]. We can apply the Lyapunov-Schmidt decomposition (see [Chossat 2000] for a review) on the Hilbert space $\mathcal{X} = \mathrm{L}^2_{per}[0, 2\pi]$, the set of 2π-periodic square integrable functions, in order to get a reduced equation

on the two-dimensional space $\mathrm{Span}(e^{ix}, e^{-ix})$. If we denote $\lambda = \mu - \mu_c$, then the neural field equation (10.1) is transformed into:

$$\partial_t v(x,t) = \mathbf{L}_{\mu_c} v(x,t) + \mathbf{R}(v(x,t), \lambda) \tag{10.17}$$

where $\mathbf{L}_{\mu_c}$ and $\mathbf{R}$ are defined by

$$\mathbf{L}_{\mu_c} v(x,t) = -v(x,t) + \mu_c s_1 \int_{\mathbb{R}} w(x-y) v(y,t) dy$$
$$\mathbf{R}(v(x,t), \lambda) = \int_{\mathbb{R}} w(x-y) \left[S_0\left((\lambda + \mu_c) v(y,t)\right) - \mu_c s_1 v(y,t) \right] dy$$

and

$$f_0(X, \lambda) = S_0\left((\lambda + \mu_c) X\right) - \mu_c s_1 X. \tag{10.18}$$

It is straightforward to check that $\mathbf{R}(0,0) = D_v \mathbf{R}(0,0) = 0$. We can write each solution of (10.17) on the form:

$$v(x,t) = Z(t) e^{ix} + \overline{Z(t)} e^{ix} + \Phi(Z(t), \overline{Z(t)}, \lambda).$$

The reduced equation is then:

$$\dot{Z}(t) = \left(\nu\lambda + \chi |Z(t)|^2\right) Z(t) + \text{h.o.t.} \tag{10.19}$$

Lemma 10.1.2. *The coefficients of the reduced equation (10.19) are:*

$$\begin{aligned} \nu &= \frac{1}{\mu_c}, \\ \chi &= \frac{\mu_c^3}{s_1} \left[\frac{s_3}{2} + \frac{\mu_c s_2^2 (19\Gamma_1 + 4\Gamma_2)}{18} \right]. \end{aligned} \tag{10.20}$$

Proof. The computation of the coefficients is postponed in appendix C.2. □

It follows that close to the bifurcation point, for $\lambda\chi < 0$, the amplitude $Z(t)$ is given by:

$$Z_\omega(t) = \sqrt{-\frac{\lambda}{\mu_c \chi}} e^{i\omega} + \mathcal{O}(|\lambda|^{\frac{3}{2}})$$

for any phase ω on the circle $\mathbf{S}^1$. This phase can be identified to the translation invariance of equation (10.1). The bifurcation to this spatially periodic branch is subcritical ($\lambda < 0$) in $\chi > 0$ and supercritical ($\lambda > 0$) in $\chi < 0$.

10.2 Reversible Hopf bifurcation with 1:1 resonance

10.2.1 PDE methods

We assume that $v \to v(\cdot, t) \in \mathcal{C}^1(\mathbb{R}^+, \mathcal{H}^4(\mathbb{R}))$ is a solution of (10.17), where $\mathcal{H}^4(\mathbb{R})$ is the Sobolev space defined as:

$$\mathcal{H}^4(\mathbb{R}) = \{u \in \mathrm{L}^2(\mathbb{R}) \mid \forall k \leq 4 \ \partial_{x^k}^k u \in \mathrm{L}^2(\mathbb{R})\}.$$

Under this assumption, an application of Fourier transform in (10.17) gives:

$$(\partial_t + 1)\,\widehat{v}(\xi,t) = \widehat{w}(\xi)\left[\widehat{f_0(v,\lambda)}(\xi,t) + \mu_c s_1 \widehat{v}(\xi,t)\right].$$

Using the inverse Fourier transform we obtain:

$$(\partial_t + 1)\,\mathcal{L}_{\mu_c}(v) = \mathcal{M}(v,\lambda) \tag{10.21}$$

with $\mathcal{L}_{\mu_c}$ and $\mathcal{M}$ defined by

$$\mathcal{L}_{\mu_c}(v) = (\sigma_1^2\sigma_2^2 - \Gamma_1\mu_c s_1)v - (\sigma_1^2 + \sigma_2^2 - \Gamma_2\mu_c s_1)\partial_{x^2}^2 v + \partial_{x^4}^4 v$$

and

$$\mathcal{M}(v,\lambda) = \Gamma_1 f_0(v,\lambda) - \Gamma_2\partial_{x^2}^2\left[f_0(v,\lambda)\right].$$

From equations (10.10) and the fact that $\mu_c = (s_1\widehat{w}_c)^{-1}$, the coefficients of $\mathcal{L}_{\mu_c}$ reduce to:

$$\begin{aligned} \sigma_1^2\sigma_2^2 - \Gamma_1\mu_c s_1 &= 1, \\ \sigma_1^2 + \sigma_2^2 - \Gamma_2\mu_c s_1 &= -2. \end{aligned}$$

Note that equation (10.21) forms a fourth order reversible dynamical system in space: the equation is invariant under spatial reflection ($x \to -x, v \to v$). We look for stationary solutions of equation (10.21) which satisfy

$$\begin{cases} \mathcal{L}_{\mu_c}(v) = \mathcal{M}(v,\lambda) \\ \qquad v \in \mathcal{H}^4(\mathbb{R}). \end{cases} \tag{10.22}$$

The spatial coordinate x is recast as the time variable and the differential equation (10.22) is now equivalent to a four-dimensional system of first order ordinary differential equations (ODEs) which can be written:

$$U' = \mathcal{A}U + \mathcal{R}(U,\lambda) \tag{10.23}$$

with $U = (u_1,u_2,u_3,u_4)^{\mathbf{T}}$ (note thet $u_1 = v$) and

$$\mathcal{A} = \begin{pmatrix} 0 & 1 & 0 & 0 \\ 0 & 0 & 1 & 0 \\ 0 & 0 & 0 & 1 \\ -1 & 0 & -2 & 0 \end{pmatrix}, \quad \mathcal{R}(U,\lambda) = \begin{pmatrix} 0 \\ 0 \\ 0 \\ \mathcal{R}_4\left(u_1,u_2,u_3,u_4,\lambda\right) \end{pmatrix}.$$

The fourth component of the nonlinear function $\mathcal{R}$ is given by

$$\begin{aligned} \mathcal{R}_4\left(u_1,u_2,u_3,u_4,\lambda\right) = \Gamma_1 f_0(u_1,\lambda) - \Gamma_2\Big[&(\lambda+\mu_c)^2 u_2^2 S_0''\left((\lambda+\mu_c)u_1\right) - \mu_c s_1 u_3 \\ &+ (\lambda+\mu_c)u_3 S_0'\left((\lambda+\mu_c)u_1\right)\Big]. \end{aligned} \tag{10.24}$$

Furthermore, we have the following Taylor expansion of $\mathcal{R}$ at $(U = 0_{\mathbb{R}^4}, \lambda = 0)$

$$\begin{aligned}
\mathcal{R}_{1,1}(U,\lambda) &= \lambda s_1 \left(0,0,0,\Gamma_1 u_1 - \Gamma_2 u_3\right)^{\mathbf{T}} \\
\mathcal{R}_{2,0}(U,U) &= \frac{\mu_c^2 s_2}{2}\left(0,0,0,\Gamma_1 u_1^2 - \Gamma_2(2u_2^2 + 2u_1 u_3)\right)^{\mathbf{T}} \\
\mathcal{R}_{3,0}(U,U,U) &= \frac{\mu_c^3 s_3}{6}\left(0,0,0,\Gamma_1 u_1^3 - \Gamma_2(6u_1 u_2^2 + 3u_1^2 u_3)\right)^{\mathbf{T}}.
\end{aligned}$$

10.2.2 Reversible-Hopf bifurcation

The associated linear problem of equation (10.23) is

$$U' = \mathcal{A}U + \mathcal{R}_{1,1}(U,\lambda).$$

Eigenvalues of the linear problem satisfy the characteristic equation:

$$X^4 + (2 + s_1\lambda\Gamma_2)\,X^2 + 1 - s_1\lambda\Gamma_1 = 0. \tag{10.25}$$

To the leading order in λ the discriminant of equation (10.25) seen as a quadratic equation in X^2 is

$$\Delta(\lambda) = 4s_1(\Gamma_1 + \Gamma_2)\lambda + o(\lambda).$$

From equation (10.8), we have $\operatorname{sign}(\Gamma_1 + \Gamma_2) = \operatorname{sign}(\widehat{w}_c) > 0$. Then, for $\lambda < 0$ there exists four complex eigenvalues with real part symmetric with respect to the imaginary axis, such that the trivial state is hyperbolic with two stables eigenvalues and two unstable eigenvalues. In contrast, for $\lambda > 0$ all the eigenvalues lie on the imaginary axis and the trivial state is no longer hyperbolic. At $\lambda = 0$, there is a pair of imaginary eigenvalues $\pm i$ of double multiplicity. The bifurcation at $\lambda = 0$ is thus a Hopf bifurcation in a reversible system with 1:1 (spatial) resonance.

10.2.3 Normal form theory

In the following, we adopt the formalism of [Iooss 1993, Haragus 2010] to study the reversible Hopf bifurcation. We start by constructing a suitable basis of $\mathbb{R}^4$ and we denote $\mathbf{S}$ the symmetry:

$$\mathbf{S} = \begin{pmatrix} 1 & 0 & 0 & 0 \\ 0 & -1 & 0 & 0 \\ 0 & 0 & 1 & 0 \\ 0 & 0 & 0 & -1 \end{pmatrix} \text{ with } \mathbf{S}^2 = \mathbb{I}_{\mathbb{R}^4}.$$

Let $\zeta_0 = (1, i, -1, -i)^{\mathbf{T}}$ be an eigenvector of $\mathcal{A}$ which satisfies:

$$(\mathcal{A} - i\mathbb{I}_{\mathbb{R}^4})\zeta_0 = 0 \text{ and } \mathbf{S}\zeta_0 = \bar{\zeta}_0$$

and let $\zeta_1 = (0, 1, 2i, -3)^{\mathbf{T}}$ be a generalized eigenvector that is:

$$(\mathcal{A} - i\mathbb{I}_{\mathbb{R}^4})\zeta_1 = \zeta_0 \text{ and } \mathbf{S}\zeta_1 = -\bar{\zeta}_1.$$

Then $(Re\zeta_0, Im\zeta_0, Re\zeta_1, Im\zeta_1)$ is a basis of $\mathbb{R}^4$ with ζ_0, ζ_1 generalized eigenvectors of $\mathcal{A}$. In this basis, we represent a vector $U \in \mathbb{R}^4$ by $(A, B, \bar{A}, \bar{B})$,

$$U = A\zeta_0 + B\zeta_1 + \overline{A\zeta_0} + \overline{B\zeta_1}$$

with $A, B \in \mathbb{C}$.

Lemma 10.2.1 (Normal form). *If we rewrite equation* (10.23) *as*

$$U' = \mathcal{A}U + \mathcal{R}(U, \lambda) = \mathbf{F}(U, \lambda)$$

then the vector field $\mathbf{F}$ *is of class* $\mathbb{C}^k$, $k \geq 3$, *in a neighborhood of* $(0,0) \in \mathbb{R}^4 \times \mathbb{R}$ *satisfying* $\mathbf{F}(0,0) = 0$ *and such that* $\mathbf{S}$ *anticommutes with* $\mathbf{F}$. *For any integer* p, $2 \leq p \leq k$, *there exist neighborhoods* $\mathcal{V}_1$ *and* $\mathcal{V}_2$ *of 0 in* $\mathbb{R}^4$ *and* $\mathbb{R}$, *respectively, and for any* $\lambda \in \mathcal{V}_2$ *there is a polynomial map* $\Psi(\cdot, \lambda) : \mathbb{R}^4 \to \mathbb{R}^4$ *of degree* p *with the following properties:*

1. *The coefficients of the monomials of degree* q *in* $\Psi(\cdot, \lambda)$ *are functions of* λ *of class* $\mathbb{C}^{k-q}$,

$$\Psi(0,0,0,0,0) = 0, \quad \partial_{(A,B,\bar{A},\bar{B})}\Psi(0,0,0,0,0) = 0,$$

and

$$\mathbf{S}\Psi(A, B, \bar{A}, \bar{B}, \lambda) = \Psi(\bar{A}, -\bar{B}, A, -B, \lambda).$$

2. *For* $(A, B, \bar{A}, \bar{B}) \in \mathcal{V}_1$, *the changes of variables*

$$U = A\zeta_0 + B\zeta_1 + \overline{A\zeta_0} + \overline{B\zeta_1} + \Psi(A, B, \bar{A}, \bar{B}, \lambda)$$

transforms the equation (10.23) *into the normal form:*

$$\begin{aligned}
\frac{dA}{dt} &= iA + B + iAP\left(|A|^2, \frac{i}{2}(A\bar{B} - \bar{A}B), \lambda\right) + \rho_A(A, B, \bar{A}, \bar{B}, \lambda) \\
\frac{dB}{dt} &= iB + iBP\left(|A|^2, \frac{i}{2}(A\bar{B} - \bar{A}B), \lambda\right) + AQ\left(|A|^2, \frac{i}{2}(A\bar{B} - \bar{A}B), \lambda\right) \\
&\quad + \rho_B(A, B, \bar{A}, \bar{B}, \lambda)
\end{aligned} \tag{10.26}$$

where P *and* Q *are real-valued polynomials of degree* $p-1$ *in* $(A, B, \bar{A}, \bar{B})$. *The remainders* ρ_A *and* ρ_B *are of class* $\mathbb{C}^k$, *and satisfy*

$$\begin{aligned}
\rho_A(\bar{A}, -\bar{B}, A, -B, \lambda) &= -\rho_A(A, B, \bar{A}, \bar{B}, \lambda), \\
\rho_B(\bar{A}, -\bar{B}, A, -B, \lambda) &= \rho_B(A, B, \bar{A}, \bar{B}, \lambda)
\end{aligned}$$

with the estimate

$$|\rho_A(A, B, \bar{A}, \bar{B}, \lambda)| + |\rho_B(A, B, \bar{A}, \bar{B}, \lambda)| = o\left((|A| + |B|)^p\right).$$

Proof. See Haragus-Iooss [Haragus 2010]. □

Moreover, the expansions of P and Q in the normal form are given by:

$$P\left(|A|^2, \frac{i}{2}(A\bar{B}-\bar{A}B), \lambda\right) = \alpha\lambda+\beta|A|^2+\frac{i\gamma}{2}\left(A\bar{B}-\bar{A}B\right)+0\left((|\lambda|+(|A|+|B|)^2)^2\right) \tag{10.27}$$

$$Q\left(|A|^2, \frac{i}{2}(A\bar{B}-\bar{A}B), \lambda\right) = c_1^1\lambda+c_3^0|A|^2+\frac{ic}{2}\left(A\bar{B}-\bar{A}B\right)+0\left((|\lambda|+(|A|+|B|)^2)^2\right). \tag{10.28}$$

We wish to determine the different coefficients that appear in the expansions of P and Q. The expression of each coefficient is given in the following lemma.

Lemma 10.2.2. *The coefficients $\alpha, \beta, \gamma, c_1^1, c_3^0$ and c in the expansions of P and Q in equations (10.27) and (10.28) are*

$$\begin{aligned}
\alpha &= \frac{s_1(\Gamma_2-\Gamma_1)}{8},\\
\beta &= \frac{\mu_c^3}{32}\left[3s_3(\Gamma_2-\Gamma_1)-\frac{\mu_c s_2^2(4\Gamma_2^2+187\Gamma_1^2+29\Gamma_1\Gamma_2)}{27}\right],\\
\gamma &= -\frac{\mu_c^4 s_2^2(36\Gamma_1^2+4\Gamma_1\Gamma_2+7\Gamma_2^2)}{162},\\
c_1^1 &= -\frac{s_1(\Gamma_1+\Gamma_2)}{4},\\
c_3^0 &= -\frac{\mu_c^3(\Gamma_1+\Gamma_2)}{4}\left[\frac{s_3}{2}+\frac{\mu_c s_2^2(19\Gamma_1+4\Gamma_2)}{18}\right],\\
c &= \frac{\mu_c^3}{16}\left[s_3(\Gamma_2-\Gamma_1)-\frac{\mu_c s_2^2(41\Gamma_1^2-209\Gamma_1\Gamma_2-52\Gamma_2^2)}{27}\right].
\end{aligned}$$

The proof of lemma 10.2.2 is let in appendix C.3. We can note that, as expected, $\chi = \frac{c_3^0}{\mu_c c_1^1}$. Moreover, the coefficients are in agreement with those computed for the Swift-Hohenberg equation with quadratic/cubic nonlinearity [Burke 2006, Burke 2007a, Burke 2007b].

10.2.4 Existence of homoclinic orbits

We are now able to state the main result of this part.

Theorem 10.2.1 (Existence). *If $c_3^0 < 0$ and $\lambda < 0$, in a neighborhood of the symmetric equilibrium a_0 and for sufficiently small λ, there is a pair of reversible homoclinic orbits to a_0.*

Proof. The proof is a direct application of Theorem 3.21 in [Haragus 2010] with $c_1^1 < 0$ in Lemma 10.2.1. □

Under the conditions stated in the theorem, the homoclinic orbits of the normal form (10.26) truncated at cubic order are given in polar coordinates $A = r_0 e^{i(t+\varphi_0)}$,

$B = r_1 e^{i(t+\varphi_1)}$ by

$$r_0(t) = \sqrt{\frac{-2c_1^1\lambda}{c_3^0}}\operatorname{sech}\left(t\sqrt{c_1^1\lambda}\right), \quad r_1 = |r_0'|$$
$$\varphi_1 - \varphi_0 \in \{0, \pi\}, \quad \varphi_0(t) = \alpha\lambda t - \frac{2\beta\sqrt{c_1^1\lambda}}{c_3^0}\tanh\left(t\sqrt{c_1^1\lambda}\right) + \phi.$$

For sufficiently small λ, $\lambda < 0$, the localized solution of (10.1) can be approximated by

$$a(x) = 2\sqrt{\frac{-2c_1^1\lambda}{c_3^0}}\operatorname{sech}\left(t\sqrt{c_1^1\lambda}\right)\cos(x+\phi) + \mathcal{O}(\lambda). \tag{10.29}$$

This family of localized solutions is parametrized by $\phi \in \mathbf{S}^1$, which controls the phase of the pattern within the sech $(\cdot)$ envelope. Within the asymptotics this phase remains arbitrary, however it is known that this is no longer the case once terms beyond all orders are included [Melbourne 1998, Kozyreff 2006, Chapman 2009]. These terms break the rotational invariance of the envelope equation and result in a weak flow on the circle $\mathbf{S}^1$. This flow in turn selects specific values of the phase $\phi = 0$ and $\phi = \pi$. Indeed these phases are the only that preserve the reversbility symmetry $(x \to -x, v \to v)$. It follows that the two branches of homoclinic orbits given in Theorem 10.2.1 or equivalently the two branches of localized states bifurcate subcritically from $\lambda = 0$ ($c_1^1 < 0$ in Lemma 10.2.1). This is illustrated in Figure 10.2. Along the $\phi = 0$ branch, also called *up branch*, the midpoint ($x = 0$) of the localized state is always a local maximum, while along the $\phi = \pi$ branch, also called *down branch*, the midpoint is always a local minimum.

Finally, as $\chi = \frac{c_3^0}{\mu_c c_1^1}$ and $c_1^1 < 0$, we deduce that the condition $c_3^0 < 0$ is equivalent to $\chi > 0$. From the discussion in 10.1.3, there is also a subcritical bifurcation from the trivial state of a branch of spatially periodic solutions at $\lambda = 0$ of equation (10.1).

10.3 Stability of localized solutions

10.3.1 Asymptotic stability

In this section we denote $U_0^\mu \in \mathcal{H}^4(\mathbb{R})$ a localized solution of equation (10.4) for a fixed value μ of the slope of the sigmoidal function. We linearize equation (10.1) around this localized solution:

$$\partial_t a(x,t) = -a(x,t) + \mu\int_{\mathbb{R}} w(x-y)S_0'(\mu U_0^\mu(y))a(y,t)dy.$$

We look for perturbation of the form $a(x,t) = p(x)e^{\sigma t}$, with $p \in \mathcal{H}^4(\mathbb{R})$, and obtain

$$(\sigma+1)\,p(x) = \mu\int_{\mathbb{R}} w(x-y)S_0'(\mu U_0^\mu(y))p(y)dy. \tag{10.30}$$

Due to the translation invariance of equation (10.1) ($\sigma = 0, \partial_x U_0^\mu$) is always solution of the above equation. It follows that U_0^μ cannot be asymptotically stable. Nevertheless, it is possible to define a notion of stability adapted to this problem as we will now show. Let $\mathcal{T}_\rho$ be the transformation on $u \in \mathcal{H}^4(\mathbb{R})$ such that $\mathcal{T}_\rho u(x) = u(x+\rho)$ ($\rho \in \mathbb{R}$). Then $\mathcal{T}_\rho$ commutes with equation (10.1) for all $\rho \in \mathbb{R}$. We define the "$\mathcal{T}$-orbit" of the stationary localized solution $U_0^\mu \in \mathcal{H}^4(\mathbb{R})$ of equation (10.4) by

$$\mathcal{O} = \{\mathcal{T}_\rho U_0^\mu \mid \rho \in \mathbb{R}\}. \tag{10.31}$$

For all $u, v \in \mathrm{L}^2(\mathbb{R})$, we set:

$$\langle u, v\rangle = \int_{\mathbb{R}} u(x)v(x)dx. \tag{10.32}$$

We can now define the *normal slice* $\mathcal{N}$ to $\mathcal{O}$ at U_0^μ as the set:

$$\mathcal{N} = \{v \in \mathrm{L}^2(\mathbb{R}) \mid \langle \partial_x U_0^\mu, v\rangle = 0\} \subset \mathrm{L}^2(\mathbb{R}). \tag{10.33}$$

Remark 10.3.1. *Note that $U_0^\mu \in \mathcal{N}$. Indeed:*

$$\langle \partial_x U_0^\mu, U_0^\mu\rangle = \int_{\mathbb{R}} \partial_x U_0^\mu(x) U_0^\mu(x)dx = \frac{1}{2}\left[(U_0^\mu(x))^2\right]_{-\infty}^{+\infty} = 0,$$

because $U_0^\mu \in L^2(\mathbb{R})$.

Then we have the following decomposition.

Lemma 10.3.1. *Let $\mathcal{V}$ a neighbourhood of U_0^μ in $L^2(\mathbb{R})$, then any $V \in \mathcal{V}$ can be decomposed into*

$$V = \mathcal{T}_\rho\,(U_0^\mu + Y) \tag{10.34}$$

where $Y \in \mathcal{N}$ and $\rho \in \mathbb{R}$.

Proof. For $V \in \mathcal{V}$, we define the function f as

$$f : \rho \to f(\rho) = \langle \mathcal{T}_{-\rho} U_0^\mu, V\rangle = \int_{\mathbb{R}} U_0^\mu(x-\rho)V(x)dx. \tag{10.35}$$

(i) We know that $\mathcal{C}_c^\infty(\mathbb{R})$, the set of differentiable functions of compact support, is dense in $\mathrm{L}^2(\mathbb{R})$ [Brezis 1983]. Then, there exists a sequence $V_n \in \mathcal{C}_c^\infty(\mathbb{R})$, such that $V_n \underset{n\to+\infty}{\longrightarrow} V$ in $\mathrm{L}^2(\mathbb{R})$. We define f_n as

$$f_n : \rho \to f_n(\rho) = \langle \mathcal{T}_{-\rho} U_0^\mu, V_n\rangle. \tag{10.36}$$

For all $\rho \in \mathbb{R}$, we have

$$|f_n(\rho) - f(\rho)| \leq \|U_0^\mu\|_{\mathrm{L}^2(\mathbb{R})}\|V_n - V\|_{\mathrm{L}^2(\mathbb{R})} \underset{n\to+\infty}{\longrightarrow} 0,$$

where $\|\cdot\|_{\mathrm{L}^2(\mathbb{R})}$ is the norm associated to the scalar product (10.37). This implies that f_n uniformaly converges to f. Because $V_n \in \mathcal{C}_c^\infty(\mathbb{R})$, we deduce that $f_n(\rho) \underset{\rho\to\pm\infty}{\longrightarrow} 0$ and then $f(\rho) \underset{\rho\to\pm\infty}{\longrightarrow} 0$.

(ii) Moreover, from the Sobolev inequality [Brezis 1983], the injection $\mathcal{H}^m(\mathbb{R}) \subset \mathcal{C}^{m-1}(\mathbb{R})$ with $m \geq 1$, is continuous. Then $U_0^\mu \in \mathcal{H}^4(\mathbb{R}) \subset \mathcal{C}^3(\mathbb{R}) \subset \mathrm{L}^1_{loc}(\mathbb{R})$ where $\mathrm{L}^1_{loc}(\mathbb{R})$ is the space of functions which are integrable on any compact subset of $\mathbb{R}$. As $U_0^\mu(x) = U_0^\mu(-x)$, it is straightforward that $f_n(\rho) = V_n * U_0^\mu(\rho)$, where $*$ is the convolution on the real line. From the property of the convolution, f_n is $\mathcal{C}^\infty$ on $\mathbb{R}$ for all $n \geq 1$ and it is easy to see that:

$$f_n'(\rho) = -\langle \mathcal{T}_{-\rho} \partial_x U_0^\mu, V_n \rangle.$$

For all $\rho \in \mathbb{R}$, we have

$$|f_n'(\rho) + \langle \mathcal{T}_{-\rho} \partial_x U_0^\mu, V \rangle| \leq \|\partial_x U_0^\mu\|_{\mathrm{L}^2(\mathbb{R})} \|V_n - V\|_{\mathrm{L}^2(\mathbb{R})} \underset{n \to +\infty}{\longrightarrow} 0.$$

This implies that f_n' uniformly converges to the function $\rho \to -\langle \mathcal{T}_{-\rho} \partial_x U_0^\mu, V \rangle$. As a consequence f is $\mathcal{C}^1$ and $f'(\rho) = -\langle \mathcal{T}_{-\rho} \partial_x U_0^\mu, V \rangle$.

(iii) We can now complete the proof of the lemma by introducing the function g:

$$g(\rho) = \langle \mathcal{T}_{-\rho} U_0^\mu - V, \mathcal{T}_{-\rho} U_0^\mu - V \rangle = \|U_0^\mu\|^2_{\mathrm{L}^2(\mathbb{R})} + \|V\|^2_{\mathrm{L}^2(\mathbb{R})} - 2f(\rho).$$

We know that g is $\mathcal{C}^1(\mathbb{R})$ and $g(\rho) \underset{\rho \to \pm\infty}{\longrightarrow} \|U_0^\mu\|^2_{\mathrm{L}^2(\mathbb{R})} + \|V\|^2_{\mathrm{L}^2(\mathbb{R})}$. This implies that g has a minimum at $\rho = \rho_0 \in \mathbb{R}$ where $g'(\rho_0) = 0$. This is equivalent to

$$0 = f'(\rho_0) = -\langle \mathcal{T}_{-\rho_0} \partial_x U_0^\mu, V \rangle = -\langle \partial_x U_0^\mu, \mathcal{T}_{\rho_0} V \rangle.$$

We deduce that $\mathcal{T}_{\rho_0} V - U_0^\mu \in \mathcal{N}$, this proves the existence of $Y \in \mathcal{N}$ such that $\mathcal{T}_{\rho_0} V = U_0^\mu + Y$.

□

We can apply the previous Lemma and decompose any solution $V \in \mathcal{V}$ of equation (10.1) as

$$V(x,t) = \mathcal{T}_{\rho(t)} \left(U_0^\mu(x) + Y(x,t) \right)$$

where $t \to \rho(t) \in \mathcal{C}^1(\mathbb{R})$ and $t \to Y(x,t) \in \mathcal{C}^1(\mathbb{R}, \mathcal{N})$. Replacing $V(x,t)$ into equation (10.1) and thanks to the translational equivariance of $\mathcal{F}$, we obtain the new equation

$$\partial_t Y(x,t) + \rho'(t) \partial_x U_0^\mu(x) + \rho'(t) \partial_x Y(x,t) = \mathcal{F}(U_0^\mu(x) + Y(x,t), \mu). \tag{10.37}$$

We shall now decompose equation (10.37) into two parts: one part on the tangent space $T_{U_0^\mu}\mathcal{O} = \mathrm{Span}(\partial_x U_0^\mu)$, which will solve $\rho'(t)$, and the remaining part in the normal slice $\mathcal{N}$ to $\mathcal{O}$ at U_0^μ, which will contain the relevant information about the dynamics near $\mathcal{O}$. We define a projection $\mathcal{P}$ in $\mathcal{H}^4(\mathbb{R})$ onto $T_{U_0^\mu}\mathcal{O}$ by

$$\mathcal{P} u = \langle u, \partial_x U_0^\mu \rangle \frac{\partial_x U_0^\mu}{\|\partial_x U_0^\mu\|} \tag{10.38}$$

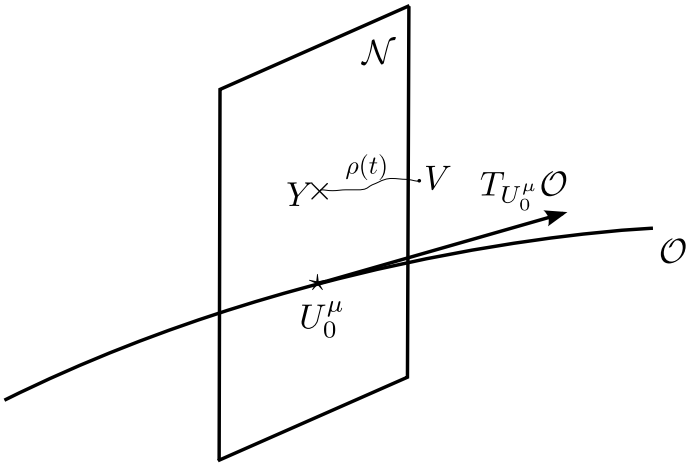

Figure 10.1: Decomposition of the flow near the relative equilibrium U_0^μ.

Let us now apply $\mathcal{P}$ to equation (10.37). Then, since $Y \perp T_{U_0^\mu}\mathcal{O}$, we obtain the following equation

$$\rho'(t)\left(1+\mathcal{P}\partial_x Y(x,t)\right) = \mathcal{P}\mathcal{F}(U_0^\mu(x)+Y(x,t),\mu). \tag{10.39}$$

Since $U_0^\mu + Y$ is taken in a neighbourhood of U_0^μ, Y is small in norm, such that the left hand side of equation (10.39) is invertible. Therefore $\rho'(t)$ can be solved in function of Y and μ:

$$\rho'(t) = \left(1+\mathcal{P}\partial_x Y(x,t)\right)^{-1}\mathcal{P}\mathcal{F}(U_0^\mu(x)+Y(x,t),\mu) \text{ for } Y \in \mathcal{V}\cap\mathcal{N}.$$

It follows that ρ is completely determined as a function of Y and μ.

The remaining equation in the normal slice $\mathcal{N}$ reads as

$$\begin{aligned}\partial_t Y(x,t) &= (Id-\mathcal{P})\left[\mathcal{F}(U_0^\mu(x)+Y(x,t),\mu) - \rho'(t)\partial_x Y(x,t)\right],\\ &= \mathcal{G}(Y(x,t),\mu).\end{aligned} \tag{10.40}$$

This decomposition is illustrated in Figure 10.1. It follows that the dynamics near the relative equilibrium U_0^μ is completely determined by the asymptotic behavior of the solutions of (10.40). If in particular $Y=0$ is asymptotically stable for (10.40), then it follows from the Lemma 10.3.1 that the $\mathcal{T}_\rho$-orbit $\mathcal{O}$ is an attractor for equation (10.1). This justifies the following definition.

Definition 10.3.1. *A localized solution $U_0^\mu \in \mathcal{H}^4(\mathbb{R})$ of equation (10.1) is orbitally stable, if for any initial condition of the form $V_0 = \mathcal{T}_{\rho_0}(U_0^\mu + Y_0)$, $\rho_0 \in \mathbb{R}$ and Y_0 close to $\mathcal{O}$ in $\mathcal{N}$, the solution $V(t)$ of (10.1) such that $V(0)=V_0$ satisfies $V(t) = \mathcal{T}_{\rho(t)}(U_0^\mu + Y(t))$ with $Y(t)$ solution of equation (10.40) and $Y(t) \underset{t\to+\infty}{\longrightarrow} 0$ in $\mathcal{N}$.*

If the spectrum of the linearized operator $D_Y\mathcal{G}(Y,\mu)|_{Y=0}$ lies entirely in the half plane $\{\Re(z) \le \xi < 0\}$, the localized solution $U_0^\mu \in \mathcal{H}^4(\mathbb{R})$ is orbitally stable. For $\mu < \mu_c$, we have already seen that the trivial solution $a_0 = 0$ is asymptotically stable

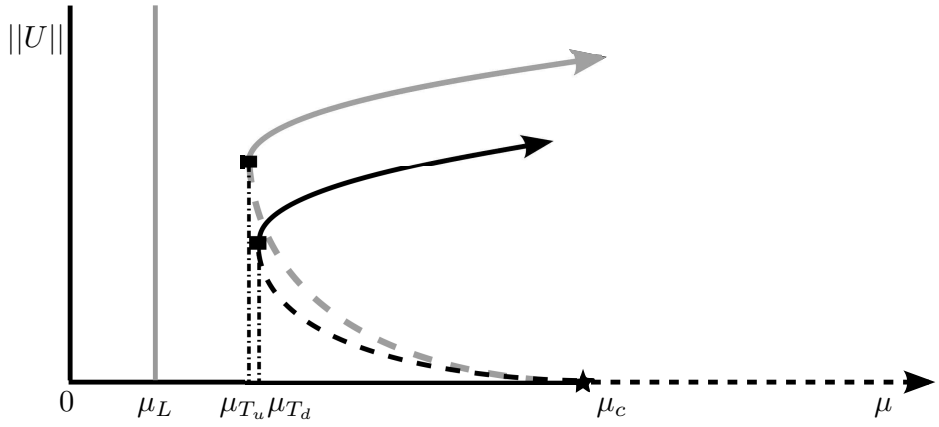

Figure 10.2: Bifurcation diagram for branches of localized stationary solutions of (10.1) with their stability. Solid (dashed) lines indicates stable (unstable) states. Grey (black) indicates the down (up) branch.

for the full neural field equation (10.1). The bifurcation at $\mu = \mu_c$ is subcritical for the reduced system (10.22) such that the two branches of homoclinic orbits are then orbitally unstable for the full neural field equation (10.1). It follows that these two branches are oriented backward. Let us follow these branches of solutions by decreasing values of μ. We introduce the following constant:

$$\mu_L = \frac{1}{\sup_{x\in\mathbb{R}} |S_0'(x)|\widehat{w}_c}.$$

An open question is to know if there exists or not a *turning point* $\mu_T \in]\mu_L, \mu_c[$ for each branch of solutions, denoted μ_{T_u} for the up branch and μ_{T_d} for the down one. At these turning points, there should be an exchange of stability and the branches should gain stability for $\mu > \mu_{T_s}$, $s \in \{u, d\}$. This is illustrated in Figure 10.2. Unfortunately, we can only conjecture the existence of such points. Nevertheless our numerical simulations support this scenario (see 10.4). A rigorous proof of the existence of orbitally stable localized solutions is a challenging problem.

10.3.2 Stability against perturbations in the connectivity function

The aim of the end of this section is to see under which conditions an orbitally stable localized solution $U_0^\mu \in \mathcal{H}^4(\mathbb{R})$ of equation (10.1) is transformed when we perturb the connectivity function w. We define a new connectivity function w^ε for all $\varepsilon \geq 0$ as

$$w^\varepsilon(x) = b_1 e^{-\sigma_1\left((1-\varepsilon)|x|+\varepsilon x^2\right)} - b_2 e^{-\sigma_2\left((1-\varepsilon)|x|+\varepsilon x^2\right)}, \tag{10.41}$$

such that w^ε is a homotopy from w to a difference of Gaussian functions.

Theorem 10.3.1. *Suppose that $U_0^\mu \in \mathcal{H}^4(\mathbb{R})$ is a solution of (10.1) and that the linearized operator $D_Y\mathcal{G}(Y,\mu)|_{Y=0}$ is invertible for a given fixed $\mu \in]\mu_L, \mu_c[$. Then, there exists $\eta > 0$ such that for all $\varepsilon \in]0, \eta[$ there exists a unique solution $U_\varepsilon^\mu \in L^2(\mathbb{R})$*

solution of

$$U_\varepsilon^\mu(x) = \int_{\mathbb{R}} w^\varepsilon(x-y) S_0(\mu U_\varepsilon^\mu(y)) dy. \tag{10.42}$$

In particular, if U_0^μ is orbitally stable than U_ε^μ is also orbitally stable.

Proof.

1. We look for solution of the form $U_\varepsilon^\mu(x) = \mathcal{T}_{\rho_\varepsilon}\left(U_0^\mu(x) + Y(x)\right)$, with $Y \in \mathcal{N}$ and $\rho_\varepsilon \in \mathbb{R}$. Replacing U_ε^μ into equation (10.42) and thanks to the translation invariance we obtain:

   $$U_0^\mu + Y = w^\varepsilon * S(\mu(U_0^\mu + Y)).$$

   Projecting onto $\mathcal{N}$ we have:

   $$0 = \mathcal{F}_\mu(U_0^\mu + Y, \varepsilon), \tag{10.43}$$

   where $\mathcal{F}_\mu(U, \varepsilon) = (Id - \mathcal{P})\left(-U + w^\varepsilon * S(\mu U)\right)$.

2. We now show that $\varepsilon \to \int_{\mathbb{R}} w^\varepsilon(x-y) S(\mu U(y)) dy$ is $\mathcal{C}^1$ on $\mathbb{R}^+$.

   - $y \to w^\varepsilon(x-y) S(\mu U(y)) \in \mathrm{L}^1(\mathbb{R})$,
   - $\varepsilon \to w^\varepsilon(x-y) S(\mu U(y)) \in \mathcal{C}^1(\mathbb{R}^+)$,
   - For all $K > 0$ and all $\varepsilon \in [0, K]$ we have that:

     $$\left|\partial_\varepsilon\left(w^\varepsilon(x)\right)\right| \leq g(x) \in \mathrm{L}^1(\mathbb{R})$$

     with

     $$g(x) = \begin{cases} |x^2 - |x||e^{-x} & x \geq 1 \\ |x^2 - |x||e^{-x\frac{K}{4}} & x \leq 1. \end{cases}$$

     Then form the theorem of differentiation under the integral sign, we have the result.

3. Equation (10.43) is an implicit equation. From the regularity of the sigmoidal function, it is clear that $y \to \mathcal{F}_\mu(U_0^\mu + Y, \varepsilon)$ is $\mathcal{C}^1$ on $\mathcal{N}$. Furthermore, we have $\mathcal{F}_\mu(U_0^\mu, 0) = 0$ and

   $$D_Y \mathcal{F}_\mu(U_0^\mu + Y, \varepsilon)|_{Y=0,\varepsilon=0} = D_Y \mathcal{G}(Y, \mu)|_{Y=0}.$$

   From our hypothesis, we have that $D_Y \mathcal{F}_\mu(U_0^\mu + Y, \varepsilon)|_{Y=0,\varepsilon=0}$ is an invertible operator from $\mathcal{N}$ to $\mathcal{N}$.

4. We can apply the implicit function theorem which says that there exists $\eta > 0$ such that for all $\varepsilon \in]0, \eta[$, $\varepsilon \to Y_\varepsilon \in \mathcal{N}$ is solution of (10.43). Then, $U_\varepsilon^\mu = \mathcal{T}_{\rho_\varepsilon}\left(U_0^\mu + Y_\varepsilon\right)$ is a solution of (10.41) for all $\rho_\varepsilon \in \mathbb{R}$.

□

10.4 Numerical results

10.4.1 Tuning the parameters

Before studying localized solutions in the model it is first necessary to identify parameter ranges for which they exist. The sign of c_3^0 in the normal form equation (10.26) governs the existence of localized solutions as discussed in section 10.2.3. The coefficient c_3^0 depends upon the connectivity function parameters $(b_1, b_2, \sigma_1, \sigma_2)$ and the threshold of the firing rate function θ. We now describe a reduction the set of parameters governing the shape of the connectivity function. Firstly, space can be rescaled such that, without loss of generality, $\sigma_1 = 1$. In our bifurcation analysis, we have seen that the important quantities for the connectivity function are $\widehat{w}_0, \widehat{w}_c$ and ξ_c, which determine the overall shape of the Fourier transform of w. In order to fix the period of the critical modes bifurcating from the trivial state $a_0 = 0$ at $\mu = \mu_c$ to 2π, we imposed that $\xi_c = 1$ in Hypothesis 10.1.2; see subsection 10.1.2. Furthermore, the connectivity function can be reparameterized in terms of $(\widehat{w}_0, \widehat{w}_c)$ by means of the following transformation:

$$\begin{aligned} \sigma_2 &= \sqrt{\frac{\widehat{w}_c}{\widehat{w}_c - \widehat{w}_0}}, \\ b_1 &= -\frac{2\widehat{w}_c(\widehat{w}_c - \widehat{w}_0)}{\widehat{w}_0}, \\ b_2 &= -\frac{(2\widehat{w}_c - \widehat{w}_0)^2}{2\widehat{w}_0}\sqrt{\frac{\widehat{w}_c}{\widehat{w}_c - \widehat{w}_0}}. \end{aligned}$$

Finally, in order to express the connectivity function in terms of a single parameter, we fix $\widehat{w}_0 = -1$. Recall that $\widehat{w}_0$ has to be negative in order to ensure the existence of a unique trivial solution a_0 of equation (10.1). The connectivity function only depends upon $\widehat{w}_c$ and can be written:

$$w(x) = 2\widehat{w}_c(\widehat{w}_c + 1)e^{-|x|} - \frac{(2\widehat{w}_c + 1)^2}{2}\sqrt{\frac{\widehat{w}_c}{\widehat{w}_c + 1}}e^{-\sqrt{\frac{\widehat{w}_c}{\widehat{w}_c+1}}|x|}.$$

It follows directly from the above discussion that, defined in this way, w satisfies the conditions $\widehat{w}_0 = -1$ and $\xi_c = 1$.

We plot the contour $c_3^0 = 0$ as a function of $(\widehat{w}_c, \theta)$ in Figure 10.3. We can see that there exists a non empty region of the parameters where the condition $c_3^0 < 0$ is satisfied; therefore, there exist branches of spatially localized solutions within this region. For small values of θ $c_3^0 > 0$ and spatially localized solutions do not exist.

10.4.2 Numerical computation of the stability of localized solutions

In order to numerically investigate the stability of a localized solution U_0^μ of equation (10.1), we have to solve the following eigenvalue problem. We start from equation (10.30) with $p \in \mathcal{H}^4(\mathbb{R})$ and apply the PDE method developed in 10.2.1. We obtain:

$$(\sigma + 1)\mathcal{L}_0\left(p(x)\right) = \mu\left(\Gamma_1 - \Gamma_2\partial_{x^2}^2\right)\left[S_0'(\mu U_0^\mu(x)p(x)\right] \tag{10.44}$$

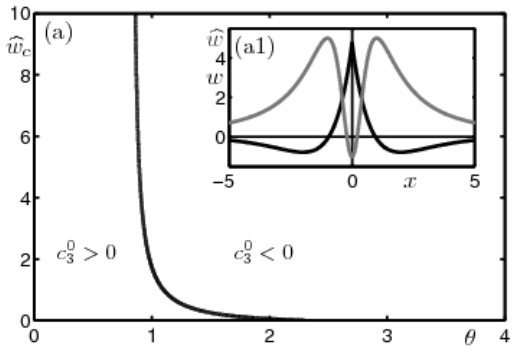

Figure 10.3: Coefficient c_3^0 and connectivity function. (a) Shows the curve $c_3^0 = 0$ in the $(\theta, \widehat{w}_c)$-plane; for values to the right of this curve $c_3^0 < 0$. Inset (a1) shows the wizard hat connectivity function w and its Fourier transform $\widehat{w}$ for $\widehat{w}_c = 5$.

where $\mathcal{L}_0 = \partial^4_{x^4} - (\sigma_1^2 + \sigma_2^2)\partial^2_{x^2} + \sigma_1^2\sigma_2^2$. For all $p \in \mathcal{H}^4(\mathbb{R})$ and $q \in \mathrm{L}^2(\mathbb{R})$, we set $\mathcal{L}_0 p = q$. As the spectrum of $\mathcal{L}_0$ is given by $\mathrm{spec}_{\mathcal{L}_0} = \{\xi^4 + (\sigma_1^2 + \sigma_2^2)\xi^2 + \sigma_1^2\sigma_2^2 \mid \xi \in \mathbb{R}\} \subset [\sigma_1^2\sigma_2^2, +\infty[$, $\mathcal{L}_0$ is an invertible operator and $p = \mathcal{L}_0^{-1} q$. It follows that equation (10.44) can be rewritten:

$$\sigma q(x) = -q(x) + \mu \left(\Gamma_1 - \Gamma_2 \partial^2_{x^2}\right) \left[S_0'(\mu U_0^\mu(x) \mathcal{L}_0^{-1} q(x)\right] = \mathcal{B}(q(x)).$$

Now, for every solution U_0^μ discretized on a domain $[-L, 0]$, we compute the eigenvalues σ of the corresponding discretized version of the linear operator $\mathcal{B}$ where we use finite differences methods to approximate the Laplacian operator $\partial^2_{x^2}$. As we numerically work on a finite domain, the 0 eigenvalue due to translation invariance in the full model is not present in the spectrum of the discretized version of the operator $\mathcal{B}$. When all eigenvalues have negative real part, then the solution is orbitally stable, otherwise it is unstable.

10.4.3 Snaking behaviour and localized solutions varying μ

In this section we use the numerical continuation package AUTO [Doedel 1997] with the extension HOMCONT to compute homoclinic solutions of the system of ODEs described by (10.23). Solutions of this system corresponds to steady states of the neural field equation (10.1) where the spatial coordinate x has been recast as the time variable in the ODE system.

Starting data for the continuation analysis is obtained by solving the system (10.23) on the half-interval $x \in [-L, 0]$ with the four boundary conditions $u_1(-L) = u_3(-L) = u_1(0) = u_3(0) = 0$; a boundary value problem (BVP) solver in the software package Matlab was used. Based on the analytical results presented in this paper, for fixed $(\widehat{w}_c, \theta)$ we set μ to a value less than but still close to μ_c, where two types of unstable localized solutions are known to exist as discussed in subsection 10.2.4. Up solutions, for which $u_1(0) > 0$, and down solutions, for which $u_1(0) < 0$, are found by providing different initial conditions to the BVP solver.

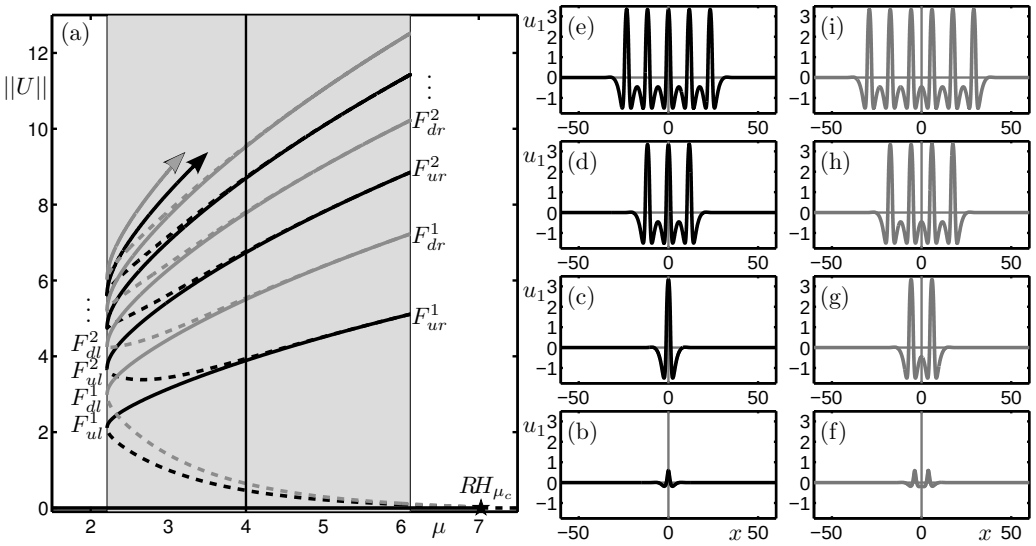

Figure 10.4: Snaking behaviour and localized solutions at $\widehat{w}_c = 5$ and $\theta = 3.5$. (a) Bifurcation diagram in μ where stable branches are solid curves and unstable branches are dashed curves. A trivial branch of solutions undergoes a reversible Hopf bifurcation at RH_{μ_c}. Bifurcating branches corresponding to up solutions are black and to down solutions are grey. These branches undergo a series of fold bifurcations that bound a μ-range (shaded gray) in which localized solutions exist; see text. A vertical gray line corresponds to $\mu = 4$. (b) Solution profile at $\mu = 4$ on the lowest unstable up solution branch. (c)–(e) Solution profiles at $\mu = 4$ on the subsequent stable up solution branch segments. (f) Solution profile at $\mu = 4$ on the lowest unstable down solution branch. (g)–(i) Solution profiles at $\mu = 4$ on the subsequent stable down solution branch segments.

Using these solutions as starting data in AUTO, branches of localized solutions were tracked under the variation of μ.

Figure 10.4 shows a bifurcation diagram in the parameter μ that gives an exact qualitative agreement with the analytical results as summarized in Figure 10.2. A branch of trivial solutions ($||U|| = 0$) is stable for $\mu < \mu_c$ and unstable after undergoing a reversible Hopf bifurcation RH_{μ_c} at $\mu = \mu_c$. There are two subcritical, unstable bifurcating branches, one corresponding to the up solution and one corresponding to the down solution. The up and down branches undergo fold bifurcations at F^1_{ul} and F^1_{dl} in which the branches gain stability as predicted analytically. A series of fold bifurcations F^n_* bound a region in which stable localized solutions persist, with additional bumps added with increasing n, moving up the diagram. In the subscript notation for the folds u and d correspond to up and down solutions, whereas l and r correspond to the left and right boundaries of the region in which stable localized solutions persist.

The panels (b)–(i) in Figure 10.4 show the solution profiles u_1 of the homoclinic

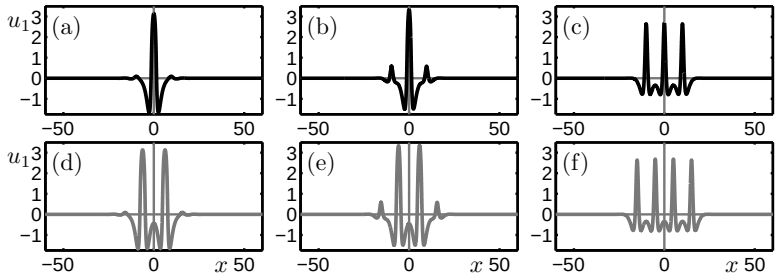

Figure 10.5: Adding of a bump through fold bifurcations. (a) Solution profile at F^1_{ur}. (b) Solution profile at $\mu = 4$ on unstable branch between F^1_{ur} and F^2_{ul}. (c) Solution profile at F^2_{ul}. (a) Solution profile at F^1_{dr}. (b) Solution profile at $\mu = 4$ on unstable branch between F^1_{dr} and F^2_{dl}. (c) Solution profile at F^2_{dl}.

cycles on the full interval $x \in [-L, L]$ by taking into account the reflectional symmetry about $x = 0$. All panels correspond to solutions at $\mu = 4$. The bottom panels (b) and (f) are from the lowest unstable up and down branches, respectively. Subsequent panels show solutions from the stable branch segments only; for example, panel (c) from the stable up branch between F^1_{ul} and F^1_{ur}, panel (g) from the stable down branch between F^1_{dl} and F^1_{dr}, and so on. In general, for the up case there are $2n - 1$ bumps on the stable branch between F^n_{ul} and F^n_{ur} and for the down case there are $2n$ bumps on the stable branch between F^n_{dl} and F^n_{dr}. The computations terminate (arrows in panel (a)) at $n = 4$; beyond this the model will no longer be valid when the localized solutions approach the limits of finite domain at $x = \pm L$.

In order to illustrate the way in which bumps are added we show in Figure 10.5 solution profiles at the right-hand folds for $n = 1$, at the left-hand folds for $n = 2$ and at the intermediate value of $\mu = 4$ on the unstable branches connecting these fold points. Panels (a)–(c) show the up case and panels (d)–(f) show the down case. One can see in panels (a) and (d) that at the right-hand fold points (F^1_{ur} and F^1_{dr}) the new bump first appears; the bumps gradually grow along the unstable branch between the fold points as shown in panels (b) and (e) and are finally the same size as the existing bumps at the left-hand fold point (F^2_{ul} and F^2_{dl}), as shown in panels (c) and (f). Note that with decreasing μ the overall range in u_1 of the solutions decreases approaching the left-hand fold points (F^2_{ul} and F^2_{dl}), but increases again on the stable branch; compare Figure 10.5(a) with Figure 10.4(d) and Figure 10.5(e) with Figure 10.4(h). The sequence described is analagous for the addition of further bumps.

10.4.4 Regions of localized solutions in the parameter plane

In the previous section, for specific values of the critical Fourier mode $\widehat{w}_c = 5$ and the threshold $\theta = 3.5$, we identified a particular range of μ for which localized solutions exist. The aim here is to show that localized solutions exist over a range of the other system parameters and are not an isolated phenomena in parameter

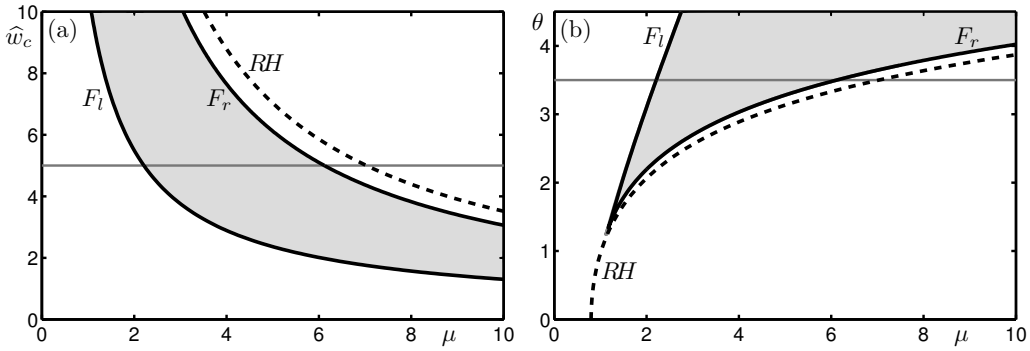

Figure 10.6: Two-parameter bifurcation diagrams. (a) Bifurcation curves in the $(\mu, \widehat{w}_c)$-plane. The locus of the reversible Hopf bifurcation *RH* is a dashed black curve. The loci of the left-hand F_l and right-hand F_r fold bifurcations in the snaking structure shown in Figure 10.4 are solid black curves. A horizontal gray line corresponds with $\widehat{w}_c = 5$, the value used in Figure 10.4. (b) Similarly indicated bifurcation curves plotted in the (μ, θ)-plane. The fold curves F_l and F_r are connected at a cusp point. A horizontal gray line corresponds with $\theta = 3.5$ the value used in Figure 10.4.

space. Further, we aim to identify exactly the ranges of the three parameters μ, $\widehat{w}_c$ and θ for which localized solutions perist. First we observe that, as shown in Figure 10.4(a), all the μ-values associated with the fold points for both the up and down solutions are aligned on the left and right boundaries as demarkated by the gray shaded region. Therefore, assuming that this is also the case when $\widehat{w}_c$ and θ are varied, we can find bounds of regions for which localized solutions exist; for example, in the $(\mu, \widehat{w}_c)$-plane it is sufficient to track the loci of the fold points F^1_{ul} and F^1_{ur} under the simultaneous variation of those two parameters. We denote the coinciding fold points at the left-hand boundary as F_l and the coinciding fold points at the right-hand boundary F_r.

Figure 10.6(a) and (b) show curves that are the loci of bifurcations in the $(\mu, \widehat{w}_c)$ and (μ, θ) parameter planes, respectively. In each panel, the curve *RH* is the locus of the reversible hopf bifurcation at μ_c, which is determined analytically by the expression $\mu_c = (s_1 \widehat{w}_c)^{-1}$. The curves F_l and F_r bound the region for which localized solutions persist (shaded in gray). A horizontal line in each panel corresponds to the default values of $\widehat{w}_c$ and θ used in Figure 10.4. Under the variation of μ and $\widehat{w}_c$, shown in Figure 10.6(a), there is a channel in parameter space for which localized solutions exist; as $\widehat{w}_c$ is increased the channel becomes narrower in μ and shifts to lower values of μ; as $\widehat{w}_c$ is decreased the channel becomes wider in μ and shifts to higher values of μ. Under the variation of μ and θ as shown in Figure 10.6(b) the range of μ for localized solutions grows and shifts to the right with increasing θ. For decreasing θ the μ range decreases and contracts to a cusp point that is effectively lower bound on θ, below which there are no localized solutions. We note

that in both cases the localized solutions always exist before the reversible Hopf. Therefore, the localized solutions coexist with a stable trivial solution.

In [Coombes 2003], the authors present a snaking diagram computed under the variation of the threshold of the sigmoidal function θ; in their formalism the sigmoid slope is $\mu = 30$. Their connectivity function was taken to be $w(x) = \frac{w_0}{4}(1-|x|)e^{-|x|}$ with Fourier transform $\widehat{w}(\xi) = w_0 \frac{\xi^2}{(1+\xi^2)^2}$, which gives $\widehat{w}_0 = 0$, $\xi_c = 1$ and $\widehat{w}_c = \frac{w_0}{4} > 0$. In Figure 10.6(b) we recover their result: for a fixed value of μ and $\widehat{w}_c$, increasing the threshold leads to a supercritical reversible Hopf bifurcation. Note that, even though the bifurcation is supercritical, the trivial solution is unstable before the bifurcation and gains stability at the *RH* point. In [Laing 2002, Elvin 2010] the authors presented a study of snaking-type behaviour; however, as was noted in [Laing 2002], the normal form theory that we have developed in this article is not applicable in their formalism, such that it is difficult to characterize their results from a bifurcation point of view. The shape of the snaking diagrams plotted in [Laing 2002, Elvin 2010] shows that, when increasing the parameter b in equation 9.4 (the equivalent of $\widehat{w}_c$ in our setting), branches of localized solutions have the opposite orientation to Figure 10.4(a). This suggests a supercritical type of bifurcation in b; we conjecture that the difference in behaviour is mainly due to the shape of nonlinearity S which is not analytical at the trivial solution in [Laing 2002, Elvin 2010].

10.5 Conclusion

In this chapter we have presented a neural field equation set on the real line with a "wizard hat" connectivity function and an analytical firing rate function. Applying successively a Fourier transform and then an inverse Fourier transform to our system, we have been able to transform our initial integro-differential equation into a partial differential equation involving spatial derivatives of even order. Time-independant spatially localized solutions of our problem satisfy a fourth order reversible dynamical system in the space variable. For some critical value of the slope of the firing rate function, a Hopf bifurcation with resonance occurs from the trivial state. We have computed the coefficients of the normal form for the 1:1 reversible Hopf bifurcation. This has allowed us to find sufficient conditions on the parameters of our model for the existence of homoclinic orbits to the trivial states and thus spatially localized states. We have also shown that our results extend to other types of connectivity function for which the PDE method cannot been applied (difference of Gaussian functions for example).

Numerical continuation was used to follow branches of homoclinic cycles corresponding to localized states and, thus, confirm the description of the system's solution structure both close to the reversible Hopf bifurcation and on the associated bifurcated branches (as described by the analytical results presented herein). Further, varying the sigmoid slope, we show that the system exhibits snaking behaviour: a series fold bifurcations accumulating at lower and upper limits bound

a parameter range over which stable localized solutions persist. The loci of these fold bifurcations, which can be followed using two-parameter continuation, form the boundaries of regions of localized solutions in the parameter plane. Importantly, we show that localized solutions are not an isolated phenomenon in parameter space, that they exist over wide ranges of three parameters and that it is possible to produce a snaking diagram in any of these parameters. Another important result is that, for small values of the threshold of the sigmoid function, there are no localized solutions.

Chapter 11

Radially symmetric localized states

Contents

11.1 Localized patterns in Euclidean geometry 220
11.1.1 The model 220
11.1.2 Linear stability analysis of the trivial state 221
11.1.3 PDE method 222
11.1.4 The equation near the core 222
11.1.5 The far-field equations 226
11.1.6 Matching the core and the far-field 228
11.2 Localized patterns in the Poincaré disk 232
11.2.1 Choice of the connectivity function 232
11.2.2 Linear stability of the trivial state 234
11.2.3 PDE methods in the Poincaré disk 234
11.2.4 The equation near the core 235
11.2.5 The far-field equations 243
11.3 Conclusion 246

In the planar Swift-Hohenberg equation, near a Turing instability, three types of radially symmetric localized solutions have been proven to exist: a localized ring decaying to almost zero at the core, a spot with a maximum at the origin (called Spot A) and a spot with minimum at the origin (called Spot B); see [Lloyd 2009, McCalla 2010, McCalla 2011]). In this chapter, we are only interested in the existence of Spot A (see figure 9.3(a)) as these localized solutions are the most relevant from a neuroscience point of view. Indeed, these spatially localized solutions can be seen as localized persistent activity and have been linked to working memory (the temporary storage of information within the brain). We will prove the existence of Spot A solutions for a neural field equation, with sigmoidal firing-rate function, set both on the Euclidean plane and the Poincaré disk.

This chapter is divided in two parts. The first section is dedicated to the Euclidean case. We study a neural field equation with a well chosen connectivity function, such that we can transform it into a partial differential equation on the Euclidean plane. We then apply techniques from Scheel, Lloyd and Sandstede [Scheel 2003, Lloyd 2009] to prove the existence of a bifurcated branch of Spot A solution near a Turing instability. The main theorem of this section is given in

11.1.1. In the second section, we study the existence of radially symmetric localized solutions for a neural field equation set on the Poincaré disk. We have adapted the PDE method developed by Troy and Laing [Laing 2003a] and the analysis conducted by Scheel, Lloyd and Sandstede in the context of hyperbolic geometry. The main theorem of this section is given in 11.2.1.

11.1 Localized patterns in Euclidean geometry

11.1.1 The model

We consider the Wilson-Cowan neural field equation for one population of neurons:

$$\frac{d}{dt}v(\mathbf{r},t) = -v(\mathbf{r},t) + \int_{\mathbb{R}^2} W(\|\mathbf{r}-\mathbf{r}'\|)S(\mu v(\mathbf{r}',t))d\mathbf{r}' \tag{11.1}$$

where $\|\cdot\|$ is the standard Euclidean norm. The nonlinearity S is defined by

$$S(x) = \frac{1}{1+e^{-x+\theta}} - \frac{1}{1+e^{\theta}}. \tag{11.2}$$

The connectivity function W is defined through its Hankel transform in the following way:

$$W(x) = \int_0^{+\infty} s\widehat{W}(s)J_0(xs)ds, \quad \widehat{W}(s) = 2\left(\frac{b_1\sigma_1}{\sigma_1^2+s^2} - \frac{b_2\sigma_2}{\sigma_2^2+s^2}\right). \tag{11.3}$$

$J_0(s)$ is the Bessel function of first kind and $(b_1, b_2, \sigma_1, \sigma_2)$ are real parameters. The connectivity function W has a "Mexican hat" shape. The Fourier transform of $W(\|\mathbf{r}\|)$ is $\widehat{W}(\|\mathbf{k}\|)$ for all $(\mathbf{r},\mathbf{k}) \in \mathbb{R}^2$. The parameters $(b_1, b_2, \sigma_1, \sigma_2)$ are chosen such that the following hypotheses are satisfied.

Hypothesis 11.1.1.

(i) $\widehat{W}(0) = \widehat{W}_0 < 0$,

(ii) $W(0) > 0$,

(iii) *there exists* $k_c > 0$ *such that* $\widehat{W}_c \overset{def}{=} \widehat{W}(k_c) = \max_{k=\|\mathbf{k}\|\in\mathbb{R}^+} \widehat{W}(k) > 0$,

(iv) $k_c = 1$.

Now, if we define

$$\begin{aligned} \Gamma_1 &= 2\sigma_1\sigma_2(b_1\sigma_2 - b_2\sigma_1), \\ \Gamma_2 &= 2(b_1\sigma_1 - b_2\sigma_2), \end{aligned} \tag{11.4}$$

then $\widehat{W}_c$ can be written:

$$\widehat{W}_c = \frac{\Gamma_1+\Gamma_2}{1+\sigma_1^2+\sigma_2^2+\sigma_1^2\sigma_2^2}. \tag{11.5}$$

The condition $k_c = 1$, which is equivalent to $\frac{d}{ds}\widehat{W}(s)|_{s=1} = 0$, reduces to

$$\Gamma_1(\sigma_1^2 + \sigma_2^2 + 2) + \Gamma_2(1 - \sigma_1^2\sigma_2^2) = 0. \tag{11.6}$$

It is a straightforward computation to see that equations (11.5) and (11.6) imply that:

$$\begin{aligned} \sigma_1^2\sigma_2^2 - \Gamma_1\widehat{W}_c^{-1} &= 1 \\ \sigma_1^2 + \sigma_2^2 - \Gamma_2\widehat{W}_c^{-1} &= -2. \end{aligned} \tag{11.7}$$

We denote for all $k \geq 1$, $S^{(k)}(0) = s_k$.

11.1.2 Linear stability analysis of the trivial state

Equation (11.1) has the trivial solution $v = 0$. The linearized equation around this trivial solution is:

$$\frac{d}{dt}u(\mathbf{r},t) = -u(\mathbf{r},t) + \mu s_1 \int_{\mathbb{R}^2} W(\|\mathbf{r}-\mathbf{r}'\|)u(\mathbf{r}',t)d\mathbf{r}'. \tag{11.8}$$

Looking at linear stability with $u(\mathbf{r},t) = e^{\sigma t}e^{i\mathbf{k}\cdot\mathbf{r}}$ we obtain the following dispersion relation:

$$\sigma(\|\mathbf{k}\|) = -1 + \mu s_1 \widehat{W}(\|\mathbf{k}\|). \tag{11.9}$$

Then the critical value μ_c is given by:

$$\mu_c = \frac{1}{s_1\widehat{W}_c}, \tag{11.10}$$

and for all $\mu < \mu_c$, the trivial solution $v = 0$ is stable.

We set $\lambda = \mu - \mu_c$ and rewrite equation (11.1):

$$\frac{d}{dt}v(\mathbf{r},t) = \mathbf{L}_{\mu_c}v(\mathbf{r},t) + \mathbf{R}(v(\mathbf{r},t),\lambda) \tag{11.11}$$

where $\mathbf{L}_{\mu_c}$ and $\mathbf{R}$ are defined by

$$\begin{aligned} \mathbf{L}_{\mu_c}v(\mathbf{r},t) &= -v(\mathbf{r},t) + \mu_c s_1 \int_{\mathbb{R}^2} W(\|\mathbf{r}-\mathbf{r}'\|)v(\mathbf{r}',t)d\mathbf{r}', \\ \mathbf{R}(v(\mathbf{r},t),\lambda) &= \int_{\mathbb{R}^2} W(\|\mathbf{r}-\mathbf{r}'\|)\left[S\left((\lambda+\mu_c)v(\mathbf{r}',t)\right) - \mu_c s_1 v(\mathbf{r}',t)\right]d\mathbf{r}' \end{aligned}$$

with $\mathbf{R}(0,0) = D_v\mathbf{R}(0,0) = 0$. We define $f(X,\lambda)$ by:

$$f(X,\lambda) = S\left((\lambda+\mu_c)X\right) - \mu_c s_1 X$$

where $f(0,0) = \partial_X f(0,0) = 0$.

11.1.3 PDE method

We assume that $v \to v(\cdot,t) \in \mathcal{C}^1(\mathbb{R}^+, \mathcal{H}^4(\mathbb{R}^2))$ is a solution of (11.11), where $\mathcal{H}^4(\mathbb{R}^2)$ is the Sobolev space defined as:

$$\mathcal{H}^4(\mathbb{R}^2) = \{u \in \mathrm{L}^2(\mathbb{R}^2) \mid \forall\ 0 \leq |\alpha| \leq 4\ D^\alpha u \in \mathrm{L}^2(\mathbb{R}^2)\}.$$

Under this assumption, an application of Fourier transform of equation (11.11), we obtain:

$$(\partial_t + 1)\,\widehat{v}(\mathbf{k},t) = \widehat{W}(\|\mathbf{k}\|)\left[\mu_c s_1 \widehat{v}(\mathbf{k},t) + \widehat{f(v,\lambda)}(\mathbf{k},t)\right]$$

Using the inverse Fourier transform we obtain:

$$(\partial_t + 1)\,\mathcal{L}_{\mu_c}(v) = \mathcal{M}(v,\lambda) \tag{11.12}$$

with $\mathcal{L}_{\mu_c}$ and $\mathcal{M}$ defined by

$$\mathcal{L}_{\mu_c}(v) = (\sigma_1^2\sigma_2^2 - \Gamma_1\mu_c s_1)v - (\sigma_1^2 + \sigma_2^2 - \Gamma_2\mu_c s_1)\Delta v + \Delta^2 v$$

and

$$\mathcal{M}(v,\lambda) = \Gamma_1 f(v,\lambda) - \Gamma_2 \Delta f(v,\lambda),$$

where Δ denotes the Laplcian on $\mathbb{R}^2$. From equations (11.7) and the fact that $\mu_c = (s_1\widehat{w}_c)^{-1}$, the coefficients of $\mathcal{L}_{\mu_c}$ reduce to:

$$\begin{aligned} \sigma_1^2\sigma_2^2 - \Gamma_1\mu_c s_1 &= 1, \\ \sigma_1^2 + \sigma_2^2 - \Gamma_2\mu_c s_1 &= -2. \end{aligned}$$

We look for stationary radial solutions of equation (11.11), that is:

$$v(r) + 2\Delta_r v(r) + \Delta_r^2 v(r) = \Gamma_1 f(v(r),\lambda) - \Gamma_2 \Delta_r f(v(r),\lambda) \tag{11.13}$$

with $r = \|\mathbf{r}\| \in \mathbb{R}^+$ and $\Delta_r = \partial_r^2 + \frac{1}{r}\partial_r$. Note that $\Delta_r f(v(r),\lambda)$ can be expressed as:

$$\Delta_r f(v,\lambda) = (\Delta_r v)\, f'(v,\lambda) + (\partial_r v)^2\, f''(v,\lambda).$$

11.1.4 The equation near the core

We rewrite equation (11.13) as a four dimensional system of non-autonomous differential equations. We set:

$$\begin{aligned} \partial_r u_1 &= u_3, \\ \partial_r u_2 &= u_4, \\ \left(\partial_r^2 + \frac{1}{r}\partial_r + 1\right) u_1 &= u_2, \\ \left(\partial_r^2 + \frac{1}{r}\partial_r + 1\right) u_2 &= \Gamma_1 f(u_1,\lambda) - \Gamma_2 \Delta_r f(u_1,\lambda). \end{aligned}$$

$$\partial_r U = \mathcal{A}(r)U + \mathcal{F}(U,\lambda), \tag{11.14}$$

where

$$\mathcal{A}(r) = \begin{pmatrix} 0 & 0 & 1 & 0 \\ 0 & 0 & 0 & 1 \\ -1 & 1 & -\frac{1}{r} & 0 \\ 0 & -1 & 0 & -\frac{1}{r} \end{pmatrix} \text{ and } \mathcal{F}(U,\lambda) = \begin{pmatrix} 0 \\ 0 \\ 0 \\ \mathcal{F}_4\left(u_1,u_2,u_3,u_4,\lambda\right) \end{pmatrix}$$

with $U = (u_1,u_2,u_3,u_4)^T$ and

$$\mathcal{F}_4\left(u_1,u_2,u_3,u_4,\lambda\right) = \Gamma_1 f(u_1,\lambda) - \Gamma_2\left[(u_2-u_1)f'(u_1,\lambda) + u_3^2 f''(u_1,\lambda)\right].$$

Furthermore the quadratic term in U of $\mathcal{F}(U,\lambda)$ at $(0,0)$ is given by:

$$\mathcal{F}_{20}(U,U) = \frac{\mu_c^2 s_2}{2}\begin{pmatrix} 0 \\ 0 \\ 0 \\ (\Gamma_1+2\Gamma_2)u_1^2 - 2\Gamma_2 u_1 u_2 - 2\Gamma_2 u_3^2 \end{pmatrix}.$$

We can now apply the theory developed in [Scheel 2003, Lloyd 2009]. First, we set $\lambda = 0$ and linearize (11.14) about $U = 0$ to get the linear system $\partial_r U = \mathcal{A}(r)U$ which has four linearly independent solutions

$$\begin{aligned} V_1(r) &= \sqrt{2\pi}\left(J_0(r), 0, -J_1(r), 0\right)^{\mathbf{T}} \\ V_2(r) &= \sqrt{2\pi}\left(rJ_1(r), 2J_0(r), rJ_0(r), -2J_1(r)\right)^{\mathbf{T}} \\ V_3(r) &= \sqrt{2\pi}\left(Y_0(r), 0, -Y_1(r), 0\right)^{\mathbf{T}} \\ V_4(r) &= \sqrt{2\pi}\left(rY_1(r), 2Y_0(r), rY_0(r), -2Y_1(r)\right)^{\mathbf{T}}. \end{aligned}$$

Lemma 11.1.1. *Fix $r_0 > 0$, then there are constants δ_0, δ_1 so that the set $\mathcal{W}^{cu}_-(\lambda)$ of solutions $U(r)$ of (11.14) for which $\sup_{0\le r\le r_0}|U(r)| < \delta_0$ is, for $|\lambda| < \delta_0$, a smooth two-dimensional manifold. Furthermore, $U \in \mathcal{W}^{cu}_-(\lambda)$ with $|P^{cu}_-(r_0)U(r_0)| < \delta_1$ if only if*

$$\begin{aligned} U(r_0) = {} & \tilde{d}_1 V_1(r_0) + \tilde{d}_2 V_2(r_0) + V_3(r_0)O_{r_0}(|\lambda||\tilde{d}| + |\tilde{d}|^2) \\ & + V_4(r_0)\left(\Theta_{\tilde{d}_1^2}\tilde{d}_1^2 + \Theta_{\tilde{d}_1\tilde{d}_2}\tilde{d}_1\tilde{d}_2 + O(_{r_0})(|\lambda||\tilde{d}| + |\tilde{d}_2|^2 + |\tilde{d}|^3)\right) \end{aligned} \tag{11.15}$$

where

$$\begin{aligned} \Theta_{\tilde{d}_1^2} &= \sqrt{2\pi}\mu_c^2 s_2 \frac{\Gamma_1+\Gamma_2}{4}\left[\frac{1}{\sqrt{3}} + O(r_0^{-1/2})\right], \\ \Theta_{\tilde{d}_1\tilde{d}_2} &= -\sqrt{2\pi}\mu_c^2 s_2 \Gamma_2\left[\frac{1}{\sqrt{3}} + O(r_0^{-1/2})\right], \end{aligned}$$

for some $\tilde{d} = (\tilde{d}_1,\tilde{d}_2) \in \mathbb{R}^2$ with $|\tilde{d}| < \delta_1$, where the right hand side in (11.15) depends smoothly on $(\tilde{d},\lambda)$.

Proof. We observe that four independent solutions to the adjoint problem $\partial_r U = -\mathcal{A}^T(r)U$ are given by

$$\begin{aligned}
W_1(r) &= \frac{\sqrt{2\pi}}{8}\left(-2rY_1(r), r^2Y_0(r), -2rY_0(r), -r^2Y_1(r)\right)^{\mathbf{T}},\\
W_2(r) &= \frac{\sqrt{2\pi}}{8}\left(0, -rY_1(r), 0, -rY_0(r)\right)^{\mathbf{T}},\\
W_3(r) &= \frac{\sqrt{2\pi}}{8}\left(2rJ_1(r), -r^2J_0(r), 2rJ_0(r), r^2J_1(r)\right)^{\mathbf{T}},\\
W_4(r) &= \frac{\sqrt{2\pi}}{8}\left(0, rJ_1(r), 0, rJ_0(r)\right)^{\mathbf{T}}.
\end{aligned}$$

It follows from

$$\frac{\pi}{2}r\left(J_1(r)Y_0(r) - J_0(r)Y_1(r)\right) = 1$$

that

$$\langle V_i(r), W_j(r)\rangle_{\mathbb{R}^4} = \delta_{i,j} \quad i,j = 1,\dots,4$$

is independent of r. For given $\tilde{d} = (\tilde{d}_1, \tilde{d}_2) \in \mathbb{R}^2$, we consider the fixed-point equation:

$$\begin{aligned}
U(r) &= \sum_{j=1}^{2}\tilde{d}_jV_j(r) + \sum_{j=1}^{2}V_j(r)\int_{r_0}^{r}\langle W_j(s), \mathcal{F}(U(s),\lambda)\rangle ds\\
&\quad + \sum_{j=3}^{4}V_j(r)\int_{0}^{r}\langle W_j(s), \mathcal{F}(U(s),\lambda)\rangle ds\\
&= \sum_{j=1}^{2}\tilde{d}_jV_j(r) + \sum_{j=1}^{2}V_j(r)\int_{r_0}^{r}W_{j,4}(s)\mathcal{F}_4(U(s),\lambda) ds\\
&\quad + \sum_{j=3}^{4}V_j(r)\int_{0}^{r}W_{j,4}(s)\mathcal{F}_4(U(s),\lambda) ds
\end{aligned} \tag{11.16}$$

on $\mathcal{C}^0([0,r_0],\mathbb{R}^4)$, where $W_{j,4}(r)$ (resp. $\mathcal{F}_4(U(r),\lambda)$)denotes the fourth component of $W_j(r)$ (resp. $\mathcal{F}(U(r),\lambda)$). A direct adaptation of Lemma 1 in [Lloyd 2009] gives:

- Each solution $U \in \mathcal{C}^0([0,r_0],\mathbb{R}^4)$ of (11.16) gives a solution of (11.14) that is bounded on $[0,r_0]$.
- Every bounded solution $U \in \mathcal{C}^0([0,r_0],\mathbb{R}^4)$ of (11.14) satisfies (11.16) provided we add $\tilde{d}_3V_3(r) + \tilde{d}_4V_4(r)$ to the right hand side for an appropriate $\tilde{d} \in \mathbb{R}^4$.
- Existence of solutions of (11.16) is given by the uniform contracting mapping principle for sufficiently small $(\tilde{d}_1, \tilde{d}_2)$ and λ.
- The resulting solution U satisfies on $[0,r_0]$:

$$U(r) = \sum_{j=1}^{2}\tilde{d}_jV_j(r) + O_{r_0}(|\lambda||\tilde{d}| + |\tilde{d}|^2).$$

As in [Lloyd 2009], we need to calculate the quadratic coefficient in $\tilde{d}$ in front of $V_4(r_0)$, denoted Θ. We recall that:

$$\mathcal{F}_{2,0}(U,U) = \frac{\mu_c^2 s_2}{2}\left(0,0,0,(\Gamma_1+2\Gamma_2)u_1^2 - 2\Gamma_2 u_1 u_2 - 2\Gamma_2 u_3^2\right)^{\mathbf{T}}.$$

If we evaluate (11.16) at $r = r_0$, we arrive at (11.15) except that we need to calculate the quadratic coefficients in front of $V_4(r_0)$: using a Taylor expansion, we find that these coefficients are given by:

$$\Theta_{\tilde{d}_1^2} = \int_0^{r_0} W_{4,4}(s)\pi\mu_c^2 s_2\left[(\Gamma_1+2\Gamma_2)J_0(s)^2 - 2\Gamma_2 J_1(s)^2\right]ds$$

and

$$\Theta_{\tilde{d}_1\tilde{d}_2} = -4\int_0^{r_0} W_{4,4}(s)\pi\mu_c^2 s_2\Gamma_2 J_0(s)^2 ds.$$

Then we have:

$$\begin{aligned}
\Theta_{\tilde{d}_1^2} &= \frac{\sqrt{2\pi}\pi\mu_c^2 s_2(\Gamma_1+2\Gamma_2)}{8}\int_0^{r_0} sJ_0(s)^3 ds - \frac{\sqrt{2\pi}\pi\mu_c^2 s_2\Gamma_2}{4}\int_0^{r_0} sJ_0(s)J_1(s)^2 ds \\
&= \frac{\sqrt{2\pi}\pi\mu_c^2 s_2(\Gamma_1+2\Gamma_2)}{8}\left(\frac{2}{\pi\sqrt{3}} + O(r_0^{-1/2})\right) - \frac{\sqrt{2\pi}\pi\mu_c^2 s_2\Gamma_2}{4}\left(\frac{1}{\pi\sqrt{3}} + O(r_0^{-1/2})\right) \\
&= \frac{\sqrt{2\pi}\mu_c^2 s_2(\Gamma_1+\Gamma_2)}{4}\left(\frac{1}{\sqrt{3}} + O(r_0^{-1/2})\right)
\end{aligned}$$

and

$$\begin{aligned}
\Theta_{\tilde{d}_1\tilde{d}_2} &= -\frac{\sqrt{2\pi}\pi\mu_c^2 s_2\Gamma_2}{2}\int_0^{r_0} sJ_0(s)^3 ds \\
&= -\sqrt{2\pi}\mu_c^2 s_2\Gamma_2\left(\frac{1}{\sqrt{3}} + O(r_0^{-1/2})\right).
\end{aligned}$$

We have used the following two formulas on integral of Bessel functions:

$$\begin{aligned}
\int_0^{+\infty} J_\nu(as)J_\nu(bs)J_\nu(cs)s^{1-\nu}ds &= \frac{2^{\nu-1}\triangle^{2\nu-1}}{(abc)^\nu\Gamma(\nu+\frac{1}{2})\Gamma(\frac{1}{2})} \\
\int_0^{+\infty} J_\mu(as)J_\nu(bs)J_\nu(cs)s^{1-\mu}ds &= \frac{(bc)^{\mu-1}\sin(A)^{\mu-1/2}}{\sqrt{2\pi}a^\mu}P^{\frac{1}{2}-\mu}_{\nu-\frac{1}{2}}(\cos(A))
\end{aligned}$$

where $\triangle$ is the area of triangle with lengths a, b and c, $A = \arccos\left(\frac{b^2+c^2-a^2}{2bc}\right)$ and P is associated Legendre function. The first integral with $a = b = c = 1$ and $\nu = 0$ gives ($\triangle = \frac{\sqrt{3}}{4}$ and $\Gamma(\frac{1}{2}) = \sqrt{\pi}$):

$$\int_0^{+\infty} sJ_0(s)^3 ds = \frac{2}{\pi\sqrt{3}}$$

and the second integral with $a = b = c = 1$, $\mu = 0$ and $\nu = 1$ gives ($A = \frac{\pi}{3}$ and $P^{\frac{1}{2}}_{\frac{1}{2}}(z) = \sqrt{\frac{2}{\pi}}\frac{z}{(1-z^2)^{\frac{1}{4}}}$):

$$\int_0^{+\infty} sJ_0(s)J_1(s)^2 ds = \frac{1}{\pi\sqrt{3}}.$$

We have also used the estimations (see [McCalla 2011])

$$\int_{r_0}^{+\infty} sJ_0(s)^3 ds = O(r_0^{-1/2})$$

and

$$\int_{r_0}^{+\infty} sJ_0(s)J_1(s)^2 ds = O(r_0^{-1/2}).$$

□

11.1.5 The far-field equations

We make equation (11.14) autonomous by adding the variable $\alpha = \frac{1}{r}$ which satisfies $\partial_r \alpha = -\alpha^2$. equation (11.14) becomes:

$$\frac{d}{dr}\begin{pmatrix} u_1 \\ u_2 \\ u_3 \\ u_4 \\ \alpha \end{pmatrix} = \begin{pmatrix} u_3 \\ u_4 \\ -u_1 + u_2 - \alpha u_3 \\ -u_2 - \alpha u_4 + \mathcal{F}_4\left(u_1, u_2, u_3, u_4, \lambda\right) \\ -\alpha^2 \end{pmatrix}. \tag{11.17}$$

We use the normal-form coordinates:

$$U = \widetilde{A}\zeta_0 + \widetilde{B}\zeta_1 + \text{c.c.}, \quad U = (u_1, u_2, u_3, u_4)^T$$

or equivalently

$$\begin{pmatrix} \widetilde{A} \\ \widetilde{B} \end{pmatrix} = \frac{1}{4}\begin{pmatrix} 2u1 - i(2u_3 + u_4) \\ -u_4 - iu_2 \end{pmatrix}$$

where $\mathcal{A}(\infty)\zeta_0 = i\zeta_0$ and $\mathcal{A}(\infty)\zeta_1 = i\zeta_1 + \zeta_0$ with:

$$\mathcal{A}(\infty) = \begin{pmatrix} 0 & 0 & 1 & 0 \\ 0 & 0 & 0 & 1 \\ -1 & 1 & 0 & 0 \\ 0 & -1 & 0 & 0 \end{pmatrix}, \quad \zeta_0 = \begin{pmatrix} 1 \\ 0 \\ i \\ 0 \end{pmatrix}, \quad \zeta_1 = \begin{pmatrix} 0 \\ 2i \\ 1 \\ -2 \end{pmatrix}.$$

In these coordinates, equation (11.17) becomes

$$\begin{aligned} \partial_r \widetilde{A} &= \left(i - \frac{\alpha}{2}\right)\widetilde{A} + \widetilde{B} + \frac{\alpha}{2}\overline{\widetilde{A}} + O((|\lambda| + |\widetilde{A}| + |\widetilde{B}|)(|\widetilde{A}| + |\widetilde{B}|)) \\ \partial_r \widetilde{B} &= \left(i - \frac{\alpha}{2}\right)\widetilde{B} - \frac{\alpha}{2}\overline{\widetilde{B}} + O((|\lambda| + |\widetilde{A}| + |\widetilde{B}|)(|\widetilde{A}| + |\widetilde{B}|)) \\ \partial_r \alpha &= -\alpha^2. \end{aligned} \tag{11.18}$$

Lemma 11.1.2. *Fix $0 < m < \infty$, then there exists a change of coordinates*

$$\begin{pmatrix} A \\ B \end{pmatrix} = e^{i\phi(r)}[1 + \mathcal{T}(\alpha)]\begin{pmatrix} \widetilde{A} \\ \widetilde{B} \end{pmatrix} + O((|\lambda| + |\widetilde{A}| + |\widetilde{B}|)(|\widetilde{A}| + |\widetilde{B}|)) \tag{11.19}$$

so that (11.18) *becomes*

$$\begin{aligned}\partial_r A &= -\frac{\alpha}{2}A + B + \mathcal{R}_A(A,B,\alpha,\lambda)\\ \partial_r B &= -\frac{\alpha}{2}B + c_1^1\lambda A + c_3^0|A|^2A + \mathcal{R}_B(A,B,\alpha,\lambda)\\ \partial_r \alpha &= -\alpha^2\end{aligned} \tag{11.20}$$

The constants c_1^1 *and* c_3^0 *are given by:*

$$c_1^1 = -\frac{s_1(\Gamma_1+\Gamma_2)}{4} \tag{11.21}$$

and

$$c_3^0 = -\frac{\mu_c^3(\Gamma_1+\Gamma_2)}{4}\left[\frac{s_3}{2} + \frac{\mu_c s_2^2(19\Gamma_1+4\Gamma_2)}{18}\right]. \tag{11.22}$$

The coordinate change is polynomial in (A,B,α) *and smooth in* λ *and* $\mathcal{T}(\alpha) = O(\alpha)$ *is linear and upper triangular for each* α*, while* $\phi(r)$ *satisfies*

$$\partial_r\phi(r) = 1 + O(|\lambda| + |\alpha|^3 + |A|^2), \quad \phi(0) = 0$$

The remainder terms are given by

$$\begin{aligned}\mathcal{R}_A(A,B,\alpha,\lambda) &= O\left(\sum_{j=0}^{2}|A^jB^{3-j}| + |\alpha|^3|A| + |\alpha|^2|B| + (|A|+|B|)^5\right.\\ &\qquad \left.+|\lambda||\alpha|^m(|A|+|B|)\right)\\ \mathcal{R}_B(A,B,\alpha,\lambda) &= O\left(\sum_{j=0}^{1}|A^jB^{3-j}| + |\alpha|^3|B| + |\lambda|(|\lambda| + |\alpha|^3 + |A|^2)|A|\right.\\ &\qquad \left.+(|A|+|B|)^5 + |\lambda||\alpha|^m|B|\right).\end{aligned}$$

Proof. See [Scheel 2003] and [Lloyd 2009] for the change of variables. The coefficients c_1^1 and c_3^0 have been computed in chapter 10. □

First of all, we rescale (A,B,α) with the anticipated amplitude which is of the order of $\sqrt{|\lambda|}$. We set $\lambda = -\varepsilon$, $\varepsilon > 0$ and $c_1^0 = -c_1^1$. We define

$$A = \sqrt{\varepsilon}a, \quad B = \varepsilon b, r = \frac{\rho}{\sqrt{\varepsilon}}, \tag{11.23}$$

for which (11.20) becomes

$$\begin{aligned}\partial_\rho a &= b - \frac{a}{2\rho} + \mathcal{R}_1(a,b,\rho,\varepsilon)\\ \partial_\rho b &= -\frac{b}{2\rho} + c_1^0 a + c_3^0|a|^2a + \mathcal{R}_2(a,b,\rho,\varepsilon)\end{aligned} \tag{11.24}$$

where

$$\begin{aligned}\mathcal{R}_1(a,b,\rho,\varepsilon) &= \varepsilon^{-1}\mathcal{R}_A(\sqrt{\varepsilon}a,\varepsilon b,\frac{\sqrt{\varepsilon}}{\rho},\varepsilon) = O(\varepsilon(|a|+|b|))\\ \mathcal{R}_2(a,b,\rho,\varepsilon) &= \varepsilon^{-3/2}\mathcal{R}_B(\sqrt{\varepsilon}a,\varepsilon b,\frac{\sqrt{\varepsilon}}{\rho},\varepsilon) = O(\varepsilon(|a|+|b|))\end{aligned} \tag{11.25}$$

uniformally in $\rho \geq \rho_1$ for each fixed $\rho_1 > 0$. We also use the variables

$$\begin{pmatrix} a \\ b \end{pmatrix} = \frac{1}{\sqrt{\rho}} \begin{pmatrix} \hat{a} \\ \hat{b} \end{pmatrix} \tag{11.26}$$

in which (11.24) becomes

$$\begin{aligned}\partial_\rho \hat{a} &= \hat{b} + O(\varepsilon(|\hat{a}|+|\hat{b}|))\\ \partial_\rho \hat{b} &= c_1^0 \hat{a} + c_3^0|\hat{a}|^2\hat{a} + O(\varepsilon(|\hat{a}|+|\hat{b}|)).\end{aligned} \tag{11.27}$$

The estimates for the remainder terms given above are valid for $\rho \geq \rho_1$ for each fixed $\rho_1 > 0$. To capture the region $r_0\sqrt{\varepsilon} \leq \rho \leq \rho_1$, we use the variables

$$\begin{pmatrix} \tilde{a} \\ \tilde{b} \end{pmatrix} = \begin{pmatrix} a \\ \rho(b - \frac{a}{2\rho}) \end{pmatrix}, \quad \tau = \log\rho \tag{11.28}$$

so that $\rho = e^\tau$ and $\rho \to 0$ corresponds to $\tau \to -\infty$. In these variables, (11.27) becomes

$$\begin{aligned}\partial_\tau \tilde{a} &= \tilde{b} + \tilde{\mathcal{R}}_1(\tilde{a},\tilde{b},\rho,\varepsilon)\\ \partial_\tau \tilde{b} &= \frac{\tilde{a}}{4} + \rho^2\left(c_1^0\tilde{a} + c_3^0|\tilde{a}|^2\tilde{a}\right) + \tilde{\mathcal{R}}_2(\tilde{a},\tilde{b},\rho,\varepsilon)\\ \partial_\tau \rho &= \rho\end{aligned} \tag{11.29}$$

with $(\tilde{a},\tilde{b},\rho) \in \mathbb{C}^2 \times \mathbb{R}^+$.

11.1.6 Matching the core and the far-field

We start by linearizing the far-field equation (11.27) about $(\hat{a},\hat{b}) = 0$ to get the equation

$$\partial_\rho \begin{pmatrix} \hat{a} \\ \hat{b} \end{pmatrix} = \begin{pmatrix} 0 & 1 \\ c_1^0 & 0 \end{pmatrix} \begin{pmatrix} \hat{a} \\ \hat{b} \end{pmatrix} + O(\varepsilon) \begin{pmatrix} \hat{a} \\ \hat{b} \end{pmatrix}. \tag{11.30}$$

For $\varepsilon = 0$, the general solution of (11.30) is given by:

$$\begin{pmatrix} \hat{a} \\ \hat{b} \end{pmatrix}(\rho) = q_1 e^{-\rho\sqrt{c_1^0}} \begin{pmatrix} 1 \\ -\sqrt{c_1^0} \end{pmatrix} + q_2 e^{\rho\sqrt{c_1^0}} \begin{pmatrix} 1 \\ \sqrt{c_1^0} \end{pmatrix}.$$

Thus, for each $\rho = \rho_1 > 0$ and for sufficiently small $\varepsilon > 0$, we can write the $\rho = \rho_1$-fiber of the stable manifold $W_+^s(\varepsilon)$ of (11.27) near 0 as

$$\mathcal{W}_+^s(\varepsilon)\,|_{\rho=\rho_1} \;:\; \begin{pmatrix} \hat{a} \\ \hat{b} \end{pmatrix} = \eta \begin{pmatrix} 1 \\ -\sqrt{c_1^0} \end{pmatrix} + 0_{\rho_1}(\varepsilon|\eta| + |\eta|^3) \begin{pmatrix} 1 \\ \sqrt{c_1^0} \end{pmatrix},$$

where $\eta \in \mathbb{C}$. Using (11.26) and (11.28) and redefining η, we obtain the expression

$$\mathcal{W}^s_+(\varepsilon)\,|_{\rho=\rho_1} \;:\; \begin{pmatrix} \tilde a \\ \tilde b \end{pmatrix} = \eta \begin{pmatrix} 1 \\ -\frac{1}{2} - \rho_1\sqrt{c_1^0} \end{pmatrix} + 0_{\rho_1}(\varepsilon|\eta| + |\eta|^3) \begin{pmatrix} 1 \\ -\frac{1}{2} + \rho_1\sqrt{c_1^0} \end{pmatrix}$$

for $\mathcal{W}^s_+(\varepsilon)$ in the $(\tilde a, \tilde b)$-coordinates. We introduce the coordinates:

$$u = \begin{pmatrix} u_1 \\ u_2 \end{pmatrix} = \frac{1}{2}\begin{pmatrix} 1 & 2 \\ 1 & -2 \end{pmatrix} \begin{pmatrix} \tilde a \\ \tilde b \end{pmatrix} \tag{11.31}$$

and get

$$\mathcal{W}^s_+(\varepsilon)\,|_{\rho=\rho_1} \;:\; \begin{pmatrix} u_1 \\ u_2 \end{pmatrix} = \eta \begin{pmatrix} -\rho_1\sqrt{c_1^0} \\ 1 + \rho_1\sqrt{c_1^0} \end{pmatrix} + 0_{\rho_1}(\varepsilon|\eta| + |\eta|^3) \begin{pmatrix} \rho_1\sqrt{c_1^0} \\ 1 - \rho_1\sqrt{c_1^0} \end{pmatrix}.$$

The (u_1, u_2)-coordinates transform equation (11.29) into

$$\partial_\tau u = \left[D + O(\varepsilon e^{-2\tau})\right] u + O((\sqrt{\varepsilon} + e^\tau)e^\tau |u|), \quad D = \begin{pmatrix} \frac{1}{2} & 0 \\ 0 & -\frac{1}{2} \end{pmatrix}. \tag{11.32}$$

Lemma 11.1.3. *The linear equation*

$$\partial_\tau u = \left[D + O(\varepsilon e^{-2\tau})\right] u \tag{11.33}$$

has an exponential dichotomy with exponents $\pm\frac{1}{2}$ *on* $[\tau_0, \tau_1]$. *Furthermore, the coordinate transformation* $u \to \tilde u$ *that brings* (11.33) *into the form*

$$\partial_\tau \tilde u = \left[D + O(\varepsilon e^{-2\tau})Id\right] \tilde u \tag{11.34}$$

can be chosen such that

$$u(\tau_0) = \tilde u(\tau_0), \quad u(\tau_1) = \begin{pmatrix} 1 & O(\varepsilon) \\ O(r_0^{-2}) & 1 \end{pmatrix} \tilde u(\tau_1). \tag{11.35}$$

Proof. See [Lloyd 2009]. □

We recall that we have

$$\mathcal{W}^s_+(\varepsilon)\,|_{\rho=\rho_1} \;:\; \begin{pmatrix} u_1 \\ u_2 \end{pmatrix} = \eta \begin{pmatrix} -\rho_1\sqrt{c_1^0} \\ 1 + \rho_1\sqrt{c_1^0} \end{pmatrix} + 0_{\rho_1}(\varepsilon|\eta| + |\eta|^3) \begin{pmatrix} \rho_1\sqrt{c_1^0} \\ 1 - \rho_1\sqrt{c_1^0} \end{pmatrix}.$$

for the stable manifold in the u-variables, which, thanks to (11.35), becomes

$$\mathcal{W}^s_+(\varepsilon)\,|_{\rho=\rho_1} \;:\; \begin{pmatrix} \tilde u_1 \\ \tilde u_2 \end{pmatrix} = \eta \begin{pmatrix} -\rho_1\sqrt{c_1^0} + O_{\rho_1}(\varepsilon) \\ 1 + \rho_1\sqrt{c_1^0}(1 + O(r_0^{-2})) \end{pmatrix} + 0_{\rho_1}(\varepsilon|\eta| + |\eta|^3) \begin{pmatrix} \rho_1\sqrt{c_1^0} + O_{\rho_1}(\varepsilon) \\ 1 - \rho_1\sqrt{c_1^0}(1 + O(r_0^{-2})) \end{pmatrix}$$

in the $\tilde{u}$-variables. Choosing $0 < \rho_1 \ll 1$ sufficiently small, we can solve

$$\eta\left(1+\rho_1\sqrt{c_1^0}(1+O(r_0^{-2}))\right)+0_{\rho_1}(\varepsilon|\eta|+|\eta|^3)\left(1-\rho_1\sqrt{c_1^0}(1+O(r_0^{-2}))\right)=\tilde{\eta}$$

for η so that

$$\eta=\frac{\tilde{\eta}}{1+\rho_1\sqrt{c_1^0}\left(1+O(r_0^{-2})\right)}+0_{\rho_1}(\varepsilon|\tilde{\eta}|+|\tilde{\eta}|^3)$$

and consequently

$$\mathcal{W}_+^s(\varepsilon)\mid_{\rho=\rho_1}\ :\ \begin{pmatrix}\tilde{u}_1\\ \tilde{u}_2\end{pmatrix}=\tilde{\eta}\begin{pmatrix}-\rho_1\sqrt{c_1^0}(1+O(\rho_1+r_0^{-2}))\\ 1\end{pmatrix}+0_{\rho_1}(\varepsilon|\tilde{\eta}|+|\tilde{\eta}|^3)\begin{pmatrix}1\\0\end{pmatrix}. \tag{11.36}$$

Using (11.36) and (11.35), we find that the stable manifold $\mathcal{W}_+^s(\varepsilon)$ at $r=r_0$ is given by

$$\mathcal{W}_+^s(\varepsilon)\mid_{r=r_0}\ :\ u=\sqrt{\varepsilon}r_0\hat{\eta}\begin{pmatrix}-\sqrt{c_1^0}+O(\rho_1+r_0^{-2})+O_{\rho_1}(\varepsilon+\sqrt{\varepsilon}|\hat{\eta}|^2)\\ 0\end{pmatrix}+\hat{\eta}\begin{pmatrix}0\\1\end{pmatrix}.$$

We apply successive changes of variables to transform this expression into the (A,B)-coordinates and obtain

$$\mathcal{W}_+^s(\varepsilon)\mid_{r=r_0}\ :\ \begin{pmatrix}A\\B\end{pmatrix}=\varepsilon\hat{\eta}\left[-\sqrt{c_1^0}+O(\rho_1+r_0^{-2})+O_{\rho_1}(\varepsilon+\sqrt{\varepsilon}|\hat{\eta}|^2)\right]\begin{pmatrix}r_0\\1\end{pmatrix}+\sqrt{\varepsilon}\hat{\eta}\begin{pmatrix}1\\0\end{pmatrix}. \tag{11.37}$$

Our goal is to find nontrivial intersections of the stable manifold $\mathcal{W}_+^s(\varepsilon)$ with the center-unstable manifold $\mathcal{W}_-^{cu}(\varepsilon)$. To this end, we write the expansion (11.15) for each fixed $r_0 \gg 1$ in the $(\tilde{A},\tilde{B})$ coordinates and afterwards in the coordinates (A,B). Using the expansions of Bessel functions and using the variables $(d_1,d_2)=(\tilde{d}_1/\sqrt{r_0},\sqrt{r_0}\tilde{d}_2)$ we arrive at the expression

$$\begin{pmatrix}\tilde{A}\\ \tilde{B}\end{pmatrix}=e^{i(r_0-\pi/4)}\begin{pmatrix}d_1(1+0(r_0^{-1}))+d_2(-i+0(r_0^{-1}))\\ -d_2r_0^{-1}(i+0(r_0^{-1}))-\left(\frac{1}{\sqrt{3}}+O(\frac{1}{\sqrt{r_0}})\right)\left(C_1\sqrt{r_0}d_1^2+\frac{C_2}{\sqrt{r_0}}d_1d_2\right)\end{pmatrix}$$
$$+e^{i(r_0-\pi/4)}\begin{pmatrix}O_{r_0}(\varepsilon|d|+|d|^2)\\ O_{r_0}(\varepsilon|d|+|d_2|^2+|d_1|^3)\end{pmatrix} \tag{11.38}$$

with $C_1=\sqrt{2\pi}\mu_c^2 s_2\frac{\Gamma_1+\Gamma_2}{4}$ and $C_2=-\sqrt{2\pi}\mu_c^2 s_2\Gamma_2$. We can apply the transformation (11.19) and obtain the expression

$$\mathcal{W}_-^{cu}(\varepsilon)\mid_{r=r_0}\ :\ \begin{pmatrix}A\\B\end{pmatrix}=e^{i(-\pi/4+O(r_o^{-2})+O_{r_0}(\varepsilon|d|+|d|^2)}\begin{pmatrix}O_{r_0}(\varepsilon|d|+|d|^2)\\ O_{r_0}(\varepsilon|d|+|d_2|^2+|d_1|^3)\end{pmatrix}$$
$$+e^{i(-\frac{\pi}{4}+O(r_o^{-2})+O_{r_0}(\varepsilon|d|+|d|^2)}\begin{pmatrix}d_1(1+0(r_0^{-1}))+d_2(-i+0(r_0^{-1}))\\ -d_2r_0^{-1}(i+0(r_0^{-1}))\end{pmatrix}$$

$$+ e^{i(-\frac{\pi}{4}+O(r_o^{-2})+O_{r_0}(\varepsilon|d|+|d|^2)} \begin{pmatrix} 0 \\ -\left(\frac{1}{\sqrt{3}}+O(\frac{1}{\sqrt{r_0}})\right)\left(C_1\sqrt{r_0}d_1^2+\frac{C_2}{\sqrt{r_0}}d_1d_2\right) \end{pmatrix}. \tag{11.39}$$

After redefining $\hat{\eta}$ to η to remove the phase in $\mathcal{W}_-^{cu}(\varepsilon)\mid_{r=r_0}$, it remains to solve:

$$\begin{cases} \sqrt{\varepsilon}\eta+\varepsilon r_0\eta\left[-\sqrt{c_1^0}+O(\rho_1+r_0^{-2})+O_{\rho_1}(\sqrt{\varepsilon})\right]=d_1(1+0(r_0^{-1}))+d_2(-i+0(r_0^{-1})) \\ \qquad\qquad +O_{r_0}(\varepsilon|d|+|d|^2) \\ \varepsilon\eta\left[-\sqrt{c_1^0}+O(\rho_1+r_0^{-2})+O_{\rho_1}(\sqrt{\varepsilon})\right]=-d_2r_0^{-1}(i+0(r_0^{-1}))+O_{r_0}(\varepsilon|d|+|d_2|^2+|d_1|^3) \\ \qquad\qquad -\left(\frac{1}{\sqrt{3}}+O(r_0^{-1/2})\right)\left(C_1\sqrt{r_0}d_1^2+\frac{C_2}{\sqrt{r_0}}d_1d_2\right). \end{cases}$$

If we set $d_j=\sqrt{\varepsilon}\hat{d}_j$ and write $\eta=\eta_1+i\eta_2$, we obtain

$$\hat{d}_1-i\hat{d}_2-i\eta_2+0(r_0^{-1})\hat{d}+O_{r_0}(\varepsilon|\hat{d}|+\sqrt{\varepsilon}|\hat{d}|^2)=\eta_1+\sqrt{\varepsilon}r_0O(\eta)$$

and

$$\sqrt{\varepsilon}r_0\eta\left[-\sqrt{c_1^0}+O(\rho_1+r_0^{-2})+O_{\rho_1}(\sqrt{\varepsilon})\right]=-i\hat{d}_2+0(r_0^{-1})\hat{d}_2$$
$$+O_{r_0}(\varepsilon|\hat{d}|+\sqrt{\varepsilon}|\hat{d}_2|^2+\varepsilon|\hat{d}_1|^3)-\left(\frac{1}{\sqrt{3}}+O(r_0^{-1/2})\right)\left(C_1r_0^{3/2}\sqrt{\varepsilon}\hat{d}_1^2+C_2\sqrt{\varepsilon}\sqrt{r_0}\hat{d}_1\hat{d}_2\right).$$

We have the expansion

$$\hat{d}_1=\eta_1+O_{r_0}(\sqrt{\varepsilon}\eta_1),\quad \hat{d}_2=O_{r_0}(\sqrt{\varepsilon}\eta_1),\quad \eta_2=O(r_0^{-1})\eta_1+O_{r_0}(\sqrt{\varepsilon}\eta_1)$$

and we can solve the equation:

$$\sqrt{\varepsilon}r_0\eta_1\left[-\sqrt{c_1^0}+O(r_0^{-1})+O(\rho_1)+O_{\rho_1}(\sqrt{\varepsilon})\right]$$
$$=-\left(\frac{1}{\sqrt{3}}+O(r_0^{-1/2})\right)C_1r_0^{3/2}\sqrt{\varepsilon}\eta_1^2+O_{r_0}(\varepsilon\eta_1)$$

which has two solutions $\eta_1=0$ and η_1 small given to leading order by:

$$\eta_1=\frac{1}{C_1}\sqrt{\frac{3c_1^0}{r_0}}+O(\rho_1)+O(r_0^{-1})+O_{\rho_1}(\sqrt{\varepsilon}).$$

This gives $\tilde{d}_1$ and $\tilde{d}_2$:

$$\tilde{d}_1=\frac{s_1}{\mu_c^2s_2}\sqrt{\frac{3\varepsilon}{2\pi c_1^0}},\quad \tilde{d}_2=O(\varepsilon)$$

or equivalently ($\varepsilon=-\lambda, c_1^0=-c_1^1$):

$$\tilde{d}_1=\frac{s_1}{\mu_c^2s_2}\sqrt{\frac{3\lambda}{2\pi c_1^1}},\quad \tilde{d}_2=O(\lambda).$$

We can now state the main result of this section.

Theorem 11.1.1 (Existence of spot solutions). *Fix $\theta \geq 0$ for the threshold of the nonlinearity S and $(b_1, b_2, \sigma_1, \sigma_2) \in \mathbb{R}^4$ such that the connectivity function W defined in equation (11.3) satisfies hypotheses 11.1.1. Then there exists $\mu_* < \mu_c$ such that the planar neural field equation (11.1) has a stationary localized radial solution $v(r)$ for each $\mu \in]\mu_*, \mu_c[$: these solutions stay close to $v = 0$ and, for each fixed $r_* > 0$, we have the asymptotics*

$$v(r) = \alpha\sqrt{\mu_c - \mu} J_0(r) + O(\mu - \mu_c) \text{ as } \mu \to \mu_c \tag{11.40}$$

uniformly in $0 \leq r \leq r_*$ for an appropriate constant α with $sign(\alpha) = sign(s_2)$.

11.2 Localized patterns in the Poincaré disk

In this section, we consider the following neural field equation set on the Poincaré disk

$$\frac{d}{dt}v(z,t) = -v(z,t) + \int_{\mathbb{D}} W(d_{\mathbb{D}}(z,z'))S(\mu v(z',t))\mathrm{dm}(z') \tag{11.41}$$

where $d_{\mathbb{D}}$ is the hyperbolic distance defined in (3.9). The nonlinearity S is defined in equation (11.2), with $\theta \geq 0$. The first step is to construct a connectivity function which can lead to a PDE when applying a suitable transformation as in subsection 11.1.3 for the Euclidean case.

11.2.1 Choice of the connectivity function

We work in geodesic polar coordinates $z = (\tau, \varphi) \in \mathbb{D}$, with $z = \tanh(\tau/2)e^{i\varphi}$. As we want to prove the existence of radial solutions (τ being the radial coordinate), we have to find the equivalent of Hankel transform for the hyperbolic disk. It is given by the Mehler-Fock transform, and we adopt the notations defined in [González 1997]. Let $f : [0, +\infty) = \mathbb{R}_+^* \to \mathbb{R}$ such that $f(\tau)e^{\tau/2} \in \mathrm{L}^1(\mathbb{R}_+^*)$, then we define for all $\rho > 0$ and all $\tau > 0$ the Mehler-Fock transform of f as:

$$\mathcal{M} \cdot f(\rho) = \int_0^{+\infty} f(\tau)\mathcal{P}_{-\frac{1}{2}+i\rho}(\cosh\tau)\sinh\tau d\tau. \tag{11.42}$$

The inversion formula states that:

$$f(\tau) = \int_0^{+\infty} \mathcal{M} \cdot f(\rho)\mathcal{P}_{-\frac{1}{2}+i\rho}(\cosh\tau)\rho\tanh(\pi\rho)d\rho. \tag{11.43}$$

Moreover, we denote $L_{\mathbb{D}}^{\tau}$ the radial part of the Laplace-Beltrami operator on $\mathbb{D}$ defined in equation (8.11):

$$L_{\mathbb{D}}^{\tau} = \frac{1}{\sinh\tau}\frac{d}{d\tau}\left(\sinh\tau\frac{d}{d\tau}\right). \tag{11.44}$$

It is shown in [González 1997] that for all $k \geq 1$

$$\begin{cases} (-1)^k \left(\frac{1}{4} + \rho^2\right)^k \mathcal{M} \cdot f(\rho) = \int_0^{+\infty} (L_{\mathbb{D}}^{\tau})^k f(\tau) \mathcal{P}_{-\frac{1}{2}+i\rho}(\cosh \tau) \sinh \tau d\tau \\ (-1)^k (L_{\mathbb{D}}^{\tau})^k f(\tau) = \int_0^{+\infty} \left(\frac{1}{4} + \rho^2\right)^k \mathcal{M} \cdot f(\rho) \mathcal{P}_{-\frac{1}{2}+i\rho}(\cosh \tau) \rho \tanh(\pi\rho) d\rho. \end{cases} \tag{11.45}$$

Furthermore, for $\Re a > 0$ the following formula holds (pp. 788 [Ryzhik 2007]):

$$\int_0^{+\infty} \frac{1}{a^2 + \rho^2} \mathcal{P}_{-\frac{1}{2}+i\rho}(\cosh \tau) \rho \tanh(\pi\rho) d\rho = \mathcal{Q}_{a-\frac{1}{2}}(\cosh \tau)$$

where $\mathcal{Q}_\nu$ is the associated Legendre function of the second kind. From equations (11.42) and (11.43), this implies that:

$$\frac{1}{a^2 + \rho^2} = \int_0^{+\infty} \mathcal{Q}_{a-\frac{1}{2}}(\cosh \tau) \mathcal{P}_{-\frac{1}{2}+i\rho}(\cosh \tau) \sinh \tau d\tau. \tag{11.46}$$

A natural choice for the connectivity function W is then:

$$\mathbf{W}(z) = W(d_{\mathbb{D}}(z, 0)) = \alpha_1 \mathcal{Q}_{a_1-\frac{1}{2}}(\cosh d_{\mathbb{D}}(z, 0)) - \alpha_2 \mathcal{Q}_{a_2-\frac{1}{2}}(\cosh d_{\mathbb{D}}(z, 0)) \tag{11.47}$$

with $(\alpha_1, \alpha_2, a_1, a_2)$ satisfying the relations:

$$\begin{cases} \alpha_1 = 2\sigma_1 b_1, \\ \alpha_2 = 2\sigma_2 b_2, \\ a_1 = \sqrt{\sigma_1^2 + \frac{1}{4}}, \\ a_2 = \sqrt{\sigma_2^2 + \frac{1}{4}}. \end{cases} \tag{11.48}$$

From equation (11.46) and the definition of the Mehler-Fock transform, we have that for all $\rho > 0$

$$\widetilde{W}(\rho) \overset{def}{=} \mathcal{M} \cdot \mathbf{W}(\rho) = 2 \left(\frac{b_1 \sigma_1}{\sigma_1^2 + \frac{1}{4} + \rho^2} - \frac{b_2 \sigma_2}{\sigma_2^2 + \frac{1}{4} + \rho^2} \right). \tag{11.49}$$

As in the first section, we impose some conditions on the coefficients $(b_1, b_2, \sigma_1, \sigma_2)$.

Hypothesis 11.2.1.

(i) $\widetilde{W}(0) = \widetilde{W}_0 < 0$,

(ii) $W(0) > 0$,

(iii) *there exists* $\rho_c > 0$ *such that* $\widetilde{W}_c \overset{def}{=} \widetilde{W}(\rho_c) = \max_{\rho \in \mathbb{R}^+} \widetilde{W}(\rho) > 0$,

(iv) $\rho_c = \frac{\sqrt{3}}{2}$.

In this case, for Γ_1 and Γ_2 defined in equation (11.4), $\widetilde{W}_c$ can be written:

$$\widetilde{W}_c = \frac{\Gamma_1 + \Gamma_2}{1 + \sigma_1^2 + \sigma_2^2 + \sigma_1^2\sigma_2^2}. \tag{11.50}$$

The condition $\rho_c = \frac{\sqrt{3}}{2}$, reduces to equatin (11.6). It is also straightforward to see that equations (11.50) and (11.6) imply the relation given in equation (11.7).

11.2.2 Linear stability of the trivial state

Equation (11.41) has the trivial solution $v = 0$. The linearized equation around this trivial solution is:

$$\frac{d}{dt}u(z,t) = -u(z,t) + \mu s_1 \int_{\mathbb{D}} W(d_{\mathbb{D}}(z,z'))u(z',t)\mathrm{dm}(z'). \tag{11.51}$$

Looking at linear stability with $u(z,t) = e^{\sigma t}e^{\left(\frac{1}{2}+i\rho\right)\langle z,b\rangle}$ we obtain the following dispersion relation:

$$\sigma(\rho) = -1 + \mu s_1 \mathcal{M}\cdot\mathbf{W}(\rho). \tag{11.52}$$

Then the critical value μ_c is given by:

$$\mu_c = \frac{1}{s_1\widetilde{W}_c}, \tag{11.53}$$

and for all $\mu < \mu_c$, the trivial solution $v = 0$ is stable.

We set $\lambda = \mu - \mu_c$ and rewrite equation (11.41):

$$\frac{d}{dt}v(z,t) = \mathbf{L}_{\mu_c}v(z,t) + \mathbf{R}(v(z,t),\lambda) \tag{11.54}$$

where $\mathbf{L}_{\mu_c}$ and $\mathbf{R}$ are defined by

$$\begin{aligned}
\mathbf{L}_{\mu_c}v(z,t) &= -v(z,t) + \mu_c s_1 \int_{\mathbb{D}} W(d_{\mathbb{D}}(z,z'))v(z',t)\mathrm{dm}(z'),\\
\mathbf{R}(v(z,t),\lambda) &= \int_{\mathbb{D}} W(d_{\mathbb{D}}(z,z'))\left[S\left((\lambda+\mu_c)v(z',t)\right) - \mu_c s_1 v(z',t)\right]\mathrm{dm}(z')
\end{aligned}$$

with $\mathbf{R}(0,0) = D_v\mathbf{R}(0,0) = 0$. We define $f(X,\lambda)$ by:

$$f(X,\lambda) = S\left((\lambda+\mu_c)X\right) - \mu_c s_1 X$$

where $f(0,0) = \partial_X f(0,0) = 0$.

11.2.3 PDE methods in the Poincaré disk

We assume that v is a sufficiently smooth radially symmetric solution of equation (11.54) such that if we apply the Mehler-Fock transform we obtain

$$\left(\frac{d}{dt}+1\right)\mathcal{M}\cdot v(\rho,t) = \widetilde{W}(\rho)\left[\mu_c s_1 \mathcal{M}\cdot v(\rho,t) + \mathcal{M}\cdot f(v,\lambda)(\rho,t)\right].$$

We also assume that we can apply an inverse Mehler-Fock transform, this yields

$$\left(\frac{d}{dt}+1\right)(1+L^\tau_{\mathbb{D}})^2\, v = \Gamma_1 f(v,\lambda) - \Gamma_2 L^\tau_{\mathbb{D}} f(v,\lambda). \tag{11.55}$$

where we used the fact that:

$$\begin{aligned}\sigma_1^2\sigma_2^2 - \Gamma_1\mu_c s_1 &= 1,\\ \sigma_1^2+\sigma_2^2 - \Gamma_2\mu_c s_1 &= -2.\end{aligned}$$

We look for stationary radial solutions of equation (11.54), that is:

$$(1+L^\tau_{\mathbb{D}})^2\, v(\tau) = \Gamma_1 f(v(\tau),\lambda) - \Gamma_2 L^\tau_{\mathbb{D}} f(v(\tau),\lambda). \tag{11.56}$$

Note that $L^\tau_{\mathbb{D}} f(v(\tau),\lambda)$ can be expressed as:

$$L^\tau_{\mathbb{D}} f(v,\lambda) = (L^\tau_{\mathbb{D}} v)\, f'(v,\lambda) + (\partial_\tau v)^2\, f''(v,\lambda).$$

11.2.4 The equation near the core

We rewrite equation (11.56) as a four dimensional system of non-autonomous differential equations. We set:

$$\begin{aligned}\partial_\tau u_1 &= u_3,\\ \partial_\tau u_2 &= u_4,\\ \left(\partial_\tau^2 + \coth(\tau)\partial_\tau + 1\right) u_1 &= u_2,\\ \left(\partial_\tau^2 + \coth(\tau)\partial_\tau + 1\right) u_2 &= \Gamma_1 f(u_1,\lambda) - \Gamma_2 L^\tau_{\mathbb{D}} f(u_1,\lambda).\end{aligned}$$

$$\partial_\tau U = \mathcal{A}(\tau)U + \mathcal{F}(U,\lambda), \tag{11.57}$$

where

$$\mathcal{A}(r) = \begin{pmatrix} 0 & 0 & 1 & 0\\ 0 & 0 & 0 & 1\\ -1 & 1 & -\coth(\tau) & 0\\ 0 & -1 & 0 & -\coth(\tau)\end{pmatrix} \text{ and } \mathcal{F}(U,\lambda) = \begin{pmatrix} 0\\ 0\\ 0\\ \mathcal{F}_4\left(u_1,u_2,u_3,u_4,\lambda\right)\end{pmatrix}$$

with $U = (u_1,u_2,u_3,u_4)^T$ and

$$\mathcal{F}_4\left(u_1,u_2,u_3,u_4,\lambda\right) = \Gamma_1 f(u_1,\lambda) - \Gamma_2\left[(u_2-u_1)f'(u_1,\lambda) + u_3^2 f''(u_1,\lambda)\right].$$

Furthermore the quadratic term in U of $\mathcal{F}(U,\lambda)$ at $(0,0)$ is given by:

$$\mathcal{F}_{20}(U,U) = \frac{\mu_c^2 s_2}{2}\begin{pmatrix} 0\\ 0\\ 0\\ (\Gamma_1+2\Gamma_2)u_1^2 - 2\Gamma_2 u_1u_2 - 2\Gamma_2 u_3^2\end{pmatrix}.$$

First, we set $\lambda = 0$ and linearize (11.57) about $U = 0$ to get the linear system $\partial_\tau U = \mathcal{A}(\tau)U$.

Proposition 11.2.1. *The linear system $\partial_\tau U = \mathcal{A}(\tau)U$ has four linearly independent solutions given by*

$$\begin{aligned} V_1(\tau) &= \big(\mathcal{P}_\nu(\cosh\tau), 0, \mathcal{P}^1_\nu(\cosh\tau), 0\big)^{\mathbf{T}} \\ V_2(\tau) &= \big(V_2^1(\tau), \mathcal{P}_\nu(\cosh\tau), V_2^3(\tau), \mathcal{P}^1_\nu(\cosh\tau)\big)^{\mathbf{T}} \\ V_3(\tau) &= \big(\mathcal{Q}_\nu(\cosh\tau), 0, \mathcal{Q}^1_\nu(\cosh\tau), 0\big)^{\mathbf{T}} \\ V_4(\tau) &= \big(V_4^1(\tau), \mathcal{Q}_\nu(\cosh\tau), V_4^3(\tau), \mathcal{Q}^1_\nu(\cosh\tau)\big)^{\mathbf{T}} \end{aligned}$$

where

$$\nu = -\frac{1}{2} + i\frac{\sqrt{3}}{2} \tag{11.58}$$

and

$$V_2^1(\tau) = \mathcal{P}_\nu(\cosh\tau)\int_0^\tau \mathcal{P}_\nu(\cosh s)\mathcal{Q}_\nu(\cosh s)\sinh(s)ds - \mathcal{Q}_\nu(\cosh\tau)\int_0^\tau \big(\mathcal{P}_\nu(\cosh s)\big)^2\sinh(s)ds$$

$$V_2^3(\tau) = \mathcal{P}^1_\nu(\cosh\tau)\int_0^\tau \mathcal{P}_\nu(\cosh s)\mathcal{Q}_\nu(\cosh s)\sinh(s)ds - \mathcal{Q}^1_\nu(\cosh\tau)\int_0^\tau \big(\mathcal{P}_\nu(\cosh s)\big)^2\sinh(s)ds$$

$$V_4^1(\tau) = \mathcal{P}_\nu(\cosh\tau)\int_0^\tau \big(\mathcal{Q}_\nu(\cosh s)\big)^2\sinh(s)ds - \mathcal{Q}_\nu(\cosh\tau)\int_0^\tau \mathcal{P}_\nu(\cosh s)\mathcal{Q}_\nu(\cosh s)\sinh(s)ds$$

$$V_4^3(\tau) = \mathcal{P}^1_\nu(\cosh\tau)\int_0^\tau \big(\mathcal{Q}_\nu(\cosh s)\big)^2\sinh(s)ds - \mathcal{Q}^1_\nu(\cosh\tau)\int_0^\tau \mathcal{P}_\nu(\cosh s)\mathcal{Q}_\nu(\cosh s)\sinh(s)ds.$$

Proof. First of all, we recall that the associated Legendre function $\mathcal{P}_\nu(\cosh\cdot)$ and $\mathcal{Q}_\nu(\cosh\cdot)$ form a basis of solutions of:

$$\partial_\tau^2\Psi(\tau) + \coth(\tau)\partial_\tau\Psi(\tau) - \nu(\nu+1)\Psi(\tau) = 0.$$

If $\nu = -\frac{1}{2} + i\frac{\sqrt{3}}{2}$ then we have $\nu(\nu+1) = -1$. This implies that $\mathcal{P}_{-\frac{1}{2}+i\frac{\sqrt{3}}{2}}(\cosh\tau)$ and $\mathcal{Q}_{-\frac{1}{2}+i\frac{\sqrt{3}}{2}}(\cosh\tau)$ are solutions of

$$\partial_\tau^2\Psi(\tau) + \coth(\tau)\partial_\tau\Psi(\tau) + \Psi(\tau) = 0.$$

From now on $\nu = -\frac{1}{2} + i\frac{\sqrt{3}}{2}$. The solution of $\partial_\tau U = \mathcal{A}(\tau)U$ can be found by inspecting the equivalent system

$$\left(\partial_\tau^2 + \coth(\tau)\partial_\tau + 1\right) u_1 = u_2, \quad \left(\partial_\tau^2 + \coth(\tau)\partial_\tau + 1\right) u_2 = 0.$$

As a consequence solutions $V_1(\tau) = \left(\mathcal{P}_\nu(\cosh\tau), 0, \mathcal{P}_\nu^1(\cosh\tau), 0\right)^{\mathbf{T}}$ and $V_3(\tau) = \left(\mathcal{Q}_\nu(\cosh\tau), 0, \mathcal{Q}_\nu^1(\cosh\tau), 0\right)^{\mathbf{T}}$ are two linearly independent solutions. Note that we have used the useful relations:

$$\partial_\tau\left(\mathcal{P}_\nu(\cosh\tau)\right) = \mathcal{P}_\nu^1(\cosh\tau), \quad \partial_\tau\left(\mathcal{Q}_\nu(\cosh\tau)\right) = \mathcal{Q}_\nu^1(\cosh\tau).$$

In order to find two other linearly independent solutions, we first solve the following equation:

$$\left(\partial_\tau^2 + \coth\tau\partial_\tau + 1\right) u(\tau) = \mathcal{P}_\nu(\cosh\tau).$$

We search solutions of the form $u(\tau) = c_1(\tau)\mathcal{P}_\nu(\cosh\tau) + c_2(\tau)\mathcal{Q}_\nu(\cosh\tau)$, where the derivatives $(\dot{c}_1(\tau), \dot{c}_2(\tau))$ satisfy:

$$\begin{cases} \dot{c}_1(\tau)\mathcal{P}_\nu(\cosh\tau) + \dot{c}_2(\tau)\mathcal{Q}_\nu(\cosh\tau) &= 0 \\ \dot{c}_1(\tau)\mathcal{P}_\nu^1(\cosh\tau) + \dot{c}_2(\tau)\mathcal{Q}_\nu^1(\cosh\tau) &= \mathcal{P}_\nu(\cosh\tau) \end{cases}$$

which we rewrite in a matrix form:

$$\begin{pmatrix} \mathcal{P}_\nu(\cosh\tau) & \mathcal{Q}_\nu(\cosh\tau) \\ \mathcal{P}_\nu^1(\cosh\tau) & \mathcal{Q}_\nu^1(\cosh\tau) \end{pmatrix} \begin{pmatrix} \dot{c}_1(\tau) \\ \dot{c}_2(\tau) \end{pmatrix} = \begin{pmatrix} 0 \\ \mathcal{P}_\nu(\cosh\tau) \end{pmatrix}.$$

From formula in [Erdelyi 1985] page 123, we obtain that:

$$W(\tau) = \mathcal{P}_\nu(\cosh\tau)\mathcal{Q}_\nu^1(\cosh\tau) - \mathcal{P}_\nu^1(\cosh\tau)\mathcal{Q}_\nu(\cosh\tau) = -\frac{1}{\sinh\tau},$$

where $W(\tau)$ is non vanishing for all $\tau \in]0; +\infty[$ such that we can inverse the matrix in left hand side of the previous system and obtain:

$$\begin{aligned} \dot{c}_1(\tau) &= \sinh\tau\mathcal{P}_\nu(\cosh\tau)\mathcal{Q}_\nu(\cosh\tau) \\ \dot{c}_2(\tau) &= -\sinh\tau\left(\mathcal{P}_\nu(\cosh\tau)\right)^2 \end{aligned}$$

which gives

$$u(\tau) = c_1\mathcal{P}_\nu(\cosh\tau) + c_2\mathcal{Q}_\nu(\cosh\tau) + \mathcal{P}_\nu(\cosh\tau)\int_0^\tau \mathcal{P}_\nu(\cosh s)\mathcal{Q}_\nu(\cosh s)\sinh(s)ds - \mathcal{Q}_\nu(\cosh\tau)\int_0^\tau \left(\mathcal{P}_\nu(\cosh s)\right)^2\sinh(s)ds,$$

with two constants $c_1, c_2 \in \mathbb{R}$. Equivalently, the solutions of

$$\left(\partial_\tau^2 + \coth\tau\partial_\tau + 1\right) u(\tau) = \mathcal{Q}_\nu(\cosh\tau)$$

are given by

$$u(\tau) = c_3\mathcal{P}_\nu(\cosh\tau) + c_4\mathcal{Q}_\nu(\cosh\tau) + \mathcal{P}_\nu(\cosh\tau)\int_0^\tau \left(\mathcal{Q}_\nu(\cosh s)\right)^2 \sinh(s)ds \\ - \mathcal{Q}_\nu(\cosh\tau)\int_0^\tau \mathcal{P}_\nu(\cosh s)\mathcal{Q}_\nu(\cosh s)\sinh(s)ds,$$

with two constants $c_3, c_4 \in \mathbb{R}$.

Choosing only linearly independent solutions, we finally obtain the result stated in the proposition. □

In table 11.1, we summarize know expansions of the associated Legendre functions in the limits $\tau \to 0$ and $\tau \to \infty$. Thus, $V_1(\tau)$ and $V_2(\tau)$ stay bounded as $\tau \to 0$, while norms of $V_3(\tau)$ and $V_4(\tau)$ behave like $\ln\tau$ as $\tau \to 0$. We expect that the set of solutions of (11.57) that are bounded as $\tau \to 0$ forms a two-dimensional manifold in $\mathbb{R}^4$ for each fixed $\tau > 0$. We denote $P_-^{cu}(\tau_0)$ onto the space spanned by $V_1(\tau_0), V_2(\tau_0)$ with null space given by the span of $V_3(\tau_0), V_4(\tau_0)$.

	$\tau \to 0$	$\tau \to \infty$
$\mathcal{P}_\nu(\cosh\cdot)$	$1 + O(\tau^2)$	$C_0\cos(\frac{\sqrt{3}\tau}{2} + \Phi_0)e^{-\frac{\tau}{2}} + O(e^{-\frac{3\tau}{2}})$
$\mathcal{P}^1_\nu(\cosh\cdot)$	$\tau\left(-\frac{1}{2} + O(\tau^2)\right)$	$C_0\cos(\frac{\sqrt{3}\tau}{2} + \Phi_0 + \frac{2\pi}{3})e^{-\frac{\tau}{2}} + O(e^{-\frac{3\tau}{2}})$
$\mathcal{Q}_\nu(\cosh\cdot)$	$(-1 + O(\tau^2))\ln\tau + O(1)$	$C_1\cos(\frac{\sqrt{3}\tau}{2} - \Phi_1)e^{-\frac{\tau}{2}} + O(e^{-\frac{3\tau}{2}})$
$\mathcal{Q}^1_\nu(\cosh\cdot)$	$(1 + O(\tau^2))\tau\ln\tau - \frac{1}{\tau} + O(1)$	$C_1\cos(\frac{\sqrt{3}\tau}{2} - \Phi_1 + \frac{2\pi}{3})e^{-\frac{\tau}{2}} + O(e^{-\frac{3\tau}{2}})$

Table 11.1: Expansions of associated Legendre functions $\mathcal{P}^k_\nu(\cosh\cdot)$ and $\mathcal{Q}^k_\nu(\cosh\cdot)$ for $\tau \to 0$ and $\tau \to \infty$; see [Erdelyi 1985, Virchenko 2001]. C_0, C_1, Φ_0 and Φ_1 are real constants.

Proposition 11.2.2. *The constants C_0, C_1, Φ_0 and Φ_1 given in table 11.1 are*

$$C_0 = \frac{2}{\sqrt{\pi}}\left|\frac{\Gamma\left(i\frac{\sqrt{3}}{2}\right)}{\Gamma\left(\frac{1}{2} + i\frac{\sqrt{3}}{2}\right)}\right|, \quad \Phi_0 = \arg\left(\frac{\Gamma\left(i\frac{\sqrt{3}}{2}\right)}{\Gamma\left(\frac{1}{2} + i\frac{\sqrt{3}}{2}\right)}\right),$$

$$C_1 = \sqrt{\pi}\left|\cot\left(\pi\left(-\frac{1}{2} + i\frac{\sqrt{3}}{2}\right)\right)\frac{\Gamma\left(-i\frac{\sqrt{3}}{2}\right)}{\Gamma\left(\frac{1}{2} - i\frac{\sqrt{3}}{2}\right)}\right|,$$

$$\Phi_1 = \arg\left[\sqrt{\pi}\cot\left(\pi\left(-\frac{1}{2} + i\frac{\sqrt{3}}{2}\right)\right)\frac{\Gamma\left(-i\frac{\sqrt{3}}{2}\right)}{\Gamma\left(\frac{1}{2} - i\frac{\sqrt{3}}{2}\right)}\right].$$

Proof. The proof of this proposition is based on the asymptotics as $z \to \infty$

[Virchenko 2001]:

$$\mathcal{P}_\nu^m(z) \approx \frac{z^{m/2}}{\sqrt{\pi}(z-1)^{m/2}}\left(\frac{(2z)^\nu\Gamma(\nu+1/2)}{\Gamma(\nu-m+1)}\left(1+O(z^{-1})\right)\right.$$
$$\left.+\frac{(2z)^{-\nu-1}\Gamma(-\nu-1/2)}{\Gamma(-m-\nu)}\left(1+O(z^{-1})\right)\right),$$

and

$$\mathcal{Q}_\nu^m(z) \approx \frac{2^{-\nu-2}z^{-\nu-1}}{\sqrt{\pi}\Gamma(-m-\nu)\Gamma(\nu-m+1)}\left(\frac{1+z}{z-1}\right)^{m/2}\left((2z)^{2\nu+1}\Gamma(-m-\nu)\Gamma(\nu+1/2)\right.$$
$$\times\left(\ln(1+z)-\ln(z-1)\right)\left(1+O(z^{-1})\right)+\Gamma(-m+\nu+1)\Gamma(-\nu-1/2)$$
$$\left.\times\left(2\pi+\ln(1+z)-\ln(z-1)\right)\left(1+O(z^{-1})\right)\right).$$

□

Proposition 11.2.3. *The following formulas are satisfied*

$$\Phi_0+\Phi_1=-\frac{\pi}{2}, \tag{11.59}$$

$$C_0=2\sqrt{\frac{2\sqrt{3}}{3\pi\tanh\left(\frac{\sqrt{3}\pi}{2}\right)}}\ \text{and}\ C_1=\sqrt{\frac{2\pi\sqrt{3}\tanh\left(\frac{\sqrt{3}\pi}{2}\right)}{3}}. \tag{11.60}$$

Proof. Relation (11.59) is straightforward to verifiy from the definition of Φ_0 and Φ_1. The formulas for C_0 and C_1 are obtained with the software *Maple* by noticing that

$$\frac{\sqrt{3}C_0}{6}=\frac{C_1C_0^2}{8}, \tag{11.61}$$

which automatically gives

$$\left|\frac{\Gamma\left(i\frac{\sqrt{3}}{2}\right)}{\Gamma\left(\frac{1}{2}+i\frac{\sqrt{3}}{2}\right)}\right|=\sqrt{\frac{2\sqrt{3}}{3\tanh\left(\frac{\sqrt{3}\pi}{2}\right)}}.$$

The formula (11.60) is then easily obtained from the above equation. □

We are now able to present the equivalent of lemma 11.1.1 in the case of the Poincaré disk.

Lemma 11.2.1. *Fix $\tau_0>0$, then there are constants δ_0,δ_1 so that the set $\mathcal{W}_-^{cu}(\lambda)$ of solutions $U(\tau)$ of (11.14) for which $\sup_{0\le\tau\le\tau_0}|U(\tau)|<\delta_0$ is, for $|\lambda|<\delta_0$, a smooth two-dimensional manifold. Furthermore, $U\in\mathcal{W}_-^{cu}(\lambda)$ with $|P_-^{cu}(\tau_0)U(\tau_0)|<\delta_1$ if only if*

$$\begin{aligned}U(\tau_0)=&\tilde{d}_1V_1(\tau_0)+\tilde{d}_2V_2(\tau_0)+V_3(\tau_0)O_{\tau_0}(|\lambda||\tilde{d}|+|\tilde{d}|^2)\\&+V_4(\tau_0)\left(\Xi_{\tilde{d}_1^2}\tilde{d}_1^2+\Xi_{\tilde{d}_1\tilde{d}_2}\tilde{d}_1\tilde{d}_2+O_{\tau_0}(|\lambda||\tilde{d}|+|\tilde{d}_2|^2+|\tilde{d}|^3)\right)\end{aligned} \tag{11.62}$$

where

$$\begin{aligned}\Xi_{\tilde{d}_1^2} &= \frac{\mu_c^2 s_2}{2}\left[-(\Gamma_1+2\Gamma_2)\mathcal{I}_1+2\Gamma_2\mathcal{I}_2+o(1)\right],\\ \Xi_{\tilde{d}_1\tilde{d}_2} &= \mu_c^2 s_2\left[\Gamma_2\mathcal{I}_1+o(1)\right],\end{aligned}$$

with

$$\begin{aligned}\mathcal{I}_1 &= \int_0^\infty (\mathcal{P}_\nu(\cosh s))^3\sinh s ds<\infty,\\ \mathcal{I}_2 &= \int_0^\infty \mathcal{P}_\nu(\cosh s)\left(\mathcal{P}_\nu^1(\cosh s)\right)^2\sinh s ds<\infty.\end{aligned}$$

for some $\tilde{d}=(\tilde{d}_1,\tilde{d}_2)\in\mathbb{R}^2$ *with* $|\tilde{d}|<\delta_1$, *where the right hand side in* (11.62) *depends smoothly on* $(\tilde{d},\lambda)$.

Proof. The proof is also very similar to the proof of lemma 11.1.1. We observe that four independent solutions to the adjoint problem $\partial_\tau U=-\mathcal{A}^T(\tau)U$ are given by

$$\begin{aligned}W_1(\tau) &= \sinh\tau\left(\mathcal{Q}_\nu^1(\cosh\tau),W_1^2(\tau),-\mathcal{Q}_\nu(\cosh\tau),W_1^4(\tau)\right)^{\mathbf{T}},\\ W_2(\tau) &= \sinh\tau\left(0,\mathcal{Q}_\nu^1(\cosh\tau),0,-\mathcal{Q}_\nu(\cosh\tau)\right)^{\mathbf{T}},\\ W_3(\tau) &= \sinh\tau\left(\mathcal{P}_\nu^1(\cosh\tau),W_3^2(\tau),-\mathcal{P}_\nu(\cosh\tau),W_3^4(\tau)\right)^{\mathbf{T}}\\ W_4(\tau) &= \sinh\tau\left(0,\mathcal{P}_\nu^1(\cosh\tau),0,-\mathcal{P}_\nu(\cosh\tau)\right)^{\mathbf{T}},\end{aligned}$$

with

$$\begin{aligned}W_1^2(\tau)=\mathcal{P}_\nu^1(\cosh\tau)\int_0^\tau \mathcal{P}_\nu^1(\cosh s)\mathcal{Q}_\nu^1(\cosh s)\sinh(s)ds\\ -\mathcal{Q}_\nu^1(\cosh\tau)\int_0^\tau\left(\mathcal{P}_\nu^1(\cosh s)\right)^2\sinh(s)ds,\end{aligned}$$

$$\begin{aligned}W_1^4(\tau)=-\mathcal{Q}_\nu(\cosh\tau)-\mathcal{P}_\nu(\cosh\tau)\int_0^\tau \mathcal{P}_\nu^1(\cosh s)\mathcal{Q}_\nu^1(\cosh s)\sinh(s)ds\\ +\mathcal{Q}_\nu(\cosh\tau)\int_0^\tau\left(\mathcal{P}_\nu^1(\cosh s)\right)^2\sinh(s)ds,\end{aligned}$$

$$\begin{aligned}W_3^2(\tau)=\mathcal{P}_\nu^1(\cosh\tau)\int_0^\tau \left(\mathcal{Q}_\nu^1(\cosh s)\right)^2\sinh(s)ds\\ -\mathcal{Q}_\nu^1(\cosh\tau)\int_0^\tau\mathcal{P}_\nu^1(\cosh s)\mathcal{Q}_\nu^1(\cosh s)\sinh(s)ds,\end{aligned}$$

$$\begin{aligned}W_3^4(\tau)=-\mathcal{P}_\nu(\cosh\tau)-\mathcal{P}_\nu(\cosh\tau)\int_0^\tau \left(\mathcal{Q}_\nu^1(\cosh s)\right)^2\sinh(s)ds\\ -\mathcal{Q}_\nu(\cosh\tau)\int_0^\tau\mathcal{P}_\nu^1(\cosh s)\mathcal{Q}_\nu^1(\cosh s)\sinh(s)ds.\end{aligned}$$

We have used the facts that:

- the following relations are satisfied [Erdelyi 1985]:

$$\begin{aligned}\partial_\tau\left(\sinh\tau\mathcal{P}^1_\nu(\cosh\tau)\right) &= -\sinh\tau\mathcal{P}_\nu(\cosh\tau)\\ \partial_\tau\left(\sinh\tau\mathcal{Q}^1_\nu(\cosh\tau)\right) &= -\sinh\tau\mathcal{Q}_\nu(\cosh\tau),\end{aligned}$$

- the solutions of

$$\begin{aligned}\left(\partial^2_\tau-\coth\tau\partial_\tau+1\right)q_1(\tau) &= \sinh\tau\mathcal{P}^1_\nu(\cosh\tau)\\ \left(\partial^2_\tau-\coth\tau\partial_\tau+1\right)q_2(\tau) &= \sinh\tau\mathcal{Q}^1_\nu(\cosh\tau)\end{aligned}$$

are given by

$$\begin{aligned}q_1(\tau) &= c_1\sinh\tau\mathcal{P}^1_\nu(\cosh\tau)+c_2\sinh\tau\mathcal{Q}^1_\nu(\cosh\tau)\\ &+\sinh\tau\mathcal{P}^1_\nu(\cosh\tau)\int_0^\tau\mathcal{P}^1_\nu(\cosh s)\mathcal{Q}^1_\nu(\cosh s)\sinh(s)ds\\ &-\sinh\tau\mathcal{Q}^1_\nu(\cosh\tau)\int_0^\tau\left(\mathcal{P}^1_\nu(\cosh s)\right)^2\sinh(s)ds\\ q_2(\tau) &= c_3\sinh\tau\mathcal{P}^1_\nu(\cosh\tau)+c_4\sinh\tau\mathcal{Q}^1_\nu(\cosh\tau)\\ &+\sinh\tau\mathcal{P}^1_\nu(\cosh\tau)\int_0^\tau\left(\mathcal{Q}^1_\nu(\cosh s)\right)^2\sinh(s)ds\\ &-\sinh\tau\mathcal{Q}^1_\nu(\cosh\tau)\int_0^\tau\mathcal{P}^1_\nu(\cosh s)\mathcal{Q}^1_\nu(\cosh s)\sinh(s)ds,\end{aligned}$$

with four real constants $c_1, c_2, c_3, c_4 \in \mathbb{R}$.

It follows from

$$\sinh\tau\left(\mathcal{P}^1_\nu(\cosh\tau)\mathcal{Q}_\nu(\cosh\tau)-\mathcal{P}_\nu(\cosh\tau)\mathcal{Q}^1_\nu(\cosh\tau)\right)=1$$

that

$$\langle V_i(\tau),W_j(\tau)\rangle_{\mathbb{R}^4}=\delta_{i,j}\quad i,j=1,\dots,4$$

is independent of τ. For given $\tilde{d}=(\tilde{d}_1,\tilde{d}_2)\in\mathbb{R}^2$, we consider the fixed-point equation:

$$\begin{aligned}U(\tau) &= \sum_{j=1}^2\tilde{d}_jV_j(\tau)+\sum_{j=1}^2V_j(\tau)\int_{\tau_0}^\tau\langle W_j(s),\mathcal{F}(U(s),\lambda)\rangle ds\\ &+\sum_{j=3}^4V_j(\tau)\int_0^\tau\langle W_j(s),\mathcal{F}(U(s),\lambda)\rangle ds\\ &= \sum_{j=1}^2\tilde{d}_jV_j(\tau)+\sum_{j=1}^2V_j(\tau)\int_{\tau_0}^\tau W_{j,4}(s)\mathcal{F}_4(U(s),\lambda)ds\\ &+\sum_{j=3}^4V_j(\tau)\int_0^\tau W_{j,4}(s)\mathcal{F}_4(U(s),\lambda)ds\end{aligned}\tag{11.63}$$

on $\mathcal{C}^0([0,\tau_0],\mathbb{R}^4)$, where $W_{j,4}(\tau)$ (resp. $\mathcal{F}_4(U(\tau),\lambda)$)denotes the fourth component of $W_j(\tau)$ (resp. $\mathcal{F}(U(\tau),\lambda)$). We have:

- Each solution $U \in \mathcal{C}^0([0,\tau_0],\mathbb{R}^4)$ of (11.63) gives a solution of (11.57) that is bounded on $[0,\tau_0]$.
- Every bounded solution $U \in \mathcal{C}^0([0,\tau_0],\mathbb{R}^4)$ of (11.57) satisfies (11.63) provided we add $\tilde{d}_3 V_3(\tau) + \tilde{d}_4 V_4(\tau)$ to the right hand side for an appropriate $\tilde{d} \in \mathbb{R}^4$.
- Existence of solutions of (11.63) is given by the uniform contracting mapping principle for sufficiently small $(\tilde{d}_1, \tilde{d}_2)$ and λ.
- The resulting solution U satisfies on $[0,\tau_0]$:

$$U(\tau) = \sum_{j=1}^{2} \tilde{d}_j V_j(\tau) + O_{\tau_0}(|\lambda||\tilde{d}| + |\tilde{d}|^2).$$

We also need to compute the quadratic coefficient in $\tilde{d}$ in front of $V_4(\tau_0)$, denoted Ξ.We recall that:

$$\mathcal{F}_{2,0}(U,U) = \frac{\mu_c^2 s_2}{2}\left(0,0,0,(\Gamma_1+2\Gamma_2)u_1^2 - 2\Gamma_2 u_1 u_2 - 2\Gamma_2 u_3^2\right)^{\mathbf{T}}.$$

If we evaluate (11.63) at $\tau = \tau_0$, we arrive at (11.62) except that we need to calculate the quadratic coefficients in front of $V_4(\tau_0)$: using a Taylor expansion, we find that these coefficients are given by:

$$\Xi_{\tilde{d}_1^2} = \frac{\mu_c^2 s_2}{2}\int_0^{\tau_0} W_{4,4}(s)\left[(\Gamma_1+2\Gamma_2)\left(\mathcal{P}_\nu(\cosh s)\right)^2 - 2\Gamma_2\left(\mathcal{P}_\nu^1(\cosh s)\right)^2\right] ds$$

and

$$\Xi_{\tilde{d}_1\tilde{d}_2} = -\mu_c^2 s_2 \Gamma_2 \int_0^{\tau_0} W_{4,4}(s)\left(\mathcal{P}_\nu(\cosh s)\right)^2 ds.$$

Then we have:

$$\begin{aligned}
\Xi_{\tilde{d}_1^2} &= \frac{\mu_c^2 s_2}{2}\left[-(\Gamma_1+2\Gamma_2)\mathcal{I}_1 + 2\Gamma_2\mathcal{I}_2 + o(1)\right] \\
\Xi_{\tilde{d}_1\tilde{d}_2} &= \mu_c^2 s_2\left[\Gamma_2\mathcal{I}_1 + o(1)\right],
\end{aligned}$$

with

$$\begin{aligned}
\mathcal{I}_1 &= \int_0^\infty \left(\mathcal{P}_\nu(\cosh s)\right)^3 \sinh s ds < \infty, \\
\mathcal{I}_2 &= \int_0^\infty \mathcal{P}_\nu(\cosh s)\left(\mathcal{P}_\nu^1(\cosh s)\right)^2 \sinh s ds < \infty.
\end{aligned}$$

□

11.2.5 The far-field equations

We make equation (11.57) autonomous by adding the variable $\alpha = \coth\tau - 1$ wich satisfies $\partial_\tau \alpha = -\alpha(2+\alpha)$. Equation (11.57) becomes

$$\frac{d}{d\tau}\begin{pmatrix} u_1 \\ u_2 \\ u_3 \\ u_4 \\ \alpha \end{pmatrix} = \begin{pmatrix} u_3 \\ u_4 \\ -u_1 + u_2 - (1+\alpha)u_3 \\ -u_2 - (1+\alpha)u_4 + \mathcal{F}_4\left(u_1, u_2, u_3, u_4, \lambda, \alpha\right) \\ -\alpha(2+\alpha) \end{pmatrix}. \tag{11.64}$$

In the remainder of this section, we focus on the regime $\alpha \approx 0$ which corresponds to the far field $\tau \gg 1$. If we denote $\mathcal{A}(\infty, \lambda)$ the following matrix

$$\mathcal{A}(\infty,\lambda) = \begin{pmatrix} 0 & 0 & 1 & 0 \\ 0 & 0 & 0 & 1 \\ -1 & 1 & -1 & 0 \\ s_1(\Gamma_1+\Gamma_2)\lambda & -1 - s_1\Gamma_2\lambda & 0 & -1 \end{pmatrix}$$

then $\mathcal{A}(\infty, 0)$ has eigenvalues $\nu, \bar{\nu}$ with multiplicity two (ν is defined in equation (11.58)). As $\Re(\nu) = -1/2$, the trivial state $U = 0$ is asymptotically stable at $\lambda = 0$ and then there is no bifurcation at the far field. Remember that in the Euclidean case a Turing instability occurs at infinity. In figure 11.1, we summarize how the eigenvalues ℓ of $\mathcal{A}(\infty, \lambda)$ split close to $\lambda = 0$. For $\lambda > 0$, there exist four complex conjugate eigenvalues with $\Re(\ell) = -1/2$. For $\lambda < 0$, there exist also four complex conjugate eigenvalues with $\Re(\ell) \neq -1/2$.

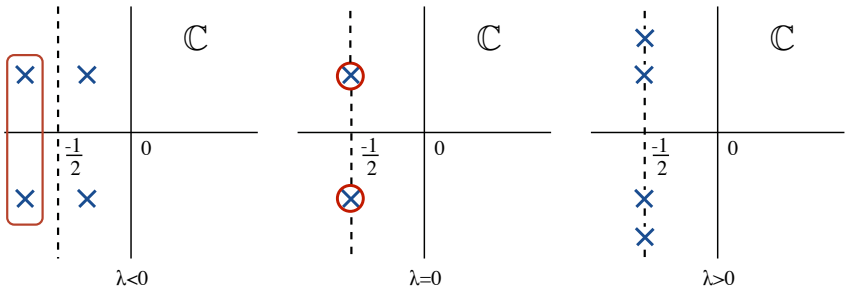

Figure 11.1: Schematic splitting of the eigenvalues ℓ of $\mathcal{A}(\infty, \lambda)$ for different values of λ. At $\lambda = 0$, the multiplicity is two. Eigenvalues in the red box correspond to the stable fast manifold $\mathcal{W}^{sf}_+(\lambda)$.

Firstly, we can use the following formal argument. We have that $V_1(\tau)$ and $V_3(\tau)$ decay like $e^{-\tau/2}$, while $V_2(\tau)$ and $V_4(\tau)$ decay like $\tau e^{-\tau/2}$ as $\tau \to \infty$. Hence the tangent space of the stable manifold at $(u, \lambda) = 0$ is spanned by $(V_1(\tau), V_2(\tau), V_3(\tau), V_4(\tau))$. On the other hand, we showed in lemma 11.2.1 that the tangent space of the core manifold is spanned by $V_1(\tau)$ and $V_2(\tau)$. Then these tangent spaces would intersect along the two-dimensional subspace spanned by $V_1(\tau)$ and $V_2(\tau)$.

As in the Euclidean case we use successive well chosen change of variables. We can first use the linear change of coordinates

$$U = \widetilde{A}\begin{pmatrix}1\\0\\\nu\\0\end{pmatrix} + \widetilde{B}\begin{pmatrix}0\\2\nu+1\\1\\\nu(2\nu+1)\end{pmatrix} + \text{c.c.}$$

or equivalently,

$$\begin{pmatrix}\widetilde{A}\\\widetilde{B}\end{pmatrix} = \begin{pmatrix}\frac{1}{2}u_1 + i\frac{\sqrt{3}}{3}\left(-\frac{1}{2}u_1 - \frac{1}{3}u_2 - u_3 - \frac{2}{3}u_4\right)\\ -\frac{1}{3}\left(\frac{1}{2}u_2 + u_4\right) - i\frac{\sqrt{3}}{6}u_2\end{pmatrix}, \quad U = (u_1, u_2, u_3, u_4)^T.$$

In these coordinates, (11.64) becomes, without the high order terms, at $\lambda = 0$,

$$\begin{aligned}
\partial_\tau \widetilde{A} &= \left(-\frac{1}{2} - \frac{\alpha}{2} + i\left[\frac{\sqrt{3}}{2} - \frac{\alpha\sqrt{3}}{6}\right]\right)\widetilde{A} + \left(1 + \frac{\alpha}{3}\right)\widetilde{B} + \alpha\left(\frac{1}{2} - \frac{\alpha\sqrt{3}}{6}\right)\overline{\widetilde{A}} - \frac{\alpha}{3}\overline{\widetilde{B}}\\
\partial_\tau \widetilde{B} &= \left(-\frac{1}{2} - \frac{\alpha}{2} + i\left[\frac{\sqrt{3}}{2} - \frac{\alpha\sqrt{3}}{6}\right]\right)\widetilde{B} + \alpha\left(-\frac{1}{2} + \frac{\alpha\sqrt{3}}{6}\right)\overline{\widetilde{B}}\\
\partial_\tau \alpha &= -\alpha(2+\alpha).
\end{aligned} \tag{11.65}$$

We can also find a transformation of the form of (11.19).

Lemma 11.2.2. *Fix $0 < m < \infty$, then there exists a change of coordinates*

$$\begin{pmatrix}A\\B\end{pmatrix} = e^{-i\phi(r)}[1 + \mathcal{T}(\alpha)]\begin{pmatrix}\widetilde{A}\\\widetilde{B}\end{pmatrix} + O((|\lambda| + |\widetilde{A}| + |\widetilde{B}|)(|\widetilde{A}| + |\widetilde{B}|)) \tag{11.66}$$

so that (11.65) *becomes*

$$\begin{aligned}
\partial_\tau A &= \left(-\frac{1}{2} - \frac{\alpha}{2}\right)A + B + h.o.t.\\
\partial_\tau B &= \left(-\frac{1}{2} - \frac{\alpha}{2}\right)B + c_1\lambda A + h.o.t.\\
\partial_\tau \alpha &= -\alpha(2+\alpha).
\end{aligned} \tag{11.67}$$

The constant c_1 is given by

$$c_1 = -s_1\frac{\Gamma_1 + \Gamma_2}{3}.$$

The coordinate change is polynomial in (A, B, α) and smooth in λ and $\mathcal{T}(\alpha) = O(\alpha)$ is linear and upper triangular for each α, while $\phi(r)$ satisfies

$$\partial_r\phi(r) = \frac{\sqrt{3}}{2} + O(|\lambda| + |\alpha| + |A|^2), \quad \phi(0) = 0.$$

Note that at $(\alpha, \lambda) = (0, 0)$, the trivial state $(A, B) = (0, 0)$ is hyperbolic such that the higher order terms in equation (11.67) are exponentially small for $\tau \gg 1$ and λ small enough and can be neglected. We can also directly solve the linear part of equation (11.67) and obtain:

$$\begin{pmatrix} A(\tau) \\ B(\tau) \end{pmatrix} = \frac{1}{\sqrt{\sinh(\tau)}} \left[q_1 e^{-\tau\sqrt{c_1\lambda}} \begin{pmatrix} 1 \\ -\sqrt{c_1\lambda} \end{pmatrix} + q_2 e^{\tau\sqrt{c_1\lambda}} \begin{pmatrix} 1 \\ \sqrt{c_1\lambda} \end{pmatrix} \right]. \quad (11.68)$$

We want to find solutions which have a finite energy density with respect to the hyperbolic measure, *i.e.* functions that are in $\mathrm{L}^2(\mathbb{R}^+, \sinh(\tau)d\tau)$. This restriction implies that we need to track the stable fast $\mathcal{W}_+^{sf}(\lambda)$ of equation (11.68) which corresponds to eigenvalues ℓ of $\mathcal{A}(\infty, \lambda)$ with real part less than $-\frac{1}{2}$ as shown in figure 11.1. Thus, for each fixed $\tau_0 \gg 1$ and for all sufficiently small $\lambda < 0$, we can write the $\tau = \tau_0$-fiber of the stable fast manifold $\mathcal{W}_+^{sf}(\lambda)$ of equation (11.68) near $U = 0$ as

$$\mathcal{W}_+^{sf}(\lambda)\,|_{\tau=\tau_0} \;:\; \begin{pmatrix} A \\ B \end{pmatrix} = e^{-\tau_0/2} \left[-\eta\sqrt{c_1\lambda}\,(1 + O_{\tau_0}(|\lambda|)) \begin{pmatrix} \tau_0 \\ 1 \end{pmatrix} + \sqrt{c_1\lambda}\eta \begin{pmatrix} 1 \\ 0 \end{pmatrix} \right] \quad (11.69)$$

for $\eta \in \mathbb{C}$.

Our goal is now to find nontrivial intersections of the stable fast manifold $\mathcal{W}_+^{sf}(\lambda)$ with the center-unstable manifold $\mathcal{W}_-^{cu}(\lambda)$. To this end, we write the expansion (11.62) for each fixed $\tau_0 \gg 1$ in the $(\tilde{A}, \tilde{B})$ coordinates and afterwards in the coordinates (A, B). Using the expansions of the associated Legendre functions given in table 11.1 we arrive at the expression

$$\begin{pmatrix} \tilde{A} \\ \tilde{B} \end{pmatrix} = e^{-\tau_0/2} \left[e^{i\left(\frac{\sqrt{3}}{2}\tau_0 + \Phi_0\right)} \begin{pmatrix} \frac{C_0}{2}\tilde{d}_1(1 + O(1)) + \tau_0\tilde{d}_2\left(-i\frac{\sqrt{3}C_0}{6} + O(1)\right) \\ -\tilde{d}_2(i\frac{\sqrt{3}C_0}{6} + O(1)) + \frac{C_1\sqrt{3}}{6}\left(\Xi_{\tilde{d}_1^2}\tilde{d}_1^2 + \Xi_{\tilde{d}_1\tilde{d}_2}\tilde{d}_1\tilde{d}_2\right) \end{pmatrix} \right.$$
$$\left. + e^{i\left(\frac{\sqrt{3}}{2}\tau_0 + \Phi_0\right)} \begin{pmatrix} O_{\tau_0}(\lambda|\tilde{d}| + |\tilde{d}|^2) \\ O_{\tau_0}(\lambda|\tilde{d}| + |\tilde{d}_2|^2 + |\tilde{d}_1|^3) \end{pmatrix} \right]. \quad (11.70)$$

We can apply the transformation (11.66) to equation (11.70) and obtain the expansion:

$$\mathcal{W}_-^{cu}(\lambda)\,|_{\tau=\tau_0} \;:\; \begin{pmatrix} A \\ B \end{pmatrix} = e^{i(\Phi_0 + O(\tau_0^{-2}) + O_{\tau_0}(\lambda|\tilde{d}| + |\tilde{d}|^2)} \begin{pmatrix} O_{\tau_0}(\lambda|\tilde{d}| + |\tilde{d}|^2) \\ O_{\tau_0}(\lambda|\tilde{d}| + |\tilde{d}_2|^2 + |\tilde{d}_1|^3) \end{pmatrix}$$
$$+ e^{i(\Phi_0 + O(\tau_0^{-2}) + O_{\tau_0}(\lambda|\tilde{d}| + |\tilde{d}|^2)} \begin{pmatrix} \frac{C_0}{2}\tilde{d}_1(1 + O(1)) + \tau_0\tilde{d}_2(-i\frac{\sqrt{3}C_0}{6} + O(1)) \\ -\tilde{d}_2(i\frac{\sqrt{3}C_0}{6} + O(1)) \end{pmatrix}$$
$$+ e^{i(\Phi_0 + O(\tau_0^{-2}) + O_{\tau_0}(\lambda|\tilde{d}| + |\tilde{d}|^2)} \begin{pmatrix} 0 \\ \frac{C_1\sqrt{3}}{6}\left(\Xi_{\tilde{d}_1^2}\tilde{d}_1^2 + \Xi_{\tilde{d}_1\tilde{d}_2}\tilde{d}_1\tilde{d}_2\right) \end{pmatrix}. \quad (11.71)$$

As in the Euclidean case, the final step of the analysis consists in finding nontrivial intersections of the stable fast manifold $\mathcal{W}_+^{sf}(\lambda)$ given above in equation (11.69) and the core manifold $\mathcal{W}_-^{cu}(\lambda)$ given in (11.71). We can easily solve this problem in $(\tilde{d}_1, \tilde{d}_2)$ and we find that:

$$\tilde{d}_1 = -\frac{C_0}{C_1 \Xi_{\tilde{d}_1^2}} \sqrt{3\lambda c_1}, \quad \tilde{d}_2 = O(\lambda).$$

We can now state the main result of this section.

Theorem 11.2.1 (Existence of spot solutions). *Fix $\theta \geq 0$ for the threshold of the nonlinearity S and $(b_1, b_2, \sigma_1, \sigma_2) \in \mathbb{R}^4$ such that the connectivity function W defined in equation (11.47) satisfies hypotheses 11.2.1. Then there exists $\mu_* < \mu_c$ such that the planar neural field equation (11.41) has a stationary localized radial solution $v(\tau)$ for each $\mu \in]\mu_*, \mu_c[$: these solutions stay close to $v = 0$ and, for each fixed $\tau_* > 0$, we have the asymptotics*

$$v(\tau) = \beta \sqrt{\mu_c - \mu}\, \mathcal{P}_{-\frac{1}{2}+i\frac{\sqrt{3}}{2}}(\cosh \tau) + O(\mu - \mu_c) \text{ as } \mu \to \mu_c \tag{11.72}$$

uniformly in $0 \leq \tau \leq \tau_*$ for an appropriate constant β with $sign(\beta) = -sign(\Xi_{\tilde{d}_1^2})$.

11.3 Conclusion

In this chapter we have presented the mechanisms of formation of Spot A solutions of neural field equations for the two geometries: Euclidean and hyperbolic. The main idea is to transform the initial neural field equations into a PDE and look for stationary radially symmetric solutions. We have applied techniques from Scheel, Lloyd and Sandstede [Scheel 2003, Lloyd 2009] to prove the existence of a bifurcated branch of Spot A solution near a Turing instability for the Euclidean case and adapted the proofs for the hyperbolic case. In the Poincaré disk, the analysis near the core manifold is much more involved as it requires the knowledge of the asymptotics of the associated Legendre functions. It turns out that the main difference between the two geometries comes from the far field. At infinity, Bessel function J_0 scales as $1/\sqrt{r}$ whereas associated Legendre function $\mathcal{P}_\nu$ scales as $e^{-\tau/2}$. Moreover, at infinity, there is a Turing instability at $\lambda = 0$ while in the hyperbolic state the trivial state $U = 0$ is always asymptotically stable.

This chapter is actually formal and a rigorous numerical study should be done to highlight the theoretical results. Moreover, for neural field equations set on the Euclidean plane, we also expect the bifurcation of Spots B and localized rings from the spatially homogeneous state provided that the coefficient $c_3^0 < 0$ in lemma 10.2.2 in chapter 10: the one dimensional Turing bifurcation is subcritical (see [McCalla 2010, McCalla 2011] for the planar Swift-Hohenberg equation).

Part IV

Conclusion

Chapter 12

General conclusion

In this Thesis, we have applied tools from dynamical systems to study, from a theoretical point of view, the spontaneous activity of neural field equations. We decided to focus our analysis on the symmetries given by the models and study the different cortical states that can be produced because of these symmetries. After the general introduction in part I, this Thesis splits in two mains parts, one being dedicated to spatially periodic solutions and symmetry-breaking mechanism on different kind of lattices, in different geometries, and the other one being centered on the study of localized solutions.

In the part concerning spatially periodic solutions, we have developped an analysis of nonlinear pattern formation in the Poincaré disk, motivated by a model of texture perception in the visual cortex. Functions that are periodic in the Poincaré disk are, by definition, invariant under the action of a discrete subgroup of the group of isometries of the Poincaré disk whose fundamental domain is a polygon. Tilings of the Poincaré disc have very different properties from tilings of the Euclidean plane. In particular tilings exist with polygons having an arbitrary number of sides, while in the Euclidean plane only rhombic, square and hexagonal periodic tilings exist. In this Thesis we have studied the case where the Poincaré disk is tiled with regular octagons. In this case, the quotient of the Poincaré disk by the tiling group is a double torus (genus 2 surface) hence a compact manifold and techniques from equivariant bifurcation theory can be applied. Solutions which generically bifurcate are called "H-planforms", by analogy with the "planforms" introduced for pattern formation in Euclidean space. We have presented a complete classification all possible H-planforms satisfying the hypotheses of the Equivariant Branching Lemma. However, these patterns are not easy to compute, even numerically, and we presented several methods for their computation. All the irreducible representations of the octagonal tiling group were described: four representations have dimension one, two have dimension two, four have dimension three and three have dimension four. Each of these cases leads to a different bifurcation diagram. We have shown that the bifurcation problem for the 2D cases is equivalent to problem with triangular symmetry, and in the 3D cases, to problem with octahedral symmetry. It follows that the bifurcation diagrams in these cases are known and show generically no other bounded dynamics than the trivial ones associated with the equilibria with maximal isotropy. The 4D case is much more involved. We have studied separately the bifurcation diagrams and local dynamics in the 4D irreducible representation spaces of the octagonal tiling group. We have also demonstrated that in one of these cases, there is a generic bifurcation of a heteroclinic network connecting equilibria with two different orbit types. We have also shown that bifurcation with

submaximal isotropy could occur generically.

In the last chapter of the part concerning spatially periodic solutions, we have considered a spatial extension of the structure tensor model. We have conducted a mathematical analysis of interacting hypercolumns that takes into account the functional geometry of local and lateral connections in the primary visual cortex. We have explicitly written down the lateral coupling function that incorporates recent experimental data. The network topology of the hypercolumn was taken to be that of the Poincaré disk. We investigated the spontaneous formation of cortical activity patterns and addressed to two different problems. Firstly, natural images can only produce a bounded set of structure tensors and, as suggested by microelectrode recordings, the lateral connections modulate rather than drive the cortical activity. The aim was to study the case of no lateral coupling (model of a single hypercolumn) and to infer properties when anisotropic coupling is added, when the feature space is reduced to a compact disk in the Poincaré disk. The second problem was based on the fact that anisotropy in lateral connections can be small depending on the animal studied. This suggests that the isotropic case should be studied and the properties of the anisotropic case inferred. The strategy adopted in order to solve this problem was to determine solutions to symmetry-breaking bifurcations in the isotropic case and study how these solutions may change when anisotropy is introduced as a forced symmetry-breaking parameter.

In the last part we have theoretically investigated stationary spatially localized solutions of neural field equations set on unbounded domains with smooth firing rate function. In the neuroscience community, these solutions are believed to be the analog of short-term memory and thus are of particular interest. The main results of this work are (i) a rigorous proof of the existence of localized states via homoclinic bifurcation in the scalar case and a numerical analysis exhibiting "snaking" bifurcation diagrams, (ii) a proof of the existence of localized radial solutions in the Euclidean plane, (iii) an extension of the results to the Poincaré disk. The study of localized solutions in the Euclidean plane and the Poincaré disk draws on the methods developed in [Scheel 2003, Lloyd 2009, McCalla 2010] for the Swift-Hohenberg equation, but which had not been applied previously to neural field equations.

Perspectives

The work concerning pattern formation in neural field equations can be pushed further. One could pursue the analysis of pattern formation in the Poincaré disk and look, for example, at non-octagonal tilings and pseudoscalar actions. We think that chapters 6, 7 and 8 provide most of the methods required to tackle such studies. Furthermore, concerning localized solutions in the 2D case, the analysis initiated in chapter 11 should be extended. The next step would be to study, for the Euclidean case, the bifurcation of hexagonal localized solutions form the radially symmetric solution along the lines of [Lloyd 2008]. And the second natural step would be to

apply the same ideas in the context of the Poincaré disk.

One of the major remaining issues in neural field equations is the impact of the external visual inputs on the dynamics. Typically, external inputs are simply ignored and only spontaneous cortical activity is studied [Bressloff 2001b, Chossat 2011]. External inputs can have various forms and depend upon time, space or features [Ermentrout 2010b, Rankin 2011]. It is also reasonable to think that inputs are source of external noise [Hutt 2008]. Without any input, neural field equations with convolutional coupling function have naturally some symmetry properties which are broken when the input is turned on. The simplest example is the ring model of orientation [Ben-Yishai 1995, Veltz 2011]: the amplitude, ε, of the thalamic external input is seen as forced symmetry-breaking parameter: without any input ($\varepsilon = 0$) the model presents an $\mathbf{O}(2)$-symmetry which is broken when the input is switched on ($\varepsilon > 0$). We see two different challenging issues. The first one is to analyse the effects of a localized visual input in spatially extended neural field models, like the spatialized model in chapter 8, and compare the mathematical results to experimental data. The second challenge is the question of noisy external input and the analysis of the related stochastic neural field equations.

Presently, there is no biological evidence for the existence of structure tensors encoded in the primary visual cortex. This is why we need to make predictions that can be easily recovered by experimentalists. So far, it has been explained in details in chapter 3 how the structure tensor model encompasses the well-known ring model of orientation [Ben-Yishai 1995] and in 8 it has been shown that it was possible to recover all the geometric visual hallucinations found by Bressloff et al [Bressloff 2001b]. In order to further pursue the validation of the model, it was also explained how to identify a point in the Poincaré disk to a point in a polar map (see chapter 3). Having done this identification, one can ask the question of formation of map of structure tensors during cortical development. This problem is directly related to the work of Wolf [Wolf 1998, Kaschube 2008, Kaschube 2010] for cortical map of orientation and the work of Bressloff and Oster for ocular dominance map [Oster 2006, Bressloff 2010]. It would be very interesting to model a structure tensor map on a growing cortex with different topolgy (disk, square and sphere) using an evolution equation similar to those proposed in [Kaschube 2008, Bressloff 2010]. The maps obtained from the model could be then compared to those obtained experimentally by optical imaging techniques.

In the past decade, there has been a growing interest to what is called the neurogeometry of the visual cortex [Petitot 2003b, Sarti 2008, Petitot 2009] where the group of Euclidean transformations of the plane plays an important role. The functional architecture of the primary visual cortex is modeled as a principal fiber bundle where the two-dimensional retinal plane is the base manifold and hyprecolumns of orientations constitute the vertical fibers over each point. Such an approach has been successfully applied in computer vision for completion problem and in psychophysics for Kaniza's illusory contours. It could be interesting to study a model of neurogeometry where the primary visual cortex is modeled as a principal fiber bundle where the base manifold is abstracted by $\mathbb{R}^2$ and hypercolumns of struc-

ture tensors constitute the vertical fibers over each point and apply it to surface completion problem.

In chapter 7, it was shown that there is a generic bifurcation of a heteroclinic network connecting equilibria with two different orbit types. So far, only sufficient conditions on the parameters for essential stability of this network have been given. The question of the stability of this network, in a more general setting, remains open. It would be very interesting for a mathematical point of view to pursue the analysis of this heteroclinic network.

Part V

Appendix

Appendix A

Appendix for the four-dimensional representations

Contents

A.1 Computation of low-order equivariants 255
A.1.1 Computational part of the proof of theorem 7.2.1 255
A.1.2 Computational part of the proof of theorem 7.3.1 257
A.2 Fixed-point subspaces 258
A.2.1 Proof of Lemma 7.2.3 258
A.2.2 Proof of Lemma 7.3.3 259

A.1 Computation of low-order equivariants

A.1.1 Computational part of the proof of theorem 7.2.1

Proposition A.1.1. *For the irreductible representation χ_{12}, the two cubic equivariant maps are:*

$$E_1(\mathbf{z}) = \mathbf{z}\left(|z_1|^2 + |z_2|^2\right) \text{ and } E_2(\mathbf{z}) = \begin{bmatrix} \sqrt{3}\left(3z_1^2 + \bar{z}_2^2\right)\bar{z}_1 - \mathbf{i}\left(z_2^2 + 3\bar{z}_1^2\right)z_2 \\ \sqrt{3}\left(3\bar{z}_1^2 + z_2^2\right)z_1 + \mathbf{i}\left(\bar{z}_2^2 + 3z_1^2\right)\bar{z}_2 \\ \sqrt{3}\left(3z_2^2 + \bar{z}_1^2\right)\bar{z}_2 + \mathbf{i}\left(z_1^2 + 3\bar{z}_2^2\right)z_1 \\ \sqrt{3}\left(3\bar{z}_2^2 + z_1^2\right)z_2 - \mathbf{i}\left(\bar{z}_1^2 + 3z_2^2\right)\bar{z}_1 \end{bmatrix} \tag{A.1}$$

Proof. Let E denote a homogeneous equivariant mapping. We want to deduce the restrictions placed on the form of E by the symmetry group $\mathcal{G}$. We first choose appropriate coordinates. Thanks to proposition 7.1.2 of subsection 7.1.4 we have a presentation of $\mathcal{G}$ with 4×4 real matrices with generators ρ, σ, κ given by equation 7.2. The eigenvalues of ρ are $\exp(\pm\frac{\mathbf{i}\pi}{4}), \exp(\pm\frac{3\mathbf{i}\pi}{4})$ (where $\mathbf{i}^2 = -1$). And we have the following decomposition:

$$\rho_P = P^{-1}\rho P = \begin{bmatrix} \exp(\frac{\mathbf{i}\pi}{4}) & 0 & 0 & 0 \\ 0 & \exp(-\frac{\mathbf{i}\pi}{4}) & 0 & 0 \\ 0 & 0 & \exp(\frac{3\mathbf{i}\pi}{4}) & 0 \\ 0 & 0 & 0 & \exp(-\frac{3\mathbf{i}\pi}{4}) \end{bmatrix}$$

$$\text{with } P = \begin{bmatrix} \mathbf{i} & -\mathbf{i} & \mathbf{i} & -\mathbf{i} \\ -1 & -1 & 1 & 1 \\ -\mathbf{i} & \mathbf{i} & \mathbf{i} & -\mathbf{i} \\ 1 & 1 & 1 & 1 \end{bmatrix}.$$

Then we can express in this basis the other generators:

$$\sigma_P = P^{-1}\sigma P = \frac{\sqrt{2}}{4}\begin{bmatrix} 1 & \mathbf{i}\sqrt{3} & 1 & -\mathbf{i}\sqrt{3} \\ -\mathbf{i}\sqrt{3} & 1 & \mathbf{i}\sqrt{3} & 1 \\ 1 & -\mathbf{i}\sqrt{3} & -1 & -\mathbf{i}\sqrt{3} \\ \mathbf{i}\sqrt{3} & 1 & \mathbf{i}\sqrt{3} & -1 \end{bmatrix},$$

$$\text{and } \kappa_P = P^{-1}\kappa P = \begin{bmatrix} 0 & \mathbf{i} & 0 & 0 \\ -\mathbf{i} & 0 & 0 & 0 \\ 0 & 0 & 0 & \mathbf{i} \\ 0 & 0 & -\mathbf{i} & 0 \end{bmatrix}.$$

We denote $\mathbf{z} = (z_1, \bar{z}_1, z_2, \bar{z}_2)$ the complex coordinates associated to the eigenvectors of ρ i.e the columns of P. Write E in components as $(f_1, \bar{f}_1, f_2, \bar{f}_2)^{\mathbf{T}}$. We begin by describing the action of ρ_P on the equivariant map E.

For all $\mathbf{z}$, the action is given by $\rho_P \cdot \mathbf{z} = (e^{\frac{\mathbf{i}\pi}{4}} z_1, e^{-\frac{\mathbf{i}\pi}{4}} \bar{z}_1, e^{\frac{3\mathbf{i}\pi}{4}} z_2, e^{-\frac{3\mathbf{i}\pi}{4}} \bar{z}_2)$ and the equivariance yields

$$\begin{cases} e^{\frac{\mathbf{i}\pi}{4}} f_1(z_1, \bar{z}_1, z_2, \bar{z}_2) = f_1(e^{\frac{\mathbf{i}\pi}{4}} z_1, e^{-\frac{\mathbf{i}\pi}{4}} \bar{z}_1, e^{\frac{3\mathbf{i}\pi}{4}} z_2, e^{-\frac{3\mathbf{i}\pi}{4}} \bar{z}_2) \\ e^{\frac{\mathbf{i}3\pi}{4}} f_2(z_1, \bar{z}_1, z_2, \bar{z}_2) = f_2(e^{\frac{\mathbf{i}\pi}{4}} z_1, e^{-\frac{\mathbf{i}\pi}{4}} \bar{z}_1, e^{\frac{3\mathbf{i}\pi}{4}} z_2, e^{-\frac{3\mathbf{i}\pi}{4}} \bar{z}_2) \end{cases} \tag{A.2}$$

We are looking for cubic equivariants of the form $\alpha z_1^{k_1} \bar{z}_1^{l_1} z_2^{k_2} \bar{z}_2^{l_2}$ satisfying the relation $k_1 + k_2 + l_1 + l_2 = 3$. So with the first equation of (A.2) we simply get

$$\alpha e^{\frac{\mathbf{i}\pi}{4}} z_1^{k_1} \bar{z}_1^{l_1} z_2^{k_2} \bar{z}_2^{l_2} = \alpha e^{\mathbf{i}\frac{\pi}{4}[(k_1 - l_1) + 3(k_2 - l_2)]} z_1^{k_1} \bar{z}_1^{l_1} z_2^{k_2} \bar{z}_2^{l_2}$$

In order that this is equivariant under the action of ρ_P we have to impose:

$$(k_1 - l_1 - 1) + 3(k_2 - l_2) = 8n \text{ with } n \in \mathbb{Z}$$

which gives 5 elements in f_1.

$$f_1(z_1, \bar{z}_1, z_2, \bar{z}_2) = a_1 z_1^2 \bar{z}_1 + a_2 z_1 z_2 \bar{z}_2 + a_3 z_2^3 + a_4 \bar{z}_1^2 z_2 + a_5 \bar{z}_1 \bar{z}_2^2$$

with $(a_i)_{i=1\ldots5} \in \mathbb{C}^5$. In the same fashion the second equation of (A.2) gives 5 elements in f_2.

$$f_2(z_1, \bar{z}_1, z_2, \bar{z}_2) = b_1 z_2^2 \bar{z}_2 + b_2 z_1 \bar{z}_1 z_2 + b_3 z_1^3 + b_4 z_1 \bar{z}_2^2 + b_5 \bar{z}_1^2 \bar{z}_2$$

with $(b_i)_{i=1\ldots5} \in \mathbb{C}^5$.

The action of κ_P on $\mathbf{z}$ is given by $\kappa_P \cdot \mathbf{z} = (\mathbf{i}\bar{z}_1, -\mathbf{i}z_1, \mathbf{i}\bar{z}_2, -\mathbf{i}z_2)$. It is straightforward to see that this action imposes that $a_1, a_2, a_5, b_1, b_2, b_5$ are real and that a_3, a_4, b_3, b_4 are imaginary numbers. Then we can rewrite f_1 and f_2 as:

$$f_1(z_1, \bar{z}_1, z_2, \bar{z}_2) = \alpha_1 z_1^2 \bar{z}_1 + \alpha_2 z_1 z_2 \bar{z}_2 + \mathbf{i}\alpha_3 z_2^3 + \mathbf{i}\alpha_4 \bar{z}_1^2 z_2 + \alpha_5 \bar{z}_1 \bar{z}_2^2$$

$$f_2(z_1,\bar{z}_1,z_2,\bar{z}_2)=\beta_1 z_2^2\bar{z}_2+\beta_2 z_1\bar{z}_1 z_2+\mathbf{i}\beta_3 z_1^3+\mathbf{i}\beta_4 z_1\bar{z}_2^2+\beta_5\bar{z}_1^2\bar{z}_2$$

with $(\alpha_i,\beta_i)_{i=1\ldots5}\in(\mathbb{R}\times\mathbb{R})^5$.

Action of σ_P:

The action of σ_P on $\mathbf{z}$ is given by

$$\sigma_P\cdot\mathbf{z}=\begin{pmatrix}\frac{\sqrt{2}}{4}\left(z_1+z_2+\mathbf{i}\sqrt{3}(\bar{z}_1-\bar{z}_2)\right)\\ \frac{\sqrt{2}}{4}\left(\bar{z}_1+\bar{z}_2-\mathbf{i}\sqrt{3}(z_1-z_2)\right)\\ \frac{\sqrt{2}}{4}\left(z_1-z_2-\mathbf{i}\sqrt{3}(\bar{z}_1+\bar{z}_2)\right)\\ \frac{\sqrt{2}}{4}\left(\bar{z}_1-\bar{z}_2+\mathbf{i}\sqrt{3}(z_1+z_2)\right)\end{pmatrix}^{\mathbf{T}}$$

and we find:

$$f_1(z_1,\bar{z}_1,z_2,\bar{z}_2)=az_1(|z_1|^2+|z_2|^2)+b\left(3\sqrt{3}z_1|z_1|^2-\mathbf{i}z_2^3-3\mathbf{i}\bar{z}_1^2z_2+\sqrt{3}\bar{z}_1\bar{z}_2^2\right)$$

$$f_2(z_1,\bar{z}_1,z_2,\bar{z}_2)=az_2(|z_1|^2+|z_2|^2)+b\left(3\sqrt{3}z_2|z_2|^2+\mathbf{i}z_1^3+3\mathbf{i}z_1\bar{z}_2^2+\sqrt{3}\bar{z}_1^2\bar{z}_2\right)$$

with $(a,b)\in\mathbb{R}^2$.

□

A.1.2 Computational part of the proof of theorem 7.3.1

Proposition A.1.2. *For the irreductible representation χ_{11}, the four quintic equivariant maps are:*

$$E_{5,1}(\mathbf{z})=\mathbf{z}\|\mathbf{z}\|^4,\quad E_{5,2}=\begin{bmatrix}z_1^4\bar{z}_2+4z_2^3|z_1|^2-z_2^3|z_2|^2\\ \bar{z}_1^4z_2+4\bar{z}_2^3|z_1|^2-\bar{z}_2^3|z_2|^2\\ -\bar{z}_1z_2^4-4z_1^3|z_2|^2+z_1^3|z_1|^2\\ -z_1\bar{z}_2^4-4\bar{z}_1^3|z_2|^2+\bar{z}_1^3|z_1|^2\end{bmatrix}$$

$$E_{5,3}=\begin{bmatrix}3\bar{z}_1^2z_2|z_2|^2-z_1^2\bar{z}_2^3-2\bar{z}_1^2|z_1|^2z_2\\ 3z_1^2\bar{z}_2|z_2|^2-\bar{z}_1^2z_2^3-2z_1^2|z_1|^2\bar{z}_2\\ -3z_1\bar{z}_2^2|z_1|^2+\bar{z}_1^3z_2^2+2z_1\bar{z}_2^2|z_2|^2\\ -3\bar{z}_1z_2^2|z_1|^2+z_1^3\bar{z}_2^2+2\bar{z}_1z_2^2|z_2|^2\end{bmatrix},\quad E_{5,4}=\begin{bmatrix}-5\bar{z}_1^4\bar{z}_2+\bar{z}_2^5\\ -5z_1^4z_2+z_2^5\\ 5\bar{z}_1\bar{z}_2^4-\bar{z}_1^5\\ 5z_1z_2^4-z_1^5\end{bmatrix}$$

Proof. Let E denote a homageneous cubic equivariant mapping. Thanks to proposition 7.1.3 of subsection 7.1.4 the generators of $\mathcal{G}$ are given in matrix form in equation (7.3). The eigenvalues of ρ are still $\exp(\pm\frac{\mathbf{i}\pi}{4}),\exp(\pm\frac{3\mathbf{i}\pi}{4})$. And we have the following decomposition:

$$\rho_P=P^{-1}\rho P=\begin{bmatrix}\exp(\frac{\mathbf{i}\pi}{4})&0&0&0\\ 0&\exp(-\frac{\mathbf{i}\pi}{4})&0&0\\ 0&0&\exp(\frac{3\mathbf{i}\pi}{4})&0\\ 0&0&0&\exp(-\frac{3\mathbf{i}\pi}{4})\end{bmatrix}\text{ with }P=\begin{bmatrix}\mathbf{i}&-\mathbf{i}&-\mathbf{i}&\mathbf{i}\\ -1&-1&1&1\\ \mathbf{i}&-\mathbf{i}&\mathbf{i}&-\mathbf{i}\\ 1&1&1&1\end{bmatrix}$$

Then we can express in this basis the other generators:

$$\sigma_P = P^{-1}\sigma P = \frac{\sqrt{2}}{2}\begin{bmatrix} -1 & 0 & -\mathbf{i} & 0 \\ 0 & -1 & 0 & \mathbf{i} \\ \mathbf{i} & 0 & 1 & 0 \\ 0 & -\mathbf{i} & 0 & 1 \end{bmatrix} \text{ and } \kappa_P = P^{-1}\kappa P = \begin{bmatrix} 0 & \mathbf{i} & 0 & 0 \\ -\mathbf{i} & 0 & 0 & 0 \\ 0 & 0 & 0 & -\mathbf{i} \\ 0 & 0 & \mathbf{i} & 0 \end{bmatrix}$$

We denote $\mathbf{z} = (z_1, \bar{z}_1, z_2, \bar{z}_2)$ the complex coordinates associated to the eigenvectors of ρ i.e the columns of P. Write E in components as $(f_1, \bar{f}_1, f_2, \bar{f}_2)^{\mathbf{T}}$. The action of ρ_P on a quintic equivariant map of the form $\alpha z_1^{k_1}\bar{z}_1^{l_1}z_2^{k_2}\bar{z}_2^{l_2}$ with the relation $k_1+k_2+l_1+l_2=5$ implies that $(k_1-l_1-1)+3(k_2-l_2)=8n$ with $n\in\mathbb{Z}$, which gives 14 elements in f_1.

$$f_1(z_1,\bar{z}_1,z_2,\bar{z}_2) = a_1 z_1^3\bar{z}_1^2 + a_2 z_1 z_2^2\bar{z}_2^2 + a_3 z_1^2\bar{z}_1 z_2\bar{z}_2 + a_4 z_1^4\bar{z}_2 + a_5\bar{z}_1^2 z_2^2\bar{z}_2 + a_6 z_1\bar{z}_1 z_2^3 + a_7 z_1^3 z_2^2$$
$$+ a_8 z_2^4\bar{z}_2 + a_9 z_1^2\bar{z}_2^3 + a_{10} z_1\bar{z}_1^2\bar{z}_2^2 + a_{11}\bar{z}_1 z_2\bar{z}_2^3 + a_{12}\bar{z}_1^4\bar{z}_2 + a_{13}\bar{z}_2^5 + a_{14} z_1\bar{z}_1^3 z_2$$

And we also obtain 14 elements in f_2 with the same method:

$$f_2(z_1,\bar{z}_1,z_2,\bar{z}_2) = b_1 z_1^2\bar{z}_1^2 z_2 + b_2 z_1\bar{z}_1 z_2^2\bar{z}_2 + b_3 z_2^3\bar{z}_2^2 + b_4 z_1^4\bar{z}_1 + b_5 z_1^3 z_2\bar{z}_2 + b_6\bar{z}_1^3 z_2^2 + b_7 z_1^2 z_2^3$$
$$+ b_8\bar{z}_1 z_2^4 + b_9 z_1 z_2\bar{z}_2^3 + b_{10} z_1^2\bar{z}_1\bar{z}_2^2 + b_{11} z_1\bar{z}_1^3\bar{z}_2 + b_{12}\bar{z}_1^2 z_2\bar{z}_2^2 + b_{13}\bar{z}_1^5 + b_{14}\bar{z}_1\bar{z}_2^4$$

where $(a_j)_{j=1\dots14}\in\mathbb{C}^{14}$ and $(b_j)_{j=1\dots14}\in\mathbb{C}^{14}$.

The action of κ_P implies that the coefficients $(a_j, b_j)_{j=1\dots14}$ are real. The action of σ_P is $\sigma_P\cdot\mathbf{z} = \frac{\sqrt{2}}{2}(-z_1 - \mathbf{i}z_2, -\bar{z}_1 + \mathbf{i}\bar{z}_2, \mathbf{i}z_1 + z_2, -\mathbf{i}\bar{z}_1 + \bar{z}_2)$ and we obtain:

$$f_1(z_1,\bar{z}_1,z_2,\bar{z}_2) = a(z_1|z_1|^4 + z_1|z_2|^4 + 2z_1|z_1|^2|z_2|^2) + b(z_1^4\bar{z}_2 + 4z_2^3|z_1|^2 - z_2^3|z_2|^2)$$
$$+ c(3\bar{z}_1^2 z_2|z_2|^2 - z_1^2\bar{z}_2^3 - 2\bar{z}_1^2|z_1|^2 z_2) + d(-5\bar{z}_1^4\bar{z}_2 + \bar{z}_2^5)$$
$$f_2(z_1,\bar{z}_1,z_2,\bar{z}_2) = a(z_2|z_2|^4 + z_2|z_1|^4 + 2z_2|z_1|^2|z_2|^2) + b(-\bar{z}_1 z_2^4 - 4z_1^3|z_2|^2 + z_1^3|z_1|^2)$$
$$+ c(-3z_1\bar{z}_2^2|z_1|^2 + \bar{z}_1^3 z_2^2 + 2z_1\bar{z}_2^2|z_2|^2) + d(5\bar{z}_1\bar{z}_2^4 - \bar{z}_1^5)$$

with $(a,b,c,d)\in\mathbb{R}^4$. Thus, we find 4 equivariant maps which is in agreement with computation of the Molien serie of subsection 7.1.5. □

A.2 Fixed-point subspaces

A.2.1 Proof of Lemma 7.2.3

To complete the proof of Lemma 7.2.3 we give the matrix of $\sigma, \tilde{\sigma}, \varepsilon, \kappa, \kappa'$ and κ'' in the basis associated to coordinates $(z_1, \bar{z}_1, z_2, \bar{z}_2)$.

$$\sigma = \frac{\sqrt{2}}{4}\begin{bmatrix} 1 & \mathbf{i}\sqrt{3} & 1 & -\mathbf{i}\sqrt{3} \\ -\mathbf{i}\sqrt{3} & 1 & \mathbf{i}\sqrt{3} & 1 \\ 1 & -\mathbf{i}\sqrt{3} & -1 & -\mathbf{i}\sqrt{3} \\ \mathbf{i}\sqrt{3} & 1 & \mathbf{i}\sqrt{3} & -1 \end{bmatrix}, \quad \tilde{\sigma} = \frac{\sqrt{2}}{4}\begin{bmatrix} 1 & -\mathbf{i}\sqrt{3} & -1 & -\mathbf{i}\sqrt{3} \\ \mathbf{i}\sqrt{3} & 1 & \mathbf{i}\sqrt{3} & -1 \\ -1 & -\mathbf{i}\sqrt{3} & -1 & \mathbf{i}\sqrt{3} \\ \mathbf{i}\sqrt{3} & -1 & -\mathbf{i}\sqrt{3} & -1 \end{bmatrix}$$

$$\varepsilon = \frac{1}{4}\begin{bmatrix} 1-\mathbf{i} & \sqrt{3}(\mathbf{i}-1) & -1-\mathbf{i} & \sqrt{3}(1+\mathbf{i}) \\ -\sqrt{3}(1+\mathbf{i}) & 1+\mathbf{i} & \sqrt{3}(1-\mathbf{i}) & \mathbf{i}-1 \\ 1-\mathbf{i} & \sqrt{3}(1-\mathbf{i}) & 1+\mathbf{i} & \sqrt{3}(1+\mathbf{i}) \\ \sqrt{3}(1+\mathbf{i}) & 1+\mathbf{i} & \sqrt{3}(1-\mathbf{i}) & 1-\mathbf{i} \end{bmatrix}, \quad \kappa = \begin{bmatrix} 0 & \mathbf{i} & 0 & 0 \\ -\mathbf{i} & 0 & 0 & 0 \\ 0 & 0 & 0 & \mathbf{i} \\ 0 & 0 & -\mathbf{i} & 0 \end{bmatrix}$$

$$\kappa' = \frac{\sqrt{2}}{2}\begin{bmatrix} 0 & \mathbf{i}-1 & 0 & 0 \\ -1-\mathbf{i} & 0 & 0 & 0 \\ 0 & 0 & 0 & -1-\mathbf{i} \\ 0 & 0 & -1+\mathbf{i} & 0 \end{bmatrix}, \quad \kappa'' = \frac{\sqrt{2}}{4}\begin{bmatrix} \sqrt{3} & \mathbf{i} & -\sqrt{3} & \mathbf{i} \\ -\mathbf{i} & \sqrt{3} & -\mathbf{i} & -\sqrt{3} \\ -\sqrt{3} & \mathbf{i} & -\sqrt{3} & -\mathbf{i} \\ -\mathbf{i} & -\sqrt{3} & \mathbf{i} & -\sqrt{3} \end{bmatrix}$$

A.2.2 Proof of Lemma 7.3.3

To complete the proof of Lemma 7.3.3 we give the matrix of σ, κ, κ' and κ'' in the basis associated to coordinates $(z_1, \bar{z}_1, z_2, \bar{z}_2)$.

$$\sigma = \frac{\sqrt{2}}{2}\begin{bmatrix} -1 & 0 & -\mathbf{i} & 0 \\ 0 & -1 & 0 & \mathbf{i} \\ \mathbf{i} & 0 & 1 & 0 \\ 0 & -\mathbf{i} & 0 & 1 \end{bmatrix}, \quad \kappa = \begin{bmatrix} 0 & \mathbf{i} & 0 & 0 \\ -\mathbf{i} & 0 & 0 & 0 \\ 0 & 0 & 0 & -\mathbf{i} \\ 0 & 0 & \mathbf{i} & 0 \end{bmatrix}$$

$$\kappa' = \frac{\sqrt{2}}{2}\begin{bmatrix} 0 & \mathbf{i}-1 & 0 & 0 \\ -1-\mathbf{i} & 0 & 0 & 0 \\ 0 & 0 & 0 & 1+\mathbf{i} \\ 0 & 0 & 1-\mathbf{i} & 0 \end{bmatrix}, \quad \kappa'' = \frac{\sqrt{2}}{2}\begin{bmatrix} 0 & -\mathbf{i} & 0 & -1 \\ \mathbf{i} & 0 & -1 & 0 \\ 0 & -1 & 0 & -\mathbf{i} \\ -1 & 0 & \mathbf{i} & 0 \end{bmatrix}$$

Appendix B

Appendix for chapter 8

Contents

B.1 Computation of ϖ in 8.2.2.2 261
B.2 Proof of Lemma 8.3.1 263
B.3 Calculation of cubic equivariants 265

B.1 Computation of ϖ in 8.2.2.2

We use methods developped in [Haragus 2010] in order to compute the coefficient ϖ in the normal form (8.17). We use the scalar product:

$$\langle \zeta_1, \zeta_j \rangle = \frac{1}{\pi} \int_0^{\omega} \int_0^{2\pi} \zeta_i(\tau,\theta)\zeta_j(\tau,\theta)\sinh(\tau) d\tau d\theta = \delta_{i,j}.$$

If we rewrite equation (8.14) as

$$V' = \mathbf{L}V + \mathcal{R}(V,\lambda)$$

with $\lambda = \mu - \mu_c$ and

$$\begin{aligned}
\mathbf{L}V(\tau,\theta) &= -V(\tau,\theta) + \mu_c s_1 \int_0^{\omega} \int_0^{2\pi} W_{loc}\left(\tau,\tau' \mid \theta-\theta'\right) V(\tau',\theta')\sinh(\tau') d\tau' d\theta' \\
\mathcal{R}(V,\lambda) &= \int_0^{\omega} \int_0^{2\pi} W_{loc}\left(\tau,\tau' \mid \theta-\theta'\right) S((\lambda+\mu_c)V(\tau',\theta'))\sinh(\tau') d\tau' d\theta' \\
&\quad - \mu_c s_1 \int_0^{\omega} \int_0^{2\pi} W_{loc}\left(\tau,\tau' \mid \theta-\theta'\right) V(\tau',\theta')\sinh(\tau') d\tau' d\theta'.
\end{aligned}$$

Taylor expanding the map Ψ:

$$\Psi(A,B,\lambda) = \sum_{1 \le s+l+m \le 3} A^s B^l \lambda^m \Psi_{slm}$$

and $\mathcal{R}$:

$$\mathcal{R}(V,\lambda) = \mathcal{R}_{11}(V,\lambda) + \mathcal{R}_{20}(V,V) + \mathcal{R}_{30}(V,V,V) + \text{h.o.t.}$$

with

$$\mathcal{R}_{11}(V,\lambda) = \lambda s_1 \int_0^\omega \int_0^{2\pi} W_{loc}\left(\tau,\tau' \mid \theta-\theta'\right) V(\tau',\theta')\sinh(\tau')d\tau' d\theta'$$
$$\mathcal{R}_{20}(U,V) = \frac{\mu_c^2 s_2}{2} \int_0^\omega \int_0^{2\pi} W_{loc}\left(\tau,\tau' \mid \theta-\theta'\right) UV(\tau',\theta')\sinh(\tau')d\tau' d\theta'$$
$$\mathcal{R}_{30}(U,V,W) = \frac{\mu_c^3 s_3}{6} \int_0^\omega \int_0^{2\pi} W_{loc}\left(\tau,\tau' \mid \theta-\theta'\right) UVW(\tau',\theta')\sinh(\tau')d\tau' d\theta'$$

where $s_2 = S''(0)$ and $s_3 = S'''(0)$ we obtain the following system of equations:

$$\begin{aligned} 0 &= \mathbf{L}\Psi_{200} + \mathcal{R}_{20}(\zeta_1,\zeta_1) \\ \varpi &= \langle 2\mathcal{R}_{20}(\Psi_{200},\zeta_1) + \mathcal{R}_{30}(\zeta_1,\zeta_1,\zeta_1),\zeta_1\rangle. \end{aligned} \tag{B.1}$$

We strat by evaluating $\mathcal{R}_{20}(\zeta_1,\zeta_1)$:

$$\begin{aligned} \mathcal{R}_{20}(\zeta_1,\zeta_1) &= \frac{\mu_c^2 s_2}{2} \int_0^\omega \int_0^{2\pi} W_{loc}\left(\tau,\tau' \mid \theta-\theta'\right) \left(\mathcal{Y}_N^1(\tau')\right)^2 \cos(\theta')^2 \sinh(\tau')d\tau' d\theta' \\ &= \frac{\mu_c^2 s_2}{2}\pi \sum_{n\in\mathbb{N}^*} \mathcal{Y}_n^0(\tau)\widehat{W}_{0,n} \int_0^\omega \mathcal{Y}_n^0(\tau')\left(\mathcal{Y}_N^1(\tau')\right)^2 \sinh(\tau')d\tau' \\ &\quad + \frac{\mu_c^2 s_2}{2}\frac{\pi}{2}\cos(2\theta) \sum_{n\in\mathbb{N}^*} \mathcal{Y}_n^2(\tau)\widehat{W}_{2,n} \int_0^\omega \mathcal{Y}_n^2(\tau')\left(\mathcal{Y}_N^1(\tau')\right)^2 \sinh(\tau')d\tau' \\ &= \frac{\mu_c^2 s_2}{2} \sum_{n\in\mathbb{N}^*} \left[\pi\mathcal{Y}_n^0(\tau)\widehat{W}_{0,n}\gamma_{0,n} + \frac{\pi}{2}\cos(2\theta)\mathcal{Y}_n^2(\tau)\widehat{W}_{2,n}\gamma_{2,n}\right] \end{aligned}$$

where

$$\gamma_{k,n} = \int_0^\omega \mathcal{Y}_n^k(\tau')\left(\mathcal{Y}_1^1(\tau')\right)^2 \sinh(\tau')d\tau'.$$

This implies that:

$$\Psi_{200} = \mathrm{Span}(\zeta_1,\zeta_2) + \sum_{n\in\mathbb{N}^*} \left[c_n^0\mathcal{Y}_n^0(\tau) + c_n^2\cos(2\theta)\mathcal{Y}_n^2(\tau)\right]$$
$$\text{with} \quad c_n^0 = \frac{\mu_c^2 s_2 \pi\widehat{W}_{0,n}\gamma_{0,n}}{2\left(1-\mu_c s_1 2\pi\widehat{W}_{0,n}\right)} \text{ and } c_n^2 = \frac{\mu_c^2 s_2 \pi\widehat{W}_{2,n}\gamma_{2,n}}{4\left(1-\mu_c s_1 \pi\widehat{W}_{2,n}\right)}.$$

It is now possible to compute coefficient ϖ:

$$\begin{aligned} \langle\mathcal{R}_{20}(\Psi_{200},\zeta_1),\zeta_1\rangle &= \frac{\mu_c^2 s_2}{2}\widehat{W}_{1,1}\langle\Psi_{200},\zeta_1\zeta_1\rangle \\ &= \frac{\mu_c^4 s_2^2\pi}{4}\widehat{W}_{1,1} \sum_{n\in\mathbb{N}^*} \left[\frac{\pi\widehat{W}_{0,n}\left(\gamma_{0,n}\right)^2}{\left(1-\mu_c s_1 2\pi\widehat{W}_{0,n}\right)} + \frac{\pi\widehat{W}_{2,n}\left(\gamma_{2,n}\right)^2}{4\left(1-\mu_c s_1\pi\widehat{W}_{2,n}\right)}\right] \end{aligned}$$

and

$$\begin{aligned}\langle \mathcal{R}_{300}(\zeta_1,\zeta_1,\zeta_1),\zeta_1\rangle &= \frac{\mu_c^3 s_3}{6}\widehat{W}_{1,1}\langle \zeta_1\zeta_1,\zeta_1\zeta_1\rangle \\ &= \frac{\mu_c^3 s_3 \pi}{8}\widehat{W}_{1,1}\Lambda \\ \text{with} \quad \Lambda &= \int_0^\omega \left(\mathcal{Y}_1^1(\tau)\right)^4 \sinh(\tau)d\tau\end{aligned}$$

which implies

$$\varpi = \frac{\mu_c^3\pi\widehat{W}_{1,1}}{4}\left(\frac{s_3\Lambda}{2} + \mu_c s_2^2 \sum_{n\in\mathbb{N}^*}\left[\frac{\pi\widehat{W}_{0,n}\left(\gamma_{0,n}\right)^2}{\left(1-\mu_c s_1 2\pi\widehat{W}_{0,n}\right)} + \frac{\pi\widehat{W}_{2,n}\left(\gamma_{2,n}\right)^2}{4\left(1-\mu_c s_1\pi\widehat{W}_{2,n}\right)}\right]\right).$$

B.2 Proof of Lemma 8.3.1

We compute each term in the expression of a and b in (8.32).

$$\begin{aligned}\langle \mathcal{R}_{30}(\Psi_1,\Psi_3,\Psi_3),\Psi_1\rangle &= \frac{\mu_c^3 s_3}{6}\langle W_{loc}\star\left(\Psi_1\Psi_3\Psi_3\right),\Psi_1\rangle \\ &= \frac{\mu_c^3 s_3}{6}\langle \Psi_1\Psi_3\Psi_3, W_{loc}\star\Psi_1\rangle \\ &= \frac{\mu_c^3 s_3}{6}W_{loc}^c\langle\frac{1}{\sqrt{3}}\Psi_{\chi_{10}}^{\mathbf{D}'_{2\kappa}},\frac{1}{\sqrt{3}}\Psi_{\chi_{10}}^{\mathbf{D}'_{2\kappa}}\rangle \\ &= \frac{\mu_c^3 s_3}{18}W_{loc}^c\end{aligned}$$

$$\begin{aligned}\langle \mathcal{R}_{30}(\Psi_3,\Psi_3,\Psi_3),\Psi_3\rangle &= \frac{\mu_c^3 s_3}{6}\langle W_{loc}\star\left(\Psi_3\Psi_3\Psi_3\right),\Psi_3\rangle \\ &= \frac{\mu_c^3 s_3}{6}W_{loc}^c\langle \Psi_3\Psi_3\Psi_3,\Psi_3\rangle \\ &= \frac{\mu_c^3 s_3}{6}W_{loc}^c\langle\frac{6}{5}\Psi_{\chi_6}^{\widetilde{\mathbf{D}}_{8\kappa}}(z)+1,\frac{6}{5}\Psi_{\chi_6}^{\widetilde{\mathbf{D}}_{8\kappa}}(z)+1\rangle \\ &= \frac{61\mu_c^3 s_3}{150}W_{loc}^c\end{aligned}$$

$$\begin{aligned}\langle \mathcal{R}_{20}(\Phi_{1010},\Psi_3),\Psi_1\rangle &= \frac{\mu_c^2 s_2}{2}\langle W_{loc}\star(\Phi_{1010}\Psi_3),\Psi_1\rangle\\ &= \frac{\mu_c^2 s_2}{2}W_{loc}^c\langle \Phi_{1010}\Psi_3,\Psi_1\rangle\\ &= \frac{\mu_c^4 s_2^2}{2}\frac{\widetilde{W}_{loc}^{\chi_{10},\mathbf{D}'_{2\kappa}}}{1-\widetilde{W}_{loc}^{\chi_{10},\mathbf{D}'_{2\kappa}}/\widetilde{W}_{loc}^c}W_{loc}^c\langle\frac{1}{\sqrt{3}}\Psi_{\chi_{10}}^{\mathbf{D}'_{2\kappa}},\frac{1}{\sqrt{3}}\Psi_{\chi_{10}}^{\mathbf{D}'_{2\kappa}}\rangle\\ &= \frac{\mu_c^4 s_2^2}{6}\frac{\widetilde{W}_{loc}^{\chi_{10},\mathbf{D}'_{2\kappa}}}{1-\widetilde{W}_{loc}^{\chi_{10},\mathbf{D}'_{2\kappa}}/\widetilde{W}_{loc}^c}W_{loc}^c\end{aligned}$$

$$\begin{aligned}\langle \mathcal{R}_{20}(\Phi_{0020},\Psi_3),\Psi_3\rangle &= \frac{\mu_c^2 s_2}{2}\langle W_{loc}\star(\Phi_{0020}\Psi_3),\Psi_3\rangle\\ &= \frac{\mu_c^2 s_2}{2}W_{loc}^c\langle \Phi_{0020}\Psi_3,\Psi_3\rangle\\ &= \frac{\mu_c^4 s_2^2}{4}W_{loc}^c\left[\frac{\widetilde{W}_{loc}^{\chi_1}}{1-\widetilde{W}_{loc}^{\chi_1}/\widetilde{W}_{loc}^c}\langle\Psi_3,\Psi_3\rangle\right.\\ &\left.+\frac{\widetilde{W}_{loc}^{\chi_6,\widetilde{\mathbf{D}}_{8\kappa}}}{1-\widetilde{W}_{loc}^{\chi_6,\widetilde{\mathbf{D}}_{8\kappa}}/\widetilde{W}_{loc}^c}\langle\frac{6}{5}\Psi_{\chi_6}^{\widetilde{\mathbf{D}}_{8\kappa}},\Psi_3^2\rangle\right]\\ &= \frac{\mu_c^4 s_2^2}{4}W_{loc}^c\left[\frac{\widetilde{W}_{loc}^{\chi_1}}{1-\widetilde{W}_{loc}^{\chi_1}/\widetilde{W}_{loc}^c}+\frac{36}{25}\frac{\widetilde{W}_{loc}^{\chi_6,\widetilde{\mathbf{D}}_{8\kappa}}}{1-\widetilde{W}_{loc}^{\chi_6,\widetilde{\mathbf{D}}_{8\kappa}}/\widetilde{W}_{loc}^c}\right]\end{aligned}$$

and

$$\begin{aligned}\langle \mathcal{R}_{20}(\Phi_{0020},\Psi_1),\Psi_1\rangle &= \frac{\mu_c^2 s_2}{2}\langle W_{loc}\star(\Phi_{0020}\Psi_1),\Psi_1\rangle\\ &= \frac{\mu_c^2 s_2}{2}W_{loc}^c\langle \Phi_{0020}\Psi_1,\Psi_1\rangle\\ &= \frac{\mu_c^4 s_2^2}{4}W_{loc}^c\left[\frac{\widetilde{W}_{loc}^{\chi_1}}{1-\widetilde{W}_{loc}^{\chi_1}/\widetilde{W}_{loc}^c}\langle\Psi_1,\Psi_1\rangle\right.\\ &\left.+\frac{\widetilde{W}_{loc}^{\chi_6,\widetilde{\mathbf{D}}_{8\kappa}}}{1-\widetilde{W}_{loc}^{\chi_6,\widetilde{\mathbf{D}}_{8\kappa}}/\widetilde{W}_{loc}^c}\langle\frac{6}{5}\Psi_{\chi_6}^{\widetilde{\mathbf{D}}_{8\kappa}},\Psi_1^2\rangle\right]\\ &= \frac{\mu_c^4 s_2^2}{4}W_{loc}^c\left[\frac{\widetilde{W}_{loc}^{\chi_1}}{1-\widetilde{W}_{loc}^{\chi_1}/\widetilde{W}_{loc}^c}-\frac{2}{3}\frac{\widetilde{W}_{loc}^{\chi_6,\widetilde{\mathbf{D}}_{8\kappa}}}{1-\widetilde{W}_{loc}^{\chi_6,\widetilde{\mathbf{D}}_{8\kappa}}/\widetilde{W}_{loc}^c}\right]\end{aligned}$$

where $\langle\frac{6}{5}\Psi_{\chi_6}^{\widetilde{\mathbf{D}}_{8\kappa}},\Psi_1^2\rangle = \langle\Psi_3^2-1,\Psi_1^2\rangle = \langle\Psi_1\Psi_3,\Psi_1\Psi_3\rangle - \langle\Psi_1,\Psi_1\rangle = \frac{1}{3}-1 = -\frac{2}{3}$.

It is now a simple calculation to obtain the coefficients a and b in the reduced equation (8.31).

B.3 Calculation of cubic equivariants

We want to compute the cubic equivariants for the action group defined in (8.39). First of all, we adopt the following notations:

$$C = (c_1, c_2, c_3) \text{ and } D = (d_1, d_2, d_3)$$

such that a cubic equivariant $\mathbf{E}$ is a cubic complex polynomial of $\mathbb{C}^6$ which we write:

$$\mathbf{E}(C, D, \bar{C}, \bar{D}) = \begin{pmatrix} f_1(C, D, \bar{C}, \bar{D}) \\ f_2(C, D, \bar{C}, \bar{D}) \\ f_3(C, D, \bar{C}, \bar{D}) \\ g_1(C, D, \bar{C}, \bar{D}) \\ g_2(C, D, \bar{C}, \bar{D}) \\ g_3(C, D, \bar{C}, \bar{D}) \end{pmatrix}$$

It is straightforward to check that of all the possible cubic terms only $c_k|c_l|^2, c_k|d_l|^2$ and $d_k|c_l|^2, d_k|d_l|^2$ are transformed in the appropriate way by the translation $\Theta = [\theta_1, \theta_2]$ such that we have:

$$f_m(C, D, \bar{C}, \bar{D}) = \sum_{k=1}^{3} c_k \sum_{l=1}^{3} \left[a_m^{kl}|c_l|^2 + b_m^{kl}|d_l|^2 \right]$$
$$g_m(C, D, \bar{C}, \bar{D}) = \sum_{k=1}^{3} d_k \sum_{l=1}^{3} \left[\tilde{a}_m^{kl}|c_l|^2 + \tilde{b}_m^{kl}|d_l|^2 \right]$$

with $a_m^{kl}, b_m^{kl}, \tilde{a}_m^{kl}$ and $\tilde{b}_m^{kl}$ are complex constants. Now using the reflection equivariance κ shows that:

$$-\sum_{k=1}^{3} c_k \sum_{l=1}^{3} \left[a_1^{kl}|c_l|^2 + b_1^{kl}|d_l|^2 \right] = -c1 \sum_{l=1}^{3} \left[a_1^{1l}|c_l|^2 + b_1^{1l}|d_l|^2 \right] + \sum_{k=2}^{3} c_k \sum_{l=1}^{3} \left[a_1^{kl}|c_l|^2 + b_1^{kl}|d_l|^2 \right]$$

and

$$-\sum_{k=1}^{3} d_k \sum_{l=1}^{3} \left[\tilde{a}_1^{kl}|c_l|^2 + \tilde{b}_1^{kl}|d_l|^2 \right] = -d1 \sum_{l=1}^{3} \left[\tilde{a}_1^{1l}|c_l|^2 + \tilde{b}_1^{1l}|d_l|^2 \right] + \sum_{k=2}^{3} d_k \sum_{l=1}^{3} \left[\tilde{a}_1^{kl}|c_l|^2 + \tilde{b}_1^{kl}|d_l|^2 \right]$$

which implies that $a_1^{kl} = b_1^{kl} = \tilde{a}_1^{kl} = \tilde{b}_1^{kl} = 0$ for all $k = 2, 3$ and $l = 1, 2, 3$ and:

$$f_1(C, D, \bar{C}, \bar{D}) = c1 \sum_{l=1}^{3} \left[a_1^{1l}|c_l|^2 + b_1^{1l}|d_l|^2 \right]$$
$$g_1(C, D, \bar{C}, \bar{D}) = d1 \sum_{l=1}^{3} \left[\tilde{a}_1^{1l}|c_l|^2 + \tilde{b}_1^{1l}|d_l|^2 \right].$$

Extending similar arguments for conjugate reflections of κ we finally have:

$$f_m(C,D,\bar{C},\bar{D}) = c_m \sum_{l=1}^{3} \left[a_m^{ml}|c_l|^2 + b_m^{ml}|d_l|^2 \right]$$
$$g_m(C,D,\bar{C},\bar{D}) = d_m \sum_{l=1}^{3} \left[\tilde{a}_m^{ml}|c_l|^2 + \tilde{b}_m^{ml}|d_l|^2 \right].$$

Now using reflection equivariance Δ and $\xi^2\Delta$ leads to the requirement that a_m^{ml}, b_m^{ml}, $\tilde{a}_m^{ml}$ and $\tilde{b}_m^{ml}$ are real. The rotation equivariance ξ imposes the conditions that:

$$a_m^{ml} = \tilde{b}_m^{ml} \text{ and } b_m^{ml} = \tilde{a}_m^{ml}.$$

This reduces the form the equivariant map $\mathbf{E}$ to:

$$f_m(C,D,\bar{C},\bar{D}) = c_m \sum_{l=1}^{3} \left[a_m^{ml}|c_l|^2 + b_m^{ml}|d_l|^2 \right]$$
$$g_m(C,D,\bar{C},\bar{D}) = d_m \sum_{l=1}^{3} \left[b_m^{ml}|c_l|^2 + a_m^{ml}|d_l|^2 \right]$$

with real coefficients. To conclude the computation, we use the result about cubic equivariants with octaheddral symmetry [Melbourne 1986] that we used for the normal form in equation (8.17) (equivariance with respect to ρ, σ and ε) and find that the following conditions have to be satisfied:

$$\begin{aligned}
a_1^{11} &= a_2^{22} = a_3^{33} \\
b_1^{11} &= b_2^{22} = b_3^{33} \\
a_1^{12} &= a_1^{13} = a_2^{21} = a_2^{23} = a_3^{31} = a_3^{32} \\
b_1^{12} &= b_1^{13} = b_2^{21} = b_2^{23} = b_3^{31} = b_3^{32}.
\end{aligned}$$

This gives:

$$\mathbf{E}(C,D,\bar{C},\bar{D}) = \begin{pmatrix}
c_1\left[\alpha_1|c_1|^2 + \alpha_2\left(|c_2|^2+|c_3|^2\right) + \alpha_3|d_1|^2 + \alpha_4\left(|d_2|^2+|d_3|^2\right)\right] \\
c_2\left[\alpha_1|c_2|^2 + \alpha_2\left(|c_1|^2+|c_3|^2\right) + \alpha_3|d_2|^2 + \alpha_4\left(|d_1|^2+|d_3|^2\right)\right] \\
c_3\left[\alpha_1|c_3|^2 + \alpha_2\left(|c_1|^2+|c_2|^2\right) + \alpha_3|d_3|^2 + \alpha_4\left(|d_2|^2+|d_1|^2\right)\right] \\
d_1\left[\alpha_1|d_1|^2 + \alpha_2\left(|d_2|^2+|d_3|^2\right) + \alpha_3|c_1|^2 + \alpha_4\left(|c_2|^2+|c_3|^2\right)\right] \\
d_2\left[\alpha_1|d_2|^2 + \alpha_2\left(|d_1|^2+|d_3|^2\right) + \alpha_3|c_2|^2 + \alpha_4\left(|c_2|^2+|c_3|^2\right)\right] \\
d_3\left[\alpha_1|d_3|^2 + \alpha_2\left(|d_2|^2+|d_1|^2\right) + \alpha_3|c_3|^2 + \alpha_4\left(|c_2|^2+|c_1|^2\right)\right]
\end{pmatrix}$$

with $(\alpha_1,\alpha_2,\alpha_3,\alpha_4) \in \mathbb{R}^4$.

Appendix C

Proofs of chapter 10

Contents

C.1 Proof of Lemma 10.1.1 267
C.2 Proof of Lemma 10.1.2 268
C.2.1 Computation of ν 268
C.2.2 Computation of χ 268
C.3 Proof of Lemma 10.2.2 269
C.3.1 Computation of c_3^0 270
C.3.2 Computation of β and c 271
C.3.3 Computation of γ 273

C.1 Proof of Lemma 10.1.1

We recall the Lemma 10.1.1 stated in subsection 10.1.2.

Lemma C.1.1. *There exists a unique solution $(\mu_c, v_c = v_0(\mu_c))$ of:*

$$\left\{ \begin{array}{rcl} v_c & = & \widehat{w}_0 S(\mu_c v_c) \\ 1 & = & \mu_c S'(\mu_c v_c)\widehat{w}_c. \end{array} \right. \tag{C.1}$$

It is possible to express (μ_c, v_c) with the following analytic formulas:

$$\begin{aligned} \mu_c &= \frac{\widehat{w}_0^2}{v_c \widehat{w}_c(\widehat{w}_0 - v_c)}, \\ v_c &= \frac{\widehat{w}_0\widehat{w}_c W\left(-\widehat{w}_0 e^{-\frac{-\widehat{w}_0+\theta\widehat{w}_c}{\widehat{w}_c}}/\widehat{w}_c\right)}{\widehat{w}_c W\left(-\widehat{w}_0 e^{-\frac{-\widehat{w}_0+\theta\widehat{w}_c}{\widehat{w}_c}}/\widehat{w}_c\right) - \widehat{w}_0}. \end{aligned} \tag{C.2}$$

W is the Lambert function which satisfies $W(x)e^{W(x)} = x$.

Proof. It has been shown in [Veltz 2010a] that if $\widehat{w}_0 < 0$ then system (C.1) has a unique solution $(\mu_c, v_c = v_0(\mu_c))$. Formulas for v_c and μ_c are related to the properties of the sigmoidal function S defined in equation (10.2). Using the fact that S satisfies the ordinary differential equations $S' = S(1-S)$ and combining the two equations of (C.1), we find:

$$\mu_c = \frac{\widehat{w}_0^2}{v_c \widehat{w}_c(\widehat{w}_0 - v_c)}.$$

If $m = \dfrac{\widehat{w}_c}{\widehat{w}_0}$ and $x = v_c/\widehat{w}_0$, from $v_c = \widehat{w}_0 S(\mu_c v_c)$, x is solution of the equation:

$$\begin{aligned}
\frac{1}{x} &= 1 + \exp\left(-\frac{1}{m(1-x)} + \theta\right) \\
\Leftrightarrow x &= (1-x)\exp\left(+\frac{1}{m(1-x)} - \theta\right) \\
\Leftrightarrow \frac{x}{m(x-1)}\exp\left(\frac{x}{m(x-1)}\right) &= -\frac{1}{m}\exp\left(-\frac{-1+\theta m}{m}\right) \\
\Leftrightarrow \frac{x}{m(x-1)} &= W\left(-\frac{1}{m}\exp\left(-\frac{-1+\theta m}{m}\right)\right) \\
\Leftrightarrow x &= \frac{mW\left(-\frac{1}{m}\exp\left(-\frac{-1+\theta m}{m}\right)\right)}{mW\left(-\frac{1}{m}\exp\left(-\frac{-1+\theta m}{m}\right)\right) - 1}
\end{aligned}$$

which gives the desired formula. □

C.2 Proof of Lemma 10.1.2

This section is devoted to the proof of Lemma 10.1.2.

C.2.1 Computation of ν

We recall that the linear operator $\mathbf{L}_\mu$ is given by:

$$\mathbf{L}_\mu v = -v + \mu s_1 w * v.$$

It is straightforward to see that $\mathbf{L}_\mu e^{ix} = (-1+\mu s_1 \widehat{w}_c)e^{ix} = \frac{\lambda}{\mu_c}e^{ix}$. As a consequence $\nu = \frac{1}{\mu_c}$.

C.2.2 Computation of χ

We have defined $\mathbf{R}$ as the following nonlinear operator:

$$\mathbf{R}(v,\lambda) = w * f_0(v,\lambda).$$

We can Taylor expand $\mathbf{R}$ at $(v=0,\lambda=0)$ and if we denote:

$$\begin{aligned}
\mathbf{R}_{11}(v,\lambda) &= \lambda s_1 w * v, \\
\mathbf{R}_{20}(v,w) &= \frac{\mu_c^2 s_2}{2} w * (vw), \\
\mathbf{R}_{30}(u,v,w) &= \frac{\mu_c^3 s_3}{6} w * (uvw),
\end{aligned}$$

then, we find that $\mathbf{R}(v,\lambda) = \mathbf{R}_{11}(v,\lambda) + \mathbf{R}_{20}(v,v) + \mathbf{R}_{30}(v,v,v) + \text{h.o.t.}$ We also Taylor expand Φ:

$$\Phi(Z,\bar{Z},\lambda) = \sum_{s,l,m} Z^s \bar{Z}^l \lambda^m \Phi_{slm}.$$

Applying classical techniques [Chossat 2000, Haragus 2010] we obtain the following equations:

$$\begin{aligned} 0 &= \mathbf{L}_{\mu_c}\Phi_{200} + \mathbf{R}_{20}(e^{ix}, e^{ix}) \\ 0 &= \mathbf{L}_{\mu_c}\Phi_{110} + 2\mathbf{R}_{20}(e^{ix}, e^{-ix}) \\ \chi &= \langle 2\mathbf{R}_{20}(e^{-ix}, \Phi_{200}) + 2\mathbf{R}_{20}(e^{ix}, \Phi_{110}) + 3\mathbf{R}_{30}(e^{ix}, e^{ix}, e^{-ix}), e^{ix}\rangle_{\mathrm{L}^2_{per}[0,2\pi]}. \end{aligned}$$

If we denote $\widehat{w}_2 = \widehat{w}(2)$, the two first equations are solved with:

$$\begin{aligned} \Phi_{200} &= \mu_c^2 s_2 \frac{\widehat{w}_2}{2(1-\widehat{w}_2/\widehat{w}_c)} e^{2ix} + \mathrm{Span}(e^{ix}, e^{-ix}) \\ \Phi_{110} &= \mu_c^2 s_2 \frac{\widehat{w}_0}{1-\widehat{w}_0/\widehat{w}_c} + \mathrm{Span}(e^{ix}, e^{-ix}). \end{aligned}$$

It follows that χ is given by:

$$\chi = \mu_c^3 \widehat{w}_c \left[\frac{s_3}{2} + \mu_c s_2^2 \left(\frac{\widehat{w}_2}{2(1-\widehat{w}_2/\widehat{w}_c)} + \frac{\widehat{w}_0}{1-\widehat{w}_0/\widehat{w}_c} \right) \right].$$

Relations (10.10) give the formula for χ, as stated in the Lemma.

C.3 Proof of Lemma 10.2.2

This section is devoted to the proof of Lemma 10.2.2. Firstly, the four eigenvalues of $D_0\mathbf{F}$, when $\lambda > 0$, are given by:

$$X = \pm i \left(1 \pm \sqrt{\frac{\lambda s_1(\Gamma_1+\Gamma_2)}{4}} + \frac{\lambda s_1(\Gamma_2-\Gamma_1)}{8} + 0(|\lambda|^{3/2}) \right).$$

We observe that the eigenvalues of the linearization at the origin of the normal form (10.26) are given by:

$$i \left(1 \pm \sqrt{-c_1^1 \lambda} + \alpha\lambda + 0(|\lambda|^{3/2}) \right),$$

where c_1^1 and α are the coefficients in the expensions of P and Q which implies that:

$$c_1^1 = -\frac{s_1(\Gamma_1+\Gamma_2)}{4}, \quad \alpha = \frac{s_1(\Gamma_2-\Gamma_1)}{8}.$$

It remains to compute the coefficients c_3^0, β, c, γ of the expansions P and Q which requires the Taylor expansion of $\mathbf{F}$. First of all, we have for the nonlinearity defined in equation (10.24):

$$\mathcal{R}(U,\lambda) = \mathcal{R}_{1,1}(U,\lambda) + \mathcal{R}_{2,0}(U,U) + \mathcal{R}_{3,0}(U,U,U) + \text{h.o.t.}$$

and if $U=(u_1,u_2,u_3,u_4), V=(v_1,v_2,v_3,v_4)$ and $W=(w_1,w_2,w_3,w_4)$ we have:

$$\begin{aligned}\mathcal{R}_{2,0}(U,V) &= \frac{\mu_c^2 s_2}{2}\left(0,0,0,\Gamma_1 u_1 v_1 - \Gamma_2(2u_2v_2+u_1v_3+u_3v_1)\right)^{\mathbf{T}}\\ \mathcal{R}_{3,0}(U,V,W) &= \frac{\mu_c^3 s_3}{6}\left(0,0,0,\Gamma_1 u_1v_1w_1 - \Gamma_2(u_1v_1w_3+u_1w_1v_3\right.\\ &\quad \left.+u_3v_1w_1+2(u_1v_2w_2+u_2v_1w_2+u_2v_2w_1))\right)^{\mathbf{T}}.\end{aligned}$$

The Taylor expansion of Ψ in the normal form (10.26) is given by:

$$\Psi(A,B,\bar{A},\bar{B},\lambda) = \sum_{1\leq r+s+q+l+m\leq p} A^r B^s \bar{A}^q \bar{B}^l \lambda^m \Psi_{rsqlm}.$$

Using the expansions of $\mathcal{R}$, Ψ, P and Q, we end up with equations at different orders.

C.3.1 Computation of c_3^0

Applying the method describes in the appendix of Haragus-Iooss [Haragus 2010], we have first to solve the two following equations:

$$\mathcal{O}(A^2): \quad 0 = (\mathcal{A}-2i\,\mathbb{I}_{\mathbb{R}^4})\Psi_{20000}+\mathcal{R}_{2,0}(\zeta_0,\zeta_0) \tag{C.3}$$

$$\mathcal{O}(A\bar{A}): \quad 0 = \mathcal{A}\Psi_{10100}+2\mathcal{R}_{2,0}(\zeta_0,\bar{\zeta}_0) \tag{C.4}$$

$$\begin{aligned}\mathcal{O}(A^2\bar{A}): \quad c_3^0\zeta_1 + i\beta\zeta_0 &= (\mathcal{A}-i\,\mathbb{I}_{\mathbb{R}^4})\Psi_{20100}+2\mathcal{R}_{2,0}(\zeta_0,\Psi_{10100})\\ &\quad +2\mathcal{R}_{2,0}(\bar{\zeta}_0,\Psi_{20000})+3\mathcal{R}_{3,0}(\zeta_0,\zeta_0,\bar{\zeta}_0).\end{aligned} \tag{C.5}$$

The invertibility of the operators $\mathcal{A}, \mathcal{A}-2i\,\mathbb{I}_{\mathbb{R}^4}$ implies that solutions of equations (C.3) and (C.4) are given by

$$\Psi_{20000} = -(\mathcal{A}-2i\,\mathbb{I}_{\mathbb{R}^4})^{-1}\mathcal{R}_{2,0}(\zeta_0,\zeta_0) = \frac{\mu_c^2 s_2((\Gamma_1+4\Gamma_2)}{18}\left(1,2i,-4,-8i\right)^{\mathbf{T}}$$

and as

$$\mathcal{R}_{2,0}(\zeta_0,\bar{\zeta}_0) = \frac{\mu_c^2 s_2\Gamma_1}{2}\left(0,0,0,1\right)^{\mathbf{T}}$$

we automatically have:

$$\Psi_{10100} = -2\mathcal{A}^{-1}\mathcal{R}_{2,0}(\zeta_0,\bar{\zeta}_0) = \mu_c^2 s_2\Gamma_1\left(1,0,0,0\right)^{\mathbf{T}}.$$

In order to compute the expression of c_3^0 in equation (C.5), we need to define a vector orthogonal to $(\zeta_0,\bar{\zeta}_1,\bar{\zeta}_0)$ for the natural Hermitian scalar product $\langle\cdot,\cdot\rangle$. Let be ζ_1^* the vector in the kernel of $(\mathcal{A}-i)^*$,

$$\zeta_1^* = -\frac{1}{4}\left(-i,1,-i,1\right)^{\mathbf{T}}$$

which satisfies

$$\langle\zeta_1,\zeta_1^*\rangle = 1, \quad \langle\zeta_0,\zeta_1^*\rangle = 0, \quad \langle\bar{\zeta}_1,\zeta_1^*\rangle = 0, \quad \langle\bar{\zeta}_0,\zeta_1^*\rangle = 0.$$

Taking the scalar product of equation (C.5) with ζ_1^* we obtain a relation for c_3^0

$$c_3^0 = \langle 2\mathcal{R}_{2,0}(\zeta_0, \Psi_{10100}) + 2\mathcal{R}_{2,0}(\bar{\zeta_0}, \Psi_{20000}) + 3\mathcal{R}_{3,0}(\zeta_0, \zeta_0, \bar{\zeta_0}), \zeta_1^* \rangle$$

with

$$\begin{aligned}
\mathcal{R}_{2,0}(\zeta_0, \Psi_{10100}) &= \frac{\mu_c^4 s_2^2 \Gamma_1(\Gamma_1+\Gamma_2)}{2}(0,0,0,1)^{\mathbf{T}} \\
\mathcal{R}_{2,0}(\bar{\zeta_0}, \Psi_{20000}) &= \frac{\mu_c^4 s_2^2 (\Gamma_1+\Gamma_2)(\Gamma_1+4\Gamma_2)}{36}(0,0,0,1)^{\mathbf{T}} \\
\mathcal{R}_{3,0}(\zeta_0, \zeta_0, \bar{\zeta_0}) &= \frac{\mu_c^3 s_3 (\Gamma_1+\Gamma_2)}{6}(0,0,0,1)^{\mathbf{T}}.
\end{aligned}$$

We deduce that

$$c_3^0 = -\frac{\mu_c^3(\Gamma_1+\Gamma_2)}{4}\left[\frac{s_3}{2} + \frac{\mu_c s_2^2(19\Gamma_1+4\Gamma_2)}{18}\right]. \tag{C.6}$$

C.3.2 Computation of β and c

If decompose $\widetilde{\Psi}_{20100}$ on (ζ_0, ζ_1) such that

$$\Psi_{20100} = \widetilde{\Psi}_{20100} + i\beta\zeta_1 + \psi_{20100}\zeta_0, \text{ with } \psi_{20100} \in \mathbb{R}$$

then equation (C.5) can be rewritten with $\widetilde{\Psi}_{20100}$ only:

$$\begin{aligned}
c_3^0\zeta_1 = (\mathcal{A} - i\,\mathbb{I}_{\mathbb{R}^4})\widetilde{\Psi}_{20100} &+ 2\mathcal{R}_{2,0}(\zeta_0, \Psi_{10100}) + 2\mathcal{R}_{2,0}(\bar{\zeta_0}, \Psi_{20000}) \\
&+ 3\mathcal{R}_{3,0}(\zeta_0, \zeta_0, \bar{\zeta_0}).
\end{aligned}$$

Knowing each terms of the previous equation allows us to calculate $\widetilde{\Psi}_{20100}$:

$$\widetilde{\Psi}_{20100} = c_3^0(0,0,1,3i)^{\mathbf{T}}.$$

The coefficients β and c are obtained from orders $\mathcal{O}(A^2\bar{B})$ and $\mathcal{O}(A\bar{A}B)$:

$$\begin{aligned}
\frac{ic}{2}\zeta_1 - \frac{\gamma}{2}\zeta_0 + \Psi_{20100} = (\mathcal{A} - i\,\mathbb{I}_{\mathbb{R}^4})\widetilde{\Psi}_{20010} &+ 2\mathcal{R}_{2,0}(\zeta_0, \Psi_{10010}) \\
&+ 2\mathcal{R}_{2,0}(\bar{\zeta_1}, \Psi_{20000}) + 3\mathcal{R}_{3,0}(\zeta_0, \zeta_0, \bar{\zeta_1})
\end{aligned} \tag{C.7}$$

$$\begin{aligned}
\left(i\beta - \frac{ic}{2}\right)\zeta_1 + \frac{\gamma}{2}\zeta_0 + 2\Psi_{20100} = (\mathcal{A} - i\,\mathbb{I}_{\mathbb{R}^4})\widetilde{\Psi}_{11100} &+ 2\mathcal{R}_{2,0}(\zeta_0, \Psi_{01100}) \\
&+ 2\mathcal{R}_{2,0}(\bar{\zeta_0}, \Psi_{11000}) + 2\mathcal{R}_{2,0}(\zeta_1, \Psi_{10100}) \\
&+ 6\mathcal{R}_{3,0}(\zeta_0, \zeta_1, \bar{\zeta_0}).
\end{aligned} \tag{C.8}$$

Taking scalar product with ζ_1^* equations (C.7) and (C.8) now give

$$\begin{aligned}
i\beta + \frac{ic}{2} = \langle 2\mathcal{R}_{2,0}(\zeta_0, \Psi_{10010}) + 2\mathcal{R}_{2,0}(\bar{\zeta_1}, \Psi_{20000}) + 3\mathcal{R}_{3,0}(\zeta_0, \zeta_0, \bar{\zeta_1}), \zeta_1^* \rangle \\
- \langle \widetilde{\Psi}_{20100}, \zeta_1^* \rangle
\end{aligned} \tag{C.9}$$

and

$$3i\beta - \frac{ic}{2} = \langle 2\mathcal{R}_{2,0}(\zeta_0, \Psi_{01100}) + 2\mathcal{R}_{2,0}(\bar{\zeta_0}, \Psi_{11000})\zeta_1^* \rangle + \langle 2\mathcal{R}_{2,0}(\zeta_1, \Psi_{10100}) + 6\mathcal{R}_{3,0}(\zeta_0, \zeta_1, \bar{\zeta_0}) - 2\widetilde{\Psi}_{20100}, \zeta_1^* \rangle. \tag{C.10}$$

$\Psi_{10010}, \Psi_{01100}$ and Ψ_{11000} satisfy the following set of equations

$$\begin{aligned} \mathcal{O}(AB): \quad & 2\Psi_{20000} &=& (\mathcal{A} - 2i)\Psi_{11000} + 2\mathcal{R}_{2,0}(\zeta_0, \zeta_1) \\ \mathcal{O}(A\bar{B}): \quad & \Psi_{10100} &=& \mathcal{A}\Psi_{10010} + 2\mathcal{R}_{2,0}(\zeta_0, \bar{\zeta_1}) \\ \mathcal{O}(B\bar{B}): \quad & \Psi_{10010} + \Psi_{01100} &=& \mathcal{A}\Psi_{01010} + 2\mathcal{R}_{2,0}(\zeta_1, \bar{\zeta_1}). \end{aligned}$$

The first equation gives:

$$\begin{aligned} \Psi_{11000} &= (\mathcal{A} - 2i\ \mathbb{I}_{\mathbb{R}^4})^{-1}(2\Psi_{20000} - 2\mathcal{R}_{2,0}(\zeta_0, \zeta_1)) \\ &= \frac{\mu_c^2 s_2}{27}\left(i(8\Gamma_1 + 20\Gamma_2), -(13\Gamma_1 + 28\Gamma_2), -i(20\Gamma_1 + 32\Gamma_2), 28\Gamma_1 + 16\Gamma_2\right)^{\mathbf{T}}. \end{aligned}$$

The second one yiels

$$\begin{aligned} \Psi_{10010} &= \mathcal{A}^{-1}\left(\Psi_{10100} - 2\mathcal{R}_{2,0}(\zeta_0, \bar{\zeta_1})\right) \\ &= \mathcal{A}^{-1}\Psi_{10100} \text{ as } R_{2,0}(\zeta_0, \bar{\zeta_1}) = 0 \\ &= \mu_c^2 s_2 \Gamma_1 (0, 1, 0, 0)^{\mathbf{T}} \end{aligned}$$

which implies that:

$$\Psi_{01100} = -\mathbf{S}\Psi_{10010} = \mu_c^2 s_2 \Gamma_1 (0, 1, 0, 0)^{\mathbf{T}}.$$

Finally, the last equation is just:

$$\begin{aligned} \Psi_{01010} &= \mathcal{A}^{-1}\left(2\Psi_{10010} - 2\mathcal{R}_{2,0}(\zeta_1, \bar{\zeta_1})\right) \\ &= \mu_c^2 s_2(-(4\Gamma_1 + 2\Gamma_2), 0, 2\Gamma_1, 0)^{\mathbf{T}}. \end{aligned}$$

It is now possible to compute each term of the form $\mathcal{R}_{2,0}(\cdot,\cdot)$ and $\mathcal{R}_{3,0}(\cdot,\cdot)$ of equations (C.9) and (C.10). They are summerize in the following set of equations:

$$\begin{aligned} \mathcal{R}_{2,0}(\zeta_0, \Psi_{10010}) &= -i\mu_c^4 s_2^2 \Gamma_1\Gamma_2 (0, 0, 0, 1)^{\mathbf{T}} \\ \mathcal{R}_{2,0}(\bar{\zeta_1}, \Psi_{20000}) &= -\frac{i\mu_c^4 s_2^2 \Gamma_2(\Gamma_1 + 4\Gamma_2)}{18}(0, 0, 0, 1)^{\mathbf{T}} \\ \mathcal{R}_{3,0}(\zeta_0, \zeta_0, \bar{\zeta_1}) &= -\frac{i\mu_c^3 s_3 \Gamma_2}{3}(0, 0, 0, 1)^{\mathbf{T}} \\ \mathcal{R}_{2,0}(\zeta_0, \Psi_{01100}) &= -i\mu_c^4 s_2^2 \Gamma_1\Gamma_2 (0, 0, 0, 1)^{\mathbf{T}} \\ \mathcal{R}_{2,0}(\bar{\zeta_0}, \Psi_{11000}) &= \frac{i\mu_c^4 s_2^2 (4\Gamma_1^2 + 11\Gamma_1\Gamma_2 - 2\Gamma_2^2)}{27}(0, 0, 0, 1)^{\mathbf{T}} \\ \mathcal{R}_{2,0}(\zeta_1, \Psi_{10100}) &= (0, 0, 0, 0)^{\mathbf{T}} \\ \mathcal{R}_{3,0}(\zeta_0, \zeta_1, \bar{\zeta_0}) &= -\frac{i\mu_c^3 s_3 \Gamma_2}{3}(0, 0, 0, 1)^{\mathbf{T}}. \end{aligned}$$

Finally formula for β and c are

$$\beta = \frac{\mu_c^3}{32}\left[3s_3(\Gamma_2-\Gamma_1) - \frac{\mu_c s_2^2(4\Gamma_2^2+187\Gamma_1^2+29\Gamma_1\Gamma_2)}{27}\right], \tag{C.11}$$

$$c = \frac{\mu_c^3}{16}\left[s_3(\Gamma_2-\Gamma_1) - \frac{\mu_c s_2^2(41\Gamma_1^2-209\Gamma_1\Gamma_2-52\Gamma_2^2)}{27}\right]. \tag{C.12}$$

C.3.3 Computation of γ

Now, it remains to compute the last coefficient γ. First of all, we decompose Ψ_{20010} and Ψ_{11100} such that we have

$$\begin{aligned}\Psi_{20010} &= \widetilde{\Psi}_{20010} + (\psi_{20100}-\gamma/2)\zeta_1\\ \Psi_{11100} &= \widetilde{\Psi}_{11100} + (2\psi_{20100}+\gamma/2)\zeta_1 + \psi_{11100}\zeta_0 \text{ with } \psi_{11100}\in\mathbb{R}.\end{aligned}$$

It will be enough to know the expression of the difference $\widetilde{\Psi}_{11100} - 2\widetilde{\Psi}_{20010}$ and its scalar product with ζ_1^*. Substracting from equation (C.8) two times equation (C.7), we obtain the following relation

$$\begin{aligned}i\left(\beta-\frac{3c}{2}\right)\zeta_1 = (\mathcal{A}-i\,\mathbb{I}_{\mathbb{R}^4})\left(\widetilde{\Psi}_{11100}-2\widetilde{\Psi}_{20010}\right) &+ 2\mathcal{R}_{2,0}(\zeta_0,\Psi_{01100})\\ &+ 2\mathcal{R}_{2,0}(\bar{\zeta}_0,\Psi_{11000}) + 6R_{3,0}(\zeta_0,\zeta_1,\bar{\zeta}_0) - 4\mathcal{R}_{2,0}(\zeta_0,\Psi_{10010})\\ &- 4\mathcal{R}_{2,0}(\bar{\zeta}_1,\Psi_{20000}) - 6\mathcal{R}_{3,0}(\zeta_0,\zeta_0,\bar{\zeta}_1),\end{aligned}$$

where we have used the fact that $\mathcal{R}_{2,0}(\zeta_1,\Psi_{10100}) = 0_{\mathbb{R}^4}$. We have already computed some of the terms that appear in the right hand side of the previous equation. We can easily deduce from our above calculations that

$$\begin{aligned}\mathcal{R}_{2,0}(\zeta_0,\Psi_{01100}) = \mathcal{R}_{2,0}(\zeta_0,\Psi_{10010}) &= -i\mu_c^4 s_2^2\Gamma_1\Gamma_2\,(0,0,0,1)^{\mathbf{T}}\\ \mathcal{R}_{3,0}(\zeta_0,\zeta_0,\bar{\zeta}_1) = \mathcal{R}_{3,0}(\zeta_0,\zeta_1,\bar{\zeta}_0) &= -\frac{i\mu_c^3 s_3\Gamma_2}{3}\,(0,0,0,1)^{\mathbf{T}}\\ \mathcal{R}_{2,0}(\bar{\zeta}_0,\Psi_{11000}) &= \frac{i\mu_c^4 s_2^2(4\Gamma_1^2+11\Gamma_1\Gamma_2-2\Gamma_2^2)}{27}\,(0,0,0,1)^{\mathbf{T}}\\ \mathcal{R}_{2,0}(\bar{\zeta}_1,\Psi_{20000}) &= -\frac{i\mu_c^4 s_2^2\Gamma_2(\Gamma_1+4\Gamma_2)}{18}\,(0,0,0,1)^{\mathbf{T}}.\end{aligned}$$

This implies that:

$$\begin{aligned}-2\mathcal{R}_{2,0}(\zeta_0,\Psi_{01100}) + 2\mathcal{R}_{2,0}(\bar{\zeta}_0,\Psi_{11000}) - 4\mathcal{R}_{2,0}(\bar{\zeta}_1,\Psi_{20000})&\\ = \frac{4i\mu_c^4 s_2^2\left(4\Gamma_1^2+41\Gamma_1\Gamma_2+10\Gamma_2^2\right)}{54}\,(0,0,0,1)^{\mathbf{T}}&.\end{aligned}$$

From equations (C.11) and (C.12) we have

$$i\left(\beta-\frac{3c}{2}\right) = \frac{-i\mu_c^4 s_2^2(4\Gamma_1^2+41\Gamma_1\Gamma_2+10\Gamma_2^2)}{54}.$$

Then we can conclude that

$$\widetilde{\Psi}_{11100} - 2\widetilde{\Psi}_{20010} = \frac{-i\mu_c^4 s_2^2(4\Gamma_1^2 + 41\Gamma_1\Gamma_2 + 10\Gamma_2^2)}{54}\,(0,0,1,3i)^{\mathbf{T}}$$

and

$$\Rightarrow \langle \widetilde{\Psi}_{11100} - 2\widetilde{\Psi}_{20010}, \zeta_1^* \rangle = -\frac{\mu_c^4 s_2^2(4\Gamma_1^2 + 41\Gamma_1\Gamma_2 + 10\Gamma_2^2)}{54}.$$

A linear combination of equations of orders $\mathcal{O}(\bar{A}B^2)$ and $\mathcal{O}(AB\bar{B})$ projected on ζ_1 gives the following relation for γ

$$\begin{aligned} 3\gamma = &\langle 4\mathcal{R}_{2,0}(\bar{\zeta}_0, \Psi_{02000}) + 4\mathcal{R}_{2,0}(\zeta_1, \Psi_{01100}) + 6\mathcal{R}_{30}(\zeta_1, \zeta_1, \bar{\zeta}_0), \zeta_1^* \rangle \\ &- \langle 2\mathcal{R}_{2,0}(\zeta_0, \Psi_{01010}) + 2\mathcal{R}_{2,0}(\bar{\zeta}_1, \Psi_{11000}) + 2\mathcal{R}_{2,0}(\zeta_1, \Psi_{10010}), \zeta_1^* \rangle \\ &- \langle 6\mathcal{R}_{30}(\zeta_0, \zeta_1, \bar{\zeta}_1) - 2\widetilde{\Psi}_{20010} + \widetilde{\Psi}_{11100}, \zeta_1^* \rangle. \end{aligned} \tag{C.13}$$

The equation for Ψ_{02000} is obtained at order $\mathcal{O}(B^2)$

$$\Psi_{11000} \;=\; (\mathcal{A} - 2i\ \mathbb{I}_{\mathbb{R}^4})\Psi_{02000} + 2\mathcal{R}_{2,0}(\zeta_1, \zeta_1)$$

$$\begin{aligned} \Rightarrow \Psi_{02000} &= (\mathcal{A} - 2i\ \mathbb{I}_{\mathbb{R}^4})^{-1}(\Psi_{11000} - 2\mathcal{R}_{2,0}(\zeta_1, \zeta_1)) \\ &= \frac{\mu_c^2 s_2}{27}\,(-(14\Gamma_1 + 30\Gamma_2), -i(20\Gamma_1 + 40\Gamma_2), 27\Gamma_1 + 52\Gamma_2, i(34\Gamma_1 + 72\Gamma_2))^{\mathbf{T}}. \end{aligned}$$

We are now able to finish the proof of the lemma as all terms of the right hand side of equation (C.13) are easily calculable. As stated in the lemma, the expression of γ is

$$\gamma = -\frac{\mu_c^4 s_2^2(36\Gamma_1^2 + 4\Gamma_1\Gamma_2 + 7\Gamma_2^2)}{162}. \tag{C.14}$$

Bibliography

[Aguiar 2005] M.A.D. Aguiar, S.B.S.D. Castro and I.S. Labouriau. *Dynamics near a heteroclinic network*. Nonlinearity, vol. 18, 2005. 141

[Allaire 2005] G. Allaire. Analyse numérique et optimisation. Éd. de l'Ecole Polytechnique, 2005. 101

[Amari 1975] S.I. Amari. *Homogeneous nets of neuron-like elements*. Biological Cybernetics, vol. 17, no. 4, pages 211–220, 1975. 17

[Amari 1977] S.-I. Amari. *Dynamics of pattern formation in lateral-inhibition type neural fields*. Biological Cybernetics, vol. 27, no. 2, pages 77–87, June 1977. 17, 23, 191, 192, 196

[Angelucci 2002] A. Angelucci, J.B. Levitt, E.J. Walton, J.M. Hupe, J. Bullier and J.S. Lund. *Circuits for local and global signal integration in primary visual cortex*. The Journal of Neuroscience, vol. 22, no. 19, pages 8633–8646, October 2002. 192

[Appell 2006] J. Appell and C.-J Chen. *How to solve Hammerstein equations*. Journal of integral equations and applications, vol. 18, no. 3, pages 287–296, 2006. 23

[Armbruster 1988] D. Armbruster, J. Guckenheimer and P. Holmes. *Heteroclinic cycles and modulated travelling waves in systems with O (2) symmetry*. Physica D: Nonlinear Phenomena, vol. 29, no. 3, pages 257–282, 1988. 141

[Ashwin 1999] P. Ashwin and M. Field. *Heteroclinic networks in coupled cell systems*. Archive for Rational Mechanics and Analysis, vol. 148, no. 2, pages 107–143, 1999. 142

[Aurich 1989] R. Aurich and F. Steiner. *Periodic-orbit sum rules for the Hadamard-Gutzwiller model*. Physica D, vol. 39, pages 169–193, 1989. 99, 101, 104

[Aurich 1993] R. Aurich and F. Steiner. *Statistical properties of highly excited quantum eigenstates of a strongly chaotic system*. Physica D, vol. 64, pages 185–214, 1993. 99, 107

[Baker 2009] T.I. Baker and J.D. Cowan. *Spontaneous pattern formation and pinning in the primary visual cortex*. Journal of Physiology-Paris, vol. 103, no. 1-2, pages 52–68, 2009. 33, 186

[Baladron 2011] Javier Baladron, Diego Fasoli, Olivier Faugeras and Jonathan Touboul. *Mean Field description of and propagation of chaos in recurrent multipopulation networks of Hodgkin-Huxley and FitzHugh-Nagumo neurons*.

Rapport technique, arXiv, 2011. Submitted to the Journal of Mathematical Neuroscience. 22

[Balazs 1986] N.L. Balazs and A. Voros. *Chaos on the pseudosphere*. Physics Reports, vol. 143, no. 3, pages 109–240, 1986. 38, 89, 99, 100, 101

[Ben-Shahar 2003a] O. Ben-Shahar, P.S. Huggins, T. Izo and S.W. Zucker. *Cortical connections and early visual function: intra-and inter-columnar processing*. Journal of Physiology-Paris, vol. 97, no. 2-3, pages 191–208, 2003. 27

[Ben-Shahar 2003b] O. Ben-Shahar and S.W. Zucker. *The Perceptual Organization of Texture Flow: A Contextual Inference Approach*. pami, vol. 25, no. 4, pages 401—417, April 2003. 27

[Ben-Shahar 2004] O. Ben-Shahar and S. Zucker. *Geometrical computations explain projection patterns of long-range horizontal connections in visual cortex*. Neural Computation, vol. 16, no. 3, pages 445—476, 2004. 27, 31

[Ben-Yishai 1995] R. Ben-Yishai, RL Bar-Or and H. Sompolinsky. *Theory of orientation tuning in visual cortex*. Proceedings of the National Academy of Sciences, vol. 92, no. 9, pages 3844–3848, 1995. 17, 25, 27, 32, 33, 172, 251

[Bigun 1987] J. Bigun and G. Granlund. *Optimal Orientation Detection of Linear Symmetry*. In Proc. First Int'l Conf. Comput. Vision, pages 433–438. EEE Computer Society Press, 1987. 25, 27

[Blasdel 1986] G.G. Blasdel and G. Salama. *Voltage-sensitive dyes reveal a modular organization in monkey striate cortex*. Nature, vol. 321, pages 579—585, 1986. 10, 12, 30

[Blasdel 1992] G.G. Blasdel. *Orientation selectivity, preference, and continuity in monkey striate cortex*. Journal of Neuroscience, vol. 12, no. 8, pages 3139–3161, 1992. 30

[Blomquist 2005] P. Blomquist, J. Wyller and G.T. Einevoll. *Localized activity patterns in two-population neuronal networks*. Physica D, vol. 206, pages 180–212, 2005. 23

[Blumenfeld 2006] B. Blumenfeld, D. Bibitchkov and M. Tsodyks. *Neural network model of the primary visual cortex: From functional architecture to lateral connectivity and back*. Journal of computational neuroscience, vol. 20, no. 2, pages 219–241, 2006. 186

[Bonhoeffer 1991] T. Bonhoeffer and A. Grinvald. *Orientation columns in cat are organized in pinwheel like patterns*. Nature, vol. 364, no. 353, pages 429–431, 1991. 12

[Bonhoeffer 1995] T. Bonhoeffer, D.S. Kim, D. Malonek, D. Shoham and A. Grinvald. *Optical Imaging of the layout of functional domains in area 17/18 border in cat visual cortex*. European J. Neurosci., vol. 7, no. 9, pages 1973–1988, 1995. 30

[Bonnabel 2009] S. Bonnabel and R. Sepulchre. *Riemannian Metric and Geometric Mean for Positive Semidefinite Matrices of Fixed Rank*. SIAM Journal on Matrix Analysis and Applications, vol. 31, pages 1055–1070, 2009. 28

[Bosch Vivancos 1995] I. Bosch Vivancos, P. Chossat and I. Melbourne. *New planforms in systems of partial differential equations with Euclidean symmetry*. Archive for rational mechanics and analysis, vol. 131, no. 3, pages 199–224, 1995. 185, 186

[Bosking 1997] W.H. Bosking, Y. Zhang, B. Schofield and D. Fitzpatrick. *Orientation Selectivity and the Arrangement of Horizontal Connections in Tree Shrew Striate Cortex*. The Journal of Neuroscience, vol. 17, no. 6, pages 2112–2127, 1997. 12, 14

[Bosking 2002] W.H. Bosking, J.C. Crowley, D. Fitzpatrick*et al.* *Spatial coding of position and orientation in primary visual cortex*. Nature neuroscience, vol. 5, no. 9, pages 874–882, 2002. 31

[Bressloff 2000] P.C. Bressloff, N.W. Bressloff and J.D. Cowan. *Dynamical mechanism for sharp orientation tuning in an integrate-and-fire model of a cortical hypercolumn*. Neural computation, vol. 12, no. 11, pages 2473–2511, 2000. 25, 111

[Bressloff 2001a] P.C. Bressloff, J.D. Cowan, M. Golubitsky and P.J. Thomas. *Scalar and pseudoscalar bifurcations motivated by pattern formation on the visual cortex*. Nonlinearity, vol. 14, page 739, 2001. 17, 153, 166, 178, 184, 186

[Bressloff 2001b] P.C. Bressloff, J.D. Cowan, M. Golubitsky, P.J. Thomas and M.C. Wiener. *Geometric visual hallucinations, Euclidean symmetry and the functional architecture of striate cortex*. Phil. Trans. R. Soc. Lond. B, vol. 306, no. 1407, pages 299–330, March 2001. 27, 31, 32, 62, 74, 111, 152, 153, 155, 161, 166, 178, 184, 186, 251

[Bressloff 2002a] P.C. Bressloff and J.D. Cowan. *SO(3) Symmetry Breaking Mechanism for Orientation and Spatial Frequency Tuning in the Visual Cortex*. Phys. Rev. Lett., vol. 88, no. 7, February 2002. 27

[Bressloff 2002b] P.C. Bressloff and J.D. Cowan. *The visual cortex as a crystal*. Physica D: Nonlinear Phenomena, vol. 173, no. 3–4, pages 226–258, December 2002. 27, 32, 152, 155

[Bressloff 2002c] P.C. Bressloff, J.D. Cowan, M. Golubitsky, P.J. Thomas and M.C. Wiener. *What Geometric Visual Hallucinations Tell Us about the Visual Cortex*. Neural Computation, vol. 14, no. 3, pages 473–491, 2002. 27, 85

[Bressloff 2003a] P. Bressloff and J. Cowan. *The functional geometry of local and horizontal connections in a model of V1*. Journal of Physiology, Paris, vol. 97, pages 221–236, 2003. 30, 33, 155

[Bressloff 2003b] P. C. Bressloff and J. D. Cowan. *A spherical model for orientation and spatial frequency tuning in a cortical hypercolumn*. Philosophical Transactions of the Royal Society B, 2003. 25, 27, 30, 33, 155

[Bressloff 2003c] P.C. Bressloff. *Spatially periodic modulation of cortical patterns by long-range horizontal connections*. Physica D: Nonlinear Phenomena, vol. 185, no. 3-4, pages 131–157, 2003. 33, 186

[Bressloff 2009] P.C. Bressloff. *Stochastic neural field theory and the system-size expansion*. SIAM J. Appl. Math, vol. 70, pages 1488–1521, 2009. 22

[Bressloff 2010] P.C. Bressloff and A.M. Oster. *Theory for the alignment of cortical feature maps during development*. Physical Review E, vol. 82, no. 2, page 021920, 2010. 187, 251

[Bressloff 2012] P.C. Bressloff. *Spatiotemporal dynamics of continuum neural fields*. Journal of Physics A: Mathematical and Theoretical, vol. 45, 2012. 17, 20, 23

[Brezis 1983] H. Brezis. Analyse fonctionnelle. théorie et applications. Masson, 1983. 206, 207

[Brodmann 1909] K. Brodmann. Vergleichende lokalisationslehre der grobhirnrinde. J.A.Barth, Leipzig, 1909. 7

[Broughton 1991] S.A. Broughton. *Classifying finite group actions on surfaces of low genus*. Journal of Pure and Applied Algebra, vol. 69, no. 3, pages 233–270, 1991. 89

[Broughton 2001] S.A. Broughton, R.M. Dirks, M.T. Sloughter and C.R. Vinroot. *Triangular surface tiling groups for low genus*. Rapport technique, MSTR, 2001. 84

[Burke 2006] J. Burke and E. Knobloch. *Localized states in the generalized Swift-Hohenberg equation*. Physical Review E, vol. 73, no. 5, page 056211, 2006. 191, 196, 204

[Burke 2007a] J. Burke and E. Knobloch. *Homoclinic snaking: structure and stability*. Chaos, vol. 17, no. 3, page 7102, 2007. 193, 196, 204

[Burke 2007b] J. Burke and E. Knobloch. *Normal form for spatial dynamics in the Swift-Hohenberg equation*. DYNAMICAL SYSTEMS, pages 170–180, 2007. 193, 195, 204

[Buser 1992] P. Buser. Geometry and spectra of compact riemann surfaces, volume 106. Springer, 1992. 85

[Buxhoeveden 2002] D.P. Buxhoeveden and M.F. Casanova. *The minicolumn hypothesis in neuroscience*. Brain, vol. 125, pages 935–951, 2002. 9, 10

[Casagrande 2004] V. Casagrande and X. Xu. Parallel visual pathways: a comparative perspective, chapitre 31, pages 494–506. In Chalupa & Werner [Chalupa 2004], 2004. Two volumes. 30

[Chalupa 2004] L. M. Chalupa and J.S. Werner, editeurs. The visual neurosciences. MIT Press, 2004. Two volumes. 22, 279, 285

[Champneys 1998] AR Champneys. *Homoclinic orbits in reversible systems and their applications in mechanics, fluids and optics*. Physica D: Nonlinear Phenomena, vol. 112, no. 1-2, pages 158–186, 1998. 191, 196

[Chapman 2009] SJ Chapman and G. Kozyreff. *Exponential asymptotics of localised patterns and snaking bifurcation diagrams*. Physica D: Nonlinear Phenomena, vol. 238, no. 3, pages 319–354, 2009. 205

[Chavel 1984] I. Chavel. Eigenvalues in riemannian geometry, volume 115. Academic Press, 1984. 158

[Chemla 2010a] S. Chemla and F. Chavane. *Voltage-sensitive dye imaging: Technique review and models*. Journal of Physiology-Paris, vol. 104, no. 1-2, pages 40–50, 2010. 39

[Chemla 2010b] Sandrine Chemla. *A biophysical cortical column model for optical signal analysis*. PhD thesis, School of Information and Communication Sciences, 2010. 3

[Chossat 1990] P. Chossat, R. Lauterbach and I. Melbourne. *Steady-state bifurcation with 0 (3)-symmetry*. Archive for Rational Mechanics and Analysis, vol. 113, no. 4, pages 313–376, 1990. 121

[Chossat 2000] P. Chossat and R. Lauterbach. Methods in Equivariant Bifurcations and Dynamical Systems. World Scientific Publishing Company, 2000. 50, 61, 87, 88, 114, 121, 124, 128, 141, 166, 178, 199, 269

[Chossat 2009] Pascal Chossat and Olivier Faugeras. *Hyperbolic planforms in relation to visual edges and textures perception*. Plos Comput Biol, vol. 5, no. 12, page e1000625, December 2009. 25, 26, 27, 34, 45

[Chossat 2011] Pascal Chossat, Grégory Faye and Olivier Faugeras. *Bifurcations of hyperbolic planforms*. Journal of Nonlinear Science, vol. 21, no. 4, pages 465–498, August 2011. x, xii, 251

[Ciarlet 1991] P.G. Ciarlet and J.L. Lions, editeurs. Handbook of numerical analysis. volume ii. finite element methods (part1). North-Holland, 1991. 101

[Conway 2003] J.H Conway and D.A Smith. On quaternions and octonions, their geometry, arithmetic, and symmetry. AK Peters, 2003. 123

[Coombes 2003] S. Coombes, G.J. Lord and M.R. Owen. *Waves and bumps in neuronal networks with axo-dendritic synaptic interactions*. Physica D: Nonlinear Phenomena, vol. 178, no. 3-4, pages 219–241, 2003. 23, 192, 196, 216

[Coombes 2005a] S. Coombes and M. R. Owen. *Bumps, Breathers, and Waves in a Neural Network with Spike Frequency Adaptation*. Phys. Rev. Lett., vol. 94, no. 14, 2005. 23

[Coombes 2005b] Stephen Coombes. *Waves, bumps, and patterns in neural fields theories*. Biological Cybernetics, vol. 93, no. 2, pages 91–108, 2005. 17, 23, 191, 192

[Coombes 2010] S. Coombes. *Large-scale neural dynamics: Simple and complex*. NeuroImage, vol. 52, no. 3, pages 731–739, 2010. 17

[Cornish 1998] N.J Cornish and N.G Turok. *Ringing the eigenmodes from compact manifolds*. Rapport technique, arXiv, 1998. 99

[Cornish 1999] N.J. Cornish and D.N Spergel. *On the eigenmodes of compact hyperbolic 3-manifolds*. Rapport technique, arXiv, 1999. 99, 100

[Curtu 2004] R. Curtu and B. Ermentrout. *Pattern Formation in a Network of Excitatory and Inhibitory Cells with Adaptation*. SIAM Journal on Applied Dynamical Systems, vol. 3, page 191, 2004. 23

[Das 1999] A. Das and C.D. Gilbert. *Topography of contextual modulations mediated by short-range interactions in primary visual cortex*. Nature, vol. 399, no. 6737, pages 655–661, 1999. 14

[Das 2000] A. Das. *Optimizing coverage in the cortex*. Nature neuroscience, vol. 3, pages 750–751, 2000. 31

[Dayan 2001] P. Dayan and L.F. Abbott. Theoretical neuroscience : Computational and mathematical modeling of neural systems. MIT Press, 2001. 111

[DeAngelis 1995a] G.C. DeAngelis, I. Ohzawa and R.D. Freeman. *Neuronal mechanisms underlying stereopsis: how do simple cells in the visual cortex encode binocular disparity?* Perception, vol. 24, no. 1, pages 3–31, 1995. 27

[DeAngelis 1995b] G.C. DeAngelis, I. Ohzawa and R.D. Freeman. *Receptive-field dynamics in the central visual pathways*. Trends in Neurosciences, vol. 18, no. 10, pages 451–458, 1995. 7

[Deco 2008] Gustavo Deco, Viktor K. Jirsa, Peter A. Robinson, Michael Breakspear and Karl Friston. *The Dynamic Brain: From Spiking Neurons to Neural Masses and Cortical Fields*. PLoS Comput. Biol., vol. 4, no. 8, 2008. 22

[Dionne 1992] B. Dionne and M. Golubitsky. *Planforms in two and three dimensions*. ZAMP, vol. 43, pages 36–62, 1992. 65, 85

[Dionne 1997] B. Dionne, M. Silber and A.C. Skeldon. *Stability results for steady, spatially periodic planforms*. Nonlinearity, vol. 10, page 321, 1997. 67, 71, 72

[Doedel 1997] E.J. Doedel, A.R. Champneys, T.F. Fairgrieve, Y.A. Kuznetsov, B. Sandstede and X. Wang. *AUTO 97: Continuation and bifurcation software for Ordinary Differential Equations (with HomCont)*. -, 1997. 196, 212

[Edwards 1995] D.P. Edwards, K.P. Purpura and E. Kaplan. *Contrast sensitivity and spatial frequency response of primate cortical neurons in and around the cytochrome oxidase blobs*. Vision Research, vol. 35, pages 1501–1523, 1995. 30

[Elvin 2010] AJ Elvin, CR Laing, RI McLachlan and MG Roberts. *Exploiting the Hamiltonian structure of a neural field model*. Physica D: Nonlinear Phenomena, vol. 239, no. 9, pages 537–546, 2010. 192, 193, 195, 216

[Erdelyi 1985] Erdelyi. Higher transcendental functions, volume 1. Robert E. Krieger Publishing Company, 1985. 157, 237, 238, 241

[Ermentrout 1979] GB Ermentrout and JD Cowan. *A mathematical theory of visual hallucination patterns*. Biological Cybernetics, vol. 34, no. 3, pages 137–150, 1979. 17, 61, 69, 74, 151, 155, 178

[Ermentrout 1991] B. Ermentrout. *Stripes or spots? Nonlinear effects in bifurcation of reaction-diffusion equations on the square*. Proceedings: Mathematical and Physical Sciences, vol. 434, no. 1891, pages 413–417, 1991. 72

[Ermentrout 1998] Bard Ermentrout. *Neural networks as spatio-temporal pattern-forming systems*. Reports on Progress in Physics, vol. 61, pages 353–430, 1998. 17, 20, 21, 24, 111

[Ermentrout 2010a] G. Bard Ermentrout and David Terman. Foundations of mathematical neuroscience. Interdisciplinary Applied Mathematics. Springer, 2010. 20

[Ermentrout 2010b] G.B. Ermentrout, J.Z. Jalics and J.E. Rubin. *Stimulus-driven traveling solutions in continuum neuronal models with a general smooth firing rate function.* SIAM Journal of Applied Mathematics, vol. 70, no. 8, pages 3039–3064, 2010. 251

[Fässler 1992] A. Fässler and E.L. Stiefel. Group theoretical methods and their applications. Birkhäuser, 1992. 100

[Faugeras 2008] O. Faugeras, F. Grimbert and J.-J. Slotine. *Abolute stability and complete synchronization in a class of neural fields models.* SIAM Journal of Applied Mathematics, vol. 61, no. 1, pages 205–250, September 2008. 23, 192

[Faugeras 2009a] Olivier Faugeras, Jonathan Touboul and Bruno Cessac. *A constructive mean field analysis of multi population neural networks with random synaptic weights and stochastic inputs.* Frontiers in Computational Neuroscience, vol. 3, no. 1, 2009. 22

[Faugeras 2009b] Olivier Faugeras, Romain Veltz and Francois Grimbert. *Persistent neural states: stationary localized activity patterns in nonlinear continuous n-population, q-dimensional neural networks.* Neural Computation, vol. 21, no. 1, pages 147–187, 2009. 23, 44

[Faye 2010] Grégory Faye and Olivier Faugeras. *Some theoretical and numerical results for delayed neural field equations.* Physica D, vol. 239, no. 9, pages 561–578, May 2010. Special issue on Mathematical Neuroscience. 23

[Faye 2011a] Grégory Faye and Pascal Chossat. *Bifurcation diagrams and heteroclinic networks of octagonal H-planforms.* Journal of Nonlinear Science, 2011. x, xiii

[Faye 2011b] Grégory Faye, Pascal Chossat and Olivier Faugeras. *Analysis of a hyperbolic geometric model for visual texture perception.* The Journal of Mathematical Neuroscience, vol. 1, no. 4, 2011. x, xii, 41, 42, 44

[Faye 2012a] G. Faye. *Reduction method for studying localized solutions of neural field equations on the Poincaré disk.* Comptes Rendus de l'Académie des Sciences, Mathématique, 2012. x, xiii

[Faye 2012b] G. Faye and P.Chossat. *A spatialized model of textures perception using structure tensor formalism.* Submitted, page 49, 2012. x, xiii

[Faye 2012c] G. Faye, J. Rankin and P. Chossat. *Localized states in an unbounded neural field equation with smooth firing rate function: a multi-parameter analysis.* Journal of Mathematical Biology, 2012. x, xiii

[Field 1989a] M. Field. *Equivariant bifurcation theory and symmetry breaking.* Journal of Dynamics and Differential Equations, vol. 1, no. 4, pages 369–421, 1989. 128

[Field 1989b] M. Field and R.W. Richardson. *Symmetry breaking and the maximal isotropy subgroup conjecture for reflection groups*. Archive for rational Mechanics and Analysis, vol. 105, no. 1, pages 61–94, 1989. 88

[Field 1991] M. Field and J.W. Swift. *Stationary bifurcation to limit cycles and heteroclinic cycles*. Nonlinearity, vol. 4, page 1001, 1991. 144

[Florack 1996] L. Florack, Bart ter Haar Romeny, M. Viergever and J. Koenderink. *The Gaussian scale-space paradigm and the multiscale local jet*. The International Journal of Computer Vision, vol. 18, pages 61–75, 1996. 27

[Folias 2004] Stefanos E. Folias and Paul C. Bressloff. *Breathing Pulses in an Excitatory Neural Network*. SIAM Journal on Applied Dynamical Systems, vol. 3, no. 3, pages 378–407, 2004. 194

[Folias 2005] S.E. Folias and P.C. Bressloff. *Breathers in Two-Dimensional Neural Media*. Physical Review Letters, vol. 95, no. 20, page 208107, 2005. 23

[Goldberg 2004] J.A. Goldberg, U. Rokni and H. Sompolinsky. *Patterns of ongoing activity and the functional architecture of the primary visual cortex*. Neuron, vol. 42, no. 3, pages 489–500, 2004. 149

[Golubitsky 1988] M. Golubitsky, I. Stewart and D.G. Schaeffer. Singularities and groups in bifurcation theory, volume II. Springer, 1988. 61, 85, 88, 97, 166, 178, 179, 180

[Golubitsky 2003] M. Golubitsky, L.J. Shiau and A. Török. *Bifurcation on the visual cortex with weakly anisotropic lateral coupling*. SIAM Journal on Applied Dynamical Systems, vol. 2, no. 2, pages 97–143, 2003. 74, 152, 155, 156, 166, 178, 185

[González 1997] B.J. González and E.R. Negrin. *Mehler-Fock transforms of generalized functions via the method of adjoints*. PROCEEDINGS-AMERICAN MATHEMATICAL SOCIETY, vol. 125, pages 3243–3254, 1997. 232, 233

[Gorenstein 1980] D. Gorenstein. Finite groups. Chelsea Pub Co, 1980. 92

[Grimbert 2008] F. Grimbert. *Mesoscopic models of cortical structures*. PhD thesis, University of Nice Sophia-Antipolis, February 2008. 3

[Grinvald 1986] A. Grinvald, E. Lieke, R.D. Frostig, C.D. Gilbert and T.N. Wiesel. *Functional architecture of cortex revealed by optical imaging of intrinsic signals*. Nature, 1986. 10

[Guckenheimer 1987] J. Guckenheimer and P. Holmes. Structurally stable heteroclinic cycles, volume 87. Cambridge University Press, 1987. 141

[Guillemin 2010] V. Guillemin and A. Pollack. Differential topology. Chelsea Pub Co, 2010. 129

[Guo 2005a] Y. Guo and C.C. Chow. *Existence and Stability of Standing Pulses in Neural Networks: II Stability.* SIAM Journal on Applied Dynamical Systems, vol. 4, pages 249–281, 2005. 23, 192, 197

[Guo 2005b] Yixin Guo and Carson C. Chow. *Existence and Stability of Standing Pulses in Neural Networks: I. Existence.* SIAM Journal on Applied Dynamical Systems, vol. 4, no. 2, pages 217–248, 2005. 23, 191, 192, 197

[Gutkin 2000] B.S. Gutkin, G.B. Ermentrout and J. O'Sullivan. *Layer 3 patchy recurrent excitatory connections may determine the spatial organization of sustained activity in the primate prefrontal cortex.* Neurocomputing, vol. 32-33, pages 391–400, 2000. 23

[Hammerstein 1930] A. Hammerstein. *Nichtlineare Integralgleichungen nebst Anwendungen.* Acta Math., vol. 54, pages 117–176, 1930. 23

[Hannula 2005] D.E. Hannula, D.J. Simons and N.J. Cohen. *Imaging implicit perception: promise and pitfalls.* Nature Reviews Neuroscience, vol. 6, no. 3, pages 247–255, 2005. 5

[Hansel 1997] D. Hansel and H. Sompolinsky. *Modeling feature selectivity in local cortical circuits.* Methods of neuronal modeling, pages 499–567, 1997. 25, 27, 32, 33, 111, 172

[Haragus 2010] M. Haragus and G. Iooss. Local bifurcations, center manifolds, and normal forms in infinite dimensional systems. EDP Sci. Springer Verlag UTX series, 2010. 50, 114, 195, 199, 202, 204, 261, 269, 270

[Hartshorne 1977] R. Hartshorne. Algebraic geometry, volume 52. Springer, 1977. 84

[Hazewinkel 2001] Michiel Hazewinkel, editeur. Encyclopaedia of mathematics. Springer, 2001. 23

[Helgason 2000] S. Helgason. Groups and geometric analysis, volume 83 of *Mathematical Surveys and Monographs.* American Mathematical Society, 2000. 78, 80, 81, 108

[Hoyle 2006] R.B. Hoyle. Pattern formation: an introduction to methods. Cambridge Univ Pr, 2006. 61, 180

[Hubel 1962] D.H. Hubel and T.N. Wiesel. *Receptive fields, binocular interaction and functional architecture in the cat visual cortex.* J Physiol, vol. 160, pages 106–154, 1962. 7, 8, 10, 11

[Hubel 1965] D.H. Hubel and T.N. Wiesel. *Receptive fields and functional architecture in two nonstriate visual areas (18 and 19) of the cat.* Journal of Neurophysiology, vol. 28, pages 229–289, 1965. 8, 10, 11

[Hubel 1968] D.H. Hubel and T.N. Wiesel. *Receptive fields and functional architecture of monkey striate cortex*. The Journal of Physiology, vol. 195, no. 1, page 215, 1968. 25

[Hubel 1977] D.H. Hubel and T.N. Wiesel. *Functional architecture of macaque monkey*. Proceedings of the Royal Society, London [B], pages 1–59, 1977. 8, 10, 11, 13

[Hubener 1997] M. Hubener, D. Shoham, A. Grinvald and T. Bonhoeffer. *Spatial Relationships among Three Columnar Systems in Cat Area 17*. Journal of Neuroscience, vol. 17, no. 23, pages 9270–9284, 1997. 13

[Hutt 2006] A. Hutt and F.M. Atay. *Effects of distributed transmission speeds on propagating activity in neural populations*. Physical Review E, vol. 73, no. 021906, pages 1–5, 2006. 23

[Hutt 2008] A. Hutt, A. Longtin and L. Schimansky-Geier. *Additive noise-induced Turing transitions in spatial systems with application to neural fields and the Swift-Hohenberg equation*. Physica D: Nonlinear Phenomena, vol. 237, no. 6, pages 755–773, 2008. 251

[Inoue 1999] K.T Inoue. *Computation of eigenmodes on a compact hyperbolic 3-space*. Rapport technique, arXiv, 1999. 99, 100

[Iooss 1993] G. Iooss and MC PerouEME. *Perturbed homoclinic solutions in reversible 1:1 resonance vector fields*. Journal of differential equations, vol. 102, no. 1, pages 62–88, 1993. 195, 202

[Issa 2000] N.P. Issa, C. Trepel and M.P. Stryker. *Spatial frequency maps in cat visual cortex*. J. Neurosci., vol. 20, pages 8504–8514, 2000. 30

[Iwaniec 2002] H. Iwaniec. Spectral methods of automorphic forms, volume 53 of *AMS Graduate Series in Mathematics*. AMS Bookstore, 2002. 38, 85

[Kandel 2000] E.R. Kandel, J.H. Schwartz and T.M. Jessel. Principles of neural science. McGraw-Hill, 4th édition, 2000. 3, 6, 9, 10, 11, 22

[Kaplan 2004] E. Kaplan. The M, P, and K pathways of the primate visual system, chapitre 30, pages 481–493. In Chalupa & Werner [Chalupa 2004], 2004. Two volumes. 30

[Kaschube 2008] M. Kaschube, M. Schnabel and F. Wolf. *Self-organization and the selection of pinwheel density in visual cortical development*. New Journal of Physics, vol. 10, page 015009, 2008. 32, 187, 251

[Kaschube 2010] M. Kaschube, M. Schnabel, S. Löwel, D.M. Coppola, L.E. White and F. Wolf. *Universality in the evolution of orientation columns in the visual cortex*. Science, vol. 330, no. 6007, page 1113, 2010. 32, 187, 251

[Katok 1992] S. Katok. Fuchsian groups. Chicago Lectures in Mathematics. The University of Chicago Press, 1992. 37, 82, 83, 168

[Kenet 2003] T. Kenet, D. Bibitchkov, M. Tsodyks, A. Grinvald and A. Arieli. *Spontaneously emerging cortical representations of visual attributes*. Nature, vol. 425, no. 6961, pages 954–956, 2003. 149

[Kilpatrick 2008] Z.P. Kilpatrick, S.E. Folias and P.C. Bressloff. *Traveling pulses and wave propagation failure in inhomogeneous neural media*. SIAM Journal on Applied Dynamical Systems, vol. 7, no. 1, pages 161–185, 2008. 17

[Kilpatrick 2010a] Z.P. Kilpatrick and P.C. Bressloff. *Effects of synaptic depression and adaptation on spatiotemporal dynamics of an excitatory neuronal network*. Physica D: Nonlinear Phenomena, vol. 239, no. 9, pages 547–560, 2010. 23

[Kilpatrick 2010b] Z.P. Kilpatrick and P.C. Bressloff. *Spatially structured oscillations in a two-dimensional excitatory neuronal network with synaptic depression*. Journal of computational neuroscience, vol. 28, no. 2, pages 193–209, 2010. 23

[Kilpatrick 2010c] Z.P. Kilpatrick and P.C. Bressloff. *Stability of bumps in piecewise smooth neural fields with nonlinear adaptation*. Physica D: Nonlinear Phenomena, vol. 239, no. 12, pages 1048–1060, 2010. 23

[Kirk 1994] V. Kirk and M. Silber. *A competition between heteroclinic cycles*. Nonlinearity, vol. 7, page 1605, 1994. 142, 143

[Kishimoto 1979] K. Kishimoto and S. Amari. *Existence and stability of local excitations in homogeneous neural fields*. Journal of Mathematical Biology, vol. 7, no. 4, pages 303–318, 1979. 17

[Klüver 1966] H. Klüver. Mescal, and mechanisms of hallucinations. University of Chicago Press Chicago, 1966. 61, 151

[Knutsson 1989] H. Knutsson. *Representing local structure using tensors*. In Scandinavian Conference on Image Analysis, pages 244–251, 1989. 25, 27

[Koenderink 1987] J. Koenderink and A. van Doorn. *Representation of local geometry in the visual system*. Biological Cybernetics, vol. 55, pages 367–375, 1987. 27

[Kozyreff 2006] G. Kozyreff and SJ Chapman. *Asymptotics of large bound states of localized structures*. Physical review letters, vol. 97, no. 4, page 44502, 2006. 205

[Krupa 1992] M. Krupa and I. Melbourne. *Nonasymptotically stable attractors in O(2) mode interactions*. Normal forms and homoclinic chaos (Waterloo, ON, 1992), vol. 4, pages 219–232, 1992. 142, 143, 144

[Krupa 1995] M. Krupa and I. Melbourne. *Asymptotic stability of heteroclinic cycles in systems with symmetry.* Ergodic Theory and Dynamical Systems, vol. 15, no. 01, pages 121–147, 1995. 142, 144

[Krupa 2004] M. Krupa and I. Melbourne. *Asymptotic stability of heteroclinic cycles in systems with symmetry. II.* Proceedings of the Royal Society of Edinburgh: Section A Mathematics, vol. 134, no. 06, pages 1177–1197, 2004. 142

[Laing 2002] C.L. Laing, W.C. Troy, B. Gutkin and G.B. Ermentrout. *Multiple bumps in a neuronal model of working memory.* SIAM J. Appl. Math., vol. 63, no. 1, pages 62–97, 2002. 17, 23, 191, 192, 193, 195, 196, 216

[Laing 2003a] Carlo R. Laing and William C. Troy. *PDE Methods for Nonlocal Models.* SIAM Journal on Applied Dynamical Systems, vol. 2, no. 3, pages 487–516, 2003. 17, 192, 194, 196, 220

[Laing 2003b] C.R. Laing and W.C. Troy. *Two-bump solutions of Amari-type models of neuronal pattern formation.* Physica D, vol. 178, no. 3, pages 190–218, April 2003. 23, 194

[Laing 2005] C.R. Laing. *Spiral waves in nonlocal equations.* SIAM Journal on Applied Dynamical Systems, vol. 4, no. 3, pages 588–606, 2005. 17

[Lang 1993] S. Lang. Algebra. Addison-Wesley, third edition édition, 1993. 90

[Lauterbach 2010] R. Lauterbach and P. Matthews. *Do absolutely irreducible group actions have odd dimensional fixed point spaces?* ArXiv, no. 1011.3986, 2010. 122

[Lebedev 1972] N.N. Lebedev and R.A. Silverman. Special functions and their applications. Dover Pubns, 1972. 158

[Lehoucq 2002] R. Lehoucq, J. Weeks, J-P. Uzan, E. Gausmann and J-P. Luminet. *Eigenmodes of 3-dimensional spherical spaces and their application to cosmology.* Rapport technique, arXiv, 2002. 99, 100

[Livingstone 1984] M.S. Livingstone and D.H. Hubel. *Anatomy and physiology of a color system in the primate visual cortex.* Journal of Neuroscience, vol. 4, pages 309—356, 1984. 30

[Lloyd 2008] D.J.B. Lloyd, B. Sandstede, D. Avitabile and A.R. Champneys. *Localized hexagon patterns of the planar Swift-Hohenberg equation.* SIAM Journal on Applied Dynamical Systems, vol. 7, no. 3, pages 1049–1100, 2008. 193, 250

[Lloyd 2009] D. Lloyd and B. Sandstede. *Localized radial solutions of the Swift–Hohenberg equation.* Nonlinearity, vol. 22, page 485, 2009. x, xii, 193, 194, 196, 219, 223, 224, 225, 227, 229, 246, 250

[Lund 2003] Jennifer S. Lund, Alessandra Angelucci and Paul C. Bressloff. *Anatomical Substrates for Functional Columns in Macaque Monkey Primary Visual Cortex*. Cerebral Cortex, vol. 12, pages 15–24, 2003. 10, 15, 32, 156, 192

[Malach 1993] R. Malach, Y. Amir, M. Harel and A. Grinvald. *Relationship between intrinsic connections and functional architecture revealed by optical imaging and in vivo targeted biocytin injections in primate striate cortex*. Proceedings of the National Academy of Sciences, vol. 90, no. 22, page 10469, 1993. 15

[Mariño 2005] J. Mariño, J. Schummers, D.C. Lyon, L. Schwabe, O. Beck, P. Wiesing, K. Obermayer and M. Sur. *Invariant computations in local cortical networks with balanced excitation and inhibition*. Nature neuroscience, vol. 8, no. 2, pages 194–201, 2005. 14

[Marr 1982] D. Marr. Vision. W.H. Freeman and Co., 1982. 27

[McCalla 2010] S. McCalla and B. Sandstede. *Snaking of radial solutions of the multi-dimensional Swift-Hohenberg equation: A numerical study*. Physica D: Nonlinear Phenomena, vol. 239, no. 16, pages 1581–1592, 2010. x, xii, 193, 194, 196, 219, 246, 250

[McCalla 2011] S. McCalla. *Localized Structures in the Multi-dimensional Swift–Hohenberg Equation*. PhD thesis, Brown UNiversity, 2011. 219, 226, 246

[McCormick 1985] D.A. McCormick, B.W. Connors, J.W. Lighthall and D.A. Prince. *Comparative electrophysiology of pyramidal and sparsely spiny stellate neurons of the neocortex*. Journal of Neurophysiology, vol. 54, no. 4, page 782, 1985. 24

[Melbourne 1986] I. Melbourne. *A singularity theory analysis of bifurcation problems with octahedral symmetry*. Dynamics and Stability of Systems, vol. 1, no. 4, pages 293–321, 1986. 98, 173, 175, 266

[Melbourne 1998] I. Melbourne. *Derivation of the time-dependent Ginzburg-Landau equation on the line*. Journal of Nonlinear Science, vol. 8, no. 1, pages 1–15, 1998. 205

[Miller 1972] W. Miller. Symmetry groups and their applications. Academic Press, 1972. 95, 96, 98, 168

[Moakher 2005] M. Moakher. *A Differential Geometric Approach to the Geometric Mean of Symmetric Positive-Definite Matrices*. SIAM J. Matrix Anal. Appl., vol. 26, no. 3, pages 735–747, April 2005. 34

[Mountcastle 1957] V.B. Mountcastle. *Modality and topographic properties of single neurons of cat's somatosensory cortex*. Journal of Neurophysiology, vol. 20, pages 408–434, 1957. 8, 10

[Murray 2003] J.D. Murray. Mathematical biology ii, spatial models and biomedical applications. Springer, 2003. 61

[Nauhaus 2008] I. Nauhaus, A. Benucci, M. Carandini and D.L. Ringach. *Neuronal selectivity and local map structure in visual cortex.* Neuron, vol. 57, no. 5, pages 673–679, 2008. 14, 40

[Nolte 2001] John Nolte. The human brain. Mosby, 5th édition, 2001. 8, 9

[Ohki 2005] K. Ohki, S. Chung, Y.H. Ch'ng, P. Kara and R.C. Reid. *Functional imaging with cellular resolution reveals precise micro-architecture in visual cortex.* Nature, vol. 433, pages 597–603, 2005. 13

[Orban 1986] G.A. Orban, H. Kennedy and J. Bullier. *Velocity sensitivity and direction selectivity of neurons in areas V1 and V2 of the monkey: influence of eccentricity.* Journal of Neurophysiology, vol. 56, no. 2, pages 462–480, August 1986. 25

[Oster 1970] G. Oster. *Phosphenes.* Scientific American, vol. 222, no. 2, page 82, 1970. 61, 151

[Oster 2006] A.M. Oster and P.C. Bressloff. *A developmental model of ocular dominance column formation on a growing cortex.* Bulletin of mathematical biology, vol. 68, no. 1, pages 73–98, 2006. 187, 251

[Owen 2007] M.R. Owen, C.R. Laing and S. Coombes. *Bumps and rings in a two-dimensional neural field: splitting and rotational instabilities.* New Journal of Physics, vol. 9, no. 10, pages 378–401, 2007. 23, 194

[Petitot 2003a] J. Petitot. *An introduction to the Mumford-Shah segmentation model.* Journal of Physiology - Paris, vol. 97, pages 335–342, 2003. 27

[Petitot 2003b] J. Petitot. *The neurogeometry of pinwheels as a sub-Riemannian contact structure.* Journal of Physiology-Paris, vol. 97, no. 2-3, pages 265–309, 2003. 251

[Petitot 2009] J. Petitot. Neurogéométrie de la vision. Les Éditions de l'École polytechnique, 2009. 27, 251

[Pinto 1996] D.J. Pinto, J.C. Brumberg, D.J. Simons, G.B. Ermentrout and R. Traub. *A quantitative population model of whisker barrels: re-examining the Wilson-Cowan equations.* Journal of Computational Neuroscience, vol. 3, no. 3, pages 247–264, 1996. 21

[Pinto 2001a] D.J. Pinto and G.B. Ermentrout. *Spatially structured activity in synaptically coupled neuronal networks: 1. Traveling fronts and pulses.* SIAM J. of Appl. Math., vol. 62, pages 206–225, 2001. 17, 23

[Pinto 2001b] D.J. Pinto and G.B. Ermentrout. *Spatially structured activity in synaptically coupled neuronal networks: 2. Standing pulses.* SIAM J. of Appl. Math., vol. 62, pages 226–243, 2001. 23, 24, 191, 192

[Pollicott 1989] M. Pollicott. *Distributions at infinity for Riemann surfaces.* In Stefan Banach Center, editeur, Dynamical Systems and Ergodic Theory, volume 23, pages 91–100, 1989. 85

[Potthast 2010] R. Potthast and P. Beim Graben. *Existence and properties of solutions for neural field equations.* Mathematical Methods in the Applied Sciences, vol. 33, no. 8, pages 935–949, 2010. 42

[Rabinovich 2008] M.I. Rabinovich, R. Huerta, P. Varona and V.S. Afraimovich. *Transient cognitive dynamics, metastability, and decision making.* PLoS computational biology, vol. 4, no. 5, page e1000072, 2008. 149

[Rabinovich 2010] M.I. Rabinovich, M.K. Muezzinoglu, I. Strigo and A. Bystritsky. *Dynamical principles of emotion-cognition interaction: mathematical images of mental disorders.* PloS one, vol. 5, no. 9, page e12547, 2010. 149

[Rankin 2011] J. Rankin, E. Tlapale, R. Veltz, O. Faugeras and P. Kornprobst. *Bifurcation analysis applied to a model of motion integration with a multistable stimulus.* Rapport technique RR-7822, INRIA Research Report, 2011. 251

[Ringach 2003] D.L. Ringach. *States of mind.* Nature, vol. 425, no. 6961, 2003. 149

[Rodieck 1965] R.W. Rodieck. Quantitative analysis of cat retinal ganglion cell response to visual stimuli. *Vision Research*, 5:583–601, 1965. 4, 6

[Rubin 2004] J.E. Rubin and W.C. Troy. *Sustained spatial patterns of activity in neuronal populations without recurrent excitation.* SIAM journal on applied mathematics, vol. 64, no. 5, pages 1609–1635, 2004. 23

[Ryzhik 2007] I.M. Ryzhik, A. Jeffrey and D. Zwillinger. Table of integrals, series and products. Academic Press, 2007. 233

[Sarti 2008] A. Sarti, G. Citti and J. Petitot. *The symplectic structure of the primary visual cortex.* Biological Cybernetics, vol. 98, no. 1, pages 33–48, 2008. 251

[Sausset 2007] F. Sausset and G. Tarjus. *Periodic boundary conditions on the pseudosphere.* Journal of Physics A: Mathematical and Theoretical, vol. 40, pages 12873–12899, 2007. 89

[Scheel 2003] A. Scheel. Radially symmetric patterns of reaction-diffusion systems, volume 165. American Mathematical Society, 2003. x, xii, 194, 219, 223, 227, 246, 250

[Schmit 1991] C. Schmit. *Quantum and classical properties of some billiards on the hyperbolic plane.* Chaos and Quantum Physics, pages 335–369, 1991. 99

[Schönert 1995] M. Schönert, H.U. Besche, T. Breuer, F. Celler, B. Eick, V. Felsch, A. Hulpke, J. Mnich, W. Nickel, G. Pfeiffer*et al. GAP: Groups, Algorithms and Programming.* Lehrstuhl D für Mathematik, Rheinisch Westfälische Technische Hochschule, Aachen, 1995. 90

[Schwartz 1977] E.L. Schwartz. *Spatial mapping in the primate sensory projection: Analytic structure and relevance to perception.* Biological cybernetics, vol. 25, no. 4, pages 181–194, 1977. 7

[Series 1987] C. Series. *Some geometrical models of chaotic dynamics.* Proceedings of the Royal Society of London. Series A, Mathematical and Physical Sciences, vol. 413, no. 1844, pages 171–182, 1987. 85

[Serre 1978] J.P. Serre. Représentations linéaires des groupes finis. Hermann, 1978. 110

[Shelley 2002] M. Shelley and D. McLaughlin. *Coarse-grained reduction and analysis of a network model of cortical response: I. Drifting grating stimuli.* Journal of Computational Neuroscience, vol. 12, no. 2, pages 97–122, 2002. 14

[Sherman 1996] S.M. Sherman and R.W. Guillery. *The functional organization of thalamocortical relays.* J. Neurophysiol.,, vol. 76, pages 1367–1395, 1996. 5

[Shriki 2003] O. Shriki, D. Hansel and H. Sompolinsky. *Rate models for conductance-based cortical neuronal networks.* Neural Computation, vol. 15, no. 8, pages 1809–1841, 2003. 111

[Sincich 2002] L.C. Sincich and J.C. Horton. *Divided by cytochrome oxidase: A map of the projections from V1 to V2 in macaques.* Science, vol. 295, pages 1734—1737, 2002. 30

[Swindale 2000] N.V. Swindale, D. Shoham, A. Grinvald, T. Bonhoeffer and M. Hubener. *Visual cortex maps are optimized for uniform coverage.* nature neuroscience, vol. 3, pages 822–826, 2000. 31

[Tass 1995] P. Tass. *Cortical pattern formation during visual hallucinations.* Journal of Biological Physics, vol. 21, no. 3, pages 177–210, 1995. 17

[Terras 1988] A. Terras. Harmonic analysis on symmetric spaces and applications, volume 2. Springer-Verlag, 1988. 177

[Tootell 1988] R.B.H. Tootell, S.L. Hamilton, M.S. Silverman, E. Switkes and R.L. De Valois. *Functional anatomy of macaque striate cortex. V. Spatial Frequency.* Journal of Neuroscience, vol. 8, pages 1610—1624, 1988. 30

[Tricomi 1985] F.G. Tricomi. Integral equations. Dover, 1985. Reprint. 23

[Tsodyks 1998] Misha Tsodyks, Klaus Pawelzik and Henry Markeam. *Neural Networks with Dynamic Synapses*. Neural Computation, vol. 10, pages 821–835, 1998. 23

[Tyler 1978] C.W. Tyler. *Some new entoptic phenomena*. Vision Research, vol. 18, no. 12, pages 1633–1639, 1978. 61, 62

[Veltz 2010a] Romain Veltz and Olivier Faugeras. *Illusions in the Ring Model of visual orientation selectivity*. Rapport technique, arXiv, 2010. Submitted to Plos Comp Bio. 162, 267

[Veltz 2010b] Romain Veltz and Olivier Faugeras. *Local/Global Analysis of the Stationary Solutions of Some Neural Field Equations*. SIAM Journal on Applied Dynamical Systems, vol. 9, no. 3, pages 954–998, August 2010. 23, 111, 114, 162

[Veltz 2011] Romain Veltz. *Nonlinear analysis methods in neural field models*. PhD thesis, Univ Paris Est ED MSTIC, 2011. 23, 186, 251

[Venkov 2007] N.A. Venkov, S. Coombes and P.C. Matthews. *Dynamic instabilities in scalar neural field equations with space-dependent delays*. Physica D: Nonlinear Phenomena, vol. 232, pages 1–15, 2007. 23

[Virchenko 2001] N.O. Virchenko and I. Fedotova. Generalized associated legendre functions and their applications. World Scientific Pub Co Inc, 2001. 238, 239

[Watson 1995] G.N. Watson. A treatise on the theory of bessel functions. Cambridge University Press, 1995. 158

[Werner 2001] Herrad Werner and Tim Richter. *Circular stationary solutions in two-dimensional neural fields*. Biological Cybernetics, vol. 85, no. 3, pages 211–217, September 2001. 23

[Wilson 1972] H.R. Wilson and J.D. Cowan. *Excitatory and inhibitory interactions in localized populations of model neurons*. Biophys. J., vol. 12, pages 1–24, 1972. 17, 25

[Wilson 1973] H.R. Wilson and J.D. Cowan. *A mathematical theory of the functional dynamics of cortical and thalamic nervous tissue*. Biological Cybernetics, vol. 13, no. 2, pages 55–80, September 1973. 17, 25

[Wohrer 2008] Adrien Wohrer. *Model and large-scale simulator of a biological retina with contrast gain control*. PhD thesis, University of Nice Sophia-Antipolis, 2008. 5

[Wolf 1998] F. Wolf and T. Geisel. *Spontaneous pinwheel annihilation during visual development.* Nature, vol. 395, no. 6697, pages 73–78, 1998. 32, 187, 251

[Woods 1999] P. D. Woods and A. R. Champneys. *Heteroclinic tangles and homoclinic snaking in the unfolding of a degenerate reversible Hamiltonian-Hopf bifurcation.* Physica D: Nonlinear Phenomena, vol. 129, no. 3-4, pages 147–170, 1999. 193, 196

[Xu 2004] X. Xu, W. Bosking, G. Sáry, J. Stefansic, D. Shima and V. Casagrande. *Functional organization of visual cortex in the owl monkey.* The Journal of neuroscience, vol. 24, no. 28, page 6237, 2004. 40

[Zettl 2005] A. Zettl. Sturm-liouville theory, volume 121. American Mathematical Society, 2005. 158